AD/A-007 077

IMPROVED MANUFACTURING METHOD FOR PRODUCING HIGH INTEGRITY, MORE RELIABLE TITANIUM FORGINGS

WYMAN-GORDON COMPANY

PREPARED FOR
AIR FORCE MATERIALS LABORATORY

FEBRUARY 1974

DISTRIBUTED BY:

NTIS
National Technical Information Service
U. S. DEPARTMENT OF COMMERCE

Security Classification

DOCUMENT CONTROL DATA · R&D

(Security classification of title, body of abstract and indexing annotation must be entered when the overall report is classified)

1. ORIGINATING ACTIVITY (Corporate author)
WYMAN-GORDON COMPANY
105 Madison Street
Worcester, Massachusetts 01601

2a. REPORT SECURITY CLASSIFICATION
NOT CLASSIFIED

2b GROUP

3. REPORT TITLE
IMPROVED MANUFACTURING METHOD FOR PRODUCING HIGH INTEGRITY, MORE RELIABLE TITANIUM FORGINGS

4 DESCRIPTIVE NOTES (Type of report and inclusive dates)
FINAL REPORT

5 AUTHOR(S) (Last name, first name, initial)
SPARKS, ROBERT B.
LONG, JOSEPH R.

6 REPORT DATE
FEBRUARY 1974

7a. TOTAL NO. OF PAGES

7b. NO. OF REFS
NONE

8a. CONTRACT OR GRANT NO.
AF33(615)71-C-1560

b. PROJECT NO

c.

d.

9a. ORIGINATOR'S REPORT NUMBER(S)
NONE

9b. OTHER REPORT NO(S) (Any other numbers that may be assigned this report)
NONE

10 AVAILABILITY/LIMITATION NOTICES
APPROVED FOR PUBLIC RELEASE

11. SUPPLEMENTARY NOTES
NONE

12. SPONSORING MILITARY ACTIVITY
AIR FORCE MATERIALS LABORATORY
AIR FORCE SYSTEMS COMMAND
U. S. AIR FORCE, WRIGHT-PATTERSON AIR FORCE BASE, OHIO 45433

13. ABSTRACT

This program was aimed at the determination of the effect of certain macro and microstructural variations on the mechanical properties of Ti-6Al-4V, Ti-6Al-6V-2Sn, and Ti-6Al-2Sn-4Zr-6Mo forgings.

The first task (A) involved the effect of starting billet macrostructure on finished forging mechanical properties. The second task (B) was the evaluation of the mechanical properties of different microstructures resulting from forging and heat treating variations. The microstructures of all conditions as observed by optical microscopy are presented and described. Selected samples of thin foil transmission electron micrographs are included, and a characterization of all the structures as revealed by transmission microscopy is reported.

Fracture patterns of the fracture toughness bars are characterized by scanning electron micrographs.

A mechanical property rating system which may be used to compare the various conditions evaluated is described. Using this system, each microstructural condition is rated for various mechanical properties, and total scores are shown for comparative purposes.

A third task involved the effect of certain metallurgical flaws on the mechanical properties of the Ti-6Al-4V and Ti-6Al-6V-2Sn alloys. Type II or "soft alpha" segregation in the 6-4 alloy and "Beta Flecks" in the 6-6-2 alloy were evaluated. The same mechanical property tests used in Tasks A and B were used for evaluation.

DD FORM 1 JAN 68 1473

PRICES SUBJECT TO CHANGE

Security Classification

KEY WORDS	LINK A		LINK B		LINK C	
	ROLE	WT	ROLE	WT	ROLE	WT
RELIABLE TITANIUM FORGINGS						

INSTRUCTIONS

1. ORIGINATING ACTIVITY: Enter the name and address of the contractor, subcontractor, grantee, Department of Defense activity or other organization *(corporate author)* issuing the report.

2a. REPORT SECURITY CLASSIFICATION: Enter the overall security classification of the report. Indicate whether "Restricted Data" is included. Marking is to be in accordance with appropriate security regulations.

2b. GROUP: Automatic downgrading is specified in DoD Directive 5200.10 and Armed Forces Industrial Manual. Enter the group number. Also, when applicable, show that optional markings have been used for Group 3 and Group 4 as authorized.

3. REPORT TITLE: Enter the complete report title in all capital letters. Titles in all cases should be unclassified. If a meaningful title cannot be selected without classification, show title classification in all capitals in parenthesis immediately following the title.

4. DESCRIPTIVE NOTES: If appropriate, enter the type of report, e.g., interim, progress, summary, annual, or final. Give the inclusive dates when a specific reporting period is covered.

5. AUTHOR(S): Enter the name(s) of author(s) as shown on or in the report. Enter last name, first name, middle initial. If military, show rank and branch of service. The name of the principal author is an absolute minimum requirement.

6. REPORT DATE: Enter the date of the report as day, month, year, or month, year. If more than one date appears on the report, use date of publication.

7a. TOTAL NUMBER OF PAGES: The total page count should follow normal pagination procedures, i.e., enter the number of pages containing information.

7b. NUMBER OF REFERENCES: Enter the total number of references cited in the report.

8a. CONTRACT OR GRANT NUMBER: If appropriate, enter the applicable number of the contract or grant under which the report was written.

8b, 8c, & 8d. PROJECT NUMBER: Enter the appropriate military department identification, such as project number, subproject number, system numbers, task number, etc.

9a. ORIGINATOR'S REPORT NUMBER(S): Enter the official report number by which the document will be identified and controlled by the originating activity. This number must be unique to this report.

9b. OTHER REPORT NUMBER(S): If the report has been assigned any other report numbers *(either by the originator or by the sponsor)*, also enter this number(s).

10. AVAILABILITY/LIMITATION NOTICES: Enter any limitations on further dissemination of the report, other than those imposed by security classification, using standard statements such as:

(1) "Qualified requesters may obtain copies of this report from DDC."

(2) "Foreign announcement and dissemination of this report by DDC is not authorized."

(3) "U. S. Government agencies may obtain copies of this report directly from DDC. Other qualified DDC users shall request through _____."

(4) "U. S. military agencies may obtain copies of this report directly from DDC. Other qualified users shall request through _____."

(5) "All distribution of this report is controlled. Qualified DDC users shall request through _____."

If the report has been furnished to the Office of Technical Services, Department of Commerce, for sale to the public, indicate this fact and enter the price, if known.

11. SUPPLEMENTARY NOTES: Use for additional explanatory notes.

12. SPONSORING MILITARY ACTIVITY: Enter the name of the departmental project office or laboratory sponsoring *(paying for)* the research and development. Include address.

13. ABSTRACT: Enter an abstract giving a brief and factual summary of the document indicative of the report, even though it may also appear elsewhere in the body of the technical report. If additional space is required, a continuation sheet shall be attached.

It is highly desirable that the abstract of classified reports be unclassified. Each paragraph of the abstract shall end with an indication of the military security classification of the information in the paragraph, represented as (TS), (S), (C), or (U).

There is no limitation on the length of the abstract. However, the suggested length is from 150 to 225 words.

14. KEY WORDS: Key words are technically meaningful terms or short phrases that characterize a report and may be used as index entries for cataloging the report. Key words must be selected so that no security classification is required. Identifiers, such as equipment model designation, trade name, military project code name, geographic location, may be used as key words but will be followed by an indication of technical context. The assignment of links, rules, and weights is optional.

Security Classification

AFML-TR-73-301

IMPROVED MANUFACTURING METHODS FOR PRODUCING HIGH INTEGRITY MORE RELIABLE TITANIUM FORGINGS

R. B. Sparks
J. R. Long

Wyman-Gordon Company
Worcester, Massachusetts

TECHNICAL REPORT AFML-TR-73-301

FEBRUARY 1974

Air Force Material Laboratory

Air Force Systems Command

Wright-Patterson Air Force Base, Ohio

ic

ABSTRACT

This program was aimed at the determination of the effect of certain macro and microstructural variations on the mechanical properties of Ti-6Al-4V, Ti-6Al-6V-2Sn, and Ti-6Al-2Sn-4Zr-6Mo forgings.

The first task (A) involved the effect of starting billet macrostructure on finished forging mechanical properties. The second task (B) was the evaluation of the mechanical properties of different microstructures resulting from forging and heat treating variations. Twenty-three structures were investigated for the 6-4 alloy, twenty-two for the 6-6-2 alloy, and eleven for the 6-2-4-6 alloy. Smooth and notched tensile, smooth and notched high cycle fatigue, low cycle fatigue, and fracture toughness properties were established for each structure produced in tasks A and B. The microstructures of all conditions as observed by optical microscopy are presented and described. Selected samples of thin foil transmission electron micrographs are included, and a characterization of all the structures as revealed by transmission microscopy is reported.

Fracture patterns of the fracture toughness bars are characterized by scanning electron micrographs.

A mechanical property rating system which may be used to compare the various conditions evaluated is described. Using this system, each microstructural condition is rated for various mechanical properties, and total scores are shown for comparative purposes.

A third task involved the effect of certain metallurgical flaws on the mechanical properties of the Ti-6Al-4V and Ti-6Al-6V-2Sn alloys. Type II or "soft alpha" segregation in the 6-4 alloy and "Beta Flecks" in the 6-6-2 alloy were evaluated. The same mechanical property tests used in Tasks A and B were used for evaluation.

FOREWORD

This Final Technical Report covers work performed under Contract AF-33615-71-C-1560 from July 1, 1971 through August 1973.

This contract with Wyman-Gordon Company, Worcester, Massachusetts was initiated under Project 226-1. The work was begun under the technical direction of Mr. G. W. Trickett and continued under Mr. N. E. Klarquist AFML/LTP of the Manufacturing Technology Division, Air Force Materials Laboratory, Wright-Patterson Air Force Base, Ohio 45433.

The program was managed for Wyman-Gordon by Mr. R. B. Sparks assisted by Mr. J. R. Long. The contract was under the direction of Mr. J. E. Coyne, Director of Research.

Low cycle fatigue testing was conducted at Pratt & Whitney Aircraft under the direction of Mr. Duane Ruckle. High cycle fatigue and fracture toughness testing was performed at LTV Aerospace Company under Dr. Carl Dumesnil; Transmission Electron Microscopy and Scanning Electron Microscopy were carried out at the Rockwell International Science Center under Dr. James Williams.

An Advisory Committee which met regularly during the course of the contract to review the program and provide technical assistance consisted of the following:

Mr. R. G. Broadwell	Timet Company
Mr. J. E. Coyne	Wyman-Gordon Company
Mr. N. E. Klarquist	AFML
Dr. H. Margolin	Polytechnic Institute of New York
Mr. T. K. Redden	General Electric Company
Mr. D. L. Ruckle	Pratt & Whitney Aircraft
Mr. R. B. Sparks	Wyman-Gordon Company
Dr. J. C. Williams	Rockwell International Science Center

This technical report has been reviewed and is approved.

H. A. Johnson
Chief, Metals Branch
Manufacturing Technology Division

TABLE OF CONTENTS

TABLE OF CONTENTS, CONTINUED

List of Illustrations

List of Illustrations (Continued)

List of Illustrations (Continued)

List of Illustrations (Continued)

List of Illustrations (Continued)

List of Illustrations (Continued)

List of Illustrations (Continued)

List of Tables

List of Tables (Continued)

List of Tables (Continued)

List of Tables (Continued)

List of Tables (Continued)

I. INTRODUCTION

Current military aircraft such as the F-14 and F-15 and future aircraft including the B-1 will make extensive use of titanium forgings in both airframes and engines. The alloys of prime interest are Ti-6Al-4V, Ti-6Al-6V-2Sn, and Ti-6Al-2Sn-4Zr-6Mo. It has been well established that mechanical properties of these alloys are affected by both micro and macrostructure. The forger, because of the nature of his operation in heating, working, and heat treatment, bears primary responsibility for the microstructure. Basic properties of these alloys, as affected by structure, are generally established; however, there is a need to determine the effect of structure variations on the extremely important second tier properties such as fracture toughness and fatigue. Also, a number of flaws and segregates have been recently observed in titanium parts. These defects have affected properties and service life. It was the purpose of this program to establish on closed die forgings the effect of various micro and macrostructures, and certain flaws and segregates on mechanical properties including fatigue and fracture toughness.

In Phase I, the effects of various billet macrostructures and forged part microstructures on the first and second tier mechanical properties of titanium alloy forgings were determined. The alloys evaluated were Ti-6Al-4V, Ti-6Al-6V-2Sn, and Ti-6Al-2Sn-4Zr-6Mo. Two closed die forgings were used in the evaluation: a structural shape and a compressor disc shape. All forging was done in a 1500-ton hydraulic press.

Macrostructures evaluated included coarse and fine macro grain size and an intermediate size. Microstructures included those resulting from different amounts of forging reductions and different forging temperatures. Twenty-three different microstructural variations on Ti-6Al-4V, 22 structures of Ti-6Al-6V-2Sn, and 11 structures on Ti-6Al-2Sn-4Zr-6Mo were made.

Mechanical property data including smooth and notched tensile, smooth and notched high cycle fatigue, low cycle fatigue, and fracture toughness were developed for each macro and microstructural condition. The forging processes and thermal treatments used to produce the various macro and microstructures are described, and the macro and microstructures of the forgings are presented. In addition to light microscopy, transmission electron microscopy was also performed on all microstructural conditions.

Phase II included the Ti-6Al-4V and Ti-6Al-6V-2Sn alloys. The same closed die forging configurations used in Phase I were used. Metallurgical flaws including soft alpha and beta flecks were evaluated for effect on smooth and notched tensile properties, low cycle fatigue, smooth and notched high cycle fatigue, and fracture toughness.

A technical committee composed of the following individuals met regularly to review and advise on this program:

R. G. Broadwell	Timet
J. E. Coyne	Wyman-Gordon Company
N. E. Klarquist	AFML
H. Margolin	Polytechnic Institute of New York
T. K. Redden	General Electric Company
D. L. Ruckle	Pratt & Whitney Aircraft
R. B. Sparks	Wyman-Gordon Company
J. C. Williams	Rockwell International Science Science Center

Machining and testing of all specimens was performed at Wyman-Gordon Company with the following exceptions:

High cycle fatigue specimens machined at Stulen Machine Company and tested at LTV Aerospace Company. The machining technique used on the fatigue specimens is described in Appendix B.

Fracture toughness specimens were machined and tested at LTV Aerospace Company.

Low cycle fatigue specimens were machined at Gorbil Tool Company and tested at Pratt & Whitney Aircraft.

All light microscopy was performed at Wyman-Gordon; electron transmission microscopy and scanning electron microscopy were performed at Rockwell International Science Center.

II. MATERIALS

Three alloys: Ti-6Al-4V, Ti-6Al-6V-2Sn, and Ti-6Al-2Sn-4Zr-6Mo were utilized. The materials for the program supplied by Timet Company are shown in Table I. Ultrasonic inspection of all bars was performed at Timet Company and was repeated at Wyman-Gordon. Timet used immersion sonic testing on all round stock and contact sonic on all square material. Wyman-Gordon used immersion testing for all bars. Table II shows the details of the ultrasonic inspection. Although some bars showed "noise" to the extent noted, no discrete sonic indications were found. No obvious structural differences were found between the so-called high noise areas and lower noise areas. The finished forgings were also sonic inspected and compared with the starting billet stock.

Wyman-Gordon chemical analysis compared with the mill analysis of all material is shown in Table III. The beta transus as determined metallographically at Wyman-Gordon for each item is shown in Table IV.

Macroetched slices showed that all billets had the desired structures. Figures 1 - 5 show starting macrostructures.

Microexamination of starting billet stock showed that all material except the 14" square stock had been finished in the alpha + beta range. Starting microstructures are shown in Figures 6 - 10. Beta stabilized areas were confirmed in the 6Al-6V-2Sn alloy which was purposely melted to produce "flecks" (Figure 9B).

An intermediate grain size was created at Wyman-Gordon on some of the 14" square Ti-6Al-4V by annealing at 2200°F for two hours. The macro and microstructure of the intermediate grain size stock is shown in Figure 11.

Grain sizes of starting billet material used for the macrostructure study (Phase I, Task A) are shown in Table V.

III. PHASE I, TASK A

A. Processing

Phase I, Task A, was a study of the effect of starting billet macrostructure on the mechanical properties of finished forgings. Ti-6Al-4V, Ti-6Al-6V-2Sn, and Ti-6Al-2Sn-4Zr-6Mo were the alloys investigated. Depending upon the efficiency of the ingot conversion forging process, the final billet may contain a mixture of recrystallized and nonrecrystallized grains, both showing evidence of alpha-beta working. These structures may be duplexed or predominantly large or small in grain size. In this work, such a definition is applied to the terminology "coarse" and "intermediate" and "fine" macro grain size billet. An attempt was made to give a general numerical grain size measurement (as shown in Table V); however, no effort was made at a delineation of percent recrystallization versus percent nonrecrystallized grains. Coarse and fine grained billet from the same mill heat were obtained for the Ti-6Al-4V and Ti-6Al-6V-2Sn alloys. The coarse grained material was in the form of 14" square stock which was quartered to 6" square. The fine grained material was processed by the mill to the 6" square size. An intermediate grain size was created at Wyman-Gordon on some of the 14" square Ti-6Al-4V by annealing at 2200°F for two hours (see Materials). Six-inch round stock was used to evaluate the Ti-6Al-2Sn-4Zr-6Mo alloy.

For evaluation of the Ti-6Al-4V and Ti-6Al-6V-2Sn alloys, the structural shape was used (Figure 12). This forging was preformed on open dies, blocked in one set, and finished in a second set of closed dies. This processing is typical of many titanium airframe parts. All operations were performed on a 1500-ton hydraulic forging press. A typical part after the various stages of forging is shown in Figure 13. Ten forgings of this configuration were required for each condition. A total of 30 Ti-6Al-4V parts and 20 Ti-6Al-6V-2Sn parts were made for this task.

A compressor disc part was used to evaluate the Ti-6Al-2Sn-4Zr-6Mo alloy (Figure 14). This part was upset and finished in two operations on a 1500-ton hydraulic press. A typical finished part is shown in Figure 15. Five fine grained and five coarse grained wheels were forged.

All the parts made for the macrostructure study were alpha beta forged in all operations using the temperatures shown in Table VI. After forging, the parts were heat treated as shown in Table VII. Ultrasonic inspection was performed on all finished forgings using immersion techniques. No defects were found in any of the forgings. A 3/32" flat bottom hole was the inspection standard.

B. Testing

Smooth and notched (K_t = 3.9) tensiles, low cycle fatigue (using the Pratt & Whitney half bolt hole specimen), smooth and notched high cycle fatigue and fracture toughness specimens were taken from the forgings as shown in Figures 16 through 21. Table VIII shows the number of specimens of each type. All specimens from the structural part were taken from the heavy section of the forgings (as was done when this shape was used for previous Air Force material evaluations). Specimen drawings are shown in Appendix A. Pratt & Whitney low cycle fatigue testing is described in Appendix C. Machining procedures used for high cycle fatigue specimens are described in Appendix B. High cycle fatigue testing was tension-tension conducted at an R ratio of 0.1.

Longitudinal slices were taken through one structural forging representing each condition. Macrostructure of these slices are shown in Figures 22 through 26. Microstructures from the heavy section of each condition are also shown in Figures 22 through 26. Macro and microstructure of the fine and coarse grained Ti-6Al-2Sn-4Zr-6Mo discs are shown in Figures 27 and 28. All microstructures showed primary alpha in a transformed matrix typical of alpha beta alloys forged in the alpha + beta field.

Smooth and notched (K_t = 3.9) tensile results on all conditions are shown in Tables IX and X respectively. High cycle fatigue results are summarized in Table XI. Table XII shows fracture toughness results and LCF data are shown in Table XIII and Figure 29.

C. Results

Ti-6Al-4V

No significant differences were found in smooth or notched tensile properties or in NTS/UTS ratio among the three macro grain sizes evaluated.

The intermediate grain size condition showed a significantly higher endurance limit (40 ksi) at 10^7 cycles than either the coarse grained (26 ksi) or the fine grained (30 ksi).

The fine grained material showed a somewhat higher K_{IC} (67.8) than the intermediate (57.5) or coarse grained (53.9) condition.

The intermediate and fine grained conditions were superior to the coarse grained condition in both initiation and growth to 1/32" crack on the low cycle fatigue test.

Ti-6Al-6V-2Sn

The fine grained material showed slightly higher strength and ductility than the coarse grained material on smooth tensile tests. No significant difference was found in NTS/UTS between the two grain size conditions.

No difference was found in notched high cycle fatigue behavior between the coarse and fine grained conditions. Average fracture toughness of the coarse grained forgings (K_{IC} = 70) was higher than that of the fine grained (K_{IC} = 54) for this alloy.

The fine grained material was slightly better than the coarse grained in initiation and growth to 1/32" crack on the half bolt hole LCF test.

Ti-6Al-2Sn-4Zr-6Mo

For this alloy (as opposed to the 6-4 and 6-6-2) the coarse and fine grained material were not from the same mill heat so that any differences found might be somewhat influenced by slightly different chemistry. However, very little difference in properties was found.

The fine grained material showed slightly higher strength and ductility than the coarse grained on the smooth tensile results. The NTS/UTS was not significantly different between the two grain size conditions.

Both coarse and fine grained conditions showed equivalent notched high cycle fatigue life at 10^7 cycles.

Fracture toughness showed no significant differences between the two grain sizes, K_{IC} = 30.2 for the fine grained and K_{IC} = 32.2 for the coarse grained.

Low cycle fatigue data showed that the coarse grained condition gave a longer average time to both crack initiation and 1/32" crack.

D. Mechanical Property Rating System

A mechanical property rating system was applied to the data for the various macrostructure conditions. Appendix D gives the details of the system. Table XIV shows the results for Phase I, Task A. No overall trend applicable to all alloys was apparent. The 6-2-4-6 alloy showed exactly the same total point score for both coarse and fine grained material. The 6-6-2 showed only a one point difference with the coarse grained higher. The 6-4 showed both the intermediate and fine grained to be superior to coarse grained with the difference coming essentially in the fatigue behavior. Both low and high cycle fatigue appears to improve with finer grain size for the Ti-6Al-4V alloy.

E. Conclusions

Macro grain size did not appear to significantly affect any of the properties tested on the subject alloys, except for fatigue on the 6-4 alloy. Lowest fatigue strength was associated with largest grain size for 6Al-4V alloy. Typical forging practice will carry over billet grain size.

IV. PHASE I, TASK B

A. Processing

This task consisted of a study of the effect of microstructure on mechanical properties of the three subject alloys. All starting billet was fine grained to minimize any macro grainsize effect. Twenty-two different microstructures were produced in the structural part in Ti-6Al-4V and Ti-6Al-6V-2Sn alloys (Figure 12). Figure 30 shows an outline of the processing used to produce these structures. Forging temperatures are shown in Table IV. In the alpha + beta categroy, 10-20% spherical alpha, (Figures 38A and 46A) and 40-50% spherical alpha (Figures 38A-1 and 46A-1) were aimed-for structures. Coarse elongated alpha, sometimes referred to as "spaghetti" or "wormy" alpha (Figure 39), a structure which has been seen in forging billet stock and finished forgings, was created by a thermal treatment (heating high in the beta field, then transferring to a furnace operating at approximately the beta transus, holding for an hour at that temperature, then slow cooling to approximately 150°F below the beta transus and air cooling). The preforms with this structure were conventionally forged in the alpha + beta field. Grain boundary outlining (Figure 40) is another structure that was created by thermal treatment (heating to 50°F above the beta transus, holding for one hour, then transferring to a furnace at 1400°F, stabilizing at that temperature and then air cooling). Preforms with this structure were also alpha + beta forged. In the beta forging section of the program, conditions included beta blocking and alpha beta finishing with two different amounts of reduction, beta blocking and beta finishing, and beta finishing with a slow cool to produce grain boundary outlining. In addition to the forging variations, both water quenching and air cooling from the forging press and two different heat treatments were utilized to provide further structure variations. All heat treatments are also indicated in Figure 30. A total of 154 structural forgings were made for each alloy in this portion of the program. An additional group of structural forgings were made from low oxygen Ti-6Al-4V for one of the microstructural conditions (Conditions A).

The processing of the Ti-6Al-2Sn-4Zr-6Mo alloy is outlined in Figure 31. The compressor disc shape (Figure 14) was used to evaluate this alloy. Forging temperatures are shown in Table XVI. The all alpha + beta forged portion of the program evaluated two amounts of spherical alpha in the finished microstructure: 10-20% and 40-50%. In the beta forged evaluation, beta upset with finishing high (T - 25°F) in the alpha+beta field was done with two amounts of reduction in the finish operation. Two amounts of reduction in the finish operation was also performed low in the alpha+beta field (T-100°F). A completely beta forged condition (beta blocked and beta finished) was also included. Heat treating included a standard solution treat and age, a solution treat and overage, and an anneal.

B. Testing

The testing program is outlined in Table XVII. Test specimens were removed from the forgings in the same pattern as that used for Phase I, Task A.

The in-process and final microstructures are shown in Figures 32-37. The final microstructures are shown and described in Figures 38-56 .

For the purposes of this report, the following definitions apply:

Primary (prior) β grain size
β grain size of billet prior to forging or β grain size resulting from processing in the β field

Secondary β grain size
β grain size smaller than the primary grain size produced by thermomechanical treatment in the α-β field

Measurements of percent alpha and alpha particle size are shown in Tables XVIII-XX. All of the mechanical property individual test results are included in the interim progress reports on the program. For most properties, only summary data will be presented in this report.

Smooth tensile data are summarized in Tables XXI, XXII, and XXIII. Notched tensile data are shown in Tables XXIV, XXV, and XXVI.

Table XXVII summarizes the high cycle fatigue data. S/N curves for the individual conditions are presented in the progress reports. As previously shown in interim progress reports, smooth bar data showed considerable scatter and the values given in Table XXVII are from the best curve fit of the S/N curves. Notched bar fatigue data was generally good in that the spread was small; the individual data points fell in a smooth S/N curve.

A summary of the low cycle fatigue data is shown in Table XXXI and Figures 57-59. The Pratt & Whitney report on the LCF testing is included as an appendix to this report.

C. Results and Conclusions

1. Ti-6Al-4V

Tensile Properties (Smooth) (Table XXI)

All conditions met 120 ksi minimum yield strength and 130 ksi minimum ultimate strength as required by most specifications. In general, the conditions which were alpha + beta forged in the last operation and given an STOA condition showed the highest strengths; however, the 10% primary alpha annealed condition (A) and the water quenched from a beta forge finish and annealed (S) condition showed equally good strength values.

As a group, the all-beta forged condition (Q through U) showed lower ductility than the other conditions. One alpha beta forged condition, spaghetti alpha in the STOA heat treat condition (E) also showed poor ductility. All other conditions met the typical specification of 10% elongation and 25% reduction of area.

The best combination of strength and ductility with low standard deviation occurred with condition B alpha beta forged to 10% primary alpha structure, then solution treated and overaged.

Tensile Properties (Notched) (Table XXIV)

All conditions showed a $\frac{NTS}{UTS}$ ratio greater than 1.0 at $K_t = 3.9$.

Average $\frac{NTS}{UTS}$ values ranged from 1.40 - 1.58 for all conditions. Lowest $\frac{NTS}{UTS}$ (1.40) occurred with the spaghetti alpha in the STOA condition (E).

Highest $\frac{NTS}{UTS}$ (1.58) was obtained with conditions A-1 and N.

High Cycle Fatigue (Smooth) (Table XXVII)

The data is presented and the authors' interpretation of the S/N curves are shown; however, due to the large amount of scatter in the smooth bar fatigue data, no conclusion will be drawn from this work. Endurance limits ranged from 72-90 ksi at 10^7 cycles.

The cause of scatter in the fatigue data was not isolated, but may in part be attributed to machining and testing variables such as specimen preparation, residual stress, and specimen alignment. A limited investigation of these factors did not reveal any reason for the wide spread in results.

High Cycle Fatigue (Notched) (Table XXVII)

In general, the notched fatigue data produced good S/N curves.

Endurance limit at 10^7 cycles for $K_t = 3.0$ ranged from 27 ksi to 38 ksi. Lowest notched bar fatigue life was obtained on the condition R specimen (27 ksi). This specimen was air cooled from a finish forge temperature in the beta range then given a conventional STOA treatment.

The highest endurance limit, 38 ksi at 10^7 cycles, was obtained with Condition I. This condition was produced by blocking and finishing at alpha + beta temperatures, water quenching from the press, and annealing. The starting billet had been treated to purposely produce grain boundary alpha.

Fracture Toughness (Table XXVIII)

For all conditions tested, K_{IC} ranged from 57 to 87 for the standard O_2 level 6-4.

Four conditions (D, J, R, and U) gave K_{IC} values 86-87. Two conditions (B and C) gave K_{IC} value <60. All other 16 conditions showed K_{IC} between 60 and 80.

The one condition tested for low O_2 material (condition A, alpha beta forged to 10% primary alpha structure and annealed) gave a K_{IC} of 103.

2. Ti-6Al-6V-2Sn

Tensile Properties (Smooth) (Table XXII)

All conditions met the typical specification minimum for annealed Ti-6Al-6V-2Sn of 135 ksi yield strength, 145 ksi ultimate strength, 8% elongation, and 15% reduction of area.

The highest strength condition (S) was obtained by water quenching from the finish forge operation in the beta field. Those forgings given the STOA condition or water quenched from the finish forge operation were generally higher in strength than those air cooled from the forging operation and annealed.

Those conditions which had no beta temperature exposure at any point in the forging process (at Wyman-Gordon) conditions A, A-1, B, and C showed the best ductilities, especially outstanding was reduction of area.

The all beta processed groups showed a generally lower ductility, mainly evident in reduction of area. The group which was water quenched from the final forge operation exhibited the lowest R.A. of all conditions.

Tensile Properties (Notched) (Table XXV)

All conditions showed a $\frac{NTS}{UTS}$ greater than 1 for $K_t = 3.9$. Average $\frac{NTS}{UTS}$ ranged from 1.32 - 1.53.

Lowest $\frac{NTS}{UTS}$ (1.32) occurred with the condition (S) water quenched from a finish beta forge operation and annealed.

Highest $\frac{NTS}{UTS}$ (1.53) resulted from the condition G, forging stock containing grain boundary alpha, alpha beta forged and annealed.

High Cycle Fatigue (Smooth) (Table XXVII)

As with the other alloys, in most cases, the scatter in smooth bar data was too great to provide valid comparisons. Endurance limits at 10^7 cycles as interpreted by the authors ranged from <75 to 100 ksi. The lowest values at 10^6 cycles and projected to 10^7 occurred with the "spaghetti" alpha structures water quenched off the press (Condition F) and the STOA heat treat condition (E).

High Cycle Fatigue (Notched) (Table XXVII)

The notched S/N curves in general were good. Endurance limits at 10^7 cycles ranged from 29-40 ksi. The lowest value at 10^7 cycles (29 ksi) was obtained with Condition Q, beta forged in both operations and annealed. The lowest of the alpha beta forged material (31 ksi) resulted from the grain boundary alpha stock in the annealed condition (G). Best 10^7 values (40 ksi) were obtained on grain boundary alpha stock alpha beta forged and given the STOA heat treatment (H), and the beta blocked and alpha beta finished, water quenched from the press and annealed condition (L). No major differences were apparent between the all alpha beta forged, beta + alpha forged or all beta forged condition. The grain boundary alpha and spaghetti alpha conditions were also quite comparable to those conditions without these abnormal structures.

Fracture Toughness (Table XXIX)

K_{IC} values for all conditions ranged from 41.0 to 77.1 -
12 conditions gave K_{IC} values between 60 and 77.1,
2 conditions (B and C) were below 45, and the remaining
8 conditions were between 45 and 60.

In general, the 6-6-2 values followed the same pattern as the similarly processed 6-4 samples, but at 10-20 ksi $\sqrt{\text{in.}}$ lower level.

The highest values were obtained by conditions of $\beta + \alpha\beta$ and all β forging (J, K, Q, R, S, and U. The lowest by conventional alpha beta processing (B and C) similar to the 6-4.

The lowest of the beta forged group at K_{IC} = 51.8 was Condition S (water quenched from the press after the finish operation and annealed). This condition (S) was also lowest of the 6-4 beta forged group.

Low Cycle Fatigue (Table XXXI)

The best LCF life (>20,000 cycles to 1/32" crack) was obtained with the following conditions:

A, B, C, A-1, and K (marginally)

All other conditions fall within the range of approximately 9-16,000 cycles for 1/32" long crack.

For crack initiation (cycles to pinpoint indication) only Conditions C and B exceeded 20,000 cycles. Conditions A, A-1, and K showed pinpoints between 15-20,000 cycles. All others were below 12,000 cycles.

3. Ti-6Al-2Sn-4Zr-6Mo

Tensile Properties (Smooth) (Table XXIII)

All conditions in the STA heat treated condition met 150 ksi minimum yield strength, 170 ksi minimum ultimate strength. Those conditions with two alpha beta forging operations given the STA heat treatment exceeded 10% elongation and 30% R.A. Ductility dropped with the use of beta temperatures for the first forge operation. The lowest ductility occurred with the use of beta temperatures for both forging operations (Condition G). Condition G also showed the lowest yield strength of the STA heat treated condition.

Highest strength condition was obtained by Condition B, alpha beta forged in both forging operations to a 50% spherical alpha structure and solution treated and aged.

Lower strengths were produced by the STOA and anneal only heat treat condition. In these conditions, the forgings with the higher primary alpha content (50%) (B1 and B2) were somewhat higher in yield strength (10.4 KSI) than those with the lower amount (10%) (A-1 and A-2).

The best combination of strength and ductility occurred with the alpha beta forged to 50% primary alpha then solution treated and aged.

Tensile Properties (Notched) (Table XXVI)

All conditions showed $\frac{NTS}{UTS}$ greater than 1 for $K_t = 3.9$.

Average $\frac{NTS}{UTS}$ ranged from 1.25 - 1.47.

Highest $\frac{NTS}{UTS}$ 1.47 was obtained with alpha beta forged to 10% primary alpha then given the STOA heat treatment.

Highest $\frac{NTS}{UTS}$ for the STA condition was Condition A, alpha beta forged to 10% primary alpha and Condition E beta blocked, and given a 10% finish reduction in the alpha beta field.

Lowest $\frac{NTS}{UTS}$ (1.26) resulted from the all-beta forged process with the STA heat treatment (Condition G).

High Cycle Fatigue (Smooth) (Table XXVII)

Similar to the other two alloys, excessive scatter was obtained in the smooth HCF tests; 10^7 cycle endurance limits for all conditions were between 88-109 ksi.

High Cycle Fatigue (Notched) (Table XXVII)

The 10^7 endurance limits for all conditions tested fall within a relatively narrow band of 34-42 ksi. The highest value (42 ksi) was obtained on Condition A-1, alpha beta forged to a 10% primary alpha structure and annealed. The lowest (34 ksi) was determined on Condition F beta blocked and alpha beta finished with 30% reduction from a temperature low in the alpha + beta field.

Microstructure did not appear to have a significant effect on notched HCF, the 10% primary alpha condition (A), the 50% primary alpha condition (B), and the all-beta condition (G) all showed essentially the same S/N curves.

Fracture Toughness (Table XXX)

K_{IC} values for all conditions ranged from 23.3 to 52.4 ksi $\sqrt{in.}$ the lowest values (<25 ksi $\sqrt{in.}$) were associated with Conditions B, B-1, and B-2 which were alpha beta forged to a 50% primary alpha structure and then given the STA, anneal, and STOA heat treatments respectively. The corresponding conditions A, A-1, and A-2 which were similarly processed except to a 10% primary alpha level gave higher K_{IC} values (27.9-31.1). The highest K_{IC} (52.4) was obtained with Condition G, beta forged in both operations and given the STA treatment. The conditions which were beta blocked and alpha beta finished (C, D, E, and F) gave K_{IC} values of 33.4-44.6, better than the all alpha beta forged, but not as good as the completely beta forged condition. It was noted that in the straight alpha beta forged conditions, difficulty was encountered in stopping the crack. Five specimens were lost due to failure in pre-cracking.

Low Cycle Fatigue (Table XXXI)

Highest LCF life with runouts over >60,000 cycles was obtained with an all alpha beta forged structure with 50% primary alpha in the annealed condition (Condition B-1).

Highest LCF life of the STA heat treated conditions was also obtained on the 50% primary alpha structure (Condition B), with 55,000 cycles to 1/32" crack and approximately 51,000 cycles to pinpoint indication.

Lowest LCF life and initiation was determined on the ß block, ß finish, STA, Condition G. Pinpoint indications occurred at approximately 8000 cycles and 1/32" crack at 12,000 cycles.

Notch-Time-Fracture

All conditions passed 180 ksi for five hours without failure.

D. Microstructural Comments

1. Ti-6Al-4V

a. In general, the forgings finish forged from the alpha + beta field which resulted in an elongated primary alpha structure rated highest in the mechanical property rating (Conditions I and J).

b. The classical spherical primary alpha structures (Conditions A, A-1, B, and C) ranked about midway in the mechanical property level.

c. Those forgings which were air cooled or slowly cooled from the beta finish forge operation (Conditions Q and T) resulting in a coarse Widmanstatten structure showed poor mechanical property ratings. Those forgings water quenched from a beta finish forge operation and those given a STOA heat treatment after beta forging showed a distinct improvement in mechanical property rating over the slow cooled conditions (Conditions R, S, and U). It should be noted that the beta forged sample quenched from the press did not produce the expected martensitic structure in the 6-4 alloy, but a fine Widmanstatten structure (determined by transmission electron microscopy).

d. A highly elongated "spaghetti" alpha structure given an STOA treatment (Condition E) gave the lowest mechanical property rating and all structures containing spaghetti alpha were generally poor.

e. The structures containing remnants of grain boundary alpha (G, H, I) rated high in overall properties. No detrimental effects of the residual grain boundary condition were determined.

f. The presence of an interface phase between the α and β phases resolvable only by thin film electron microscopy was found to varying extent for all conditions. (It was also found in the other alloys.) As the thickness of this phase increased, the trend was for the yield strength to decrease and toughness increase. The processing variables responsible for establishing the amount and distribution of this phase were not determined in this study.

2. Ti-6Al-6V-2Sn

a. For this alloy, the classical spherical primary alpha microstructure (Conditions A, A-1, B, and C) generally provided the best combination of properties.

b. The elongated primary alpha structures were mainly in the middle of the mechanical property rating (Conditions J through L).

c. The Widmanstatten structure resulting from air cooling from a beta finish forge operation (Q) and the martensitic structure obtained from water quenching from a beta finish forge operation (S) resulted in the poorest mechanical property rating.

d. The "spaghetti" alpha structure air cooled from the press and annealed (D) which contained no martensite had one of the highest mechanical property ratings. The similarly processed forgings with spaghetti alpha when given an STOA treatment or water quenched from the press so that some martensitic alpha was developed (E,F) were significantly lower in mechanical property ratings. All "spaghetti" alpha structures were generally poor in LCF.

3. Ti-6Al-2Sn-4Zr-6Mo

a. The structure giving the best combination of properties resulted from two alpha beta forge operations and contained approximately 50% spherical primary alpha. Heat treatment was STA (B-1).

b. The elongated primary alpha structures resulting from a single alpha + beta operation after a beta forge operation were generally lower in mechanical property rating than the all alpha + beta forged conditions (C, D, E, F). Of those which received a single alpha + beta operation, those finished high in the alpha + beta field (C, D) were superior to those finished low in the alpha + beta field (E, F).

E. Mechanical Property Rating

Using the mechanical property rating systems (described in Appendix E) which included:

Notched high cycle fatigue life to 10^7 cycles, low cycle fatigue life, and crack initiation, fracture toughness, ultimate tensile strength, reduction of area, and the notched tensile strength ratio, the following conditions appeared to show the best combination of properties: (Individual ratings are shown in Tables XXXII, XXXIII, and XXXIV.)

For the 6-4 alloy

Condition J	Beta block + $\alpha\beta$ finish (10% reduction) air cooled and annealed
Condition I	Stock which contained intermittent grain boundary alpha, alpha beta blocked, and alpha beta finished, water quenched from the press and annealed.
Condition A	Alpha beta forged to 10-20% primary alpha air cooled from the press and annealed.
Condition G	Stock which contained intermittent grain boundary alpha, alpha beta forged, air cooled from press, and annealed.

For the 6-6-2 alloy

Condition C	Alpha beta forged to 10-20% primary alpha, water quenched from the press, and annealed.
Condition D	Stock which contained spaghetti alpha $\alpha\beta$ blocked and finished, air cooled from the press, and annealed.
Condition A	Alpha beta forged to 10-20% primary alpha, air cooled from the press, and annealed.
Condition B	Alpha beta forged to 15% primary alpha air cooled from press, solution treated, and overaged.
Condition A-1	Alpha beta forged (50% primary alpha) annealed.

Condition L — Beta blocked, alpha beta finished (10% reduction), water quenched from the press, and annealed.

Condition O — Beta blocked, alpha beta finish (30% reduction), air cooled from press, solution treated, and overaged.

For the 6-2-4-6 alloy

Condition B-1 — Alpha beta forged to 50% primary alpha and annealed.

Condition B — Alpha beta forged to 50% primary alpha, solution treated, and aged.

Condition A-1 — Alpha beta forged to 10-20% primary alpha annealed.

The poorest combination of properties based on this rating system occurred in the following combinations:

For the 6-4 alloy

Condition E — Stock treated to produce spaghetti alpha, alpha beta blocked and finished, air cooled from the press. Solution treated and overaged.

For the 6-6-2 alloy

Condition Q — Beta blocked and finished, air cooled from the press, and annealed.

Condition S — Beta blocked and finished, water quenched from the press, and annealed.

For the 6-2-4-6 alloy

Condition F — Beta blocked alpha beta finished low in the alpha beta field (30% reduction on finish), solution treated and aged.

Fracture Toughness (Table XXVIII)

For all conditions tested, K_{IC} ranged from 57 to 87 for the standard O_2 level 6-4.

Four conditions (D, J, R, and U) gave K_{IC} values 86-87. Two conditions (B and C) gave K_{IC} value <60. All other 16 conditions showed K_{IC} between 60 and 80.

The one condition tested for low O_2 material (condition A, alpha beta forged to 10% primary alpha structure and annealed) gave a K_{IC} of 103.

Low Cycle Fatigue (Table XXXI)

The best LCF life (those groups including "run outs" over 100,000 cycles) was obtained with conditions:

A alpha beta forged (10-20% P.A.) air cooled and annealed

I grain boundary condition in stock, alpha beta forged. Water quenched from press and annealed.

J beta blocked, alpha beta finished, air cocled and annealed.

L beta blocked, alpha beta finished, water quenched and annealed.

S beta blocked, beta finished, water quenched from press and annealed

The lowest LCF life (<20,000 cycles to 1/32" crack) was obtained with conditions:

A (low O_2), E, Q, T, and U

Lowest crack initiation (values <20,000 cycles to pinpoint indication) was found on the following conditions:

A (low O_2), B, D, E, F, M, Q, T, and U

V. PHASE II

Phase II consisted of a study of two types of metallurgical defects found in titanium alloys - "soft alpha" segregation and "beta flecks".

A. Soft Alpha Segregation

Soft alpha segregation has been identified as regions containing higher aluminum content than matrix material which stabilizes the alpha phase in these areas. The soft alpha segregate for this investigation was created by forge bonding of strips of Ti-8Al-1V-1Mo foil (0.015" thick) between sections of Ti-6Al-4V billet. Figure 60 shows schematically how this was accomplished. Billet faces to be bonded were machined and chemically cleaned. Two strips of Ti-8Al-1V-1Mo foil (0.25" wide x .015" thick) were placed at 90° to each other overlapping at the center on half of the billets. The ends of the strips were tack welded to the billets at the O.D. to hold them in position. The billets with the strips were then joined to the remaining billets by EB welding. Sealing the edges of the mating surfaces of the billets by the EB method (welding in a vacuum chamber) insures that the mating surfaces to be bonded remain clean. After the initial upset on open dies (12" → 6"), the parts were finished in closed dies. Figure 61 shows one of the bonded discs after finish forging.

Three discs were finished in the alpha beta temperature range and three above the beta transus of the matrix 6-4 alloy. Table XXXV shows the forging and heat treating processing. After forging and heat treating, all discs were ultrasonically inspected by the immersion technique per a typical aircraft engine builder's procedures (PWA SIM-1J). All discs were inspected to 20% of a 2/64" flat bottom hole, and no indications were found in any of the parts. The "segregation" was not detectable by ultrasonic techniques. A 100% sound bond was indicated.

Figure 62 shows the macro and microstructure of a typical alpha beta forged disc containing the inclusion. Segregated area was approximately 0.0012" thick.

Figure 63 shows the macro and microstructure of a typical beta forged 6-4 disc which contained the inclusion. Segregate layer showed an alpha particle size of approximately .00025". Smooth and notched tensile bars were taken in areas with and without the inclusion. Tensile results are shown in Table XXXVI. The beta forged disc showed approximately the same tensile properties with and without the inclusion. The alpha beta forged disc, however, showed a significant reduction in both

smooth and notched strength and ductility in the axial direction (axis of the tensile bar parallel with axis of the disc, normal to the plane of the inclusion) with failure occurring through the plane of the inclusion. The tangential tests (alpha beta forged) showed tensile properties to be approximately equal both with and without the inclusion.

High and low cycle fatigue and fracture toughness tests were also taken in areas with and without the inclusion. Figure 64 shows the location of test specimens. Table XXXVII shows HCF data. Low cycle fatigue data is shown in Table XXXVIII. Fracture toughness results are shown in Table XXXIX.

B. Beta Flecks

Figure 65 shows a macroetched slice of the Ti-6Al-6V-2Sn bar used to make the forging with "beta flecks". Also shown in Figure 65 is the microstructure of the typical "flecks". Flecks are defined as areas having a lower beta transus than the matrix material so that after normal alpha + beta processing, these areas appear as islands of acicular transformed structure in a matrix of typical spherical alpha structure. The heat used for this evaluation was purposely melted to produce "flecks" for evaluation. The structural forging used for Phase I was used in this evaluation. Forgings were made by three methods as outlined in Table XL. The first group was made by typical production procedures used for the 6-6-2 alloy, all operations at 50-75°F below the beta transus of the base material. A macrosection of one of the forgings made by this process is shown in Figure 66. The flecked areas are easily seen. A photomicrograph showing the appearance of one of the flecks in the finished forging is also shown in Figure 66. The second group of forgings was produced with both closed die operations performed at approximately 125-135°F above the beta transus. In this condition, all the material showed the acicular transformed structure, and the flecks were not discernible (Figure 67). The third group was processed at very low alpha + beta temperature (225°F below the beta transus of the matrix material) in order to stay below the transus of the "fleck" areas. This provided a uniform structure of spherical alpha in a transformed matrix throughout the part. Flecked areas could not be distinguished (Figure 68). All parts were annealed at 1350°F (2 hours) and air cooled.

Tensile, fracture toughness, low and high cycle fatigue specimens were taken from the forgings as shown in Figure 69.

Tensile properties are shown in Table XLI. Table XLII gives fracture toughness results. High cycle fatigue data is shown in Table XLIII. Low cycle fatigue is presented in Table XLIV.

C. Phase II, Results and Conclusions

1. "Soft Alpha"

a. Tensiles (Table XXXVI)

Smooth bar tensile ductility and notched tensile ultimate were reduced by the presence of the "soft alpha" inclusion when tested normal to the plane of the inclusion (axial direction in disc) for alpha + beta forged discs. Failure occurred through the plane of the inclusion. Tangential tests showed no significant difference between those specimens with and without the inclusion. Beta forged discs showed no reduction in properties resulting from the inclusion in either direction.

b. High Cycle Fatigue (Table XXXVII)

No significant differences were found in the endurance limits between the material containing the inclusion and base material in smooth or notched HCF after either alpha beta or beta forging.

c. Low Cycle Fatigue (Table XXXVIII)

Alpha beta forged samples containing the "soft alpha" inclusion failed at a significantly lower number of cycles than those without. Rupture of the defect containing samples occurred with no prior indication of cracking. The beta forged samples containing the inclusions failed at approximately the same median times as those without; however, the inclusion was not at the center of the gauge length in two specimens and could not be detected in the gauge length of the other two. The actual values of the beta forged specimen containing the defect are not valid for LCF life of a soft alpha inclusion as the inclusion was not in the center of the gauge length. It is significant to note, however, that when there was an inclusion within the gauge length (not at the center), the failure initiated in normal material at the center and not at the inclusion. This type of inclusion is apparently not particularly sensitive to fatigue crack initiation in a beta forged part.

d. Fracture Toughness Table XXXIX

No significant differences were found in fracture toughness between those samples with and those without segregation either alpha beta or beta forged. Presence of the soft alpha along the fracture was confirmed metallographically.

2. Beta Flecks

a. Tensiles (Table XLI)

Beta flecks did not appear to affect tensile properties in the annealed condition. Beta forging reduced tensile ductility; however, this is attributed to overall transformed structure and not localized "fleck" area.

b. Fracture Toughness (Table XLII)

Presence of beta flecks did not reduce fracture toughness. The presence of flecks along the crack paths was verified metallographically. K_{IC} of parts forged by standard practice (1675°F forge) K_{IC} = 72-79, was equivalent to beta forged parts. Parts forged at very low alpha beta temperature (1500°F) (which eliminated visible flecks) showed significantly reduced K_{IC} values (K_{IC} = 55-58).

c. High Cycle Fatigue (Table XLIII)

In notched HCF, the low $\alpha\beta$ forge procedure and the beta forge procedure appeared to be superior to the standard forged material (with flecks) at an endurance life of 10^7 cycles. In smooth bar results, the low $\alpha + \beta$ was superior to the beta forged and standard forge practice parts.

d. Low Cycle Fatigue (Table XLIV)

Cracking in "standard forged" samples initiated in flecks. Highest median LCF life was obtained with low $\alpha\beta$ forged samples.

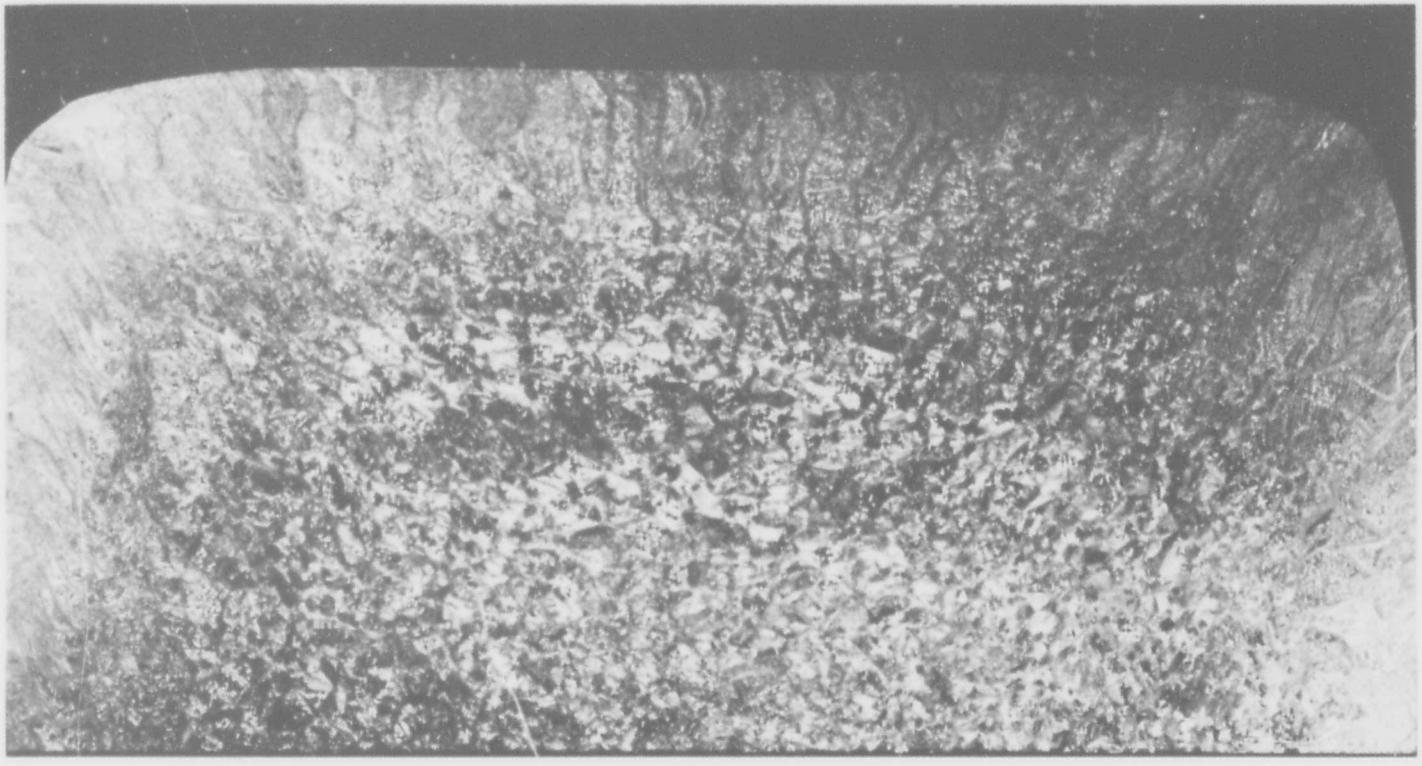

2/3X

Item #1 Macrostructure. Ti-6Al-4V 14" square coarse grained (.15-.20% O_2)

Figure 1

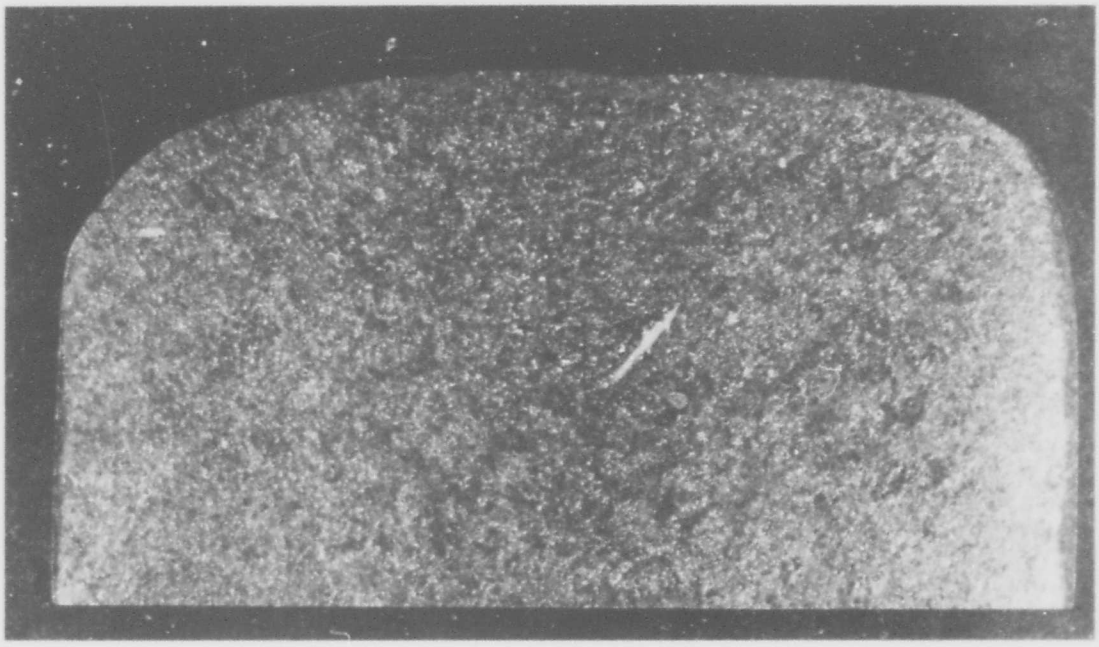

1X

Item #2. Macrostructure. Ti-6Al-4V 6" square fine grained (.15-.20% O_2)

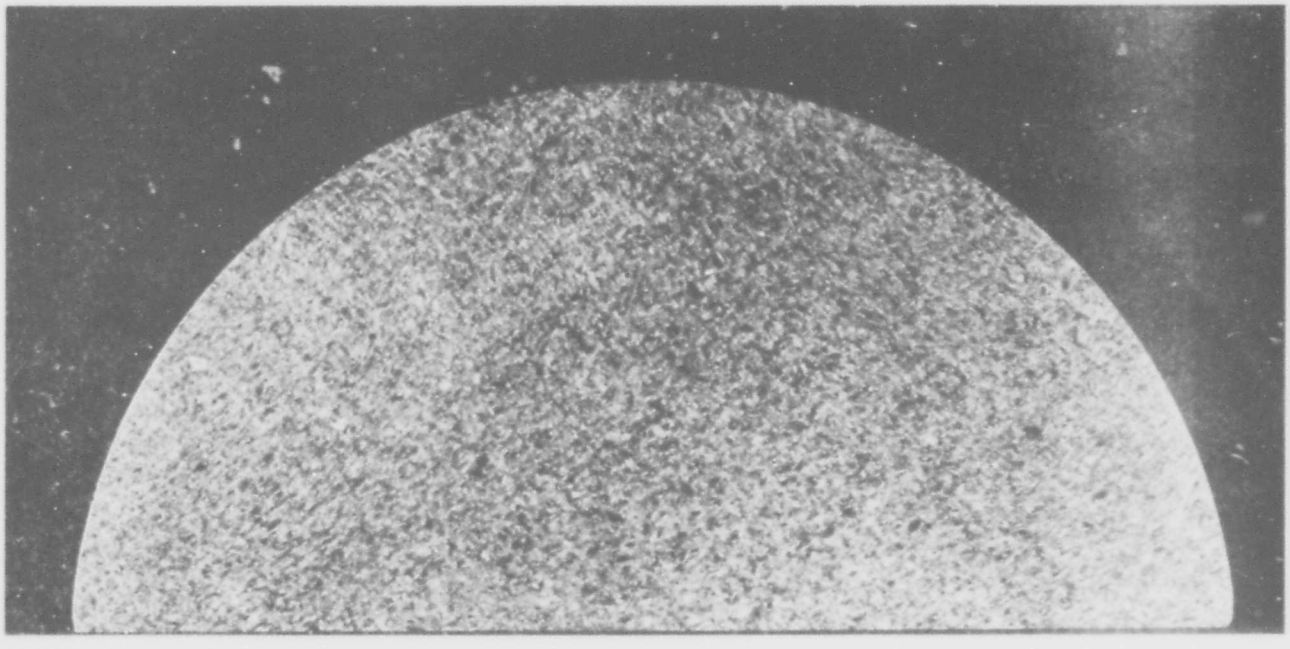

1X

Item #3 Macrostructure. Ti-6Al-4V 6" round fine grained.

Figure 2

Item #4 (Replacement)
Macrostructure Ti-6Al-4V
6" Round Fine Grained (0.12-.15% O_2)

1X

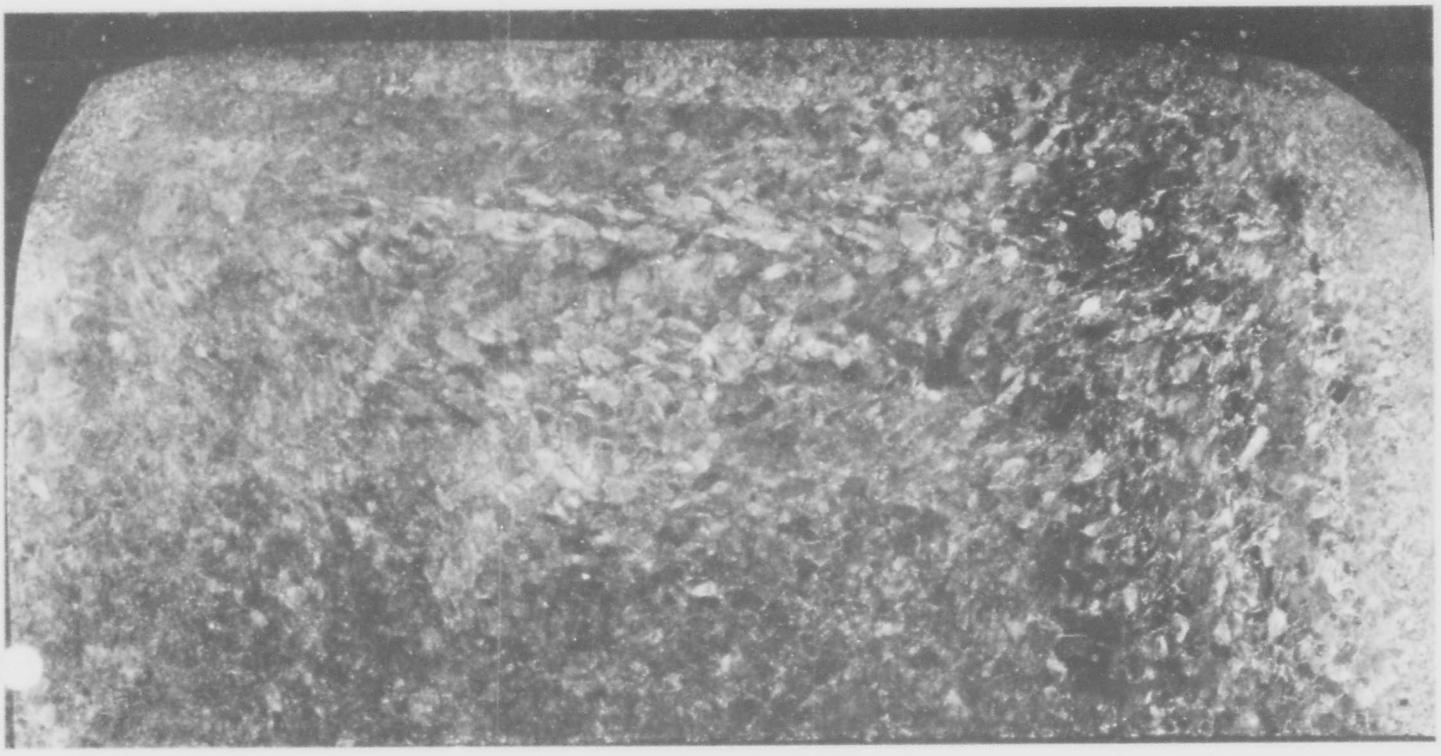

2/3X

Item #5 Macrostructure. Ti-6Al-6V-2Sn 14" square fine grained.

Figure 3

1X

Item #6 Macrostructure. Ti-6Al-6V-2Sn
6" square fine grained.

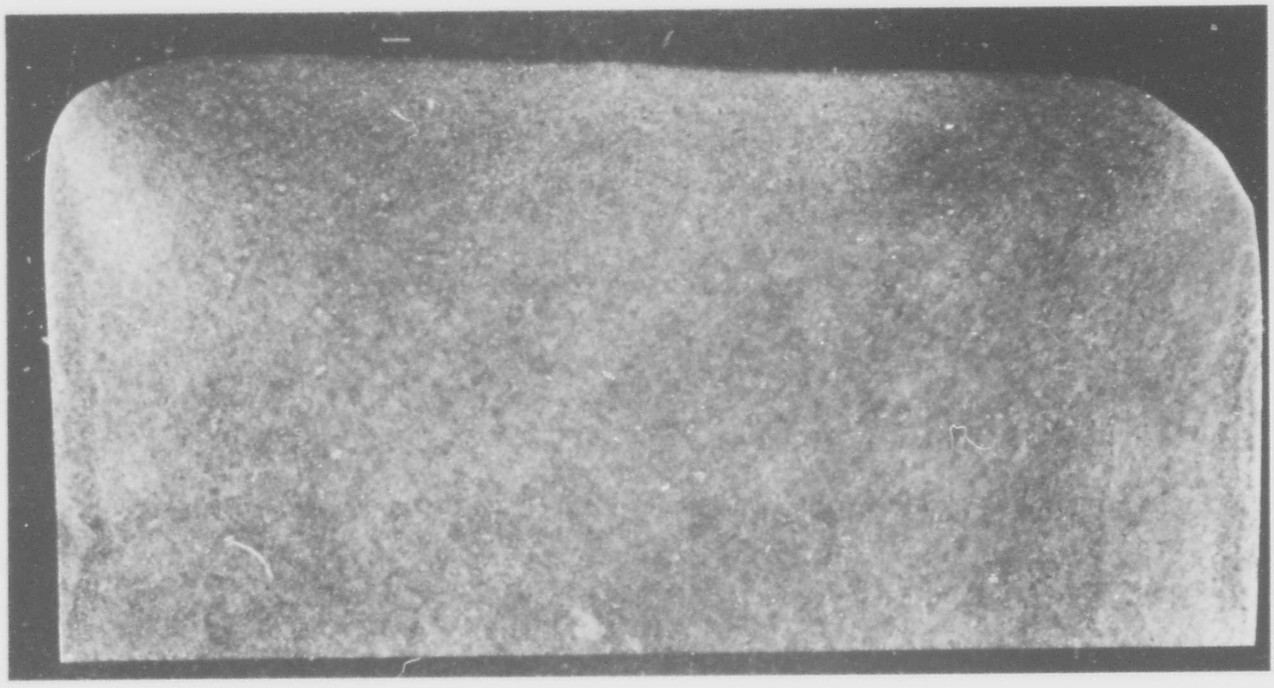

1X

Fig. 18. Item #7 Macrostructure. Ti-6Al-6V-2Sn 6" square
beta flecked fine grained.

Figure 4

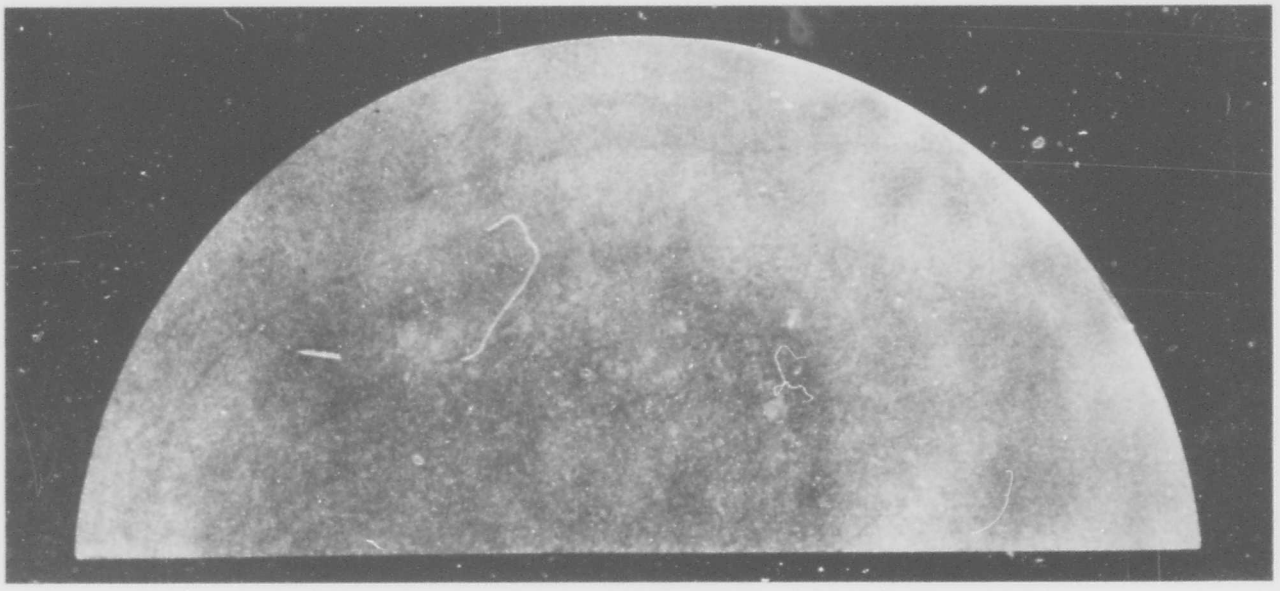

1X

Item #8 Macrostructure. Ti-6Al-2Sn-4Zr-6Mo
6" round fine grained.

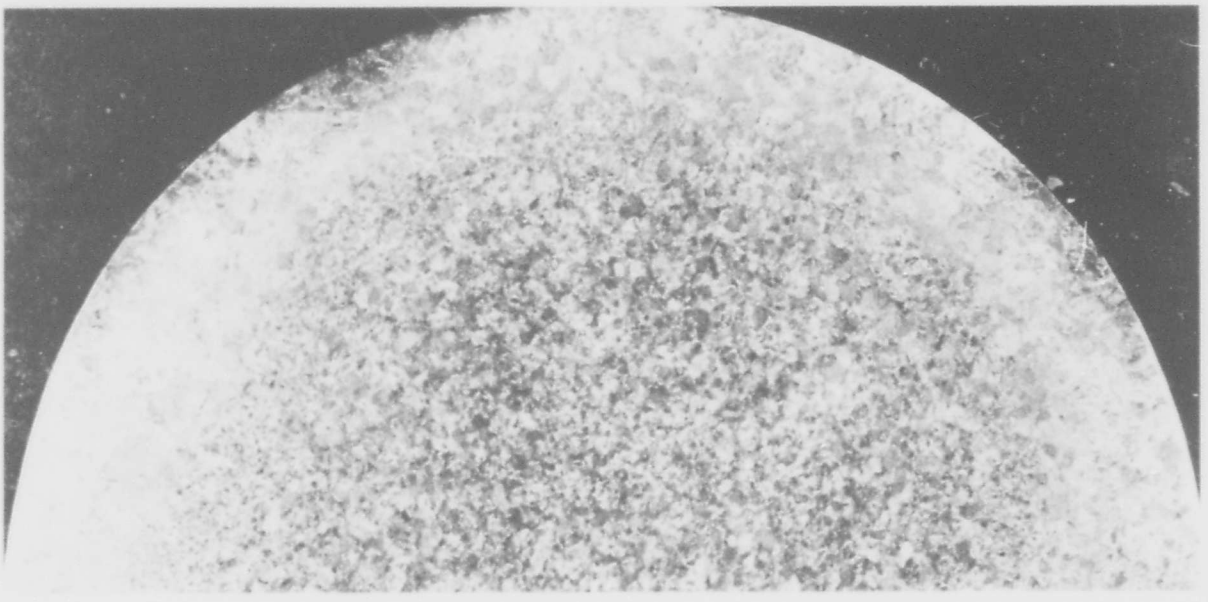

1X approx.

Item #9 (Replacement)
Ti 6Al-2Sn-4Zr-6Mo
6" Round Coarse Grained

Figure 5

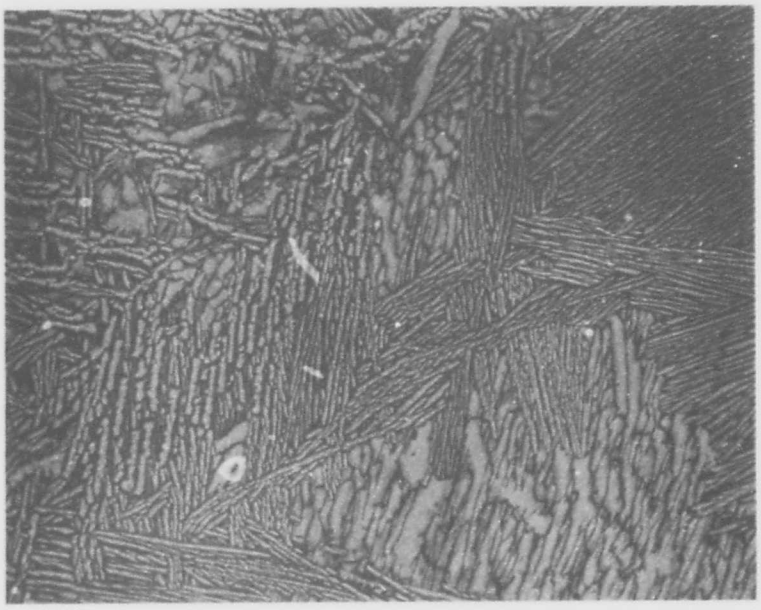

Item #1 Microstructure. Ti-6Al-4V 100 X
14 inch square coarse grained
(.15-.20% O_2).

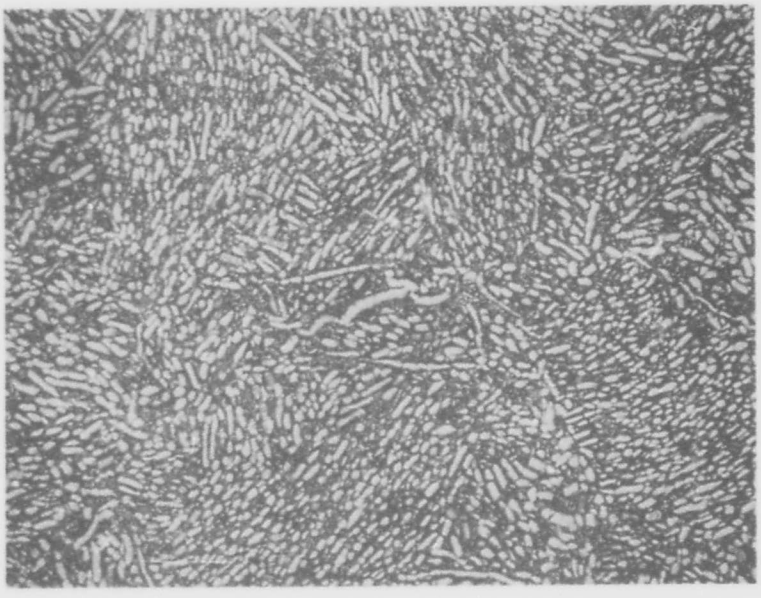

Item #2 Microstructure. Ti-6Al-4V 100 X
6 inch square fine grained.
(.15-20% O_2).

Figure 6

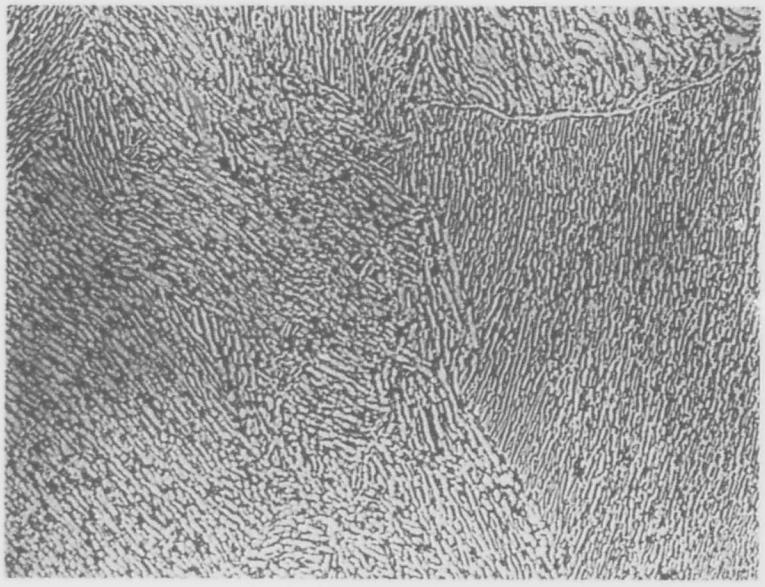

Item #3 Microstructure. Ti-6Al-4V 100 X
6 inch round fine grained.

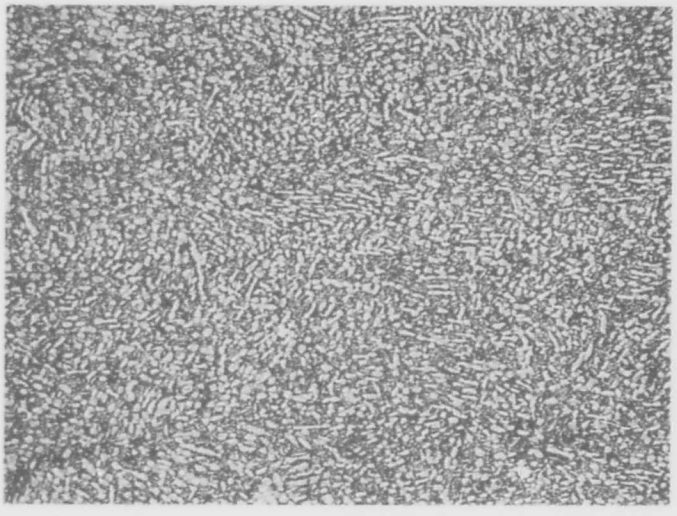

Item #4 100X
Microstructure Ti 6Al-4V
6" Round Fine Grained (.12-.15% O_2)

Figure 7

Item #5 Microstructure. Ti-6Al-6V-2Sn 100 X
14 inch square coarse grained.

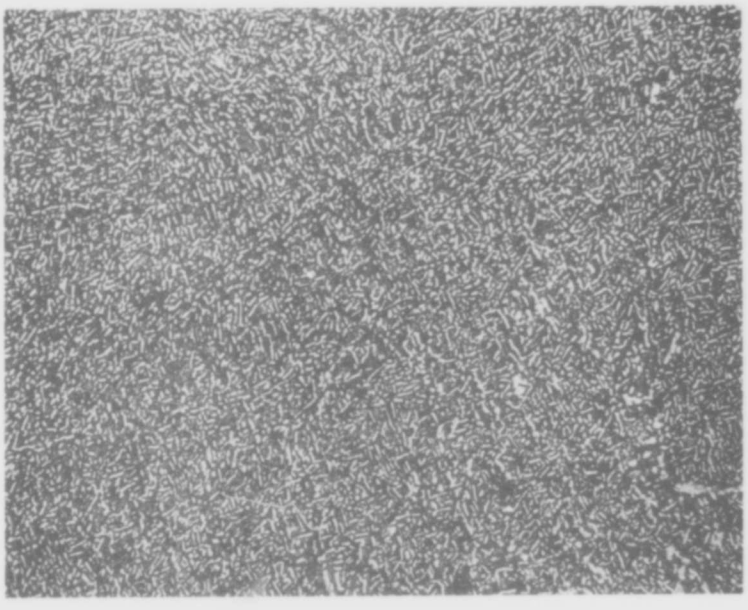

Item #6 Microstructure. Ti-6Al-6V-2Sn 100 X
6 inch square fine grained.

Figure 8

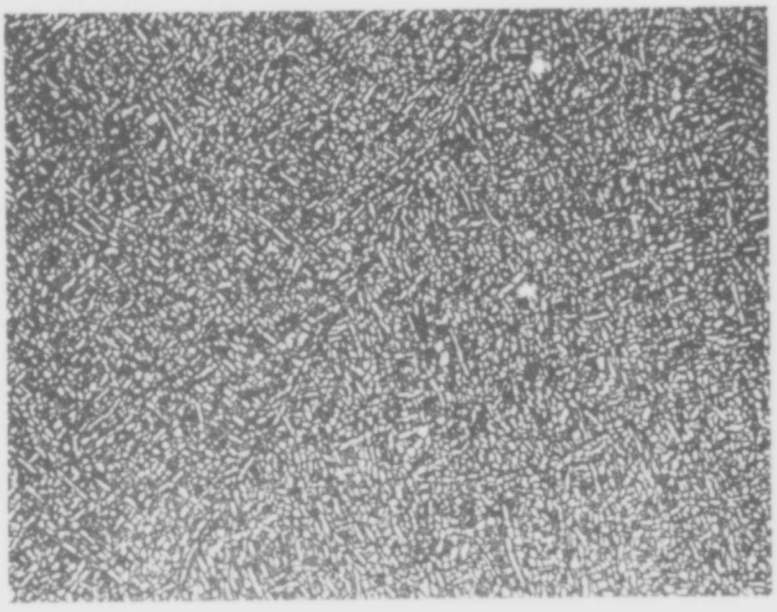

Item #7 Figure 9A 100X
Microstructure A Ti-6Al-6V-2Sn
6 inch square beta flecked fine grained
Structure illustrates a region without beta flecks

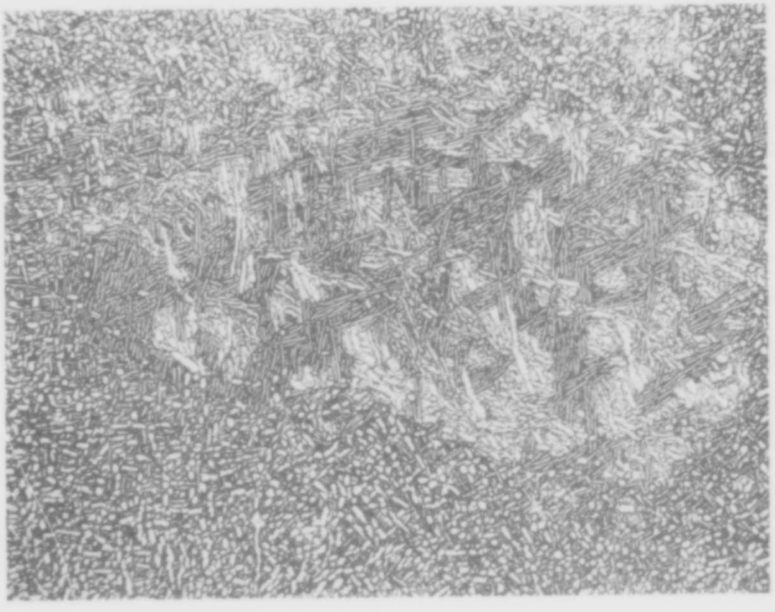

Item #7 Figure 9B 100X
Microstructure B Ti-6Al-6V-2Sn
6 inch square beta flecked fine grained
Structure illustrates a beta flecked region

Figure 9

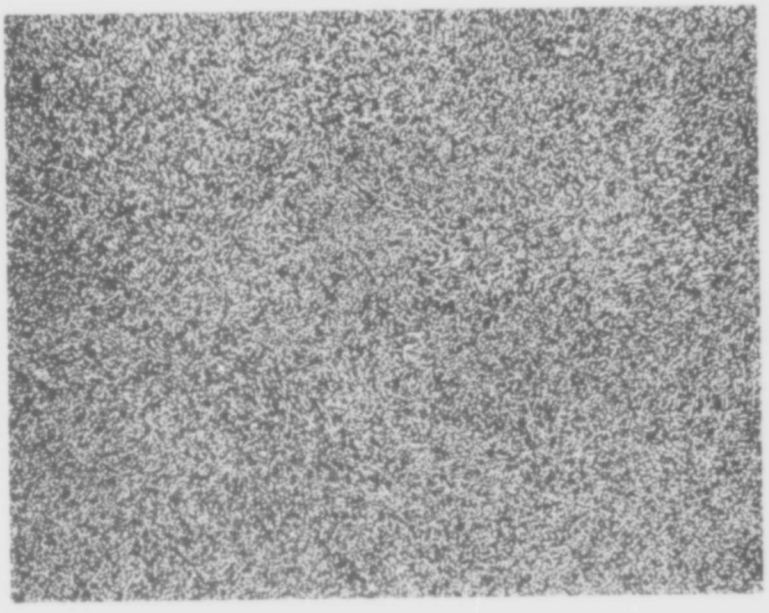

Item #8 Microstructure. Ti-6Al-2Sn-4Zr-6Mo 100 X
6 inch round fine grained.

Item #9 Microstructure. Ti-6Al-2Sn-4Zr-6Mo 100 X
6 inch round coarse grained.

Figure 10

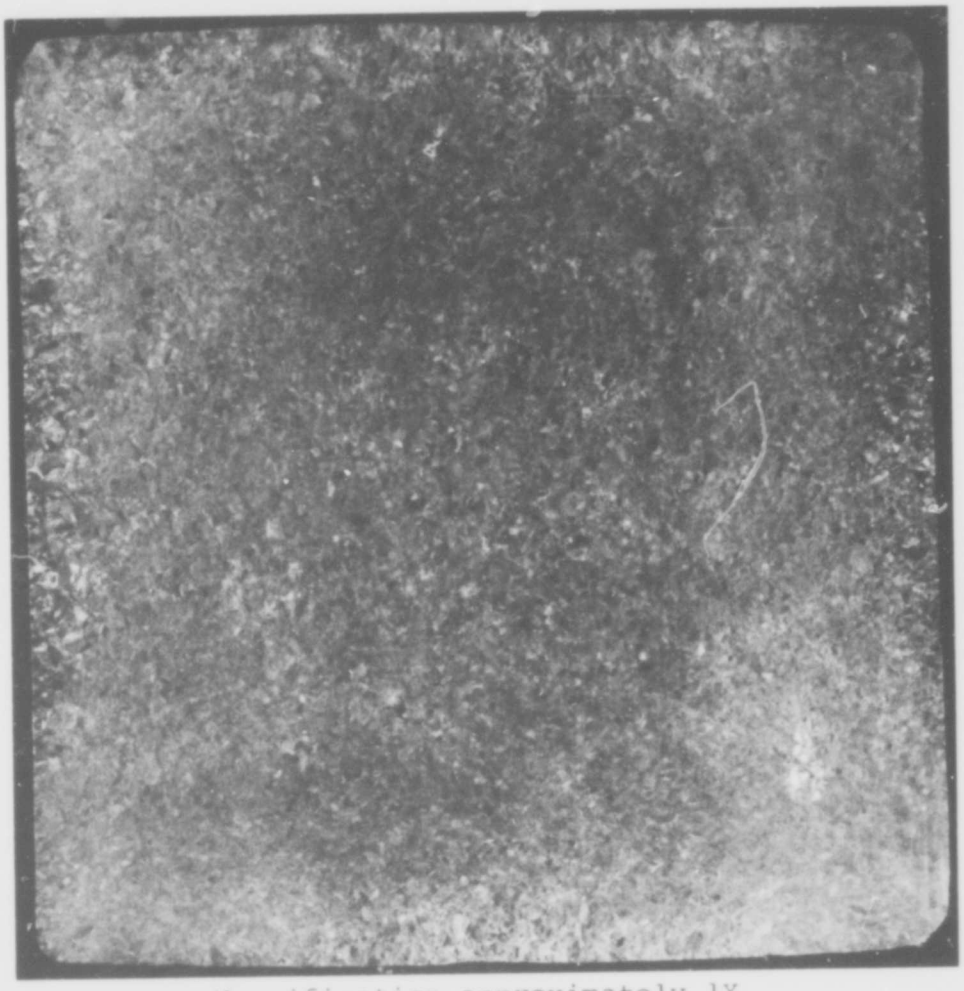

Magnification approximately 1X

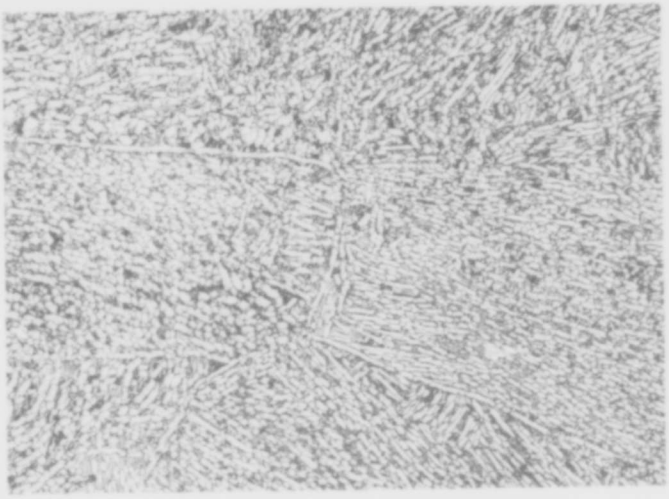

X100

Macro and microstructure of Ti-6Al-4V cut from coarse grained bar, beta annealed, and then forged at 1775°F from 7" square to 5" square to produce intermediate macro grain size

Figure 11

Structural Forging Used for Evaluation

Figure 12

PREFORM

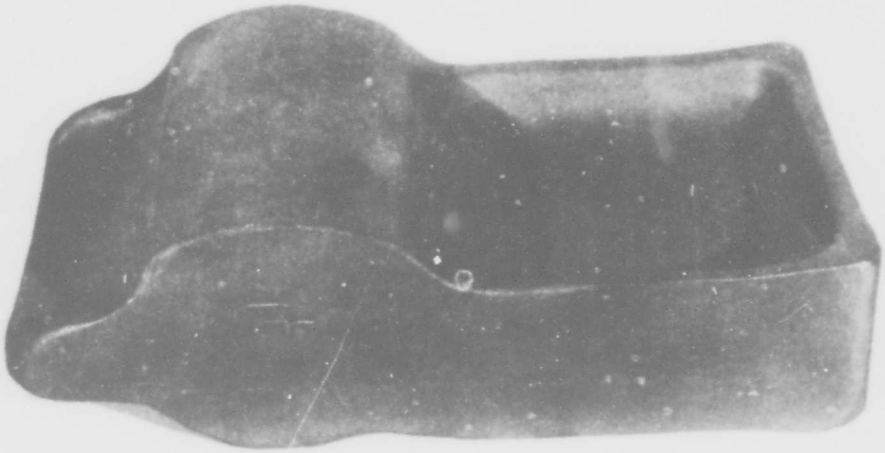

BLOCKER

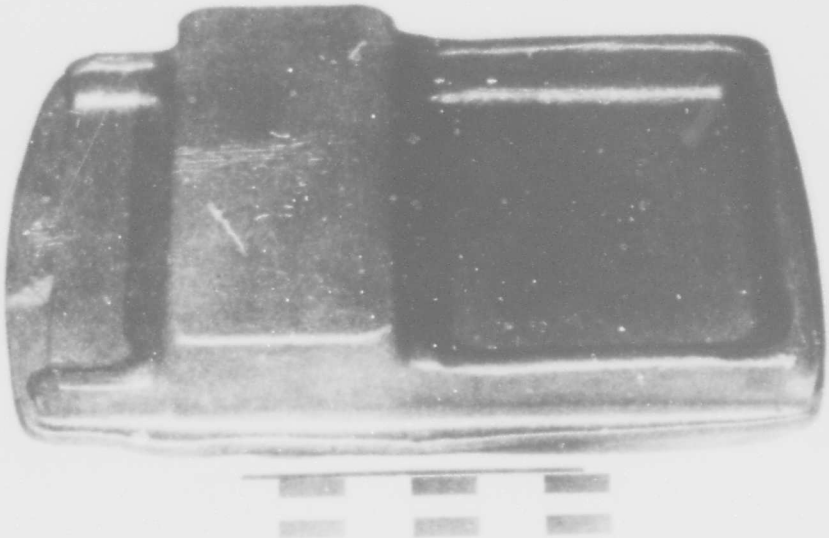

FINISH

FORGING SEQUENCE FOR TITANIUM STRUCTURAL PART

Figure 13

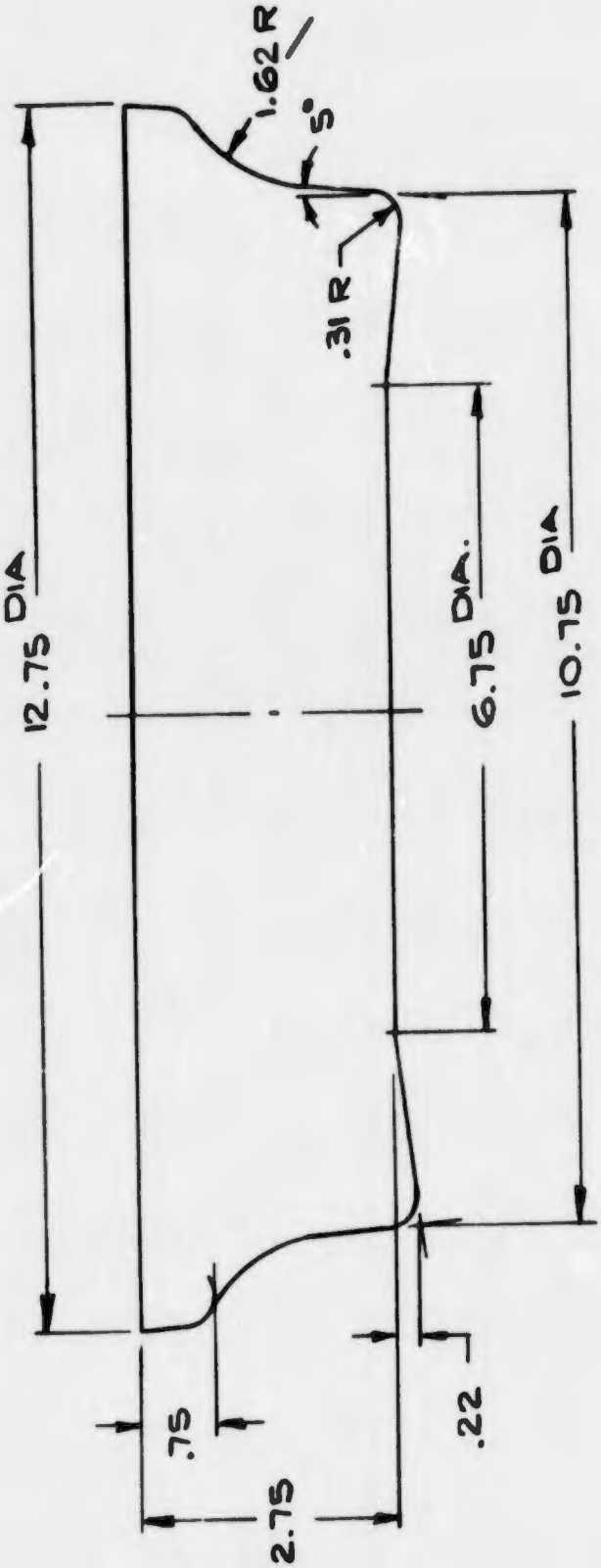

Figure 14

Compressor Disc Forging Used for Evaluation

Figure 15
Titanium Compressor Disc Forging

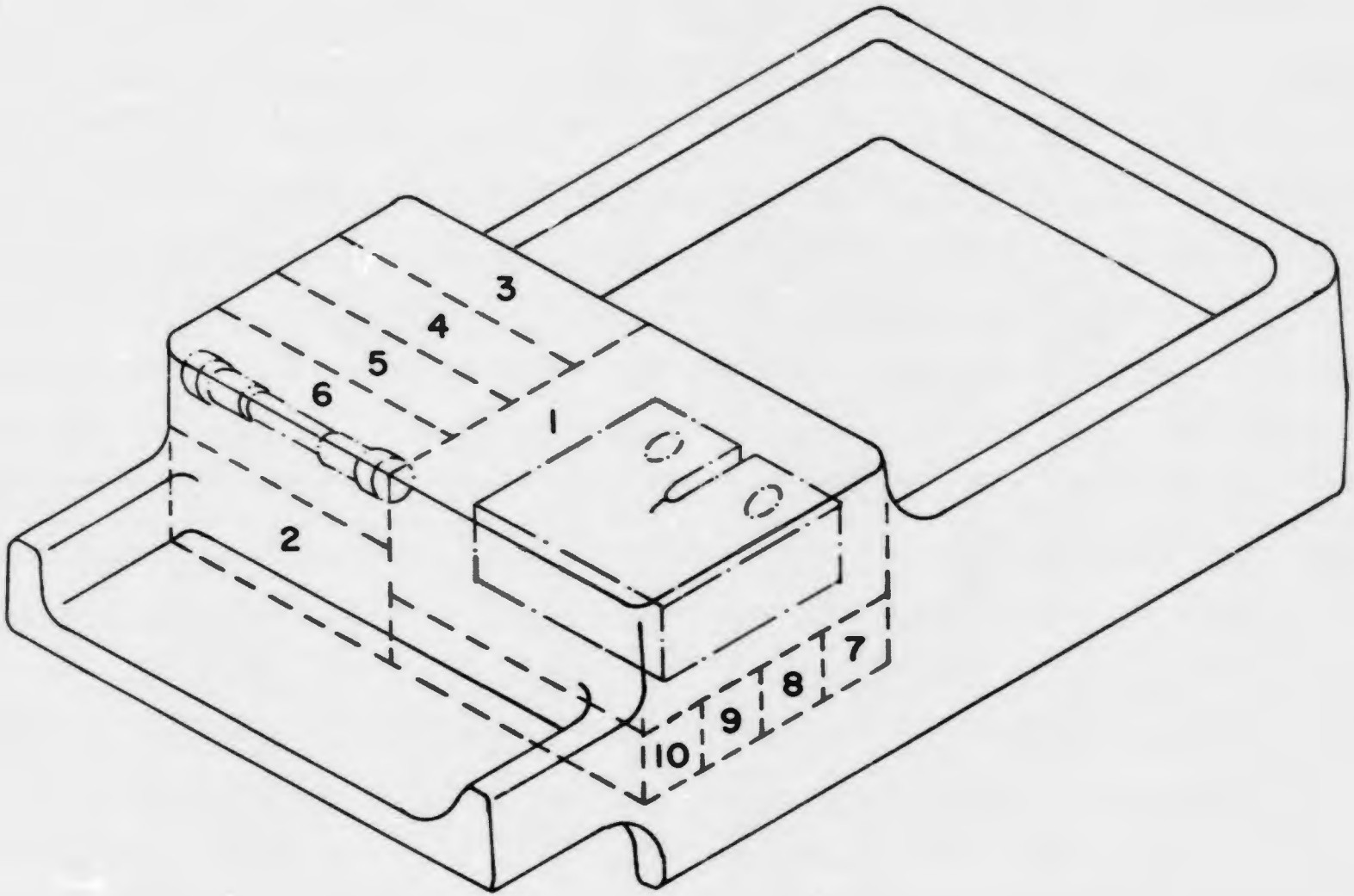

Figure 16

TITANIUM STRUCTURAL FORGING SHOWING
LOCATION OF TENSILE & FRACTURE TOUGHNESS SPECIMEN

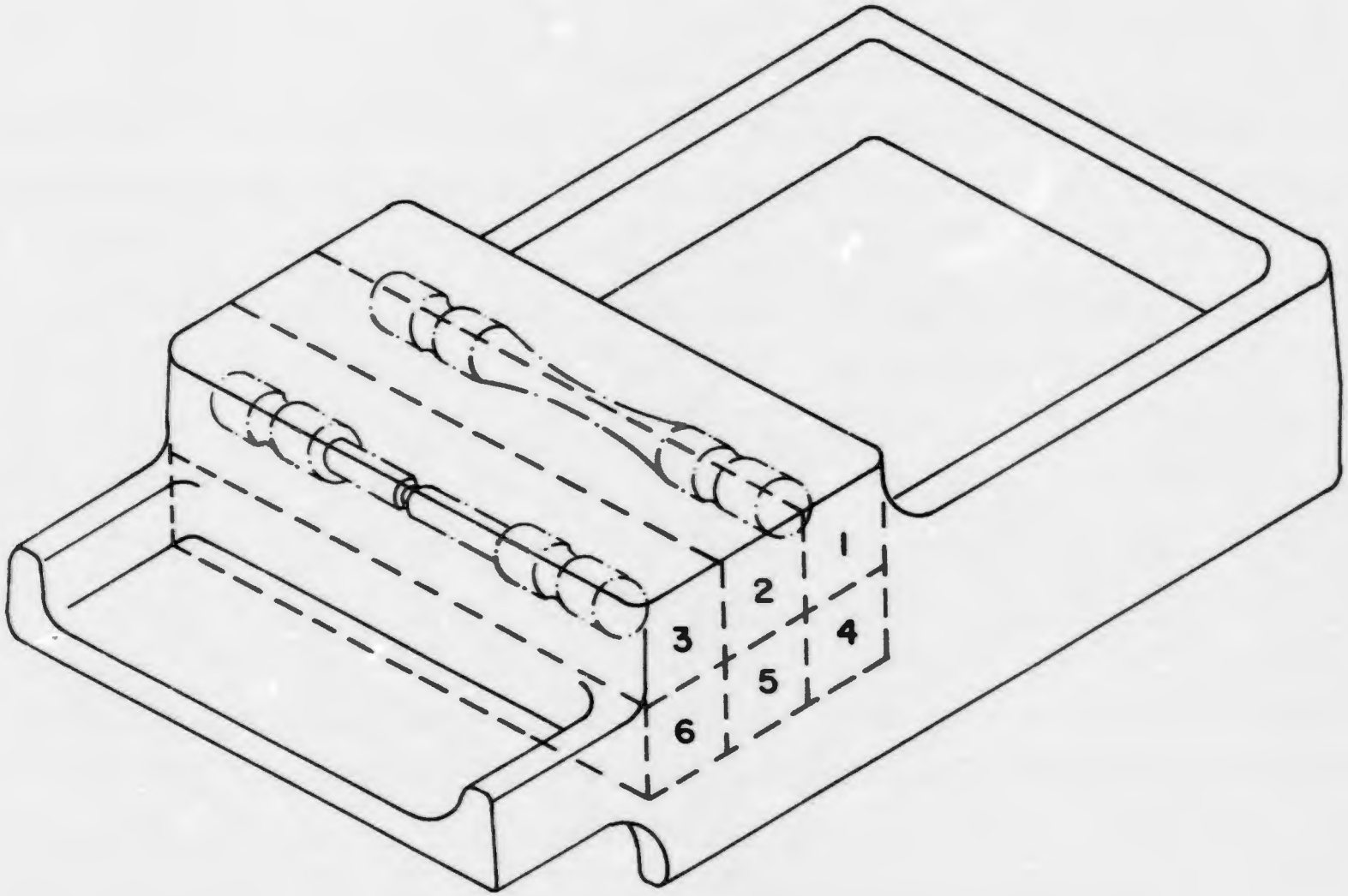

TITANIUM STRUCTURAL FORGING SHOWING
HIGH CYCLE FATIGUE SPECIMEN

Figure 17

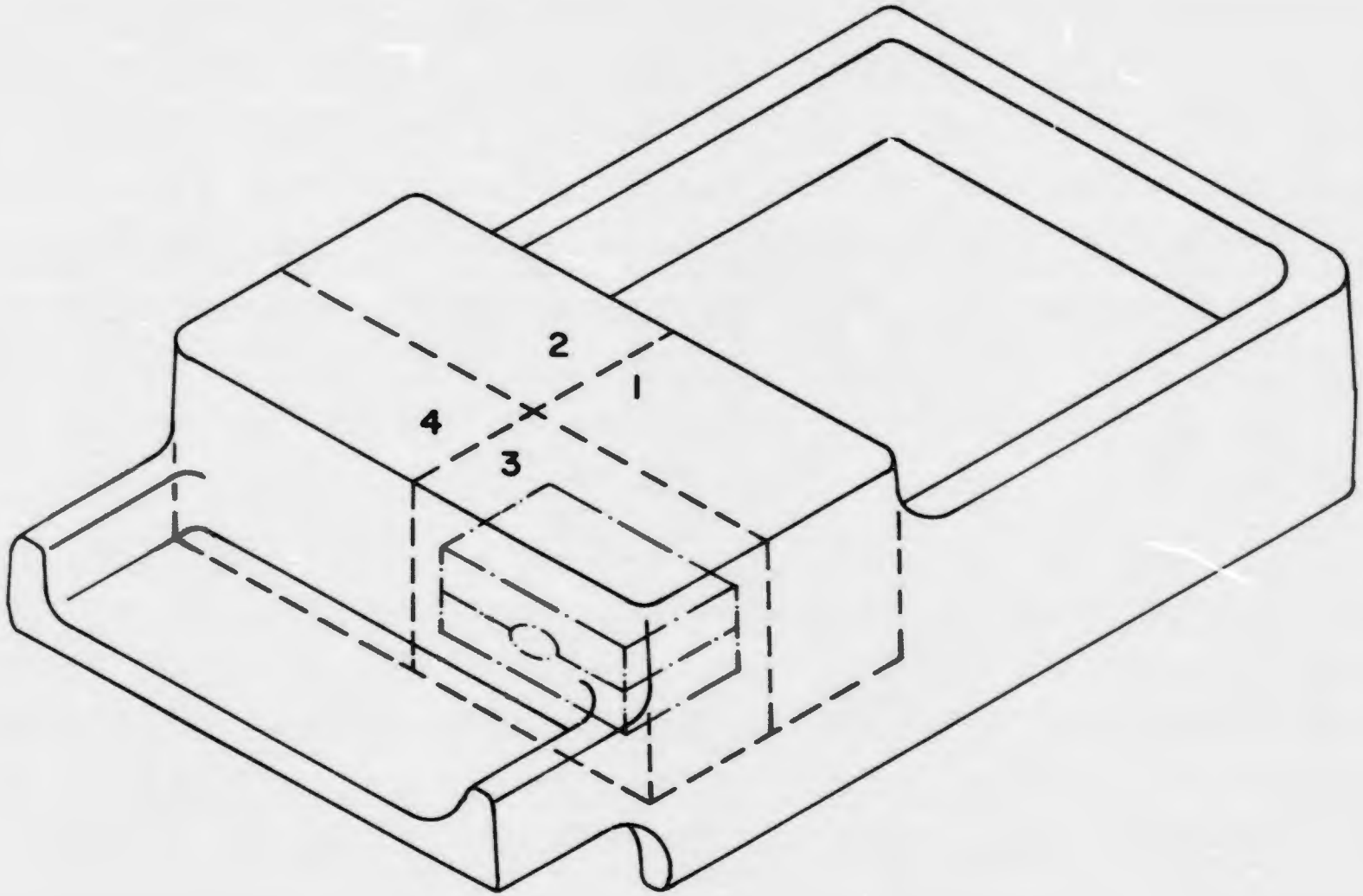

TITANIUM STRUCTURAL FORGING SHOWING
LOW CYCLE FATIGUE SPECIMEN

Figure 18

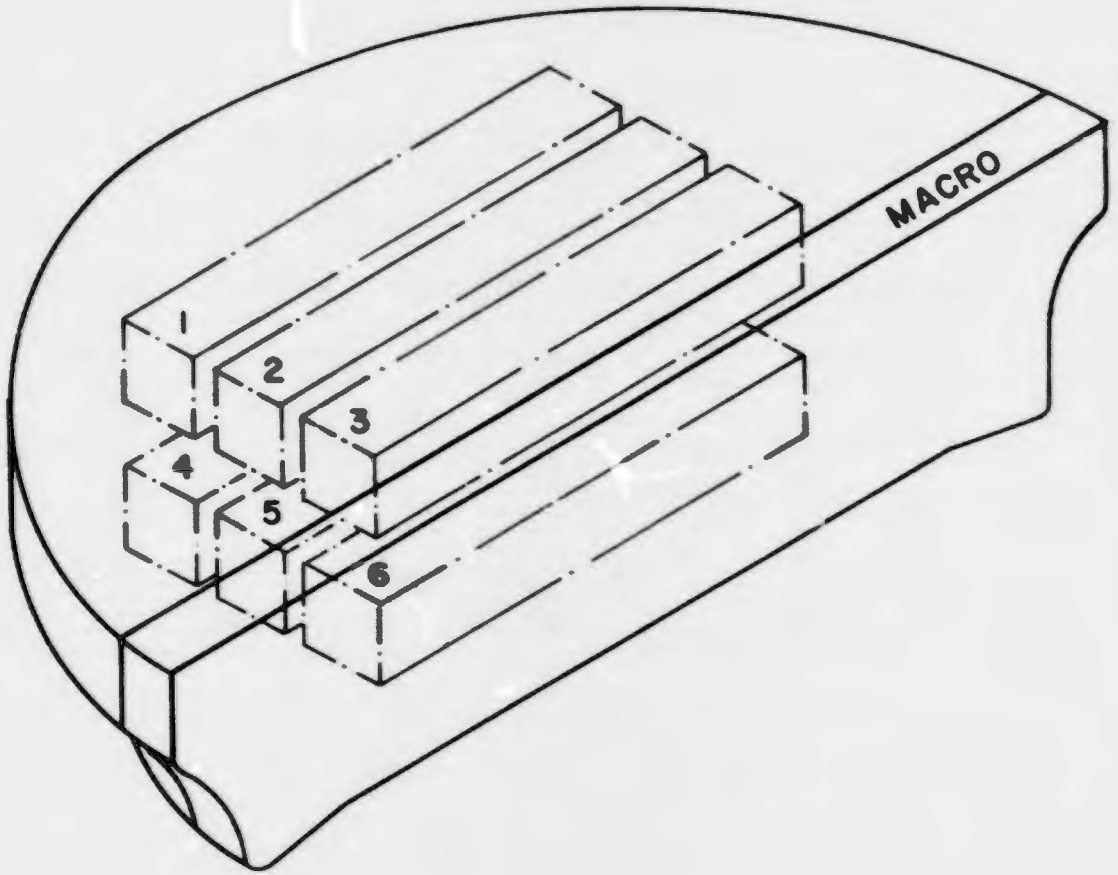

Figure 19

TITANIUM DISC FORGING SHOWING
LOCATION OF HIGH CYCLE FATIGUE SPECIMENS
AND MACRO SLICE

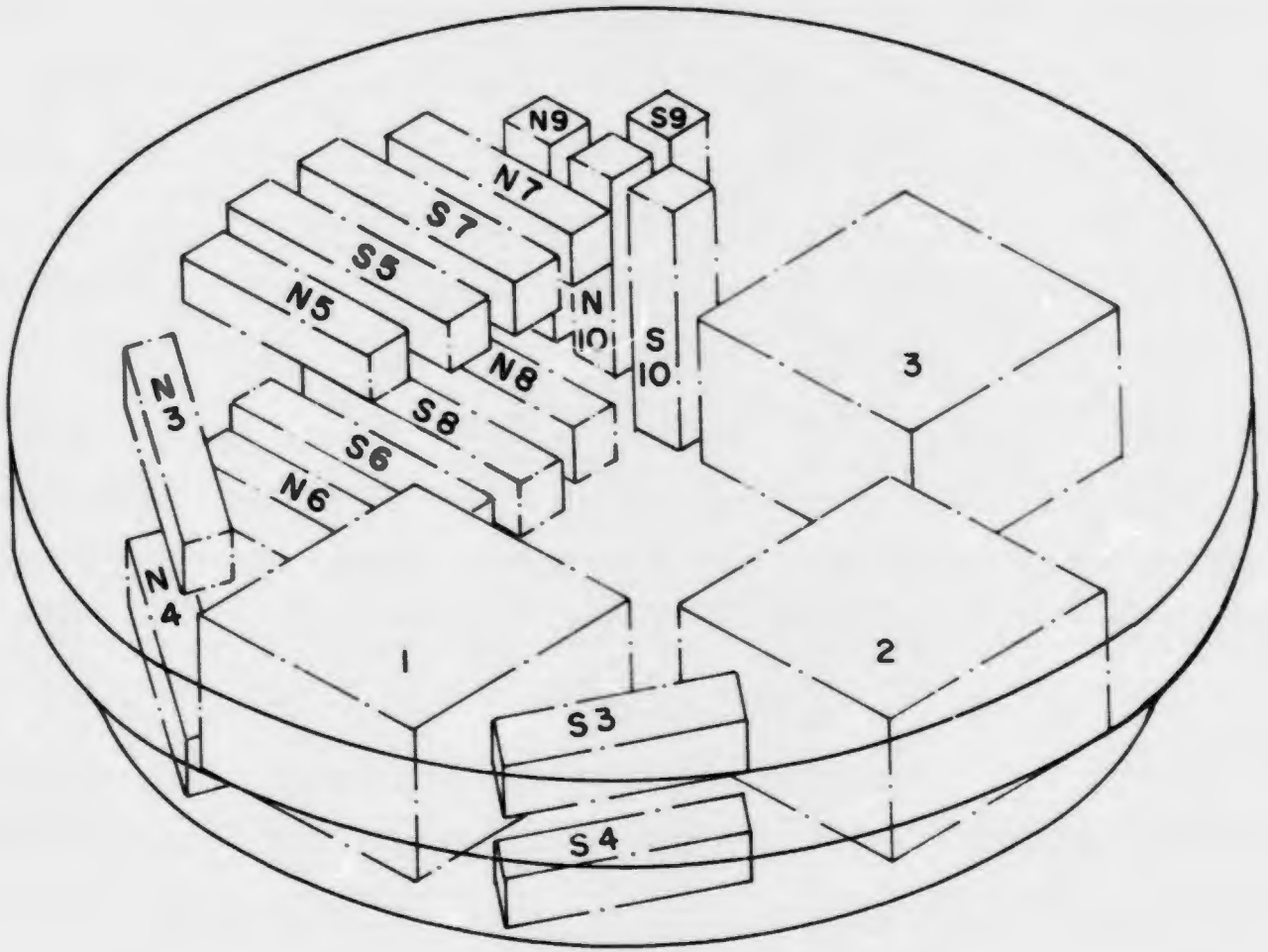

Figure 20

TITANIUM COMPRESSOR DISC
SHOWING LOCATION OF
FRACTURE TOUGHNESS AND
TENSILE SPECIMENS

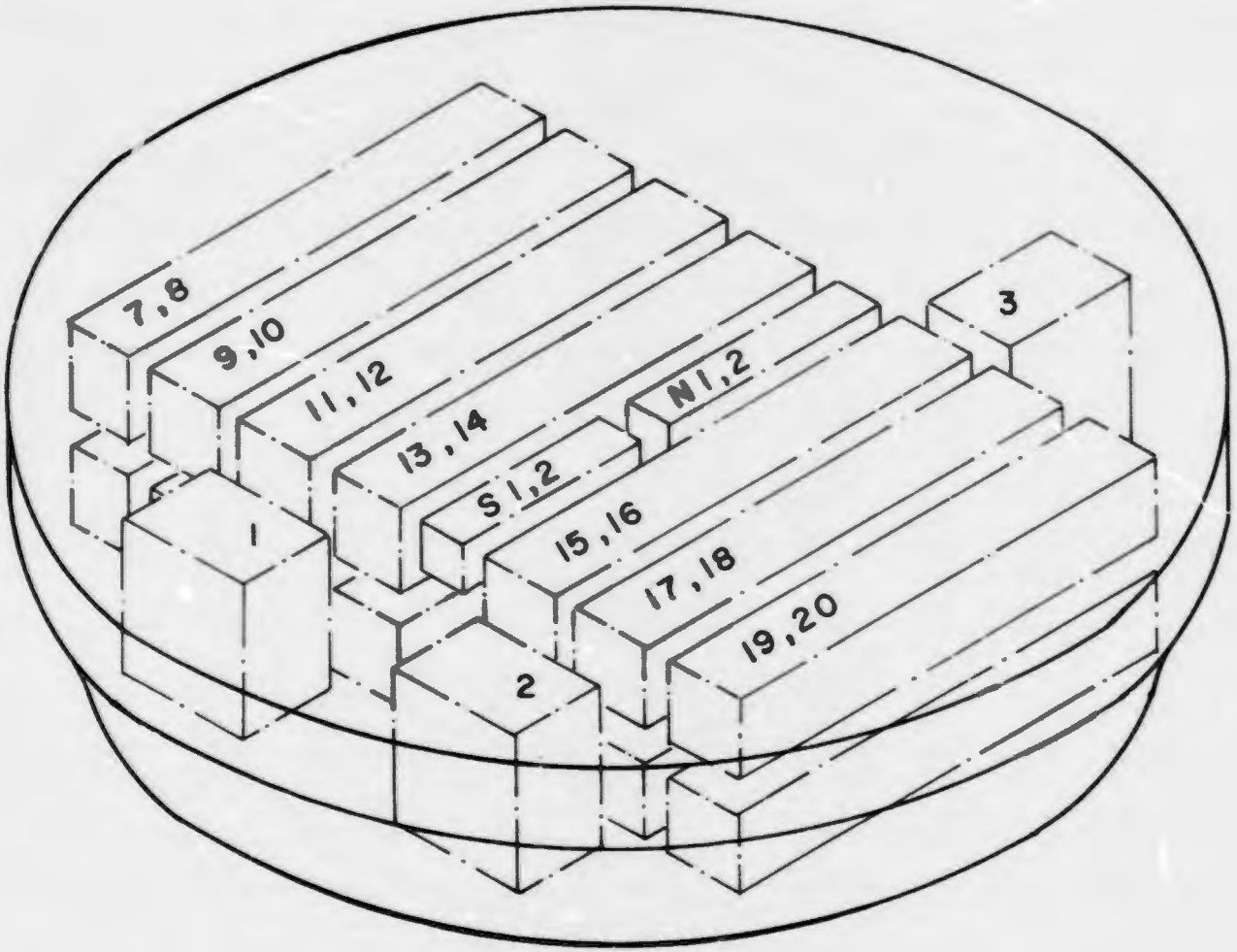

TITANIUM DISC FORGING SHOWING
LOCATION OF HIGH CYCLE AND
LOW CYCLE FATIGUE SPECIMENS
AND TENSILE BARS

Figure 21

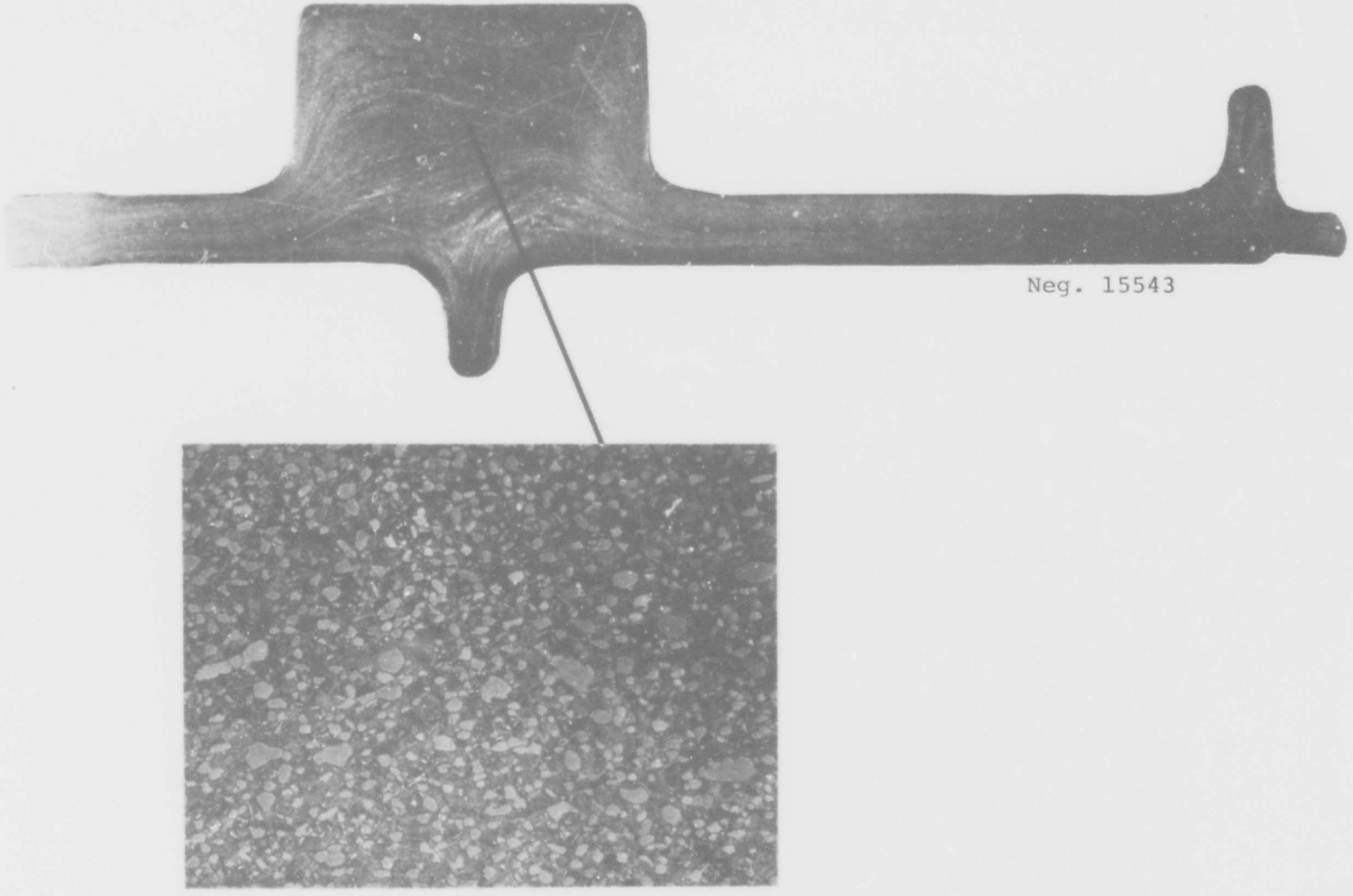

Neg. 15543

Neg. 15496

Macro section and microstructure (200X) of
structural part forged from fine grained Ti-6Al-4V

Negative 15524

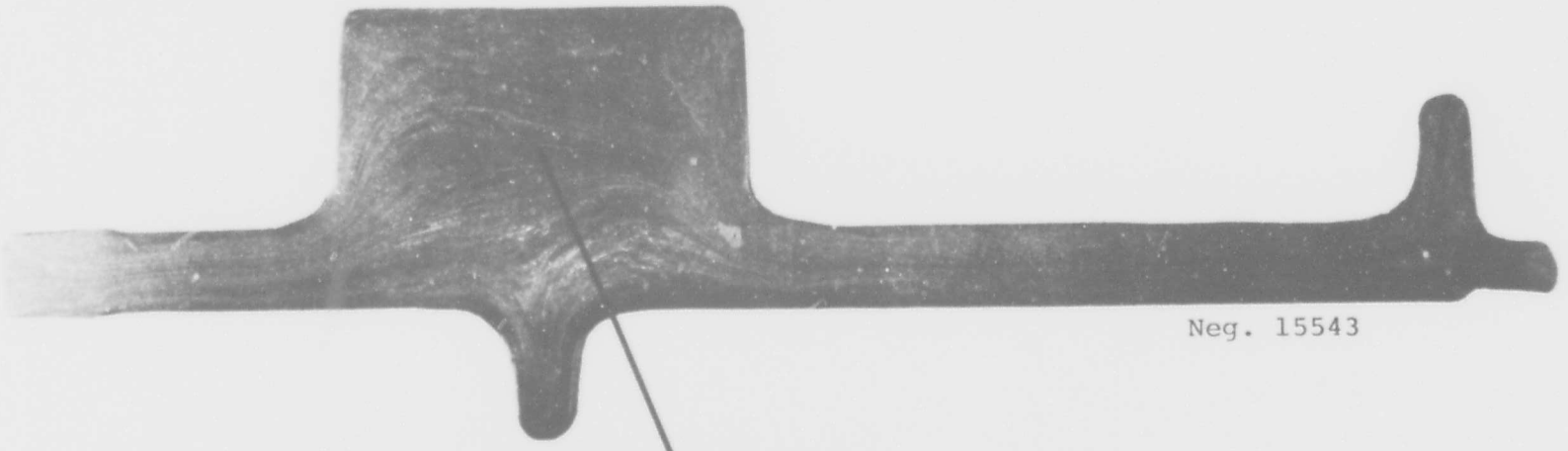

Neg. 15543

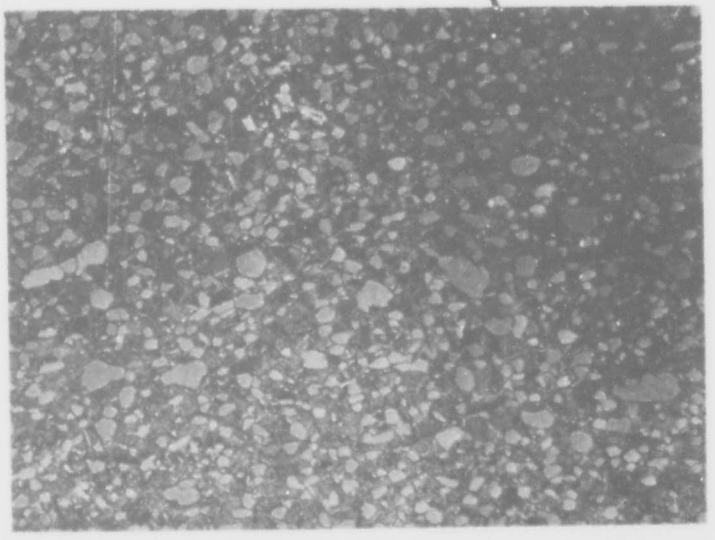

Neg. 15496

Macro section and microstructure (200X) of
structural part forged from fine grained Ti-6Al-4V

Negative 15524

Figure 23

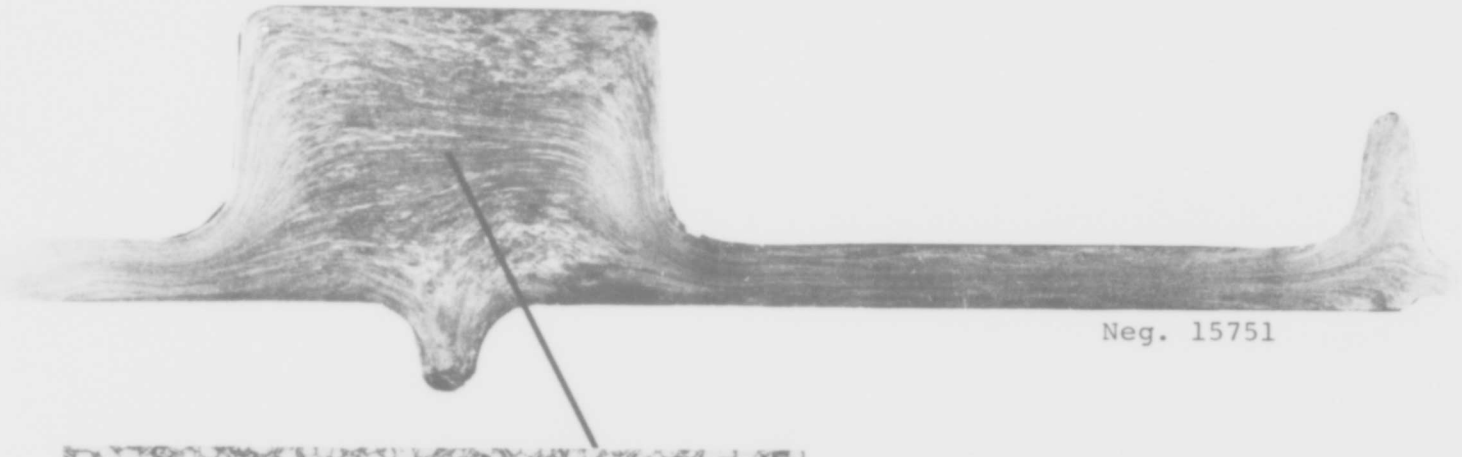

Neg. 15751

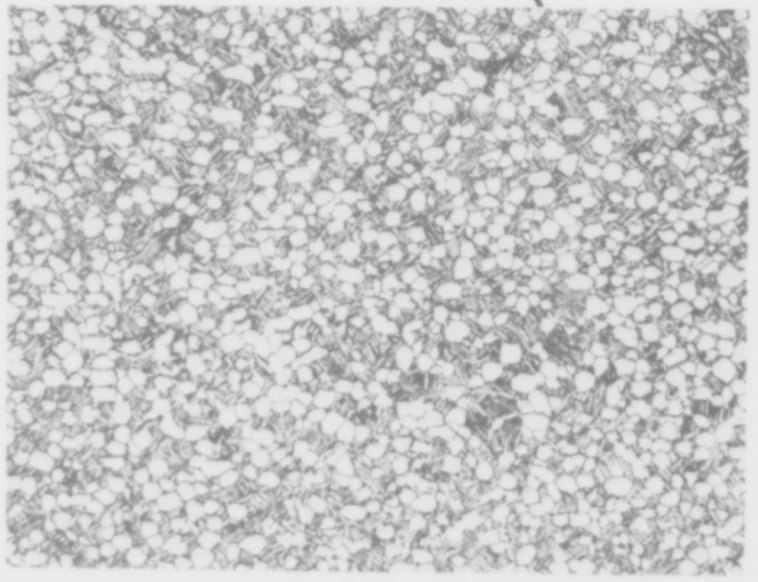

Macro section and microstructure (200X) of
structural part forged from intermediate grained Ti-6AL-4V

Negative 15752

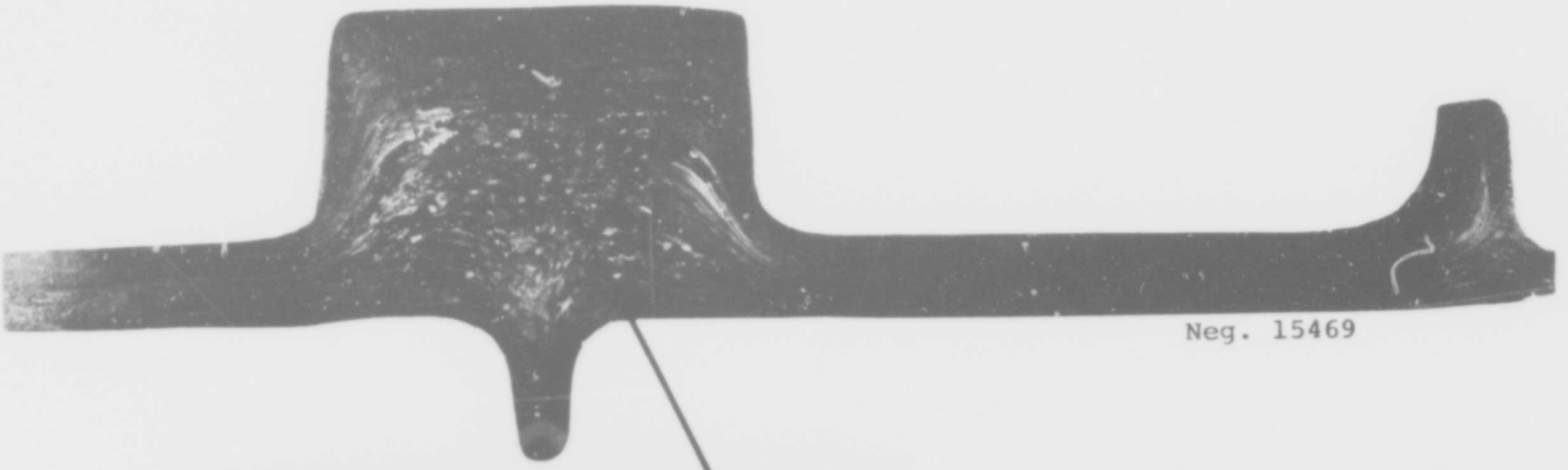

Neg. 15469

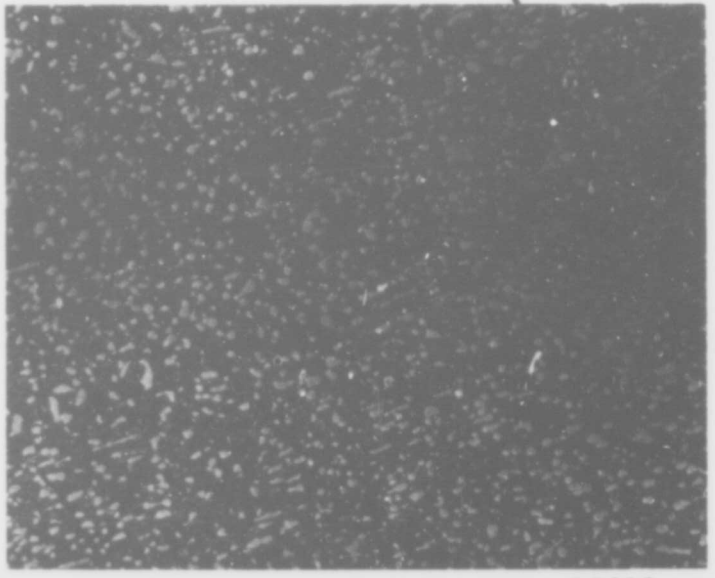

Neg. 15492

Macro section and microstructure (200X) of
structural part forged from coarse grained Ti-6Al-6V-2Sn

Negative 15521

Figure 25

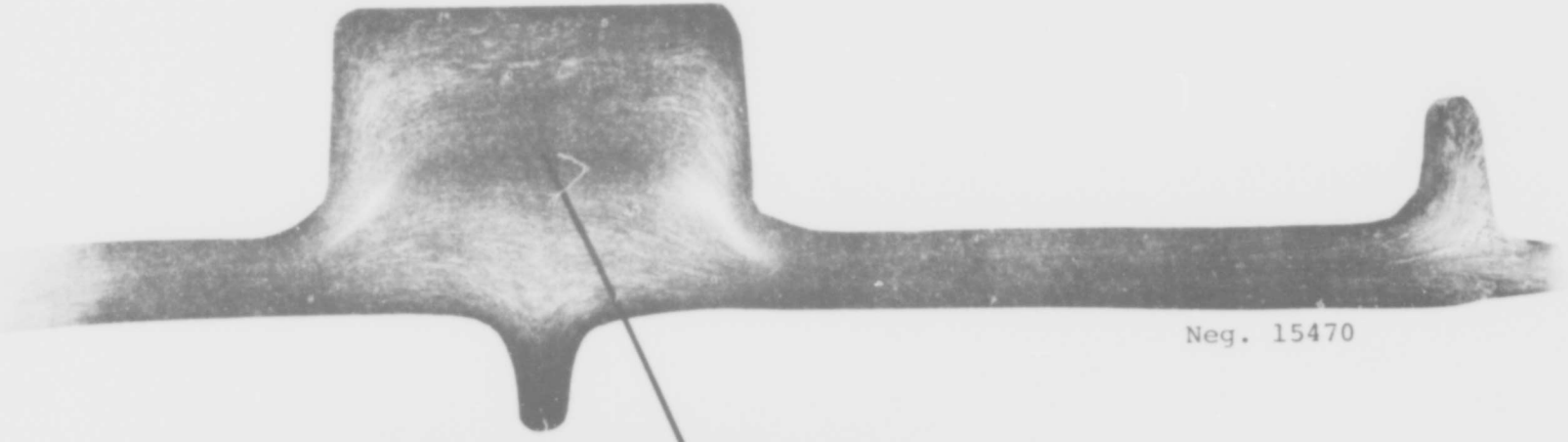

Neg. 15470

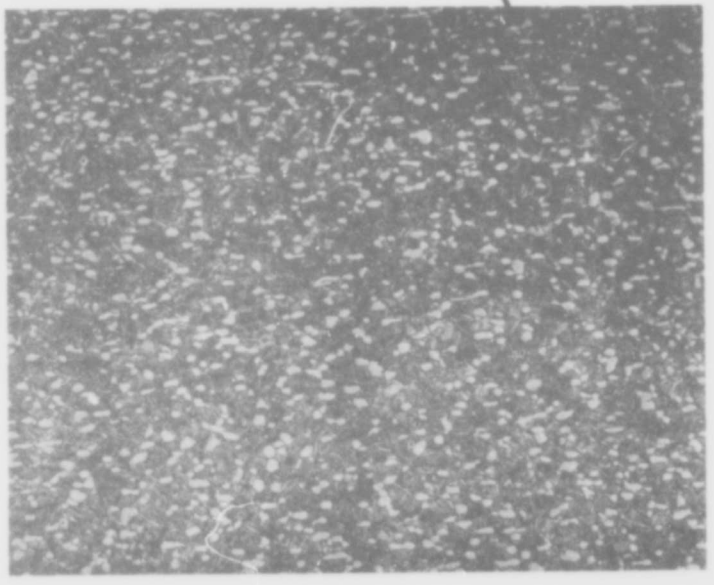

Neg. 15490

Macro section and microstructure (200X) of
structural part forged from fine grained Ti-6Al-6V-2Sn

Negative 15522

Figure 26

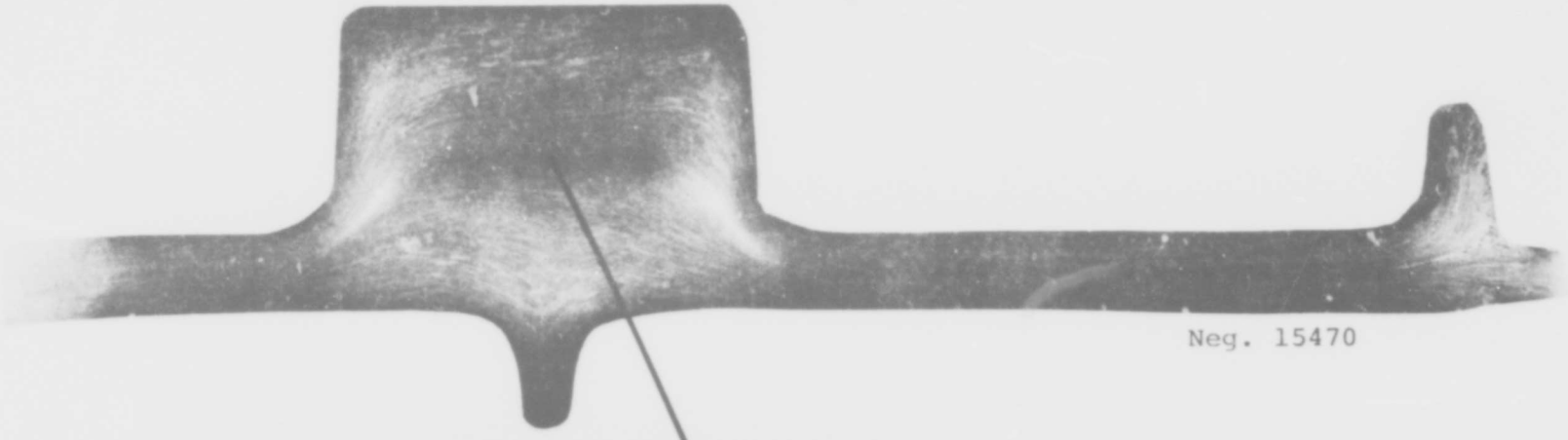

Neg. 15470

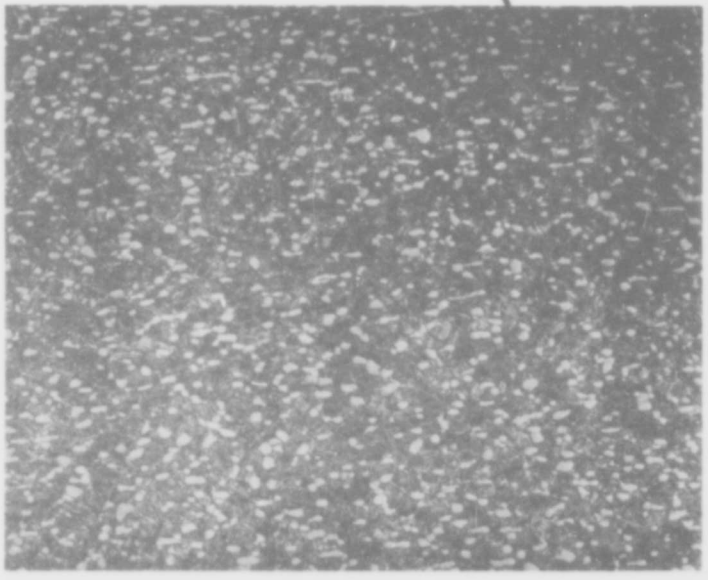

Neg. 15490

Macro section and microstructure (200X) of
structural part forged from fine grained Ti-6Al-6V-2Sn

Negative 15522

Figure 26

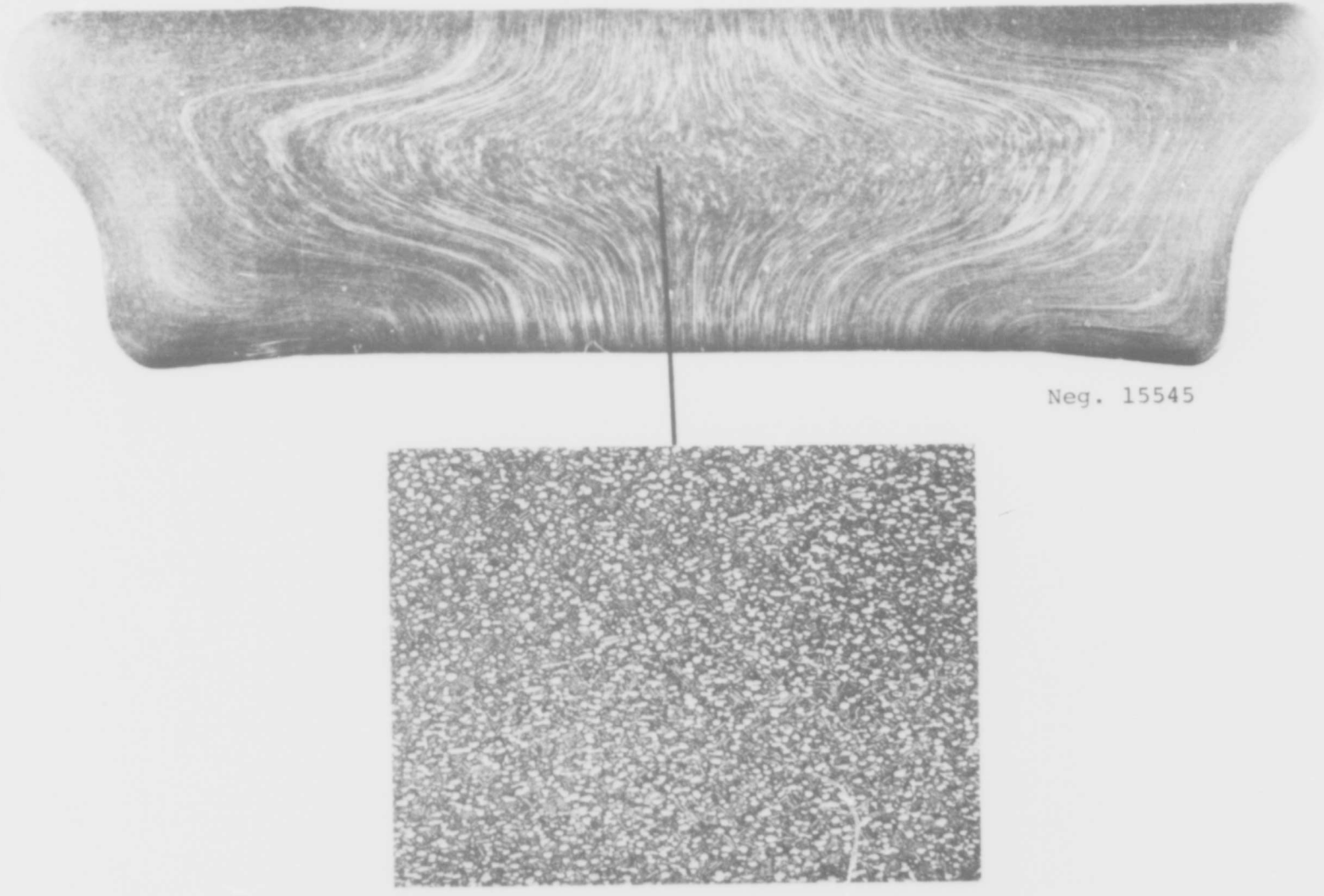

Neg. 15545

Figure 27

Macro section and microstructure (200X) of compressor disc forged from fine grained Ti-6Al-2Sn-4Zr-6Mo

Negative 15530

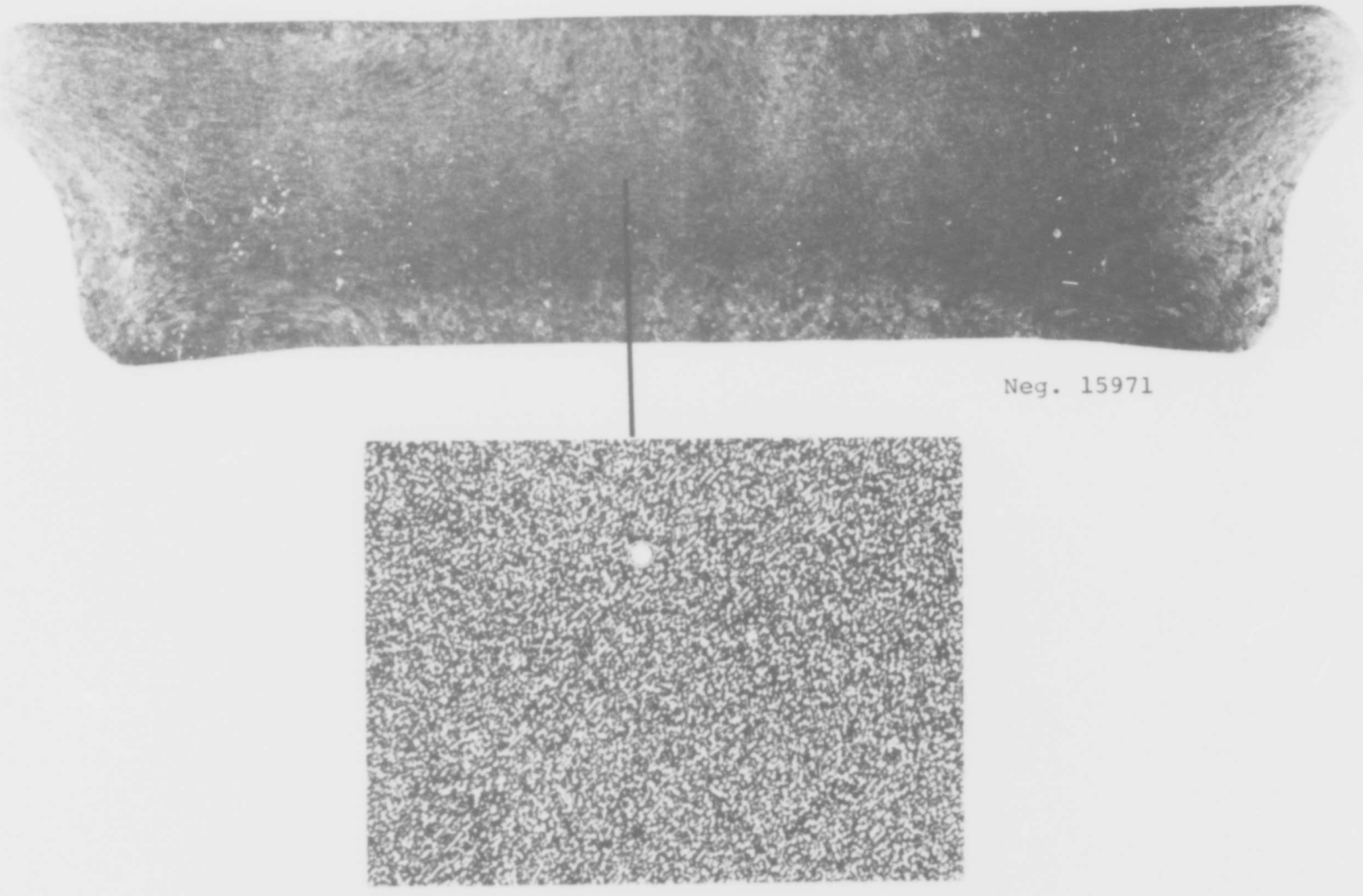

Neg. 15971

Macro section and microstructure (200X) of compressor disc forged from coarse grained Ti-6Al-2Sn-4Zr-6Mo

Negative 16010

Figure 28
54

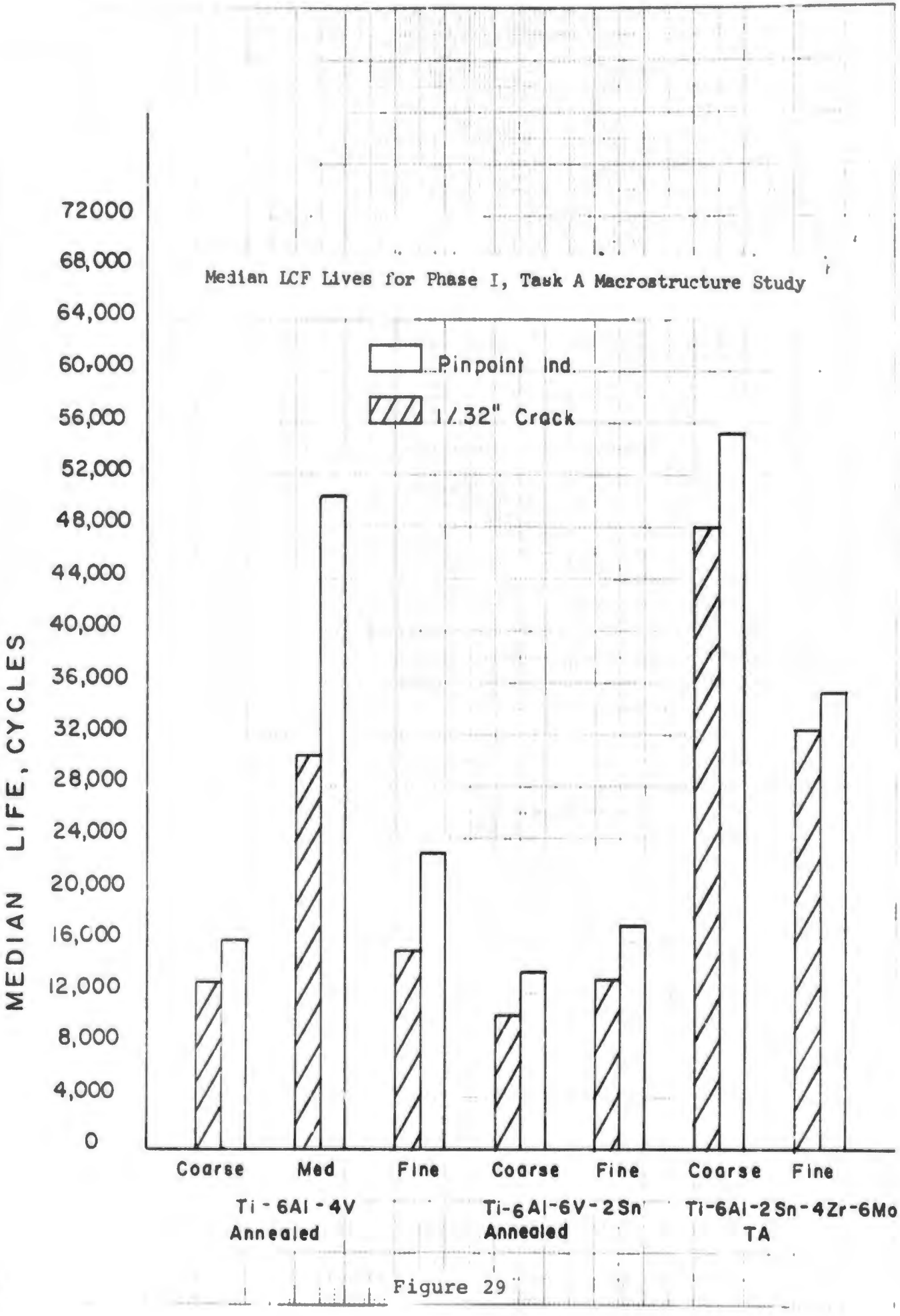
Median LCF Lives for Phase I, Task A Macrostructure Study
Pinpoint Ind.
1/32" Crack
MEDIAN LIFE, CYCLES
72000
68,000
64,000
60,000
56,000
52,000
48,000
44,000
40,000
36,000
32,000
28,000
24,000
20,000
16,000
12,000
8,000
4,000
0
Coarse
Med
Fine
Coarse
Fine
Coarse
Fine
Ti - 6Al - 4V
Annealed
Ti-6Al-6V-2Sn
Annealed
Ti-6Al-2Sn-4Zr-6Mo
TA

Figure 29

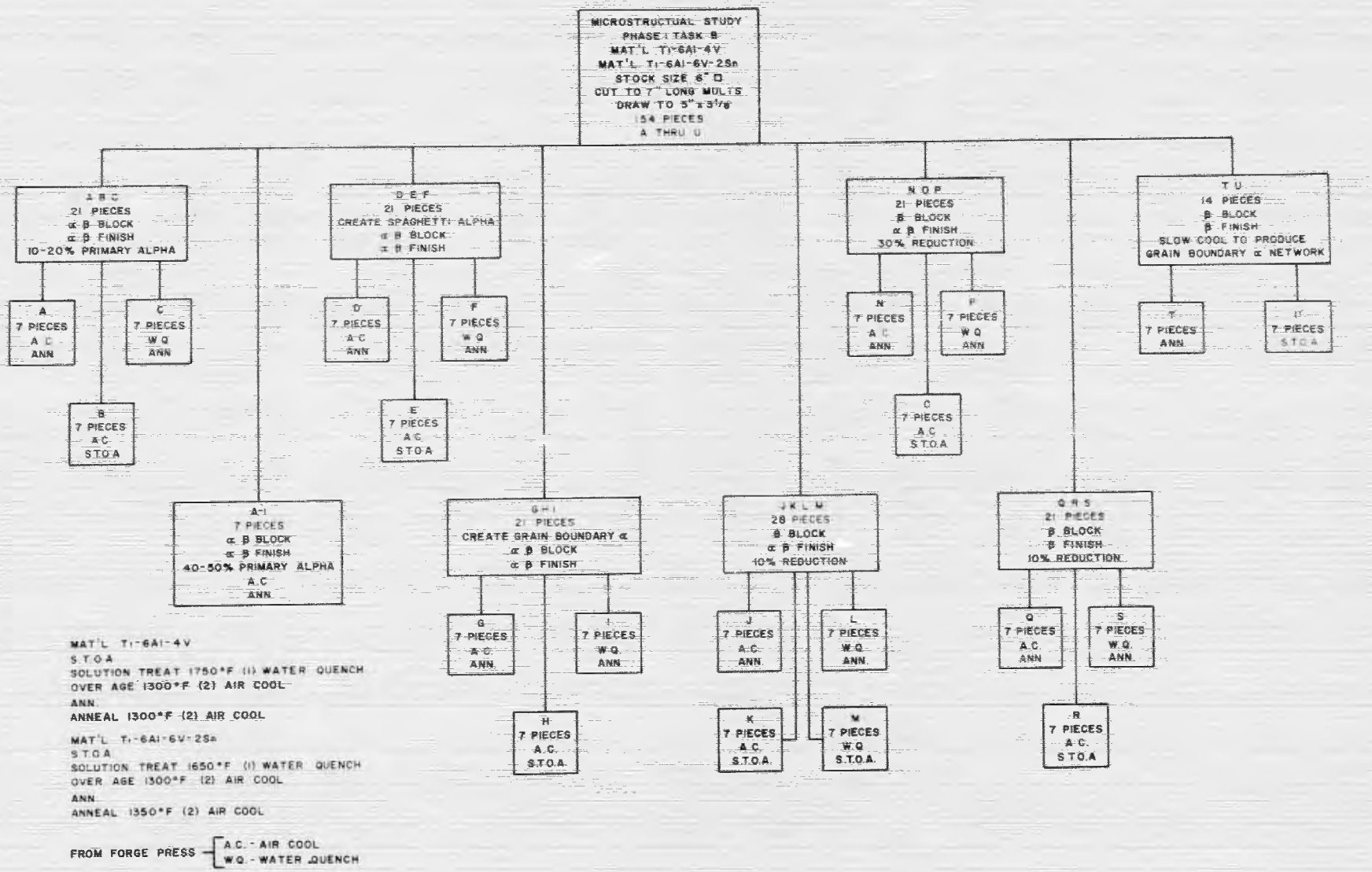
MICROSTRUCTUAL STUDY
PHASE I TASK B
MAT'L Ti-6Al-4V
MAT'L Ti-6Al-6V-2Sn
STOCK SIZE 6" □
CUT TO 7" LONG MULTS
DRAW TO 5" x 3 1/8"
154 PIECES
A THRU U
A B C
21 PIECES
α β BLOCK
α β FINISH
10-20% PRIMARY ALPHA
A
7 PIECES
A C
ANN
B
7 PIECES
A C
S T O A
C
7 PIECES
W Q
ANN
A-1
7 PIECES
α β BLOCK
α β FINISH
40-50% PRIMARY ALPHA
A C
ANN
D E F
21 PIECES
CREATE SPAGHETTI ALPHA
α β BLOCK
α β FINISH
D
7 PIECES
A C
ANN
E
7 PIECES
A C
S T O A
F
7 PIECES
W Q
ANN
G H I
21 PIECES
CREATE GRAIN BOUNDARY α
α β BLOCK
α β FINISH
G
7 PIECES
A C
ANN
H
7 PIECES
A C
S T O A
I
7 PIECES
W Q
ANN
J K L M
28 PIECES
β BLOCK
α β FINISH
10% REDUCTION
J
7 PIECES
A C
ANN
K
7 PIECES
A C
S T O A
L
7 PIECES
W Q
ANN
M
7 PIECES
W Q
S T O A
N O P
21 PIECES
β BLOCK
α β FINISH
30% REDUCTION
N
7 PIECES
A C
ANN
O
7 PIECES
A C
S T O A
P
7 PIECES
W Q
ANN
Q R S
21 PIECES
β BLOCK
β FINISH
10% REDUCTION
Q
7 PIECES
A C
ANN
R
7 PIECES
A C
S T O A
S
7 PIECES
W Q
ANN
T U
14 PIECES
β BLOCK
β FINISH
SLOW COOL TO PRODUCE
GRAIN BOUNDARY α NETWORK
T
7 PIECES
ANN
U
7 PIECES
S T O A
MAT'L Ti-6Al-4V
S T O A
SOLUTION TREAT 1750°F (1) WATER QUENCH
OVER AGE 1300°F (2) AIR COOL
ANN.
ANNEAL 1300°F (2) AIR COOL
MAT'L Ti-6Al-6V-2Sn
S T O A
SOLUTION TREAT 1650°F (1) WATER QUENCH
OVER AGE 1300°F (2) AIR COOL
ANN.
ANNEAL 1350°F (2) AIR COOL
FROM FORGE PRESS
A.C. - AIR COOL
W.Q. - WATER QUENCH

Figure 30

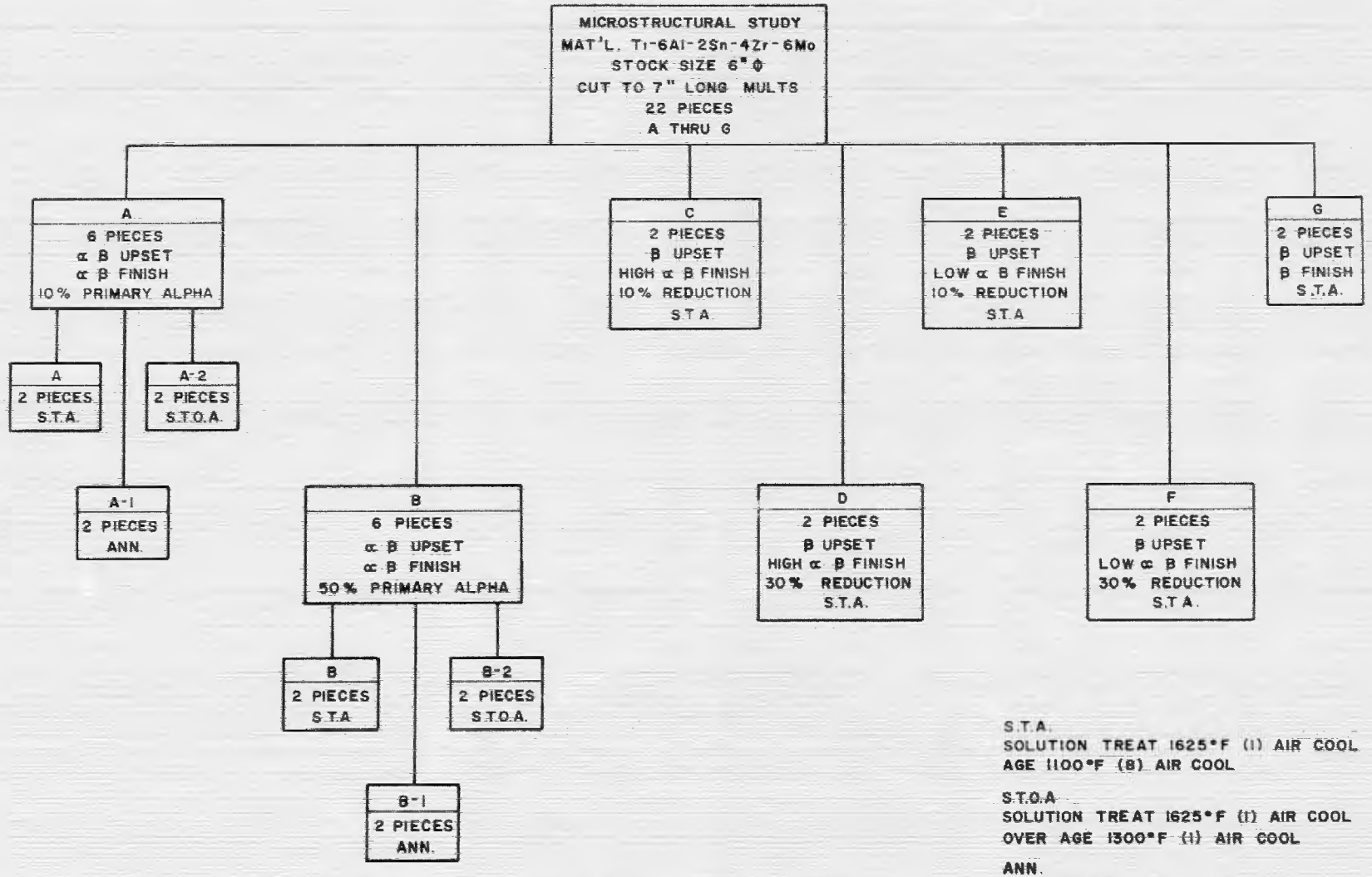
MICROSTRUCTURAL STUDY
MAT'L. Ti-6Al-2Sn-4Zr-6Mo
STOCK SIZE 6" Φ
CUT TO 7" LONG MULTS
22 PIECES
A THRU G
A
6 PIECES
α β UPSET
α β FINISH
10% PRIMARY ALPHA
A
2 PIECES
S.T.A.
A-2
2 PIECES
S.T.O.A.
A-1
2 PIECES
ANN.
B
6 PIECES
α β UPSET
α β FINISH
50% PRIMARY ALPHA
B
2 PIECES
S.T.A.
B-2
2 PIECES
S.T.O.A.
B-1
2 PIECES
ANN.
C
2 PIECES
β UPSET
HIGH α β FINISH
10% REDUCTION
S.T.A.
D
2 PIECES
β UPSET
HIGH α β FINISH
30% REDUCTION
S.T.A.
E
2 PIECES
β UPSET
LOW α β FINISH
10% REDUCTION
S.T.A.
F
2 PIECES
β UPSET
LOW α β FINISH
30% REDUCTION
S.T.A.
G
2 PIECES
β UPSET
β FINISH
S.T.A.
S.T.A.
SOLUTION TREAT 1625°F (1) AIR COOL
AGE 1100°F (8) AIR COOL
S.T.O.A.
SOLUTION TREAT 1625°F (1) AIR COOL
OVER AGE 1300°F (1) AIR COOL
ANN.
ANNEAL 1300°F (1) AIR COOL

Figure 31

Ti-6Al-4V
MICROSTRUCTUAL STUDY
INITIAL, IN-PROCESS AND
FINAL STRUCTURES

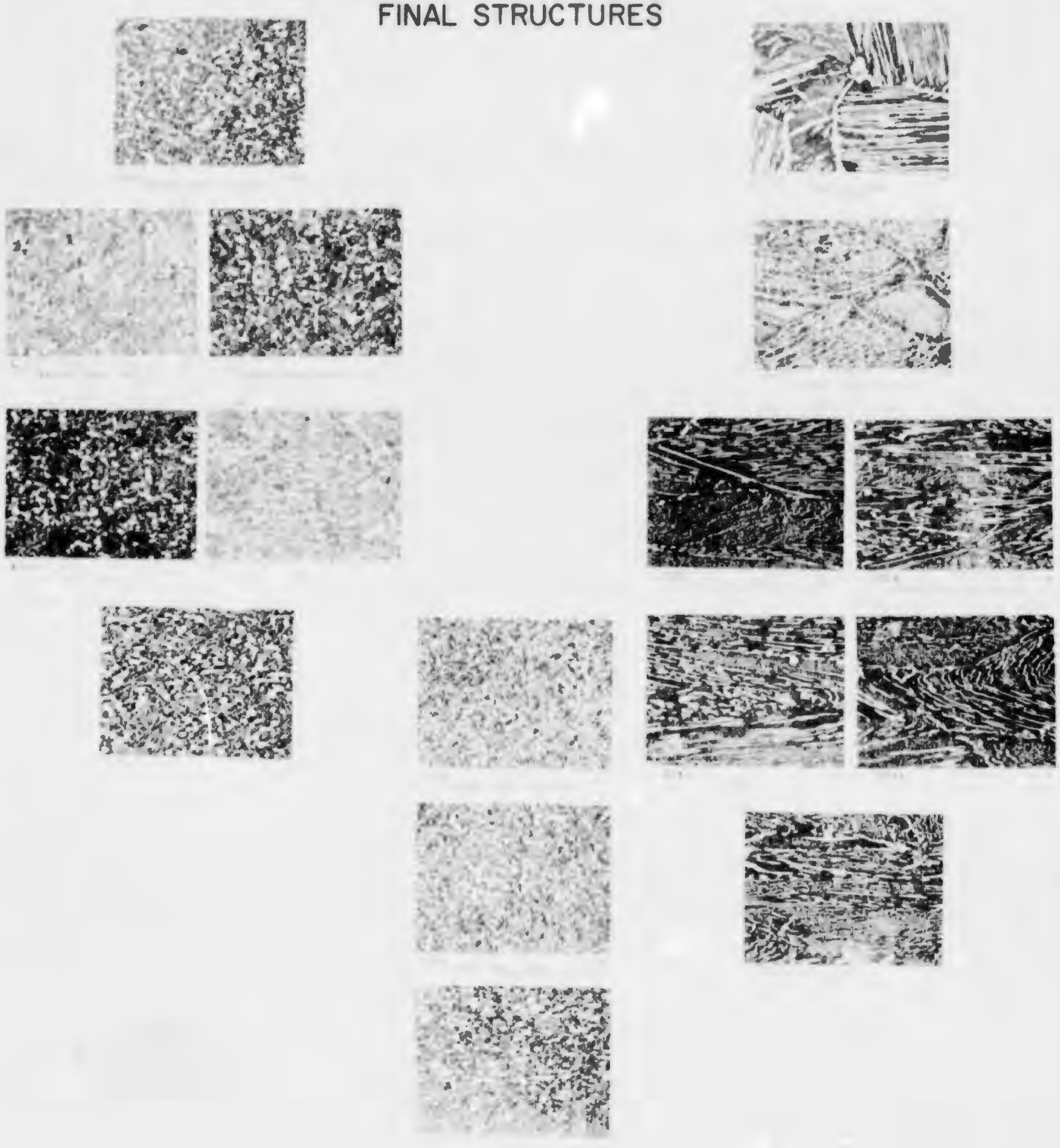

Figure 32

Ti-6Al-4V
MICROSTRUCTUAL STUDY
INITIAL, IN-PROCESS AND
FINAL STRUCTURES

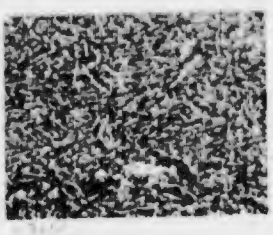

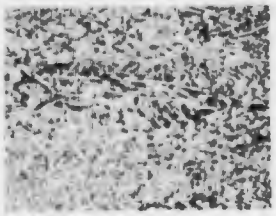

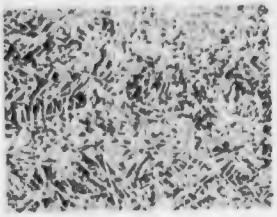

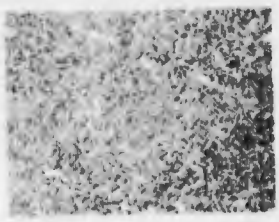

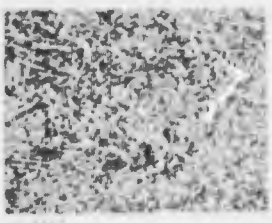

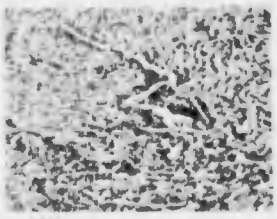

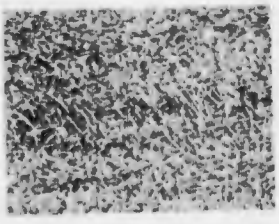

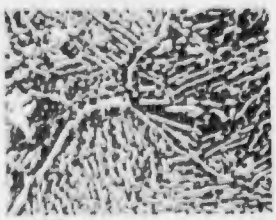

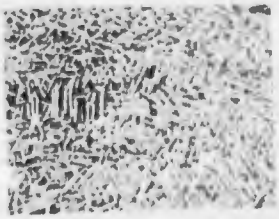

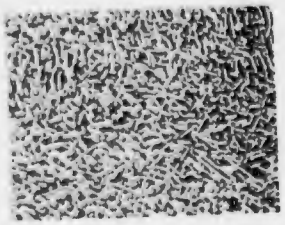

Figure 33

Ti-6Al-4V
MICROSTRUCTUAL STUDY
INITIAL, IN-PROCESS AND
FINAL STRUCTURES

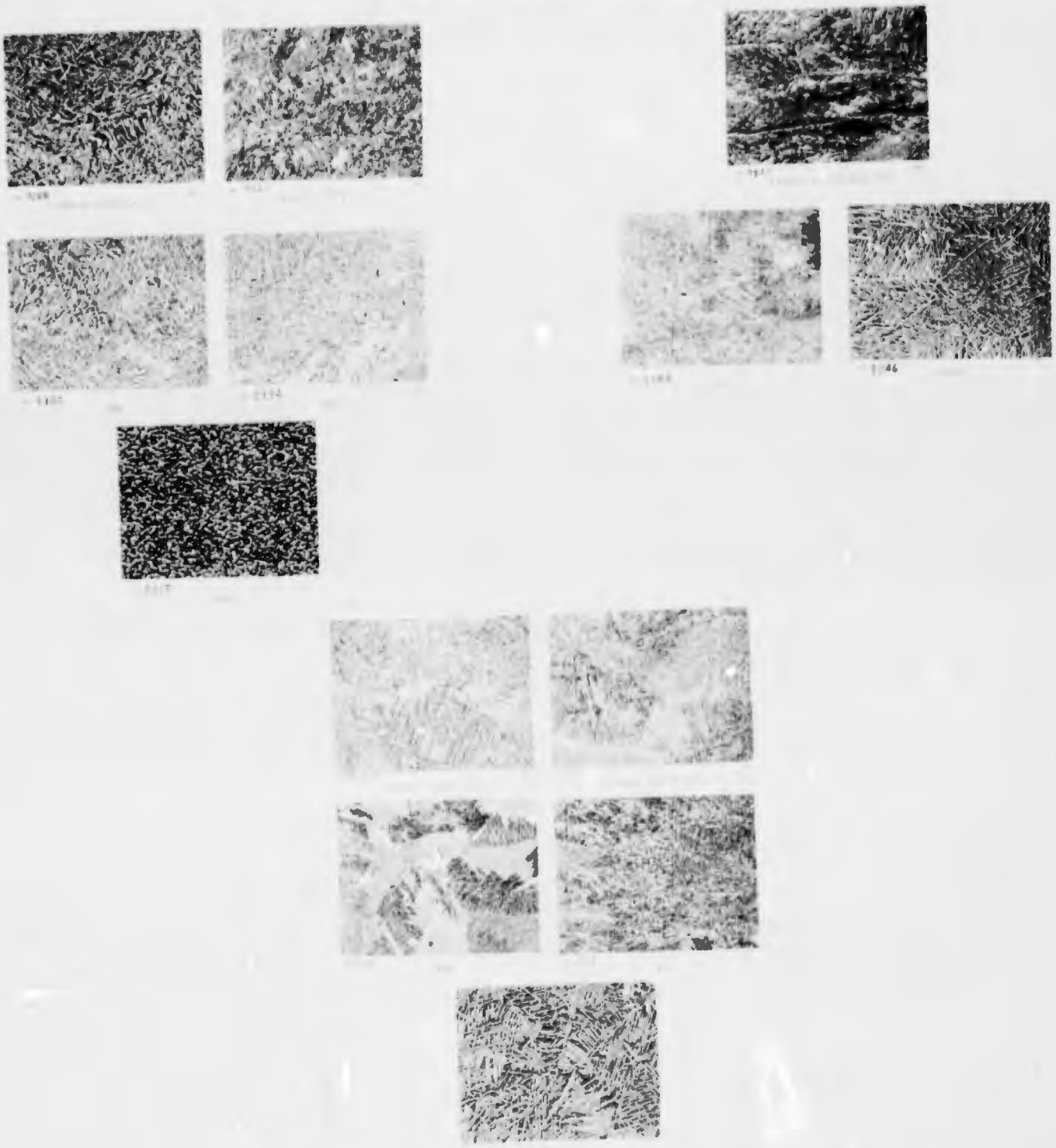

Figure 34

Ti-6Al-6V-2Sn

MICROSTRUCTUAL STUDY

INITIAL, IN-PROCESS AND

FINAL STRUCTURES

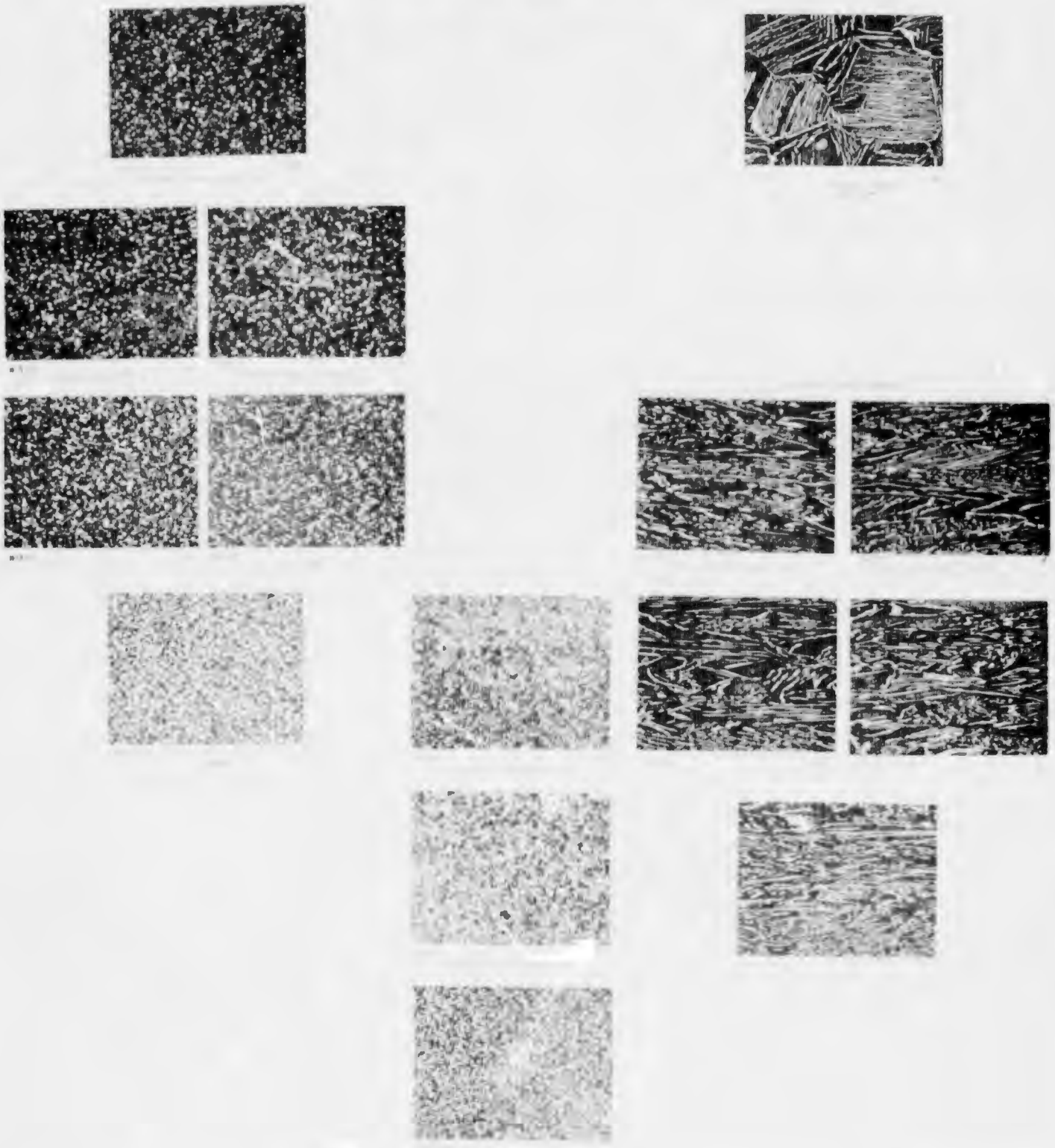

Figure 35

Ti-6Al-6V-2Sn
MICROSTRUCTUAL STUDY
INITIAL, IN-PROCESS AND
FINAL STRUCTURES

Figure 36

Ti-6Al-6V-2Sn
MICROSTRUCTUAL STUDY
INITIAL, IN-PROCESS AND
FINAL STRUCTURES

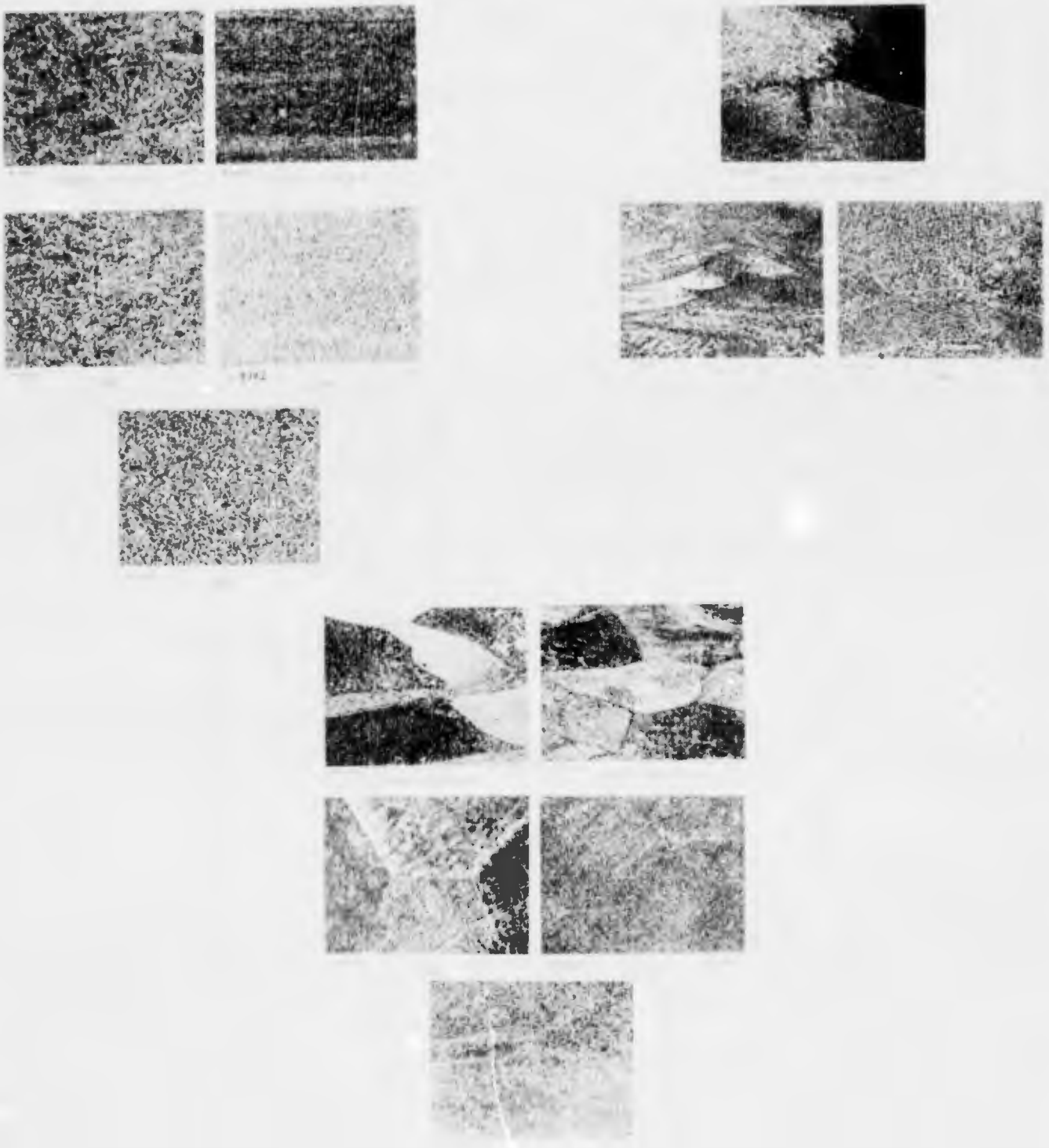

Figure 37

Condition A:
6% equiaxed α; platelet α precipitated in secondary β grains. Some outline of secondary β grains by α.

Condition B:
28% equiaxed α; platelet α precipitated in secondary β grains. Platelet α present in different sizes; resulting from different thermal treatment.

Condition C:
12% equiaxed α
Same as Condition A, but with greater outlining of secondary beta grains.

Condition A1
32% equiaxed α
Similar to Condition B, with larger amounts of the coarser platelet α.

Figure 38 Comments

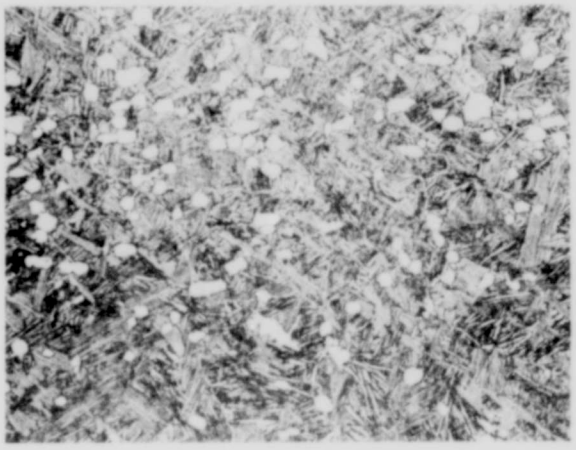

A

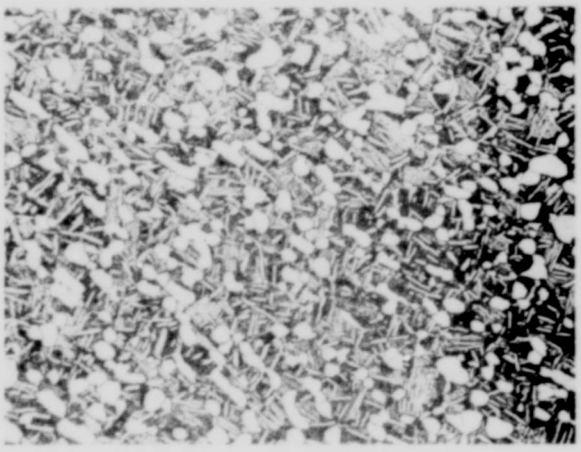

B

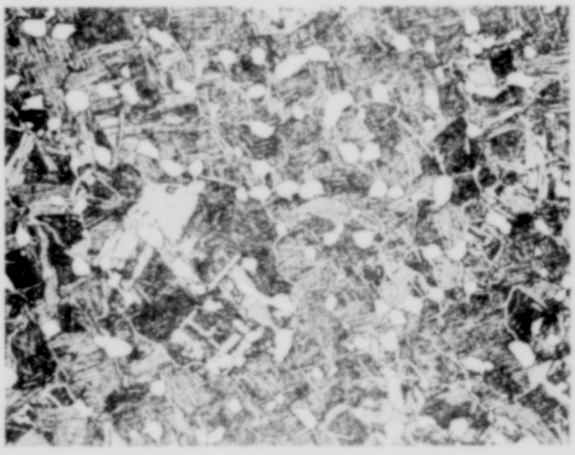

C

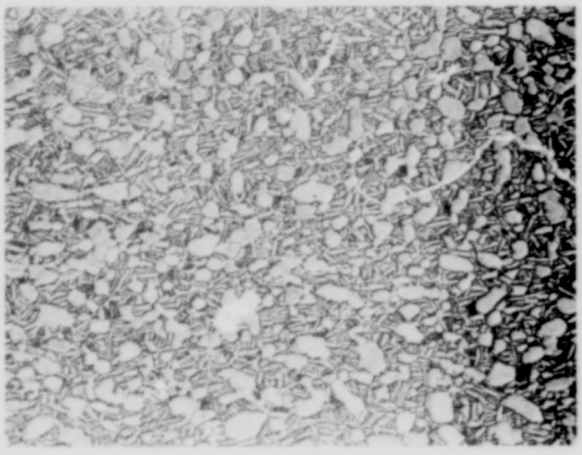

A-1

Final Structures Ti-6Al-4V
Microstructural Study
See Figure 30 for Processing Details

Magnification: All 200X

Etchant: NaOH, H_2O_2

Negative 16515

Figure 38

Condition D - 30% α. This % α determined from measurement of regions A and B. Alpha corresponding to regions A and B precipitated from primary β grains. Some evidence of recrystallization in the coarse α of region A. Alpha of region A is frequently referred to as coarse elongated α. Region B is designated a colony of aligned α. Region C platelet α formed at temperatures below those at which α of regions A and B formed.

Condition E - 25% α. α of regions similar to A, B, C, and D used to determine percentage of α Alpha of areas A-D precipitated from primary β grains. Alpha of region B precipitated at primary β grain boundary. Some evidence of recrystallization in α corresponding to A, B, and C. Secondary β grain outlined by α at region E. Matrix consists of secondary β grains in which the generally unresolved platelet α has precipitated.

Condition F - 29% α. The percentage of α determined from regions corresponding to A and B. Alpha of A and B precipitated from primary β grains. Alpha at "A" precipitated at primary β grain boundary. Aligned colony of α at B. Alpha of region C formed on cooling from temperatures below that at which regions A and B formed. Some evidence of recrystallization of regions A and B, but this is not easily detected.

Figure 39 Comments

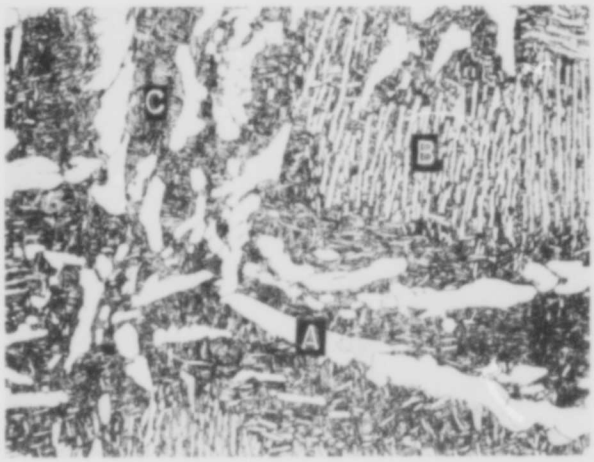

D

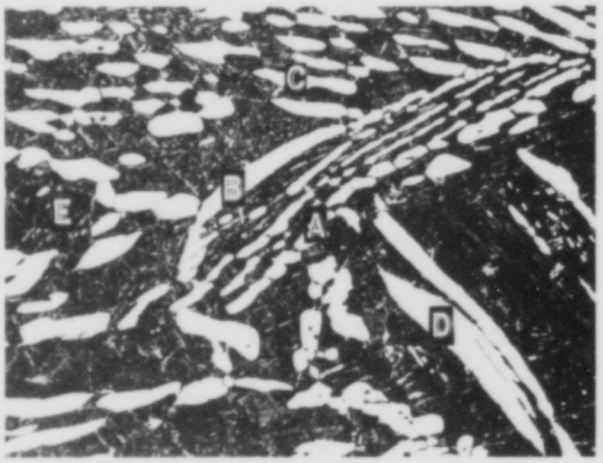

E

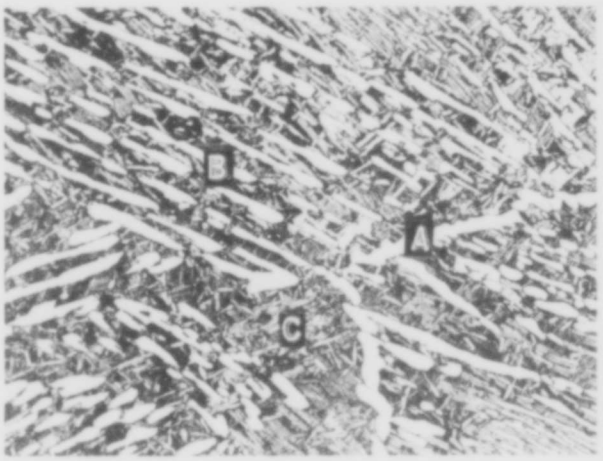

F

Final Structures Ti-6Al-4V
Microstructural Study
See Figure 30 for Processing Details

Magnification: All 200X

Etchant: NaOH, H_2O_2

Negative 16516

Figure 39

Condition G - 29% α. Alpha, formed as a result of cooling from the β field, has precipitated at primary β grain boundaries and within these grains. Working within the α-β field has produced some recrystallization of both grain boundary and intragranular α. Insufficient working and heating heating in α-β field has prevented α from becoming equiaxed as seen in Condition A, Figure 31. Platelet alpha in region A produced on cooling from temperatures below those at which the coarser α formed.

Condition H - 26% α
Similar to Condition G

Condition I - 23% α
Similar to Condition G

Figure 40 Comments

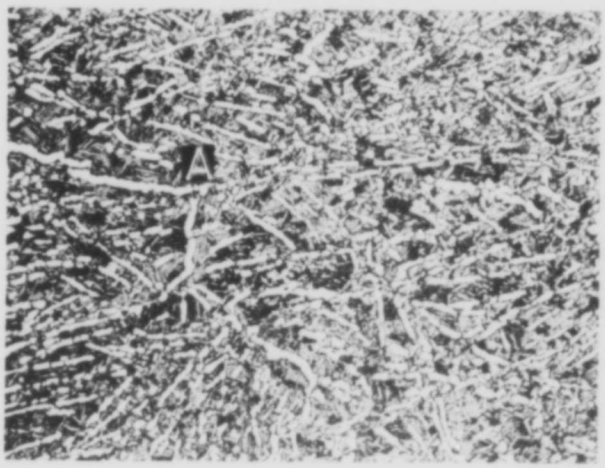

G

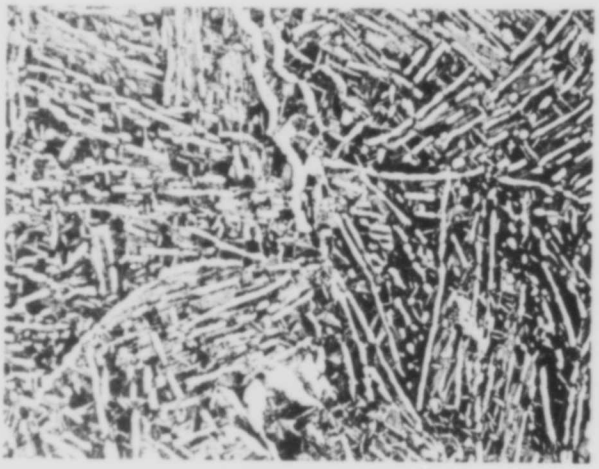

H

I

Final Structures Ti-6Al-4V
Microstructural Study
See Figure 30 for Processing Details

Magnification: All 200X

Etchant: NaOH, H_2O_2

Negative 16517

Figure 40

Condition J 63%% α, Condition K 45% α, Condition L 52% α, Condition M 43% α.

Structures J, K, L, and M are similar to Conditions G, H, and I, with the following exceptions:

Conditions J, K, L, and M have less grain boundary α as a result of more rapid cooling from the β field compared to that for Conditions G, H, and I.

Conditions J, K, L, and M reflect less alpha beta working than Conditions G, H, and I.

Alpha morphology of Condition L segments is referred to as a "basket weave" morphology.

Figure 41 Comments

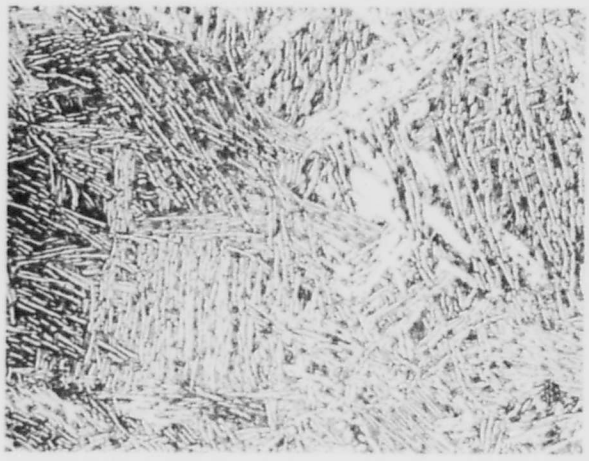

J

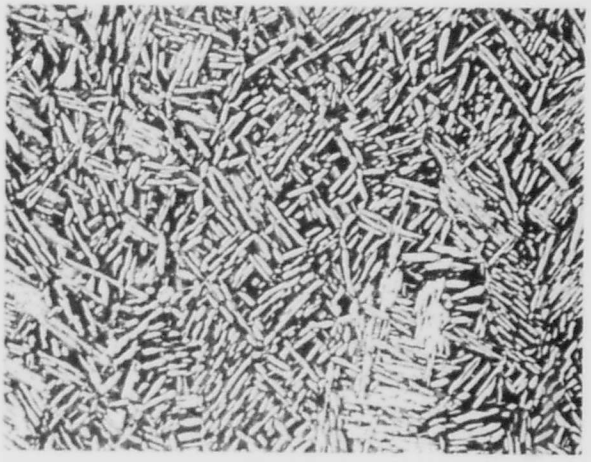

K

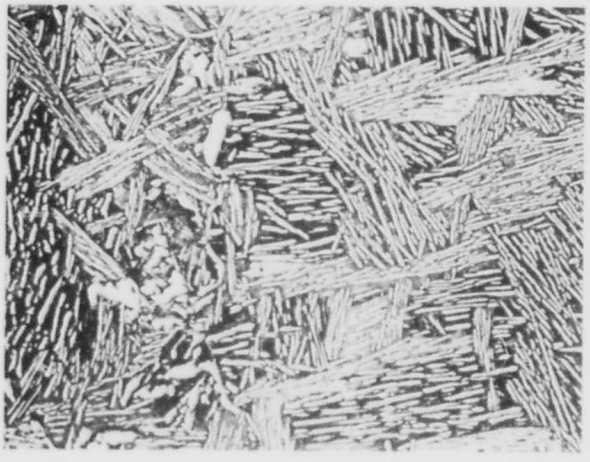

L

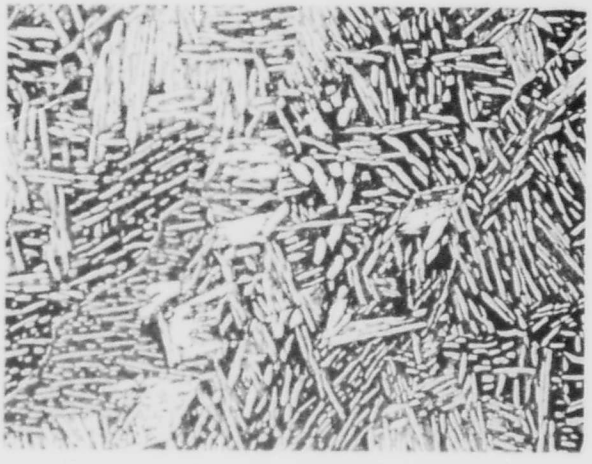

M

Final Structures Ti-6Al-4V
Microstructural Study
See Figure 30 for Processing Details

Magnification: All 200X

Etchant: NaOH, H_2O_2

Negative 16518

Figure 41

Condition N - 76% α, Condition O - 43% α, Condition P - 68% α,

Structures are essentially similar to Condition L, Figure 41, with the α in basket weave morphology. Working 30% in the α-β field has produced some raggedness in the α, particularly noticeable in Condition N. This indicates recrystallization of the alpha, which has occurred without destroying the basket weave morphology. The lower percentage of α in Condition O results from solution of alpha during the solution treatment.

Figure 42 Comments

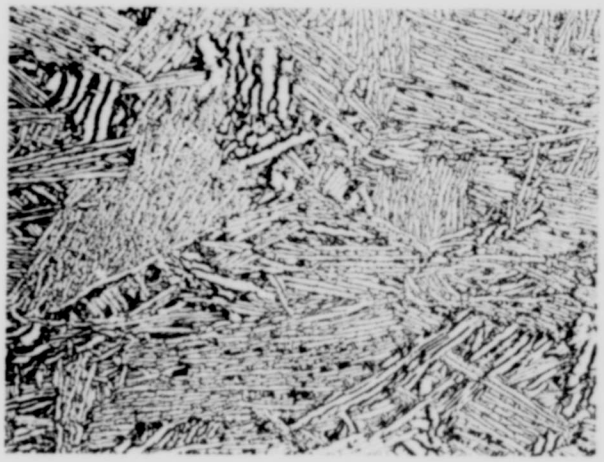

N

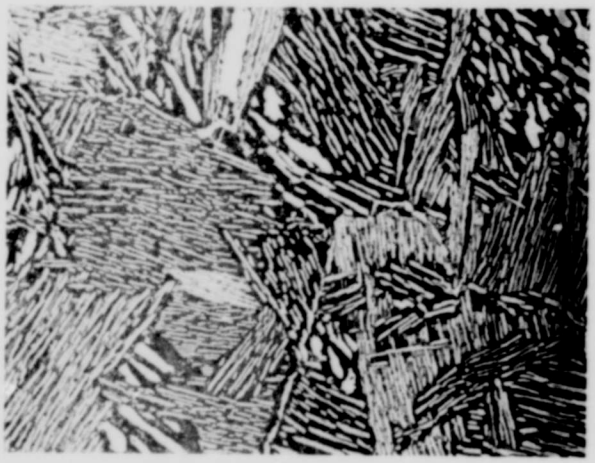

O

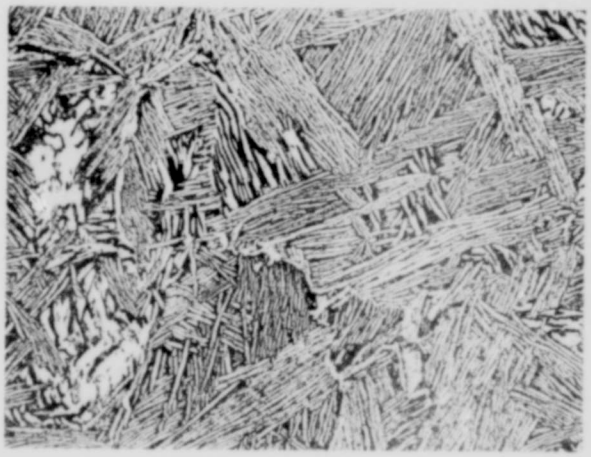

P

Final Structures Ti-6Al-4V
Microstructural Study
See Figure 30 for Processing Details

Magnification: All 200X

Etchant: NaOH, H_2O_2

Negative 16519

Figure 42

Condition Q - 75% α; Condition R - 48% α
Air cooling from the β field has produced this basket weave α morphology. Solution treatment, Condition R, has dissolved some α, and permitted some coarsening to take place without destroying the basket weave pattern.

Condition S - 58% α. Since this material was water quenched from the β field, the basket weave morphology could not form and the alpha, in platelet form, is quite fine. As Table XVIII indicates, the percentage of alpha was measured at 800X. This permitted determination of the percentage of α which would not be possible at the 200X magnification reproduced here. Cooling from the β field has produced some outlining of the prior β grains.

Figure 43 Comments

Q

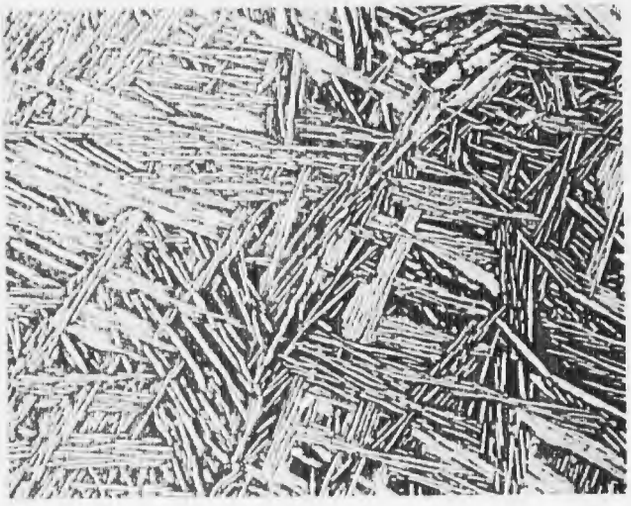

R

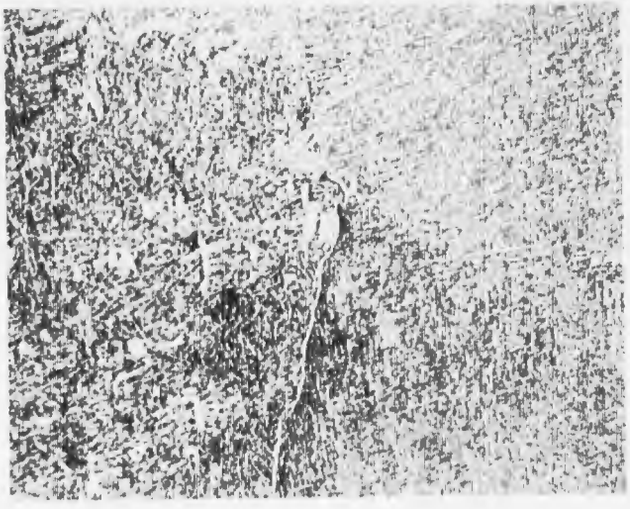

S

Final Structures Ti-6Al-4V
Microstructural Study
See Figure 30 for Processing Details

Magnification: All 200X

Etchant: NaOH, H_2O_2

Negative 16520

Figure 43

Condition T - 92% α, and Condition U - 49% α. Condition T similar to Condition Q. Condition U similar to Condition R. The increased coarseness of structures U and T over Q and R is due to slower cooling from the β field.

Figure 44 Comments

T

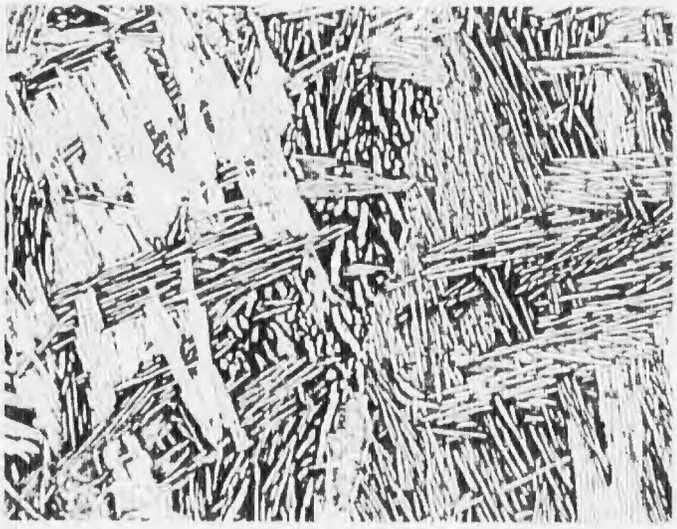

U

Final Structures Ti-6Al-4V
Microstructural Study
See Figure 30 for Processing Details

Magnification: All 200X

Etchant: NaOH, H_2O_2

Negative 16521

Figure 44

Condition A Low O_2
Structure similar to Condition A standard O_2
(Figure 38)

Figure 45 Comments

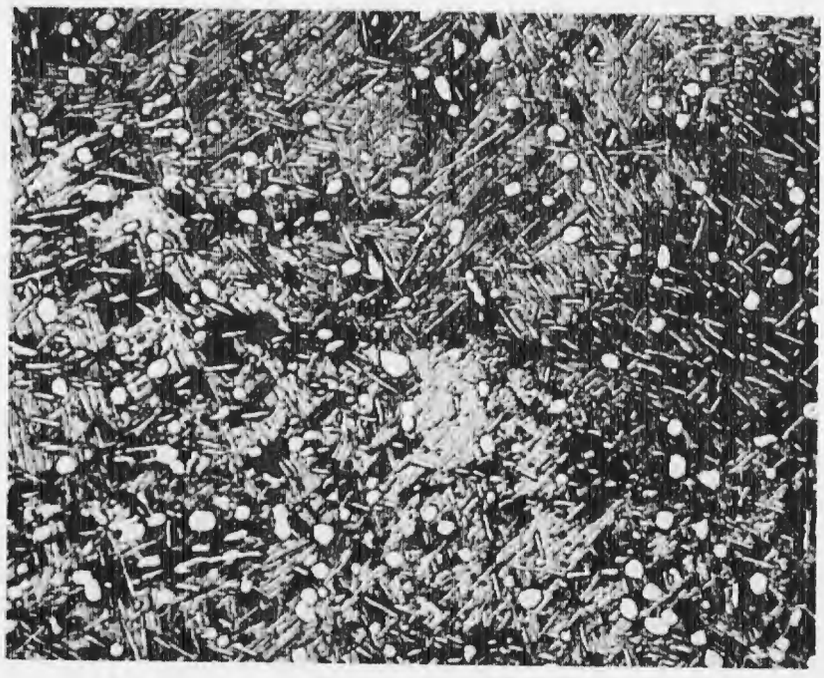

X200

Figure 45
Final Microstructure Ti-6Al-4V
Low Oxygen Condition A
See Figure 30 for Processing Details
Etchant NaOH, H_2O_2

Condition A:
15% equiaxed α; fine platelet α precipitated in secondary β grains.

Condition B:
33% equiaxed α.
Platelet α precipitated in secondary β grains.

Condition C:
23% equiaxed α
Same as Condition A, but with greater outlining of secondary beta grains.

Condition A-1:
42% equiaxed α
Platelet α coarser than Condition B.

Figure 46 Comments

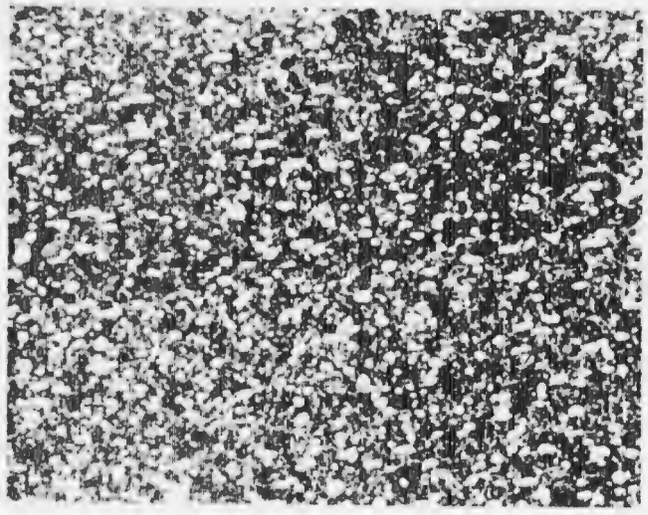

A

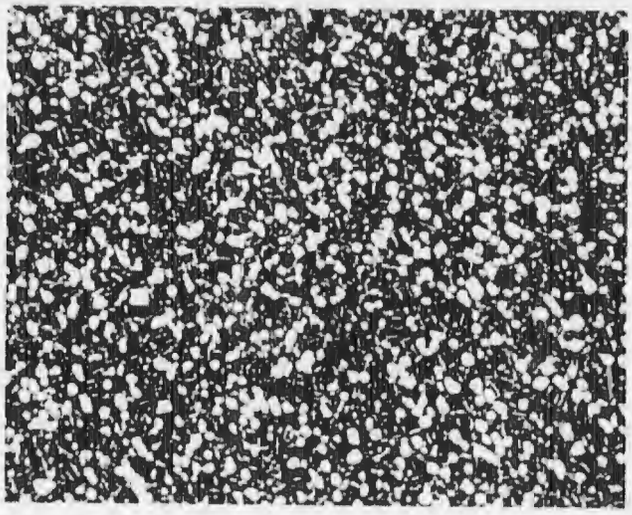

B

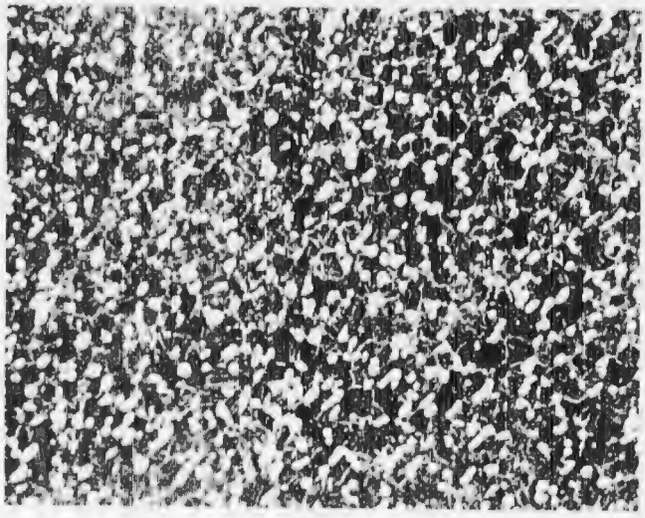

C

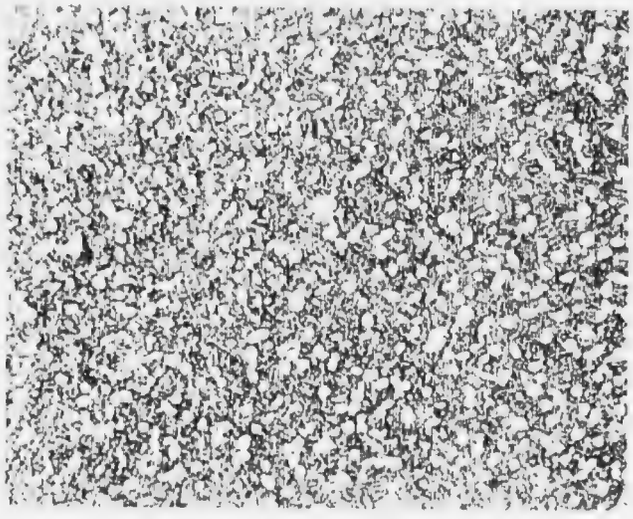

A-1

Final Structures Ti-6Al-6V-2Sn
Microstructural Study
ee Figure 30 for Processing Details

cation: All 200X

Etchant: NaOH, H_2O_2

Negative 16522

Figure 46

Condition E - 24% α. This % α determined from measurement of region A. Alpha corresponding to region A precipitated from primary β grains. Some evidence of recyrstallization in the coarse α of region A. Alpha of region A is frequently referred to as coarse elongated α. Region B platelet α formed at temperatures below those at which α of region A formed.

Condition E - 21% α. α of regions similar to A, B, and C used to determine percentage of α. Alpha of areas A-C precipitated from primary β grains. Alpha of region B precipitated at primary β grain boundary. Region D formed at temperatures below those at which α of regions A, B, and C formed.

Condition F - 23% α. The percentage of α determined from regions corresponding to A and B. Alpha of A and B precipitated from primary β grains. Alpha at "A" precipitated at primary β grain boundary. Alpha of region C formed on cooling from temperatures below that at which regions A and B formed.

Figure 47 Comments

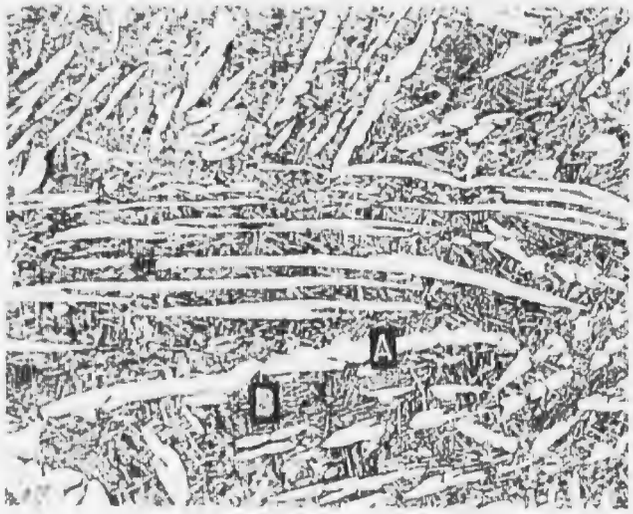

D

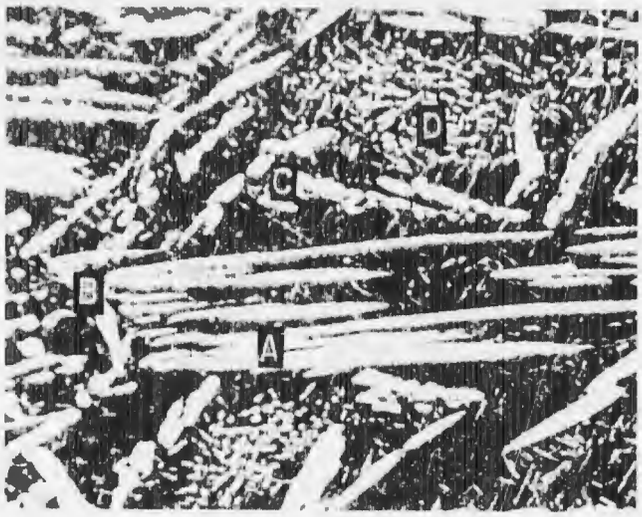

E

F

Final Structures Ti-6Al-6V-2Sn
Microstructural Study
See Figure 30 for Processing Details

Magnification: All 200X Etchant: NaOH, H_2O_2

Negative 16523

Figure 47

Condition G - 24% α. Alpha, formed as a result of cooling from the β field, has precipitated at primary β grain boundaries and within these grains. Working within the α-β field has produced some recrystallization of both grain boundary and intragranular α. Insufficient working and heating in α-β field has prevented α from becoming equiaxed as seen in Condition A, Figure 38. Platelet alpha in region A produced on cooling from temperatures below those at which the coarser α formed.

Condition H - 25% α. Similar to Condition G.

Condition I - 20% α. Similar to Condition G.

Figure 48 Comments

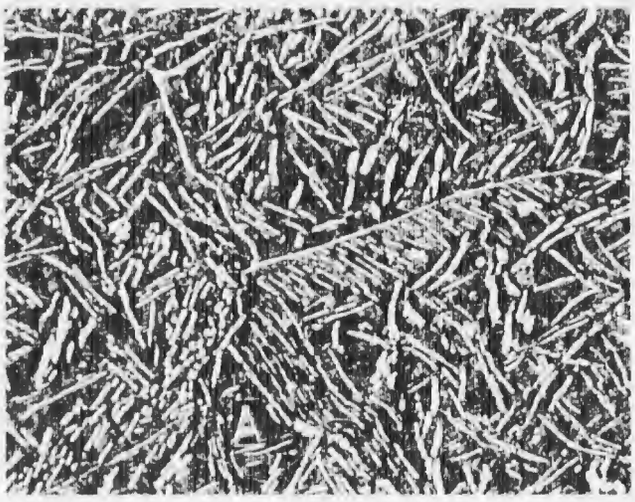

G

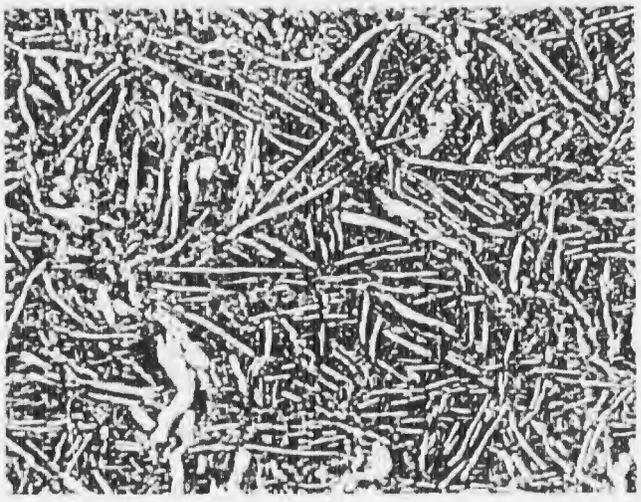

H

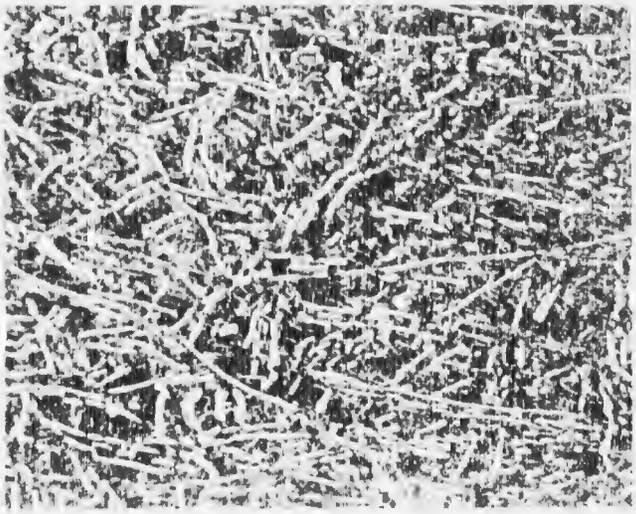

I

Final Structures Ti-6Al-6V-2Sn
Microstructural Study
[illegible] 30 for Processing Details

[illegible]: [illegible] Etchant: NaOH, H_2O_2

Negative 16524

Figure 48

Condition J 60% α, Condition K 31% α, Condition L 46% α, Condition M 26% α.

Structures J, K, L, and M are similar to Conditions G, H, and I except Conditions J, K, L, and M have less grain boundary α.

Figure 49 Comments

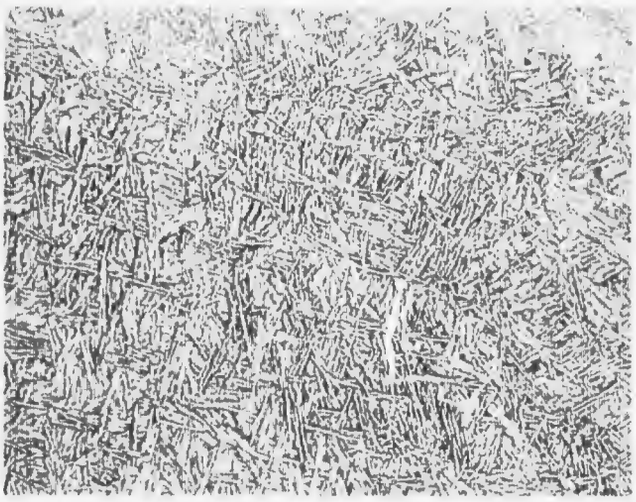

J

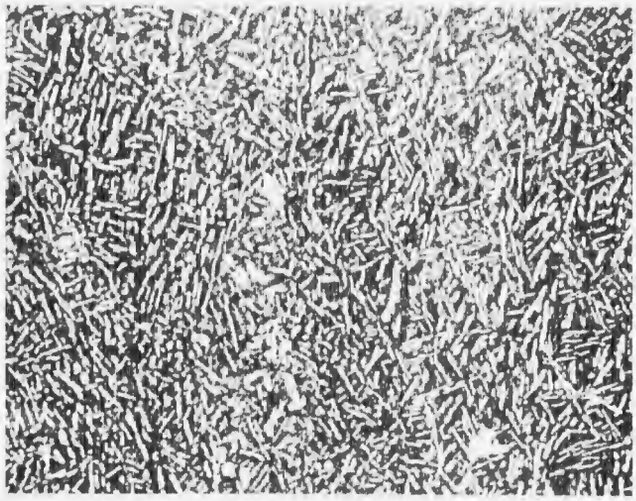

K

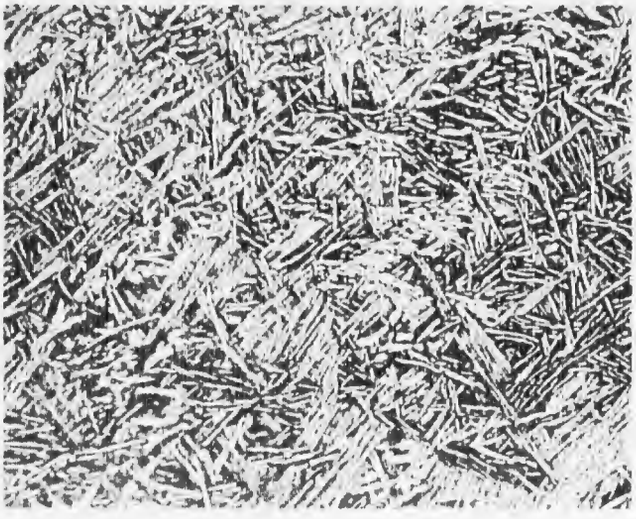

L

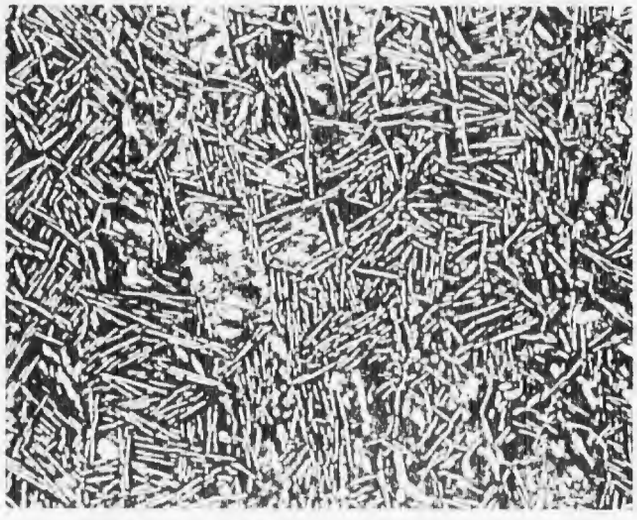

M

Final Structures Ti-6Al-6V-2Sn
Microstructural Study
See Figure 30 for Processing Details

Magnification: All 200X Etchant: NaOH, H_2O_2

Negative 16525

Figure 49

Condition N - 64% α, Condition O - 39% α, Condition P - 49% α, Structures are essentially similar to Condition L, Figure 41, with the α in basket weave morphology. The lower percentage of α in Condition O results from solution of alpha during the solution treatment.

Figure 50 Comments

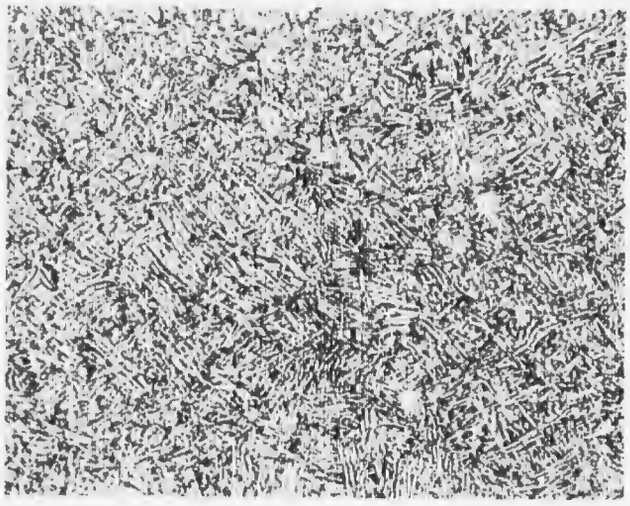

N

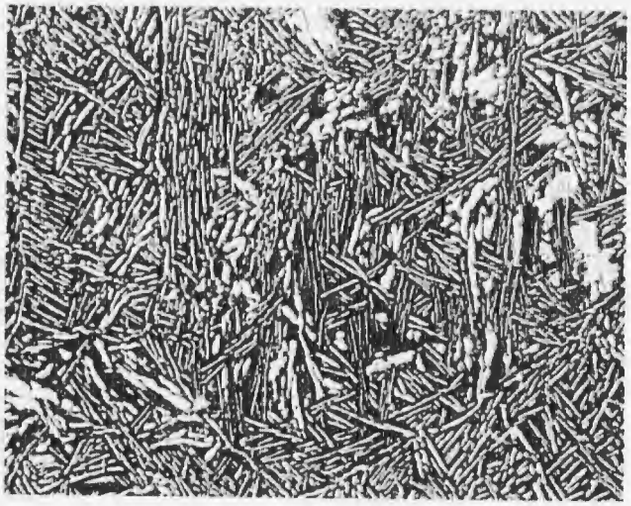

O

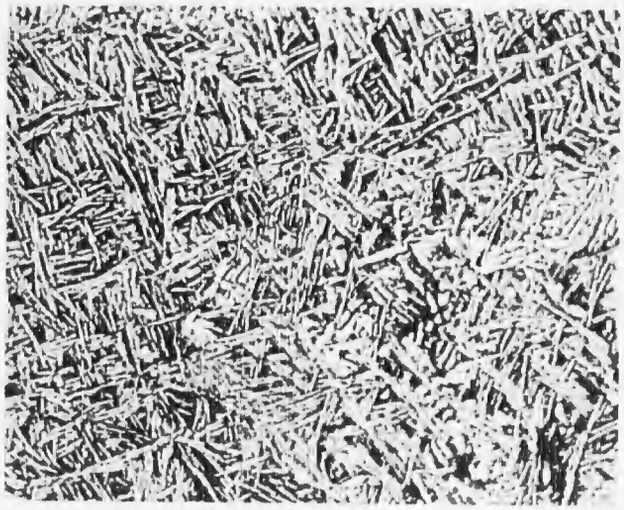

P

Final Structures Ti-6Al-6V-2Sn
Microstructural Study
See Figure 30 for Processing Details

Magnification: All 200X

Etchant: NaOH, H_2O_2

Negative 16526

Figure 50

Condition Q - 71% α; Condition R - 45% α.
Air cooling from the β field has produced this basket weave α morphology. Solution treatment (Condition R) has dissolved some α, and permitted some coarsening to take place without destroying the basket weave pattern.

Condition S - 67% α;
Since this material was water quenched from the β field, the basket weave morphology could not form and the alpha, in platelet form, is quite fine. As Table XIX indicates, the percentage of alpha was measured at 800X. This permitted determination of the percentage of α which would not be possible at the 200X magnification reproduced here. Cooling from the β field has produced some outlining of the prior β grains.

Figure 51 Comments

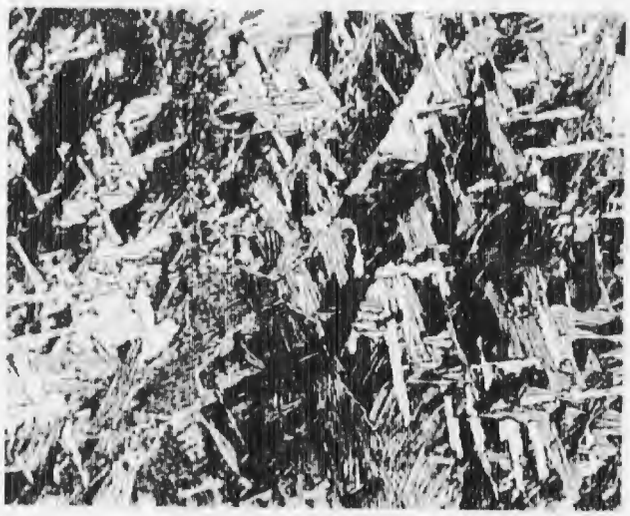

Q

R

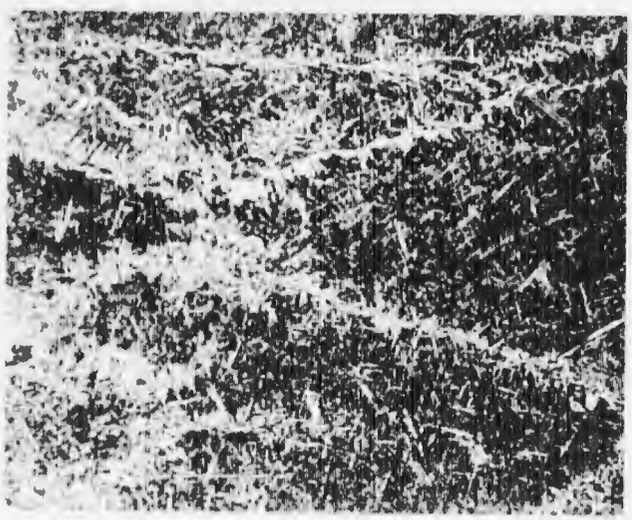

S

Final Structures Ti-6Al-6V-2Sn
Microstructural Study
See Figure 30 for Processing Details

Magnification: All 200X

Etchant: NaOH, H_2O_2

Negative 16527

Figure 51

Condition T - 41% α.
Slow cool from the beta field has produced this basket weave α morphology.

Condition U - 39% α.
Structure essentially similar to Condition R.

Figure 52 Comments

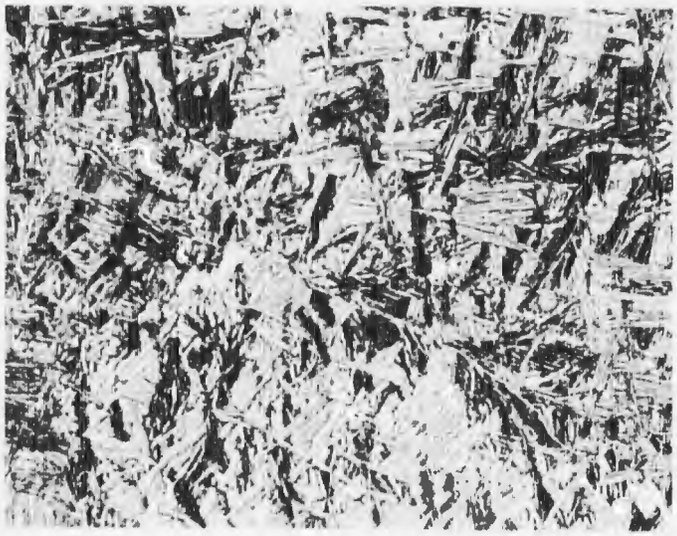

T

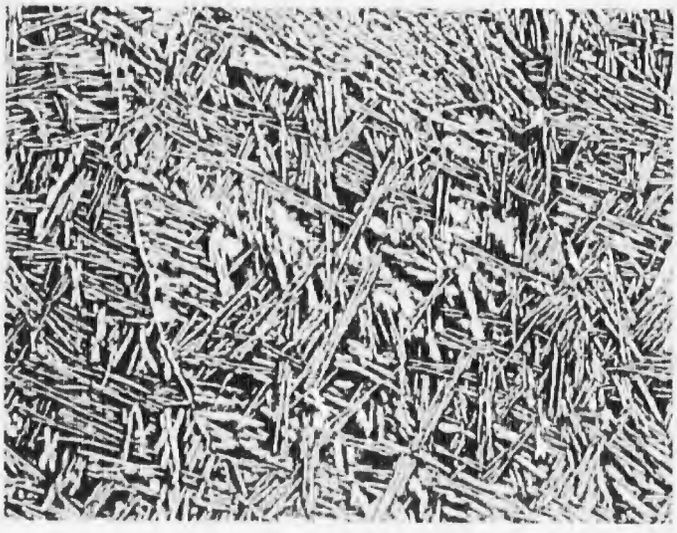

U

Final Structures Ti-6Al-6V-2Sn
Microstructural Study
See Figure 30 for Processing Details

Magnification: All 200X

Etchant: NaOH, H_2O_2

Negative 16528

Figure 52

Condition A - 11%, A-1 - 8%, and A-2 - 10% equiaxed alpha. Solution treatment has caused agglomeration of equiaxed α and coarsening of platelet α in Condition A.

Figure 53 Comments

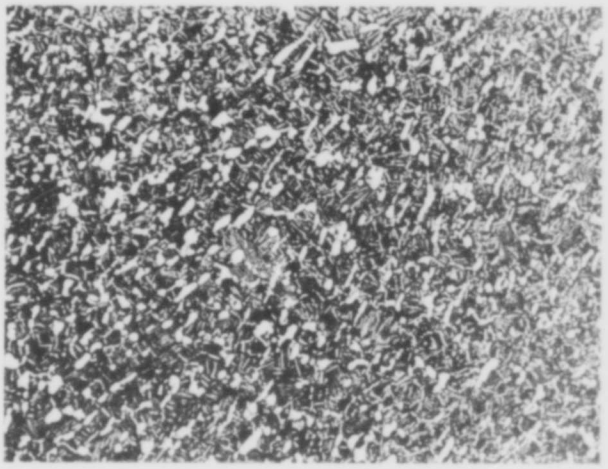

A

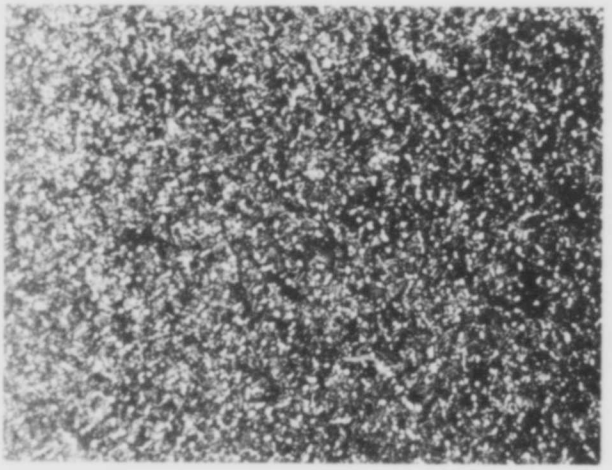

A-1

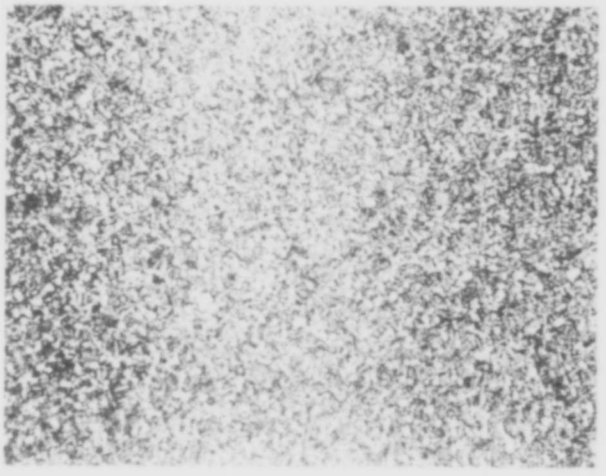

A-2

Final Structures Ti-6Al-2Sn-4Zr-6Mo
Microstructural Study
See Figure 31 for Processing Details

Magnification: All 200X

Etchant: NaOH, H_2O_2

Negative 16511

Figure 53

Condition B -
34% equiaxed α.

Condition B-1
32% equiaxed α.

Condition B-2
32% equiaxed α.

Figure 54 Comments

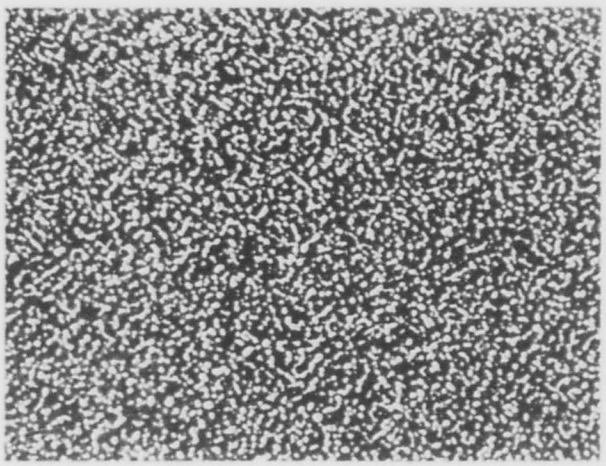

B

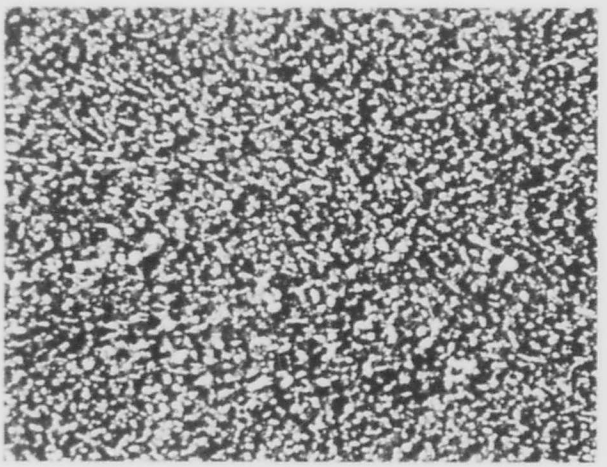

B-1

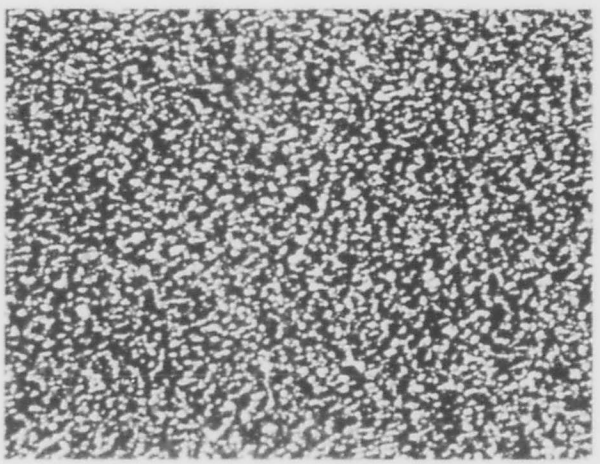

B-2

Final Structures Ti-6Al-2Sn-4Zr-6Mo
Microstructural Study
See Figure 31 for Processing Details

Magnification: All 200X Etchant: NaOH, H_2O_2

Negative 16512

Figure 54

Condition C - 49%, D - 21%, and E - 49% platelet alpha. Platelet alpha results from beta temperatures used in first forge operation.

Figure 55 Comments

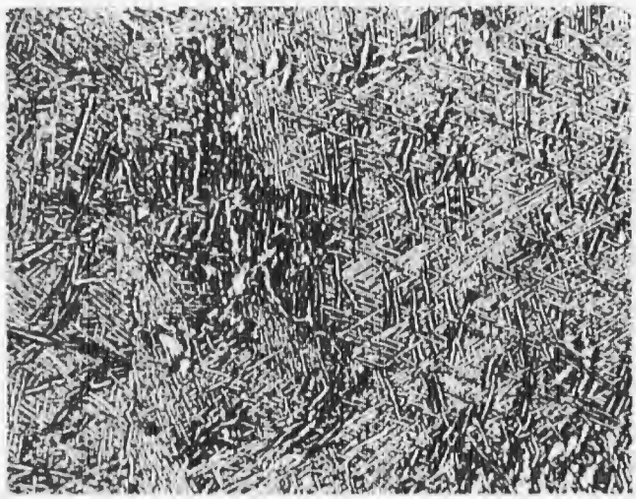

C

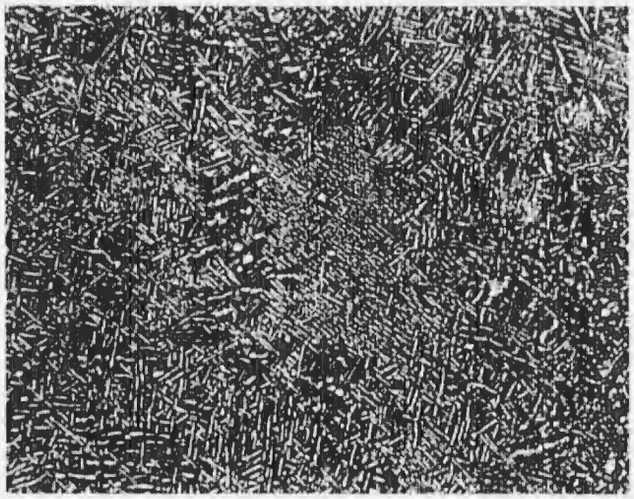

D

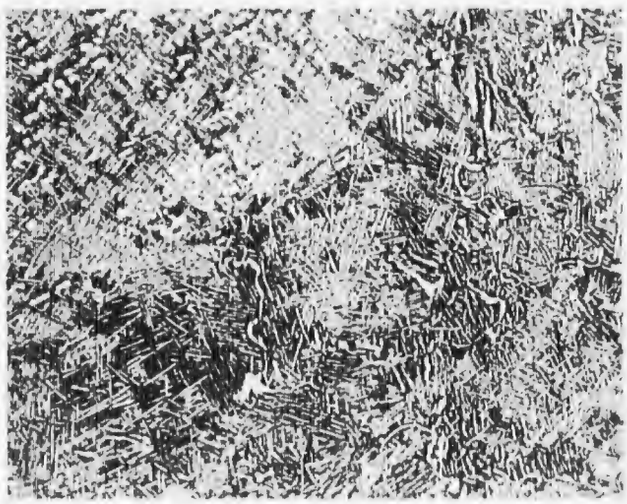

E

Final Structures Ti-6Al-2Sn-4Zr-6Mo
Microstructural Study
See Figure 31 for Processing Details

Magnification: All 200X Etchant: NaCH, H_2O_2

Negative 16513

Figure 55

Condition F - 51% and G - 47% platelet α.
Structure similar to C, D, and E.

Figure 56 Comments

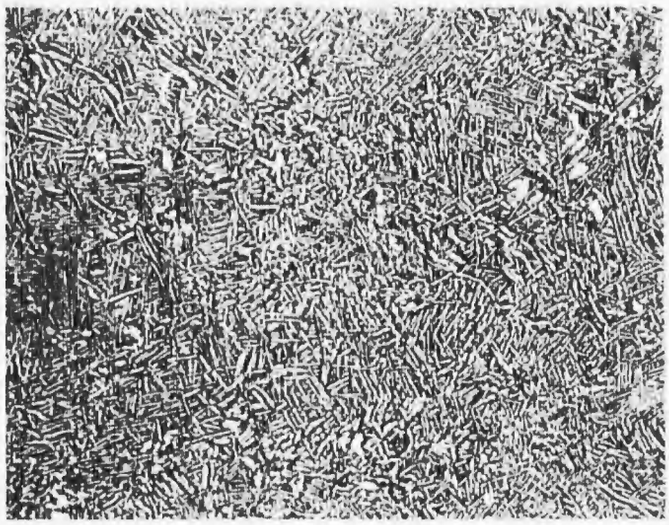

F

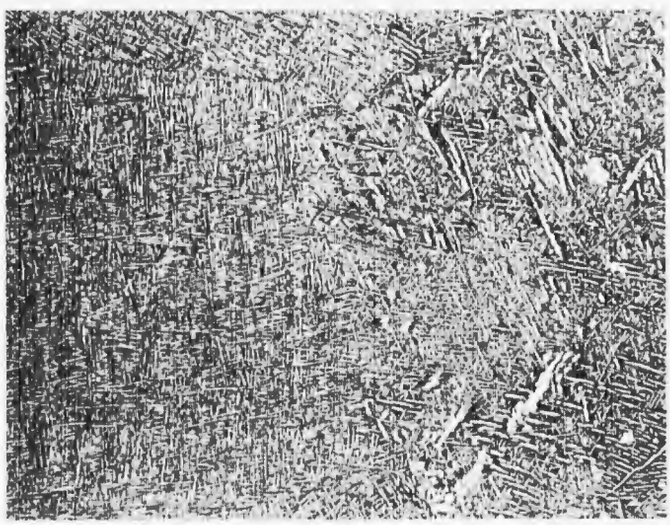

G

Final Structures Ti-6Al-2Sn-4Zr-6Mo
Microstructural Study
See Figure 31 for Processing Details

Magnification: All 200X Etchant: NaOH, H_2O_2

Negative 16514

Figure 56

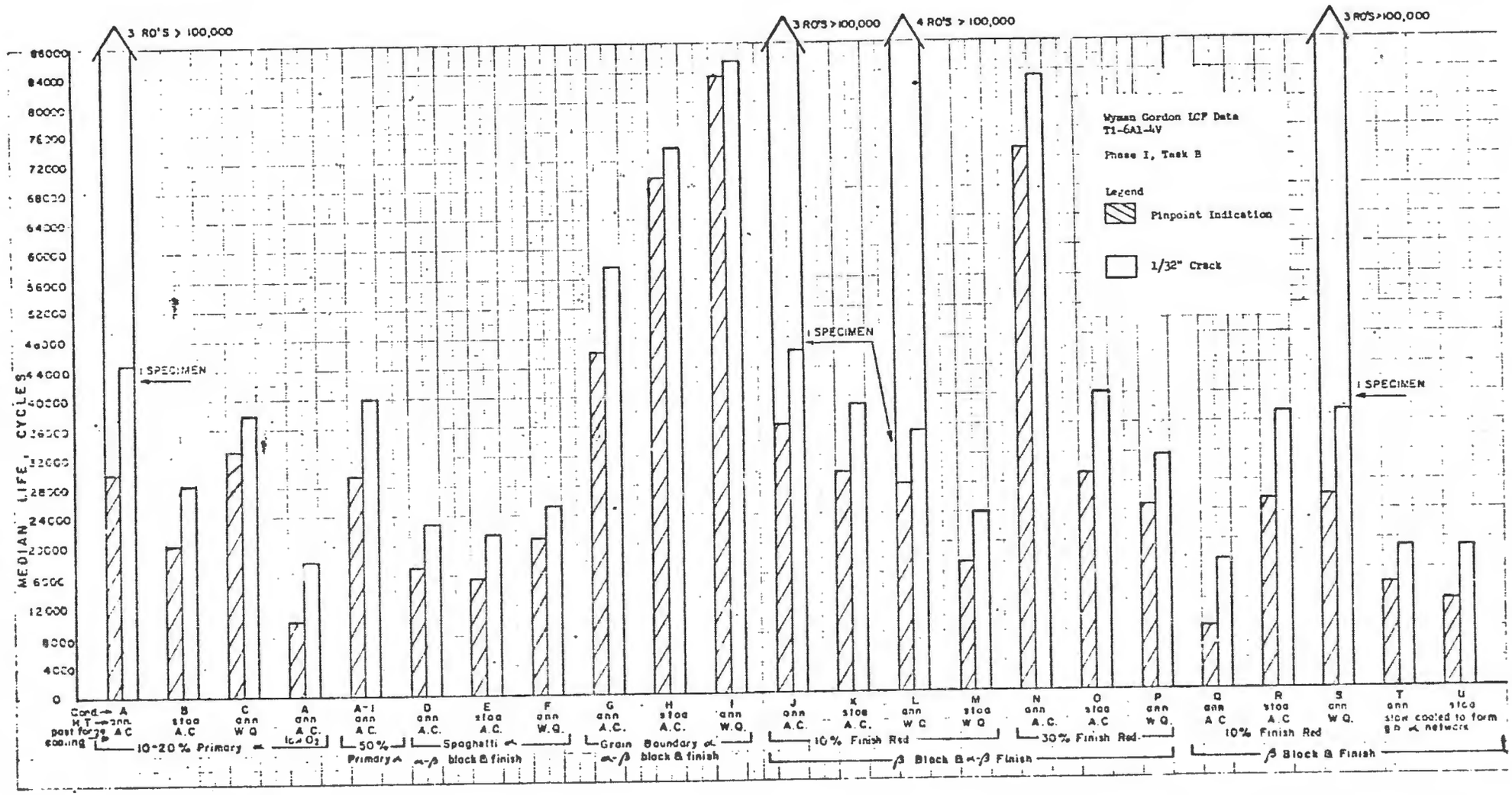

Figure 57

Low Cycle Fatigue Life versus Microstructure Ti-6Al-4V
(See Figure 30 for Processing Details)

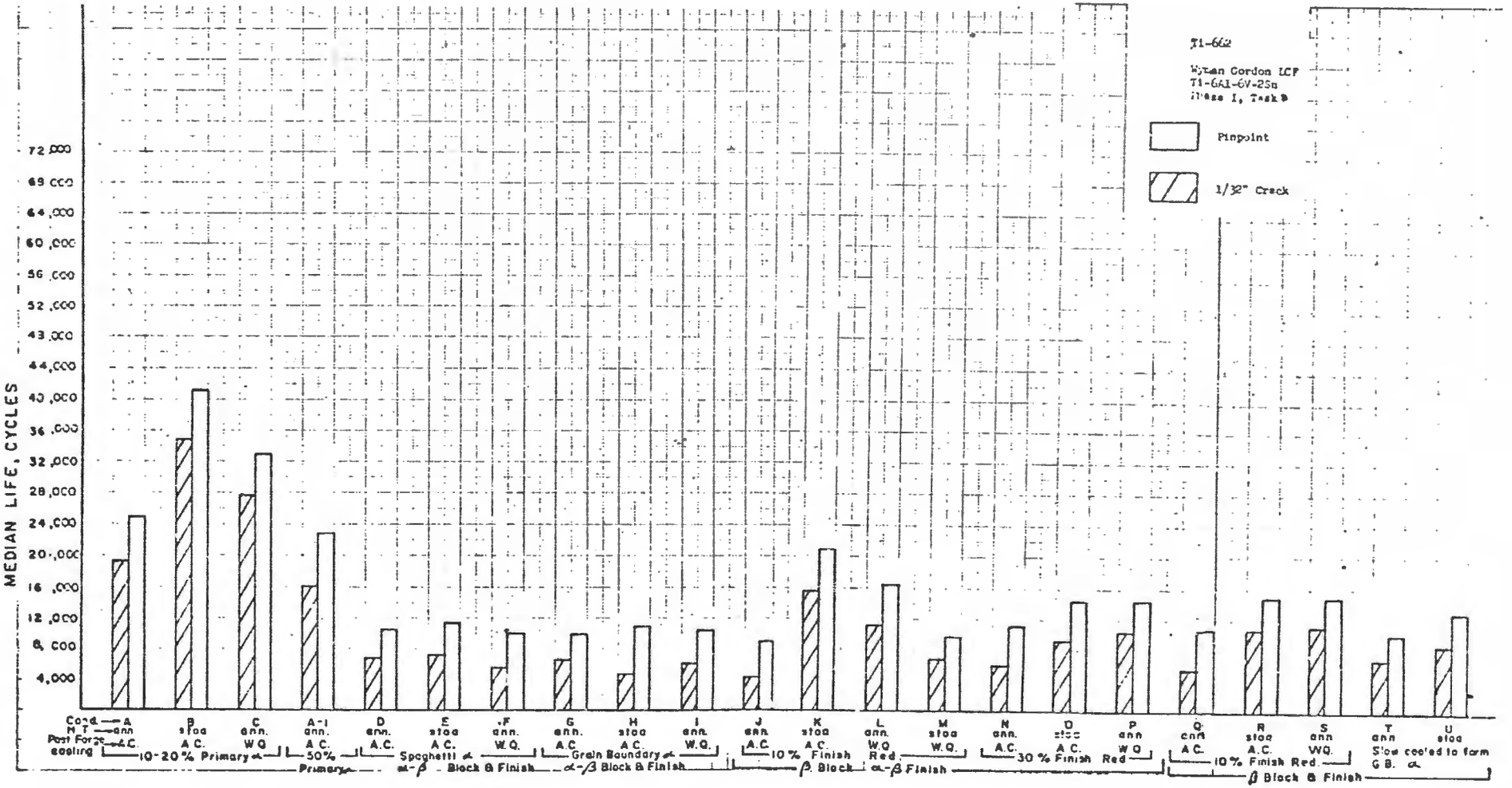

Figure 58
103

Low Cycle Fatigue Life versus Microstructure Ti-6Al-6V-2Sn
(See Figure 30 for Processing Details)

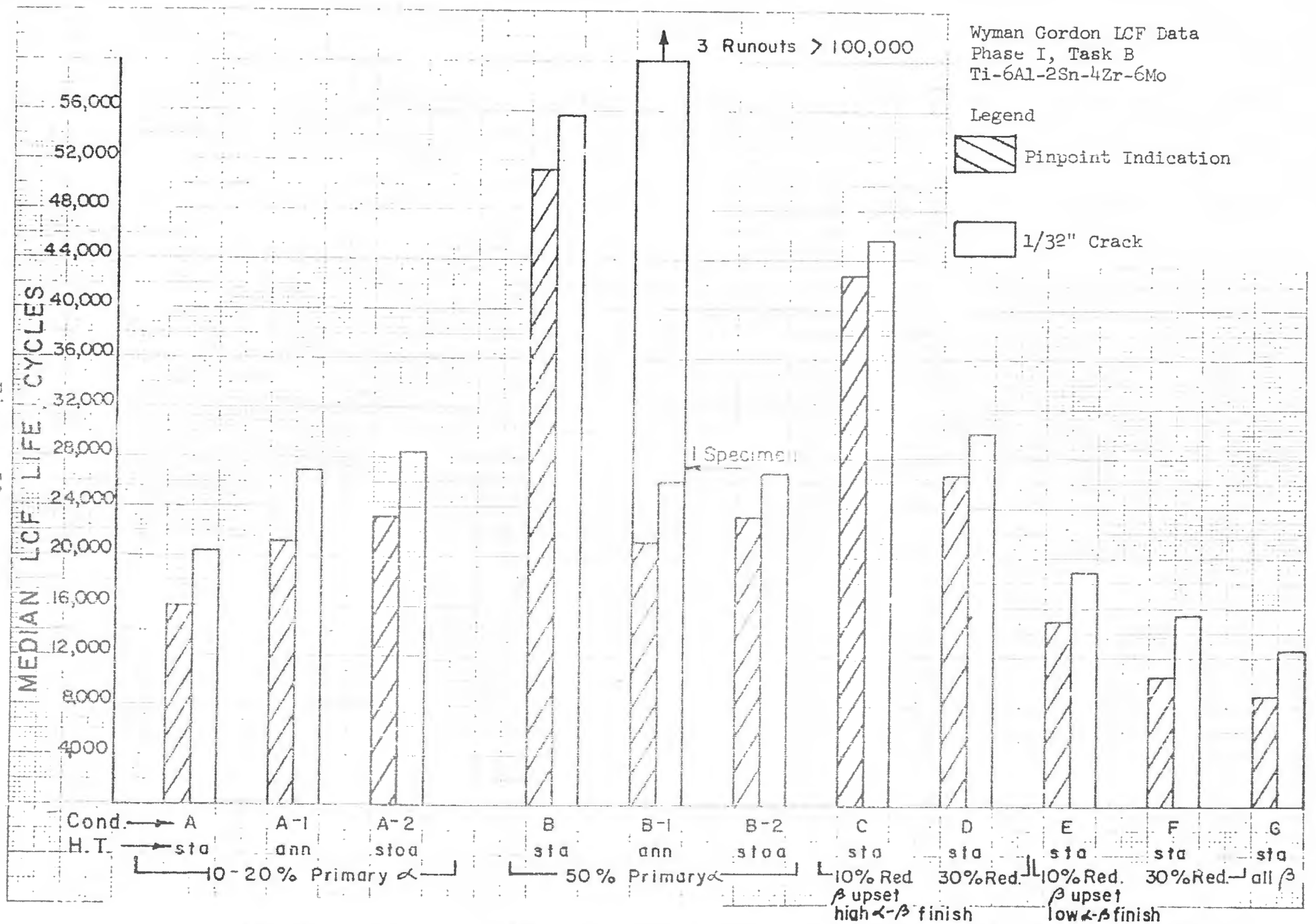

Figure 59
104

Low Cycle Fatigue Life versus Microstructure Ti-6Al-2Sn-4Zr-6Mo
(See Figure 31 for Processing Details)

6" Round Ti-6Al-4V Bar Cut to 6" Long Multiples
Cut Faces Shaped and Chemically Cleaned

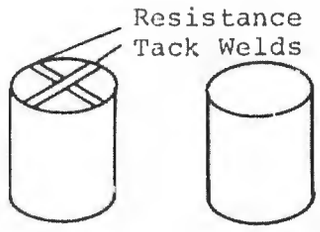

0.010" Thick x .250" Wide
Ti-8Al-1V-1Mo Foil Tacked to Billet

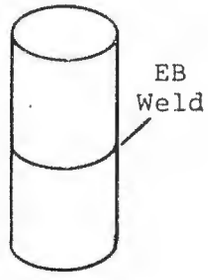

Multiples Joined by EB Welding
With 8-1-1 Foil at Interface

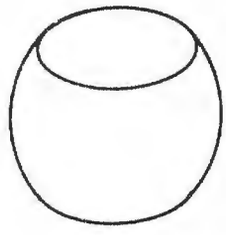

Welded Assembly Upset
from 12" to 6" Thick

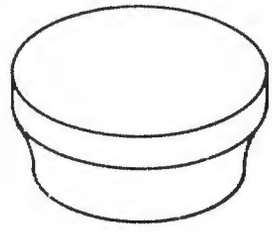

Upset Forged in Closed Dies to
Disc Configuration (3" Thick)

Schematic Diagram of Forge Bonding Method of Producing
Simulated Aluminum-Rich Stabilized Alpha Segregation

Negative 16355

Figure 60

Figure 61

Neg. 16310

Forge Bonded Ti-6Al-4V Disc Containing "Soft Alpha" Inclusion
Arrow Indicates Location of EB Weld Used to Seal Joint at Billet Stage
This is the Plane of the Segregate

Negative 16356

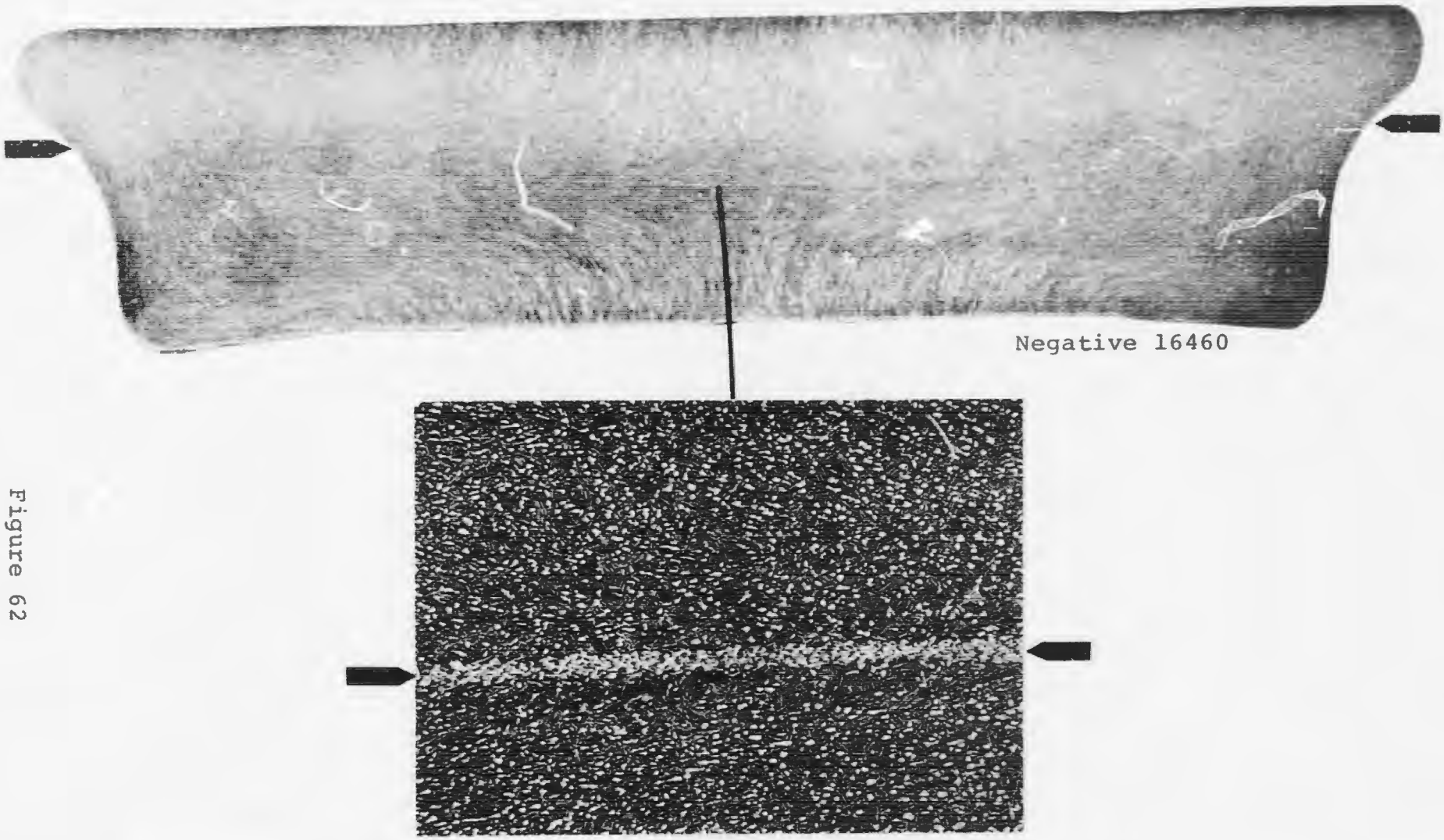

Negative 16460

Negative 16643

Macro Section and Microstructure (100X) of Compressor Disc Alpha-Beta Forged from Forge Bonded Ti-6Al-4V with Simulated "Soft Alpha" Inclusion (Light Etching Strip Indicated by Arrows)

Figure 62

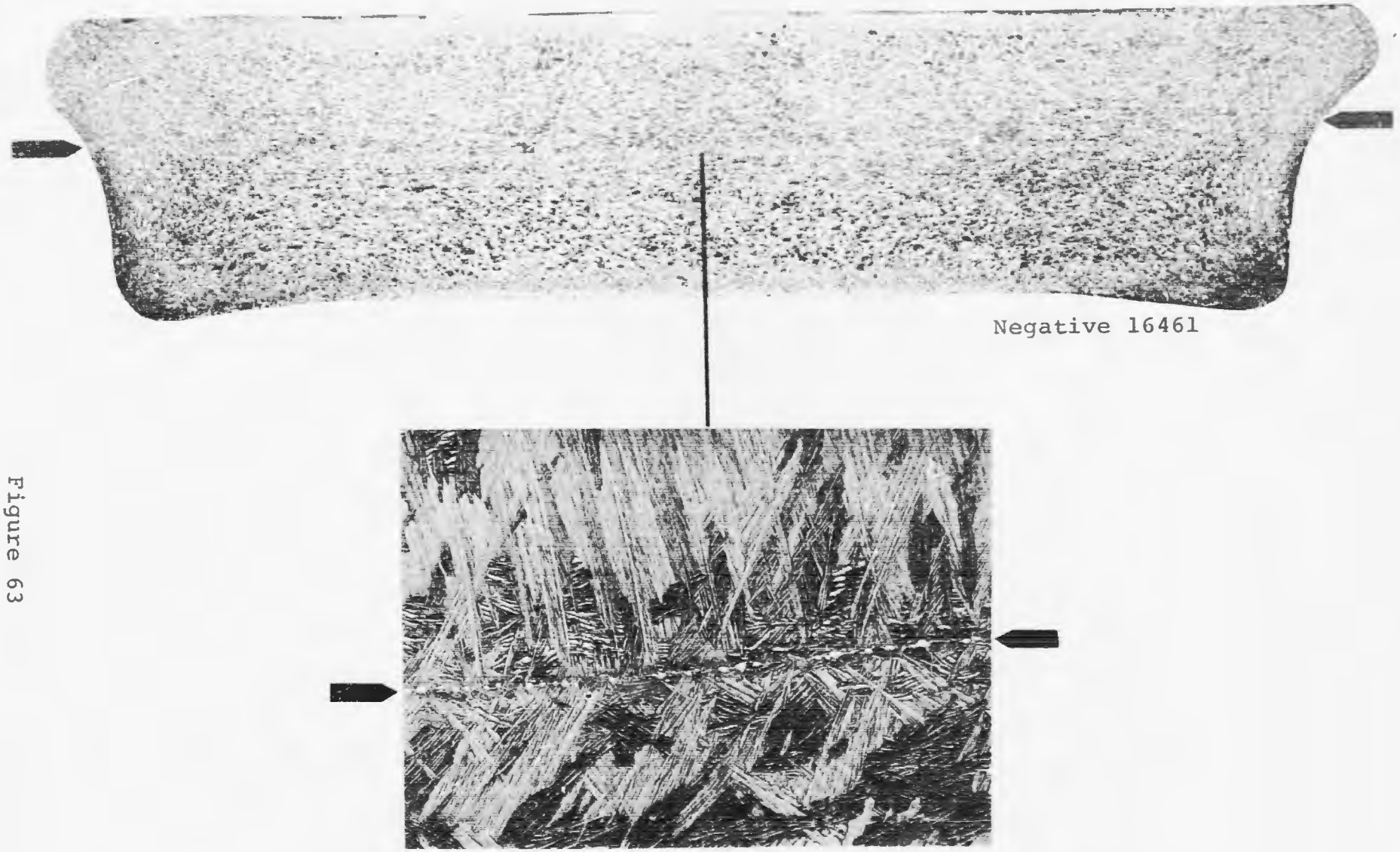

Negative 16461

Negative 16644

Figure 63

Macro Section and Microstructure (100X) of Compressor Disc Beta Forged from Forge Bonded Ti-6Al-4V with Simulated "Soft Alpha" Inclusion (Light Etching Strip Indicated by Arrows)

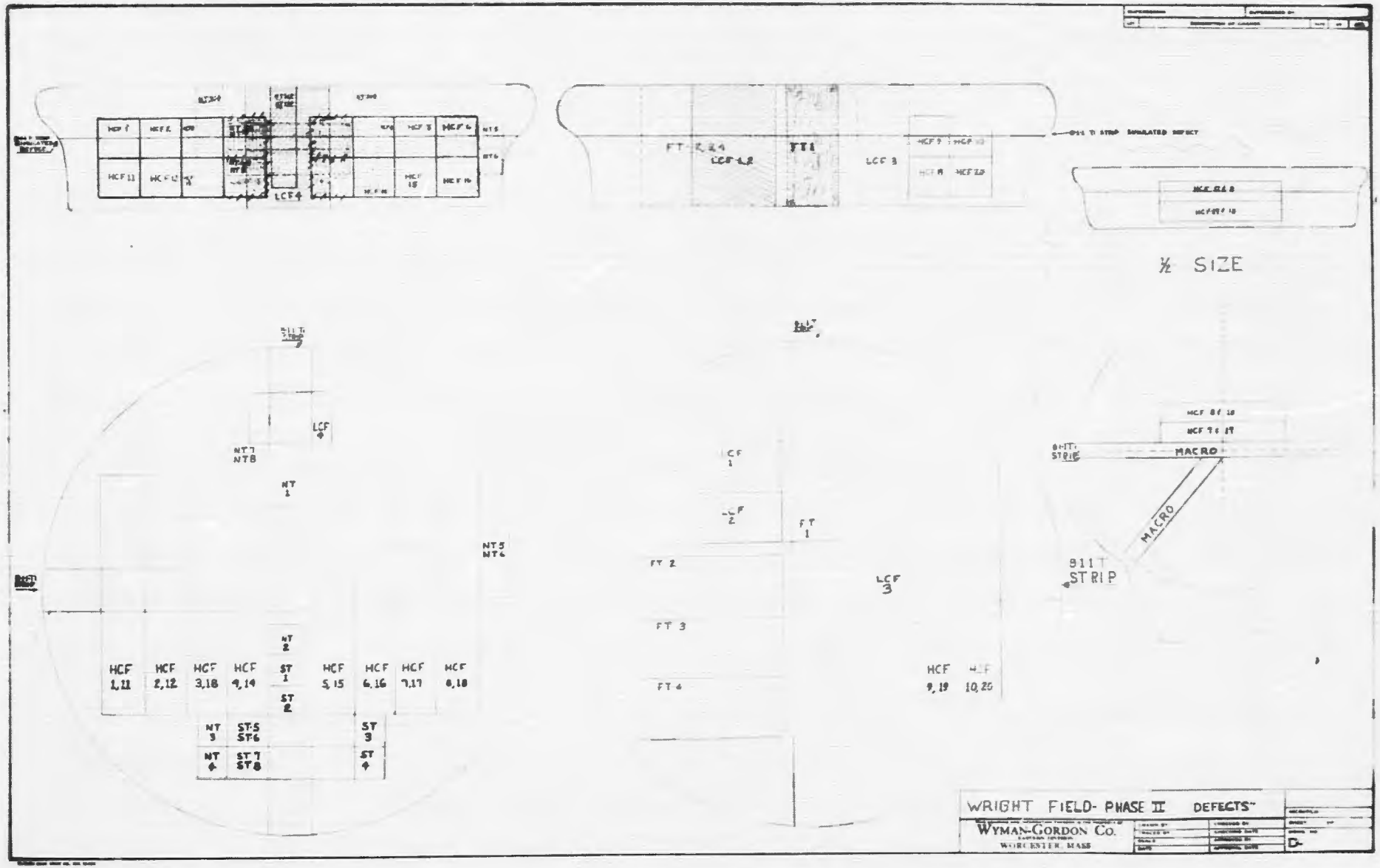

Figure 64

Sketch of Compressor Disc Forging Showing Location of Specimen for Phase II "Soft Alpha" Evaluation

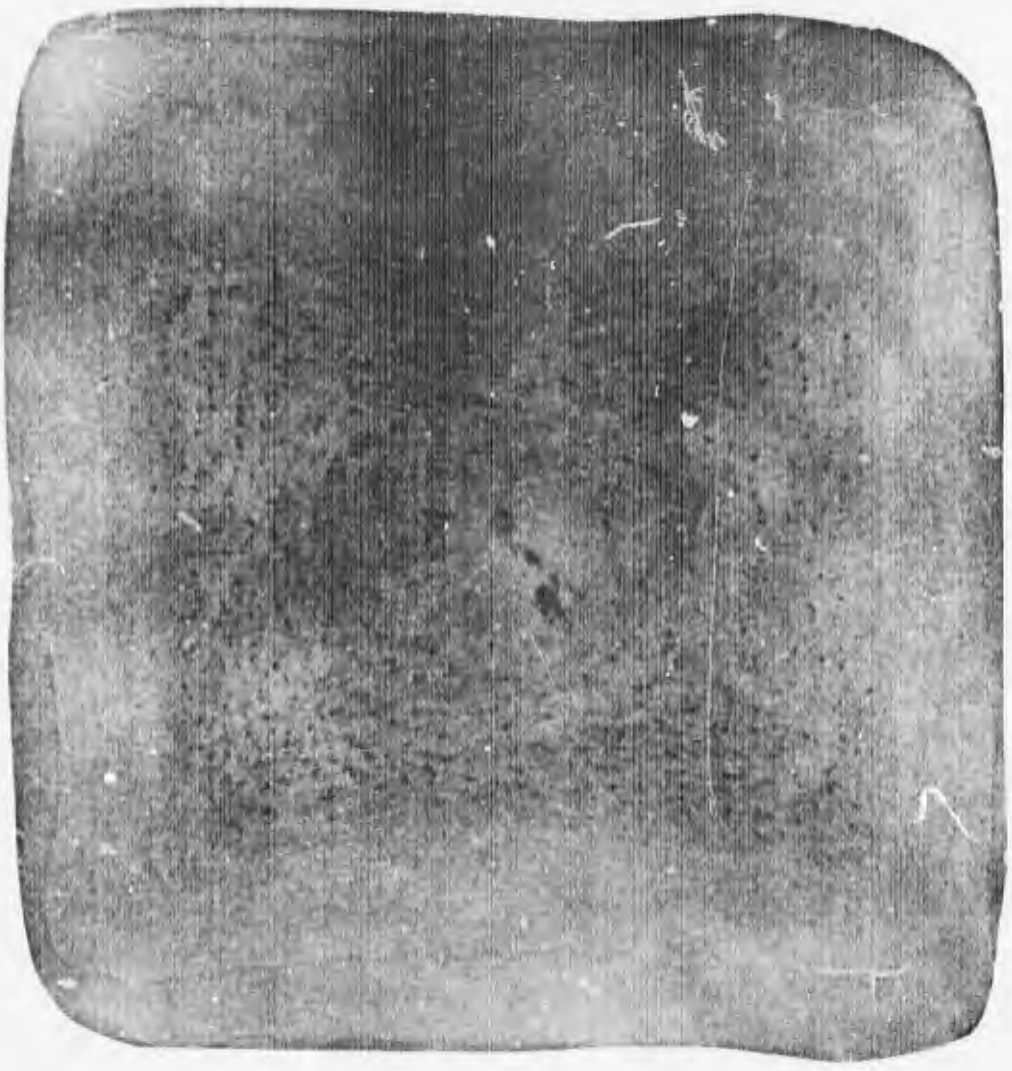

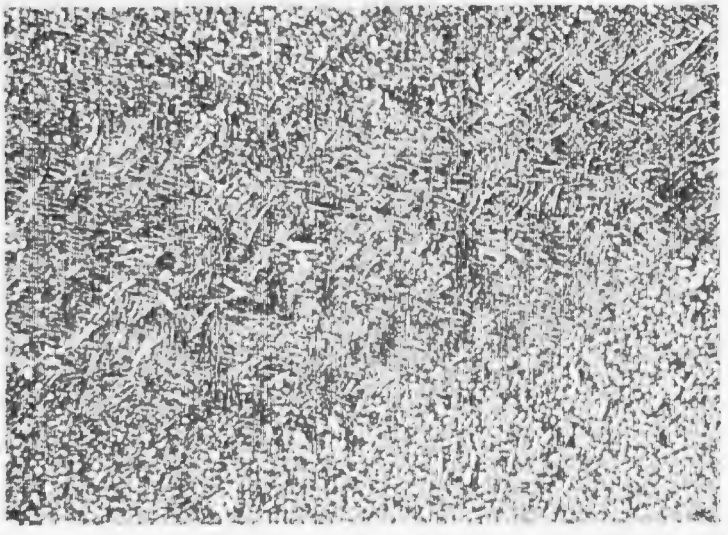

Negative 16154

Top - Macroetched Slice of As-Received Ti-6Al-6V-2Sn Billet Stock Used for "Beta Fleck" Investigation. Dark Etching Areas are "Beta Flecks".
1X

Bottom - Microstructure of As-Received Ti-6Al-6V-2Sn Billet Showing Typical "Beta Fleck" (Acicular Structure)
100X

Figure 5

Negative 16358

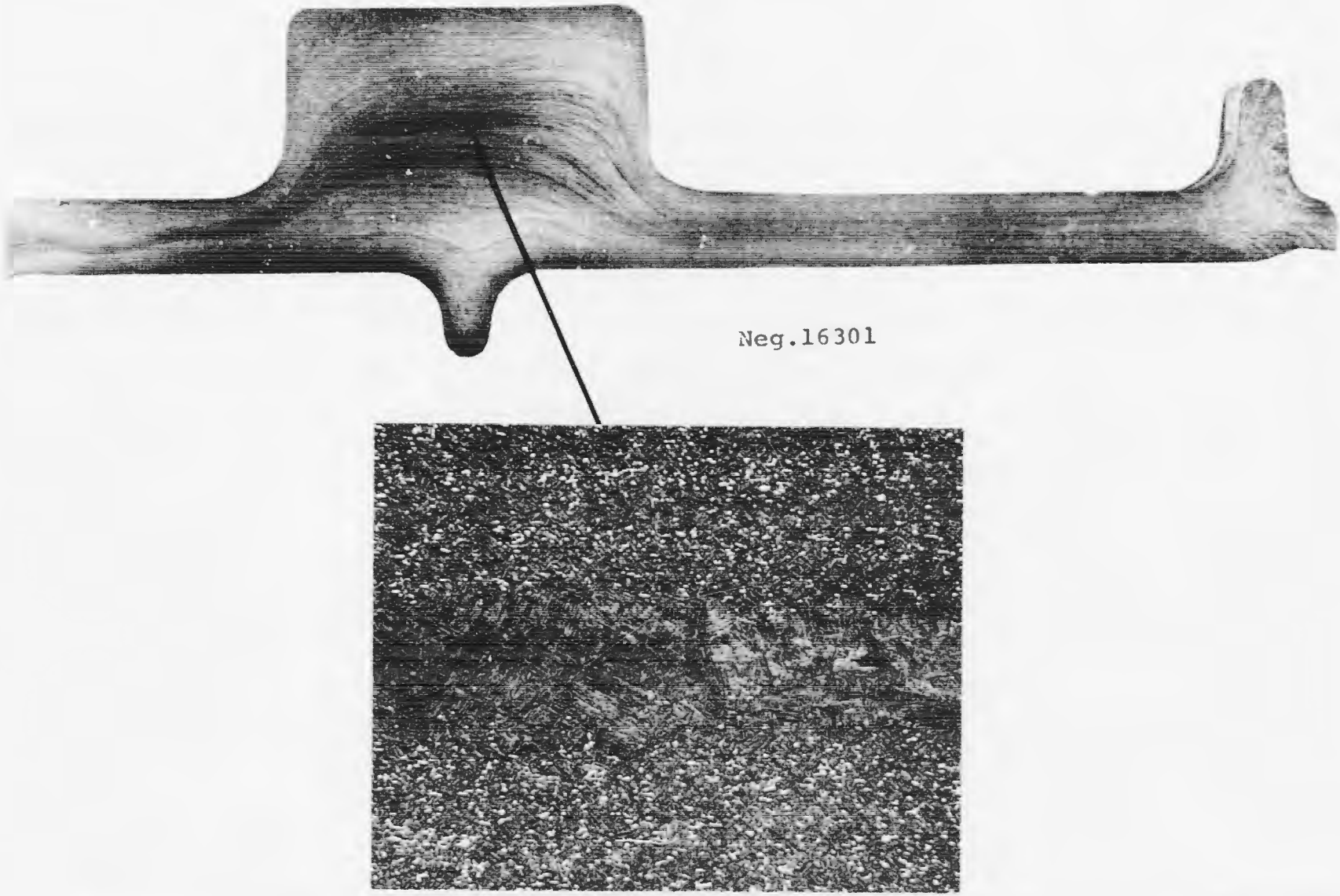

Neg.16301

Figure 66

Top - Macrosection Through Ti-6Al-6V-2Sn Structural Part Forged from Flecked Material at Transus -50°F. (Dark Etching Streaks are "Beta Flecks")

Bottom - Microstructure of Typical "Beta Fleck" After Forging at Transus -50°F. 100X

Negative 16359

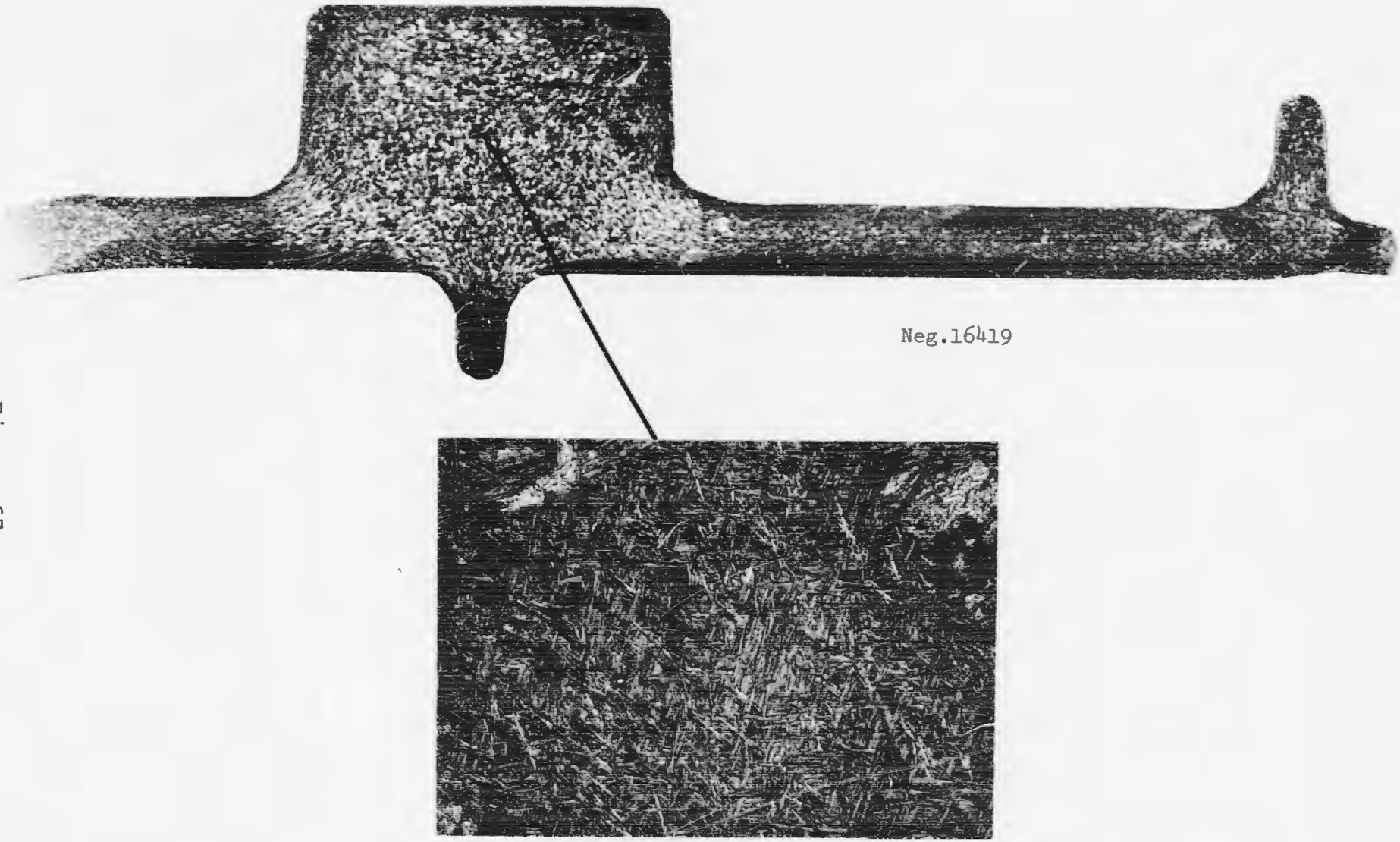

Neg.16419

Figure 67

Top - Macrosection Through Ti-6Al-6V-2Sn Structural Part Forged from Flecked Material at Transus+125°F

Bottom - Microstructure of Typical "Fleck" After Forging at Transus+125°F

100X

Negative 16646

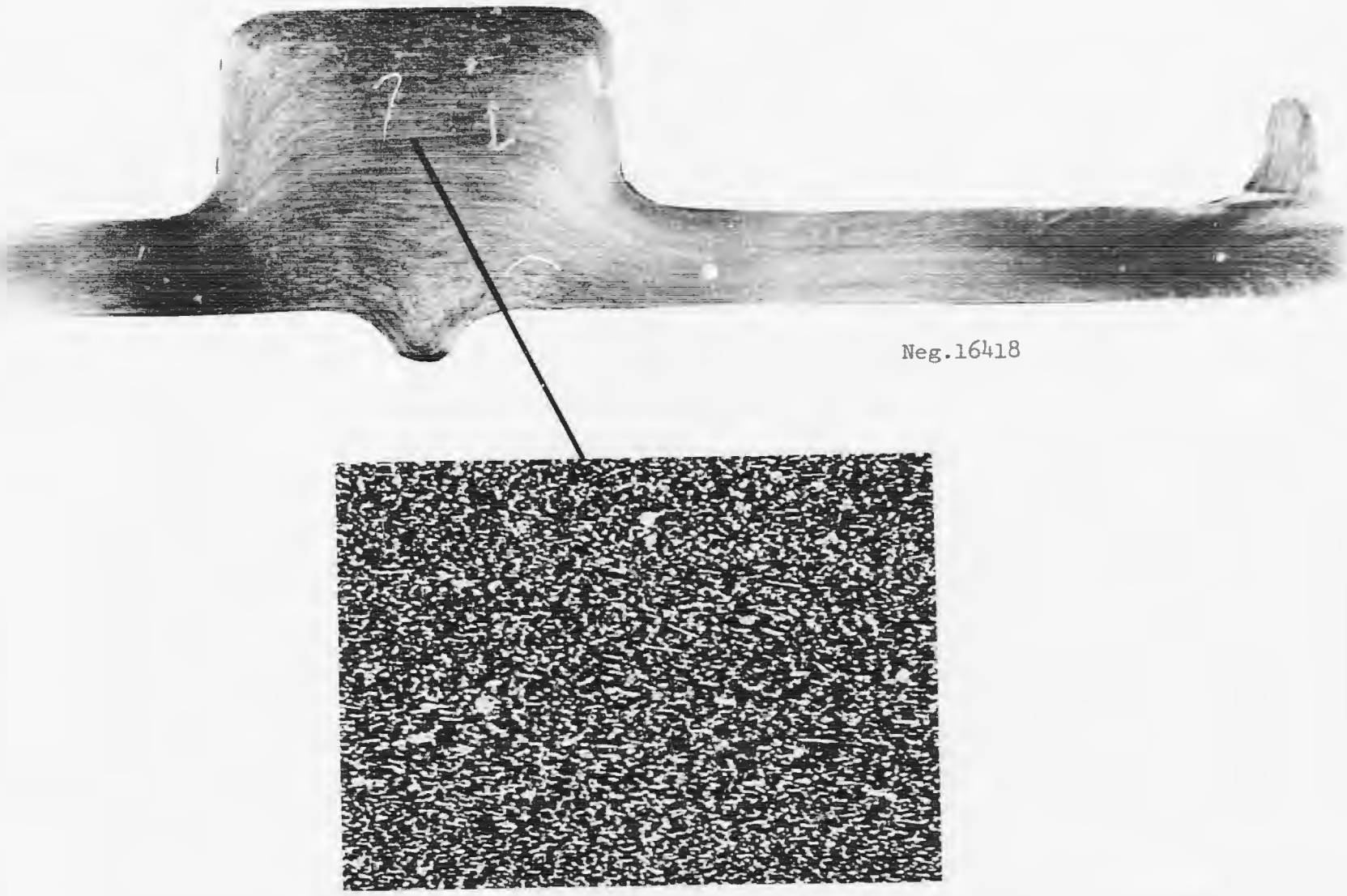

Neg.16418

Figure 68

Top - Macrosection Through Ti-6Al-6V-2Sn Structural Part Forged from Flecked Material at Transus-225°F

Bottom - Microstructure of Typical "Fleck" After Forging at Transus-225°F

100X

Negative 16645

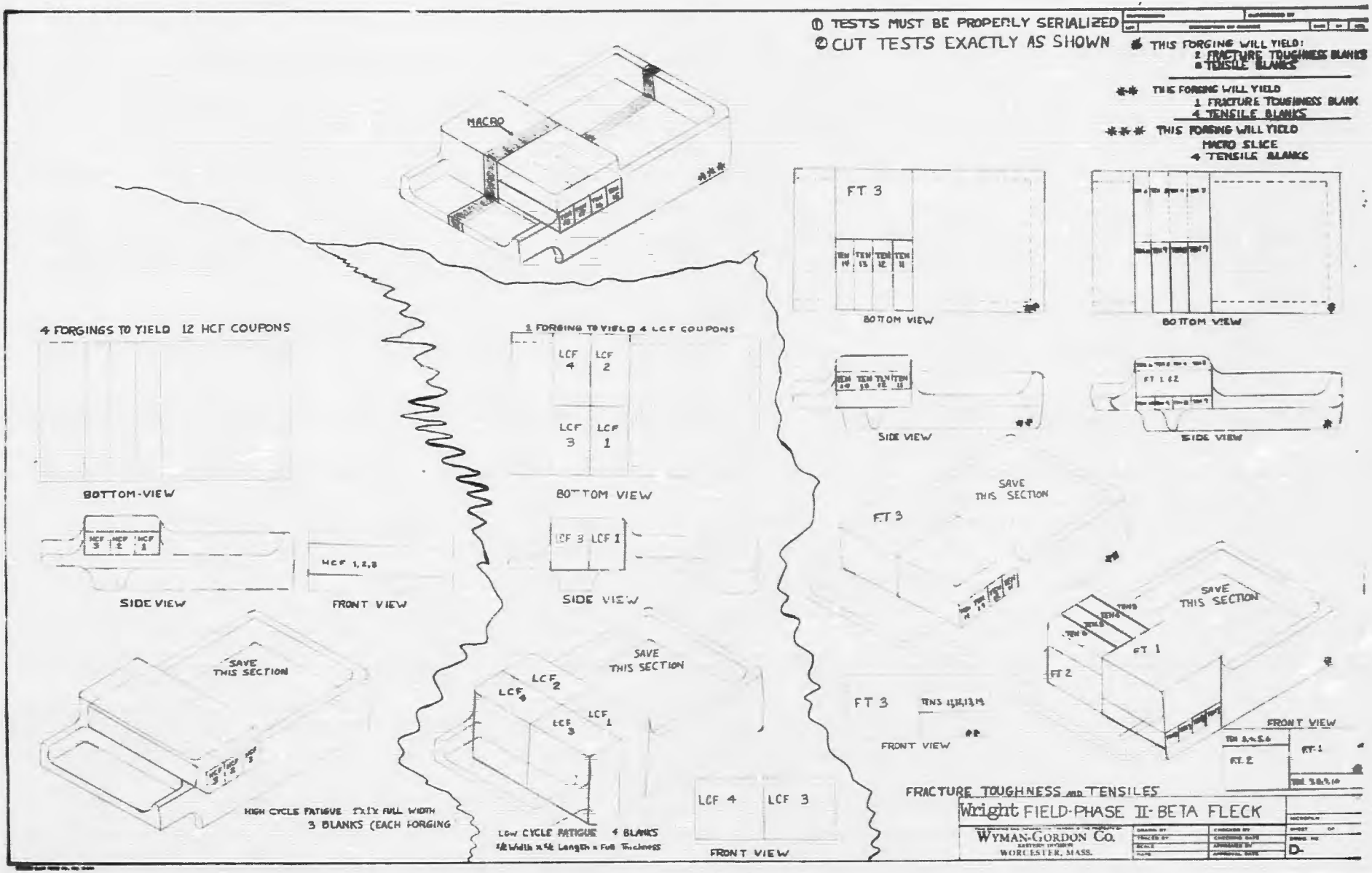

Sketch of Airframe Part Showing Location of Specimen
for Phase II "Beta Fleck" Evaluation

Table I

Starting Material for Titanium Forging Program

Item	Alloy	Size	Description
1	Ti-6Al-4V	14" Sq.	Coarse Grained (.15-.20 0_2)
2	Ti-6Al-4V	6" Sq.	Fine Grained (same heat as 1)
3	Ti-6Al-4V	6" Rd.	Fine Grained
4	Ti-6Al-4V	6" Rd.	Fine Grained (.12-.15% 0_2)
5	Ti-6Al-6V-2Sn	14" Sq.	Coarse Grained
6	Ti-6Al-6V-2Sn	6" Sq.	Fine Grained (same heat as 5)
7	Ti-6Al-6V-2Sn	6" Sq.	Flecked Fine Grained
8	Ti-6Al-2Sn-4Zr-6Mo	6" Rd	Fine Grained
9	Ti-6Al-2Sn-4Zr-6Mo	6" Rd.	Coarse Grained

Table II

Summary of Ultrasonic Test Results on Ti Billet Stock

Item	Size	Alloy	TMCA Inspection Method	TMCA Inspec. Level	TMCA Reports	W-G Inspection Method	W-G Inspec. Level	W-G Results	Comments
1	14" Sq.	Ti-6Al-4V	Contact per MIL-I-8950	#5 FBH	No Indication	Immersion per WG Stds.	#4 FBH	No Indication	
2	6" Sq.	Ti-6Al-4V	Contact per MIL-I-8950	#5 FBH	No Indication	Immersion per WG Stds.	#3 FBH	No Indication	
3	6" Rd.	Ti-6Al-4V	Immersion per PWA E-52	#2 FBH	No Indication See Comments	Immersion per PWA E-52	#2 FBH	No Indication See Comments	Both inspection sources report no defects and material okay to #3 FBH, but "noise" level of 90-120% of #2 FBH.
4	6" Rd.	Ti-6Al-4V	Immersion per PWA E-52	#2 FBH	No Indication See Comments	Immersion per PWA E-52	#3 FBH	No Indication	TMCA reports no indication okay to #3 FBH "noise" level 80-115% of #2 FBH.
5	14" Sq.	Ti-6Al-6V-2Sn	Contact per MIL-I-8950	#8 FBH	No Indication	Immersion per WG Stds.	#4 FBH	No Indication	
6	6" Sq.	Ti-6Al-6V-2Sn	Contact per MIL-I-8950	#5 FBH	No Indication	Immersion per WG Stds.	#3 FBH	No Indication	
7	6" Sq.	Ti-6Al-6V-2Sn	Contact per MIL-I-8950	#5 FBH	No Indication	Immersion per WG Stds.	#3 FBH	No Indication	
8	6" Rd.	Ti-6Al-2Sn-4Zr-6Mo	Immersion per PWA E-52	#3 FBH	No Indication See Comments	Immersion per WG Stds.	#3 FBH	No Indication	TMCA reports "noise" level of 70-115% of #3. Wyman-Gordon reports okay to #3 FBH but noise level of 120-180% of #2 FBH when inspected to #2.
9	6" Rd.	Ti-6Al-2Sn-4Zr-6Mo	Immersion per PWA E-52	#3 FBH	No Indication	Immersion per WG Stds.	#3 FBH	No Indications	

TABLE III

CHEMICAL COMPOSITION OF BILLET STOCK

Item No.	Heat Number	Analysis Source	Al	V	Sn	Zr	Mo	O_2	N_2	H_2	C	Fe	Cu	Ti
1	TMCA K9240	TMCA	6.0	4.2				.19	.010	.004	.022	.17		Bal.
		W-G	6.6	4.2				.15	.012	.003	.018	.20		"
2	TMCA K9240	TMCA	6.0	4.2				.19	.010	.007	.022	.27		"
		W-G	6.5	4.1				.19	.012	.006	.010	.16		"
3	TMCA K8623	TMCA	6.4	4.2				.20	.010	.007	.026	.20		"
		W-G	6.2	4.2				.18	.009	.006	.020	.18		"
4	TMCA K8738	TMCA	6.0	4.0				.13	.008	.010	.026	.12		"
		W-G	6.3	3.9				.13	.013	.007	.030	.14		"
5	TMCA K9200	TMCA	5.5	5.5	2.3			.19	.016	.002	.022	.66	.60	"
		W-G	5.5	5.4	2.0			.17	.020	.003	.026	.51	.50	"
6	TMCA K9200	TMCA	5.5	5.5	2.3			.19	.016	.004	.022	.66	.60	"
		W-G	5.6	5.6	1.8			.18	.015	.007	.029	.53	.51	"
7	TMCA K8583	TMCA	5.5	5.2	2.2			.18	.015	.006	.022	.67	.53	"
		W-G	5.5	5.6	1.8			.15	.011	.007	.022	.73	.87	"
8	TMCA K9056	TMCA	6.0		2.1	4.1	5.8	.12	.010	.005	.026	.08		"
		W-G	5.7		2.0	4.1	6.3	.12	.009	.004	.002	.08		"
9	TMCA K7478	TMCA	5.9		2.0	4.1	5.8	.11	.009	.010	.026	.11		"
		W-G	5.8		1.9	3.6	6.0	.09	.006	.009	.016	.10		"

Table IV

Beta Transus for Program Materials

(Determined Metallographically at Wyman-Gordon)

Item	Alloy	Beta Transus
1	Ti-6Al-4V	1825°F
2	Ti-6Al-4V	1830°F
3	Ti-6Al-4V	1835°F
4	Ti-6Al-4V	1800°F
5	Ti-6Al-6V-2Sn	1725°F
6	Ti-6Al-6V-2Sn	1735°F
7	Ti-6Al-6V-2Sn	1725°F
8	Ti-6Al-2Sn-4Zr-6Mo	1750°F
9	Ti-6Al-2Sn-4Zr-6Mo	1935°F

TABLE V

BILLET GRAIN SIZE - MACROSTRUCTURE STUDY

Alloy	Condition	Location	ASTM Macro Size	Average Size, in.	Area, in^2	ASTM Micro G.S.
6-4	Coarse	O.D.	M 2.5	1 x .35	.35	
		Center	M 4	.3 x .4	.12	
	Inter.	General	M 9.5	.05 x .05	.0025	
	Fine	General	M 13.0	.014 x .014	.0002	0
6-6-2	Coarse	General	M 6	.18 x .18	.031	
	Fine	General	M 13.5	.012 x .012	.00014	.5
6-2-4-6	Coarse	General	M 8.5	.07 x .07	.005	
	Fine	General	M 14	.01 x .01	.0001	.1

TABLE VI

FORGING TEMPERATURES USED FOR PHASE I, TASK A
(MACROSTRUCTURE EVALUATION)

Alloy	Preform Temperature (°F)	Block Temperature (°F)	Finish Temperature (°F)
Ti-6Al-4V	1775	1775	1775
Ti-6Al-6V-2Sn	1675	1675	1675
Ti-6Al-2Sn-4Zr-6Mo		1675	1675

TABLE VII

HEAT TREATMENTS USED FOR PHASE I, TASK A
(MACROSTRUCTURE EVALUATION)

Alloy	Heat Treatment
Ti-6Al-4V	1300°F (2) Air Cool
Ti-6Al-6V-2Sn	1350°F (2) Air Cool
Ti-6Al-2Sn-4Zr-6Mo	1625°F (2) Air Cool + 1100°F (8) Air Cool

TABLE VIII

PHASE I, TASK A
TITANIUM MACROSTRUCTURE STUDY MECHANICAL PROPERTY TEST PROGRAM

	Alloy	Macrostructure	Forging	Type of Test	No. of Specimens
A.	Ti-6Al-4V	Coarse Grained	Structural	70°F Smooth Tensile	10
				70°F Notched Tensile	10
				Low Cycle Fatigue	5
				High Cycle Fatigue, Smooth	20
				High Cycle Fatigue, Notched	10
				Fracture Toughness	5
B.		Intermediate Grain	Structural	Same as A	Same as A
C.		Fine Grained	Structural	Same as A	Same as A
D.	Ti-6Al-6V-2Sn	Coarse Grained	Structural	Same as A	Same as A
E.		Fine Grained	Structural	Same as A	Same as A
F.	Ti-6Al-2Sn-4Zr-6Mo	Fine Grained	Compressor Disc	70°F Smooth Tensile	10
				70°F Notched Tensile	10
				Low Cycle Fatigue	6
				High Cycle Fatigue, Smooth	10
				High Cycle Fatigue, Notched	10
				Fracture Toughness	3
G.		Coarse Grained	Compressor Disc	Same as F	Same as F

TABLE IX

TENSILE PROPERTY SUMMARY
PHASE I, TASK A
MACROSTRUCTURE STUDY

Alloy	Macrostructure	0.2% Yield Strength				Ultimate Tensile Strength				Elongation				Reduction of Area			
		Min.	Max.	Mean	Std. Dev.	Min.	Max.	Mean	Std. Dev.	Min.	Max.	Mean	Std. Dev.	Min.	Max.	Mean	Std. Dev.
6-4	Coarse Grained	134.0	144.0	139.3	3.54	146.0	156.0	150.9	3.07	13.0	15.0	14.1	.91	35.7	43.7	39.3	3.12
6-4	Intermediate Grained	134.8	147.8	140.3	4.64	146.8	159.0	151.9	4.20	11.0	15.0	14.0	1.20	28.6	42.5	38.4	3.95
6-4	Fine Grained	130.4	146.0	138.2	4.62	143.4	156.0	150.2	3.38	13.5	15.0	14.4	.58	36.3	42.5	39.6	2.10
6-6-2	Coarse Grained	136.0	150.0	142.9	4.95	150.0	164.0	156.5	4.84	10.0	15.0	13.9	1.66	34.4	52.2	43.6	6.58
6-6-2	Fine Grained	142.0	159.4	148.0	6.08	153.8	170.4	159.9	5.73	15.0	17.0	16.3	.67	46.1	49.0	47.7	1.12
6-2-4-6	Coarse Grained	157.2	168.2	163.2	2.98	169.0	178.2	175.2	2.56	7.5	12.5	10.4	1.97	19.6	35.7	27.4	5.65
6-2-4-6	Fine Grained	165.0	174.5	166.5	6.66	169.0	186.0	178.4	5.94	10.0	15.0	13.1	1.74	23.4	42.8	34.1	8.87

TABLE X

MACROSTRUCTURE PROGRAM NOTCHED (K_t = 3.9) TENSILE TEST DATA

Alloy	Grain Size	NTS			$\frac{NTS}{UTS}$		
		Min.	Max.	Ave.	Min.	Max.	Ave.
6-4	Coarse	226	231	228.4	1.50	1.58	1.53
	Fine	221	239	228.5	1.47	1.58	1.51
	Inter.	225	235	229.6	1.42	1.60	1.50
6-6-2	Coarse	231	239	236.4	1.51	1.57	1.53
	Fine	224	242	232.2	1.42	1.61	1.52
6-2-4-6	Coarse	229	255	242.6	1.30	1.43	1.38
	Fine	221	258	237.3	1.22	1.44	1.32

TABLE XI

MACROSTRUCTURE STUDY - FATIGUE STRENGTH AT INDICATED CYCLES

Alloy	Condition	Fatigue Strength (KSI) Number of Cycles — Smooth Bar 10^4	10^5	10^6	10^7	Notched Bar ($K_t = 3.0$) 10^4	10^5	10^6	10^7
Ti-6Al-4V	Coarse Grained	120	95	77	59	72	40	30	26
	Intermediate Grain	108	89	82	80	66	46	42	40
	Fine Grain	126	98	82	70	62	41	34	30
Ti-6Al-6V-2Sn	Coarse Grain	117	103	89	75	67	44	35	33
	Fine Grain	115	93	86	74	65	45	37	33
Ti-6Al-2Sn-4Zr-6Mo	Coarse Grain	117	96	92	88	66	42	39	38
	Fine Grain	119	93	83	81	66	45	38	36

TABLE XII

FRACTURE TOUGHNESS DATA - MACROSTRUCTURE STUDY

Serial Number	Alloy	Condition	K_{Ic} (KSI $\sqrt{in.}$)	Average K_{IC}
1- 7-1	Ti-6Al-4V	Coarse Grained	56.7	
1- 7-2			55.3	
1- 8-1			52.2	53.9
1- 9-1			52.1	
1- 9-2			53.2	
2- 7-1	Ti-6Al-4V	Fine Grained	64.0	
2- 7-2			69.1	
2- 8-1			67.6	
2- 8-2			59.6	67.8
2- 9-1			80.6	
2- 9-2			76.1	
1-A7-1	Ti-6Al-4V	Intermediate Grain Size	55.2	
1-A7-2			62.8	
1-A8-1			52.4	57.5
1-A8-2			58.2	
1-A9-1			58.8	
5- 7-1	Ti-6Al-6V-2Sn	Coarse Grained	65.0	
5- 7-2			73.2	
5- 8-1			65.0	
5- 8-2			75.6	70.1
5- 9-1			62.8	
5- 9-2			78.8	
6- 7-1	Ti-6Al-6V-2Sn	Fine Grained	50.3	
6- 7-2			53.8	
6- 8-1			54.4	
6- 8-2			54.6	54.0
6- 9-1			54.4	
6- 9-2			56.6	
8- 1-1	Ti-6Al-2Sn-4Zr-6Mo	Fine Grained	31.2	
8- 1-2			30.2	30.2
8- 1-3			29.2	
	Ti-6Al-2Sn-4Zr-6Mo	Coarse Grained	32.7	
			32.4	32.2
			31.6	

TABLE XIII

MEDIAN LOW CYCLE FATIGUE LIVES FOR ALL ALLOYS WITH VARIOUS BILLET GRAIN SIZE[1]

PHASE I, TASK A

Condition	Grain Size	Cycles to Pinpoint x 10^{-3}	Cycles to 1/32" Crack x 10^{-3}	Remarks
		Ti-6Al-4V		
A	Coarse	12.5	16.0	
A	Inter-mediate	30.0	50.0	
A	Fine	15.0	23.0	Banded microstructure
		Ti-6Al-6V-2Sn		
A	Coarse	10.0	13.5	
A	Fine	13.0	17.0	
		Ti-6Al-2Sn-4Zr-6Mo		
A	Coarse	47.5	55.0	
A	Fine	32.0	35.0	

[1] B_{50} Life per Weibull Analysis

TABLE XIV

MACROSTRUCTURE STUDY

MECHANICAL PROPERTY RATING

Alloy	Macro Grain Size	Billet Average Grain Size in^2	Forge Procedure	Heat Treatment	Notched HCF	LCF	Fracture Toughness	UTS	Red. of Area	NTS UTS	Total
Ti-6Al-4V	Coarse	Center .12" O.D. 35"	α + β	Ann.	1	1	2	3	3	3	13
	Medium	.0025"	α + β	Ann.	3	2	2	3	3	3	16
	Fine	.0002"	α + β	Ann.	2	2	3	3	3	3	16
Ti-6Al-6V-2Sn	Coarse	.031	α + β	Ann.	2	1	3	3	4	3	16
	Fine	.00014"	α + β	Ann.	2	1	2	3	4	3	15
Ti-6Al-2Sn-4Zr-6Mo	Coarse	.005"	α + β	STA	3	3	1	4	2	1	14
	Fine	.0001"	α + β	STA	3	2	1	4	3	1	14

TABLE XV

FORGING TEMPERATURES USED FOR PHASE I, TASK B
(MICROSTRUCTURE EVALUATION)

Alloy	Group	Preform Temp. (°F)	Block Temp. (°F)	Finish Temp. (°F)	Comments
Ti-6Al-4V	A,B,C	1775	1775	1800	10-20% spherical α
	A-1	1775	1750	1725	40-50% spherical α
	D,E,F	1775	1750	1750	Preforms treated to produce spaghetti α
	G,H,I	1775	1775	1775	Preforms treated to produce grain boundary α
	J,K,L,M	1775	1900	1775	10% reduction in finish
	N,O,P	1775	1900	1775	30% reduction in finish
	Q,R,S	1775	1900	1900	β finish
	T,U	1775	1900	1900	Slow cooled from finish forge
Ti-6Al-6V-2Sn	A,B,C	1675	1665	1700	10-20% spherical α
	A-1	1675	1625	1625	40-50% spherical α
	D,E,F	1675	1675	1675	Preforms treated to produce spaghetti α
	G,H,I	1675	1675	1675	Preforms treated to produce grain boundary α
	J,K,L,M	1675	1800	1675	10% reduction in finish
	N,O,P	1675	1800	1675	30% reduction in finish
	Q,R,S	1675	1800	1800	β finish
	T,U	1675	1800	1800	Slow cool from finish forge

TABLE XVI

FORGING TEMPERATURE USED FOR PHASE I, TASK B
(MICROSTRUCTURE EVALUATION)

Alloy	Group	Preform Temp. (°F)	Block Temp. (°F)	Finish Temp. (°F)	Comments
Ti-6Al-2Sn-4Zr-6Mo	A		1625	1700	10-20% spherical α
	B		1625	1625	40-50% spherical α
	C		1800	1725	10% reduction in finish
	D		1800	1725	30% reduction in finish
	E		1800	1625	10% reduction in finish
	F		1800	1625	30% reduction in finish
	G		1800	1800	β finish

TABLE XVII

PHASE I, TASK B
MICROSTRUCTURAL STUDY MECHANICAL TEST PROGRAM

Group Identification	Alloy	Type of Test	Number of Tests per Group	Total Number of Tests
A through U (See Figure 15)	Ti-6Al-4V	Tensiles (S)	5	110
		Tensiles (N)	5	110
		Low Cycle Fatigue	5	110
		High Cycle Fatigue (S)	10	220
		High Cycle Fatigue (N)	10	220
		Fracture Toughness	3	66
A' through U'	Ti-6Al-6V-2Sn	Same as A through U		
A" through F" (See Figure 16)	Ti-6Al-2Sn-4Zr-6Mo	Tensiles (S)	4	44
		Tensiles (N)	4	44
		Low Cycle Fatigue	6	66
		High Cycle Fatigue (S)	10	110
		High Cycle Fatigue (N)	10	110
		Fracture Toughness	3	33
		Notch Time Fracture	2	22

TABLE XVIII

PERCENT ALPHA AND ALPHA PARTICLE SIZE MEASUREMENTS* (INCHES)
PHASE I, TASK B MICROSTRUCTURAL STUDY
Ti-6Al-4V

Group	% Alpha	Equiaxed Alpha	Alpha Particle Size			
			Elongated Alpha		Blocky Alpha	
			Length	Width	Length	Width
A	6	.00058	-	-	-	-
A1	32	.00110	-	-	-	-
B	28	.00099	-	-	-	-
C	12	.00091	-	-	-	-
D	30	-	.01307	.00069	.00625	.00125
E	25	-	.01888	.00060	-	-
F	29	-	.01150	.00063	-	-
G	29	-	.00220	.00030	-	-
H	26	-	.00263	.00030	.00300	.00125
I	23	-	.00450	.00024	.00050	-
J	63	-	.00165	.00033	-	-
K	45	-	.00178	.00025	-	-
L	52	-	.00210	.00021	-	-
M	43	-	.00158	.00023	.00117	-
N	76	-	.00420	.00015	-	-
O	43	-	.00353	.00019	-	-
P	68	-	.00278	.00029	-	-
Q	75	-	.00223	.00010	-	-
R	48	-	.00215	.00021	-	-
S	58	-	.00110	.00003	-	-
T	92	-	.00350	.00013	-	-
U	49	-	.00310	.00015	-	-

*Measurements determined metallographically by point intercept method at 800X.

TABLE XIX

PERCENT ALPHA AND ALPHA PARTICLE SIZE MEASUREMENTS* (INCHES)
PHASE I, TASK B MICROSTRUCTURAL STUDY
Ti-6Al-6V-2Sn

Group	% Alpha	Equiaxed Alpha	Alpha Particle Size			
			Elongated Alpha		Blocky Alpha	
			Length	Width	Length	Width
A	15	.00055	-	-	-	-
A1	42	.00065	-	-	-	-
B	33	.00057	-	-	-	-
C	23	.00063	-	-	-	-
D	24	-	.01025	.00053	.00155	-
E	21	.00124	.01273	.00045	-	-
F	23	.00150	.01380	.00048	-	-
G	24	-	.00234	.00016	-	-
H	25	.00034	.00311	.00025	-	-
I	20	.00031	.00419	.00017	-	-
J	60	-	.00095	.00009	-	-
K	31	-	.00148	.00013	.00071	-
L	46	-	.00190	.00010	-	-
M	26	-	.00210	.00014	.00095	-
N	64	-	.00118	.00013	-	-
O	39	-	.00139	.00014	-	-
P	49	-	.00129	.00013	-	-
Q	71	-	.00175	.00006	-	-
R	45	-	.00211	.00008	.00068	-
S	67	-	.00098	.00006	-	-
T	41	-	.00174	.00008	.00075	.00025
U	39	-	.00238	.00013	.00098	.00041

*Measurements determined metallographically by the point intercept method at 800X.

TABLE Xx

PERCENT ALPHA AND ALPHA PARTICLE SIZE MEASUREMENTS* (INCHES)
PHASE I, TASK B MICROSTRUCTURAL STUDY
Ti-6Al-2Sn-4Zr-6Mo

Group	% Alpha	Alpha Particle Size				
		Equiaxed Alpha	Elongated Alpha		Blocky Alpha	
			Length	Width	Length	Width
A	11	.00041	-	-	-	-
A1	8	.00031	-	-	-	-
A2	10	.00036	-	-	-	-
B	34	.00040	-	-	-	-
B1	32	.00045	-	-	-	-
B2	32	.00046	-	-	-	-
C	47	-	.00126	.00009	-	-
D	21	-	.00086	.00009	.00035	-
E	49	-	.00250	.00006	.00075	.00031
F	51	-	.00140	.00009	.00053	-
G	47	-	.00185	.00006	-	-

*Measurements determined metallographically by point intercept method at 800X.

TABLE XXI

TENSILE PROPERTY SUMMARY
PHASE I, TASK B
MICROSTRUCTURE STUDY
Ti-6Al-4V

Condition	0.2% Yield Strength				Ultimate Tensile Strength				% Elongation				% Reduction of Area			
	Min.	Max.	Mean	Std. Dev.	Min.	Max.	Mean	Std. Dev.	Min.	Max.	Mean	Std. Dev.	Min.	Max.	Mean	Std. Dev.
A	137.2	145.2	141.2	3.40	152.0	159.0	155.0	3.21	12.0	15.0	13.8	1.25	30.5	39.5	35.4	4.49
A-1	131.8	138.4	134.6	2.93	143.4	150.6	146.7	3.15	14.0	15.0	14.6	.42	39.5	44.4	41.2	1.91
B	138.6	144.8	142.2	2.54	151.2	155.8	154.1	2.09	14.5	15.0	14.8	.27	39.4	41.7	40.9	.89
C	132.0	144.0	139.1	4.24	150.0	158.0	153.2	2.85	12.0	15.0	14.3	1.21	32.7	41.4	37.0	2.97
D	132.0	142.0	137.2	4.64	144.8	154.0	149.4	3.66	10.0	12.5	11.1	.96	22.3	31.1	28.1	3.37
E	136.8	142.4	140.8	2.32	151.8	156.0	154.3	1.66	7.5	10.5	10.9	4.19	12.2	24.5	20.2	5.19
F	133.2	138.0	134.6	1.96	147.8	150.6	149.6	1.13	12.0	13.0	12.6	.55	28.6	34.4	32.8	2.44
G	134.6	142.6	137.5	3.06	149.2	155.4	150.9	1.89	12.0	14.5	13.2	1.25	31.9	37.0	34.8	1.89
H	137.6	150.6	143.3	4.69	150.8	163.8	156.5	4.67	11.5	13.0	12.3	.67	31.1	38.2	35.8	2.80
I	136.8	143.8	139.0	2.74	149.4	154.2	150.7	2.01	13.0	14.0	13.3	.45	27.8	37.6	33.8	3.77
J	131.4	140.8	134.3	3.47	146.0	154.0	149.2	3.39	12.0	15.0	13.3	1.37	23.7	38.8	31.6	6.25
K	130.6	142.0	136.5	3.90	148.0	155.8	151.2	2.51	11.0	12.5	12.0	.50	25.9	33.8	29.6	2.67
L	132.4	138.0	136.1	1.85	146.8	156.0	151.7	3.49	11.5	12.5	11.9	.35	23.7	33.2	29.0	3.75
M	132.4	142.8	137.8	3.88	147.8	153.4	151.2	2.23	12.5	13.5	12.8	.45	27.8	38.8	32.6	4.37
N	126.0	128.4	126.7	1.17	142.0	144.0	143.0	1.15	13.0	15.0	13.5	1.00	33.8	37.0	35.2	1.42
O	131.8	141.6	136.8	3.76	143.6	156.0	150.6	5.10	13.0	15.0	13.5	.87	25.9	37.0	32.9	4.11
P	132.2	138.4	134.4	2.33	146.4	151.0	148.0	1.73	11.0	15.0	13.2	1.79	29.9	35.1	32.0	2.33
Q	126.0	132.4	128.1	2.61	141.4	149.8	144.1	3.29	8.5	13.5	10.5	1.97	15.2	27.2	19.9	4.79
R	132.2	140.0	137.6	3.13	147.8	158.0	152.9	3.67	9.0	11.0	10.2	.84	18.1	24.5	21.1	2.46
S	137.8	147.8	142.3	3.73	150.6	161.6	155.8	4.13	8.0	10.5	9.5	1.00	16.6	23.7	19.75	2.57
T	126.0	136.0	130.6	4.12	143.8	152.0	147.2	3.47	10.0	13.0	11.5	1.73	23.1	27.8	24.8	2.10
U	133.6	145.0	138.6	4.81	147.2	158.0	151.9	4.68	9.0	11.0	10.3	.76	17.4	24.5	22.6	3.82
Low O_2 A	121.0	134.0	127.5		138.0	148.0	142.9		12.5	13.5	12.7		25.9	37.6	33.1	

TABLE XXII

TENSILE PROPERTY SUMMARY
PHASE I, TASK B
MICROSTRUCTURE STUDY
Ti-6Al-6V-2Sn

Condition	0.2% Yield Strength				Ultimate Tensile Strength				% Elongation				% Reduction of Area			
	Min.	Max.	Mean	Std. Dev.	Min.	Max.	Mean	Std. Dev.	Min.	Max.	Mean	Std. Dev.	Min.	Max.	Mean	Std. Dev.
A	140.4	150.0	144.6	3.78	156.0	160.0	157.8	1.48	14.5	17.0	15.3	.97	32.7	52.2	44.6	9.59
A-1	148.0	151.8	148.8	1.66	158.0	159.8	158.8	.68	15.0	17.0	16.4	.82	46.7	50.0	48.5	1.20
B	146.0	160.0	154.2	5.40	160.0	167.6	164.9	1.34	15.0	18.0	16.1	1.34	47.2	51.8	49.7	1.91
C	148.0	154.8	152.1	2.71	160.0	166.0	164.3	2.49	15.0	17.0	15.7	.84	46.7	49.6	48.3	1.12
D	139.6	148.0	143.3	3.53	152.6	158.4	155.3	2.63	13.0	18.0	15.6	2.10	33.8	48.5	40.3	7.50
E	147.0	149.4	148.0	1.13	160.2	162.6	161.2	1.07	11.5	13.5	12.4	.89	28.6	33.8	31.0	2.23
F	148.0	150.0	149.0	1.00	161.0	164.0	162.7	1.31	12.0	12.0	12.0	0	29.2	35.1	32.9	2.38
G	140.0	144.0	141.6	1.68	154.0	156.2	155.4	.89	12.0	14.0	13.0	1.00	27.2	41.4	35.4	5.52
H	148.4	151.8	149.9	1.24	162.4	164.0	163.5	.74	11.0	13.0	12.0	1.00	23.7	35.1	31.0	4.69
I	148.0	150.6	149.5	1.03	162.0	164.0	163.6	.89	11.0	13.0	12.2	.84	26.6	38.8	31.5	5.05
J	145.0	148.3	146.7	1.37	156.2	162.0	159.9	2.51	14.5	15.0	14.9	.22	35.7	39.5	37.5	1.43
K	145.0	150.0	147.8	1.81	160.6	164.0	162.4	1.20	12.5	14.5	13.3	.76	25.1	37.0	29.3	4.57
L	139.4	146.6	143.1	2.97	156.6	161.8	159.2	2.20	13.0	15.0	14.4	.89	32.7	37.6	35.2	1.81
M	140.8	145.8	143.8	1.87	156.6	161.2	159.6	2.00	13.0	16.5	14.4	1.56	28.6	31.9	30.3	1.35
N	143.8	146.8	144.7	1.24	157.4	159.6	158.4	.89	13.0	18.0	15.1	1.88	35.1	38.8	37.7	1.54
O	146.0	148.6	147.6	.98	160.8	163.0	161.5	1.20	14.0	15.0	14.7	.45	31.9	41.4	35.0	3.76
P	144.0	148.3	146.7	1.69	158.8	161.2	161.0	1.78	13.0	15.0	13.8	1.10	33.2	43.1	38.1	3.71
Q	134.8	137.4	136.3	1.06	153.2	155.4	154.5	.81	12.0	14.0	12.8	.84	21.7	24.5	23.4	1.17
R	134.6	143.8	140.4	3.53	151.8	158.8	156.4	2.98	10.0	12.0	11.4	.82	19.6	25.1	21.7	2.57
S	153.8	157.6	155.8	1.52	169.8	173.0	171.2	1.40	6.0	10.0	8.0	1.87	12.2	21.7	15.7	3.67
T	130.2	143.6	136.2	5.25	148.0	158.0	152.7	4.24	12.0	13.5	12.8	.57	20.9	27.2	24.3	2.38
U	140.1	145.0	142.6	1.94	170.4	160.4	158.5	1.68	10.0	12.5	12.0	1.12	18.8	25.9	21.1	3.28

TABLE **XXIII**

TENSILE PROPERTY SUMMARY
PHASE I, TASK B
MICROSTRUCTURE STUDY
Ti-6Al-2Sn-4Zr-6Mo

Condition	0.2% Yield Strength				Ultimate Tensile Strength				% Elongation				% Reduction of Area			
	Min.	Max.	Mean	Std. Dev.	Min.	Max.	Mean	Std. Dev.	Min.	Max.	Mean	Std. Dev.	Min.	Max.	Mean	Std. Dev.
A	152.2	166.0	162.2	6.04	166.8	182.0	176.2	5.25	12.0	13.5	12.8	.53	30.5	47.2	36.6	5.84
A-1	140.0	161.8	147.6	3.72	154.6	166.0	160.7	3.89	10.0	17.0	14.5	2.73	25.9	47.8	39.5	8.76
A2	137.2	152.0	147.5	5.91	148.8	161.8	158.3	5.37	14.0	17.5	15.6	1.13	32.7	51.3	42.2	7.83
B	162.2	171.2	167.2	3.55	174.0	187.6	180.0	5.10	11.0	15.0	13.6	1.21	31.1	46.1	41.9	5.25
B-1	148.0	158.4	154.0	3.53	158.8	168.2	163.8	3.53	9.0	15.5	12.6	2.36	16.0	44.4	34.3	10.66
B-2	150.0	158.0	155.2	2.71	160.0	168.0	165.6	2.98	12.0	15.0	13.8	1.16	31.9	47.2	41.1	6.44
C	150.8	165.8	159.0	5.50	166.6	179.4	174.5	4.27	8.0	12.0	10.4	1.27	16.6	28.6	23.4	4.39
D	156.0	167.2	161.1	3.76	171.6	179.8	174.9	2.80	9.0	12.0	10.5	.96	20.3	30.5	25.8	3.23
E	147.0	160.6	154.6	5.07	163.6	176.0	171.4	4.18	7.0	11.5	9.8	1.44	13.7	24.5	20.1	3.93
F	159.4	164.6	161.3	2.09	174.4	179.0	177.1	1.73	9.0	10.5	9.8	.46	18.8	27.8	23.2	2.60
G	146.8	157.4	152.3	3.89	170.0	178.4	173.6	3.06	4.0	8.0	6.5	1.31	10.0	16.6	12.9	3.04

TABLE XXIV

NOTCHED TENSILE (K_t = 3.9) PROPERTY SUMMARY
PHASE I, TASK B MICROSTRUCTURAL STUDY
Ti-6Al-4V

Group	NTS			NTS/UTS		
	Min. ksi	Max. ksi	Average ksi	Min.	Max.	Average
A	231	235	233.2	1.49	1.53	1.51
A1	224	235	231.5	1.57	1.62	1.58
B	225	229	228.2	1.46	1.49	1.48
C	233	235	234.5	1.48	1.56	1.51
D	204	235	221.4	1.33	1.56	1.47
E	204	229	216.5	1.33	1.47	1.40
F	221	231	226.2	1.50	1.54	1.51
G	225	233	227.9	1.48	1.52	1.50
H	225	237	230.2	1.40	1.58	1.47
I	229	235	233.3	1.52	1.57	1.54
J	230	235	231.7	1.53	1.58	1.56
K	230	233	232.3	1.51	1.57	1.54
L	230	234	231.7	1.50	1.58	1.53
M	230	234	232.6	1.53	1.56	1.53
N	226	234	229.8	1.57	1.63	1.58
O	229	241	232.2	1.47	1.64	1.53
P	225	237	231.1	1.55	1.61	1.56
Q	217	225	222.4	1.52	1.58	1.56
R	223	234	229.8	1.47	1.57	1.51
S	225	231	228.6	1.41	1.53	1.47
T	219	231	224.9	1.50	1.55	1.52
U	223	229	226.7	1.43	1.56	1.49
Low O_2 A	219	230	224.2	1.48	1.67	1.58

TABLE XXV

NOTCHED TENSILE (K_t = 3.9) PROPERTY SUMMARY
PHASE I, TASK B MICROSTRUCTURAL STUDY
Ti-6Al-6V-2Sn

Group	NTS			NTS/UTS		
	Min. ksi	Max. ksi	Average ksi	Min.	Max.	Average
A	232	239	236.1	1.45	1.51	1.49
A1	240	243	241.4	1.51	1.54	1.52
B	241	241	241.1	1.44	1.50	1.46
C	241	247	243.5	1.45	1.50	1.48
D	229	241	237.1	1.52	1.55	1.52
E	224	233	227.6	1.38	1.45	1.41
F	228	234	231.8	1.41	1.45	1.42
G	239	243	241.5	1.50	1.56	1.53
H	238	249	245.0	1.47	1.53	1.50
I	237	245	242.7	1.46	1.49	1.48
J	240	249	243.9	1.49	1.53	1.52
K	233	239	236.4	1.42	1.48	1.45
L	236	246	241.3	1.50	1.53	1.51
M	231	237	234.0	1.44	1.50	1.46
N	240	241	241.8	1.51	1.53	1.52
O	234	243	238.9	1.44	1.50	1.48
P	235	245	237.9	1.45	1.50	1.47
Q	229	233	230.7	1.48	1.52	1.49
R	225	231	227.8	1.43	1.49	1.45
S	224	229	227.4	1.31	1.35	1.32
T	219	225	223.7	1.42	1.51	1.47
U	231	235	233.4	1.45	1.48	1.47

TABLE XXVI

NOTCHED TENSILE (K_t = 3.9) PROPERTY SUMMARY
PHASE I, TASK B MICROSTRUCTURAL STUDY
Ti-6Al-2Sn-4Zr-6Mo

Group	NTS			$\frac{NTS}{UTS}$		
	Min. ksi	Max. ksi	Average ksi	Min.	Max.	Average
A	231	255	246.6	1.37	1.44	1.40
A-1	218	241	233.4	1.38	1.48	1.43
A-2	221	237	231.7	1.43	1.57	1.47
B	225	257	242.2	1.23	1.42	1.33
B-1	215	236	228.5	1.34	1.40	1.39
B-2	221	235	227.0	1.34	1.42	1.37
C	219	253	240.4	1.27	1.42	1.36
D	217	253	240.0	1.25	1.43	1.36
E	217	255	241.5	1.33	1.47	1.40
F	202	249	230.1	1.13	1.41	1.29
G	191	237	219.7	1.13	1.36	1.26

TABLE XXVII

SUMMARY HCF DATA - MICROSTRUCTURAL STUDY
FATIGUE STRENGTH (KSI) FOR INDICATED CYCLES
SEE FIGURES 30 AND 31 FOR PROCESSING

		Cycles							
		Smooth Bar				Notched Bar K_t = 3.0			
Alloy	Condition	10^4	10^5	10^6	10^7	10^4	10^5	10^6	10^7
		Endurance Limit - KSI							
Ti-6Al-6V-2Sn	A	146	108	99	97	64	41	37	36
	A-1	136	122	110	94	58	38	34	33
	B	137	124	111	97	65	41	36	35
	C	145	126	109	92	62	41	37	36
	D	134	98	90	87	65	40	39	38
	E	121	104	78	<75	45	35	34	34
	F	126	103	80	<75	56	38	35	34
	G	120	96	87	84	59	42	35	31
	H	134	106	91	83	60	44	41	40
	I	128	105	98	91	64	44	39	38
	J	116	96	90	89	65	41	35	34
	K	120	95	90	89	66	38	33	32
	L	128	108	100	98	61	44	41	40
	M	137	105	93	91	62	42	37	34
	N	122	113	104	94	64	38	34	32
	O	126	115	105	94	65	41	38	37
	P					60	42	38	36
	Q	116	102	100	99	65	40	32	29
	R	113	101	100	100	64	41	37	36
	S	136	102	97	96	66	44	38	36
	T	125	103	96	93	63	43	38	36
	U	122	99	95	94	62	40	36	35
Ti-6Al-4V	A	105	87	81	78	66	43	36	31
	A-1	106	91	86	84	69	43	38	37
	B	112	94	82	71	64	41	35	32
	C	117	95	88	85	69	45	31	30
	D	129	88	84	80	66	42	33	32
	E	114	90	78	74	68	40	32	31
	F	126	98	84	78	65	40	35	34
	G	108	91	85	84	70	43	34	33
	H	114	86	78	76	69	45	36	34
	I	104	91	89	88	70	43	38	38

TABLE XXVII CONTINUED

Alloy	Condition	Cycles							
		Smooth Bar				Notched Bar K_t = 3.0			
		10^4	10^5	10^6	10^7	10^4	10^5	10^6	10^7
		Endurance Limit - KSI							
Ti-6Al-4V, Continued	J	103	89	85	84	68	42	34	32
	K	106	92	89	85	66	43	35	31
	L	117	104	86	72	70	43	33	30
	M	116	92	82	77	64	42	34	29
	N	103	89	82	76	68	43	36	35
	O	126	92	82	76	66	42	37	35
	P	119	96	91	90	65	40	35	33
	Q	115	95	87	82	68	41	33	32
	R	106	91	88	88	68	42	29	27
	S	114	94	86	85	70	42	33	32
	T	106	90	87	86	67	43	35	34
	U	101	92	88	87	64	41	36	35
	Low O_2	101	94	91	90	68	39	32	31
Ti Ti-6Al-2Sn-4Zr-6Mo	A	119	99	94	90	68	46	38	36
	A-1	120	98	92	90	67	50	45	42
	A-2					67	43	37	36
	B	121	102	99	98	66	48	41	38
	B-1	120	99	92	90	65	47	43	41
	B-2	124	100	92	90	63	45	40	38
	C	125	120	115	109	66	44	41	40
	D	118	95	91	90	70	56	45	41
	E	111	94	91	90	65	46	42	40
	F	122	113	105	94	68	42	35	34
	G	119	101	99	98	70	44	40	38

TABLE XXVIII

FRACTURE TOUGHNESS DATA - MICROSTRUCTURE STUDY
SEE FIGURE 30 FOR PROCESSING

Condition	Serial Number	K_{IC} (KSI $\sqrt{In}$)	Average K_{IC}
		Ti-6Al-4V	
A	2-24-1	68.0	
	2-24-2	73.1	69.4
	2-25-1	67.1	
A-1	2-17-1	71.5	
	2-17-2	70.6	69.1
	2-18-1	65.2	
B	2-168-1	56.9	
	2-168-2	61.4	59.2
	2-169-1	59.8	
C	2-128-1	60.0	
	2-128-2	52.6	57.7
	2-174-1	60.6	
D	2-70-2	87.7	87.0
	2-77-1	86.3	
	-		
E	2-97-1	70.6	
	2-97-2	71.2	69.9
	2-98-1	68.1	
F	2-156-1	75.8	
	2-156-2	76.0	75.4
	2-157-1	74.5	
G	2-52-1	75.7	
	2-52-2	79.5	79.9
	2-61-1	84.7	
H	2-73-1	63.9	
	2-73-2	75.2	69.3
	2-74-1	68.9	

TABLE XXVIII, CONTINUED

FRACTURE TOUGHNESS DATA - MICROSTRUCTURE STUDY
SEE FIGURE 30 FOR PROCESSING

Condition	Serial Number	K_{IC} (KSI $\sqrt{In}$)	Average K_{IC}
	Ti-6Al-4V, Continued		
I	2-149-1	70.6	
	2-149-2	71.1	68.7
	2-150-1	64.6	
J	2-80-1	87.6	
	2-80-2	91.0	86.3
	2-85-1	80.3	
K	2-95-1	79.0	
	2-95-2	85.5	81.5
	2-96-1	80.5	
L	2-104-1	71.9	
	2-104-2	79.5	75.5
	2-107-1	75.1	
M	2-119-1	80.4	
	2-119-2	77.7	78.0
	2-120-1	76.0	
N	2-43-1	75.9	
	2-43-2	83.4	79.6
	2-44-1	80.5	
O	2-56-1	67.4	
	2-56-2	78.0	73.0
	2-63-1	73.8	
P	2-83-1	69.7	
	2-83-2	74.9	73.4
	2-84-1	76.1	
Q	2-137-1	74.4	
	2-137-2	71.1	73.3
	2-138-1	74.5	

TABLE XXVIII, CONTINUED

FRACTURE TOUGHNESS DATA - MICROSTRUCTURE STUDY
SEE FIGURE 30 FOR PROCESSING

Condition	Serial Number	K_{IC} (KSI $\sqrt{In}$)	Average K_{IC}
	Ti-6Al-4V, Continued		
R	2-144-1	86.4	
	2-144-2	86.4	86.1
	2-147-1	85.6	
S	2-161-1	61.6	
	2-161-2	60.4	60.2
	2-162-1	58.8	
T	2-130-1	80.4	
	2-130-2	77.1	78.0
	2-131-1	76.7	
U	2-164-1	86.4	
	2-164-2	86.7	87.2
	2-165-1	88.6	
	Ti-6Al-4V (Low O_2)		
A	4-6-1	97.1	
	4-6-2	104.8	103.0
	4-7-1	107.1	

TABLE XXIX

FRACTURE TOUGHNESS DATA - MICROSTRUCTURE STUDY
SEE FIGURE 30 FOR PROCESSING

Condition	Serial Number	K_{IC} (KSI $\sqrt{In}$)	Average K_{IC}
	Ti-6Al-6V-2Sn		
A	6-107-1	50.4	50.3
	6-107-2	51.3	
A-1	6-100-1	49.4	48.7
	6-100-2	48.1	
B	6-114-1	40.4	41.0
	6-114-2	41.6	
C	6-121-1	42.4	42.2
	6-121-2	42.0	
D	6-128-1	63.6	64.1
	6-128-2	64.6	
E	6-135-1	56.4	57.4
	6-135-2	57.4	
	6-136-2	58.5	
F	6-142-1	54.8	54.8
	6-142-2	56.0	
	6-143-1	53.7	
G	6-149-1	65.4	66.7
	6-149-2	65.8	
	6-150-1	69.0	
H	6-156-1	55.2	54.9
	6-156-2	55.0	
	6-157-2	54.7	
I	6-163-1	54.3	54.5
	6-163-2	54.8	
	6-164-1	54.4	

TABLE XXIX, CONTINUED

FRACTURE TOUGHNESS DATA - MICROSTRUCTURE STUDY
SEE FIGURE 30 FOR PROCESSING

Condition	Serial Number	K_{IC} (KSI $\sqrt{In}$)	Average K_{IC}
	Ti-6Al-6V-2Sn, Continued		
J	6-16-1	74.6	
	6-16-2	84.7	77.1
	6-17-1	71.8	
K	6-23-1	68.7	
	6-23-2	76.6	72.6
L	6-30-1	63.3	
	6-30-2	69.5	66.5
	6-31-1	66.9	
M	6-37-1	66.5	
	6-37-2	67.9	65.3
	6-38-1	61.7	
N	6-79-1	64.4	
	6-79-2	64.2	64.6
	6-80-1	65.4	
O	6-86-1	60.8	
	6-86-2	64.3	61.5
	6-87-1	59.6	
P	6-93-1	56.7	
	6-93-2	59.5	58.1
Q	6-44-1	71.7	
	6-44-2	69.7	70.5
	6-45-1	70.2	
R	6-51-1	70.7	
	6-51-2	73.6	72.1
S	6-58-2	51.8	
	6-58-1	Failed	51.8
T	6-65-1	73.6	
	6-65-2	69.5	71.5
U	6-72-1	69.3	
	6-72-2	71.3	70.3

TABLE XXX

FRACTURE TOUGHNESS DATA - MICROSTRUCTURE STUDY
SEE FIGURE 31 FOR PROCESSING

Condition	Serial Number	K_{IC} (KSI $\sqrt{In}$)	Average K_{IC}
	Ti-6Al-2Sn-4Zr-6Mo		
A	8-7-1	30.4	
	8-7-2	31.6	31.1
	8-7-3	31.3	
A-1	8-9-1	26.7	
	8-9-2	28.5	27.9
	8-9-3	28.5	
A-2	8-11-2	Failed in PC*	
	8-11-1	27.1	28.4
	8-11-3	29.7	
B	8-13-1	Failed in PC	
	8-13-2	24.8	24.4
	8-13-3	24.0	
B-1	8-15-1	22.7	
	8-15-2	24.9	23.8
	8-15-3	Failed in PC	
B-2	8-17-1	23.3	
	8-17-2	Failed in PC	23.3
	8-17-3	Failed in PC	
C	8-19-1	40.5	
	8-19-2	41.5	41.1
	8-19-3	42.3	
D	8-21-1	38.9	
	8-21-2	36.4	37.4
	8-21-3	36.9	
E	8-23-1	43.6	
	8-23-2	44.8	44.6
	8-23-2	45.8	

*Precracking

TABLE XXX, CONTINUED

FRACTURE TOUGHNESS DATA - MICROSTRUCTURE STUDY
SEE FIGURE 31 FOR PROCESSING

Condition	Serial Number	K_{IC} (KSI $\sqrt{in}$)	Average K_{IC}
	Ti-6Al-2Sn-4Zr-6Mo, Continued		
F	8-25-1	31.6	
	8-25-2	31.1	33.4
	8-25-3	37.6	
G	8-27-1	51.4	
	8-27-2	52.7	52.4
	8-27-3	53.2	

TABLE XXXI

Median Low Cycle Fatigue Lives For Ti 6Al-4V and Ti 6Al-6V-2Sn(1)

Phase I, Task B

Ti 6Al-4V				Ti 6Al-6V-2Sn		
Cycles To Pinpoint x 10^{-3}	Cycles To 1/32" Crack x 10^{-3}	Remarks	Condition	Cycles To Pinpoint x 10^{-3}	Cycles To 1/32" Crack x 10^{-3}	Remarks
-	-	3 Runouts > 100.0	A	19.5	24.5	
10.0	17.6		A (Low O_2)	-	-	Not tested in Ti 662
29.7	39.8		A-1	16.0	23.0	
20.3	28.5		B	35.5	41.0	
33.1	38.7		C	27.6	32.3	
17.0	23.0		D	7.0	10.6	
15.4	21.3		E	7.1	11.6	
20.7	25.3		F	5.7	9.2	
46.2	57.6		G	6.4	9.4	
69.7	73.4		H	4.5	10.4	
83.3	85.5		I	6.0	10.4	
-	-	4 Runouts > 100.0	J	4.2	8.8	
29.0	38.9		K	15.7	20.8	
-	-	3 Runouts > 100.0	L	11.5	16.4	
17.0	23.9		M	6.7	9.8	
73.6	83.2		N	6.1	11.2	
29.0	40.0		O	8.8	14.5	
24.1	31.5		P	10.2	14.4	
8.3	17.0		Q	5.8	11.0	
25.1	36.9		R	10.6	14.8	
-	-	3 Runouts > 100.0	S	10.7	15.0	
14.4	18.8		T	6.7	10.0	
11.6	18.3		U	8.7	12.7	

(1) B_{50} Life Per Weibull Analysis

TABLE XXXI, CONTINUED

Median Low Cycle Fatigue Lives
For Ti 6Al-2Sn-4Zr-6Mo(1)

Phase I, Task B

Condition	Cycles To Pinpoint x 10^{-3}	Cycles to 1/32" Crack x 10^{-3}	Remarks
A	16.0	20.1	
A-1	21.0	26.7	
A-2	22.9	28.3	
B	51.0	55.1	
B-1	-	-	3 Runouts > 100.0
B-2	22.9	26.5	
C	42.5	45.1	
D	26.4	29.9	
E	15.1	18.7	
F	10.3	15.5	
G	8.7	12.6	

(1) B_{50} Life Per Weibull Analysis

TABLE XXXII

MECHANICAL PROPERTY RATING*
Ti-6Al-4V

Cond.	Pre-Treat on Stock	Blocker Forge Temp.	Finish Forge Temp.	Finish Forge Red.	Cooling from Finish Forge	Heat Treat.	Notched High Cycle Fatigue	Low Cycle Fatigue	Fracture Toughness	UTS	R/A	NTS/UTS	Total	Cond.
A	-	αβ	αβ		AC	ANN	2	4	3	3	3	4	19	A
A (low O_2)	-	"	"		"	"	2	1	4	2	3	4	16	A (low O_2)
B	-	"	"		"	STOA	2	2	2	3	4	3	16	B
C	-	"	"		WQ	ANN	2	2	2	3	3	4	16	C
A-1	-	"	"		AC	"	3	1	3	2	4	4	17	A-1
D	Spaghetti Alpha	"	"		"	"	2	1	4	3	2	3	15	D
E	"	"	"		"	STOA	2	1	3	3	2	2	13	E
F	"	"	"		WQ	ANN	2	1	3	3	3	4	16	F
G	Grain Boundary Alpha	"	"		AC	"	3	3	4	3	3	3	19	G
H	"	"	"		"	STOA	2	3	3	3	3	3	17	H
I	"	"	"		WQ	ANN	3	4	3	3	3	4	20	I

*Properties are rated on scale of 1-4 with 1 the low and 4 the high. Scales are described in Appendix E.

TABLE XXXII, CONTINUED

MECHANICAL PROPERTY RATING*
Ti-6Al-4V

Cond.	Pre-Treat on Stock	Blocker Forge Temp.	Finish Forge Temp.	Finish Forge Red.	Cooling from Finish Forge	Heat Treat.	Notched High Cycle Fatigue	Low Cycle Fatigue	Fracture Toughness	UTS	R/A	NTS UTS	Total	Cond.
J	-	β	αβ	10%	AC	ANN	2	4	4	3	3	4	20	J
K	-	"	"	"	"	STOA	2	2	4	3	2	4	17	K
L	-	"	"	"	WQ	ANN	2	4	3	3	2	4	18	L
M	-	"	"	"	"	STOA	1	1	3	3	3	4	15	M
N	-	"	"	30%	AC	ANN	3	3	3	2	3	4	18	N
O	-	"	"	"	"	STOA	3	2	3	3	3	4	18	O
P	-	"	"	"	WQ	ANN	2	2	3	2	3	4	16	P
Q	-	"	β	10%	AC	"	2	1	3	2	2	4	14	Q
R	-	"	"	"	"	STOA	1	2	4	3	2	4	16	R
S	-	"	"	"	WQ	ANN	2	4	3	3	1	3	16	S
T	-	"	"		Slow Cool	"	2	1	3	2	2	4	14	T
U	-	"	"		"	STOA	3	1	4	3	2	3	16	U

*Properties are rated on scale of 1-4 with 1 the low and 4 the high. Scales are described in Appendix E.

TABLE XXXIII

MECHANICAL PROPERTY RATING
Ti-6Al-6V-2Sn

Cond.	Pre-Treat on Stock	Blocker Forge Temp.	Finish Forge Temp.	Finish Forge Red.	Cooling from Finish Forge	Heat Treat.	Notched High Cycle Fatigue	Low Cycle Fatigue	Fracture Toughness	UTS	R/A	NTS UTS	Total	Cond.
A	-	αβ	αβ		AC	ANN	3	2	2	3	4	3	17	A
B	-	"	"		"	STOA	3	1	2	4	4	3	17	B
C	-	"	"		WQ	ANN	3	2	2	4	4	3	18	C
A-1	-	"	"		AC	"	2	2	2	3	4	4	17	A-1
D	Spaghetti Alpha	"	"		"	"	3	1	3	3	4	4	18	D
E	"	"	"		"	STOA	2	1	2	4	3	3	15	E
F	"	"	"		WQ	ANN	2	1	2	4	3	3	15	F
G	Grain Boundary Alpha	"	"		AC	"	2	1	3	3	3	4	16	G
H	"	"	"		"	STOA	3	1	2	4	3	3	16	H
I	"	"	"		WQ	ANN	3	1	2	4	3	3	16	I
J	-	β	"	10%	AC	"	2	1	3	3	3	4	16	J
K	-	"	"	"	"	STOA	2	1	3	4	2	3	15	K

TABLE XXXIII, CONTINUED

MECHANICAL PROPERTY RATING
Ti-6Al-6V-2Sn

Cond.	Pre-Treat on Stock	Blocker Forge Temp.	Finish Forge Temp.	Finish Forge Red.	Cooling from Finish Forge	Heat Treat.	Notched High Cycle Fatigue	Low Cycle Fatigue	Frac-ture Tough-ness	UTS	R/A	NTS/UTS	Total	Cond.
L	-	"	"	"	WQ	ANN	3	1	3	3	3	4	17	L
M	-	"	"	"	"	STOA	2	1	3	3	2	3	14	M
N	-	"	"	30%	AC	ANN	2	1	3	3	3	4	16	N
O	-	"	"	"	"	STOA	3	1	3	4	3	3	17	O
P	-	"	"	"	WQ	ANN	3	1	2	4	3	3	16	P
Q	-	"	β	10%	AC	"	1	1	3	3	2	3	13	Q
R	-	"	"	"	"	STOA	3	1	3	3	2	3	15	R
S	-	"	"	"	WQ	ANN	3	1	2	4	1	2	13	S
T	-	"	"		Slow Cool	"	3	1	3	3	2	3	15	T
U	-	"	"		"	STOA	3	1	3	3	1	3	14	U

TABLE XXXIV

MECHANICAL PROPERTY RATING
Ti-6Al-2Sn-4Zr-6Mo

Cond.	Blocker Forge Temp.	Finish Forge Temp.	Finish Forge Red.	Heat Treat.	Notched High Cycle Fatigue	Low Cycle Fatigue	Fracture Toughness	UTS	R/A	NTS UTS	Total	Cond.
A	αβ	αβ		STA	3	1	1	4	3	2	14	A
A-1	"	"		ANN	4	2	1	4	3	3	17	A-1
A-2	"	"		STOA	3	2	1	3	4	3	16	A-2
B	"	"		STA	3	3	1	4	4	2	17	B
B-1	"	"		ANN	4	4	1	4	3	2	18	B-1
B-2	"	"		STOA	3	2	1	4	4	2	16	B-2
C	β	High αβ	10%	STA	3	3	2	4	2	2	16	C
D	"	"	30%	"	4	2	1	4	3	2	15	D
E	"	Low αβ	10%	"	3	1	2	4	2	2	14	E
F	"	"	30%	"	2	1	1	4	2	1	11	F
G	"	β		"	3	1	2	4	1	1	12	G

TABLE XXXV

FORGING AND HEAT TREATING PROCEDURE
Ti-6Al-4V
"SOFT ALPHA INCLUSION" MATERIAL

(See Figure 60 for Schematic Diagram of Processing)

Serial Number	Forge #1	Forge Temp. (°F)	Forge #2	Forge Temp. (°F)	Heat Treatment
3-2 - 3-4	12" × 6"	1775	6" × 3" (closed die)	1775	1300°F (2 hours) Air Cool
3-5 - 3-7		1775		1900	1300°F (2 hours) Air Cool

TABLE XXXVI

TENSILE PROPERTIES OF Ti-6Al-4V DISC
CONTAINING "SOFT ALPHA SEGREGATION"
ANNEALED 1300°F (2 HOURS) A.C.

Direction	Condition	0.2% Y.S. (KSI)	U.T.S. (KSI)	El.%	R.A.%	NTS	NTS/UTS
Axial	αβ Forged with Inclusion	127.6	141.6	6.0	13.0		
"	"	125.0	138.0	10.0	20.9		
"	"					153.5	1.08
"	"					166.9	1.21
"	αβ Forged No Inclusion	128.2	145.2	11.5	31.9		
"	"	135.6	149.2	12.5	38.8		
"	"					211.4	1.45
"	"					223.9	1.55
Tangential	αβ Forged with Inclusion	133.0	143.6	14.5	36.3		
"	"	134.4	147.0	10.5	30.5		
"	"					224.7	1.56
"	"					214.1	1.45
"	αβ Forged No Inclusion	137.8	150.0	14.0	36.3		
"	"	135.8	147.6	15.0	40.8		
"	"					225.7	1.50
"	"					228.9	1.55
Axial	β Forged with Inclusion	130.4	143.2	10.0	17.4		
"	"	124.4	142.6	10.0	19.6		
"	"					212.1	1.48
"	"					218.1	1.53
"	β Forged No Inclusion	124.2	143.8	10.0	20.9		
"	"	130.4	146.4	9.5	20.3		
"	"					218.5	1.52
"	"					223.9	1.53
Tangential	β Forged with Inclusion	132.0	144.8	8.5	19.6		
"	"	134.6	149.2	8.5	15.2		
"	"					225.3	1.50
"	"					223.8	1.50
"	β Forged No Inclusion	132.4	146.0	8.5	18.8		
"	"	132.0	146.0	8.0	17.4		
"	"					218.9	1.49
"	"					229.6	1.57

TABLE XXXVII

HIGH CYCLE FATIGUE
Ti-6Al-4V
CONTAINING "SOFT ALPHA" INCLUSION
ANNEALED 1300°F[2] A.C.

Condition	Cycles							
	Smooth Bar				Notched Bar K_t = 3.0			
	10^4	10^5	10^6	10^7	10^4	10^5	10^6	10^7
αβ Forged								
No Inclusion	132	95	85	82	62	41	33	31
Inclusion								
β Forged								
No Inclusion	130	94	89	84	65	42	37	36
Inclusion								

TABLE XXXVIII

LCF DATA DISC ALPHA SEGREGATION

Alloy	Condition	Median Life Cycle x 10^{-3} Pinpoint	1/32" Crack	Remarks
Ti-64	Alpha-beta with inclusion	Specimens failed - no pinpoint or 1/32" crack		
Ti-64	Alpha-beta no inclusion	12.0	20.5	--
Ti-64	Beta with inclusion	8.0	9.5	Not all specimens had inclusion
Ti-64	Beta no inclusion	8.5	11.5	--

TABLE XXXIX

FRACTURE TOUGHNESS DATA - PHASE II
"SOFT ALPHA INCLUSIONS" Ti-6Al-4V DISC FORGINGS
ANNEALED 1300°F (2 HOURS) A.C.

Serial Number	Condition	K_{IC} (KSI $\sqrt{in}$)	Average K_{IC}
3-4-1	αβ Forged with inclusions	58.5	58.6
3-4-2	αβ Forged with inclusions	58.8	
3-4-3	αβ Forged no inclusions	57.2	56.2
3-4-4	αβ Forged no inclusions	55.2	
3-6-1	β Forged with inclusions	81.5	77.3
3-6-2	β Forged with inclusions	73.1	
3-6-3	β Forged no inclusions	72.9	75.3
3-6-4	β Forged no inclusions	77.7	

TABLE XL

FORGING AND HEAT TREATING PROCEDURE
Ti-6Al-6V-2Sn
"BETA FLECKED" MATERIAL

Serial Number	Preforming Temp. (°F)	Blocker Temp. (°F)	Finish Temp. (°F)	Heat Treatment
7-1 - 7-8	1650	1675	1675	1350°F (2 hours) Air Cool
7-9 - 7-16	1650	1850	1850	1350°F (2 hours) Air Cool
7-17 - 7-24	1500	1500	1500	1350°F (2 hours) Air Cool

TABLE XLI

TENSILE RESULTS
Ti-6Al-6V-2Sn ("BETA FLECKED") FORGINGS
ANNEALED 1350°F (2 HOURS) AIR COOLED
SEE FIGURE 69 FOR TEST LOCATIONS

Serial Number	Forging Procedure	0.2% Y.S. (KSI)	U.T.S. (KSI)	El.%	R.A.%	NTS	NTS/UTS
7-1-17	A	132.4	146.4	14.5	43.1	219.5	1.50
7-1-15 7-6-3		145.8	159.8	16.0	45.0	233.0	1.47
7-6-5 7-6-4		143.8	157.2	17.0	44.4	235.4	1.49
7-6-6 7-6-9		136.8	153.2	14.0	37.6	231.0	1.51
7-6-8 7-7-13 7-7-11		130.0	143.4	15.0	40.1	231.0	1.61
7-9-17	B	134.0	151.4	10.0	25.1	221.0	1.47
7-9-15 7-14-3		137.4	155.8	13.0	29.2	202.3	1.30
7-14-5 7-14-4		136.4	154.2	12.0	25.9	223.4	1.45
7-14-6 7-14-9		136.0	153.4	11.0	23.1	224.2	1.46
7-14-8 7-15-13 7-15-11		135.0	151.8	12.5	25.1	225.0	1.48
7-17-17	C	136.6	147.0	17.5	53.4	228.8	1.55
7-17-15 7-22-3		144.8	153.4	16.5	50.7	229.0	1.49
7-22-5 7-22-4		144.4	152.4	17.0	49.0	227.4	1.49
7-22-6 7-22-9		143.6	152.2	17.0	49.5	225.0	1.48
7-22-8 7-23-13 7-23-11		136.6	148.2	16.0	52.9	219.0	1.48

Forging Procedures

	Draw (°F)	Block (°F)	Finish (°F)	
A	1650	1675	1675	(Standard
B	1650	1850	1850	(Beta)
C	1500	1500	1500	(Very Low Alpha Bc

TABLE XLII

FRACTURE TOUGHNESS DATA - PHASE II
"BETA FLECKED" Ti-6Al-6V-2Sn
ANNEALED 1350°F (2 HOURS) A.C.

Serial Number	Condition	K_{IC} (KSI $\sqrt{in}$)	Average K_{IC}
7-6-1	Standard αβ forged (1675°F)	74.5	75.2
7-6-2	Standard αβ forged (1675°F)	79.3	
7-7-3	Standard αβ forged (1675°F)	72.1	
7-14-1	β forged (1850°F)	73.9	74.1
7-14-2	β forged (1850°F)	73.8	
7-15-3	β forged (1850°F)	74.7	
7-22-1	Very low αβ forged (1500°F)	58.1	56.3
7-22-2	Very low αβ forged (1500°F)	55.2	
7-23-3	Very low αβ forged (1500°F)	55.7	

TABLE XLIII

HIGH CYCLE FATIGUE
Ti-6Al-6V-2Sn
"BETA FLECKED" MATERIAL
ANNEALED 1350°F(2) A.C.

	Cycles							
	Smooth Bar				Notched Bar K_t = 3.0			
Forge Practice	10^4	10^5	10^6	10^7	10^4	10^5	10^6	10^7
Standard Forge α+β (A)	139	93	85	84	66	37	32	30
β Forge (B)	134	94	86	85	60	42	41	40
Low α+β Forge (C)	130	109	93	89	5C	43	40	39

TABLE XLIV

LCF PROPERTIES OF Ti-6Al-6V-2Sn

AIR FRAME PART (BETA FLECKED MATERIAL)

Ti-662	Standard forge	4.7	9.5	Beta flecks observed
Ti-662	Beta forge	4.2	7.0	No beta flecks observed
Ti-662	Low alpha-beta forge	9.1	17.0	No beta flecks observed

APPENDIX A

TEST SPECIMEN DRAWINGS

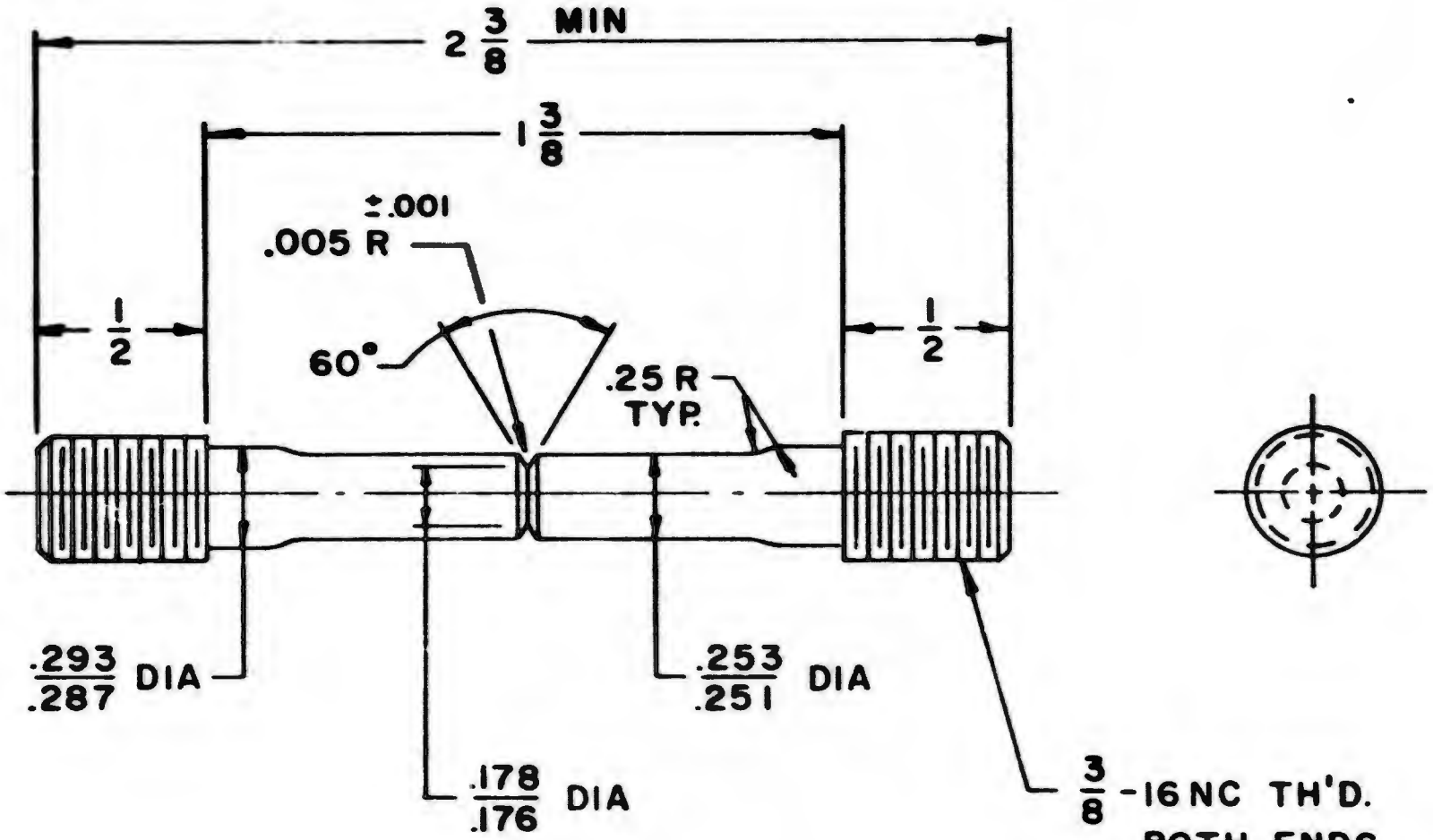

89T

NOTCHED TENSILE
TEST SPECIMEN WITH "V" GROOVE
$K_t = 3.9$

FRACTURE TOUGHNESS SPECIMEN

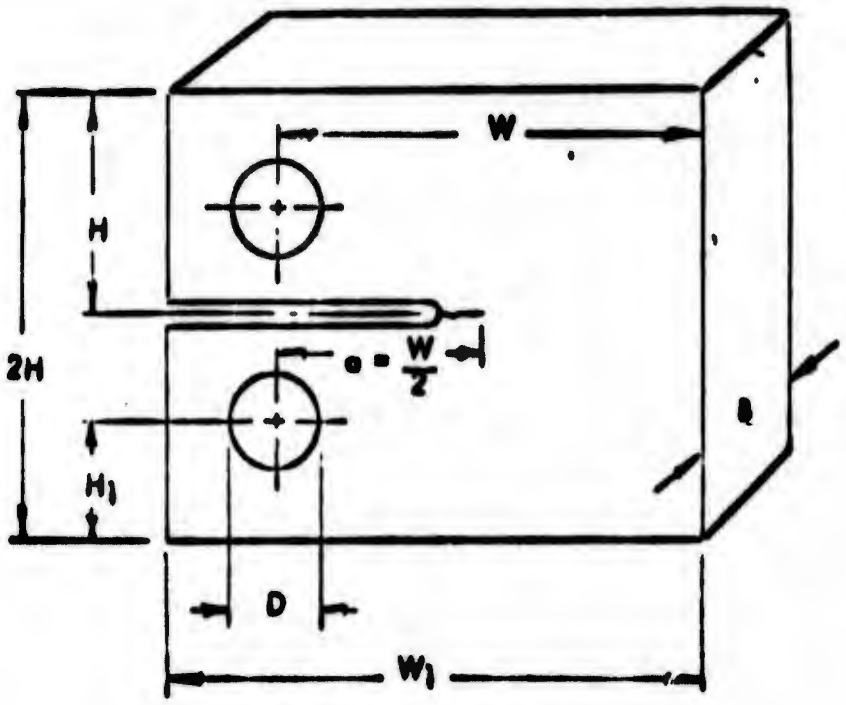

W = 2.08 D = 0.58

a = 1.08 W_1 = 2.58

H = 1.28 H_1 0.658

Type	Estimated Measurement Capacity* K_{Ic}/σ_{ys}	Estimated Measurement Capacity* $(K_{Ic}/\sigma_{ys})^2$	Tentative Overall Dimensions Thickness (in.)	Height (in.)	Width (in.)
1T-CT	0.63	0.40	1	2.4	2.5
2T-CT	0.90	0.80	2	4.8	5.0
3T-CT	1.10	1.20	3	7.2	7.5
4T-CT	1.30	1.60	4	9.6	10.0
6T-CT	1.60	2.40	6	14.4	15.0
8T-CT	1.80	3.20	8	19.2	20.0
10T-CT	2.00	4.00	10	24.0	25.0
12T-CT	2.20	4.80	12	28.8	30.0

*Based on currently suggested ASTM E-24 minimum size criterion, a and B $\geq 2.5 (K_{Ic}/\sigma_{ys})^2$

General configuration, proportions and measurement capacities of compact tension specimens for K_{Ic} fracture toughness measurement.

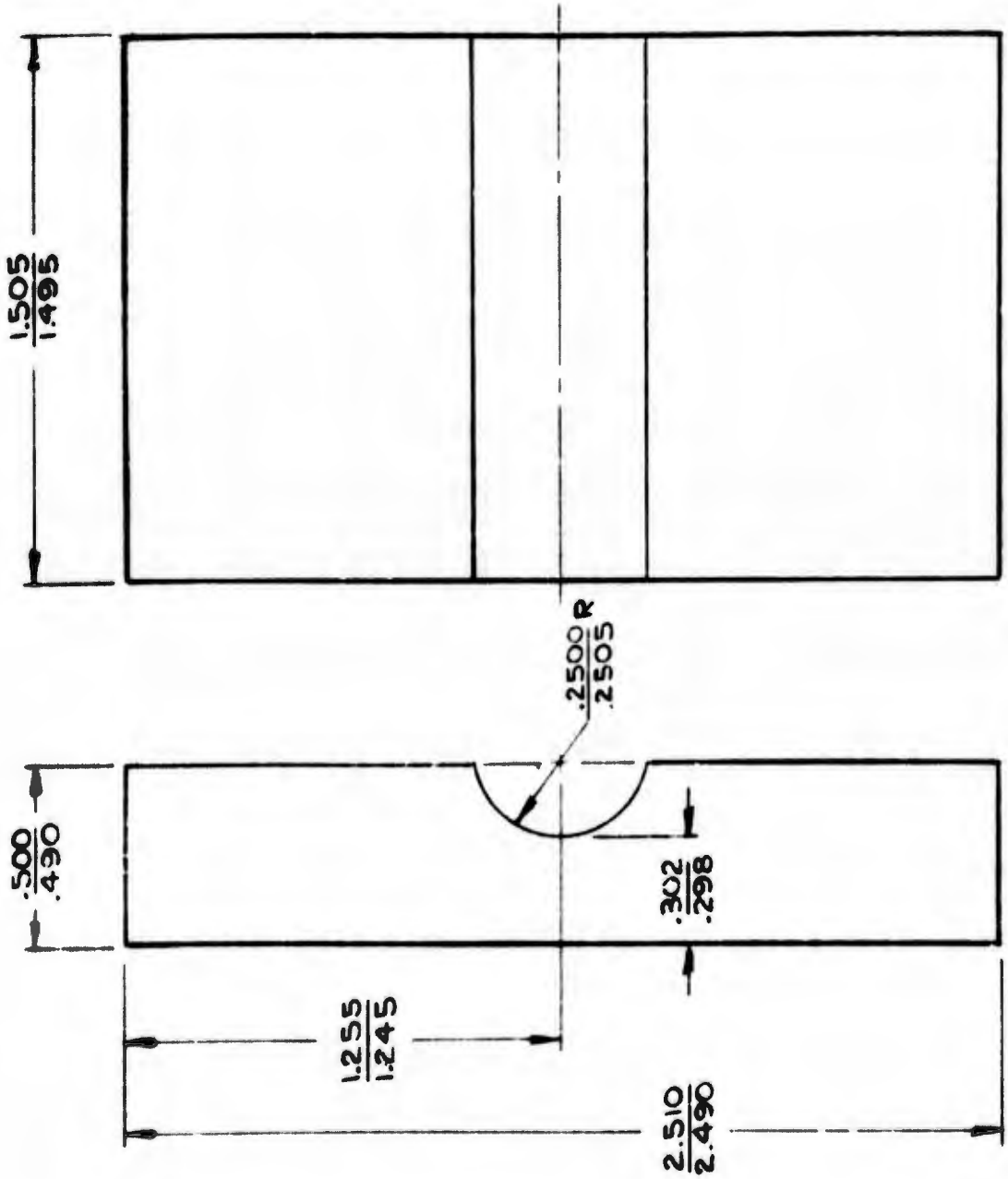

BOLT HOLE BENDING SPECIMEN

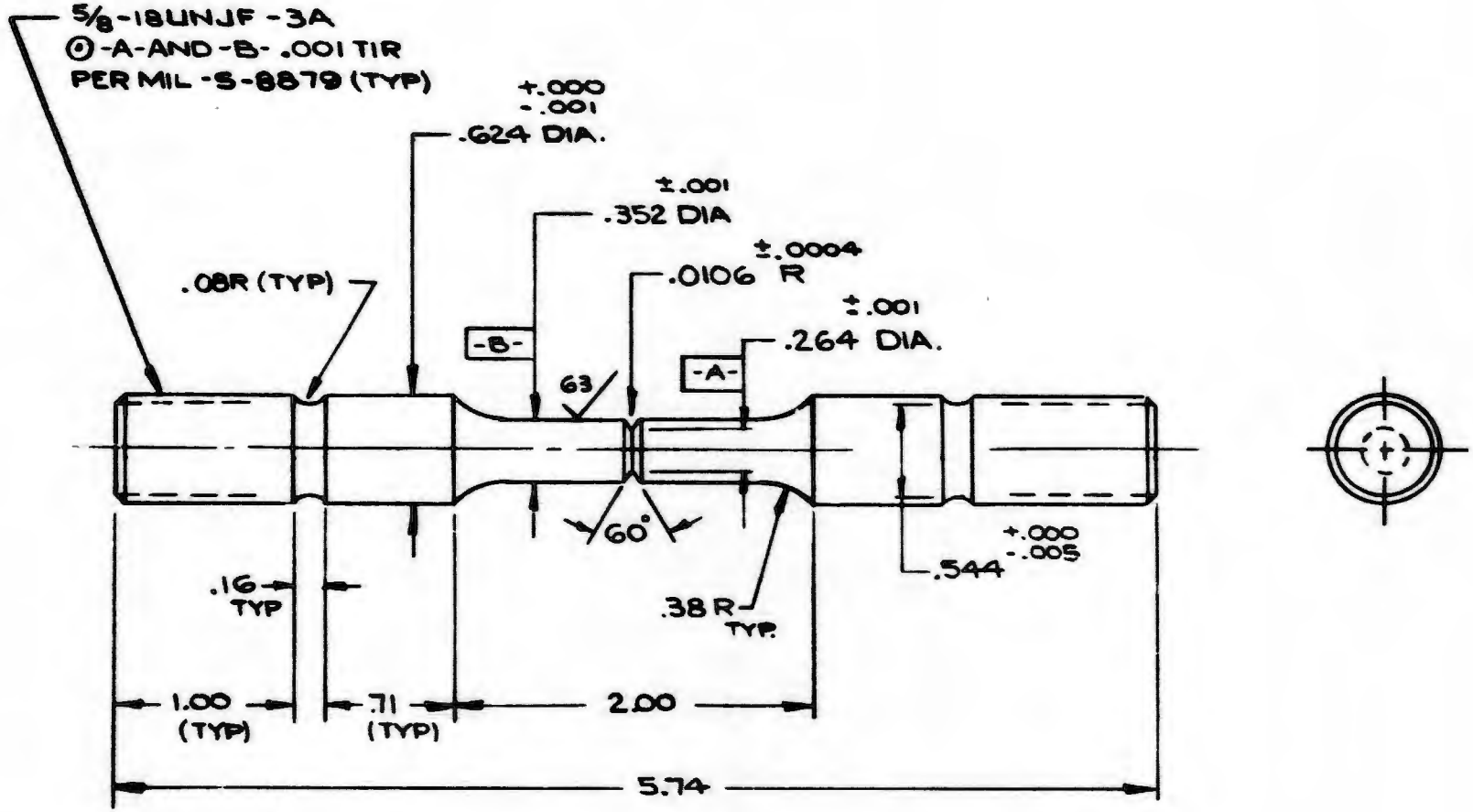

$K_t = 3.00$

NOTCHED HIGH CYCLE FATIGUE

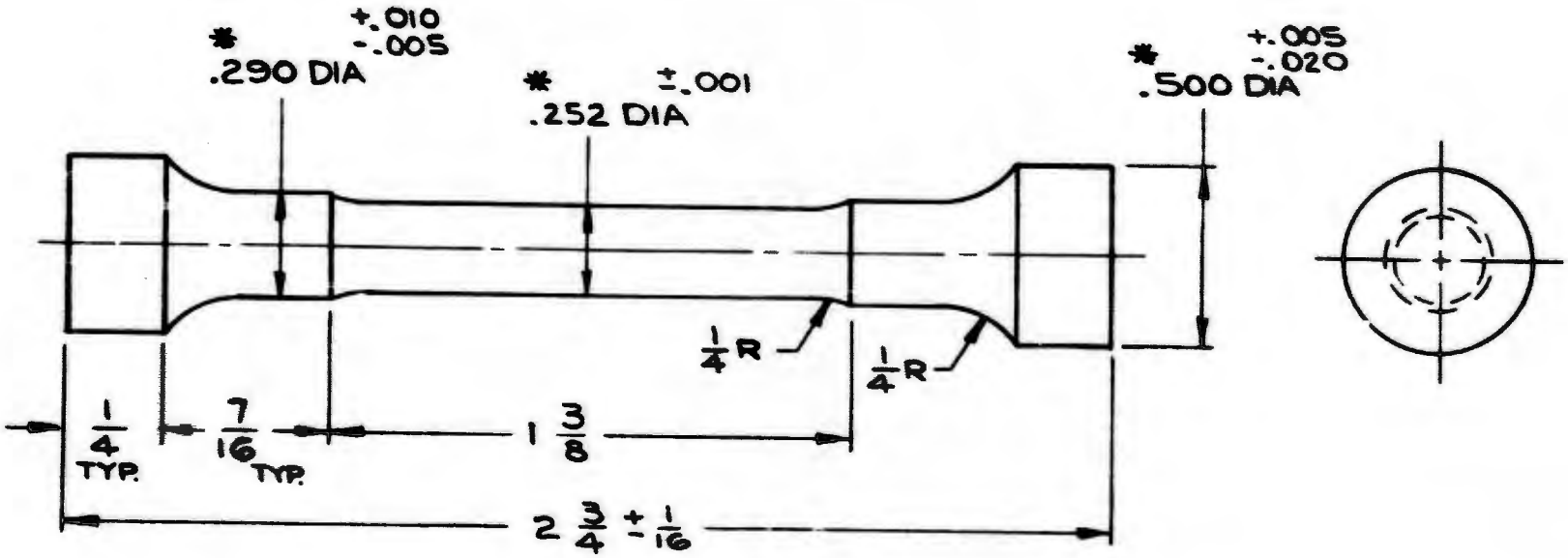

* TOLERANCE TO ACCOMODATE CRUSH WEAR

LABORATORY
.252 BUTTON HEAD
TENSILE SPECIMEN

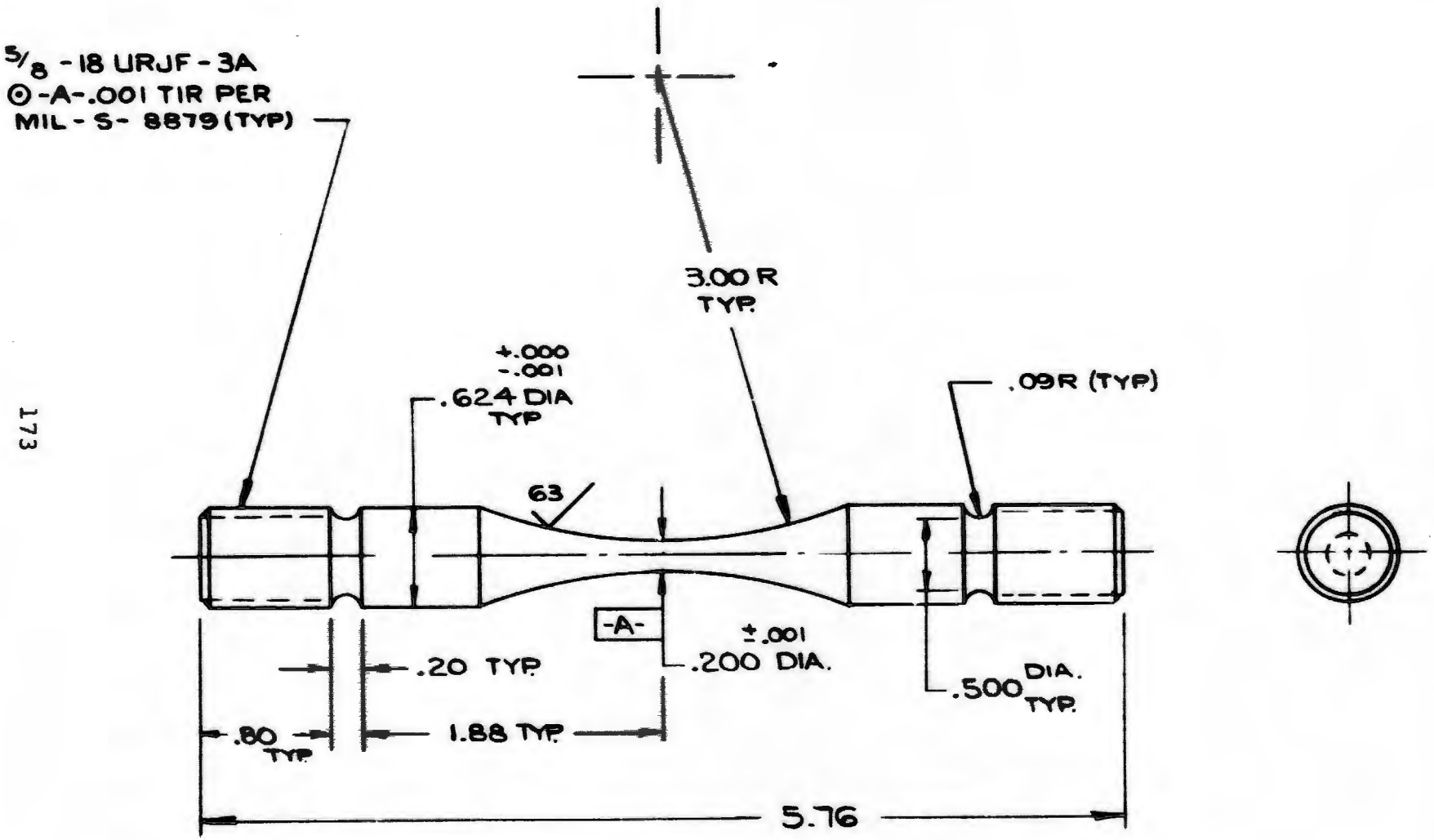

$K_t = 1.01$

SMOOTH HIGH CYCLE FATIGUE

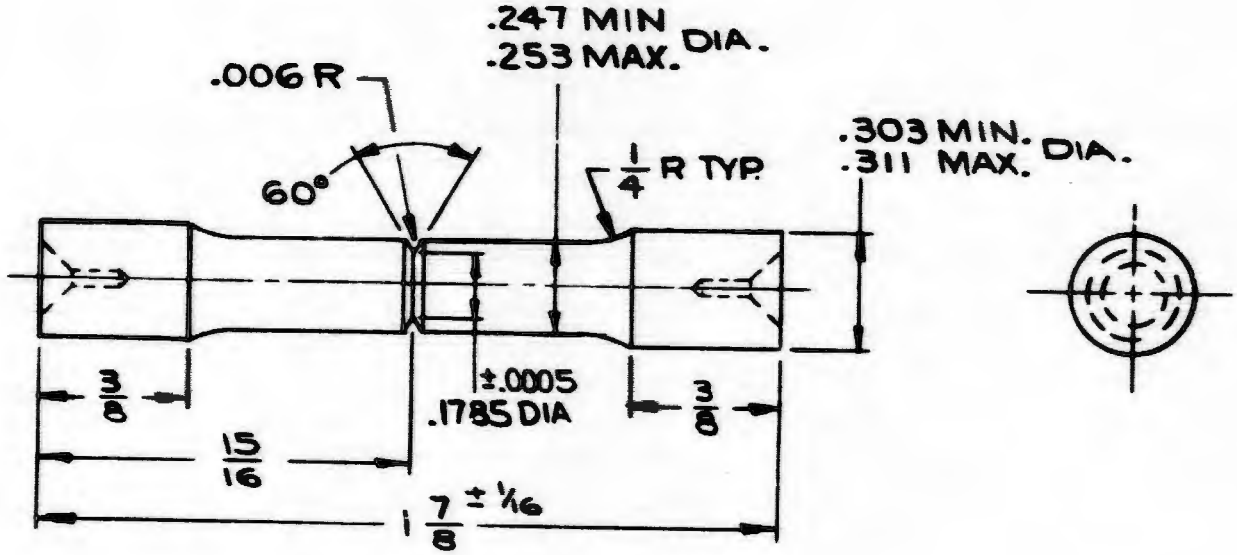

LABORATORY
STRESS RUPTURE
TEST SPECIMEN WITH "V" GROOVE

APPENDIX B

STULEN FATIGUE SPECIMEN MACHINING PROCEDURE

STULEN MACHINE COMPANY

Low Stress Grinding Methods

used in the

Preparation of Titanium Test Specimens

1. Saw to length, face and countersink, and identify.

2. These specimens are machined in three cuts to .015 over final diameter.

3. Threaded specimens - shoulders are finished round.
Fatigue specimens - shoulders are rough ground to .005.

4. Fatigue specimens are contour ground with a rough grind of .003. Grinder speed 3400 rpm, head stock speed 650 rpm, hydraulic horizontal feed 1" per 3 minutes. Grinding wheel used, GC-120-P5 VE wheel - 4" diameter. Coolant is Veedol Afton 8 supplied by Getty Oil Company.

5. Second contour grind is .002, procedure the same as Item 4.

6. Third contour grind is .002, procedure the same as Item 4.

7. The specimen is left .001 oversize for final polishing which is commercial 400 grit. The final two polishes applied to the final polishing of the specimen is a Stulen Machine Company procedure which cannot be disclosed.

8. Grinding wheel used is A80-V2-BT 4" Diameter.
Notch grinding in Feed -.0001 to .0002 in/Rev. + Spark out.

APPENDIX C

PRATT AND WHITNEY AIRCRAFT REPORT ON LOW CYCLE FATIGUE

PHASE I

Summary of Low Cycle Fatigue Testing of Titanium Alloy Forgings

As Part of AF Contract F33615-71-C-1560

Submitted to:

Wyman Gordon Company

Mr. R. B. Sparks

Prepared By:

D. L. Ruckle and M. P. Smith

1 September 1973

I. Introduction

The Pratt and Whitney Aircraft Division of United Aircraft Corporation was a subcontractor to the Wyman Gordon Company to perform low cycle fatigue testing of over 300 specimens from the Ti-6Al-4V, Ti-6Al-6V-2Sn and Ti-6Al-2Sn-4Zr-6Mo alloys. There were 23 groups of Ti-6Al-4V (Ti-64) specimens, 22 groups of Ti-6Al-6V-2Sn (Ti-662) and 11 groups of Ti-6Al-2Sn-4Zr-6Mo (Ti-6246) in Phase I. In Phase II, 40 specimens were tested representing three groups of Ti-662 and four groups of Ti-64.

The fully machined specimens were of the "half-bolthole" type which were tested in strain controlled bending as described in Section II. These specimens have been found to be very sensitive in distinguishing the low cycle fatigue capability of various microstructures and processing conditions.

Metallographic examination of crack initiation and propagation modes and statistical analysis of test data were supplied.

II. Method of Procedure

A. Testing

Six specimens of each group were received from the prime contractor. Five from each group were tested as required by the contract and the extra specimen was reserved for selective testing as deemed necessary by the subcontractor. Four specimens of each group were run with the surface in the "as-machined" condition and inspected at periodic intervals to determine lives to pinpoint indication and 1/32" crack. One of the four specimens was replicated with an acetate tape to verify the cyclic life range to pinpoint crack as determined by "Wink Zyglo" technique for the remaining three as-machined specimens. The fifth specimen of each group was electropolished and etched prior to testing and was replicated at periodic intervals to determine the mode of

crack initiation and growth. Specimen details, inspection intervals and the electropolishing technique are given in Appendix I.

Specimens were tested in a bending mode at 12 cpm over a total strain range of 0-0.9% for Ti-64 and 0-1.1% for Ti-662 and Ti-6246. Subsequent to completion of testing, all specimens were spot polished to verify that the microstructure was correct and, when required by variations in results, micros were made for more intensive analysis.

B. Data Analysis

Raw fatigue data (please refer to Tables IV through VI) were analyzed by the Weibull method of statistical analysis (Tables I, II and III) which is useful in evaluating alternate materials, microstructures or fabrication methods. It should, however, be realized that the number of specimens in this study, for each variable tested, is inadequate to fully define the scatter band and allow design minimums to be established. For a small sample of a true population, the median life which is determined is only an estimate of the true rank of the specimens tested. The median life (B50 life) was used in this study for the life comparisons shown in Figures 2 through 5. This procedure was previously utilized in LCF comparisons of various titanium microstructures in another AFML contract[1].

III. Summary and Conclusions

The following conclusions were reached after evaluation of the Phase I test results. (Refer to Section IV for Discussion.)

A. Crack initiation in three alloys investigated occurred at alpha phase/matrix interfaces, or, if coarse elongated primary alpha was present, across slip bands in the alpha. Crack growth occurred preferentially along the alpha phase interfaces.

B. Macro-grain size is less significant than microstructure in determining LCF life of the three alloys.

C. Scatter in test results was related to the amount of plastic strain applied during bending. The amount of scatter decreased as plastic strain increased.

D. Specimens which were all beta processed had the lowest fatigue lives in each alloy with the exception of the quenched and annealed Ti-64 group "S" which had a very high median fatigue life.

E. The presence of coarse elongated "spaghetti" alpha lowered fatigue life severely in alpha-beta processed Ti-64 and Ti-662 alloys.

F. The presence of grain boundary alpha in alpha-beta processed Ti-64 and Ti-662 resulted in good LCF life for the former alloy and a slight reduction in LCF life for the latter; consequently no firm LCF life correlation with the presence of grain boundary alpha alone is apparent from this study.

G. In Ti-6246, for alpha-beta forgings, the fatigue life was higher at the 50% primary alpha level compared to the 10-20% primary alpha level, while in Ti-64 and Ti-662 the reverse was true. This is probably related to the smaller average alpha particle size and absence of resolvable matrix alpha in Ti-6246 for the 50% primary alpha condition compared to similar conditions for the other alloys.

H. Thermomechanical treatment (TMT) consisting of beta upsetting or blocking followed by alpha-beta finishing had a strong effect on fatigue life in Ti-64 and Ti-6246, but had little or no effect in Ti-662. The LCF properties obtained could not be explained microstructurally. In general, higher alpha-beta finish temperature and a low amount of finish reduction gave the best lives.

I. In general, for Ti-64 and Ti-6246, annealing after forging gave better life than the STOA treatment. In Ti-662, the STOA treatment gave slight advantage over annealing.

IV. Results and Discussion

Microexamination of replicas from electropolished and etched specimens revealed that crack initiation occurred at the interfaces of the alpha phase and the matrix microstructure in all alloys (Figure 1). The cracks tended to propagate preferentially along the alpha phase/matrix interface in most conditions. However, when coarse and/or elongated primary alpha phase was present, the advancing crack would also propagate across slip bands in the alpha. This latter behavior is especially prevalent in Groups D, E and F in Ti-64 and Ti-662 which contained the "spaghetti" alpha phase. These results verify previous studies conducted by Wells and Sullivan[2] and others[3, 8] have similar crack initiation behavior was observed in Ti-64.

Phase I, Task A

The effect of billet macro-grain size on the fatigue lives of the three alloys was not great (Figure 2). There was a slight trend to increased fatigue life with the finer grain size specimens, although microstructural variables appeared to affect the fatigue behavior more strongly. For example, in the Ti-662 alloy, the microstructures of the coarse and fine macrostructure groups were very similar as were the median lives of the two groups, although the fine grain size had a very slight advantage in median life over the coarse grain size group. Conversely, in the Ti-6246 alloy, the coarse macro-grain size group had a decided fatigue life increase over those specimens from fine grain material. In this alloy, the microstructural examination revealed that the fine grain size material contained resolvable secondary platelet alpha and a lower primary alpha content than coarse grain size material. Similar fatigue behavior was reported in an AFML study[1] which revealed that the presence of resolvable alpha caused a reduction

in fatigue life in Ti-6246 and that increased primary alpha content resulting in a fine non-resolvable matrix promoted good fatigue life.

In the Ti-64 alloy, three specimen groups representing fine, intermediate and coarse billet grain size were tested. Test results (Figure 2) showed that the intermediate grain size specimens had nearly a 3:1 increase in median life over the coarse grain size specimens while the fine grain size specimens showed only a slight life increase over the coarse. The basic microstructures of the three groups were similar, but considerable scatter in data was encountered in the intermediate and fine grain size groups. Careful metallographic examination of the individual specimens revealed that the scatter in the fine grain size material could be explained by the presence of microstructural inhomogeneity in the form of beta banding or "beta flecked" areas in most specimens. The beta structure present would tend to lower LCF capability in general. The scatter in lives of the intermediate grain size group specimens, particularly in two with very long lives, could not be explained metallographically. It is thus unclear whether the resultant large increase for intermediate grain size Ti-64 is real or a result of some unknown variable. No other correlation such as differences in strength, ductility or toughness with fatigue lives measured was apparent.

In general, scatter was more severe in the Ti-64 alloy than the other two alloys studied. The Ti-64 alloy is considered a lower strength material than Ti-662 or Ti-6246 thus testing was carried out at a strain range of 0-0.9% while the Ti-6246 and Ti-662 alloys were cycled at 0-1.1%. This was in order to equalize the amount of plastic strain applied during testing of the three alloys. Previous experience in testing of compressor disk forgings has shown that nearly equivalent plastic strains were achieved by using the above strain ranges for

the subject alloys. In the current study, the strength differential between Ti-64 and the other alloys, especially Ti-662, was not as large as is normally expected. Therefore, the relative plastic strain was significantly less in Ti-64 than the other alloys resulting in a test where conditions approached those of high cycle fatigue and thus were more dependent on external variables such as surface finish. The median plastic strain in each alloy was measured from the lowest yield strength stress-strain curve for each condition and Weibull analysis for the data. The median plastic strain was 0.28% for Ti-64, 0.35% for Ti-6246 and 0.41% for Ti-662. The amount of scatter during testing of each alloy was high for Ti-64, moderate for Ti-6246 and low for Ti-662. Thus, the amount of scatter in LCF test results for each alloy appears to be related to the plastic strain applied.

Phase I, Task B

With one exception, the all-beta processed specimens had lower fatigue lives than alpha-beta groups in all three alloys (Figures 3, 4 and 5). This LCF debit due to beta processing agrees with the results in a previous study by Sattar etal[3] where the lowered LCF crack resistance was attributed to coarse elongated alpha and retained beta platelets. The annealed fine alpha platelet microstructure (water quenched condition S in Ti-64) exhibited a very high fatigue capability however. This behavior has also previously been reported by Lucas[5] and Henricks[6].

In alpha-beta processed specimen groups, the presence of coarse elongated "spaghetti" alpha phase drastically lowered LCF life of the Ti-64 and Ti-662 alloys. (This condition was not tested in Ti-6246.) The resulting lives obtained were essentially equivalent to those for all beta processed specimens discussed above (Figures 3 and 4). The coarse alpha phase nucleated cracks readily and served as a rapid path for propagation and growth. This behavior

has been confirmed in previous work in this laboratory and reported by Sprague etal[4].

The presence of grain boundary alpha in alpha-beta processed Ti-64 and Ti-662 groups did not give consistent results. In the Ti-64 alloy, the specimens with the grain boundary alpha phase had high median lives for all heat treatments; while the Ti-662 specimen groups processed to contain the grain boundary phase had low lives equal to the Ti-662 "spaghetti" containing groups. This behavior cannot be explained, although considerably more scatter existed in Ti-64 where specimens tended to have either very high or very low lives. This may have resulted from the differences in plastic strain during testing previously discussed. The grain boundary alpha phase was not completely continuous in either alloy and there was approximately 10-15% blocky alpha in a very fine matrix.

The percent equiaxed primary alpha in the alpha-beta processed specimens affected the LCF life of all alloys. In Ti-6246, specimens with 50% primary alpha and no optically resolvable secondary platelet alpha had higher lives than specimens containing 10-20% primary alpha and resolvable platelet alpha. This agrees with previous data reported by Ruckle and Smith[1] where the presence of coarse platelet alpha developed during cooling appeared to decrease LCF life compared to that of structures with a very fine alpha matrix. In Ti-64 and Ti-662 the microstructure containing 50% primary alpha had lower lives than microstructures containing 10-20% primary alpha. This may be related to the larger alpha particle size observed for Ti-64 and Ti-662 specimens containing 50% primary alpha compared to those for Ti-6246.

Thermomechanical treatment (TMT) in the form of beta upsetting or blocking following by alpha-beta finishing in the temperature region of the alpha plus beta two-phase field had a strong effect on the fatigue life of the Ti-64 and

Ti-624C alloys. TMT of the Ti-662 alloy did not improve its fatigue behavior and in most cases for Ti-662 lives of the TMT groups were equivalent to those of all-beta processed groups and below those of the alpha-beta processed groups with equiaxed primary alpha. This is in contrast to the results for Ti-64 and Ti-6246 alloys where certain of the TMT groups had better fatigue lives than the normally acceptable equiaxed alpha groups.

In Ti-6246, TMT groups C and D which were given a high temperature alpha-beta finish (1725°F) reduction had an approximately 2:1 increase in median LCF life over TMT groups E and F finished at a lower temperature (1625°F) or alpha-beta blocked and finished group A which contained resolvable matrix alpha platelets. Alpha-beta groups B and B-1 which did not contain coarse alpha matrix platelets were, however, superior to all other Ti-6246 conditions. TMT groups with small (10%) finish reductions were superior to those with large (30%) finish reductions. Quantitative metallography reported by Wyman Gordon (Tables 18, 19 Draft Report) revealed that the Ti-6246 TMT specimens with 30% reduction had an alpha particle with a much higher aspect (length/width) ratio than those with only 10% reduction. This may be related to the LCF capability of the TMT materials since alpha morphology in general appears to be related to LCF, however, the structural complexity of TMT Ti-6246 precludes firm conclusions based on the available data. The differences in LCF capability observed could not be related strongly to other mechanical properties such as yield strength, ductility of fracture toughness. The Ti-64 alloy responded strongly to the TMT schedules used, particularly in the annealed condition (Figure 5). As in Ti-6246, the lower finish reductions resulted in higher lives. (STOA treating after processing equalized lives for the two amounts of finish reduction.) The smaller finish reductions again resulted in a lower aspect ratio alpha particle as reported by Wyman Gordon (Draft Report, Table 20). Henricks[6] has previously reported that certain TMT processing followed

by annealing increased the LCF life of AMS 4928, although no explanation of the phenomenom was offered.

Based on microstructural evaluation the reason for the increased fatigue capability cannot be explained. Apparently, the LCF behavior of TMT forgings is highly sensitive to amount and temperature of reduction, cooling rate, post-forge heat treatment and resulting alpha phase/matrix morphology. Although the high fatigue life capability of some of the TMT forgings is of interest, it is unfortunate that normally determined mechanical properties and microstructure appear to be insufficient to distinguish the LCF capability resulting from slight process variations. Further study of process reproduciblity and structural characteristics of TMT forgings appears to be justified.

In Ti-64 and Ti-6246, there was a strong trend for greatly improved fatigue life in forgings which were annealed only as opposed to those which were STOA after forging. (Except for spaghetti alpha specimens and slow cooled all beta specimens.) However, in Ti-64, with normal oxygen content, conditions C and P did not fit this general pattern, but no apparent microstructural or other reasons for this could be detected.

References

1. D. L. Ruckle and M. P. Smith, "Development of Computerized Microstructure Control Procedure for Ti-6Al-2Sn-4Zr-6Mo Alloy Production Compressor Disks", AFML-TR-73-16, December 1972.
2. C. H. Wells and C. P. Sullivan, "Low Cycle Fatigue Crack Initiation in Ti-6Al-4V", Trans ASM, 62, 1969, p 263.
3. S. A. Sattar, D. H. Kellogg, H. J. Oberle and B. N. Green, "Low Cycle Fatigue of the Ti-6Al-4V Alloy", ASM Report System Paper D8-24.4, October 1968.
4. R. A. Sprague, D. L. Ruckle and M. P. Smith, "The Effect of Microstructure on the Low Cycle Fatigue Behavior of Ti-6Al-4V", Paper presented at Second International Conference on Titanium, May 2-5, 1972, Boston, Massachusetts.
5. J. J. Lucas, "Fatigue Strength Improvements in Ti-6Al-4V Forgings", Paper presented at Twenty-Seventh Annual National V/STOL Forum of the AWS, Washington, D.C., May 1971, Reprint No. 552.
6. R. J. Henricks, "Effect of High Temperature Thermomechanical Treatment on the Ti-6Al-4V Alloy", Paper presented to the AIME Spring Meeting, May 12-15, 1969, Pittsbrugh, Pennsylvania.
7. J. C. Williams, C. G. Rhodes, "Summary of Microstructural Characterization of Titanium Alloy Forgings", Draft Report Submitted to Wyman Gordon Company, August 1, 1973.
8. C. A. Stubbington, A. W. Bowen, "Some Observations on Stage I Crack Initiation in Ti-6Al-4V, and on the Synthesis of a High Fatigue Strength Microstructure in this Alloy", Royal Aircraft Establishment, TR 73036, May 1973.

A 250X

B 250X

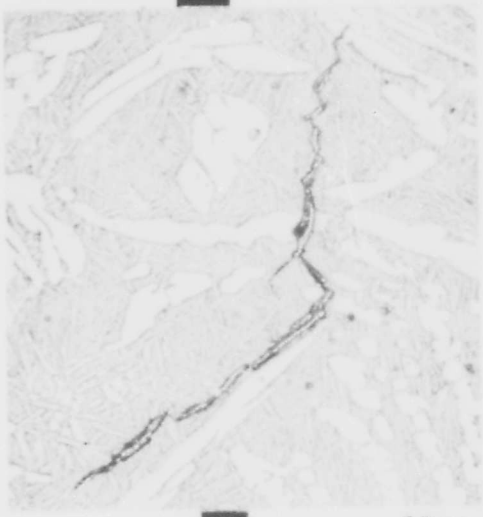

C 250X

D 500X

E 250X

F 500X

FIGURE 1

TYPICAL MODES OF CRACK INITIATION AND PROPAGATION IN TITANIUM ALLOYS.

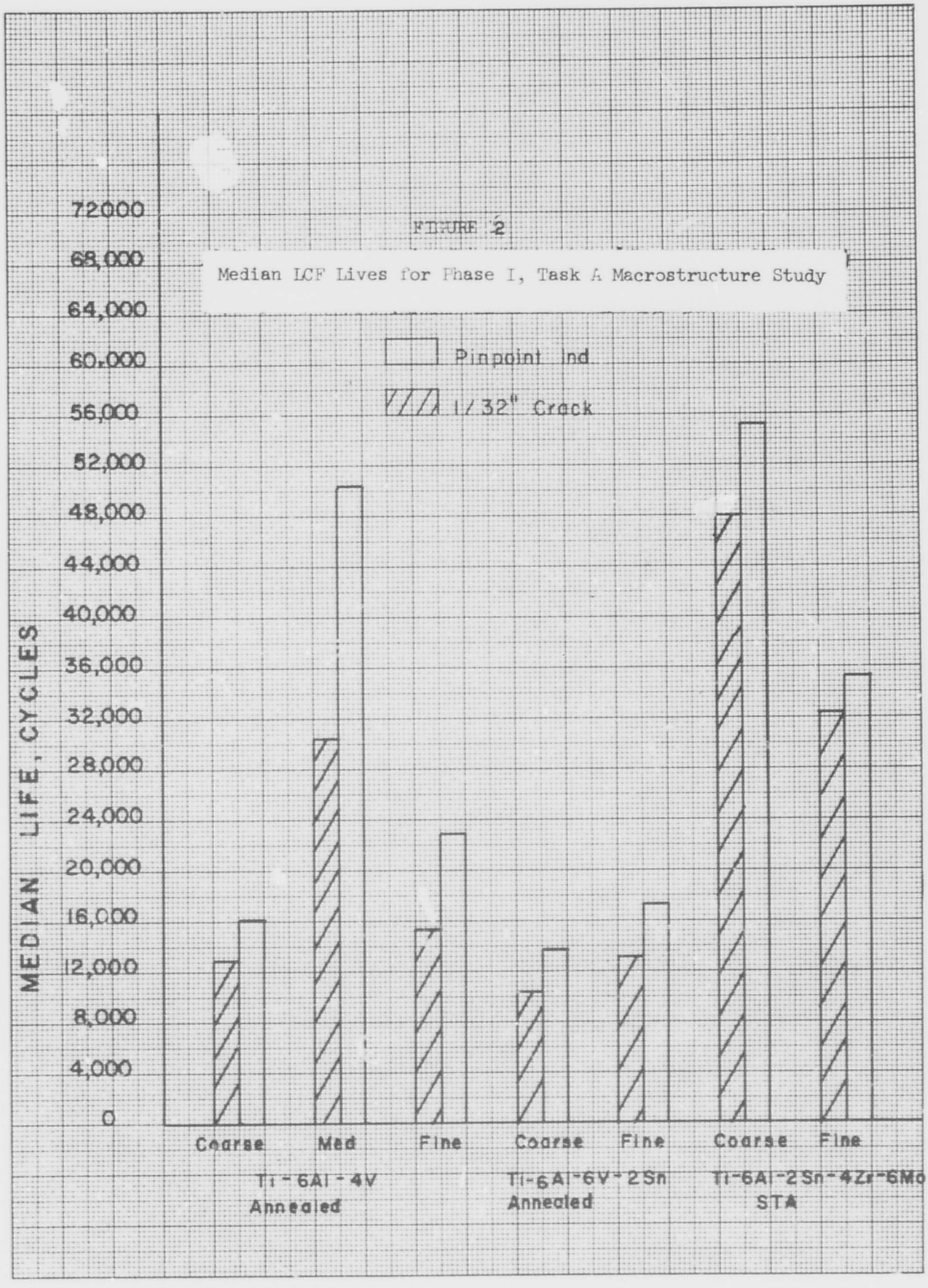

10 X 10 TO THE CM. SS—186

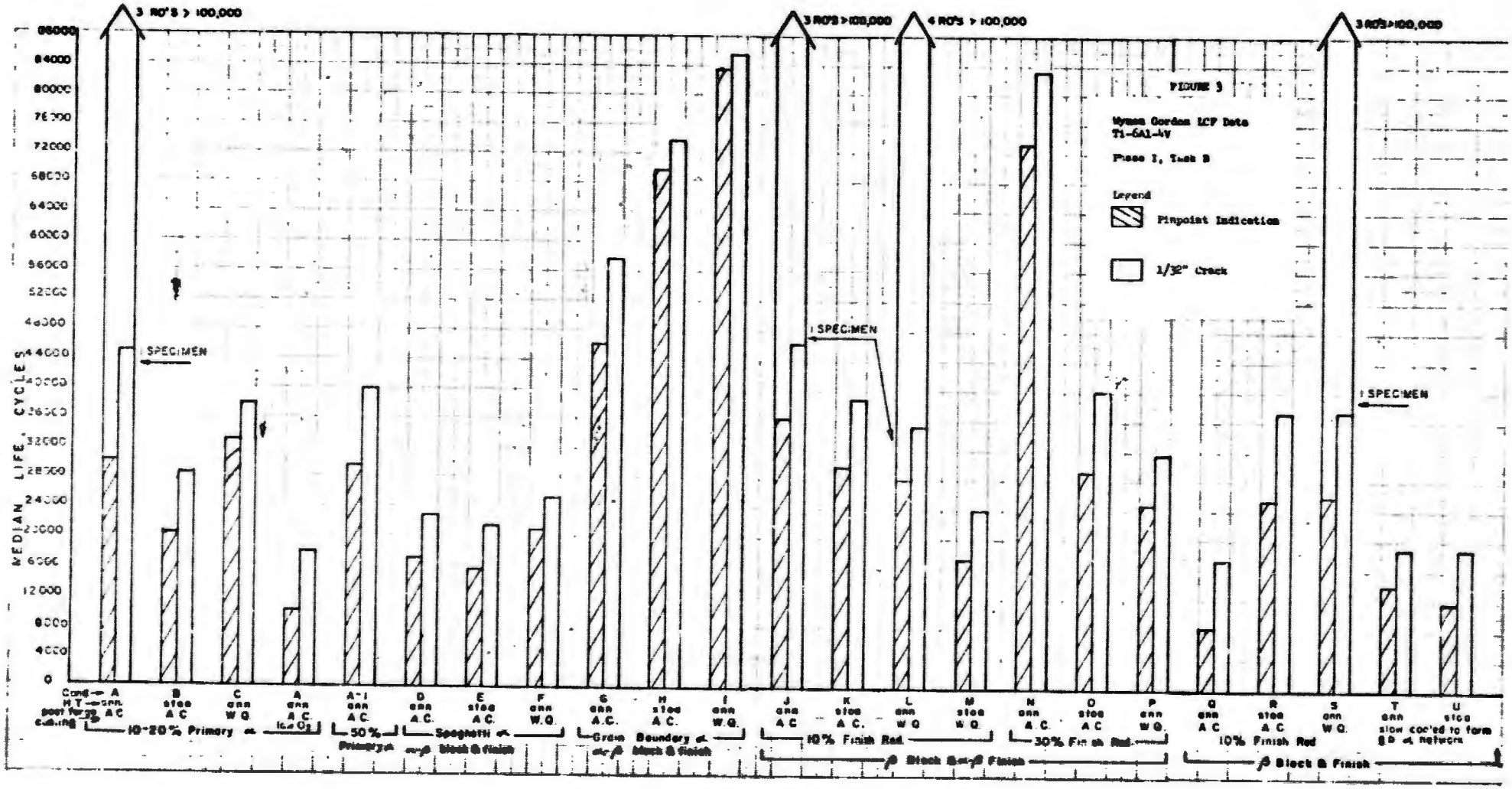
3 RO'S > 100,000
3 RO'S > 100,000
4 RO'S > 100,000
3 RO'S > 100,000
SPECIMEN
SPECIMEN
SPECIMEN
FIGURE 3
Wyman Gordon LCF Data
Ti-6Al-4V
Phase I, Task B
Legend
Pinpoint Indication
1/32" Crack
MEDIAN LIFE, CYCLES
88000
84000
80000
76000
72000
68000
64000
60000
56000
52000
48000
44000
40000
36000
32000
28000
24000
20000
16000
12000
8000
4000
0
Cond → A HT → ann. post forge AC cutting
B sta AC
C ann WQ
A ann AC
A-1 ann AC
D ann AC
E sta AC
F ann WQ
G ann AC
H sta AC
I ann WQ
J ann AC
K sta AC
L ann WQ
M sta WQ
N ann AC
O sta AC
P ann WQ
Q ann AC
R sta AC
S ann WQ
T ann
U sta
10-20% Primary
50% Primary
Spagnetti of β Block & finish
Grain Boundary α of β Block & Finish
10% Finish Rad.
β Block & β Finish
30% Finish Rad.
10% Finish Rad
β Block & Finish
slow cool to form β network

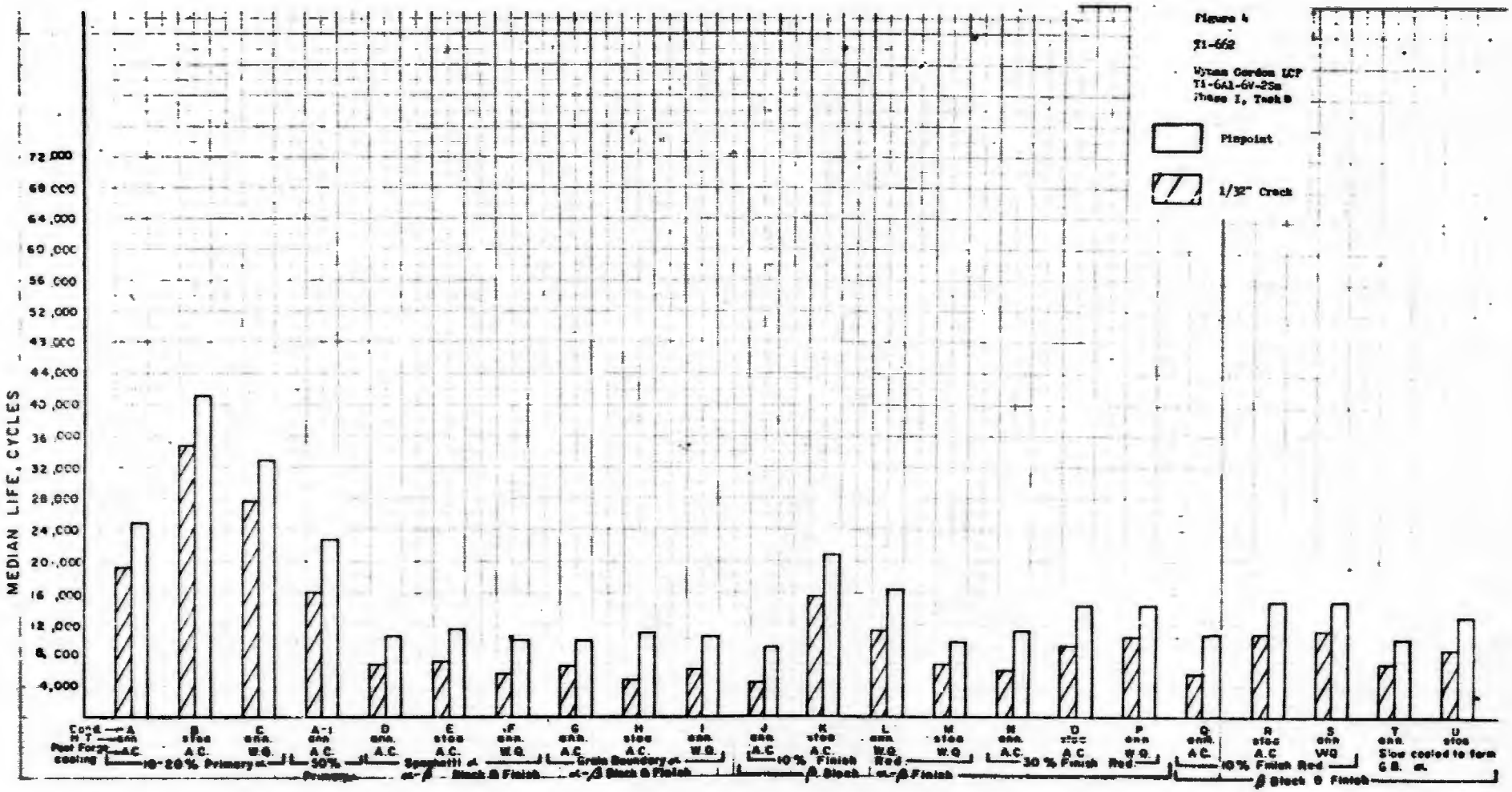
Figure 4
T1-662
Wyman Gordon UCP
Ti-6Al-6V-2Sn
Phase I, Task B
Pinpoint
1/32" Crack
MEDIAN LIFE, CYCLES
72,000
68,000
64,000
60,000
56,000
52,000
48,000
44,000
40,000
36,000
32,000
28,000
24,000
20,000
16,000
12,000
8,000
4,000
Cond. — A B C A-1 D E F G H I J K L M N O P Q R S T U
H T — sam stac sam sam sam stac sam sam stac sam sam stac sam sam stac sam sam stac sam sam stac sam sam stac
Post Forge — A.C. A.C. W.Q. A.C. A.C. A.C. W.Q. A.C. A.C. W.Q. A.C A.C W.Q. W.Q A.C. A.C A.C W.Q. A.C. A.C A.C W.Q A.C. Slow cooled to form
cooling
10-20 % Primary α
50% Primary α
Spaghetti α
Grain Boundary α
10 % Finish
30 % Finish
10% Finish
β Finish
β Block & Finish
β Block
β Block & Finish

FIGURE 5

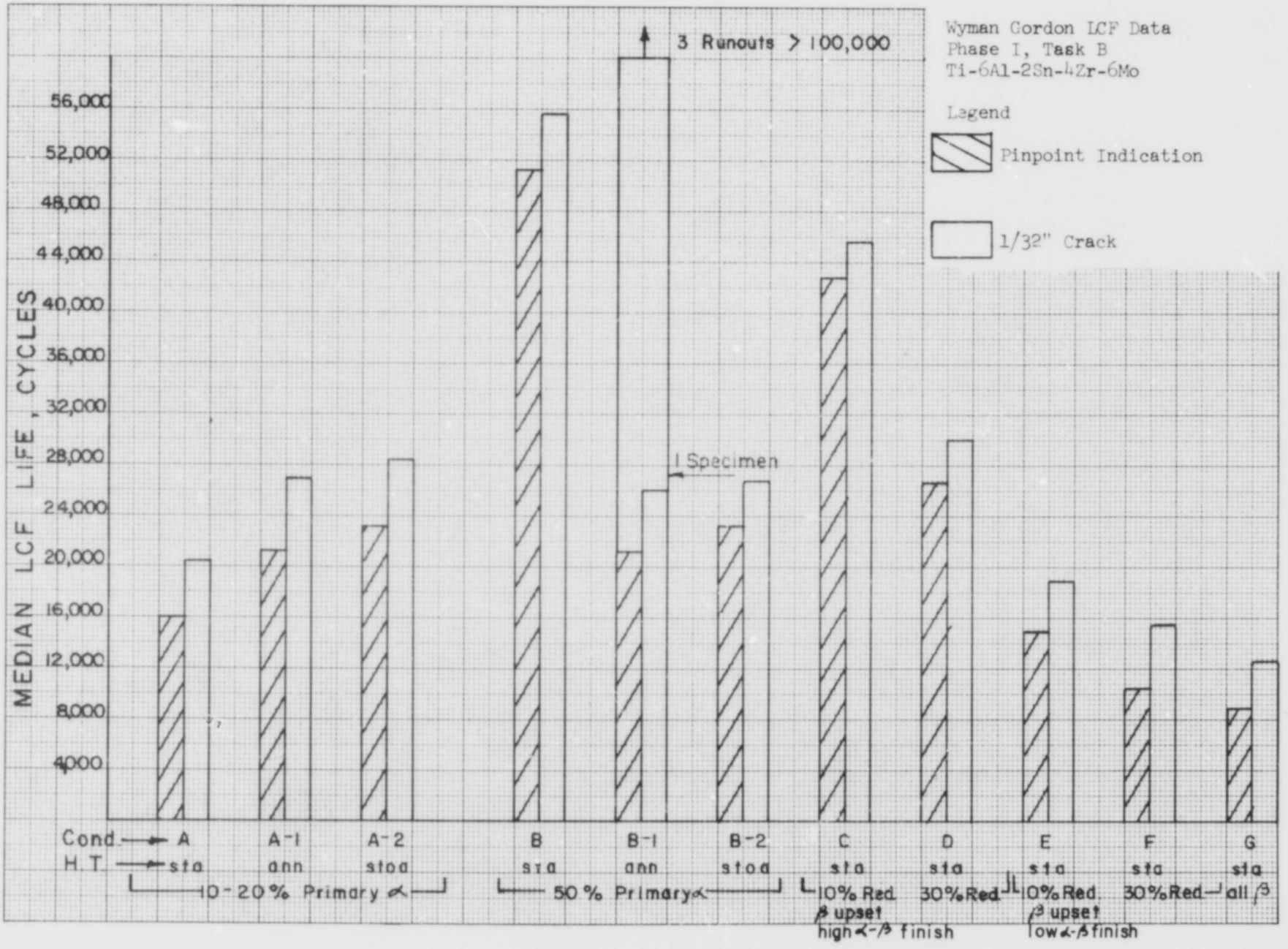

TABLE I

Median Low Cycle Fatigue Lives
For All Alloys With Various Billet Grain Size[1]

Phase I, Task A

Alloy	Condition	Grain Size	Cycles To Pinpoint x 10^{-3}	Cycles To 1/32" Crack x 10^{-3}	Remarks
Ti-64	A	Coarse	12.5	16.0	
	A	Intermediate	30.0	50.0	
	A	Fine	15.0	23.0	Banded microstructure
Ti-662	A	Coarse	10.0	13.5	
	A	Fine	13.0	17.0	
Ti-6246	A	Coarse	47.5	55.0	
	A	Fine	32.0	35.0	

[1] B50 Life Per Weibull Analysis

TABLE II

Median Low Cycle Fatigue Lives
For Ti 6Al-4V and Ti 6Al-6V-2Sn(1)

Phase I, Task B

Ti 6Al-4V				Ti 6Al-6V-2Sn		
Cycles To Pinpoint x 10^{-3}	Cycles To 1/32" Crack x 10^{-3}	Remarks	Condition	Cycles To Pinpoint x 10^{-3}	Cycles To 1/32" Crack x 10^{-3}	Remarks
-	-	3 Runouts > 100.0	A	19.5	24.5	
10.0	17.6		A (Low O_2)	-	-	Not tested in Ti 662
29.7	39.8		A-1	16.0	23.0	
20.3	28.5		B	35.5	41.0	
33.1	38.7		C	27.6	32.3	
17.0	23.0		D	7.0	10.6	
15.4	21.3		E	7.1	11.6	
20.7	25.3		F	5.7	9.2	
46.2	57.6		G	6.4	9.4	
69.7	73.4		H	4.5	10.4	
83.3	85.5		I	6.0	10.4	
-	-	4 Runouts > 100.0	J	4.2	8.8	
29.0	38.9		K	15.7	20.8	
-	-	3 Runouts > 100.0	L	11.5	16.4	
17.0	23.9		M	6.7	9.8	
73.6	83.2		N	6.1	11.2	
29.0	40.0		O	8.8	14.5	
24.1	31.5		P	10.2	14.4	
8.3	17.0		Q	5.8	11.0	
25.1	36.9		R	10.6	14.8	
-	-	3 Runouts > 100.0	S	10.7	15.0	
14.4	18.8		T	6.7	10.0	
11.6	18.3		U	8.7	12.7	

(1) B_{50} Life Per Weibull Analysis

TABLE III

Median Low Cycle Fatigue Lives
For Ti 6Al-2Sn-4Zr-6Mo[1]

Phase I, Task B

Condition	Cycles To Pinpoint x 10^{-3}	Cycles to 1/32" Crack x 10^{-3}	Remarks
A	16.0	20.1	
A-1	21.0	26.7	
A-2	22.9	28.3	
B	51.0	55.1	
B-1	-	-	3 Runouts > 100.0
B-2	22.9	26.5	
C	42.5	45.1	
D	26.4	29.9	
E	15.1	18.7	
F	10.3	15.5	
G	8.7	12.6	

(1) B_{50} Life Per Weibull Analysis

TABLE IV

WYMAN-GORDON LOW CYCLE FATIGUE DATA
PHASE I, TASK A, AS MACHINED SPECIMENS

Alloy	Condition	Grain Size	Cycles to Pinpoint X 10^{-3}	Cycles to 1/32" Crack X 10^{3}	Remarks
Ti-64	A	Fine	5.0	8.0	Microstructural banding
			10.0	15.0	" "
			52.0	68.0	No Banding Detected
			> 24.0	-	Discontinued Test No Banding Detected
Ti-64	A	Intermediate	20.0	27.0	
			8.0	16.0	
			9.0	14.0	
			No Indication @ 80.0		
			No Indication @ 90.0		
Ti-64	A	Coarse	14.0	16.0	
			10.0	16.0	
			10.0	12.0	
			16.0	14.0	
Ti-662	A	Fine	12.0	14.0	
			12.0	18.0	
			14.0	18.0	
			13.0	18.0	
Ti-662	A	Coarse	10.0	13.0	Beta Flecks Detected
			10.0	13.0	No Beta Flecks
			9.0	13.0	No Beta Flecks
			10.0	14.0	No Beta Flecks
			No Indication @ 20.0		Discontinued Test - No Beta Flecks
Ti-6246	A	Fine	23.0	24.0	
			12.0	13.0	
			36.0	38.0	
			78.0	84.0	
Ti-6246	A	Coarse	26.0	30.0	
			52.0	56.0	
			81.0	86.0	
			36.0	46.0	

TABLE V

Ti-6Al-4V Cycles to Pinpoint X 10^{-3}	Ti-6Al-4V Cycles to 1/32" X 10^{-3}	Remarks	Condition	Ti-6Al-6V-2Sn Cycles to Pinpoint X 10^{-3}	Ti-6Al-6V-2Sn Cycles to 1/32" X 10^{-3}	Remarks
No Indications @ 25.0		Discontinued Test	A	10.0	15.0	
No Indications @ 101.0				25.0	30.0	
No Indications @ 52.0				20.0	26.0	
6.0	9.0	Invalid Test Edge Crack		24.0	27.0	
30.0	44.0					
22.0	33.0		A (Low O_2)	-	-	Not Tested for Ti-662
7.0	15.0					
10.0	17.0					
5.0	9.0					
25.0	35.0		A-1	18.0	21.0	
30.0	39.0			37.0	44.0	
31.0	40.0			9.0	13.0	
32.0	44.0			10.0	16.0	
19.0	27.0		B	38.0	44.0	
9.0	17.0			53.0	57.0	
59.0	66.0			20.0	24.0	
12.0	17.0			33.0	38.0	
12.0	18.0		C	21.0	24.0	
32.0	38.0			17.0	19.0	
32.0	41.0			34.0	45.0	
39.0	46.0			40.0	44.0	
21.0	26.0		D	8.0	15.0	
11.0	20.0			3.0	6.0	
20.0				9.0	11.0	
-	-	Specimen invalid due to slippage during test		8.0	15.0	
13.0	20.0		E	4.0	8.0	
12.0	17.0			6.0	10.0	
14.0	19.0			8.0	11.0	
23.0	29.0			11.0	18.0	
12.0	18.0		F	4.0	8.0	
19.0	23.0			5.0	8.0	
21.0	25.0			6.0	8.0	
32	35.0			8.0	13.0	

TABLE V (cont.)

Ti-6Al-4V Cycles to Pinpoint X 10^{-3}	Ti-6Al-4V Cycles to 1/32" X 10^{-3}	Ti-6Al-4V Remarks	Condition	Ti-6Al-6V-2Sn Cycles to Pinpoint X 10^{-3}	Ti-6Al-6V-2Sn Cycles to 1/32" X 10^{-3}	Ti-6Al-6V-2Sn Remarks
16.0	18.0		G	1.0	3.0	
17.0	24.0			6.0	8.0	
64.0	73.0			8.0	10.0	
No Indications @ 80.0				20.0	23.0	
No Indications @ 100.0						
45.0	50.0		H	3.0	9.0	
62.0	68.0			4.0	10.0	
74.0	79.0			5.0	11.0	
No Indications @ 80.0				6.0	11.0	
61.0	66.0		I	2.0	7.0	
74.0	83.0			5.0	8.0	
No Indications @ 77.0				7.0	11.0	
No Indications @ 80.0				13.0	16.0	
No Indications @ 90.0						
No Indications @ 100.0			J	[illegible].0	11.0	
No Indications @ 100.0				3.0	7.0	
No Indications @ 113.0				4.0	8.0	
36.0	46.0			4.0	9.0	
9.0	23.0	Invalid-Edge Crack				
10.0	19.0		K	20.0	25.0	
18.0	28.0			11.0	18.0	
46.0	51.0			16.0	19.0	
60.0	66.0			5.0	-	Edge Crack
No Indications @ 75.0			L	4.0	7.0	
No Indications @ 175.0				8.0	14.0	
No Indications @ 100.0				14.0	18.0	
No Indications @ 31.0				27.0	31.0	
28.0	35.0					
12.0	18.0		M	4.0	8.0	
16.0	20.0			7.0	8.0	
17.0	23.0			7.0	11.0	
23.0	33.0			9.0	12.0	
34.0	40.0		N	4.0	8.0	
73.0	84.0			4.0	9.0	
78.0	87.0			8.0	13.0	
No Indications @ 100.0				9.0	15.0	

TABLE V (cont.)

Ti-6Al-4V Cycles to Pinpoint X 10^{-3}	Ti-6Al-4V Cycles to 1/32" X 10^{-3}	Remarks	Condition	Ti-6Al-6V-2Sn Cycles to Pinpoint X 10^{-3}	Ti-6Al-6V-2Sn Cycles to 1/32" x 10^{-3}	Remarks
27.0	35.0		O	4.0	8.0	
21.0	26.0			8.0	15.0	
17.0	29.0			9.0	15.0	
61.0	73.0			16.0	21.0	
11.0	18.0		P	8.0	12.0	
15.0	22.0			14.0	21.0	
27.0	33.0			8.0	13.0	
56.0	60.0			11.0	12.0	
5.0	11.0		Q	4.0	7.0	Two additional specimens contain machining damage and were not tested
8.0	16.0			8.0	16.0	
9.0	20.0			-	-	
11.0	21.0			-	-	
15.0	21.0		R	10.0	15.0	
22.0	32.0			17.0	19.0	
No Indications @ 54.0				9.0	14.0	
No Indications @ 108.0				7.0	11.0	
No Indications @ 108.0			S	7.0	10.0	
No Indications @ 145.0				18.0	21.0	
No Indications @ 54.0				7.0	11.0	
26.0	37.0			12.0	14.0	
2.0	4.0		T	9.0	12.0	
9.0	11.0			4.0	9.0	
25.0	29.0			8.0	10.0	
51.0	58.0			6.0	8.0	
14.0	20.0		U	.0	8.0	
6.0	10.0			6.0	8.0	
14.0	24.0			12.0	16.0	
13.0	20.0			15.0	21.0	

TABLE VI

WYMAN-GORDON LOW CYCLE FATIGUE DATA
PHASE I, TASK B, AS MACHINED SPECIMENS

Ti-6Al-2Sn-4Zr-6Mo

Condition	Cycles to Pinpoint X 10^{-3}	Cycles to 1/32" Crack X 10^{-3}	Remarks
A	13.0	16.0	
	13.0	18.0	
	17.0	22.0	
	21.0	24.0	
A-1	13.0	15.0	
	14.0	25.0	
	27.0	30.0	
	33.0	38.0	
A-2	14.0	18.0	
	23.0	28.0	
	33.0	40.0	
	3.0	-	Crack started in machining mark
B	36.0	39.6	
	43.0	47.0	
	52.0	56.0	
	No Indications @ 76.0		
	No Indications @ 80.0		
B-1	No Indications @ 80.0		
	No Indications @ 80.0		
	No Indications @ 70.0		
	21.0	26.0	
	No Indications @ 76.0		
B-2	17.0	21.0	
	18.0	24.0	
	19.0	20.0	
	41.0	43.0	
C	23.0	28.0	
	27.0	29.0	
	48.0	52.0	
	No Indications @ 80.0		
	No Indications @ 76.0		
D	11.0	14.0	
	16.0	21.0	
	29.0	31.0	
	No Indications @ 76.0		
	No Indications @ 80.0		

TABLE VI(cont.)

Condition	Cycles to Pinpoint X 10^{-3}	Cycles to 1/32" Crack X 10^{-3}	Remarks
E	9.0	13.0	
	11.0	15.0	
	19.0	23.0	
	23.0	24.0	
F	5.0	10.0	
	6.0	12.0	
	12.0	17.0	
	23.0	24.0	
G	5.0	8.0	
	6.0	10.0	
	9.0	12.0	
	17.0	22.0	

Titanium LCF Summary

Appendix I

A. Specimen Type

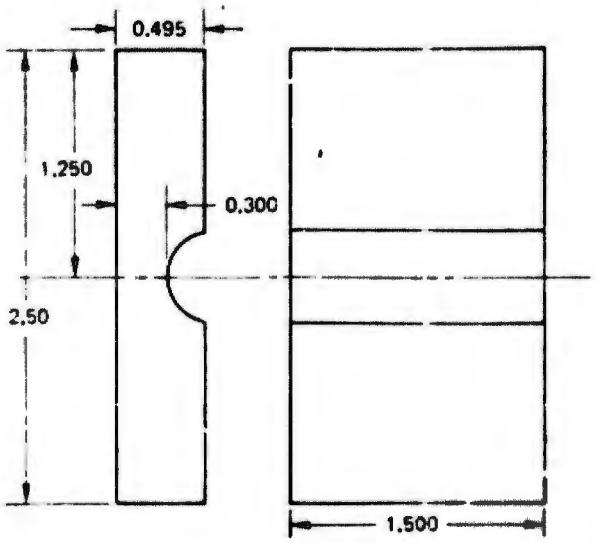

Machining Procedure for Surface of Titanium LCF Specimens

1. Hole 7/16" diameter, to be drilled at 112 rpm .005" feed.
2. Bore hole from 0.438" to 0.452" diameter, using boring tool at 112 rpm, .004 feed.
3. Bore hole from 0.452" to 0.494" diameter using boring tool at 112 rpm, .004 feed.
4. Semi-finish bore with boring tool to 0.494" diameter at 450 rpm 0.002 feed.
5. Finish bore to 0.500" diameter at 450 rpm 0.002 feed.
6. Hone at 425 rpm 10 psi pressure 80 strokes using HSU-4 stone.
7. Use PMC 9252 broaching oil. Cutting oil for above operations.
8. Remove burrs on holes; 0.0005-0.010" x 45° cham. maximum is permissible on holes.
9. Butterfly polish using 320 grit emery cloth, 1500 rpm.

B. Electropolishing Procedure for Gage Area of LCF Bending Specimen

1. Mask all areas not to be polished with stop-off laquer.
2. Clean area to be polished with acetone.

3. Place stainless steel beaker in shallow tray containing dry ice and acetone and place tray on hot plate with magnetic stirring device. Place magnetic stirring rod in beaker.

4. Add the following ingredients stirring slowly. 58 ml Butanol
   98 ml Methanol
   Allow to cool to 32°F and slowly add 13 ml perchloric acid while stirring.

5. After mixture has recooled to 32°F suspend specimen into solution with an alligator clip and connect to the anode of a DC power supply. Connect cathode wire to beaker.

6. Electropolish at 35V for 2-3 minutes while stirring, rinse with water and etch with Kroll's reagent. Strip laquer with acetone. Specimen is now ready to test.

C. Inspection Schedule

1. As machined - inspect every 1000 cycles with Zyglo until pinpoint indication occurs. Replicate one specimen every 1000 cycles for 10,000 cycles to obtain crack growth. Zyglo remaining specimens and record cycles to 1/64", 1/32", 1/16" and 1/8" crack.

2. Electropolished - replicate every 1000 cycles to 10,000 cycles, then every 2000 cycles thereafter until cracks are detected.

APPENDIX D

PRATT AND WHITNEY AIRCRAFT REPORT ON LOW CYCLE FATIGUE

PHASE II

Summary of Low Cycle Fatigue Testing of Titanium Alloy Forgings

As Part of AF Contract F33615-71-C-1560

Phase II Supplement

Submitted to:

Wyman-Gordon Company
Mr. R. B. Sparks

Prepared By:

D. L. Ruckle and M. P. Smith

1 September 1973

I. Introduction

Phase 1 of the program involved the testing of over 300 LCF specimens of the Ti-6Al-4V (Ti-64), Ti-6Al-6V-2Sn (Ti-662) and Ti-6Al-2Sn-4Zr-6Mo (Ti-6246) alloys processed by 34 different forging/heat treat conditions.

Phase II consisted of LCF testing 40 specimens of the Ti-64 and Ti-662 alloys processed to contain microstructural abnormalities encountered as a result of improper processing or melting of the alloys. The Ti-662 specimens were taken from structural forgings similar to those produced in Phase I, however, Phase II forgings were made from billet containing "beta flecks" and processed at three different temperatures. Ti-64 specimens in Phase II contained areas of simulated "soft alpha" inclusions in both beta and alpha-beta processed conditions. Ti-64 disk forgings were used in Phase II to enable the "soft alpha" inclusion to be incorporated in the section.

II. Method of Procedure

Test specimens, test procedures, inspection methods and data analyses were conducted as described in the Phase I report.

III. Summary and Conclusions

The following conclusions apply to the Ti-662 alloy after evaluating Phase II results:

A. "Beta flecks" were visually observed in standard forged material, but were indistinguishable from the bulk microstructure in beta processed or low alpha-beta processed specimens.

B. Multiple crack initiation in the standard forged specimens was observed in the beta fleck areas. Crack initiation in all conditions occurred at alpha phase/matrix interfaces.

C. Overall median lives were lower than comparable Phase I groups similarly processed.

D. Groups in order of increasing median lives were beta, standard practice and low alpha-beta.

The following conclusions apply to the Ti-64 alloy after evaluating Phase II results:

A. Not all specimens which were to contain the "soft alpha" defects did in fact contain them and crack initiation photographs from electropolished specimens were not obtained.

B. Alpha-beta specimens processed with the "soft alpha" defect failed abruptly without prior indications. Lives were lower than for specimens without the defect.

C. Beta processed specimens with and without the "soft alpha" defect had the same median lives due to the fact that the defects were either not present in the specimens or were not in the center of the gage section.

IV. Results and Discussion

Metallographic examination of electropolished and etched Ti-662 specimens revealed that crack initiation and propagation occurred, as reported in Phase I, at alpha/matrix interfaces for all forging conditions (Figure 1). The specimens with a beta or low alpha-beta finish were similar in appearance to comparable Phase I specimens while the standard forge practice specimens (10-20% primary alpha) had multiple origins occurring at the beta flecks (Figures 1 and 2).

Median lives for the three Ti-662 forging conditions were somewhat lower than for comparable Phase I conditions (compare standard practice with Group A, low alpha-beta practice in the Group A-1, and beta practice with Group Q). This may be attributable to the beta flecks present in the billet, even though not observed in two of the conditions. Phase II groups in order of increasing lives were beta, standard practice and low alpha-beta practice (Table I). The presence

of beta fleck areas in the standard alpha-beta specimens inflicted a fairly severe debit when compared to Ti-662 alpha-beta specimens without the flecks, probably as a result of the tendency for cracks to initiate preferentially in coarse beta areas.

Metallographic examination of electropolished and etched Ti-64 specimens with "soft alpha" defect revealed that the defects were in actuality not present in the electropolished and etched specimens tested. As a result the crack initiation photographs (Figures 3 and 4) for groups reportedly with and without the defects show similar results. Actual initiation mode was as previously observed, i.e., at alpha phase/matrix interfaces in both alpha-beta and beta specimens.

The remaining three Ti-64 alpha-beta specimens in the "defect group" actually contained the soft alpha area in the proper location. The results showed that two of the specimens had failure origins in the defect region (Figure 5) and each failed completely without prior indication at 708 cycles and approximately 10,000 cycles, respectively. The remaining specimen slipped during testing and was improperlycycled so that the applied stress was not normal to the bolt hole. The crack originated away from the soft alpha area but propagated rapidly to the defect and failed along the soft alpha interface (Figure 6). The alpha-beta groups without the defect had median 1/32" lives in the 20,000 to 22,000 cycle range. This is lower than the comparable Phase I group A, possibly as a result of slower cooling rates from the heavier section disk forging (Table I) compared to Phase I structural forgings.

The beta processed groups had comparable lives in groups with and without the soft alpha defects. In two of the specimens which were to have contained defects, none could be detected, while the two that did contain defects had them located

off center in the gage section in the lower stress region (Figures 7 and 8). As a result the defect containing specimen did not fail in the soft alpha area. Test results for both beta groups were equivalent to the comparable Phase I group Q. Raw LCF data for individual specimens are given in Tables II through IV.

TABLE I

Median Lives for Wyman-Gordon LCF Specimens

Phase II

Alloy	Condition	Median Life Cycle x 10^{-3} Pinpoint	1/32" Crack	Remarks
Ti-64	Alpha-beta with inclusion	Specimens failed - no pinpoint or 1/32" crack		
Ti-64	Alpha-beta no inclusion	12.0	20.5	--
Ti-64	Beta with inclusion	8.0	9.5	Not all specimens had inclusion
Ti-64	Beta no inclusion	8.5	11.5	--
Ti-662	Standard forge	4.7	9.5	Beta flecks observed
Ti-662	Beta forge	4.2	7.0	No beta flecks observed
Ti-662	Low alpha-beta forge	9.1	17.0	No beta flecks observed

TABLE II

Median Low Cycle Fatigue Lives
For Ti 6Al-4V and Ti 6Al-6V-2Sn(1)

Phase I, Task B

Ti 6Al-4V				Ti 6Al-6V-2Sn		
Cycles To Pinpoint x 10^{-3}	Cycles To 1/32" Crack x 10^{-3}	Remarks	Condition	Cycles To Pinpoint x 10^{-3}	Cycles To 1/32" Crack x 10^{-3}	Remarks
-	-	3 Runouts > 100.0	A	19.5	24.5	
10.0	17.6		A (Low O_2)	-	-	Not tested in Ti 662
29.7	39.8		A-1	16.0	23.0	
20.3	28.5		B	35.5	41.0	
33.1	38.7		C	27.6	32.3	
17.0	23.0		D	7.0	10.6	
15.4	21.3		E	7.1	11.6	
20.7	25.3		F	5.7	9.2	
46.2	57.6		G	6.4	9.4	
69.7	73.4		H	4.5	10.4	
83.3	85.5		I	6.0	10.4	
-	-	4 Runouts > 100.0	J	4.2	8.8	
29.0	38.9		K	15.7	20.8	
-	-	3 Runouts > 100.0	L	11.5	16.4	
17.0	23.9		M	6.7	9.8	
73.6	83.2		N	6.1	11.2	
29.0	40.0		O	8.8	14.5	
24.1	31.5		P	10.2	14.4	
8.3	17.0		Q	5.8	11.0	
25.1	36.9		R	10.6	14.8	
-	-	3 Runouts > 100.0	S	10.7	15.0	
14.4	18.8		T	6.7	10.0	
11.6	18.3		U	8.7	12.7	

(1) B_{50} Life Per Weibull Analysis

TABLE II

Low Cycle Fatigue Data for Wyman-Gordon Specimens

Phase II

Identity	Alloy	Condition	Strain	Inspection Method	Pinpoint	Cycles 1/64"	1/32"	1/16"	1/4"
7-8-2-1	Ti-662	Beta fleck Standard Forge Practice	0-1.1%	Zyglo	4,000	5,000	6,000	8,000	9,000
7-8-2-2					22,000	24,000	28,000	30,000	32,000
7-8-3-1					5,000	9,000	10,000	11,000	13,000
7-8-3-2					Invalid Test - Edge Crack				
7-8-4-1					4,000	6,000	8,000	9,000	9,000
7-8-4-2					5,000	6,000	9,000	10,000	14,000
7-8-1-2				Replica	4,000	---	---	---	---
7-16-2-1	Ti-662	Beta fleck Beta forge Practice	0-1.1%	Zyglo	4,000	4,000	6,000	7,000	9,000
7-16-2-2					5,000	6,000	9,000	---	14,000
7-16-3-1					4,000	6,000	9,000	---	12,000
7-16-3-2					4,000	---	5,000	6,000	10,000
7-16-4-1					4,000	4,000	4,000	5,000	7,000
7-16-4-2					5,000	6,000	9,000	10,000	13,000
7-16-1-2				Replica	4,000	---	---	---	---
7-24-2-1	Ti-662	Beta fleck Low Alpha-Beta Forge	0-1.1%	Zyglo	14,000	16,000	16,000	---	19,000
7-24-2-2					14,000	16,000	17,000	20,000	24,000
t-24-3-1					8,000	10,000	12,000	14,000	15,000
7-24-3-2					7,000	10,000	18,000	28,000	30,000
7-24-4-1					8,000	12,000	17,000	19,000	20,000
7-24-4-2					9,000	10,000	19,000	26,000	27,000
7-24-1-2				Replica	6,000	---	---	---	---

TABLE III

Low Cycle Fatigue Data for Wyman-Gordon Specimens

Phase II

Identity	Alloy	Condition	Strain	Inspection Method	Cycles Pinpoint	1/64"	1/32"	1/16"	1/4"
3-3-4-2	Ti-64	Alpha-beta with inclusion	0-0.9%	Zyglo	Invalid Test - Specimen slipped during test				
3-4-3-1					Ruptured at 708 cycles				
3-4-3-2				Replica	Ruptured at 10,000 cycles				
3-4-1-1	Ti-64	Alpha-beta No inclusion	0-0.9%	Zyglo	14,000	17,000	21,000	23,000	26,000
3-4-1-2					10,000	15,000	22,000	24,000	27,000
3-4-2-2				Replica	10,000	---	---	---	---
3-5-4-1	Ti-64	Beta forge with inclusion	0-0.9%	Zyglo	5,000	6,000	7,000	8,000	12,000
3-5-4-2					8,000	11,000	12,000	15,000	19,000
3-6-3-2				Replica	11,000	---	---	---	---
3-6-1-1	Ti-64	Beta forge No inclusion	0-0.9%	Zyglo	10,000	11,000	15,000	20,000	26,000
3-6-1-2					6,000	8,000	9,000	11,000	19,000
3-6-2-2				Replica	10,000	---	---	---	---

TABLE IV

Crack Length Versus Cycles for Wyman-Gordon LCF Specimens

Phase II

Identity	Alloy	Condition	Cycles After Pinpoint										
			Pinpoint	1,000	2,000	3,000	4,000	5,000	6,000	7,000	8,000	9,000	10,000
7-8-1-2	Ti-662	Standard forge	4,000	.005"	.010"	.018"	.040"	.060"	.120"	Multiple crack linkup			
7-16-1-2	Ti-662	Beta forge	4,000	.020"	.040"	.085"	.145"	.360"	---	Multiple crack linkup			
7-24-1-2	Ti-662	Low alpha-beta forge	6,000	---	---	.015"	.020"	.039"	.060"	.087"	.110"	.220"	---
3-4-3-2	Ti-64	Alpha-beta with inclusion	---	Failed 10,000 cycles									
3-4-2-2	Ti-64	Alpha-beta no inclusion	10,000	.007"	---	.026"	---	.037"	.085"	.110"	.178"	.250"	.420"
3-6-3-2	Ti-64	Beta forge with inclusion*	11,000	Multiple Cracks		.032"	.085" .037"	.125" .040"	.150" .040"	.198" .045"	.245" .018"	.280" .018"	.370" .020"
3-6-2-2	Ti-64	Beta forge no inclusion	10,000	.005"	---	.012"	---	.020"	.026"	.032"	.039"	.053"	.070"

*Inclusion not detected in specimen 3-6-3-2

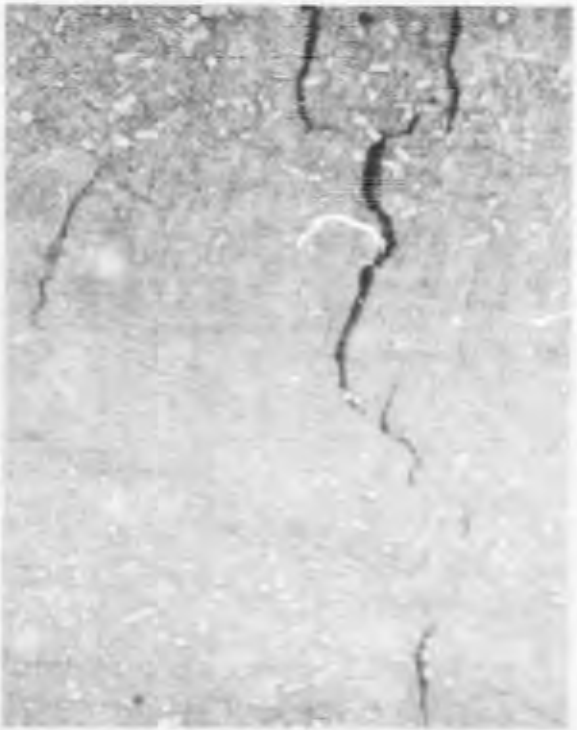

A

B

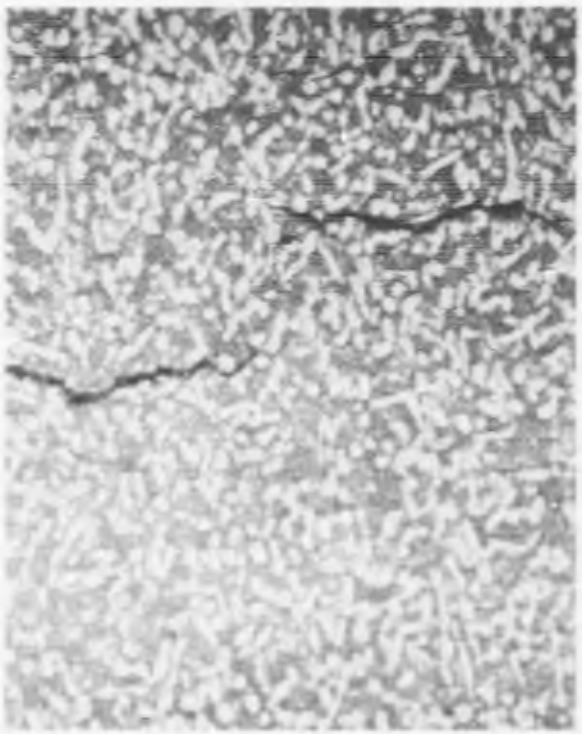

C

ETCHING REAGENT: KROLL'S FIGURE 1 MAG: A: 200X
B,C: 250X

TYPICAL CRACK INITIATION AND PROPAGATION MODES IN THE TI-662 ALLOY MADE FROM BILLET CONTAINING "BETA FLECKS". (A) STANDARD FORGE PRACTICE - NOTE MULTIPLE CRACKING IN "FLECK" AREA; (B) BETA FORGE PRACTICE; (C) LOW ALPHA-BETA FORGE PRACTICE.

EY 1822-1, 2, 3

ETCHING REAGENT: KROLL'S MAG: 150X

MICROSTRUCTURE OF TI-662 SPECIMEN NO. Y-5-7-2 FORGED BY THE STANDARD PRACTICE. NOTE PRESENCE OF "BETA FLECK" AT FAILURE ORIGIN (ARROW).

EY 1777-4

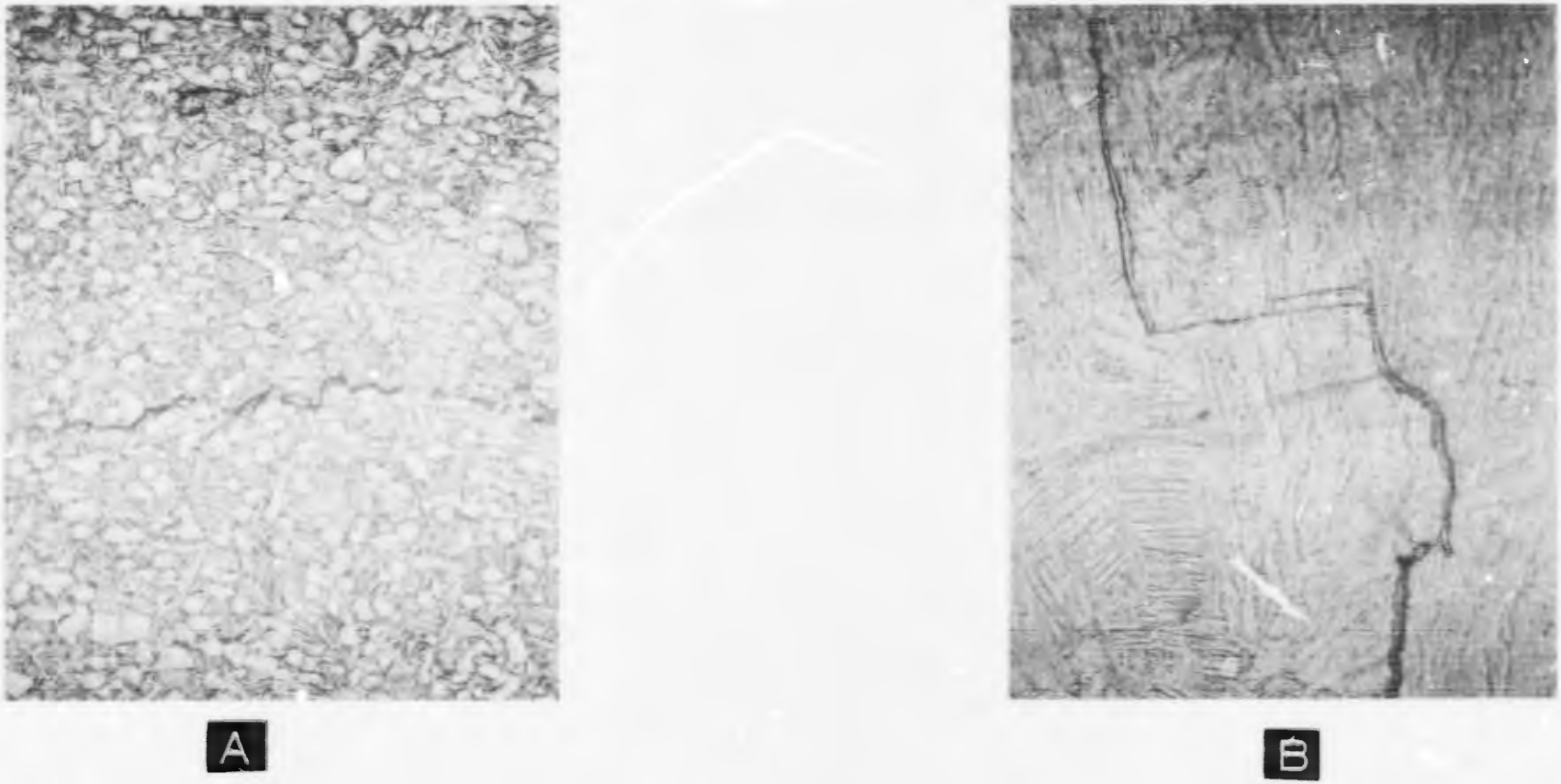

ETCHING REAGENT: KROLL'S FIGURE 3 MAG: 250X

TYPICAL MODE OF CRACK INITIATION AND PROPAGATION IN TI-64 SPECIMENS WHICH WERE TO HAVE CONTAINED "SOFT ALPHA" DEFECTS. NO AREAS OF DEFECTS WERE DETECTED IN THE SPECIMENS. (A) ALPHA-BETA FORGED; (B) BETA FORGED.

EY 1822-6, 7

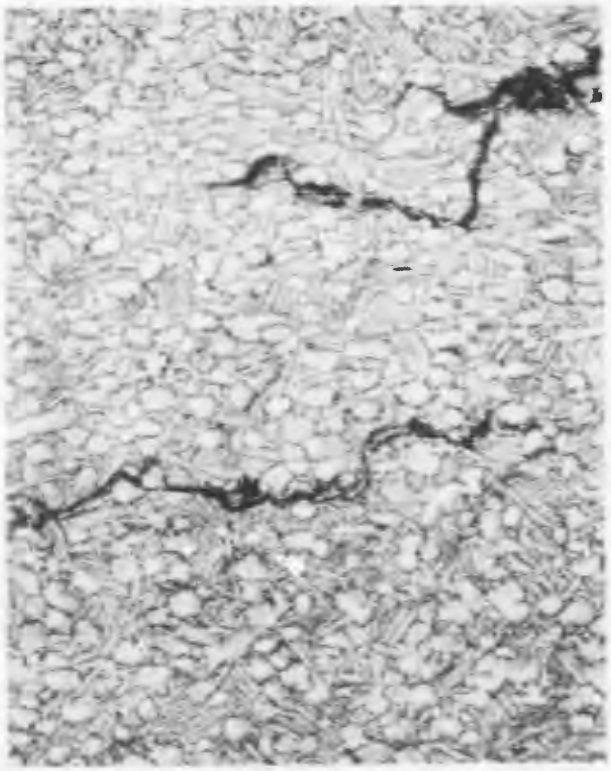

A

B

ETCHING REAGENT: KROLL'S FIGURE 4 MAG: 250X

TYPICAL MODE OF CRACK INITIATION AND PROPAGATION IN TI-64 SPECIMENS WITHOUT "SOFT ALPHA" DEFECTS. NOTE SIMILARITY TO FIGURE 3. (A) ALPHA-BETA FORGED; (B) BETA FORGED.

EY 1822-4, 5

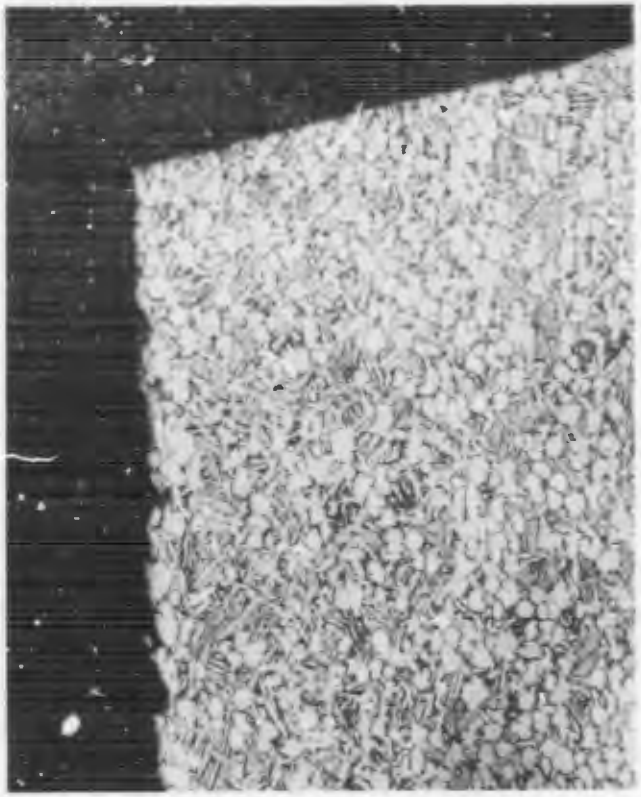

A

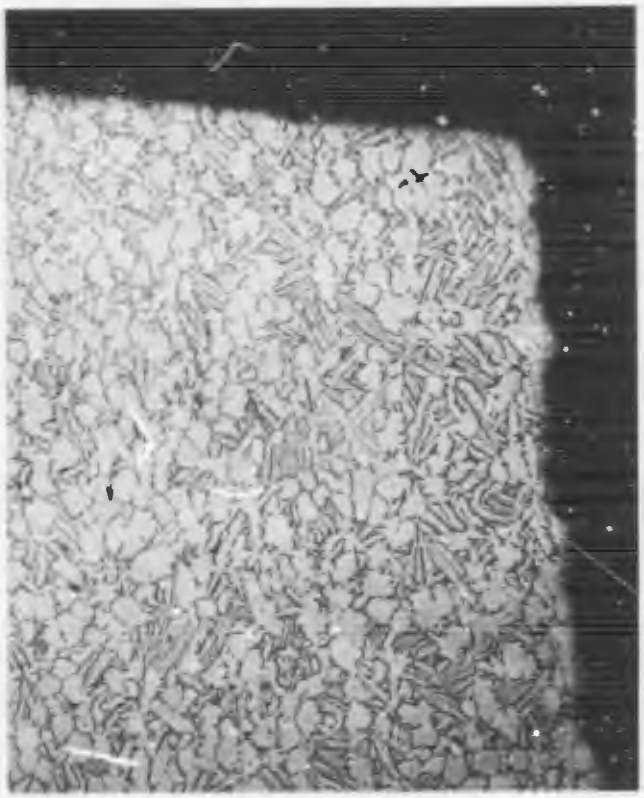

B

ETCHING REAGENT: KROLL'S

FIGURE 5

MAG: A: 200X
B: 250X

MICROSTRUCTURE AT FAILURE ORIGIN OF ALPHA-BETA PROCESSED TI-64 SPECIMENS CONTAINING "SOFT ALPHA" INCLUSION. (A) SPECIMEN NO. 3-4-3-1, FAILED AT 708 CYCLES; (B) SPECIMEN NO. 3-4-3-2, FAILED AT 10,000 CYCLES.

EY 1777-9, 3

ETCHING REAGENT: KROLL'S FIGURE 6 MAG: 100X

MICROSTRUCTURE AT FAILURE ORIGIN OF ALPHA-BETA PROCESSED TI-64 SPECIMEN CONTAINING "SOFT ALPHA" INCLUSION. THIS SPECIMEN (NO. 3-3-4-2) SLIPPED DURING TESTING AND CAUSED FAILURE TO OCCUR AT A LOWER STRESS AREA, THUS RESULTING IN A HIGH LIFE. THE DATA WAS NOT CONSIDERED VALID. NOTE THAT FAILURE OCCURRED AWAY FROM "SOFT ALPHA" THEN PROPAGATED INTO THE INCLUSION.

EY 1777-1, 2

ETCHING REAGENT: KROLL'S FIGURE 7 MAG: 100X

MICROSTRUCTURE OF TI-64 BETA FORGED SPECIMEN NO. 3-5-4-1. NOTE THAT "SOFT ALPHA" INCLUSION (ARROWS A) IS NOT IN THE CENTER OF THE SPECIMEN GAGE SECTION AND IS AWAY FROM THE FAILURE ORIGIN (ARROW B).

EY 1777-5, 6, 7

ETCHING REAGENT: KROLL'S FIGURE 8 MAG: 150X

MICROSTRUCTURE OF TI-64 BETA FORGED SPECIMEN NO. 3-4-5-2 SHOWING "SOFT ALPHA" INCLUSIONS (ARROW A) IS NOT IN CENTER OF THE SPECIMEN GAGE SECTION.

EY 1777-8

APPENDIX E

MECHANICAL PROPERTY RATING SYSTEM

APPENDIX B

MECHANICAL PROPERTY RATING SYSTEM

In order to compare the various conditions (microstructures) within each alloy group, an arbitrary rating system was established. The mechanical property values of: ultimate tensile strength, reduction of area, fracture toughness, notched tensile - unnotched tensile ratio, low cycle fatigue cycles to pinpoint and cycle to 1/32" crack and notched high cycle fatigue stress for 10^7 cycle endurance limit were divided into four categories and assigned a point value of 1 - 4, low to high value respectively. For example, reduction of area was divided as follows:

	Point Value
less than 20%	1
20 - 29.9%	2
30 - 40%	3
greater than 40%	4

Each property was similarly divided and each condition of each alloy graded. Then a cumulative total was determined as an indication of overall performance. The breakdown of the properties and point value is shown in Table I of this Appendix. The individual scores are shown in Tables XXXII, XXXIII, and XXXIV of the text.

Those tables should be useful in selecting the type of processing to be used for the particular mechanical property desired. The total score can be compared within alloy systems, but not between different alloys as similar heat treatments were not used and testing conditions were not the same for all alloys. For example, the 6-6-2 and 6-2-4-6 alloys were tested in low cycle fatigue at 0-1.1% E, whereas the 6-4 alloy was tested at 0-0.9% E. The evaluation of the 6-2-4-6 alloy included the STA condition, the 6-4 and 6-6-2 evaluation did not, but within a particular alloy group the comparative ratings of the condition tested should be helpful in choosing the desired processing. See Table XIV for mechanical property rating Phase I, Task A, Macrostructure Study. See Tables XXXII and XXXIII for mechanical property rating Phase I, Task B, Microstructural Study, Ti-6Al-4V and Ti-6Al-6V-2Sn, respectively.

MECHANICAL PROPERTY RATING SYSTEM

Property	Test Result	Point Value
Notched High Cycle Fatigue		
Stress for 10^7 cycle Life	<30 ksi	1
	30-34 ksi	2
	35-40 ksi	3
	>40 ksi	4
Low Cycle Fatigue		
Cycles to 1/32" crack		
Cycles to pinpoint	<20 ksi	1
	20-39 ksi	2
	40-80 ksi	3
	>80 with R.O.'s	4
Fracture Toughness		
K_{IC}	<40 ksi $\sqrt{in}$	1
	40-59.9	2
	60-80	3
	>80	4
Ultimate Tensile Strength		
	130-139 ksi	1
	140-149	2
	150-160	3
	>160	4

Property	Test Result	Point Value
Reduction of Area		
	<20	1
	20-29.9	2
	30-40	3
	>40	4
Notched Tensile Strength		
Ultimate Tensile Strength	<1.30	1
	1.31-1.40	2
	1.41-1.50	3
	>1.50	4

APPENDIX F

ROCKWELL INTERNATIONAL SCIENCE CENTER REPORT ON TRANSMISSION ELECTRON MICROSCOPIC EXAMINATION

SUMMARY OF MICROSTRUCTURAL CHARACTERIZATION OF Ti ALLOY FORGINGS

Received from Wyman-Gordon

As Part of Air Force Contract #F33615-71-C-1560

Submitted to:

R. B. Sparks

Prepared by:

C. G. Rhodes and J. C. Williams

1 August 1973

INTRODUCTION

The Rockwell International Science Center was subcontracted by the Wyman-Gordon Company to perform thin foil transmission electron microscopy on 56 titanium alloy samples under Air Force Contract #F33615-71-C-1560. The following were supplied by Wyman-Gordon in the form of one half of a fractured tensile specimen: 23 Ti-6Al-4V, 22 Ti-6Al-6V-2Sn, and 11 Ti-6Al-2Sn-4Zr-6Mo samples with various forging and post forging treatments. The particular treatments of samples sent to us are those outlined in the "Microstructural Study" portion of the contract and are tabulated in Interim Technical Report IR-226-II as Figures 16 and 17. In addition to those listed, we also received a low oxygen sample of Ti-6Al-4V in condition A.

The Science Center's approach to microstructural characterization was three-fold. First, all samples were examined for general features and obvious variations thereof. Second, unusual features, whether artificial or real, were documented. Finally, quantitative or semi-quantitative data of specific microstructural features were obtained from selected samples in order to correlate microstructure to mechanical properties data. The thin foil electron microscopy results will be presented here according to these categories.

EXPERIMENTAL

Samples received by the Science Center were in the form of half of a failed tensile specimen. A transverse slice 0.020" thick was cut from the grip end of each specimen at a position near the shoulder. The remaining section of the grip was sliced in half longitudinally.

All samples were examined by light microscopy prior to thin foil transmission electron microscopy. To accomplish this, the longitudinally-sliced section from the grip were mounted in epoxy and mechanically ground through

600 grit SiC. They were then electropolished for one minute at 40 volts (D.C.) in a methanolic solution containing 5% H_2SO_4 and 1.25% HF and etched.

Thin foils for transmission electron microscopy were prepared from the .020" transverse slices by mechanically grinding to 1-2 mils followed by electropolishing at -40°C at a potential of 15 volts in a solution consisting of 300 pts. methanol, 175 pts butyl alcohol and 30 pts. perchloric acid using the window method. The thin foils were examined using a Philips EM300 equipped with a double tilt goniometer stage and a high resolution dark field device. Heating stage experiments were carried out with the Philips single tilt heating holder.

RESULTS

The results will be divided into three general topics. The first of these is designated Special Features and consists of those microstructural features which occur in some samples of all alloys. The second is labelled Microstructural Characterization and contains the individual observations of all fifty-six (56) specimens examined. The third category, Properties Correlation, is the correlation of quantitative or semi-quantitative results of selected microstructural features from selected specimens to mechanical properties.

SPECIAL FEATURES

This section is separated from the Microstructural Characterization section because the particular features described herein are frequently encountered in thin foil electron microscopy of titanium alloys and the microscopist must be able to recognize and properly identify them before proceeding with the characterization. Some of these features are thin foil artifacts while others are real; this section will document both types of features.

Spontaneous Transformation

The first special feature is a thin foil artifact which occurs in the beta phase of titanium alloys. Figure 1 illustrates this effect, which has been termed "spontaneous transformation" in an earlier communication.[1] The beta phase appears to undergo a spontaneous shear process during thinning and the microstructure is typified by the linear structure seen in Fig. 1. Diffraction patterns from this structure frequently show streaking depending upon the degree of distortion of the bcc lattice. Although the precise nature of the shear is not known, it has not been investigated here since this effect is a thin foil artifact and thus does not bear any relationship to the structure of the bulk material. For the purpose of this report, it is sufficient to note that spontaneous transformation is easily recognizable by its twin-like morphology.

Hydrides

Hydrogen can be introduced into titanium alloys during processing or during thin foil preparation. In the latter case it is likely the hydrogen is picked up during mechanical thinning or during electropolishing. If hydrogen is introduced into the material during grinding or electropolishing, it will initially exist as a supersaturated solid solution. Removal of the metal during thinning reduces the volume of metal which contains the hydroger, thereby increasing the concentration. At some point the supersaturation can be relieved by nucleation of Ti hydrides. Such nucleation frequently occurs at α/β interfaces as shown in Figure 2. The reason for the α/β interface acting as a preferred nucleation site is probably related to the high hydrogen solubility in the β phase relative to the α-phase. Such a situation can result in localized sites which contain high concentrations of hydrogen and which can reject hydrogen into the adjacent α-phase resulting in hydride formation.

Because of the small size and relatively low scattering power of these

hydrides, it is difficult to obtain diffraction evidence to confirm that the plate-like features are hydrides. As a result, we have resorted to an alternate technique for identifying hydrides, namely a heating stage experiment; a typical result of which is depicted in Figure 3. This technique utilizes the strong temperature dependence of hydrogen solubility which leads to rapid dissolution of hydrides during heating. As shown in Figure 3a and b, the plate-like feature present at room temperature (3a) shrinks during heating, and eventually disappears at ~ 220°C (3b). This observation confirms that the plate-like feature is Ti hydride since 220°C is consistent with the temperature range for dissolution of titanium hydride[2] and since there are no phases in the alloys studied here which would be unstable at 220°C. Hydrides are generally recognizable by their thin platelet morphology, although, as will be discussed below, identification of all plate-like features as hydrides on the basis of their morphology can lead to serious errors.

α+β Interface Phase

In α+β Ti alloys, the interface between these two phases generally consists of a region containing a complex structure which is only resolvable by thin foil electron microscopy techniques. This complex interface structure is observed in all alloys examined and therefore can be treated as a general microstructural feature. Furthermore, this interface phase has been reported by others variously as a region of high dislocation density[3] or a hydrogen effect.[4] Since we feel this phase is neither, some detailed clarification seems warranted. Typical examples of the interface phase are shown in Fig. 4. In this aspect the interface phase appears to be made up of a very finely divided structure. However, by tilting the thin foil to a position where neither the α and β phases are near a strong diffracting condition, the interphase can be seen to be a single, continuous phase, Fig. 5.

The interface phase is generally too narrow to produce complete or intense electron diffraction patterns. However, in one instance a nearly complete pattern was obtained, as illustrated in Fig. 6. The SAD pattern obtained is a basal zone of the α-phase and, as indicated by the dark field micrographs in 6b and 6c, originates from the interface phase. The existence of a distinct type of α phase in the interface region between the α and β phases is illustrated in Fig. 7 which contains a SAD pattern from the primary α-phase adjacent to the interface phase in Fig. 6. This diffraction pattern is 16° off a $[0001]_\alpha$ zone, indicating that the α-phase in the interface has a different crystallographic orientation than the primary α.

In all cases examined, the primary α and the β phases were oriented in the well-known Burgers orientation relation, an example of which is shown in Fig. 8a and b. When the diffraction pattern includes the interface phase, it appears as in 8c, where the extra, arced reflections are from the interface phase. Note that these arced reflections do not superimpose on primary α reflections. The observations of Figs. 6, 7, and 8 lead to the conclusion that the interface phase is indeed α but that it has a different crystallographic orientation than the α phase to which it is adjacent.

Alpha Lath Internal Structure

The alpha laths which are present in these alloys sometimes contain an internal plate-like structure, Fig. 9. These internal plates occur in both Widmanstätten α and martensitic α. This structure is not present in all samples and tends to be more frequent in alloys with increasing amounts of β-stabilizing alloying additions. That is, it is more general in 6-2-4-6 than in 6-6-2 where it is more frequent than in 6-4. Furthermore, the internal structure occurs more frequently in STOA samples than in annealed samples, implying that cooling rate influences the development of this structure. The

platelets are too thin to generate complete or intense electron diffraction patterns, consequently exact identification was not accomplished. The platelets do have an appearance that makes them reminiscent of the interface phase which occurs between the alpha and beta phases as was described in the previous section. In fact, with proper tilting, they can be shown to consist of an apparent strip of beta phase bounded by the interface phase, Fig. 10. The beta strip has not been positively identified by SAD but it has been observed to be continuous with the known beta lamellae which exists between alpha laths; this strongly suggests that the internal plates are β-phase.

These platelets might be mistakenly identified as hydrides as discussed earlier but they clearly are not since the structures persist when heated to 700°C while hydrides do not. Also, these platelets have a general mottled appearance, hydrides have a continuous or monolithic appearance. Further, these platelets can be tilted to show that they consist of a central phase bounded by an interface structure, whereas hydrides do not exhibit this appearance under any contrast conditions.

The origin or mechanism of formation of the beta platelets within the alpha laths is not clear at present but has not been pursued as part of the present program.

MICROSTRUCTURAL CHARACTERIZATION

In this section the TEM observations of each of the 56 specimens will be presented. The results will be broken down by alloy. The forging and post-forging treatments for each of the alloys examined are listed in Tables I, II and III. The samples will hereafter be referred to only by their code letters and no further description of treatments will be given in the text. No light micrographs will be presented in the results inasmuch as light microscopy was performed by Wyman-Gordon.

Ti-6Al-4V

Condition A. Figure 11 is a low magnification electron micrograph illustrating the interface area between a spherical primary α particle, Widmanstätten α laths and lamellar β-phase regions. The β lamellae separate the α laths from each other and from the primary α. The interface phase (see Special Features section) is always present in the α/β interfaces.

The β-phase regions are free of any α-phase precipitation. The primary α particles show a moderate dislocation density, some of which exist in networks indicating some degree of recovery. The Widmanstätten α laths also show a low dislocation density with few or no networks.

Condition A, Low O_2. The most striking difference between this sample and the previous one is the difference in size of the Widmanstätten α laths. In this case they are about 1/2 the width of those in Treatment A, normal O_2, as illustrated in Fig. 12. The laths also have a higher dislocation density than those in the previous sample. While the difference in oxygen level may influence the microstructure, it is not likely that the small difference in oxygen can account for such extensive variations. Thus the observed changes suggest that there were also processing variations between these two Condition A specimens or that the tensile samples were taken from different locations in the forging.

Condition B. This sample contains a large fraction of martensitic α. The tempered martensite is shown in Fig. 13. Regions of retained β-phase also are present between the martensite laths with the interface phase present between the α and β phases, Fig. 14. The spherical primary α particles have a moderate dislocation density, a portion of which are contained in networks. The laths of tempered martensitic α show a low dislocation density.

Condition C. This sample exhibits Widmanstätten α rather than the martensite structure expected for a specimen water quenched off the forging press with an 1800°F finish temperature. This result may reflect either the position in the forging from which the tensile specimen was taken or a quench delay during quenching off the press. The microstructure consists of Widmanstätten α laths separated by retained β regions and interface phase in the α/β interfaces. The primary α shows dislocation networks as well as individual dislocations.

Condition A1. There is little difference between the microstructural features of this sample and those in Condition A (with the exception, of course, of the difference in amounts of primary α). This sample shows a few of the internal platelets in the α laths (see Special Features section) whereas Condition A did not.

Condition D. The microstructure of this sample consists of spaghetti α, elongated primary α, Widmanstätten α, β lamellae and interface phase. The spaghetti alpha particles have a high dislocation density, Fig. 15, while the remaining primary α and Widmanstätten α particles show lower dislocation densities with some networks appearing in both, Figs. 16 and 17. This probably reflects the higher Al content of the spaghetti α and the attendant retardation in recovery and recrystallization rates.

Condition E. The microstructural constituents present in this material are spaghetti α, elongated primary α, martensitic α, β-phase lamellae, β-phase precipitates and interface phase. The larger α phase laths have β-phase precipitates within them, Fig. 18. The laths likely are those which formed during the air cool from the press and when heated back up to 1750°F (where the equilibrium amount of α phase is less than at room temperature) equilibrate by the precipitation of β-phase within the lath as well as at the lath boundary.

The dislocation densities in the primary and spaghetti α phases are similar to those observed in Condition D, the martensitic α laths have low dislocation density.

Condition F. This sample does not have the expected martensitic α in the transformed regions. Instead there are larger, apparently Widmanstätten α, laths similar to Condition C which was also water quenched off the press. The microstructure is very similar to Condition D.

Condition G. The grain boundary α phase, much like the spaghetti α in the previous samples, has a high dislocation density, probably for the same reasons as those cited above in connection with the spaghetti α. The elongated primary α and the Widmanstätten α show lower dislocation densities with some networks present. Retained β-phase occurs between α laths with the interface phase present.

Condition H. The expected martensitic α phase is not present in this sample. The microstructure consists of elongated primary α, grain boundary α, Widmanstätten α, and β lamellae with interface phase. The elongated primary α particles have a moderately low dislocation density, as do the Widmanstätten α laths. The lack of martensitic α is probably a result of the tensile sample coming from the interior of the forging.

Condition I. Little or no martensitic α is evident in this sample, similar to results of Conditions C and F. The grain boundary α, as in Condition G, has a high dislocation density, Fig. 19. The elongated primary α and the lath α phases have a moderate dislocation density. Lamellar retained β regions are present between α laths; the α/β boundary contains the interface phase.

Condition J. The microstructure consists of elongated primary α laths, Widmanstätten α laths, β lamellae and interface phase in the α/β boundaries. The primary α and Widmanstätten α have a moderately low dislocation density

with a few networks present. The Widmanstätten α-phase also exhibits some internal plates (see Special Features section).

Condition K. The sample contains some areas of martensite but most of the α-phase has formed by nucleation and growth. The microstructure consists mainly of elongated primary α, Widmanstätten α, β lamellae, β-phase precipitates and the interface phase. The dislocation densities are similar to those observed for Condition J.

Condition L. Martensitic α, elongated primary α and β lamellae with interface phase compose the microstructure of this sample. The primary α particles show extensive dislocation networks, the martensitic α laths show moderate dislocation density.

Condition M. The sample consists of martensitic α, elongated primary α, β lamellae with interface phase, and the internal plate structure within the α laths, Fig. 20. These features are rare, as indicated in the Special Features section. Dislocation densities are moderate in these α phases.

Condition N. The most significant difference between this sample and Condition J is the much higher dislocation density, both in the primary alpha and the Widmanstätten alpha phases of this sample.

Condition O. There is very little difference in the microstructure of this sample and that of Condition K described above.

Condition P. When compared to Condition L, this sample has higher dislocation densities in the α phases. Also, the α-phase in this sample is principally Widmanstätten type, with little or no martensitic α present.

Condition Q. This sample consists of Widmanstätten α laths separated by β lamellae which contain the interface phase in the α/β boundaries. There is a fairly high dislocation density in the α phase.

Condition R. This sample contains martensitic α, elongated primary α, and β lamellae and interface phase. The primary α particles have a moderately

high dislocation density, while the martensitic α laths have a lower dislocation density.

Condition S. The prior β regions in this sample consist of fine Widmanstätten rather than the martensitic α which might be expected in material quenched from the press. Beta lamellae with interface phase separates these Widmanstätten α laths. Some of the larger laths contain β-phase precipitates similar to those seen in Condition E. Dislocation densities are moderately high in Widmanstätten α.

Condition T. Occasional grain boundary α and Widmanstätten α laths separated by β lamellae and interface phase comprise the microstructure of this sample. The dislocation densities in the α phases are fairly high.

Condition U. The microstructure consists of elongated primary α particles, Widmanstätten α, β lamellae and interface phase (grain boundary α particles were not detected). The dislocation densities in the α phases are low.

Ti-6Al-6V-2Sn

Condition A. This microstructure consists of spherical primary α, Widmanstätten α, β lamellae and interface phase. The β-phase lamellae are fairly narrow (on the order of 1000 Å) and do not contain any α precipitation. The dislocation density in the primary α is fairly high, Fig. 21, but moderately low in the Widmanstätten α.

Condition B. This sample has a microstructure consisting of martensitic α laths which contain a fine internal structure, along with β lamellae and spherical primary α. The unusual α structure is shown in Fig. 22. This structure is commonly observed in 6-2-4-6, but is infrequently seen in 6-6-2 and has not been observed at all in 6-4. As will be shown in the case of 6-2-4-6, the α laths are apparently composed of fine particles belonging to several variants of the α/β orientation relation. The β-phase does not contain

α precipitation.

Condition C. Very little martensitic α is observed in this sample; most of the transformed regions appear to consist of Widmanstätten α. The β lamellae which separate the Widmanstätten α are narrow and do not contain α-phase precipitates. Interface phase is present in the α/β boundaries. The dislocation density in the spherical primary α is moderate and many networks are present.

Condition A1. The beta lamellae between the Widmanstätten α laths are wider than in previous samples and tend to widen out near primary α particles, Fig. 23. In these broad regions of β-phase there has been precipitation of α phase. The interface phase is present between the β phase and primary α, or Widmanstätten α, regardless of whether or not α phase has precipitated in the β phase. The dislocation density in the primary α is moderate with many networks formed.

Condition D. The microstructure of this sample consists of spaghetti α, Widmanstätten α, β lamellae and interface phase. The thicker β lamellae generally contain precipitated α-phase, Fig. 24, whereas the thin β lamellae do not. The SAD pattern indicates that the α-phase which has precipitated in the β-phase does not follow the Burgers orientation relation. The spaghetti α has a moderately high dislocation density most of which have rearranged into networks, Fig. 25.

Condition E. The martensitic α laths in this condition contain a large number of internal plates (see Special Features section), Fig. 26. The β lamellae tend to be broad but contain little or no α precipitation even in the broad areas between martensitic and primary α particles. The dislocation density both in the spaghetti α and primary α tends to be high.

Condition F. This sample contains martensitic α as well as spaghetti α, elongated primary α and β lamellae with interface phase. The β-lamellae

between martensitic α laths are quite narrow and contain no α precipitation, but many of the wider β patches (near primary or spaghetti α particles) contain α precipitation. The dislocation density in the α phases is moderate.

Condition G. Widmanstätten α, elongated primary α, grain boundary α, and β lamellae with interface phase are the constituents of the microstructure. The Widmanstätten α laths contain a large number of internal plates. The broader regions of β phase contain precipitated α-phase. The dislocation density in the primary α is moderate. Grain boundary α particles were not detected in the thin foils.

Condition H. This microstructure consists of martensitic α, elongated primary α, grain boundary α, β lamellae and interface phase. The β lamellae are quite narrow, even in regions near primary α particles, and are free from α precipitation. The martensitic α laths contain little of the internal plate structure. The dislocation density in the primary α is high, a large fraction of which exists in networks, Fig. 27. Grain boundary α particles were not detected in the thin foils.

Condition I. The sample contains martensitic α, elongated primary α, β lamellae and interface phase. A few of the widest β lamellae have α precipitated within them, otherwise the β-phase is untransformed. The dislocation density in the primary α is high. No grain boundary α was detected in the thin foils.

Condition J. Widmanstätten α, elongated primary α, β lamellae and interface phase are present in this sample. There is α precipitation in the wide portions of the β lamellae. The dislocation density in the primary α is low, but somewhat higher in the Widmanstätten α.

Condition K. The martensitic α laths contain a fine internal structure similar to that observed in Condition B. Many of the smaller elongated primary

α particles contain the internal platelet structure. There is little or no α precipitation within the β phase. The interface phase is present between β and primary α particles. The dislocation density is moderate in the primary α.

Condition L. The α phase in the transformed region is a mixture of martensitic α and Widmanstätten α. The martensitic α laths contain the fine internal structure similar to that seen previously in Conditions B and K. The Widmanstätten α and some of the smaller elongated primary α particles contain the internal platelet structure. The β phase does not exhibit α-phase precipitation; the α/β interfaces contain the interface phase. The dislocation density in the primary α is fairly high.

Condition M. This microstructure consists of martensitic α, elongated primary α, and β lamellae bounded by interface phase. As in the two previous samples, the martensitic α contains the fine internal structure. The β lamellae tend to be free from α precipitate. The dislocation density in the primary α is moderate.

Condition N. The most significant difference between this sample and Condition J is that here there is a higher dislocation density in the primary α.

Condition O. This sample is different from Condition K in that here the martensitic α laths are relatively clean of the fine internal structure. Also, there is little internal platelet structure in the primary α particles.

Condition P. This microstructure is quite similar to that of Condition L, except that the α-phase contains no internal platelet structure in Condition P. Also, α precipitation occasionally is seen within some of the wider areas of β phase.

Condition Q. This sample consists of Widmanstätten α laths separated by β lamellae and interface phase. The α laths contain a high density of internal platelets. The dislocation density in the α phase is moderate.

Condition R. Elongated primary α, martensitic α, and β lamellae with interface phase comprise the microstructure of this sample. The martensitic laths contain the fine internal structure such as seen in Condition B. Some of the primary α particles contain internal platelets. The β phase shows no α precipitation. The dislocation density in the primary α is low.

Condition S. This microstructure consists of martensitic α laths separated by β lamellae with interface phase between the α and β. The α laths contain numerous internal platelets. The dislocation density in the α phase is low.

Condition T. There is little grain boundary α in this sample. The Widmanstätten α laths are separated by untransformed β lamellae and interface phase. There are numerous internal platelets in the α laths. The dislocation density is moderate in the α phases.

Condition U. This sample contains elongated primary α, martensitic α, and β lamellae with interface phase between the α and β. The β phase does not contain α precipitation. The martensitic α laths tend to have the fine internal structure seen in previous samples such as Condition B. Many of the smaller elongated primary α particles contain the internal platelet structure. The dislocation density in the α phase is moderate.

Ti-6Al-2Sn-4Zr-6Mo

Condition A. This microstructure consists of spherical primary α (produced during the forging operation), elongated "secondary" α (produced during the post forge solution treatment), and a transformed region of fine α laths (produced during the cool-down), Fig. 28. The fine laths have an acicular morphology and contain a fine structure; their morphology and substructure make them distinct from the Widmanstätten α and they will thus be termed acicular α. Some of the secondary α particles contain internal platelets (see Special Features section). The dislocation density in the α phases is moderate.

Condition A1. Spherical primary α, acicular α, and β lamellae with interface phase (see Special Features section) comprise the microstructure of this sample. The β phase is free from α precipitation. The acicular α laths have numerous internal platelets. The dislocation density in the primary α is moderate.

Condition A2. This structure is somewhat unusual in that the elongated, secondary α laths contain a fine structure which appears to consist of several variants of α phase, Fig. 29. The transformed β regions contain acicular α which is coarser than in Condition A. The β lamellae contain no α precipitate; the interface phase is present.

Condition B. When compared to Condition A, this sample shows none of the elongated secondary α particles. Also, the acicular α laths in the transformed regions are larger than those in Condition A, Fig. 30.

Condition B1. The major difference between this sample and Condition A1 is that here the acicular α laths have the fine internal structure, Fig. 31. The fine structure is composed of more than one variant of α phase, as illustrated in Fig. 32. In Fig. 32a, the dark field image arises from a $(10\bar{1}0)_\alpha$ reflection and portions of the lath can be seen to be in a strong diffracting orientation, while other portions are not. Similarly, in Fig. 32b, other portions of the lath are in a strongly diffracting orientation when a $(10\bar{1}1)_\alpha$ reflection is imaged. The accompanying diffraction pattern reveals that the $(10\bar{1}0)_\alpha$ and $(10\bar{1}1)_\alpha$ reflections are from different variants. The β phase contains no α precipitation.

Condition B2. The acicular α contains a fine structure as described in the previous sample. The β phase does not exhibit evidence of α precipitation. The dislocation density in the spherical primary α is moderate.

Condition C. The microstructure consists of elongated primary α particles separated by transformed regions. In some areas the transformed region consists of fine acicular α plates separated by β phase. In other areas the transformed region is a very fine mixture of α and β with such a high density of small particles that individual particles of either phase are very difficult to discern, Fig. 33. The α and β phases do not follow the Burgers orientation relation. The primary α particles contain numerous internal platelets.

Condition D. This microstructure is very similar to Condition C with the exception that the primary α particles in Condition D exhibit the internal platelet structure only to a limited extent.

Condition E. Elongated primary α particles separated by transformed β regions comprise this sample. In some of the transformed regions there is a fine acicular α structure, while in others there is a very fine mixture of α and β. The major difference between this sample and Condition C is the lack of internal platelet structure in the primary α in this sample.

Condition F. When compared to Condition E, this sample shows numerous internal platelets in the elongated primary α laths. Otherwise the microstructures are quite similar.

Condition G. The microstructure consists of elongated primary α laths, transformed β regions and a few β lamellae extending between primary α laths. The transformed β regions are fine acicular α in some instances and a fine mixture of α and β in other instances. As in previous samples, the α and β phases in this fine mixture do not follow the Burgers orientation relation. The primary α laths contain the internal platelet structure.

Properties Correlation

The correlation between mechanical properties and microstructure in alloys

such as 6-4, 6-6-2, and 6-2-4-6 is not simple because of the complicated microstructures which occur. The microstructures become more complex with increasing concentrations of β stabilizing alloying elements. Further, there are most certainly combined effects involving more than one microstructural feature which influence mechanical properties. The mechanical properties of the samples produced for the microstructural studies in this program extended over a fairly limited range. Consequently, the correlation between variations in microstructure and such small variations in properties may be misleading. With these limitations in mind, we none-the-less have attempted some correlations between several of the individual microstructural features and mechanical properties.

Microstructural features which could potentially influence properties and which could be quantified to some degree were selected for correlation. These features include average width of α laths, width of interface phase, volume fraction β phase (biased), and dislocation density of primary α. The correlations between these features and yield strength and K_{Ic} were examined. Correlation to elongation was arbitrarily excluded and correlation to fatigue life was not attempted.

Nine (9) samples each of 6-4 and 6-6-2, representing the high, medium, and low values of yield strength and K_{Ic} were selected. No correlations with 6-2-4-6 were attempted since the complex microstructures encountered in this alloy are not readily separated into significant individual features.

The average width of α laths for 6-4 was obtained exclusively from samples containing Widmanstätten α. In the case of 6-6-2, there were approximately 50% Widmanstätten and 50% martensitic α containing samples. The interface phase width was taken as that between α laths and β. The volume fraction β phase, as recorded, is a biased value. The measurements were made from electron micrographs taken specifically in transformed regions and exclusive

of primary α. The values, then, are those for transformed regions only and not for the entire sample. However, since the volume fraction of primary α is fairly constant, except for Condition A-1, the values are biased by a systematic error and thus are relatable to each other. These values also are meaningful in the sense of indicating the ratio of β to Widmanstätten (or martensitic) α. The dislocation densities of the primary α particles were not precisely quantified. Electron micrographs of each of the 9 samples (using the same magnifications and contrast conditions, i.e. the reflection with a two beam orientation) were compared and visually separated into groups corresponding to low, medium and high dislocation densities.

The results of microstructure-property correlations are shown in Figs. 34-41. All curves were drawn as a least squares fit to the data. Figure 34 shows there is a correlation between width of α lath and yield strength for both 6-4 and 6-6-2. No physical significance has been attached to the fact that the slopes of both curves are the same. In Fig. 35 a correlation between α lath width and K_{Ic} is apparent for 6-6-2, but K_{Ic} is independent of α lath width for 6-4.

Figures 36 and 37 demonstrate a correlation between interface phase width and both yield strength and K_{Ic} for 6-4 and 6-6-2. The interface phase width has opposite effects on the yield strength and K_{Ic} as shown in these figures.

The effects of volume fraction β phase (biased) on yield strength and K_{Ic} are shown in Figs. 38 and 39. Again the opposite effect of β phase volume fraction on these two properties is observed.

The results of dislocation density correlations are presented in Figs. 40 and 41. Here no curves are drawn because of the apparent lack of correlation. A trend which indicates yield strength decreases with increasing dislocation density is detectable for 6-4.

DISCUSSION

The beta phase spontaneous transformation, hydrides, alpha-beta interface phase, and alpha lath internal platelet structure are all microstructural features which occur to at least a limited extent in most α, α+β and metastable β titanium alloys. The degree of severity of the shear of the spontaneous transformation is a function of the composition of the beta phase. Based not only on this work but other studies at this laboratory, it has been found that β phase leaner in β-stabilizing solute(s) undergoes more severe spontaneous transformation compared to more concentrated beta phase. The transformation occurs during thinning of the alloy and as such is a thin foil artifact and not representative of the bulk material.

The presence of hydrides in the alpha phase is generally a fairly minor effect. The hydrogen may be introduced in the processing of the alloy or in the mechanical grinding portion of thin foil preparation. The amount of hydrides present in any of the 6-4, 6-6-2, or 6-2-4-6 samples was small and would be expected to have little or no effect on mechanical properties, were they present prior to thinning.

The interface phase which occurs between the β lamellae and α phase in these alloys is of special interest. The importance of the interface phase lies in its potential effect on mechanical properties. The phase could provide an easy fracture path, or conversely it could act to blunt or branch cracks, thus affecting K_{Ic} values in either case. The phase also could provide a barrier to slip across α-β interfaces and thereby affect yield strengths and elongation. When observed with particular diffraction contrast conditions described previously, the interface phase is seen to be a solid, single phase zone for most of the 6-4 and 6-6-2 samples examined in this investigation.

Strain fields are frequently observed in the α-phase near the interface. These strain fields are particularly prominent when the α-phase is strongly diffracting. In this condition, the interface phase could easily be mistaken for a region of high dislocation density. The electron diffraction evidence here indicates that the interface phase is alpha phase of a different crystallographic orientation than the alpha phase it borders. The reasons for the presence of α-phase in an α-β boundary are not entirely clear, but it is possible the interface alpha, which at times appears to grow into the lath α, may be closer to the equilibrium composition.

The platelets which occur within α laths can act as barriers to slip within the laths and in so doing should affect mechanical properties. However, comparisons of relative amounts of platelet structure to yield strength, K_{Ic}, or elongation revealed no correlation in 6-6-2 samples. This likely means that the effect of the platelets is overshadowed by other microstructural features in 6-6-2.

The variations in microstructures among samples were limited in each of the alloys. The alloys were forged to produce either spherical or elongated primary α. In the cases of 6-4 and 6-6-2 the post forging treatment generated either Widmanstätten or martensitic α. The β phase in all the 6-2-4-6 samples appears to have decomposed by nucleation and growth, resulting in a distinctive distribution of α platelet sizes.

There were few anomalies in the microstructure characterization in that comparable forging practice and thermal treatment usually produced similar final microstructures. The most frequently encountered anomaly was the lack of martensite in samples which had been quenched from high temperature. This was more prevalent in the 6-4 alloy than the 6-6-2, and occurred mainly in samples which had been water quenched from the press. In the case of 6-4 only

5 of the 14 samples quenched showed martensite; further, subdivision of these results shows that 1 of 6 quenched from the press was martensitic, while 4 of 8 quenched in the post forge treatment were martensitic. For the 6-6-2 alloy, 3 of 6 samples quenched from the press transformed to martensite and all 8 of those quenched in post forge treatments exhibited a martensitic structure. These results support the notion that the 6-4 alloy and to a lesser extent the 6-6-2 have a very limited deep hardening capability. Thus, heavy sections of these alloys will not transform to martensite thru their section thickness resulting in a microstructural gradient consisting of a martensitic structure at the surface and Widmanstätten α in the center. This seems to be especially true for those quenched from the press, suggesting that the quench delay off the press may have been consistently somewhat greater.

Attempts at rationalizing correlations of individual microstructural features with mechanical properties in alloys which have complex microstructures must be approached with great care. Apparent correlations may be actually the result of several interacting microstructural features or may not be correlations at all, since only a limited number of samples were examined. These restrictions notwithstanding, the following comments are made as regards property correlations.

The increase in yield strength with decreasing alpha lath width may be attributed at least in part to unobstructed slip length effect such as predicted by the Petch equation. Smaller α laths mean shorter slip distances, which is consistent with higher yield strengths, but in the alloys studied here dislocation interactions with the complex interphase boundaries probably also have a significant influence on the yield stress. The parallelism of the 6-4 and 6-6-2 curves is likely fortuitous when the other features of the microstructures in the two alloys, which are quite different, are considered.

The data show that the fracture toughness of 6-6-2 is a function of α lath width, whereas the 6-4 samples show K_{Ic} to be independent of α lath width. Crack propagation path has not yet been determined in these samples, making it difficult to speculate on the role of lath α in resisting crack motion. Alternatively, it may turn out that the K_{Ic} correlation to interface phase width is the correct one, in which case there is a correlation for both alloys, although the effect is much smaller for 6-4. If the crack were to follow the α-β boundaries, it is conceivable that the crack could be blunted when it moves into the interface phase. A broader phase then could provide more volume of material for crack blunting. The apparent correlation of α lath width with K_{Ic} then occurs because there is an interdependence between interface phase width and α-phase lath width.

The width of interface phase also correlates with yield strength. This could be a real effect or could be the result of the dependence of interface phase width upon lath α width. In this case it is reasonable that both interface phase width and α lath width influence the yield strength but the relative contributions of these two factors cannot be separated at present.

The dependence of yield strengths and K_{Ic} values upon the biased volume fraction beta phase in both 6-4 and 6-6-2 is similar to their dependence upon lath α width and interface phase width. The effect of increased amounts of β phase upon the yield strength can be described as similar to that of increased widths of α laths. That is, there is a longer slip distance in the β phase and fewer intersections of dislocations with interphase boundaries. As was the case for α lath widths, the correlation of biased volume fraction β with K_{Ic} is not yet clear.

No correlation could be drawn between dislocation density and either yield strength or K_{Ic} values. This is possibly because of the non-quantitative manner

in which dislocation "densities" were determined, but it is more likely that the range of dislocation densities encountered in this study was not large enough to have much effect on properties. Thus, the contributions of other microstructural variables to variations in mechanical properties may be large enough to mask any effect due to dislocation density variations.

The results have shown that trends, if not correlations, may be made between microstructural features and mechanical properties. However, relating individual microstructural features from a complex microstructure to particular mechanical properties is complicated by the fact that microstructural features interact to affect the mechanical properties more as a unit than as individual features. The trends from each of the microstructural features point up the trade-off that must be made between yield strength and K_{Ic}. For all features, as one increases, the other decreases.

SUMMARY

This report presents the results of transmission electron microscopy of 23 Ti-6Al-4V, 22 Ti-6Al-6V-2Sn, and 11 Ti-6Al-2Sn-4Zr-6Mo samples with various forging and post-forging treatments.

Special microstructural features which occur generally in α-β and metastable β Ti alloys are described. Spontaneous transformation of the β phase and hydride precipitation in the α phase are shown to be artifacts which may occur in thin foils. An interface phase which forms between α and β phases is shown to be α phase of different crystallographic orientation. Internal platelets which are present within Widmanstätten α laths or martensitic α laths have the appearance of β phase with the interface phase at the surfaces of the plates.

The microstructure of each of the 56 samples is documented. In several of the 6-4 samples and a few of the 6-6-2 samples, water quenching from the press was not sufficient to produce a martensitic structure through the cross-section. In many of the 6-2-4-6 and a few of the 6-4 samples, the acicular α laths consisted of a mixture of fine particles which appeared to be several variants of α phase.

Selected microstructural features were quantified and correlated to yield strength and K_{Ic} values. The results show trends, if not correlations, between most of the microstructural features and the mechanical properties. Also illustrated is the microstructural basis for the well-known trade-off between yield strength and fracture toughness.

REFERENCES

1. M. J. Blackburn and J. C. Williams, Trans. Met. Soc. AIME, 239 (1967) 287.
2. N. E. Paton, B. S. Hickman, and D. H. Leslie, Met. Trans. 2 (1971) 2791.
3. E. N. Levine, S. Hayden and H. Margolin, "The Deformation Behavior of Equiaxed α-β Ti-Mn Alloys as Effected by Volume Percent Alpha," paper presented at Mat. Eng. Cong., Cleveland, Ohio, October, 1972.
4. G. F. Pittinato and W. D. Hanna, Met. Trans., 3 (1974) 2905.

TABLE I. Treatments for Specimens of Ti-6Al-4V

Code	Pre-Forge Treatment	Block	Finish	Cool from Press	Comment	Post Forge Treatment
A	-----	1775°F ($\alpha+\beta$)	1800°F($\alpha+\beta$)	AC[1]	10-20% primary α	Ann[3]
B	-----	"	"	AC[1]	" "	STOA[4]
C	-----	"	"	WQ[2]	" "	Ann
A-1	-----	1750°F ($\alpha+\beta$)	1725°F ($\alpha+\beta$)	AC	40-50% primary α	Ann
D	Create spaghetti α	"	1750°F ($\alpha+\beta$)	"		Ann
E	"	"	"	"		STOA
F	"	"	"	WQ		Ann
G	Create grain boundary α	1775°F ($\alpha+\beta$)	1775°F ($\alpha-\beta$)	AC		Ann
H	"	"	"	"		STOA
I	"	"	"	WQ		Ann
J	-----	1900°F (β)	"	AC	10% reduction	Ann
K	-----	"	"	"	" "	STOA
L	-----	"	"	WQ	" "	Ann
M	-----	"	"	"	" "	STOA
N	-----	"	"	AC	30% reduction	Ann
O	-----	"	"	"	" "	STOA
P	-----	"	"	WQ	" "	Ann
Q	-----	"	1900°F (β)	AC	10% reduction	Ann
R	-----	"	"	"	" "	STOA
S	-----	"		WQ	" "	Ann
T	-----	"	"	Slow cool to produce grain boundary α		Ann
U	-----	"	"			STOA

1. AC = air cooled
2. WQ = water quenched
3. Ann = anneal 1300°F/2 hrs/AC
4. STOA = 1750°F/1 hr/WQ + 1300°F/2 hrs/AC

TABLE II. Treatments for Specimens of Ti-6Al-6V-2Sn

Code	Pre-Forge Treatment	Block	Finish	Cool from Press	Comment	Post Forge Treatment
A	-----	1665°F (α+β)	1700°F (α+β)	AC[1]	10-20% primary α	Ann[3]
B	-----	"	"	"	" "	STOA[4]
C	-----	"	"	WQ[2]	" "	Ann
A-1	-----	1625°F (α+β)	1625°F (α+β)	AC	40-50% primary α	Ann
D	Create spaghetti α	1675°F (α+β)	1675°F (α+β)	"		Ann
E	"	"	"	"		STOA
F	"	"	"	WQ		Ann
G	Create grain boundary α	"	"	AC		Ann
H	"	"	"	"		STOA
I	"	"	"	WQ		Ann
J		1800°F (β)	"	AC	10% reduction	Ann
K		"	"	"	" "	STOA
L		"	"	WQ	" "	Ann
M		"	"	"	" "	STOA
N		"	"	AC	30% reduction	Ann
O		"	"	"	" "	STOA
P		"	"	WQ	" "	Ann
Q		"	1800°F (β)	AC	10% reduction	Ann
R		"	"	"	" "	STOA
S		"	"	WQ	" "	Ann
T		"	"	Slow cool to produce grain boundary α		Ann
U		"	"			STOA

1. AC = air cooled
2. WQ = water quenched
3. Ann = 1350°F/2 hrs/AC
4. STOA = 1650°F/1 hr/WQ + 1300°F/2 hrs/AC

TABLE III

Treatments for Specimens of Ti-6Al-2Sn-4Zr-6Mo

Code		Finish	Comment	Post Forge Treatment
A	1625°F ($\alpha+\beta$)	1700°F ($\alpha+\beta$)	10-20% Spherical α	STA[1]
A-1	"	"	" "	Ann[2]
A-2	"	"	" "	STOA[3]
B	"	1625°F ($\alpha+\beta$)	40-50% Spherical α	STA
B-1	"	"	" "	Ann
B-2	"	"	" "	STOA
C	1800°F (β)	1725°F ($\alpha+\beta$)	10% reduction	STA
D	"	"	30% "	STA
E	"	1625°F ($\alpha+\beta$)	10% "	STA
F	"	"	30% "	STA
G	"	1800°F (β)		STA

1. STA = 1625°F/1 hr/air cool + 1100°F/8 hrs/a.c.
2. Ann = 1300°F/1 hr/a.c.
3. STOA = 1625°F/1 hr/a.c. + 1300°F/1 hr/a.c.

Fig. 1. Spontaneous transformation in beta phase in Ti-6Al-6V-2Sn.

Fig. 2. Titanium hydride platelets which have nucleated at α/β boundary and grown into alpha phase in Ti-6Al-2Sn-4Zr-6Al.

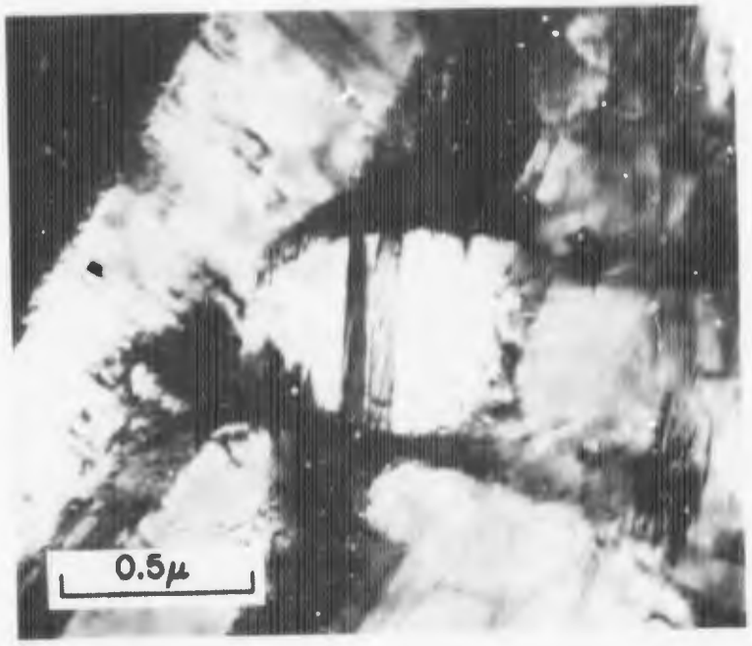

(a)

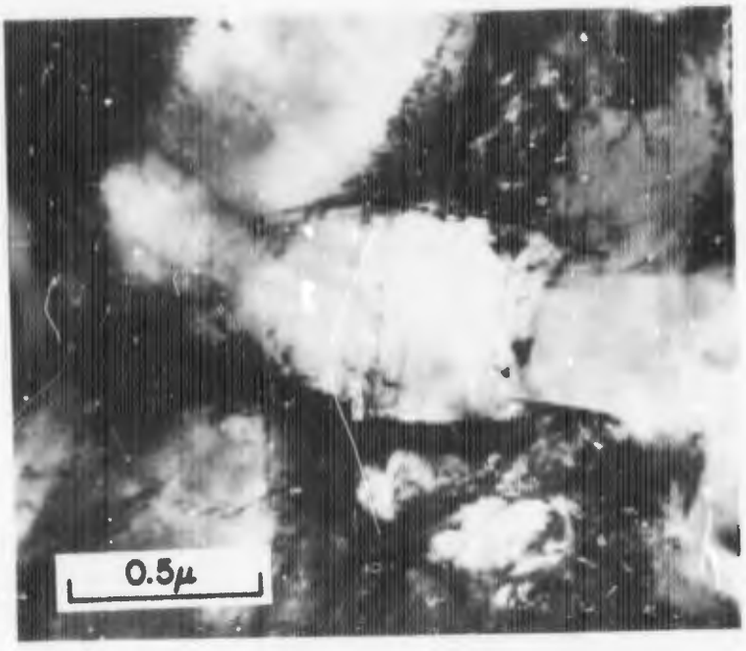

(b)

Fig. 3. Heating stage experiment demonstrating that platelets are titanium hydrides in Ti-6Al-4V. a) Thin foil micrograph taken at room temperature showing platelets in alpha phase. b) Same area after heating to 220°C, platelets have dissolved.

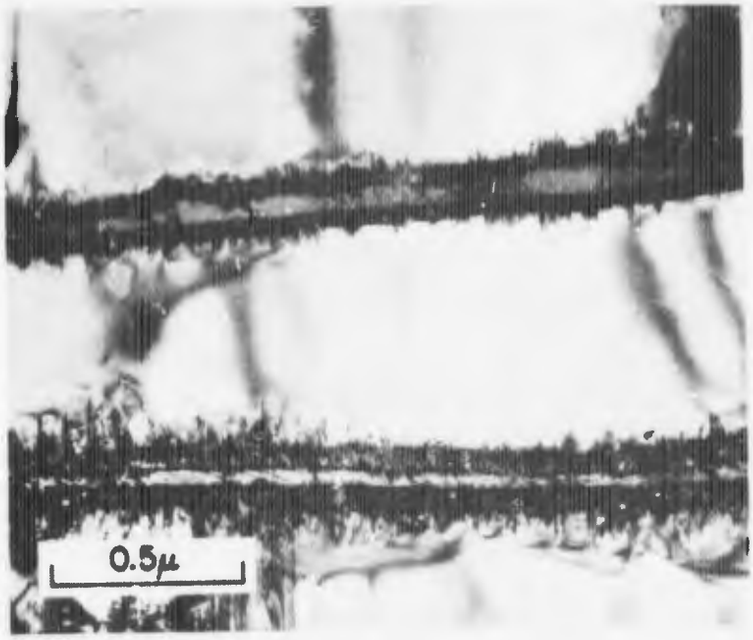

(a)

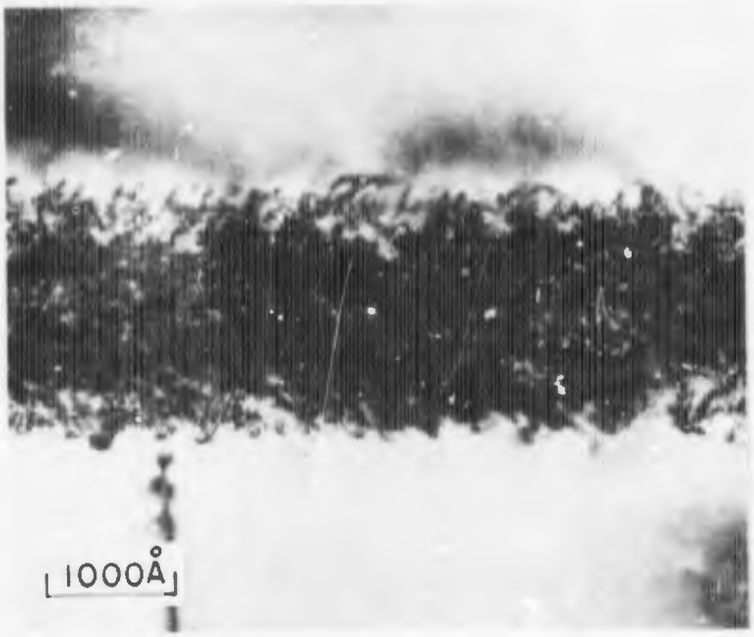

(b)

Fig. 4. α/β interface phase as it occurs in Ti-6Al-4V. a) low magnification with beta phase in contrast, b) high magnification with β phase in poor contrast.

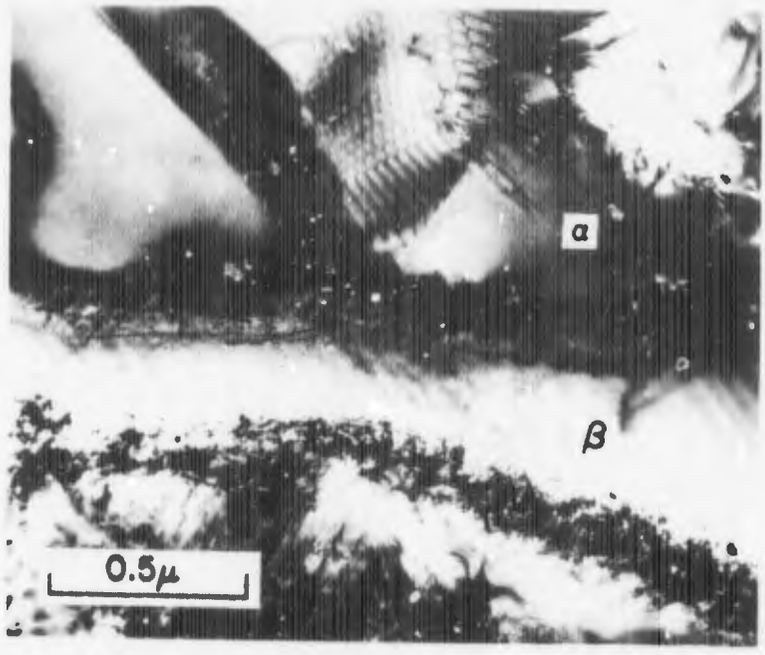

Fig. 5. Thin foil tilted to reveal continuous nature of interface phase in Ti-6Al-6V-2Sn.

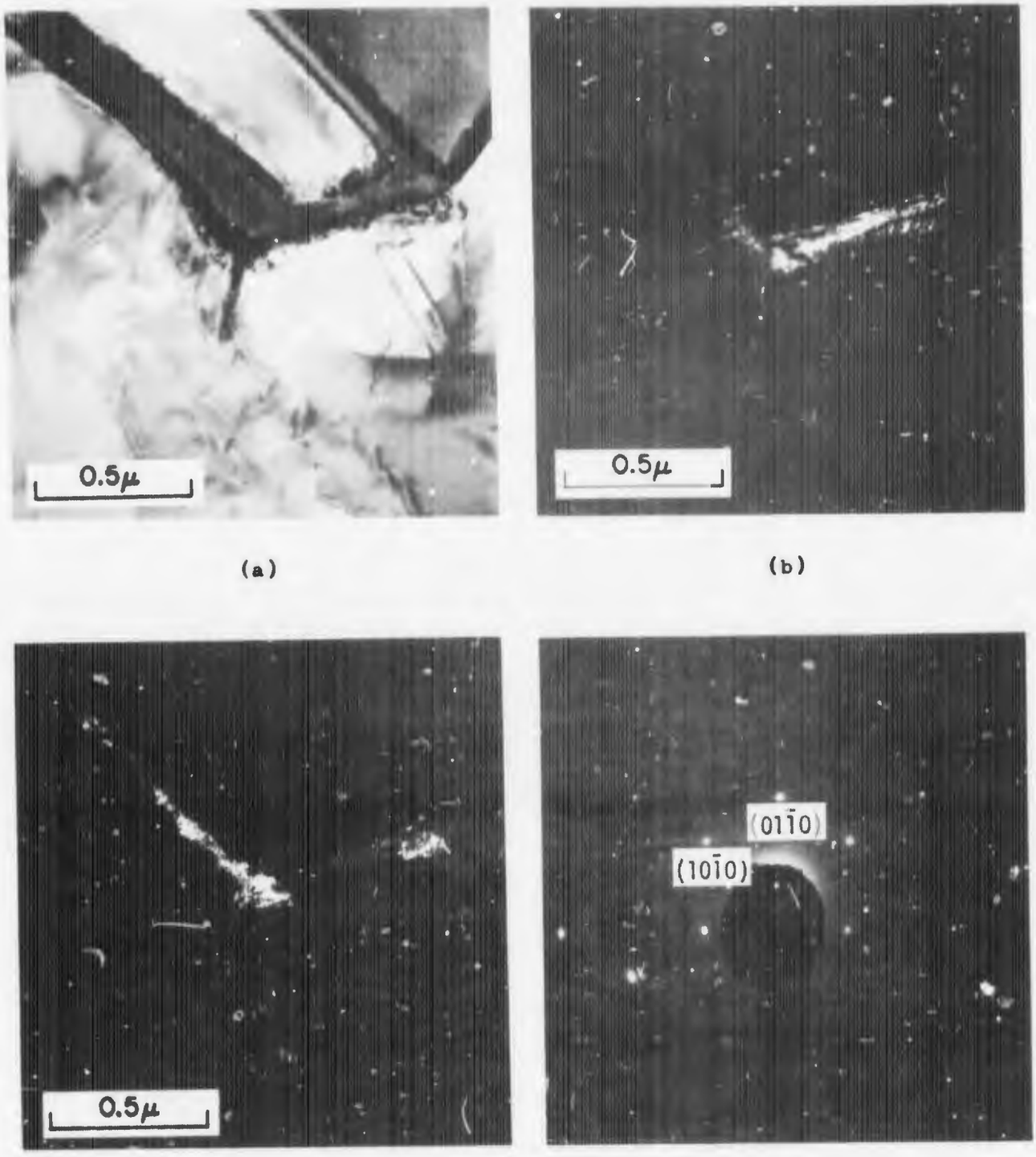

Fig. 6. Interface phase between spaghetti α and β lamella in Ti-6Al-4V. a) Bright field, b) dark field with $(10\bar{1}0)_\alpha$ reflection operating, c) dark field with $(01\bar{1}0)_\alpha$ reflection operating, d) electron diffraction pattern from interface phase indexable as $[0001]_\alpha$ zone.

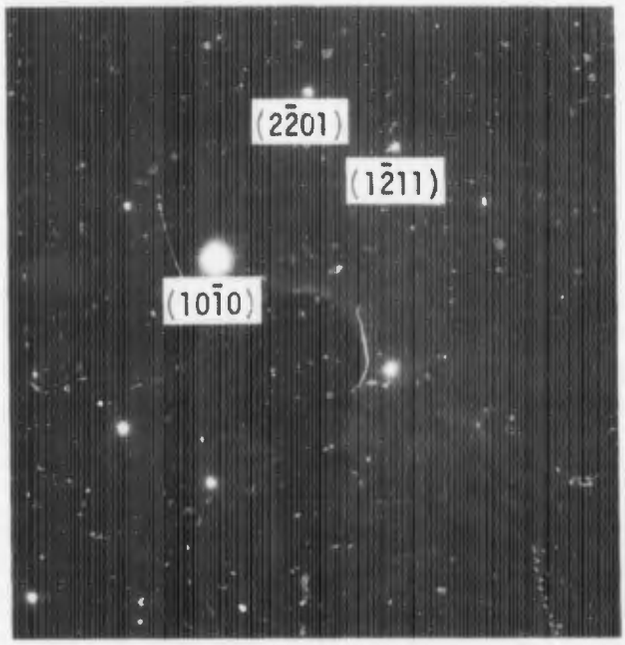

Fig. 7. Electron diffraction pattern from spaghetti alpha phase adjacent to α/β interface phase shown in Fig. 6(a). This zone is 16° from an $[0001]_\alpha$ zone.

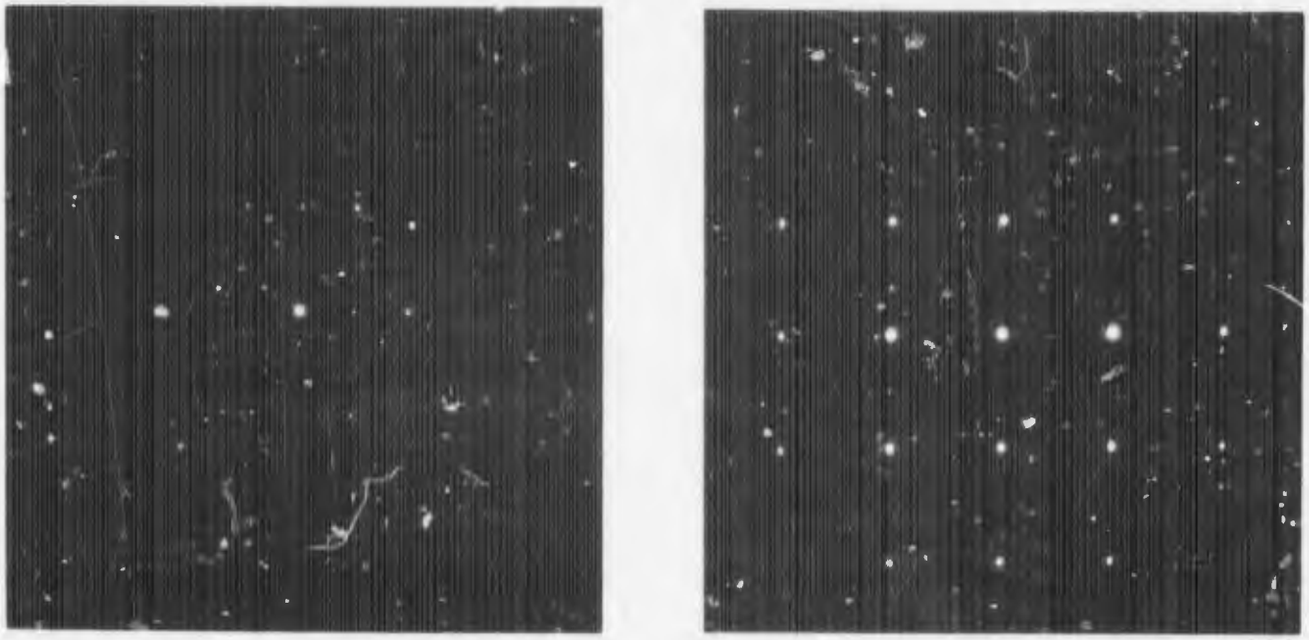

(a) (b)

(c)

Fig. 8. Electron diffraction patterns from α, β, and interface phases in Ti-6Al-6V-2Sn indicating α and β phases exhibit the Burgers orientation relation. a) $[11\bar{2}0]_\alpha$ zone; b) $(001)_\beta$ zone; c) including interface phase which produces arced reflections.

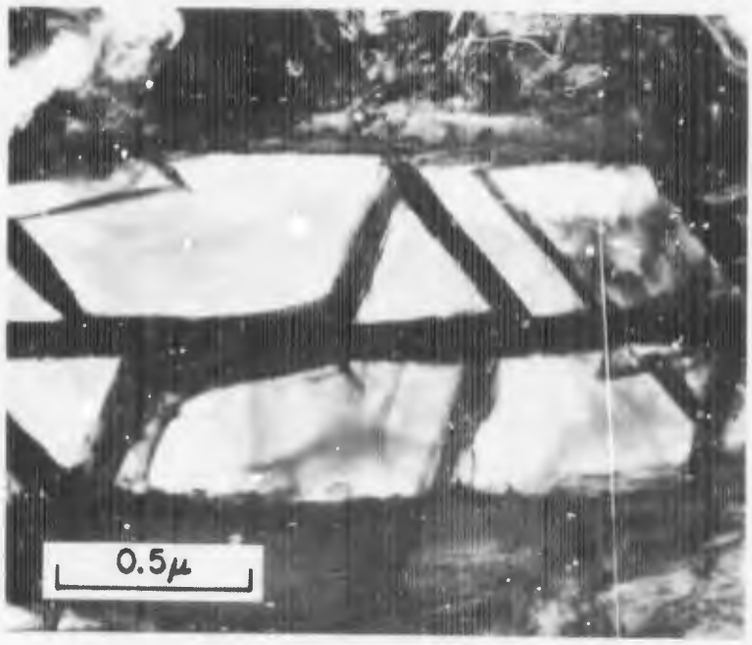

Fig. 9. Internal plates in α laths in Ti-6Al-6V-2Sn.

Fig. 10. The internal plates in the α lath consist of a β strip bounded by interface phase, as illustrated here in Ti-6Al-6V-2Sn.

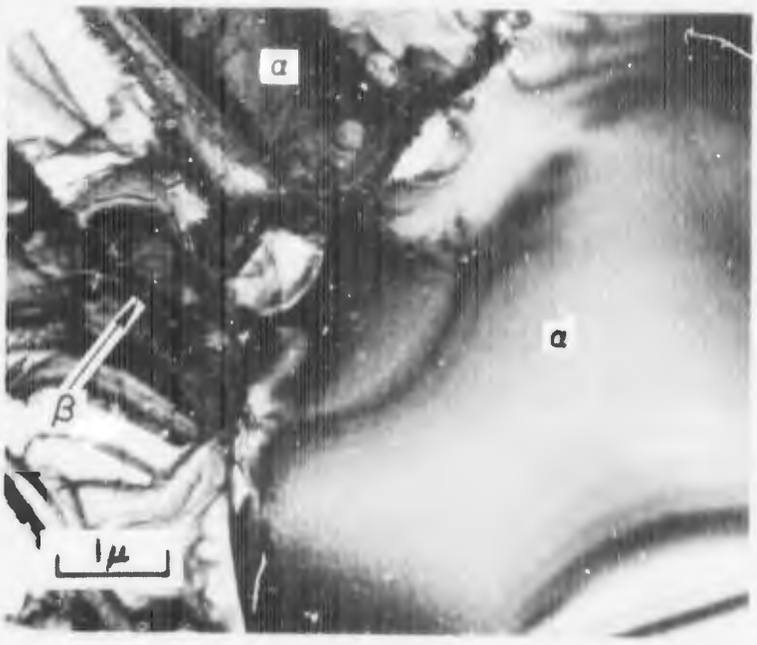

Fig. 11. Typical microstructure of Ti-6Al-4V, Condition A illustrating spherical primary α, Widmanstätten α, β-phase lamellae, and α/β interface phase.

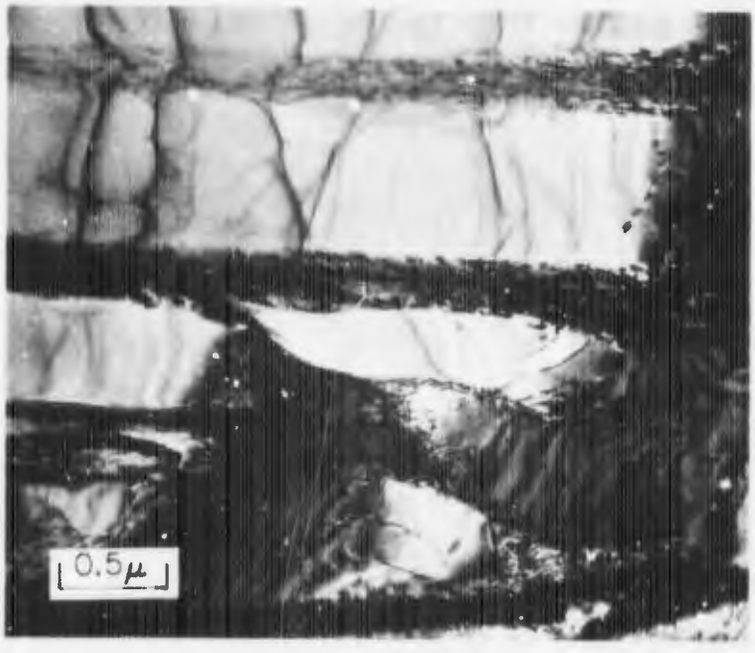

Fig. 12. Widmanstätten α laths in Ti-6Al-4V low oxygen, Condition A.

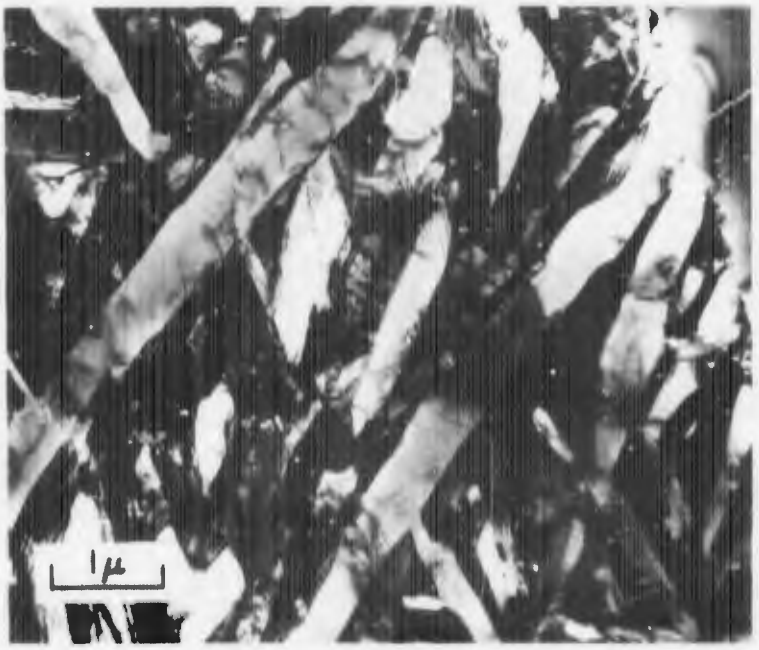

Fig. 13. Martensitic α in Ti-6Al-4V, Condition B.

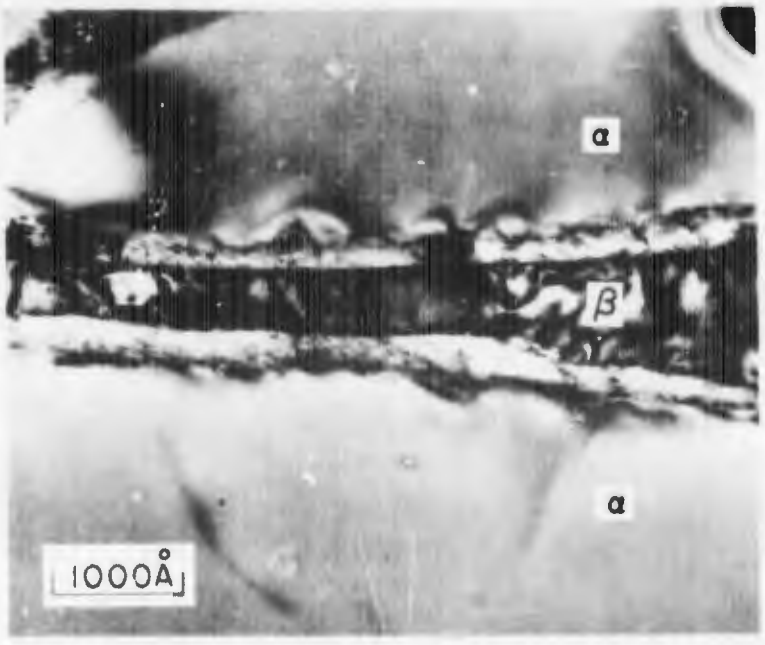

Fig. 14. Interface phase between α and β phases in Ti-6Al-4V, Condition B.

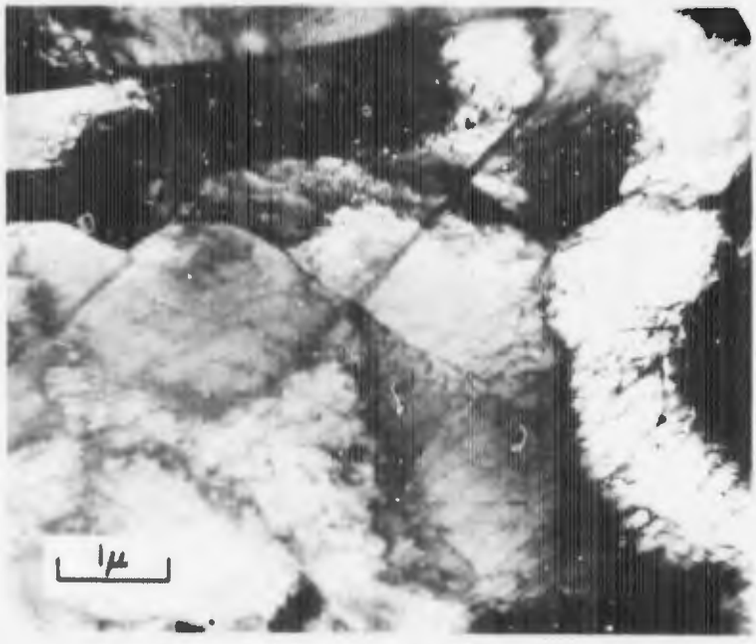

Fig. 15. Dislocation arrangements in spaghetti alpha phase in Ti-6Al-4V, Condition D.

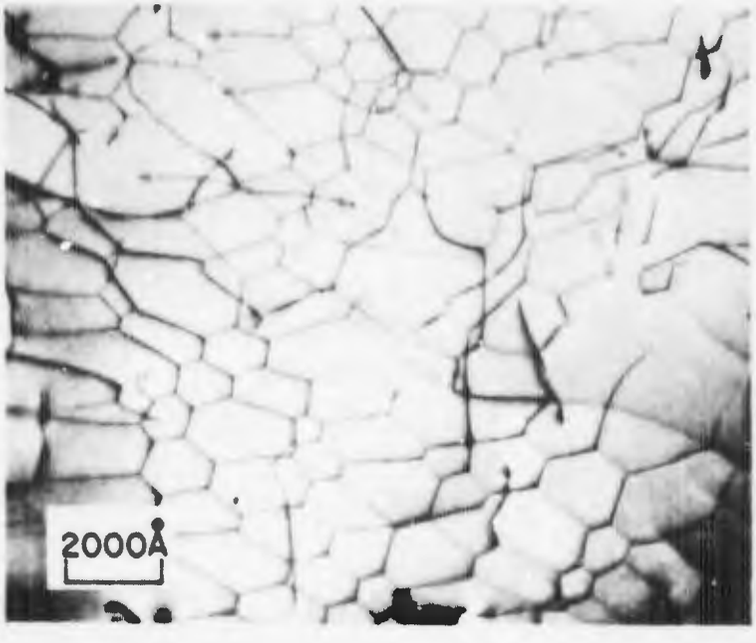

Fig. 16. Dislocation network in primary α phase in Ti-6Al-4V, Condition D.

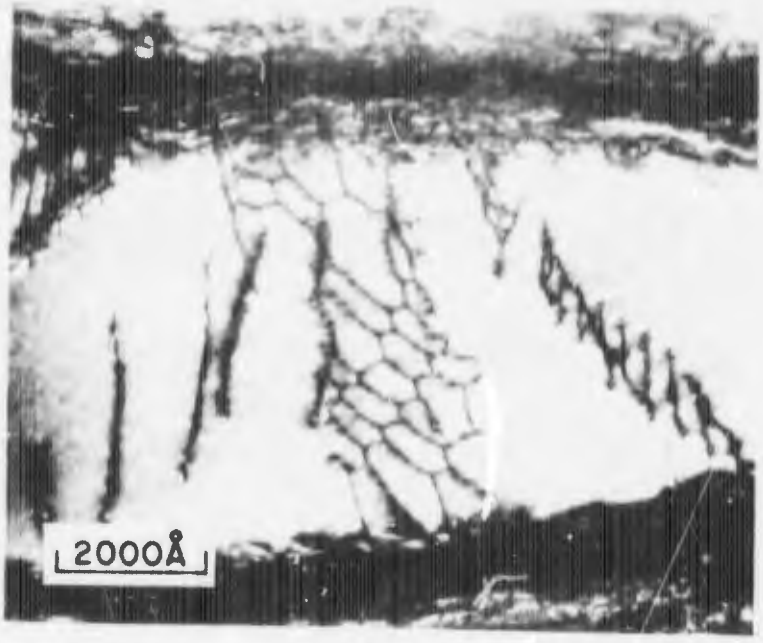

Fig. 17. Dislocation network in Widmanstätten α phase in Ti-6Al-4V, Condition D.

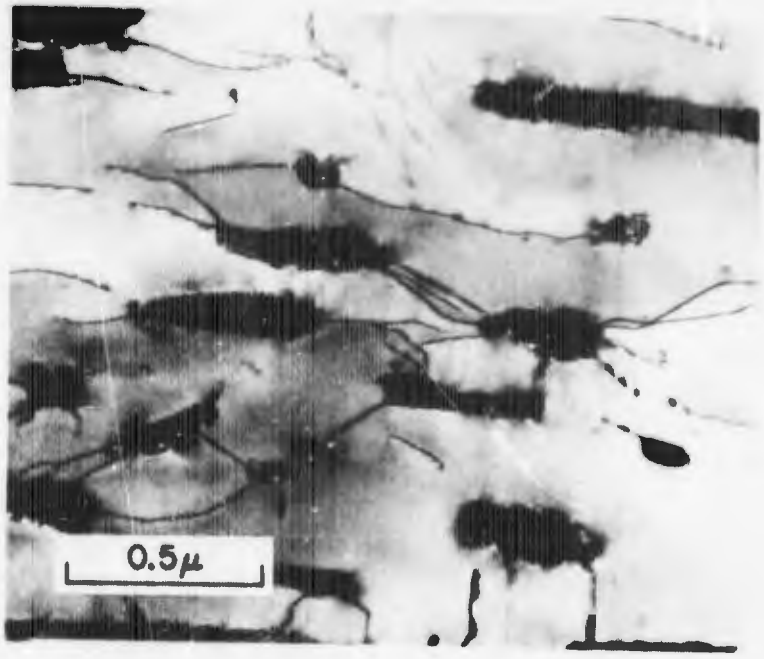

Fig. 18. Beta phase precipitates in large α phase lath in Ti-6Al-4V, Condition E.

Fig. 19. Dislocation arrangements in grain boundary α phase in Ti-6Al-4V, Condition I.

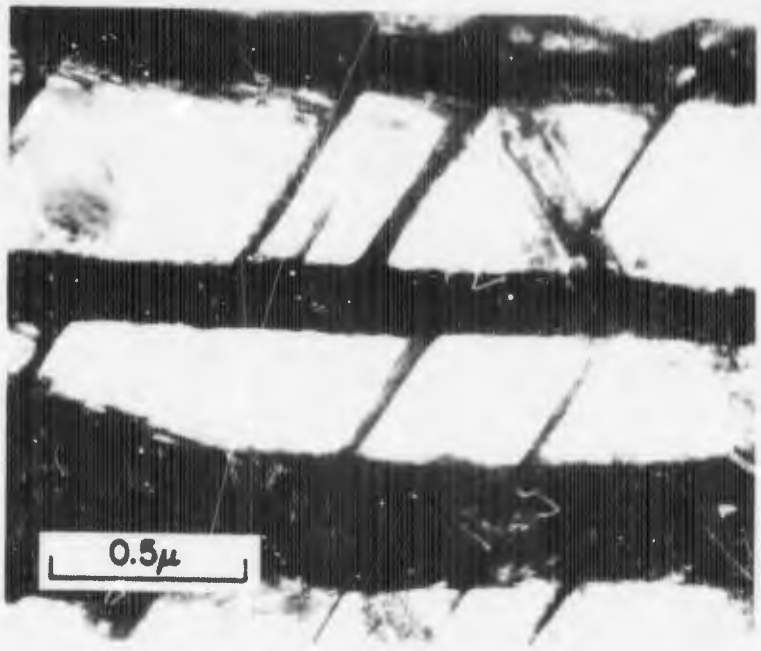

Fig. 20. Internal plate structure in martensitic α phas in Ti-6Al-4V, Condition M.

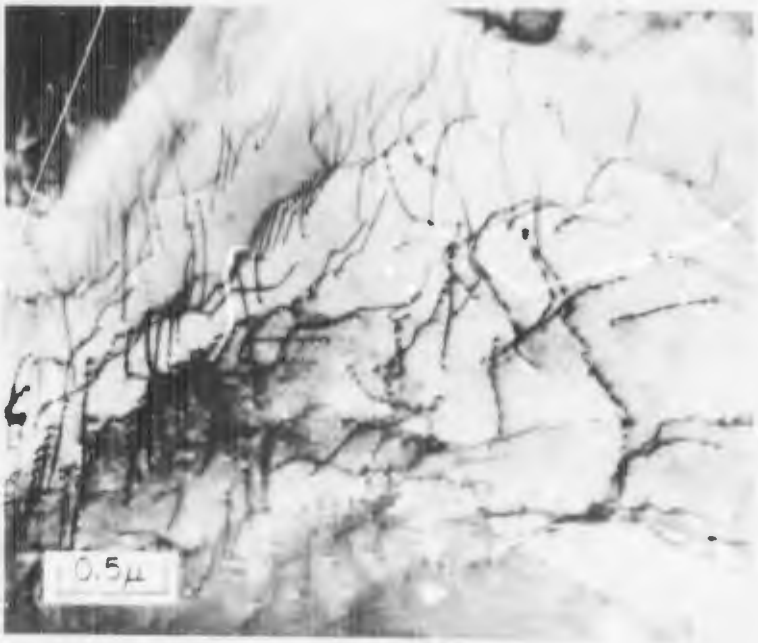

Fig. 21. Dislocations in primary α phase in Ti-6Al-6V-2Sn, Condition A.

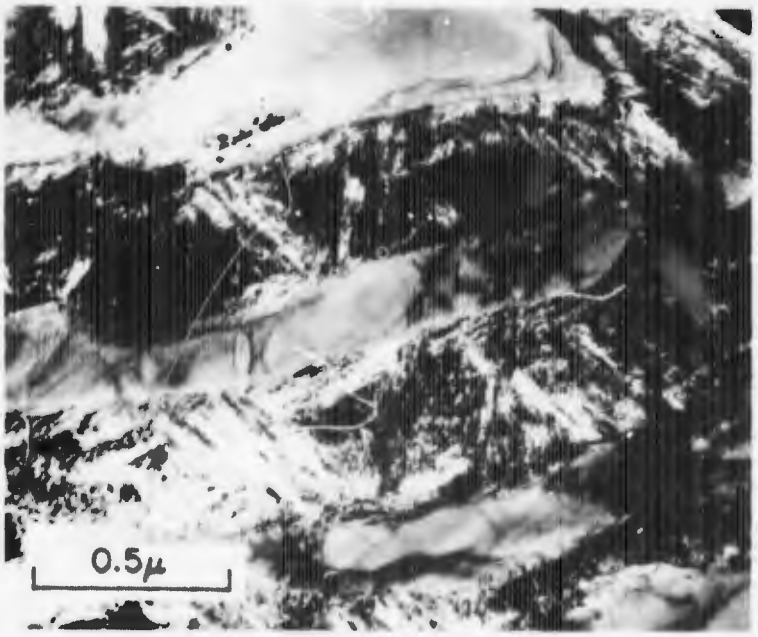

Fig. 22. Martensitic α laths containing a fine internal structure in Ti-6Al-6V-2Sn, Condition B.

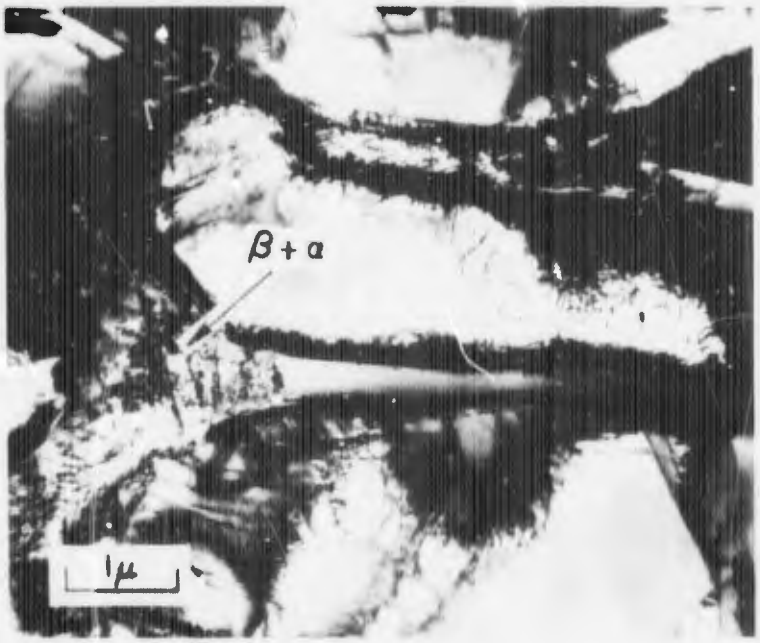

Fig. 23. Alpha phase precipitation in broad areas of beta phase in Ti-6Al-6V-2Sn, Condition A1.

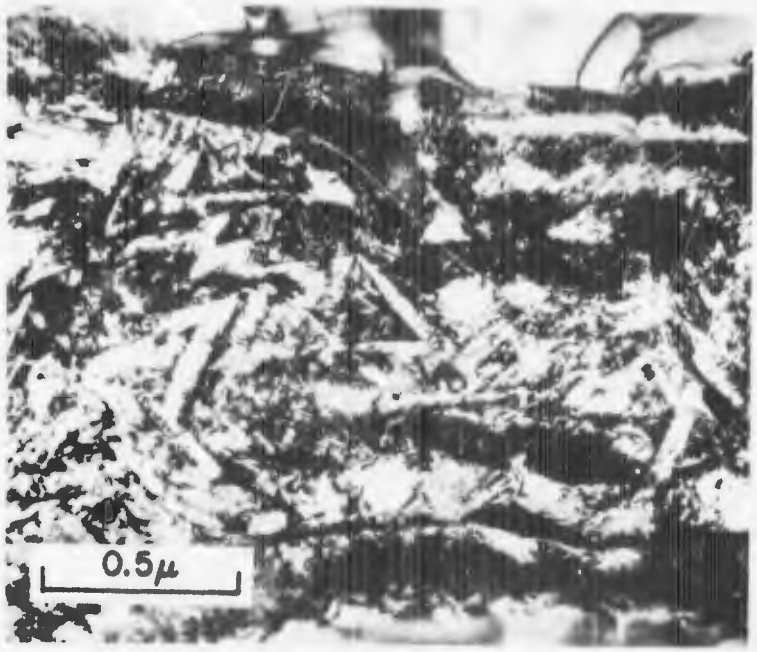

(a)

(b)

Fig. 24. A thick beta lamella in which α phase has precipitated in Ti-6Al-6V-2Sn, Condition D. The selected area diffraction pattern which is a $\langle 111 \rangle_\beta$ zone, reveals that the α-phase does not precipitate with the Burgers orientation relation.

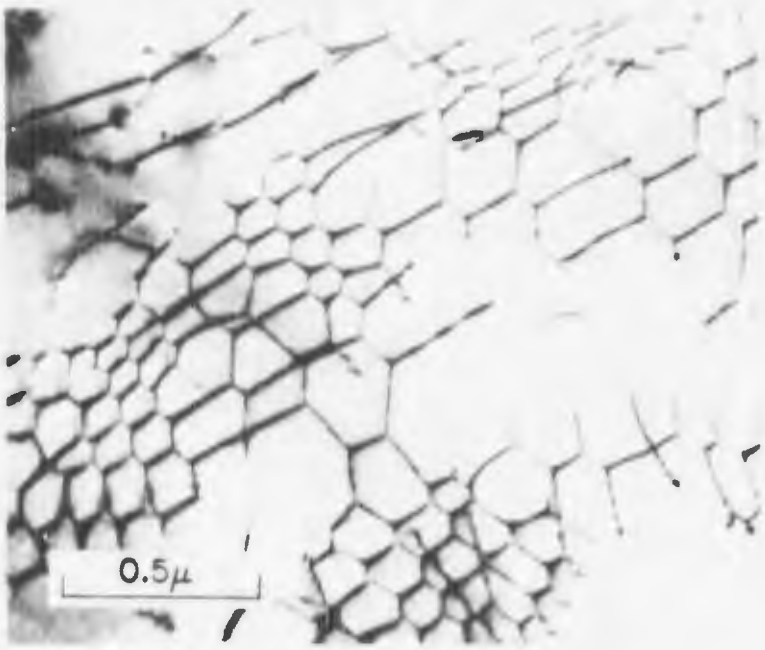

Fig. 25. Dislocation networks in spaghetti α phase in Ti-6Al-6V-2Sn, Condition D.

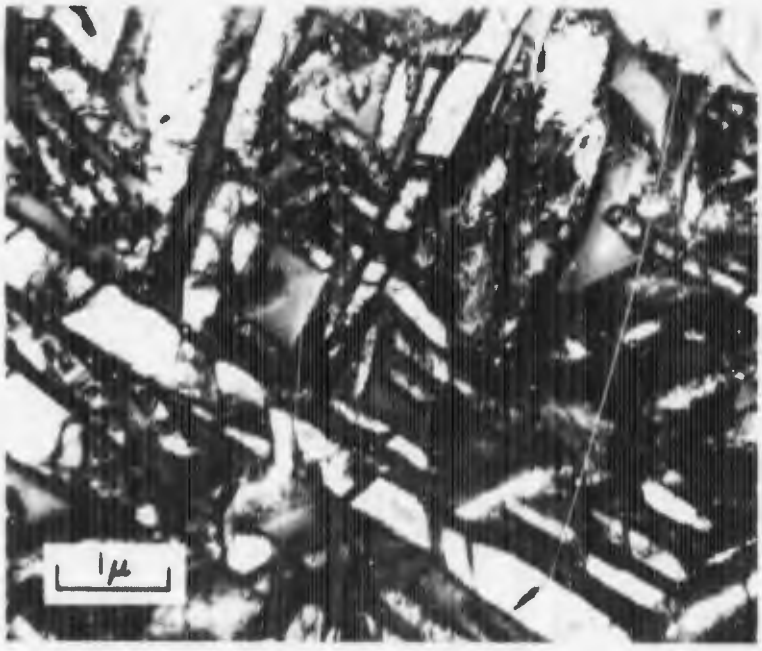

Fig. 26. Martensitic α laths containing internal plates in Ti-6Al-6V-2Sn, Condition D.

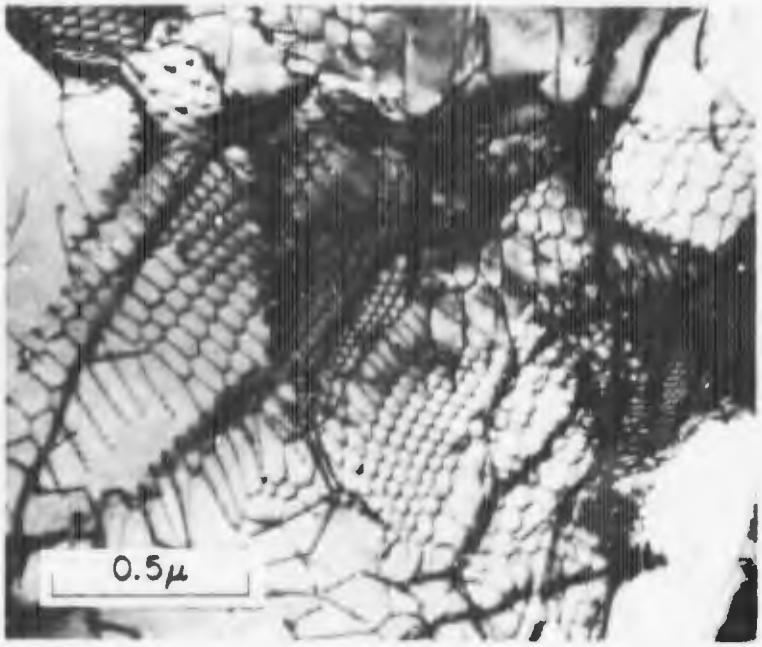

Fig. 27. Dislocation networks in primary α in Ti-6Al-6V-2Sn, Condition H.

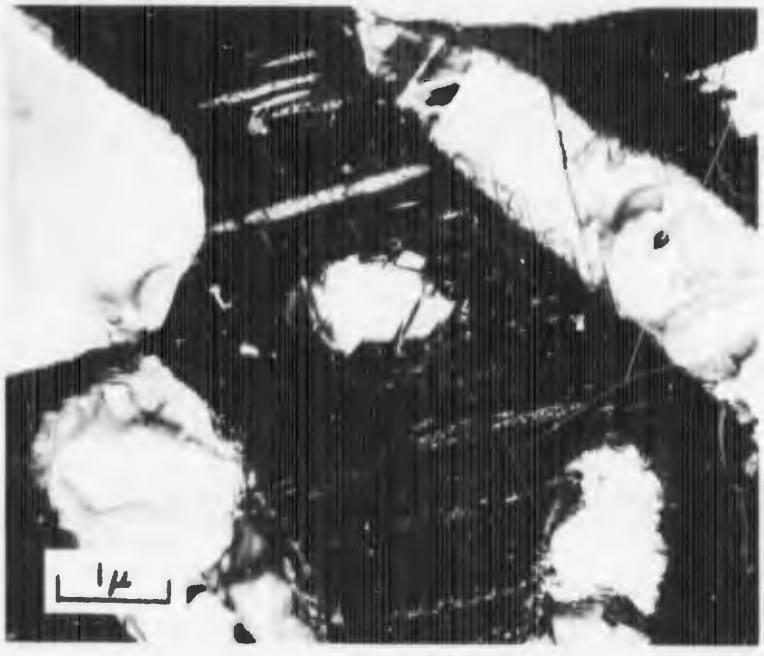

Fig. 28. Typical microstructure of Ti-6Al-2Sn-4Zr-6Mo, Condition A.

(a)

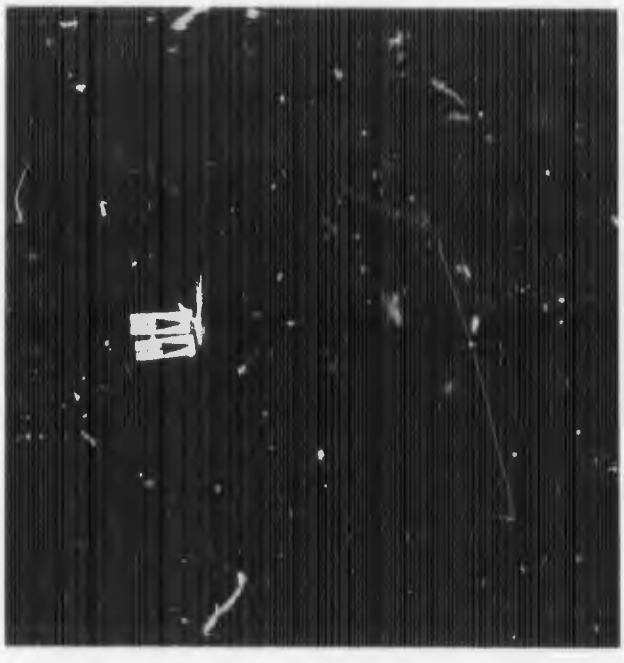

(b)

Fig. 29. Internal structure in α-phase lath in Ti-6Al-2Sn-4Zr-6Mo, Condition A2. a) Dark field electron micrograph using two relrods indicated in (b). b) SAD of α lath, near [0001] α zone with numerous relrods appearing. Arrows indicate two used for (a).

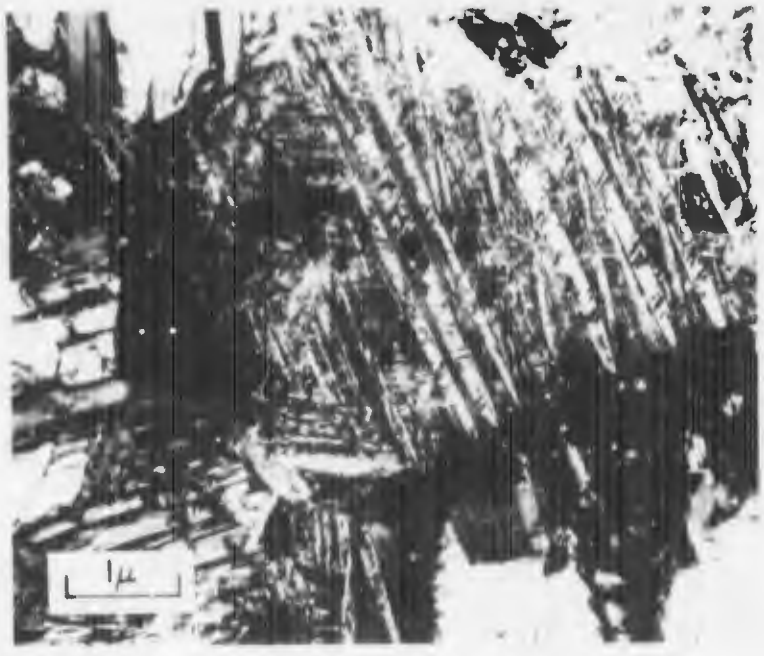

Fig. 30. Transformed region containing acicular α and β lamellae in Ti-6Al-2Sn-4Zr-6Mo, Condition B.

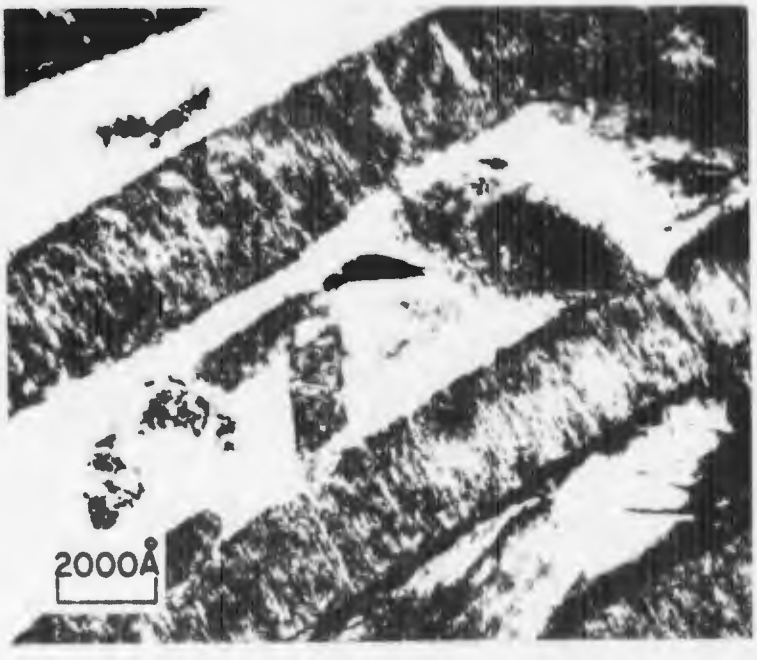

Fig. 31. Fine internal structure in α-phase laths in Ti-6Al-2Sn-4Zr-6Mo, Condition B1.

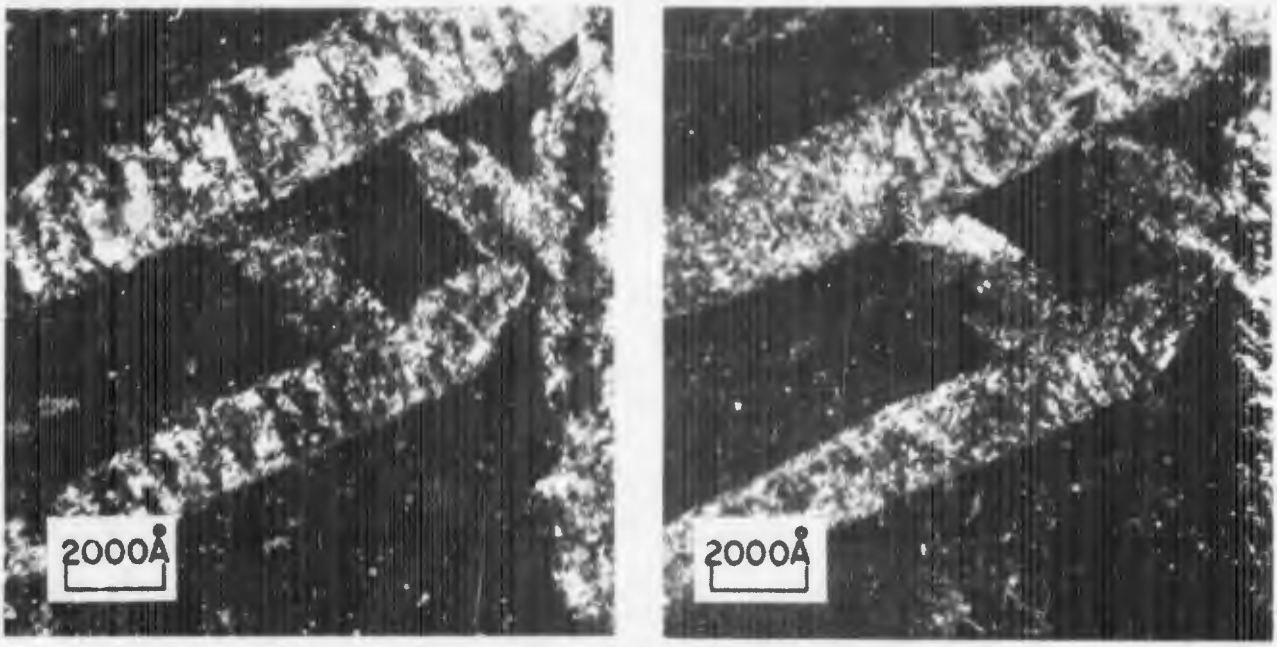

(a) (b)

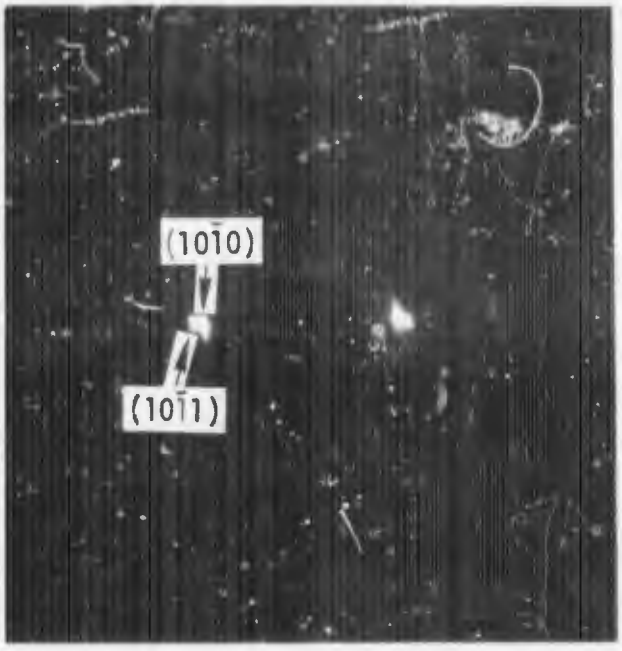

(c)

Fig. 32. Internal structure in α laths in Ti-6Al-2Sn-4Zr-6Mo, Condition B1. a) Dark field micrograph using $(10\bar{1}0)_\alpha$ reflection; b) dark field micrograph using $(10\bar{1}1)_\alpha$ reflection; c) SAD pattern with α reflections indicated.

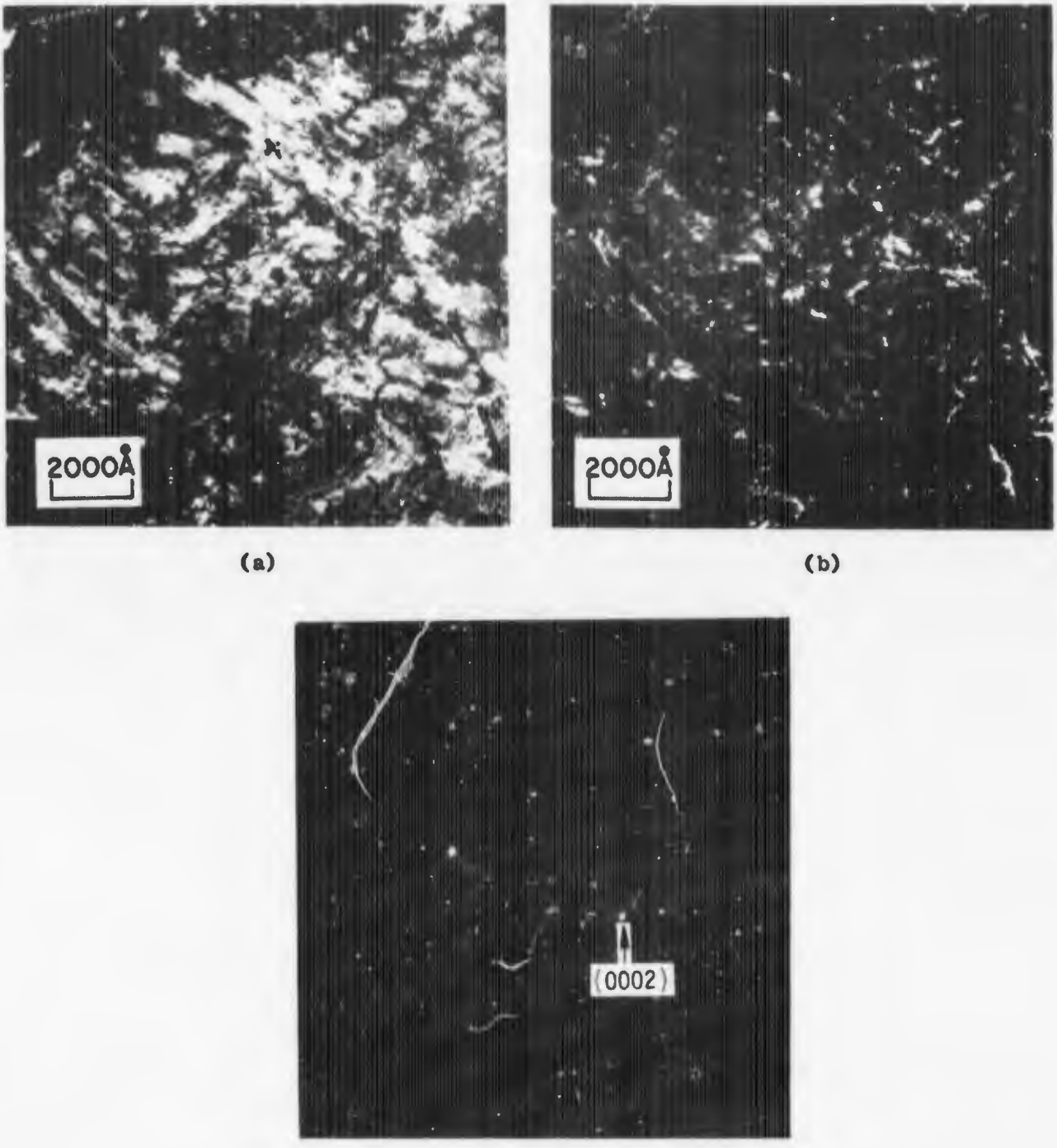

(a) (b)

(c)

Fig. 33. Transformed β region in Ti-6Al-2Sn-4Zr-6Mo, Condition C. a) Bright field showing fine mixture of α and β phases; b) Dark field using $(0002)_\alpha$ reflection; c) SAD containing α reflections from more than one variant.

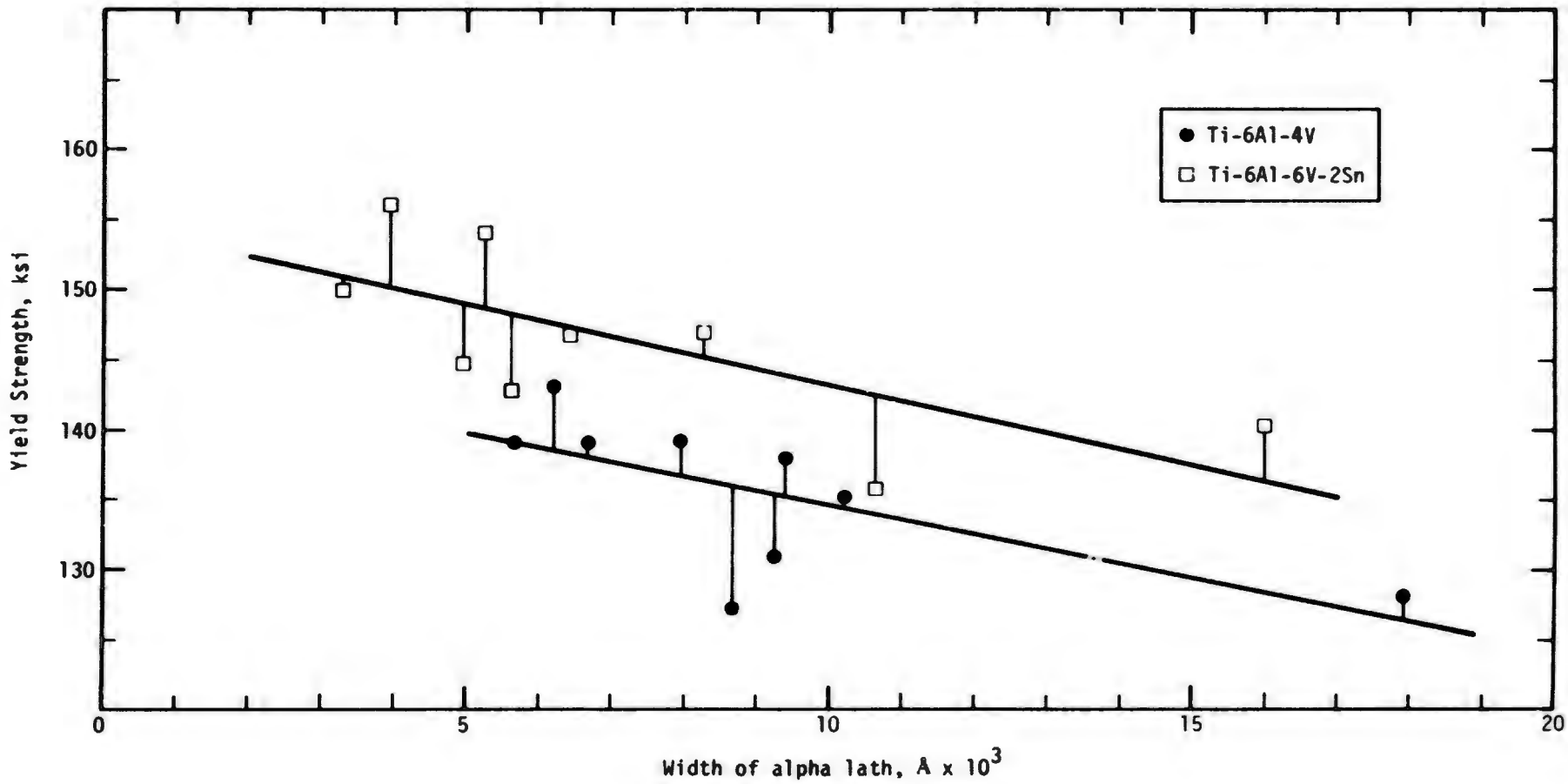

Fig. 34. Plots of the average width of alpha phase laths vs. yield strength for Ti-6Al-4V and Ti-6Al-6V-2Sn. Curves are least squares fits of the data.

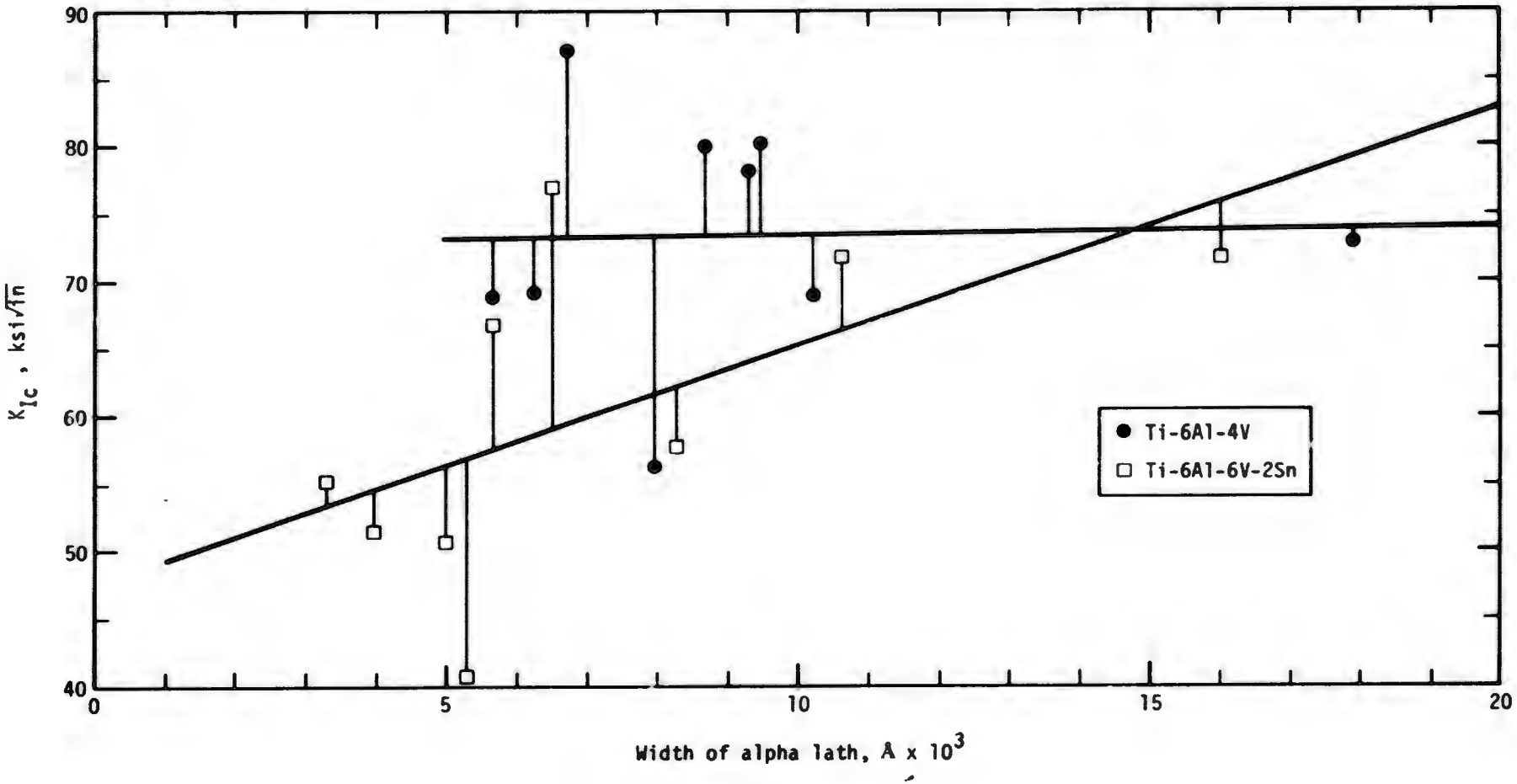

Fig. 35. Plots of the average width of alpha phase laths vs. fracture toughness for Ti-6Al-4V and Ti-6Al-6V-2Sn. Curves are least squares fits of the data.

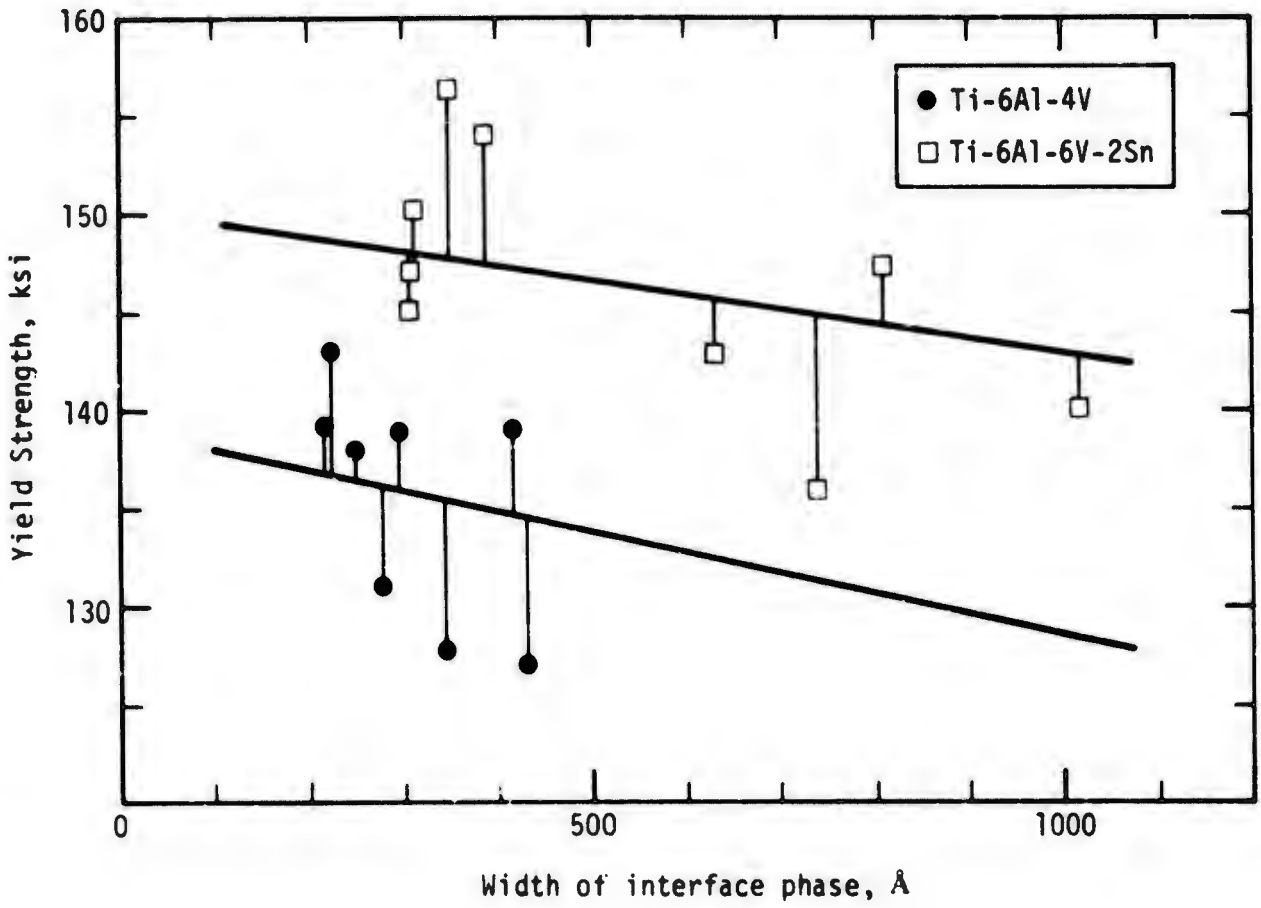

Fig. 36. Plots of the average width of the α-β interface phase vs. yield strength for Ti-6Al-4V and Ti-6Al-6V-2Sn. Curves are least squares fits of the data.

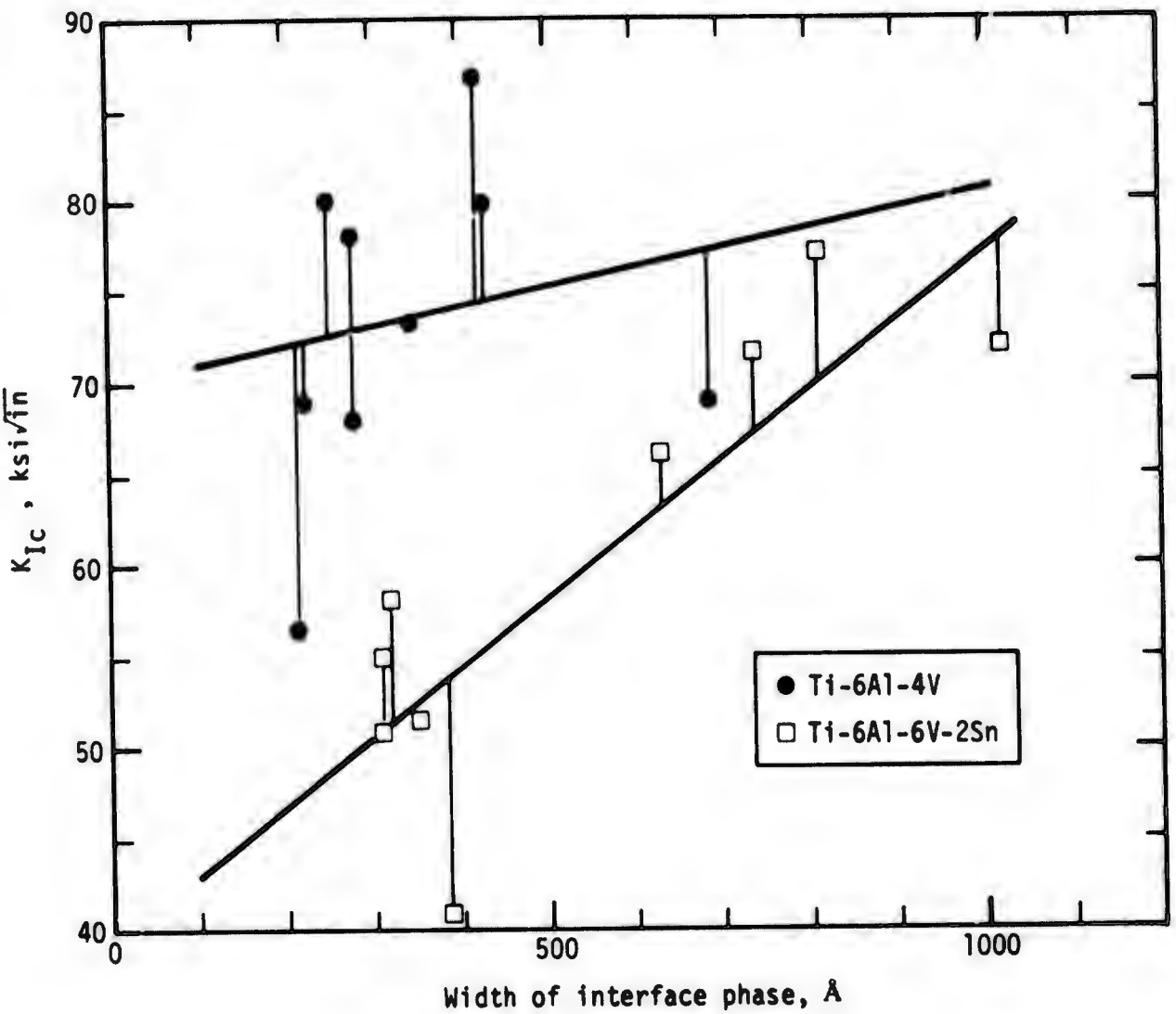

Fig. 37. Plots of the average width of the α-β interface phase vs. fracture toughness for Ti-6Al-4V and Ti-6Al-6V-2Sn. Curves are least squares fits of the data.

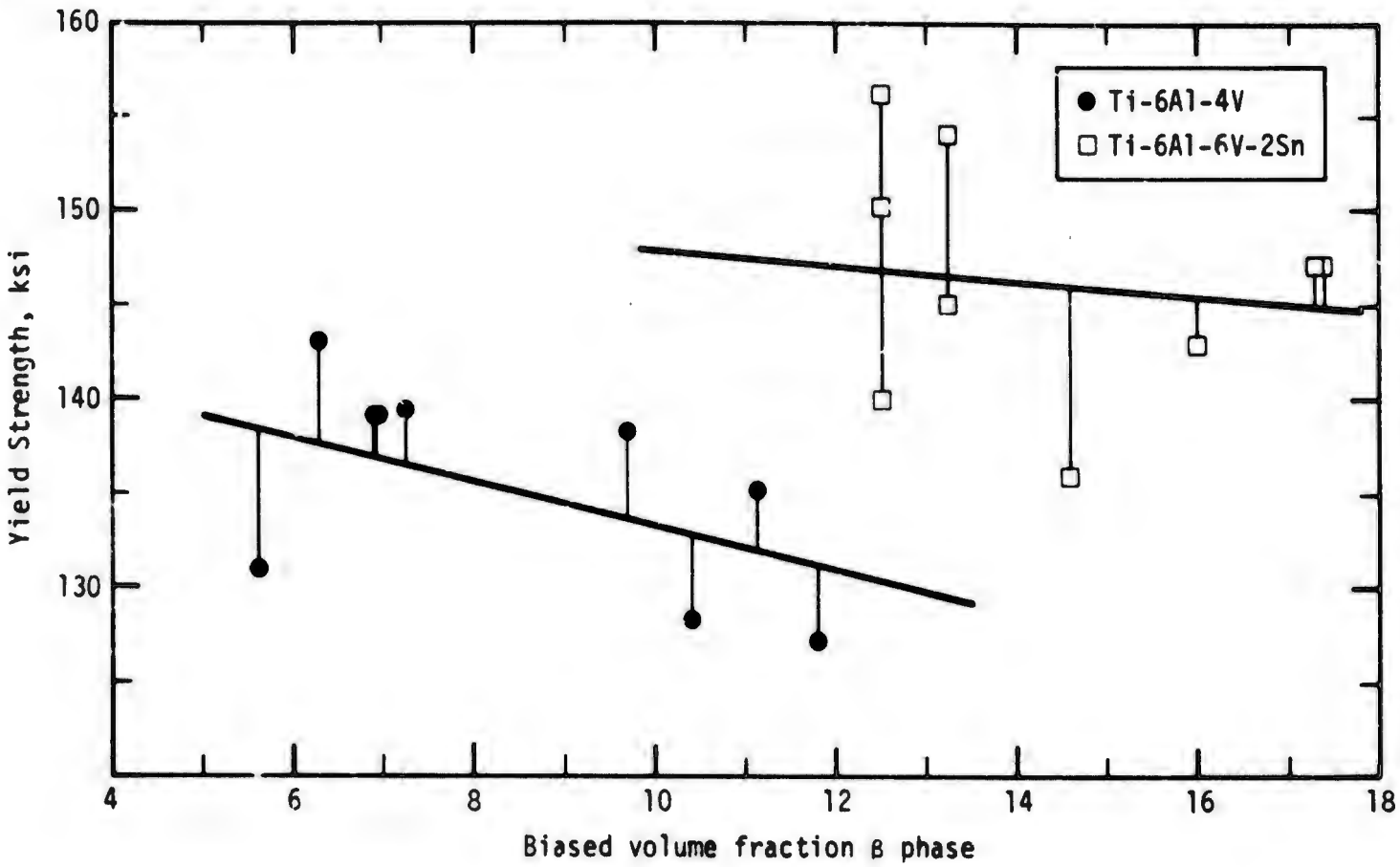

Fig. 38. Plots of the biased volume fraction β phase (see text for explanation) vs. yield strength for Ti-6Al-4V and Ti-6Al-6V-2Sn. Curves are least squares fits of the data.

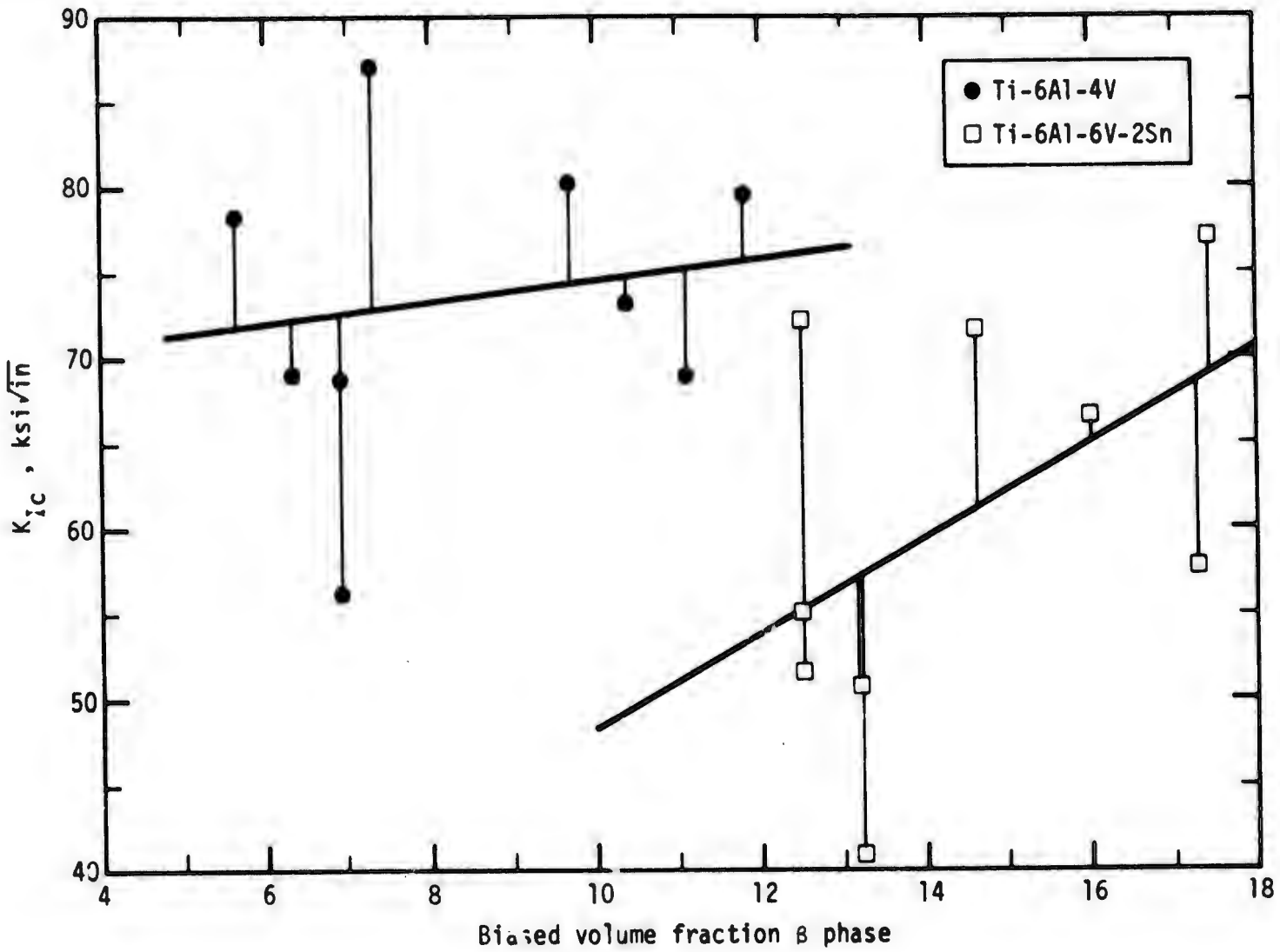

Fig. 39. Plots of the biased volume fraction β phase (see text for explanation) vs. fracture toughness for Ti-6Al-4V and Ti-6Al-6V-2Sn. Curves are least squares fits of the data.

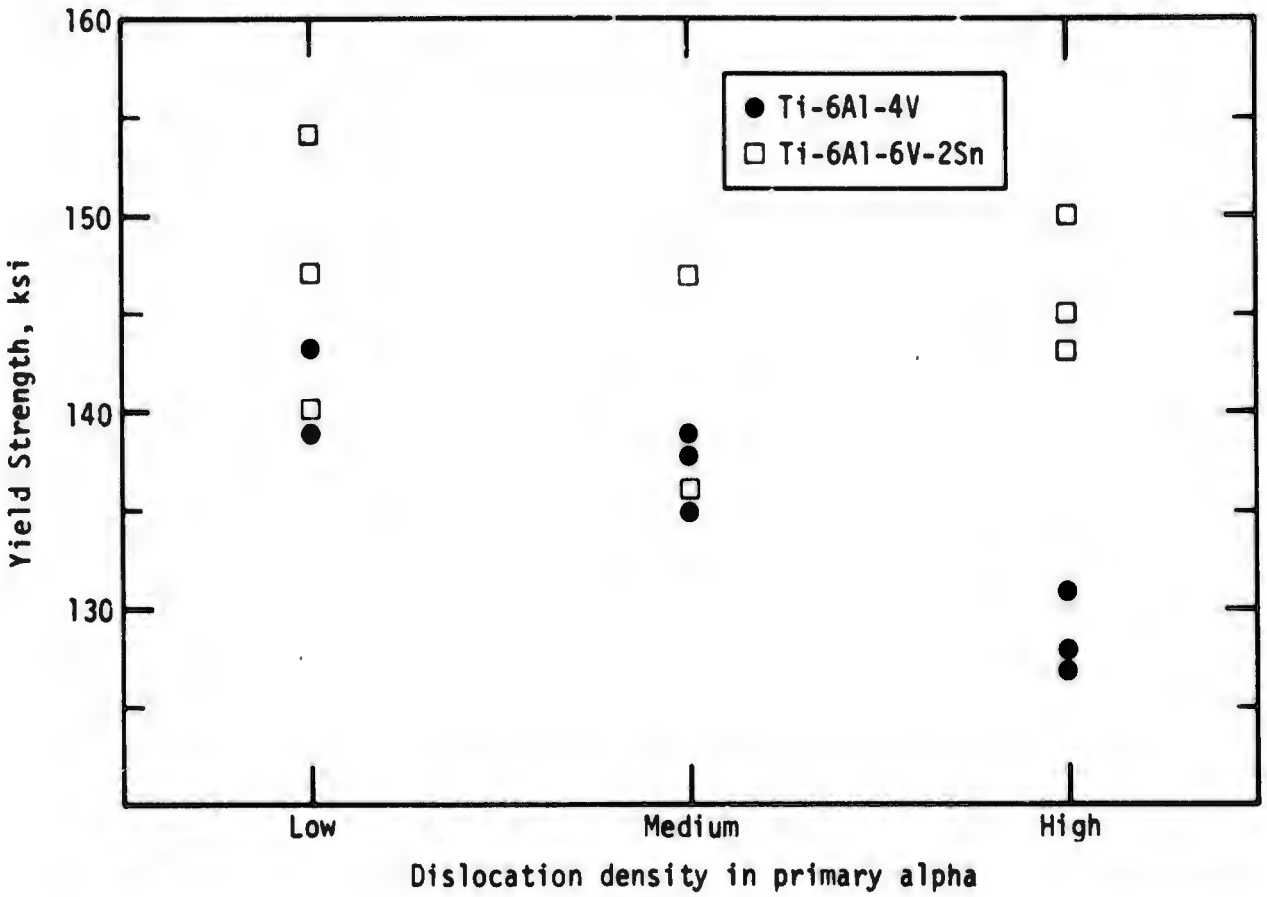

Fig. 40. Qualitative dislocation densities vs. yield strength for Ti-6Al-4V and Ti-6Al-6V-2Sn.

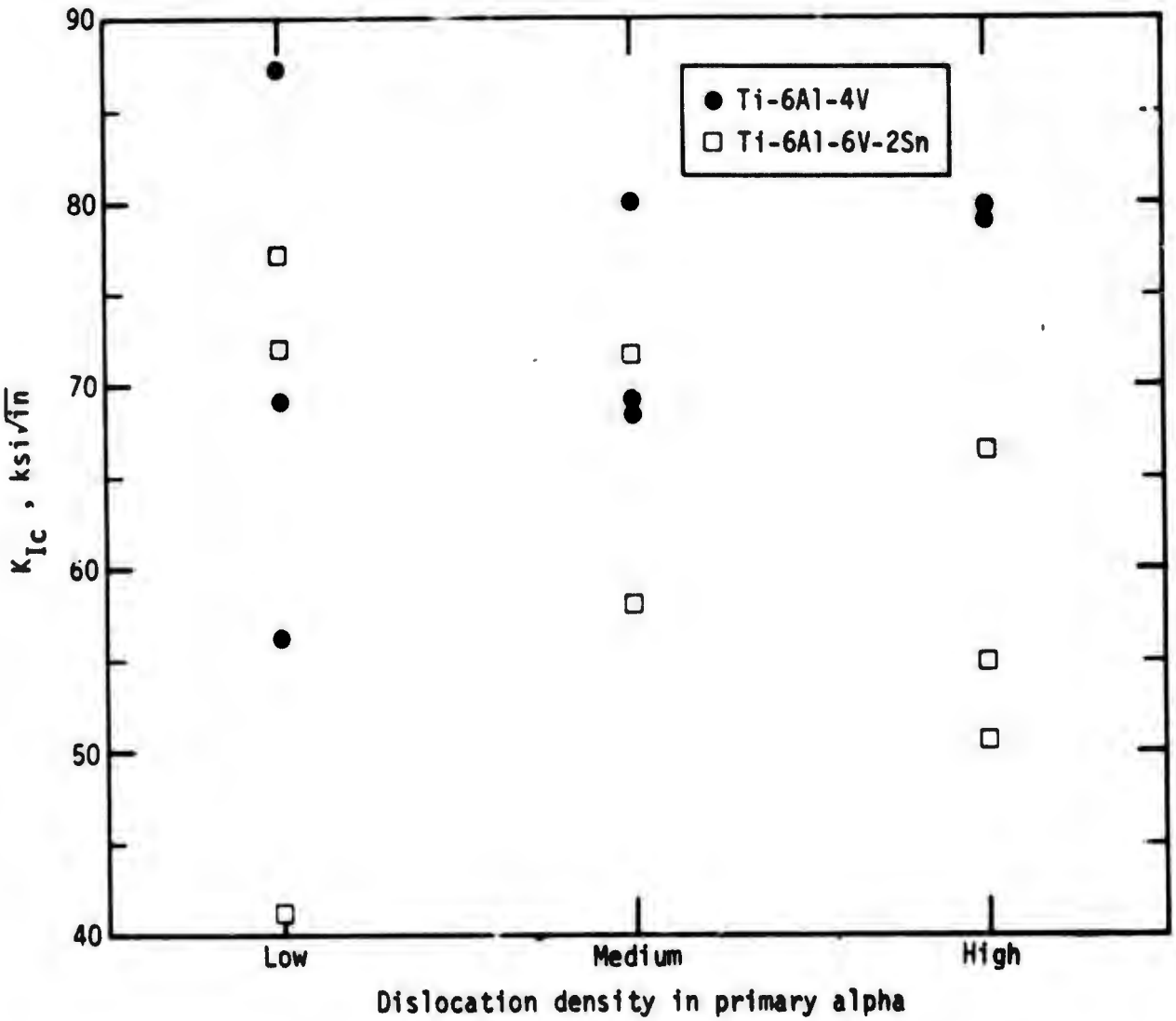

Fig. 41. Qualitative dislocation densities vs. fracture toughness for Ti-6Al-4V and Ti-6Al-6V-2Sn.

APPENDIX G

ROCKWELL INTERNATIONAL SCIENCE CENTER REPORT ON SCANNING ELECTRON MICROSCOPY STUDY OF FRACTURE PATTERNS ON FRACTURE TOUGHNESS SPECIMENS

ELECTRON FRACTOGRAPHIC STUDY OF BROKEN K_{Ic} SPECIMENS FROM Ti ALLOY FORGINGS

Received from Wyman-Gordon

As Part of Air Force Contract #F33615-71-C-1560

Submitted To:

R. B. Sparks

Prepared By:

J. C. Chesnutt and J. C. Williams

19 October 1973

INTRODUCTION

The Rockwell International Science Center was subcontracted by the Wyman-Gordon Company to perform an electron fractographic study on 42 titanium alloy samples under Air Force Contract #F33615-71-C-1560. The following broken fracture toughness (K_{Ic}) specimens were supplied: 16 Ti-6Al-4V, 15 Ti-6Al-6V-2Sn, and 11 Ti-6Al-2Sn-4Zr-6Mo in conditions representing various forging and post-forging treatments. The conditions furnished are listed in Table I; the details of the particular treatments are found in preceding sections of the contract final report.

The Science Center's approach to the electron fractographic study emphasized scanning electron microscopy (SEM) with supporting replica fractography as required as a referee technique. The irregular surface topography of the broken Ti-6Al-4V and Ti-6Al-6V-2Sn specimens coupled with the resolution obtainable with the SEM resulted in use of the SEM for examination of these specimens.

EXPERIMENTAL

Specimens received by the Science Center consisted of mating halves of the broken K_{Ic} samples. The size of these specimens necessitated sectioning prior to SEM examination. Accordingly, a 1/8 in thick slice of parallel to and containing the fracture face was cut from one half of each specimen as shown in Fig. 1. Prior to cutting, the fracture face was protected with Krylon spray which was removed by an acetone wash prior to mounting the sample. The samples were mounted on standard specimen stubs with conducting paint and were examined at 20 KV and an angle of 40 ± 5° in an ETEC Autoscan capable of resolving less than 100 Å. Areas of each sample examined included, but were

TABLE I - ALLOY CONDITIONS EXAMINED

Ti-6Al-4V	Ti-6Al-6V-2Sn	Ti-6Al-2Sn-4Zr-6Mo
A	A	A
A (low O_2)	A-1	A-1
A-1	B	A-2
B	D	B
D	E	B-1
E	G	B-2
G	H	C
H	J	D
J	M	E
M	N	F
N	O	G
O	Q	
Q	R	
R	T	
T	U	
U		

not limited to:

1) the precrack approximately one-half way between the notch and the fatigue (precrack) - fast fracture transition,
2) the fatigue to fast fracture transition, and
3) the fast fracture zone approximately 0.30 in ahead of the transition.

RESULTS AND DISCUSSION

The results, which are presented in Fig. 2 through Fig. 43, are grouped by alloy and within each alloy group the figures are presented in the order of decreasing fracture toughness. Each figure in general represents examination of the three areas discussed in the experimental section. All figures, with the exception of Fig. 12, are presented with the direction of crack propagation running from left to right. A 500X light micrograph appears in the upper left corner of each figure and the fatigue to fast fracture transition is generally located in the lower center of the figure. Different regions photographed at similar magnifications are presented horizontally. Areas photographed at increasing magnifications are connected by a solid line. The 0.2% offset yield stress (YS), ultimate tensile strength (UTS) and fracture toughness (K_{Ic}) are shown on each figure. The K_{Ic} values are for the individual specimen examined in this program.

Ti-6Al-4V

The results for this alloy are presented in four groups: 1) $K_{Ic} > 90$ KSI$\sqrt{in}$, 2) 80 KSI$\sqrt{in} \leq K_{Ic} \leq 90$ KSI$\sqrt{in}$, 3) 60 KSI$\sqrt{in} \leq K_{Ic} \leq 80$ KSI$\sqrt{in}$ and 4) $K_{Ic} < 60$ KSI$\sqrt{in}$.

K_{Ic} greater than 90 KSI$\sqrt{in}$

Only one condition, a low oxygen material processed to Condition A

resulted in this level of toughness. The fracture surface, which was predominantly transgranular had features characteristic of a high energy fracture, including considerable dimple formation (Fig. 2). The regions of ductile tearing appeared to be largely associated with the primary α particles.

K_{IC} from 80 to 90 KSI$\sqrt{in}$

The four microstructures in this group, Conditions D, J, U, R (Figs. 3-6), though having different microstructures, all exhibit considerable dimple formation. For Conditions D, J, and R the fracture is primarily transgranular with regions of ductile tearing associated with the spaghetti α in Condition D and the primary α in Conditions J and R. Condition U, which was fully β processed exhibits, in addition to the transgranular fracture, some large "facets" which appear to be associated with the prior β grain boundaries. Dimple formation on the scale of the Widmanstätten α plate size (Fig. 5h) are also observed. Condition R has some crack branching which is manifested as secondary cracks on the fracture surface, these possibly occur along prior β grain boundaries.

K_{Ic} from 60 to 80 KSI$\sqrt{in}$

This group contains ten conditions, Conditions T, M, O, N, G, Q, A-1, E, A, H (Figs. 7-16). The specimens representing microstructural conditions in this group of Ti-6Al-4V exhibit mixed fracture modes, all of which are consistent with extensive ductility. These modes include void formation and growth, ductile tearing and plastic stretching or sliding-off. The intermixing of these modes seems in part dependent on microstructure as described below but the ranking of K_{Ic} values on the basis of fracture topography is not possible at present since the relative contributions to toughness of the

three ductile fracture modes mentioned above cannot be assessed. The conditions which have equiaxed primary α show localized regions of fracture by sliding off, the distribution of these regions is similar to the distribution of equiaxed primary α particles. The transformed β matrix shows a combination of poorly developed dimples and tear ridges. In some instances the dimples (or holes) appear to form at α/β interfaces or α' (martensite) plate boundaries.

The fast fracture zone in Condition T (Fig. 7) is similar to that of Condition R (Fig. 6) but the crack branching in this condition produces some smooth appearing facets with considerable microscopic dimple formation (Fig. 7i and j). The precrack zone in Condition M (Fig. 8) exhibits regions with well-developed fatigue striations; these regions appear to correspond to the primary α platelets. These same platelets provide a fracture path in the fast fracture zone. An interesting feature is the hole (Fig. 8j) which has apparently formed at a hard particle which has subsequently been dragged across the fracture surface leaving the trail also seen in Fig. 8j.

Condition G (Fig. 11), which was processed to produce a grain boundary α network, is striking in the effect of this network on the fracture topography in the fatigue to fast-fracture transition zone and in the fast-fracture zone. The transition region is shown in a montage of 2000X micrographs (Fig. 11g) and the particles in the fast-fracture zone in Fig. 11e.

Condition A-1 (Fig. 13) which contains 40-50% primary α in the form of large spherical particles demonstrates the effect of this type of particle on the propagation of a crack in either fatigue (Fig. 13b and c) on fast fracture (Fig. 13d, g and h).

Condition E (Fig. 14) exhibits a structure which contains spaghetti α, elongated primary α and martensitic α and shows the effect of the spaghetti α and/or primary α particles on the fracture propagation. In Fig. 14 h and i

can be seen a probable interface between a large α particle and a packet of martensitic α through which the crack has propagated.

The fracture modes characteristic of the other microstructures in this group (Figs. 9, 10, 12, 15 and 16) exhibit the same general features previously described.

K_{Ic} less than 60 KSI$\sqrt{in}$

Only one condition examined, Condition B (Fig. 17) was in this group. The structure which contained 10-20% primary α also contained a large fraction of martensitic α. Fracture was characterized by extensive fracture by sliding-off; this appears to occur along the boundaries between the primary α and the regions of martensitic α. In addition, considerable secondary cracking is present in this specimen.

Ti-6Al-6V-2Sn

The results for this alloy are presented in three groups: 1) 60 KSI$\sqrt{in} \leq K_{Ic} \leq$ 75 KSI$\sqrt{in}$, 2) 45 KSI$\sqrt{in} \leq K_{Ic} <$ 60 KSI$\sqrt{in}$, and 3) $K_{Ic} <$ 45 KSI$\sqrt{in}$.

K_{Ic} from 60 to 75 KSI$\sqrt{in}$

This group contains ten conditions, Conditions J, T, R, Q, U, M, G, N, D and O (Figs. 18-27) all of which, with the exception of G and D, were β blocked and β or α+β finished. All the microstructural conditions in this group of Ti-6Al-6V-2Sn exhibit corresponding mixed fracture modes representative of considerable ductility. As in the case of Ti-6Al-4V in similar conditions, and in the same toughness range, these modes include void formation and growth, ductile tearing and plastic stretching or sliding-off. Specific features of unusual interest will be discussed in further detail.

In Condition J the elongated primary α laths can be seen to act as a preferential fracture path in both fatigue crack propagation (Fig. 18b and c) and rapid fracture (Fig. 18g and h).

Although processed to produce grain boundary α, Condition T consists of Widmanstätten α lath separated by lamellar regions of untransformed β. Fracture through or around bundles of Widmanstätten α produces the "herringbone" appearance in Fig. 19h, i and j. The grain boundary α particles in Condition G (Fig. 24) offer a preferential fracture path although one requiring high energy as seen in the dimple formation in Fig. 24i.

K_{Ic} from 45 to 59 KSI$\sqrt{in}$

This group of four specimens, Conditions E, H, A and A-1 (Figs. 28-31) all of which were α+β processed have fracture features characteristic of a lower energy fracture process. Such features include small, shallow dimples and smooth appearing regions associated with fracture through the spaghetti α primary α or grain boundary α particles.

K_{Ic} < 45 KSI$\sqrt{in}$

The lowest toughness condition in the Ti-6-6-2 alloy falls in this group. It is Condition B (Fig. 32) which contains 10-20% spherical primary α and martensitic α laths. Crack propagation around the primary α particles appears very easy with the particles exhibiting a smooth cleavage type fracture.

Ti-6Al-2Sn-4Zr-6Mo

Unlike the preceding two alloys, the fracture toughness of this alloy correlates very well with processing in that similar microstructural conditions have similar toughness values. These microstructural features will be discussed in terms of processing and will be grouped as follows: 1) β forged in both blocking and finishing operations (K_{Ic} > 50 KSI$\sqrt{in}$); 2) β blocked and α+β finished (31 KSI$\sqrt{in} \leq K_{Ic} \leq$ 45 KSI$\sqrt{in}$); 3) α+β forged in both operations to a 10% primary α level (25 KSI$\sqrt{in}$ < $K_{Ic} \leq$ 31 KSI$\sqrt{in}$) and 4) α+β forged in

both operations to a 50% primary α structure ($K_{Ic} \leq 25$ KSI$\sqrt{in}$). Most of the Ti-6Al-2Sn-4Zr-6Mo specimens had a very smooth fracture surface when observed at low magnification; in fact care had to be exercised in order to locate the fatigue to fast fracture transition in these specimens.

K_{Ic} greater than 50 KSI$\sqrt{in}$

The one specimen in this category (Condition G, Fig. 33) which was fully β processed had considerable crack branching (Fig. 33c and f) along prior β grain boundaries and dimple formation suggestive of void formation associated with fine transformed β.

K_{Ic} from 31 to 45 KSI$\sqrt{in}$

The four conditions in this group, Conditions E, C, D and F (Figs. 34-37) were all β upset and α+β finished. Condition E had considerable crack branching coupled with void formation, growth and coalescence. Conditions C, D and F exhibit void formation and coalescence characteristic of the bulk of the Ti-6Al-4V and Ti-6Al-6V-2Sn conditions.

K_{Ic} from 25-31 KSI$\sqrt{in}$

The three specimens in this group, Conditions A, A-2 and A-1 (Figs. 38-40) were α+β forged to 10-20% primary α and then given STA, anneal, and STOA heat treatments, respectively. The fatigue to fast fracture transition shows very little change in appearance. The fast fracture zone shows evidence of dimple formation although the dimples are very shallow. The fracture path in the region of primary α particles is suggestive of a very low energy fracture mode either along the boundary or through these particles. This observation is consistent with the fact that the following group containing 40-50% primary α has even lower fracture toughness.

K_{Ic} less than 25 KSI$\sqrt{in}$

The three specimens in this group, Conditions B, B-2 and B-1 (Figs. 41-43) were $\alpha+\beta$ forged to 40-50% primary α and then given STA, anneal and STOA heat treatments, respectively. The fatigue to fast fracture transition shows little change in topography and a path around the primary α particles is evident. There is a relatively poor correlation between fracture topography and microstructure in these specimens.

SUMMARY AND CONCLUSIONS

Although variations in the fracture topography as elucidated by SEM and replica fractography techniques are insufficient to permit the fracture toughness to be estimated, the current investigation has established the following points.

1. The fracture topography in the fatigue precrack region most accurately reflects the microstructure. Thus it is useful to compare the topographical variations observed in the precrack to those observed in the fast fracture zone.
2. In high K_{Ic} materials there is a noticeable variation in fracture topography between the initial rapid propagation region and the region of rapid propagation distant from the limit of the fatigue precrack. The width of this topography transition zone and the extent of variation between the initial and final fracture regions decreases with decreasing fracture toughness.

3. The fully Widmanstätten structures typically exhibited the highest K_{Ic} values. In the high strength conditions of Ti-6-6-2 and Ti-6-2-4-6 these structures exhibited primary and secondary cracking along prior β grain boundaries. In the lower strength conditions, this trend is much less pronounced.

4. The high strength low toughness conditions of Ti-6-2-4-6 are α+β finished and exhibit a uniform distribution of fine primary α particles in an α+β matrix. This type of microstructure appears to have little influence on fracture topography since these specimens exhibit a uniform distribution of small, shallow dimples, the dimensions of which do not correlate with those of any microstructural features.

5. In most of the Ti-6Al-4V and Ti-6Al-6V-2Sn specimens, those falling in the range of K_{Ic} values of 60-80 KSI$\sqrt{in}$, the fracture topography is very similar with the exception that the effect(s) of primary α, spaghetti α and grain boundary α on the fracture topography are observable. A quantitative correlation between fracture toughness, fracture topography and microstructure is not currently possible although some qualitative trends have been suggested above.

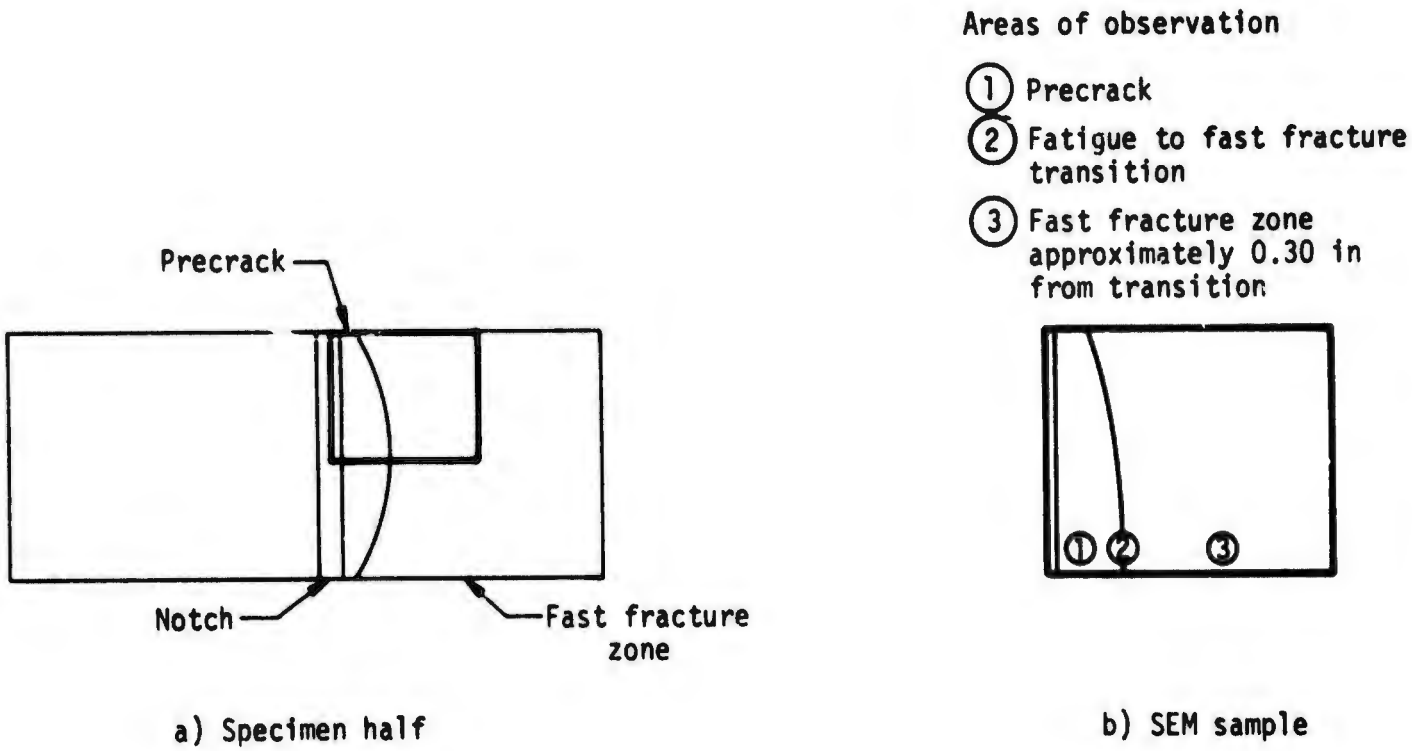

a) Specimen half

b) SEM sample

Figure 1. Schematic of specimen and SEM sample

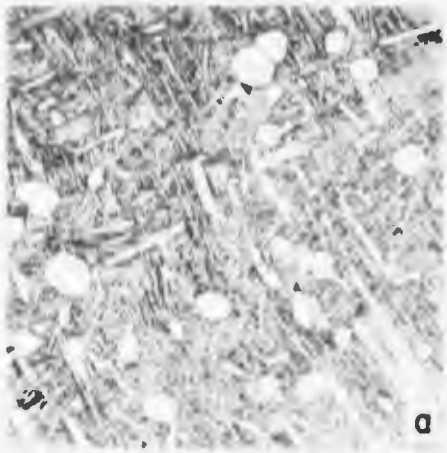

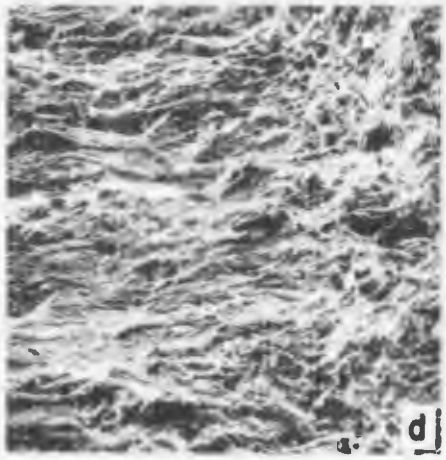

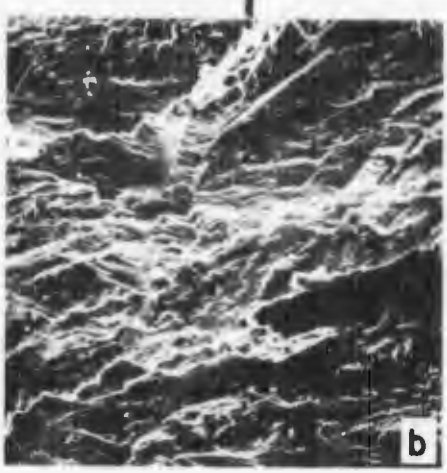

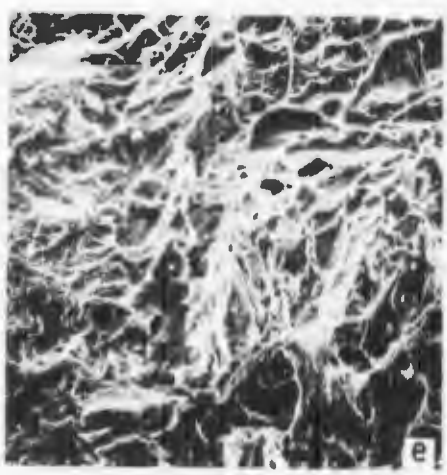

Preceding page blank

Ti-6Al-4V Condition A (Low O_2), ANN

a) Light micrograph; 500X

b,c) Precrack, 400X, 4000X

d,e) Fatigue to fast fracture transition;
80X, 400X

f,g) Fast fracture zone near the transition;
200X, 800X

h,i) Fast fracture zone; 200X, 800X

YS = N.D.

UTS = N.D.

K_{Ic} = 97.1 KSI$\sqrt{in}$

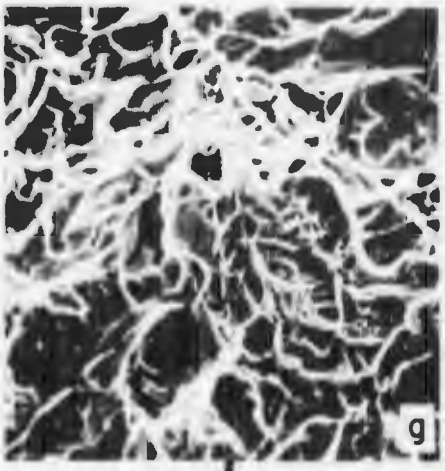

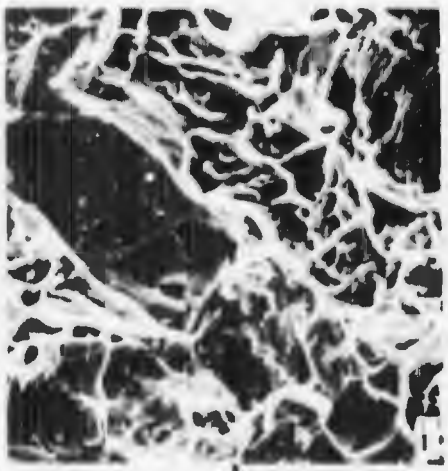

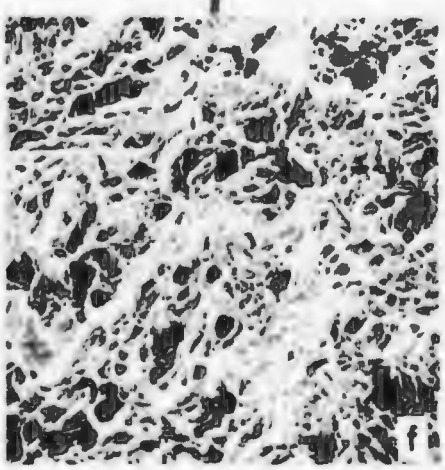

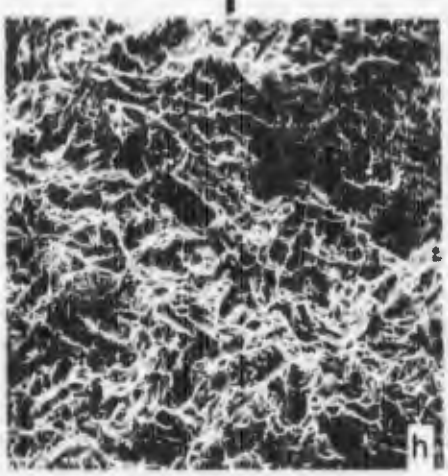

Figure 2

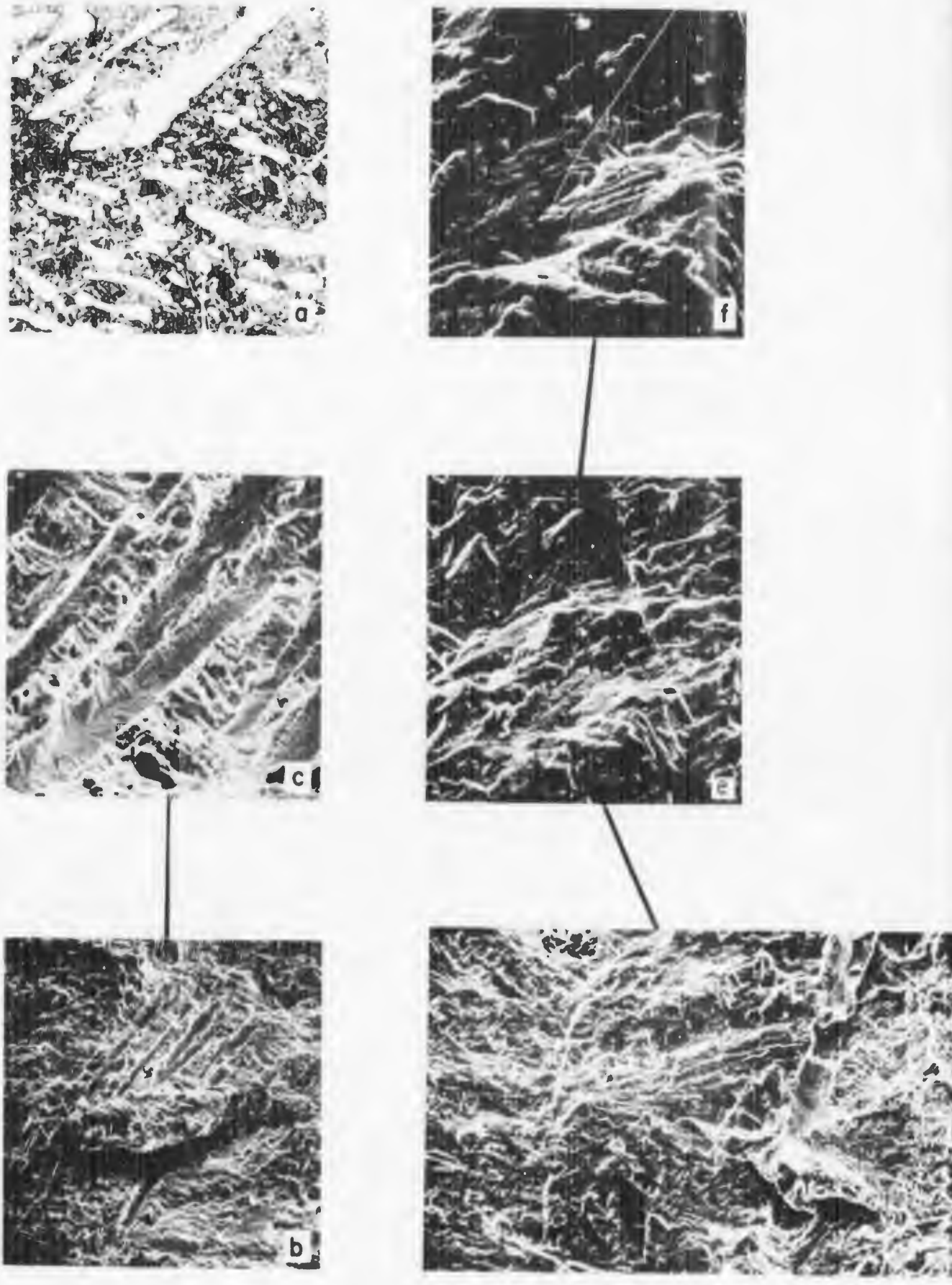

Preceding page blank

Ti-6 V Condition D, AC, ANN

a) L micrograph; 500X

b,c) crack zone; 200X, 500X

d,e, Fatigue to fast fracture transition;
400X, 800X, 2000X, 2000X

h,i) st fracture zone; 400X, 2000X

YS = 37 KSI

UTS = 49 KSI

K_{Ic} = 7.7 KSI$\sqrt{in}$

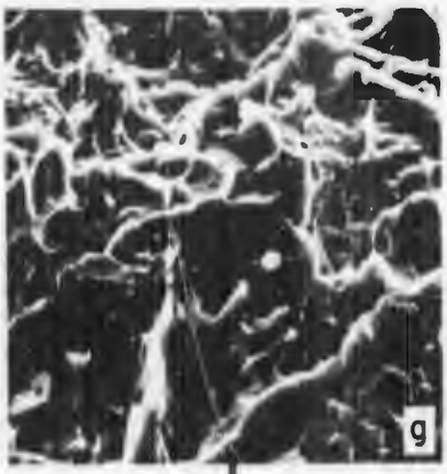

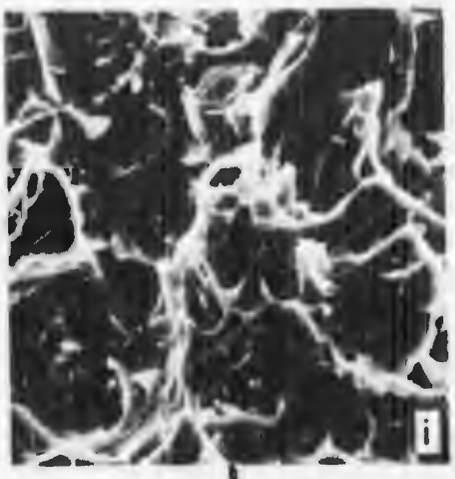

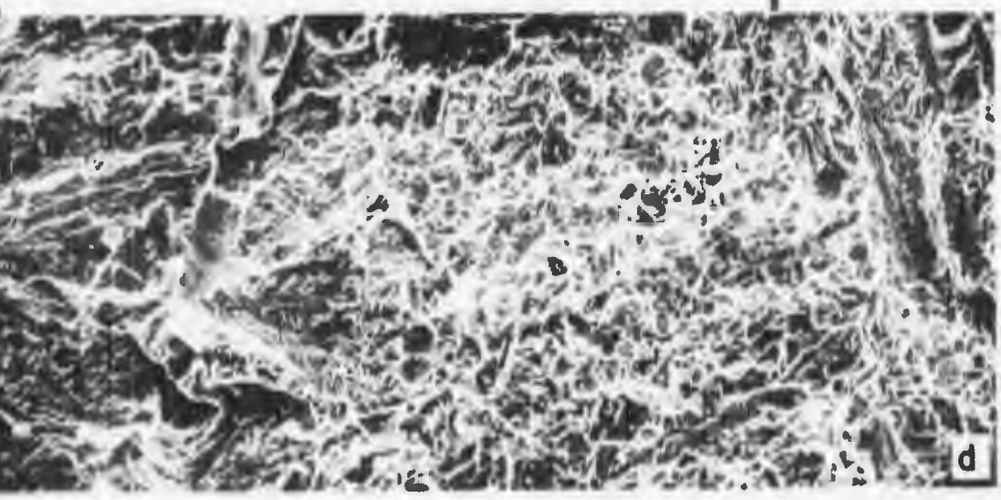

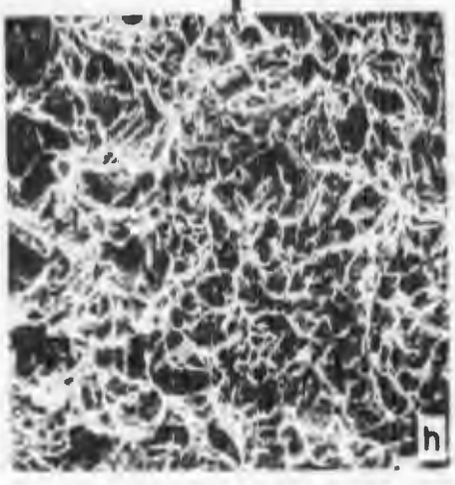

Figure 3

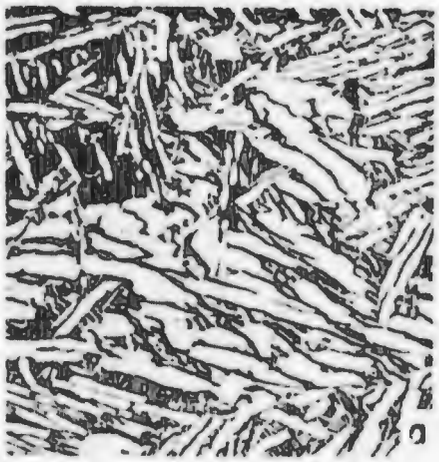

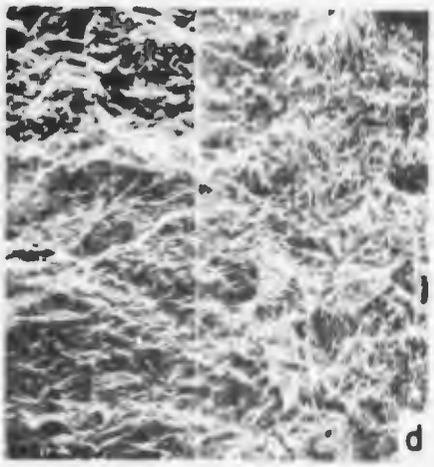

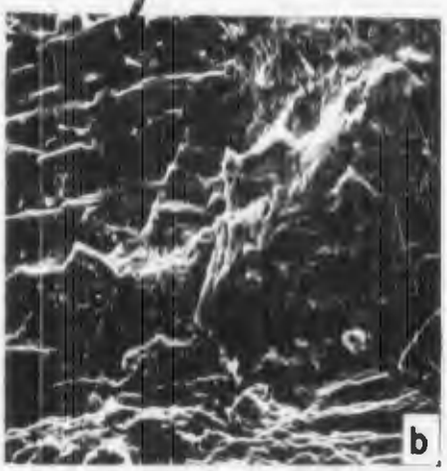

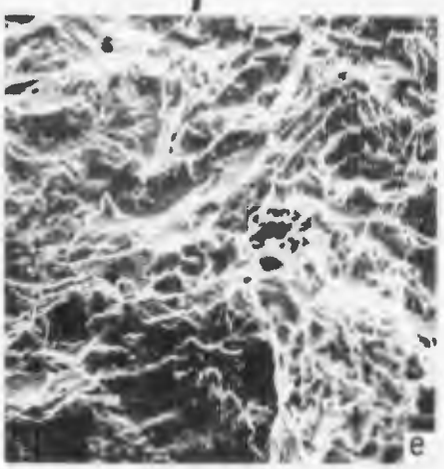

Preceding page blank

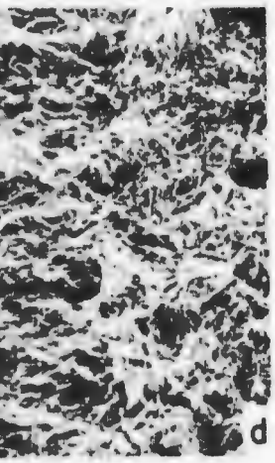

Ti-6A -4V Condition J, AC, ANN

a) Li ht micrograph; 500X

b,c) recrack zone; 800X, 2000X

d,e,f) Fatigue to fast fracture transition;
80X, 400X, 2000X

g,h) Fast fracture zone near the transition;
400X, 1600X

i,j) Fast fracture zone; 400X, 1600X

YS = 134 KSI

UTS = 149 KSI

K_{Ic} = 87.6 KSI$\sqrt{in}$

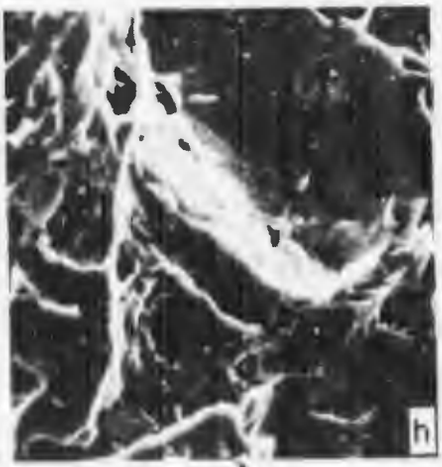

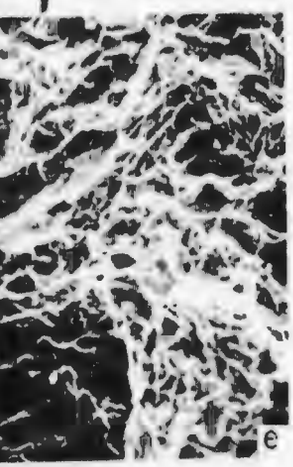

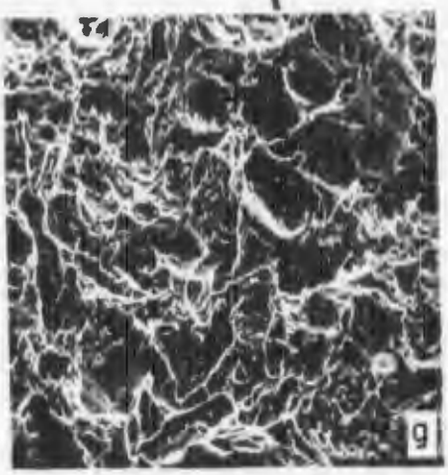

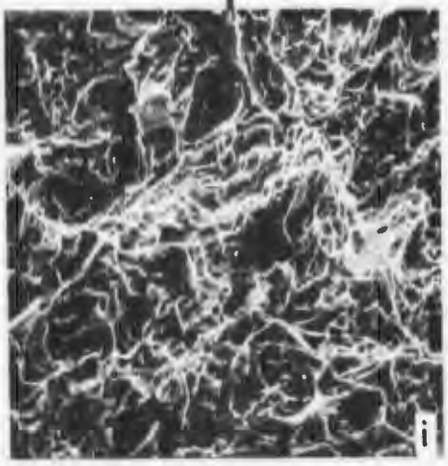

Figure 4

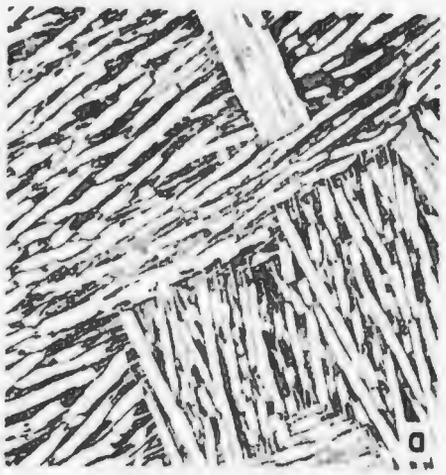

T1-6A

a) L

b) P

c,d,

f,g)

h) B

YS =

UTS =

K_{Ic} =

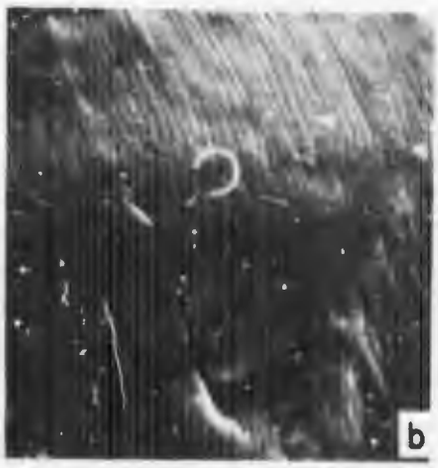

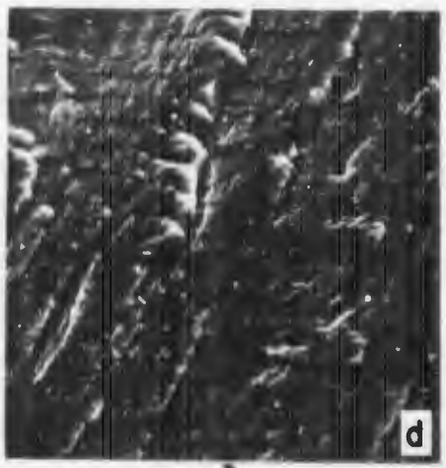

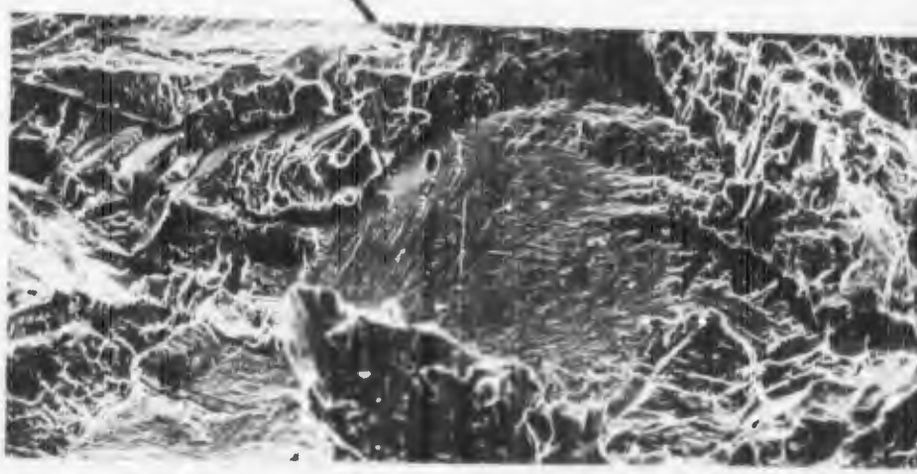

Preceding page blank

Ti-6Al-4V Condition U, STOA

a) Light micrograph; 500X

b) Precrack zone; 4000X

c,d,e) Fatigue to fast fracture transition;
400X, 2000X, 2000X

f,g) Fast fracture zone; 400X, 2000X

h) Bright "facet" in fast fracture zone; 400X

YS = 139 KSI

UTS = 152 KSI

K_{Ic} = 86.4 KSI$\sqrt{in}$

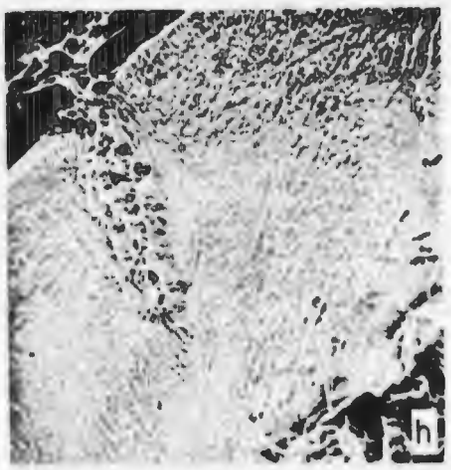

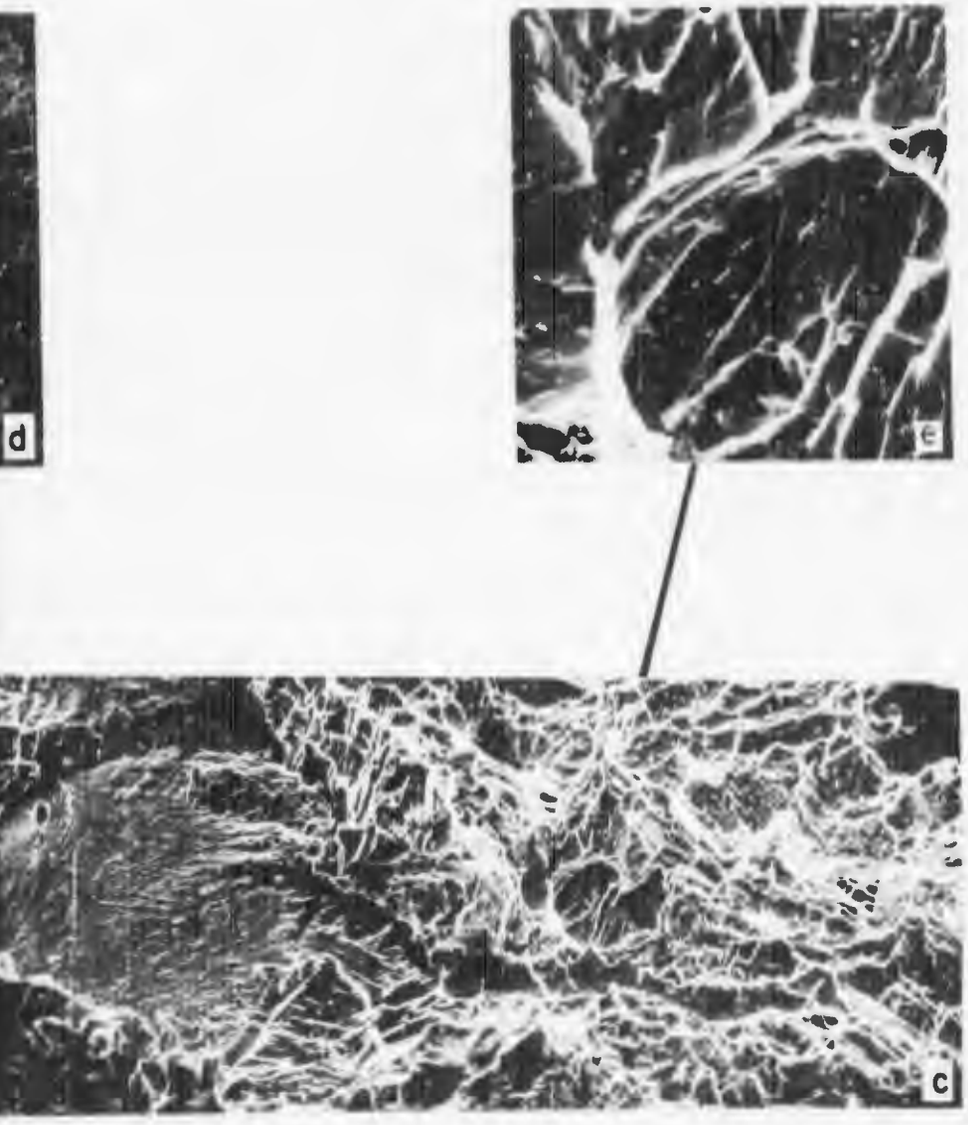

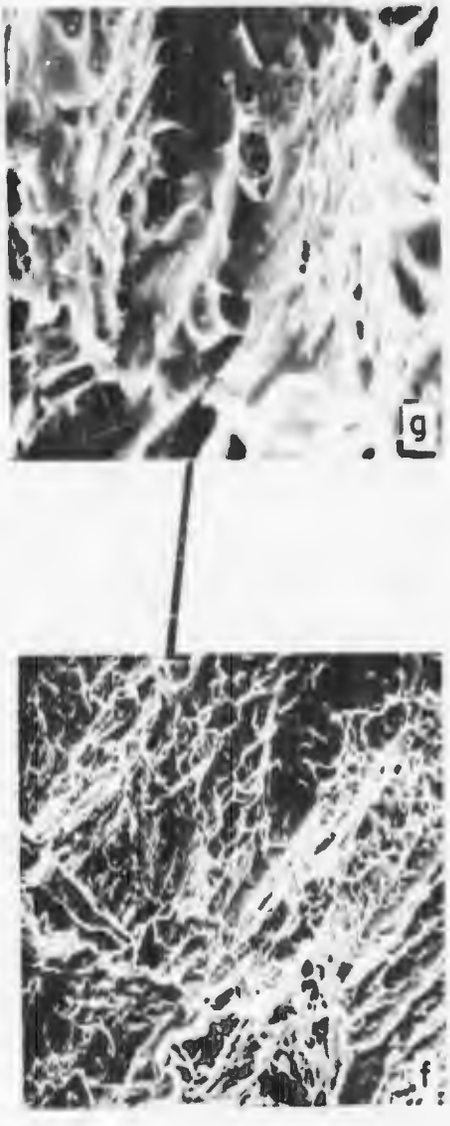

Figure 5

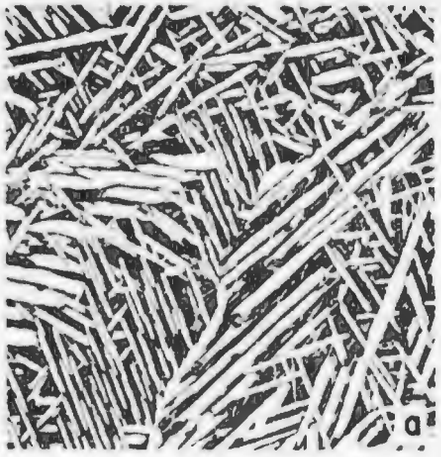

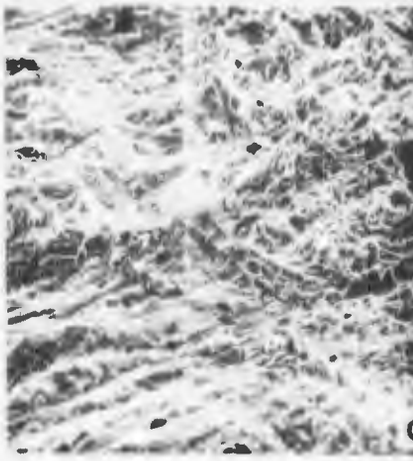

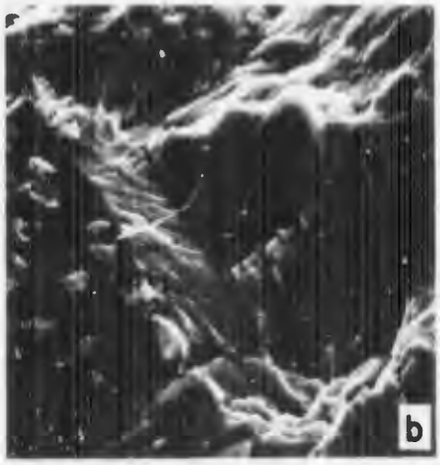

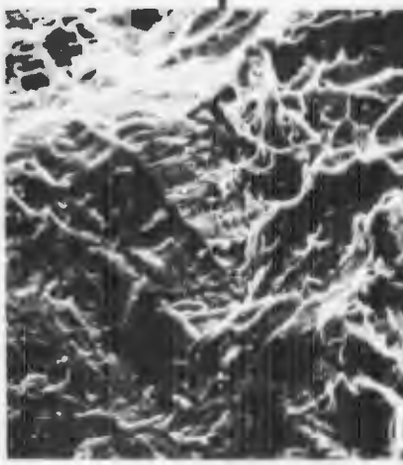

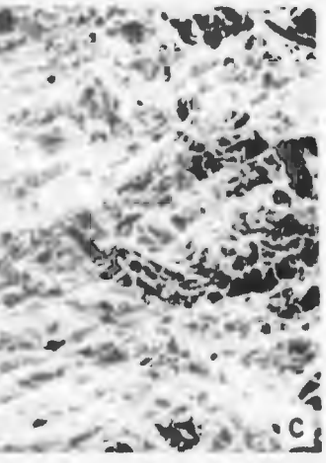

Ti-6Al-4V Condition R, AC, STOA

a) Light micrograph; 500X

b) Precrack zone; 2000X

c,d,e,f) Fatigue to fast fracture transition;
160X, 800X, 4000X, 16000X, 400X, 2000X

g,h) Fast fracture zone near the transition;
400X, 2000X

i,j,k) Fast fracture zone; 80X, 400X, 1600X

YS = 138 KSI

UTS = 153 KSI

K_{Ic} = 44.4 KSI$\sqrt{In}$

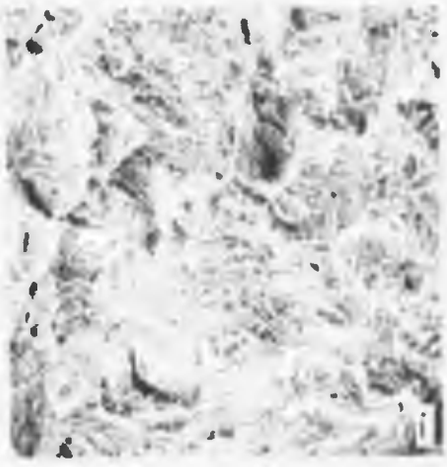

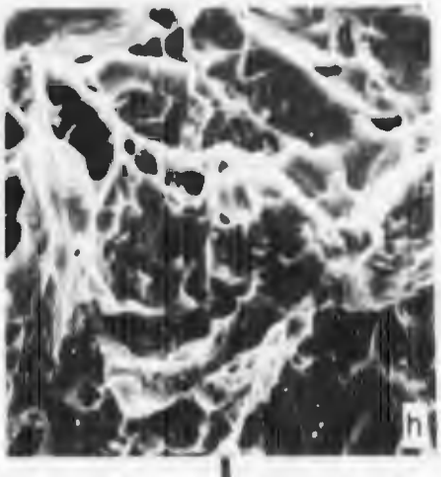

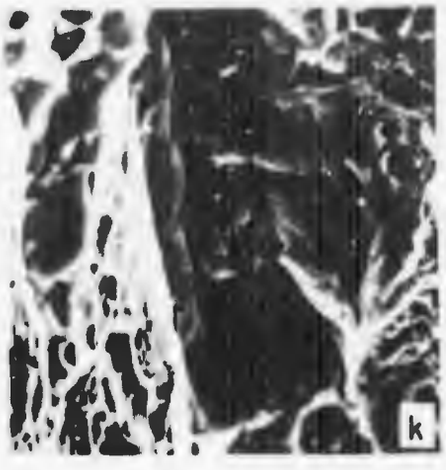

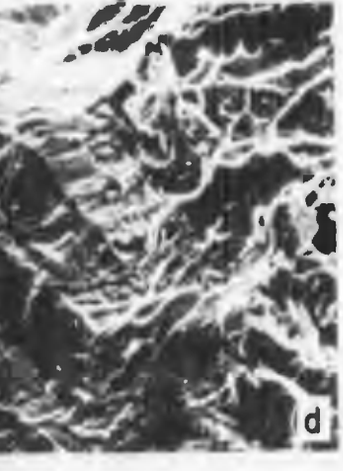

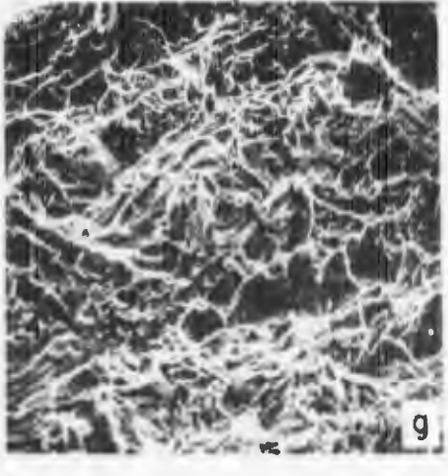

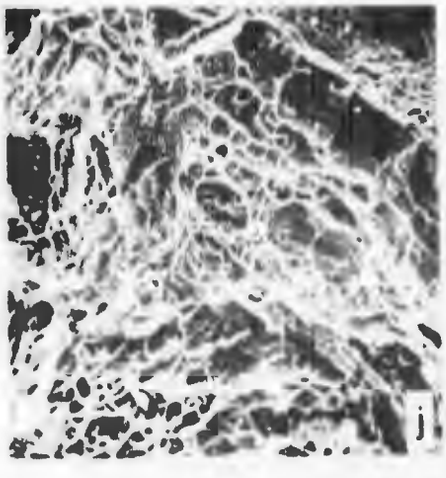

Figure 6

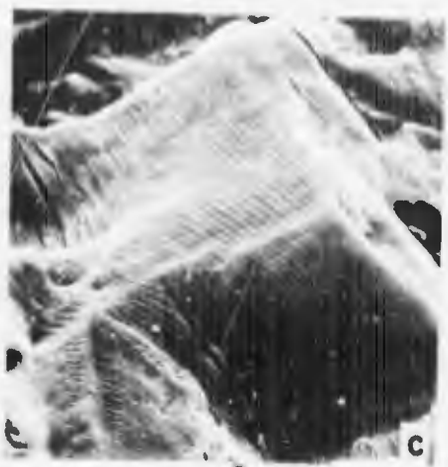

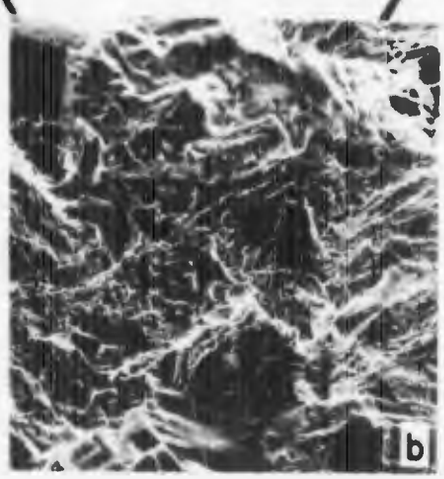

Preceding page blank

Ti-6Al-4V Condition T, ANN

a) Light micrograph; 500X

b,c,d) Precrack zone; 200X, 2000X, 2000X

e,f) Fatigue to fast fracture transition; 200X, 800X

g,h) Fast fracture zone, 200X, 800X

i,j) "Facet" in fast fracture zone near the transition; 80X, 4000X

YS = 131 KSI

UTS = 147 KSI

K_{Ic} = 80.4 KSI$\sqrt{in}$

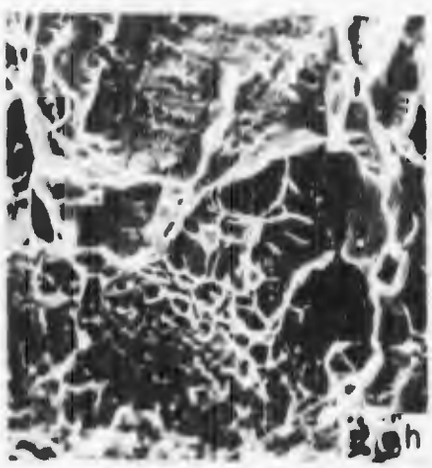

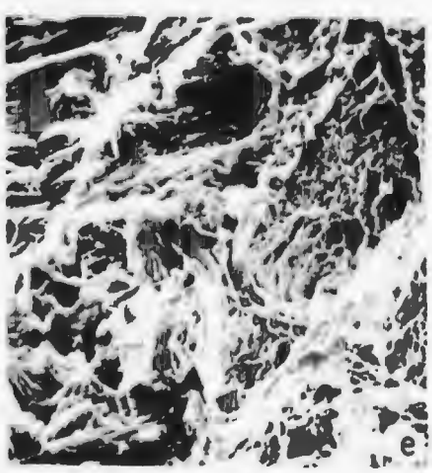

Figure 7

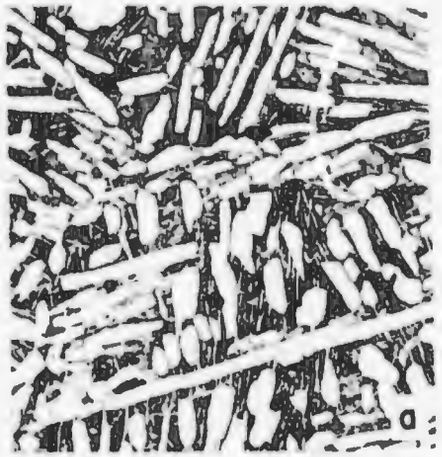

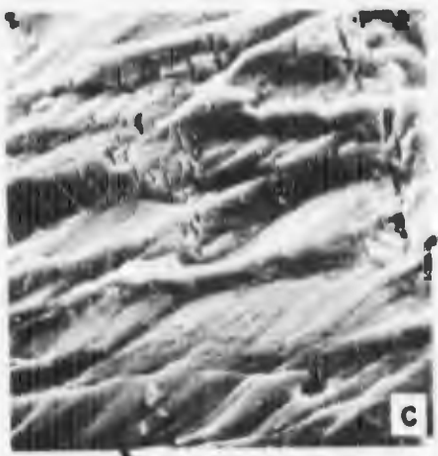

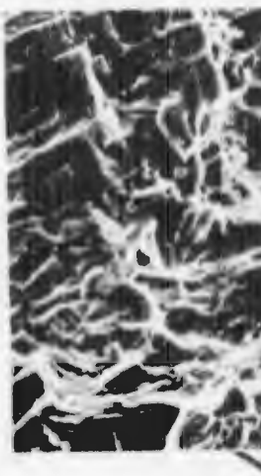

Preceding page blank

Ti-6Al-4V Condition M, WQ, STOA

a) Light micrograph; 500X

b,c,d) Precrack zone; 800X, 2000X, 8000X

e,f,g) Fatigue to fast fracture transition; 200X, 800X, 800X

h,i,j) Fast fracture zone; 400X, 2000X, 8000X

YS = 138 KSI

UTS = 151 KSI

K_{Ic} = 80.4 KSI$\sqrt{in}$

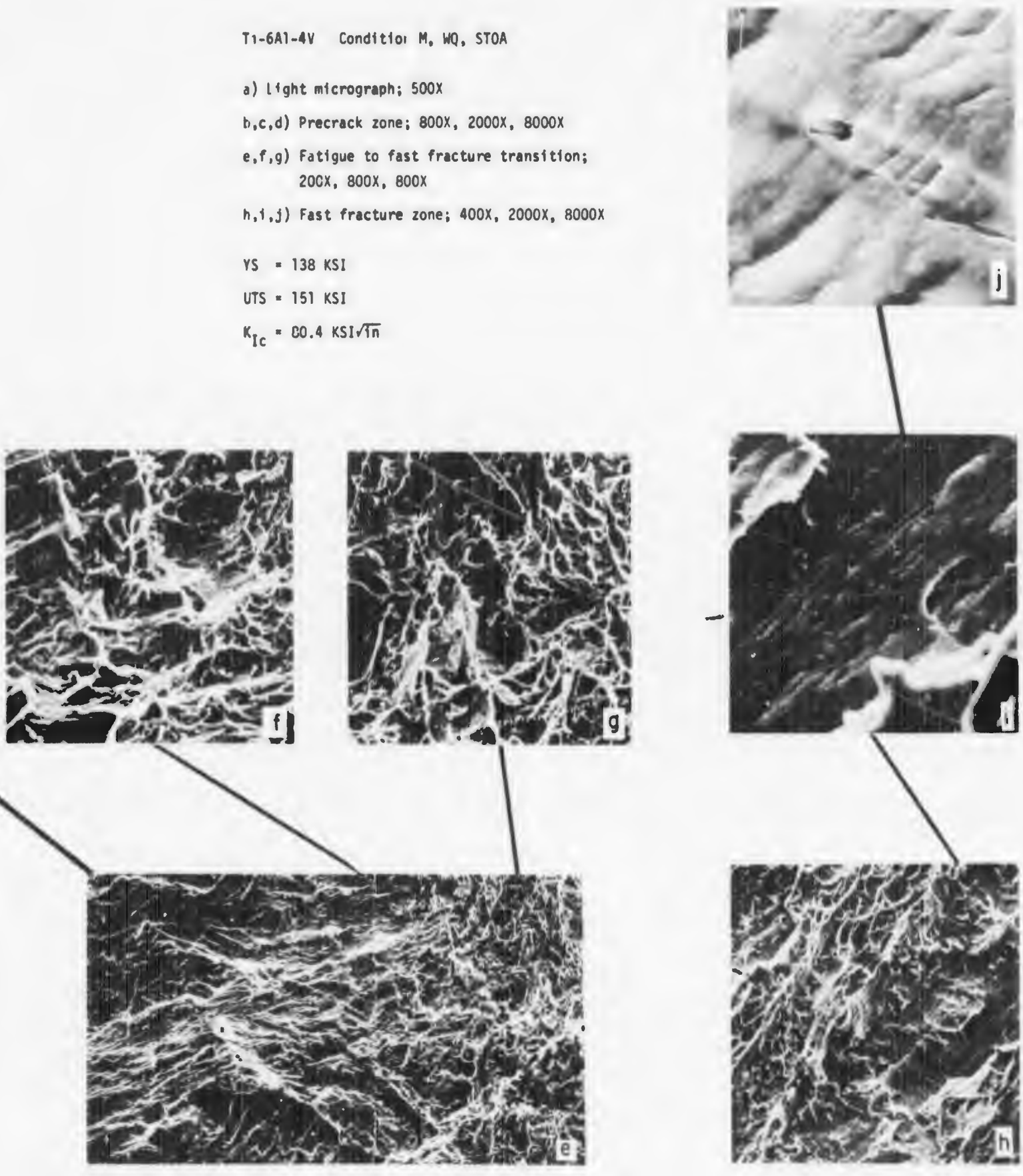

Figure 8

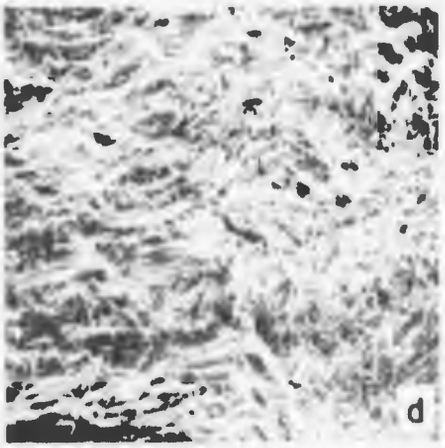

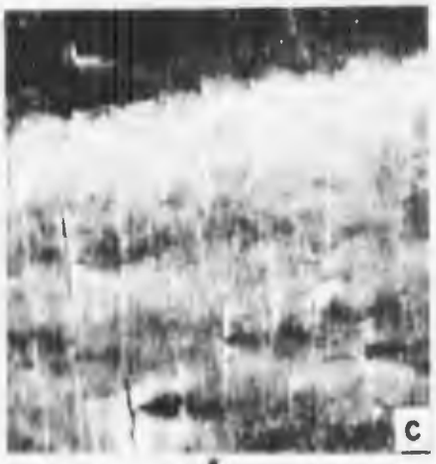

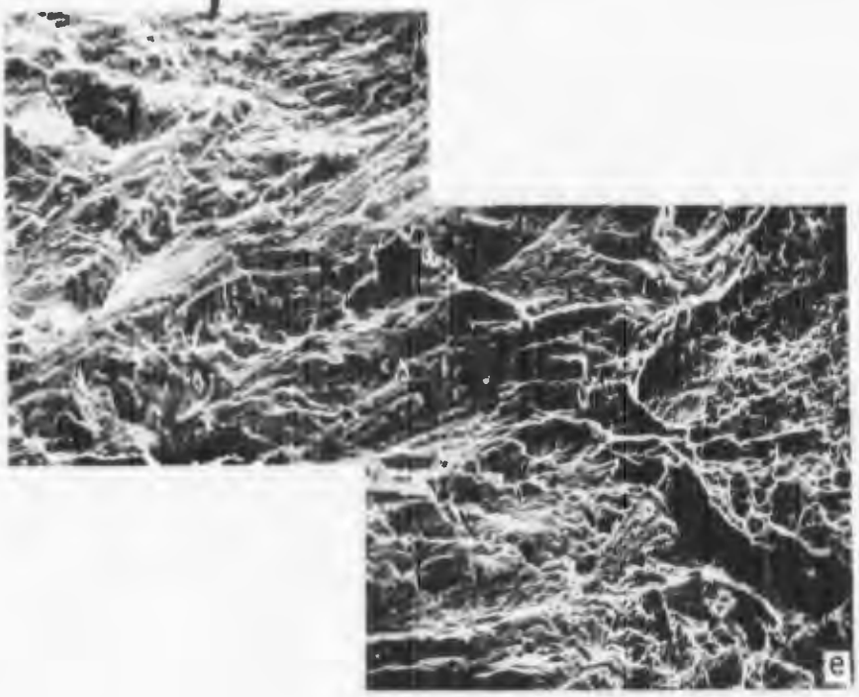

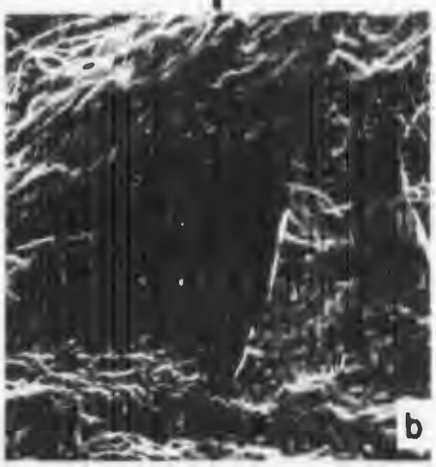

Preceding page blank

Ti-6Al-4V Condition O, AC, STOA

a) Light micrograph; 500X

b,c) Precrack zone; 400X, 2000X

d,e,f) Fatigue to fast fracture transition; 80X, 400X, 2000X

g,h) Fast fracture zone near the transition; 400X, 2000X

i,j) Fast fracture zone; 400X, 2000X

YS = 137 KSI

UTS = 151 KSI

K_{Ic} = 78.0 KSI$\sqrt{in}$

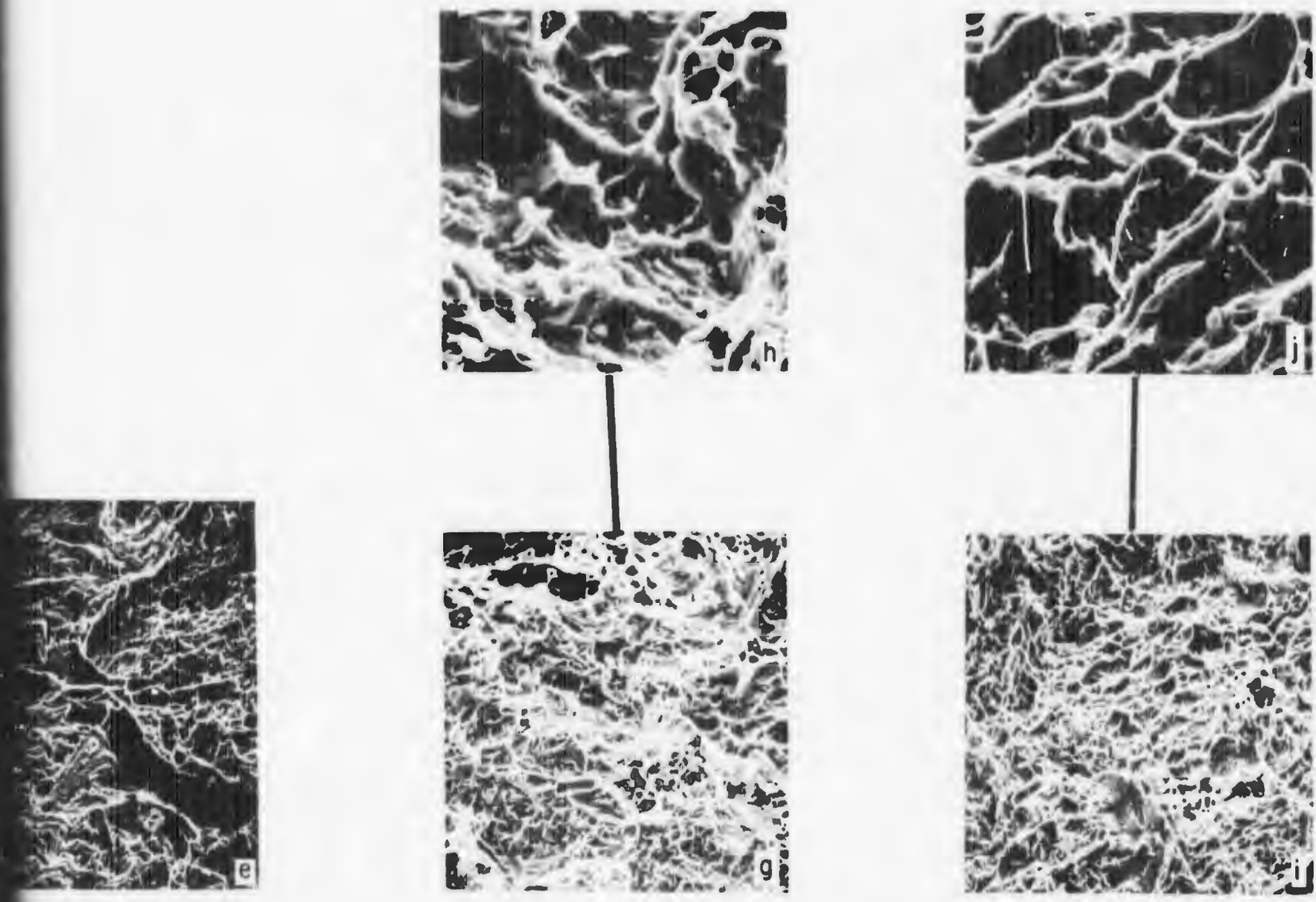

Figure 9

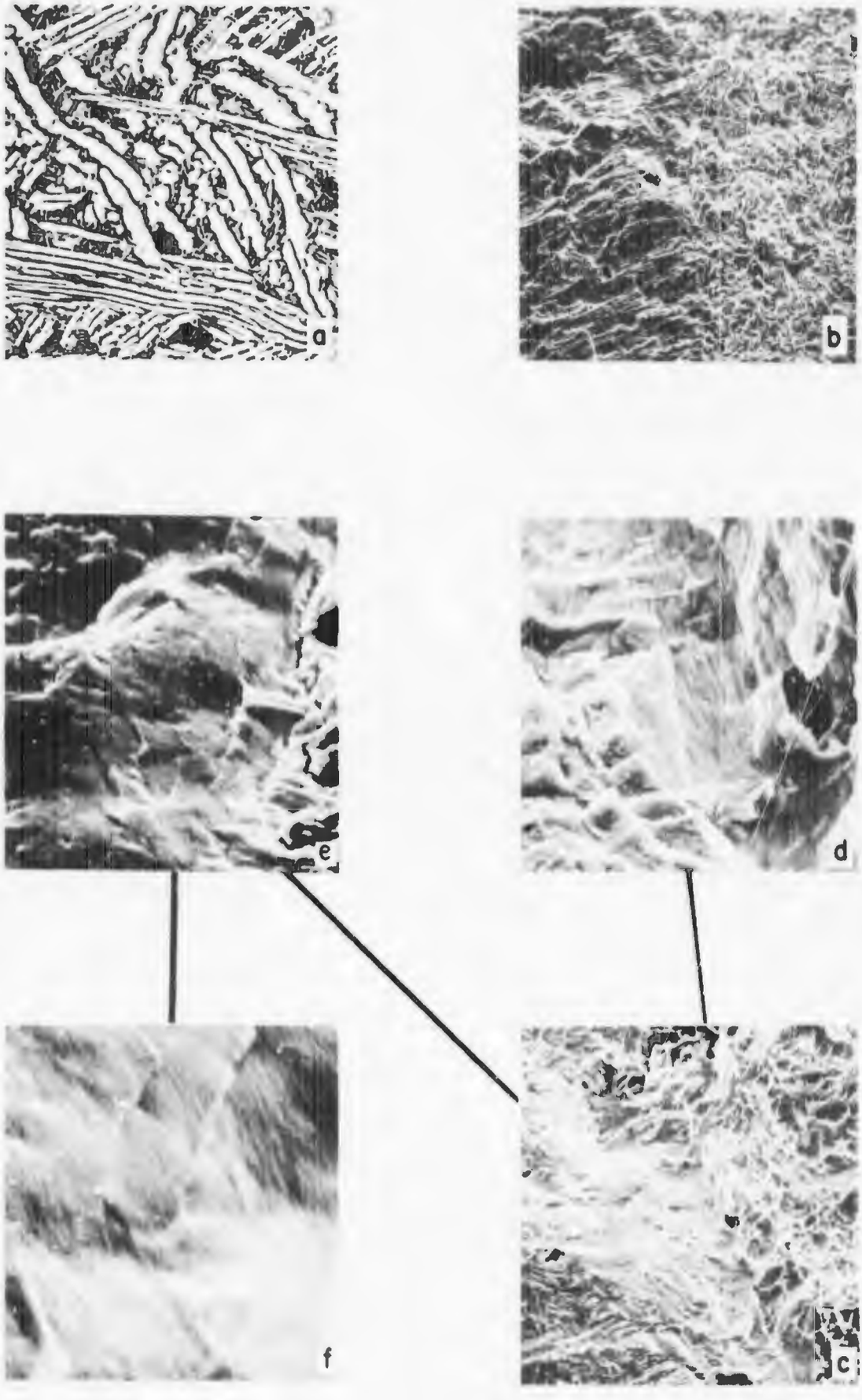

Preceding page blank

Ti-6Al-4V Condition N, AC, ANN

a) Light micrograph; 500X

b,c d,e,f) Fatigue to fast fracture transition;
80X, 400X, 2000X, 2000X, 8000X

g,h) Fast fracture zone near the transition;
400X, 2000X

i,j) Fast fracture zone; 400X, 2000X

YS = 127 KSI

UTS = 143 KSI

K_{Ic} = 75.9 KSI$\sqrt{in}$

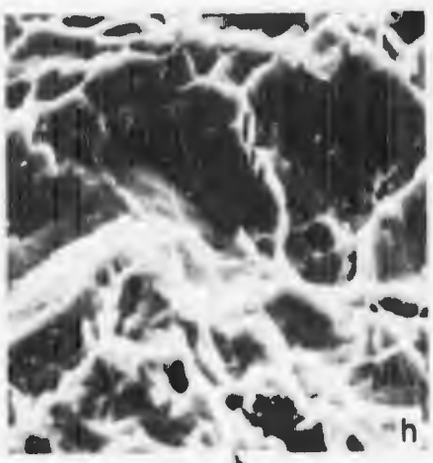

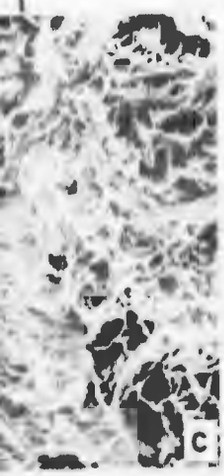

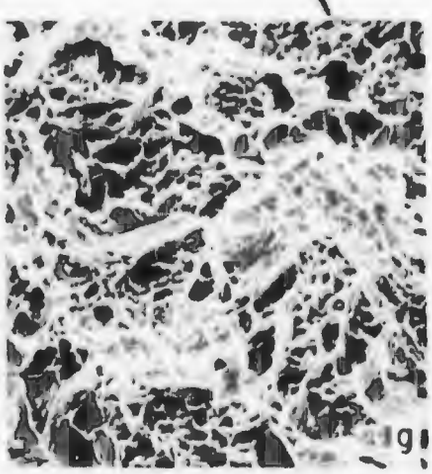

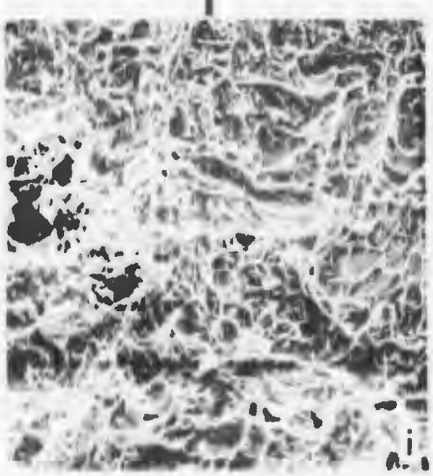

Figure 10

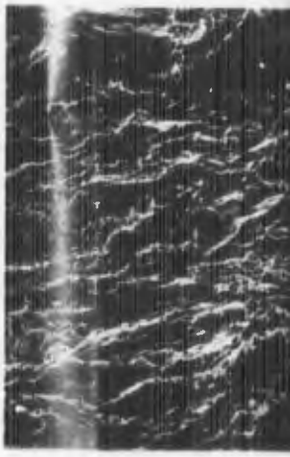

Preceding page blank

Ti-6Al-4V Condition G, AC, ANN

a) Light micrograph; 500X

b,c,d) Fatigue to fast fracture transition;
160X, 400X, 800X

e) Fast fracture zone; 400X

YS = 138 KSI

UTS = 151 KSI

K_{Ic} = 75.7 KSI$\sqrt{in}$

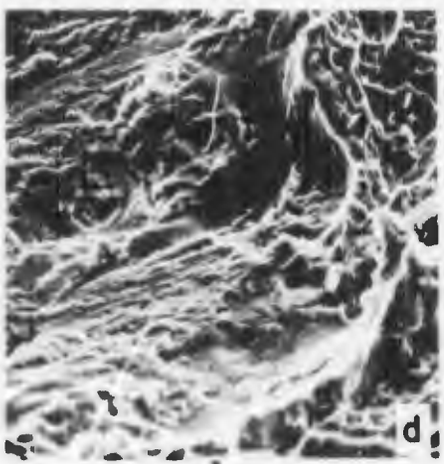

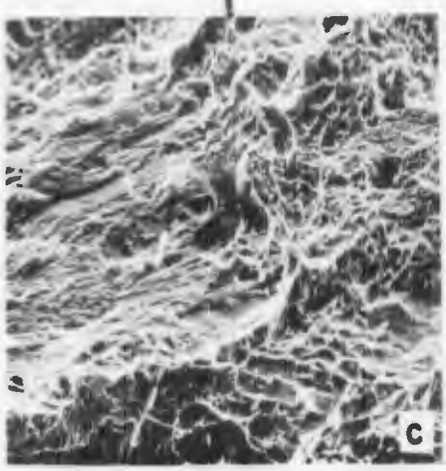

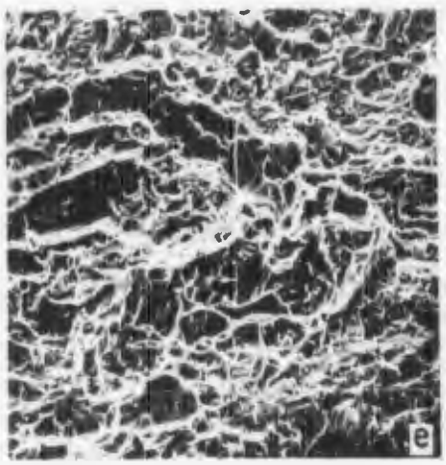

Figure 11

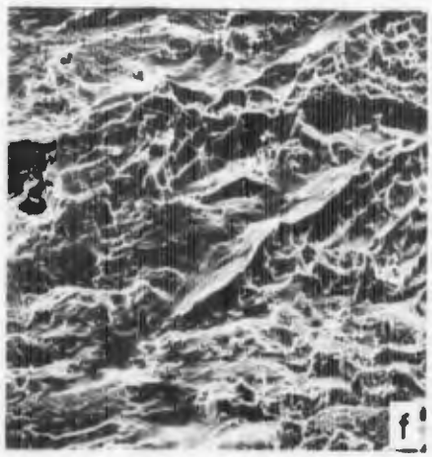

Preceding page blank

Ti-6Al-4V Condition G, AC, ANN

f,g) Fatigue to fast fracture transition;
400X, 2000X

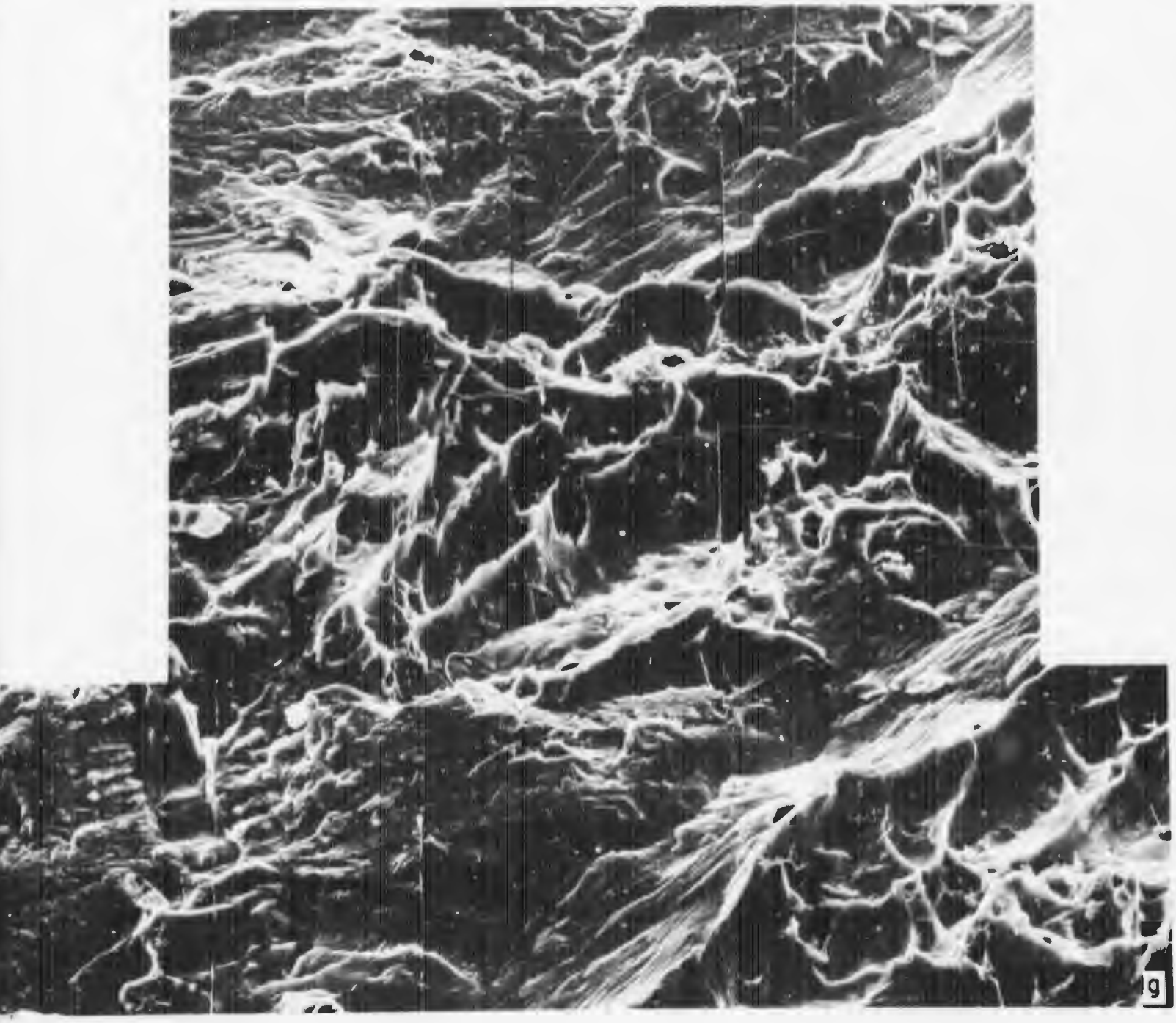

Figure 11 (Continued)

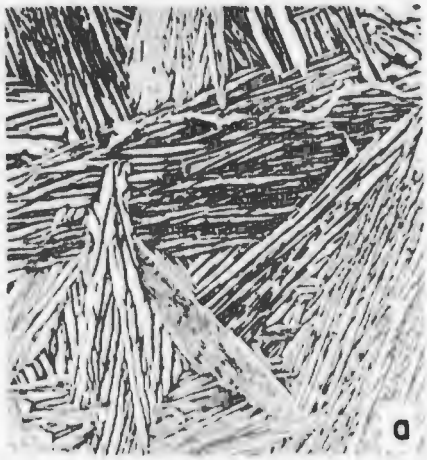

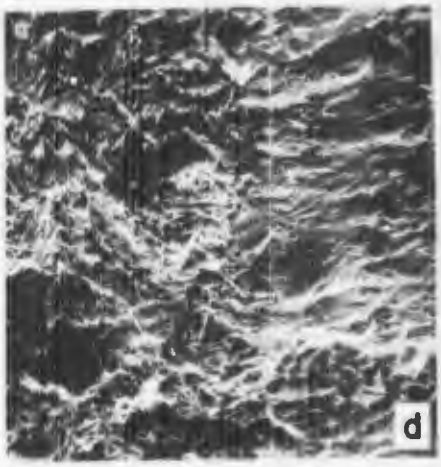

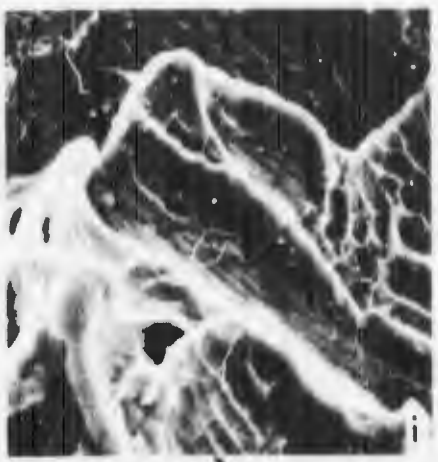

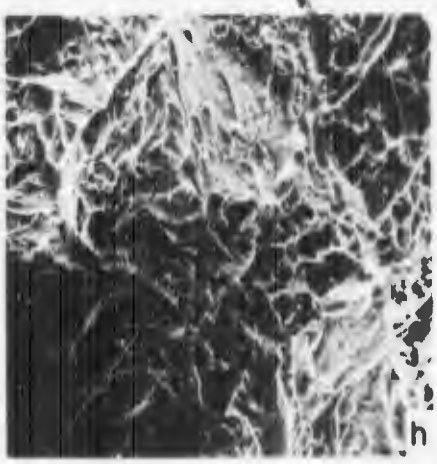

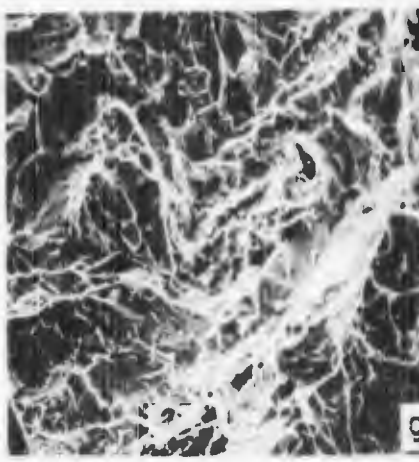

Ti-6Al-4V Condition Q, AC, ANN

a) Light micrograph; 500X

b,c, Precrack zone; 400X, 4000X

d,e,f) Fatigue to fast fracture transition;
80X, 400X 2000X

g) Fast fracture zone near the transition;
400X

h,i) Fast fracture zone; 400X, 2000X

YS = 128 KSI

UTS = 144 KSI

K_{Ic} = 71.1 KSI$\sqrt{in}$

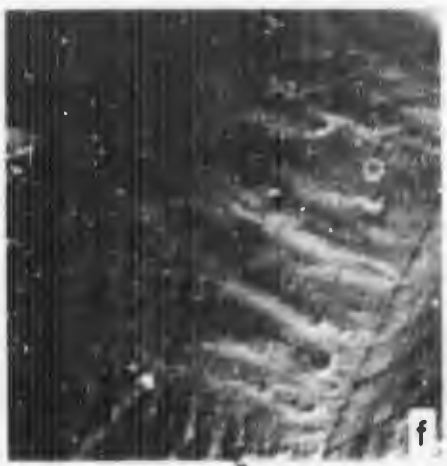

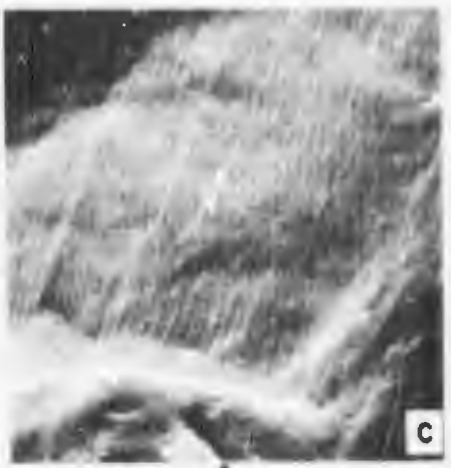

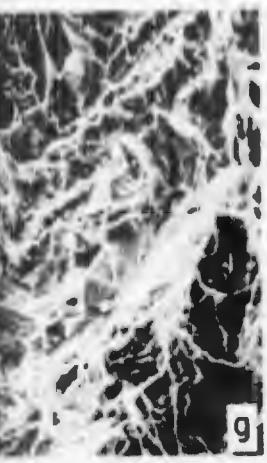

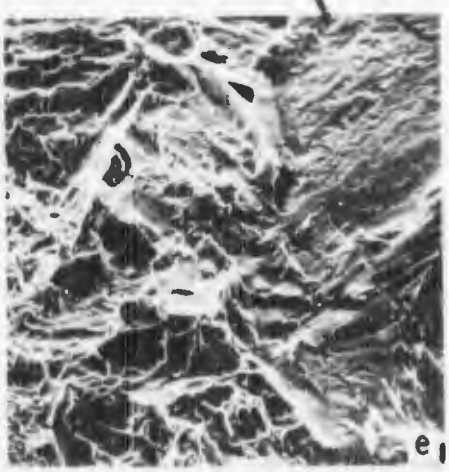

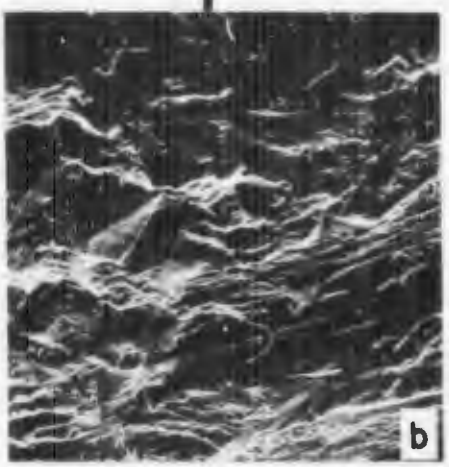

Figure 12

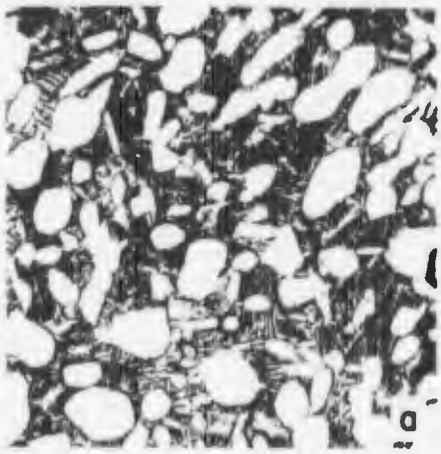

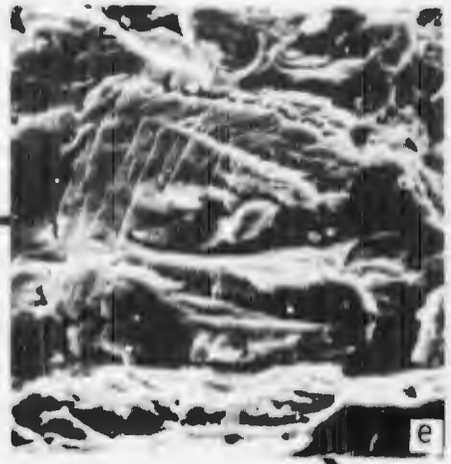

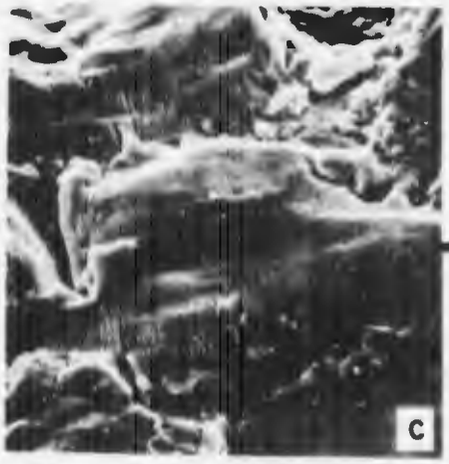

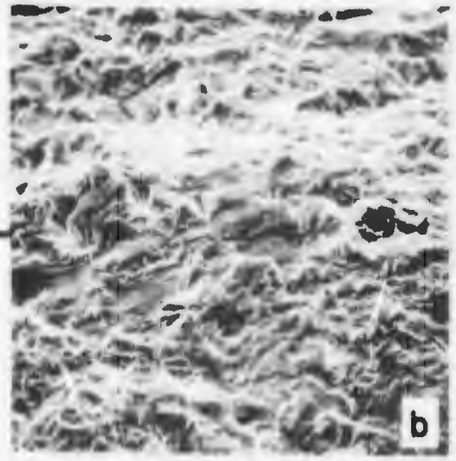

Preceding page blank

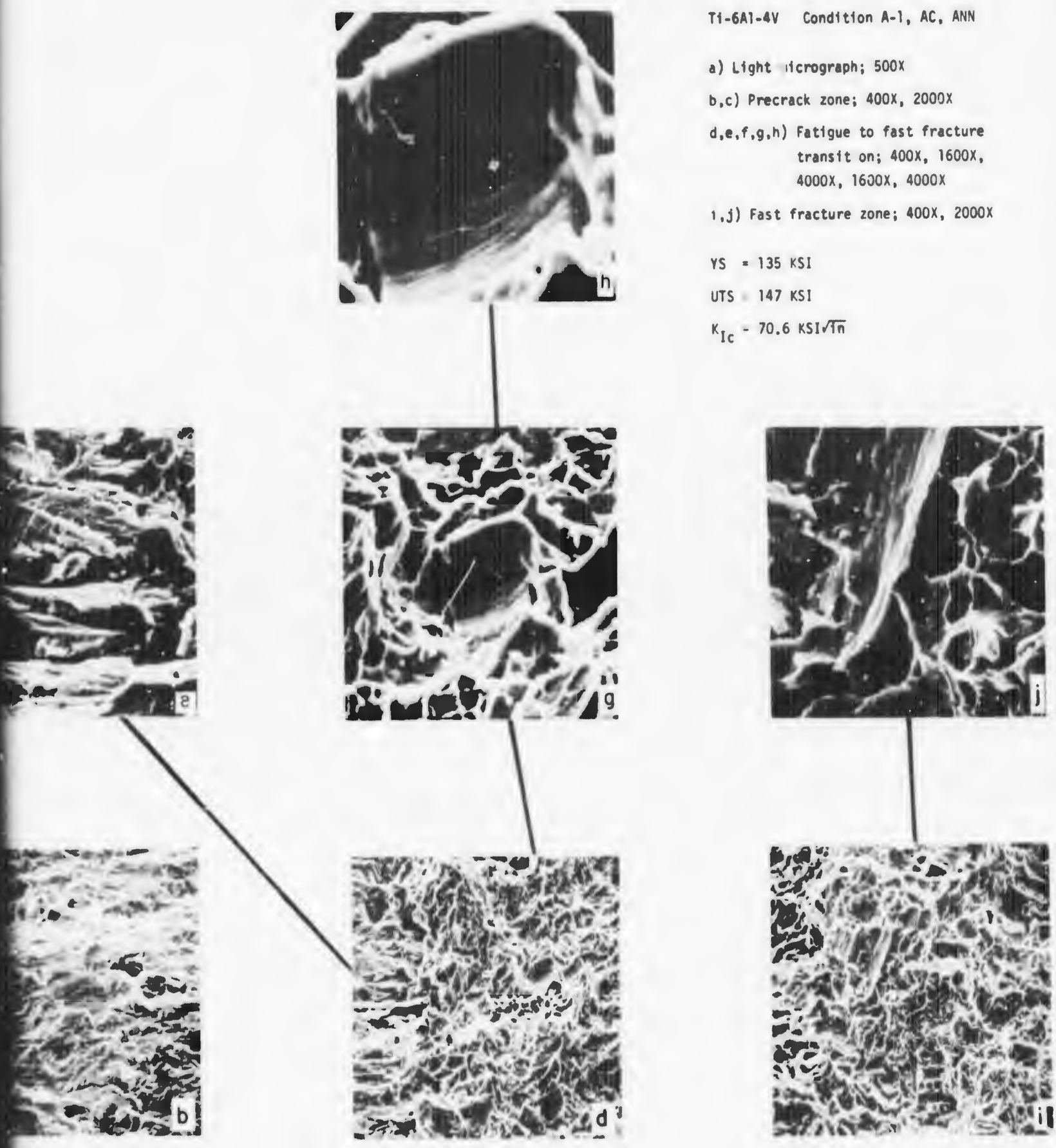

Ti-6Al-4V Condition A-1, AC, ANN

a) Light micrograph; 500X

b,c) Precrack zone; 400X, 2000X

d,e,f,g,h) Fatigue to fast fracture transit on; 400X, 1600X, 4000X, 1600X, 4000X

i,j) Fast fracture zone; 400X, 2000X

YS = 135 KSI

UTS = 147 KSI

K_{Ic} = 70.6 KSI$\sqrt{in}$

Figure 13

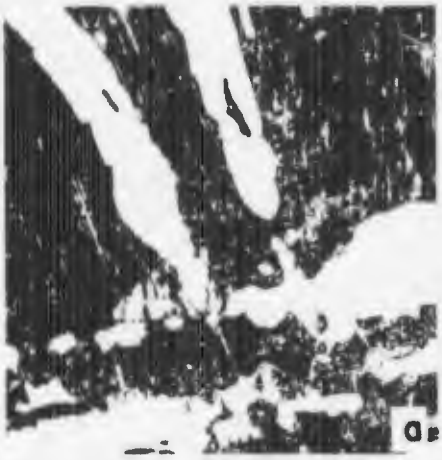

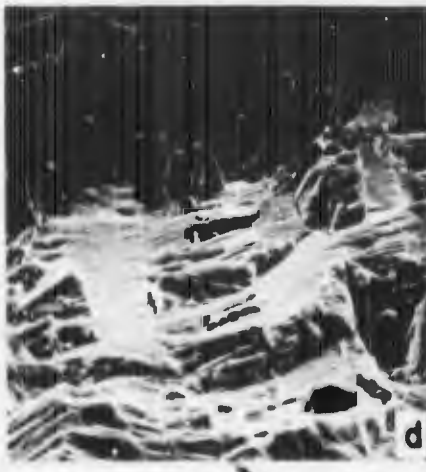

Preceding page blank

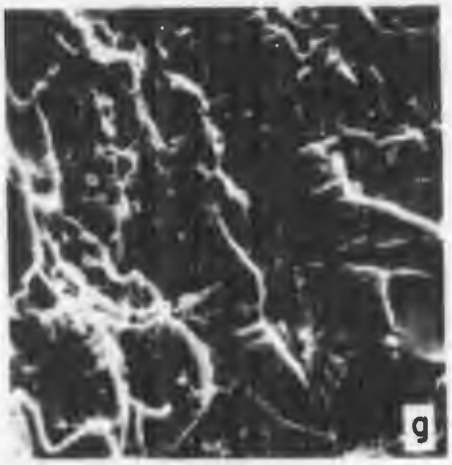

Ti-6Al-4V Condition E, AC, STOA

a) Light micrograph; 500X

b,c,d,e,f,g) Fatigue to fast fracture transition; 80X, 400X, 800X, 1600X, 800X, 1600X

h,i) Fast fracture zone; 400X, 1600X

YS = 141 KSI

UTS = 154 KSI

K_{Ic} = 68.1 KSI$\sqrt{in}$

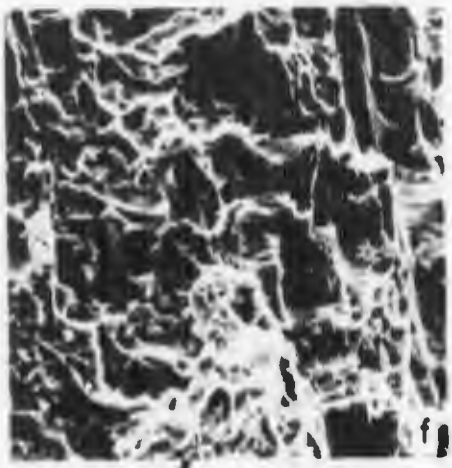

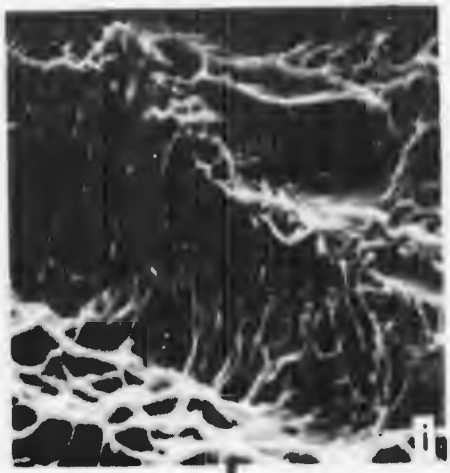

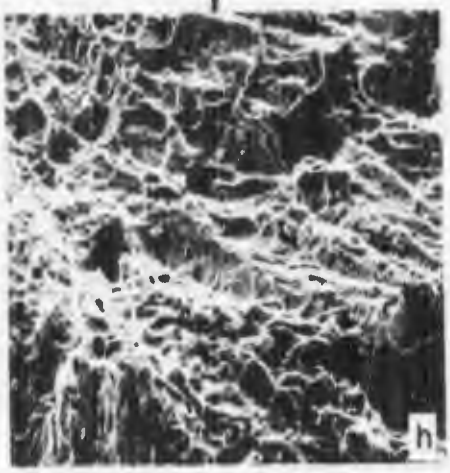

Figure 14

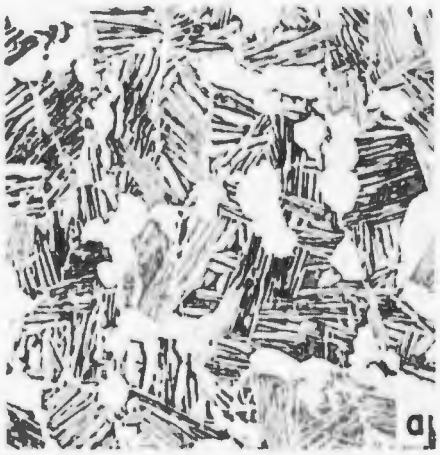

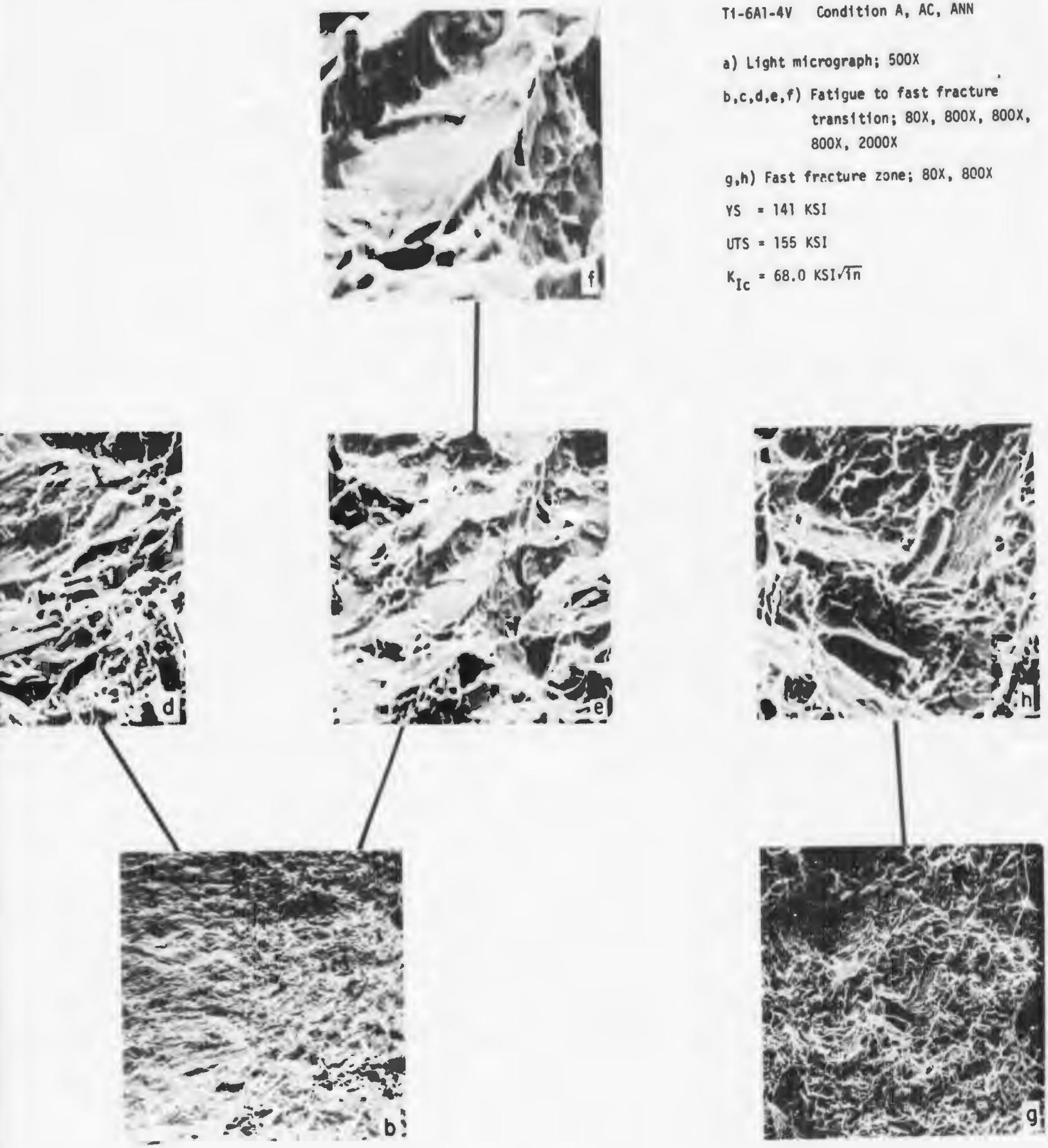

Ti-6Al-4V Condition A, AC, ANN

a) Light micrograph; 500X

b,c,d,e,f) Fatigue to fast fracture transition; 80X, 800X, 800X, 800X, 2000X

g,h) Fast fracture zone; 80X, 800X

YS = 141 KSI

UTS = 155 KSI

K_{Ic} = 68.0 KSI$\sqrt{in}$

Figure 15

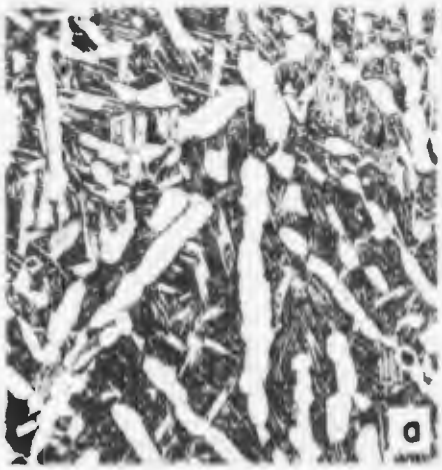

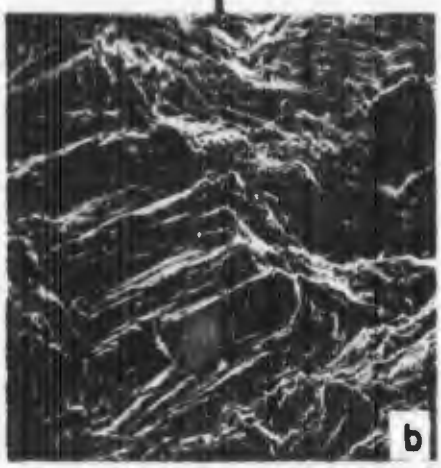

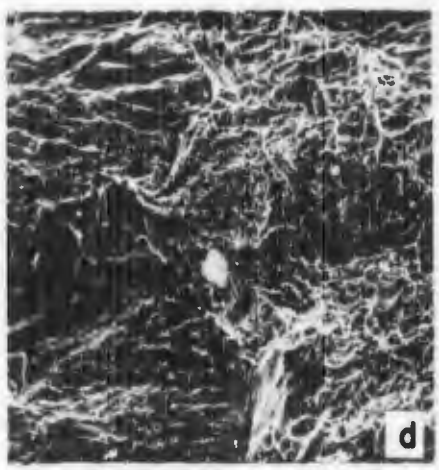

Preceding page blank

Ti-6Al-4V Condition H, AC, STOA

a) Light micrograph; 500X

b,c) Precrack zone; 200X, 2000X

d) Fatigue to fast fracture transition; 200X

e,f) Fast fracture zone near the transition; 200X, 2000X

g,h,i) Fast fracture zone; 300X, 1200X, 1500X

YS = 143 KSI

UTS = 157 KSI

K_{Ic} = 63.9 KSI$\sqrt{in}$

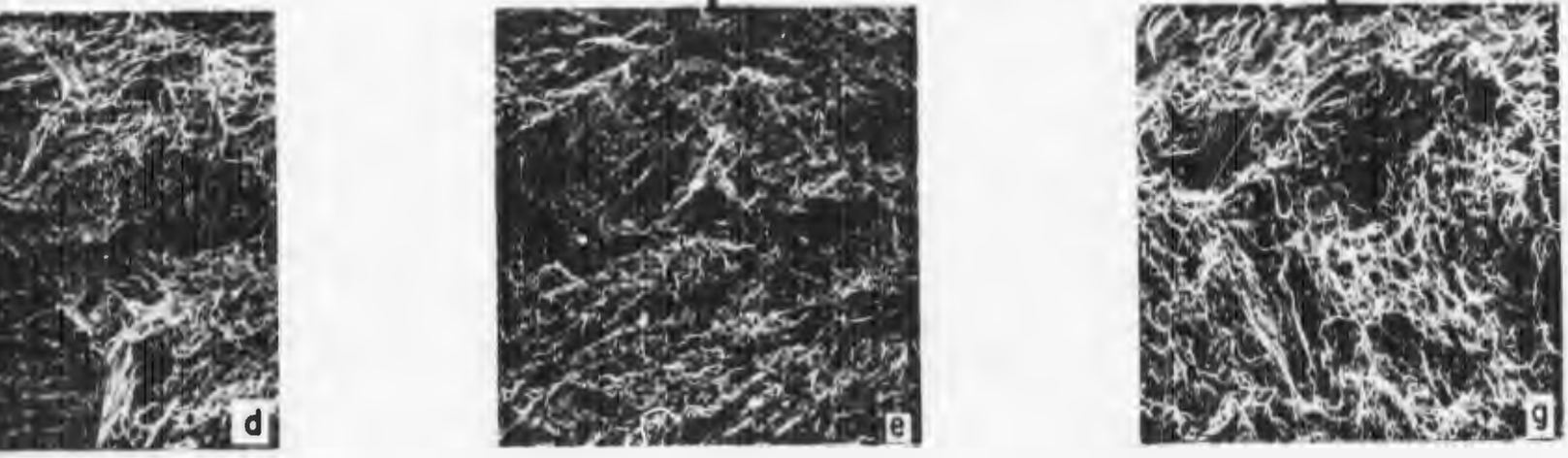

Figure 16

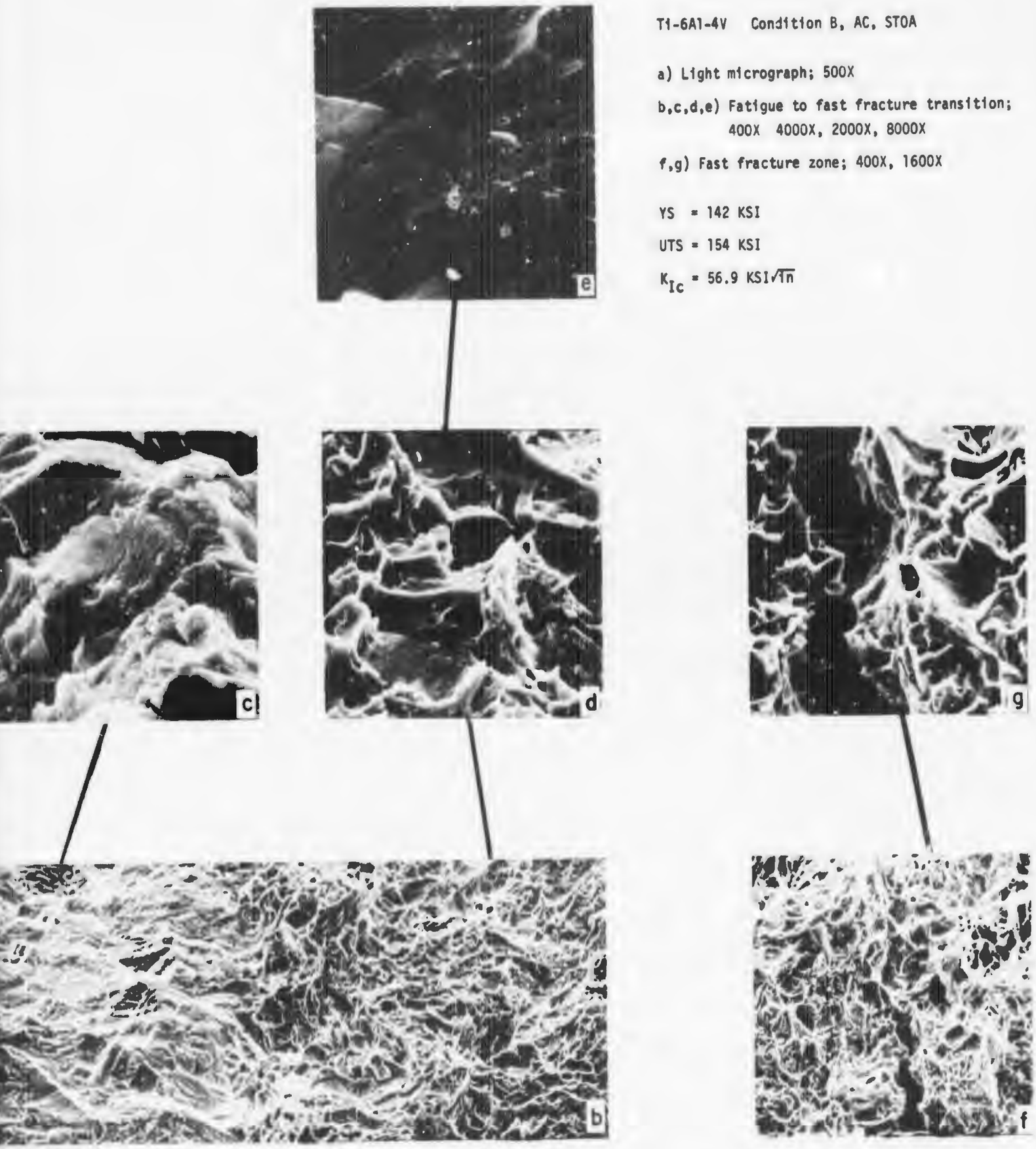

Ti-6Al-4V Condition B, AC, STOA

a) Light micrograph; 500X

b,c,d,e) Fatigue to fast fracture transition;
400X 4000X, 2000X, 8000X

f,g) Fast fracture zone; 400X, 1600X

YS = 142 KSI

UTS = 154 KSI

K_{Ic} = 56.9 KSI$\sqrt{in}$

Figure 17

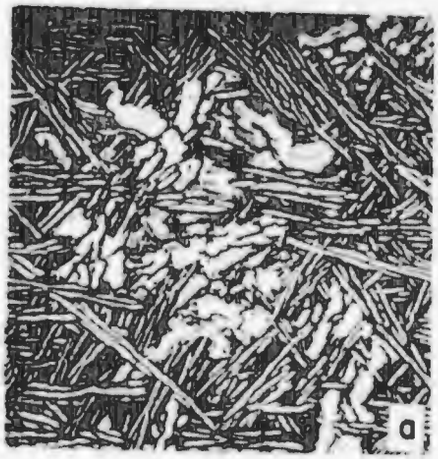

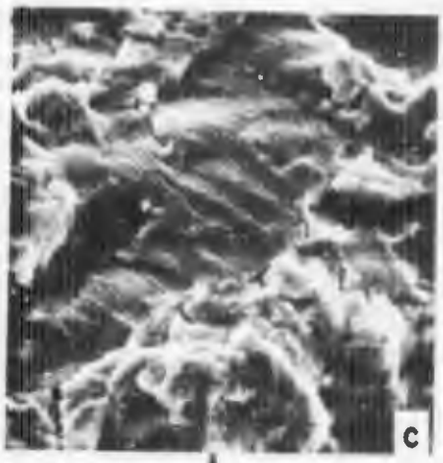

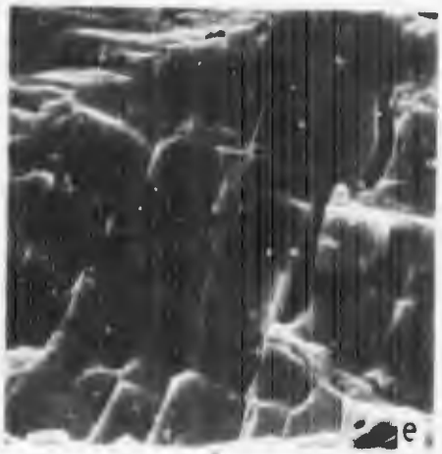

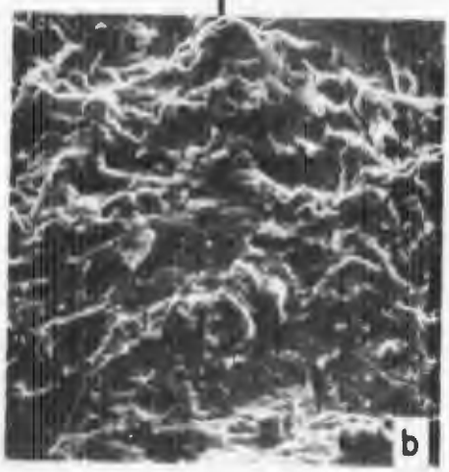

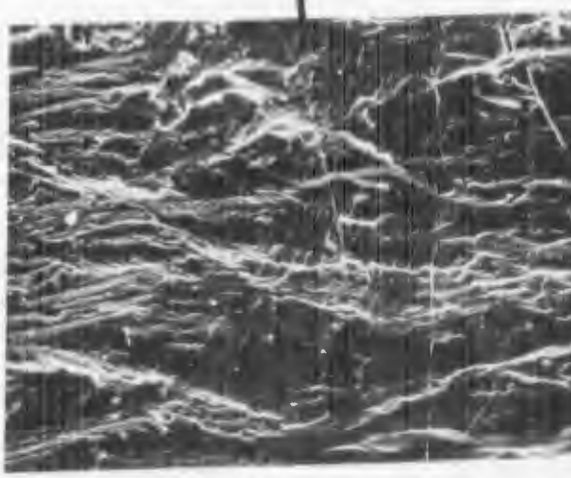

Preceding page blank

Ti-6Al-6V=2

Ti-6Al-6V-2Sn Condition J, AC, ANN

a) Light micrograph; 500X

b,c) Precrack zone; 800X, 2000X

d,e,f) Fatigue to fast fracture transition;
800X, 4000X, 2000X

g,h,i) Fast fracture zone; 800X, 2000X, 800X

YS = 147 KSI

UTS = 160 KSI

K_{Ic} = 74.6 KSI$\sqrt{in}$

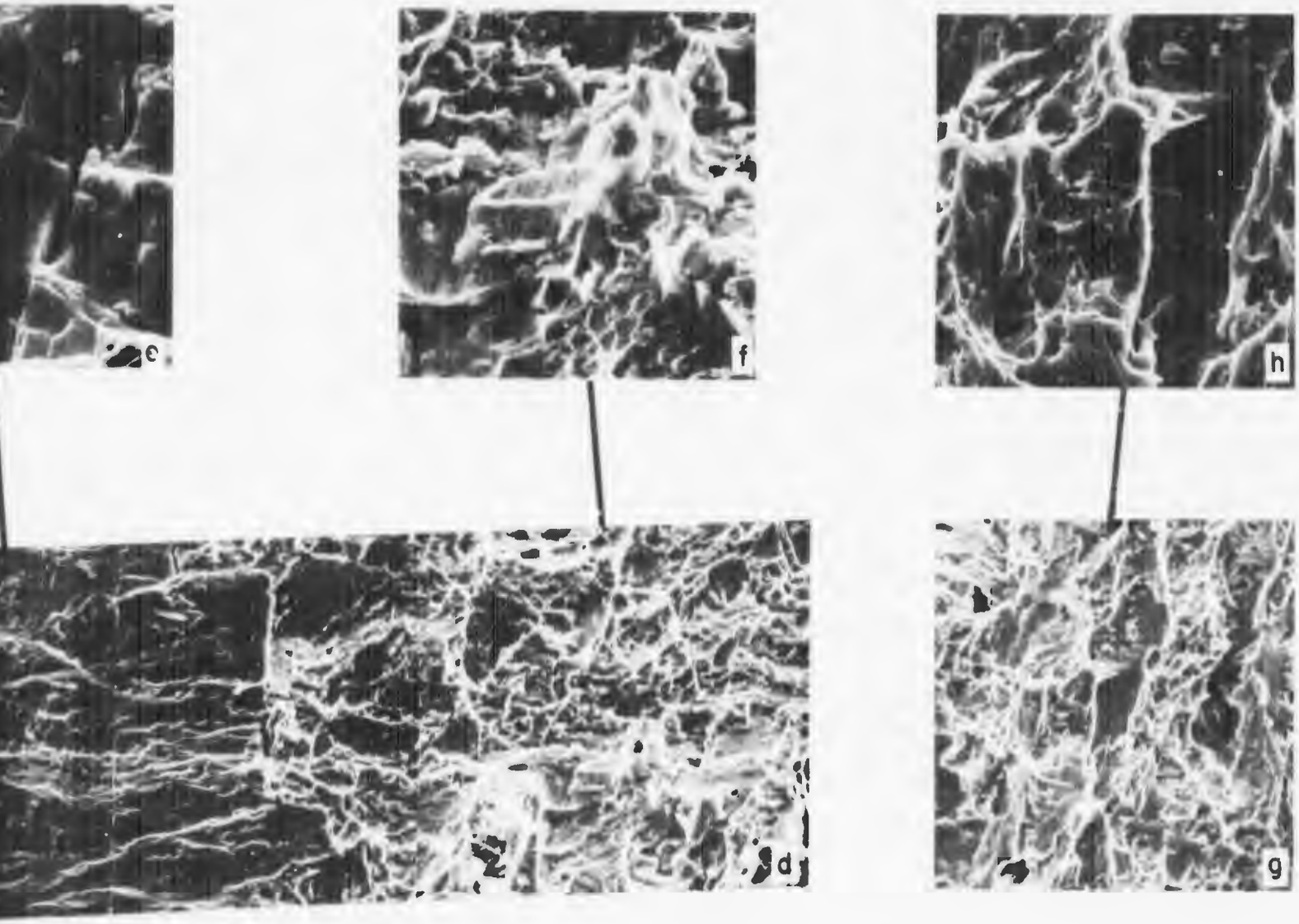

Figure 18

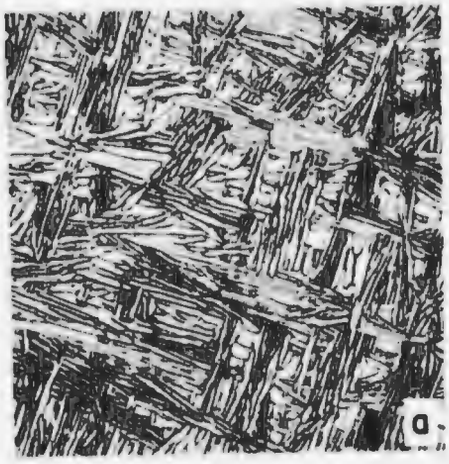

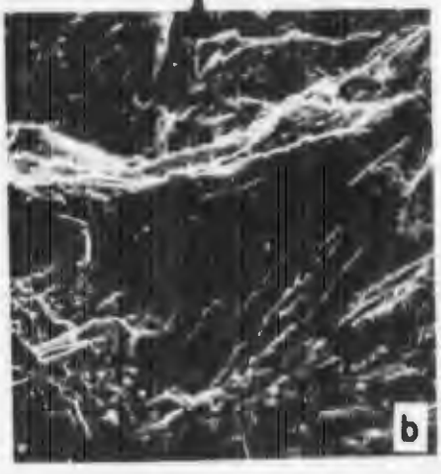

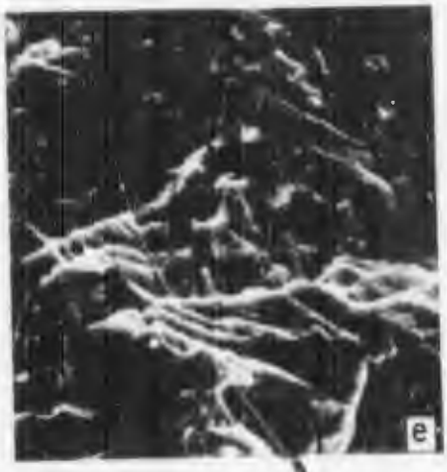

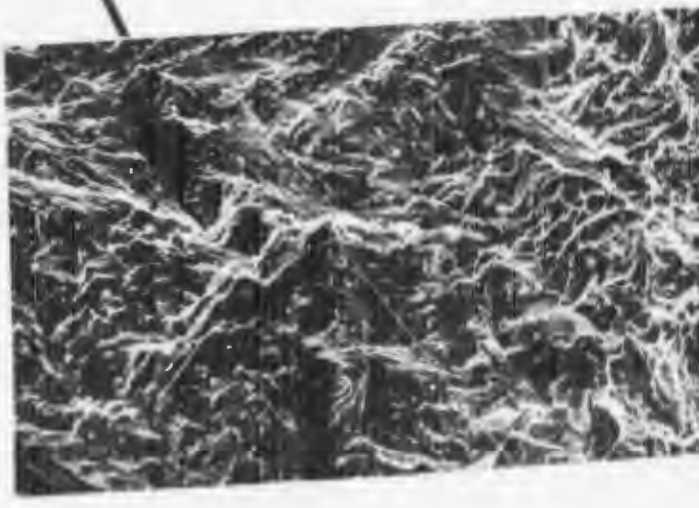

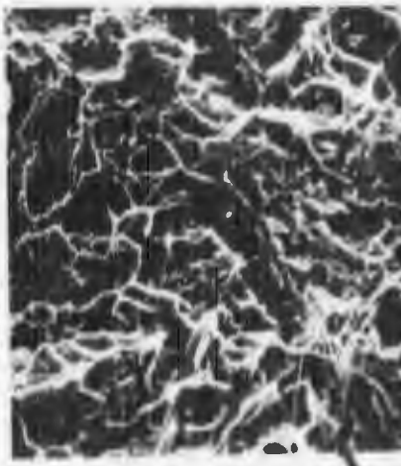

Preceding page blank

Ti-6Al-6V-2Sn Condition T, ANN

a) Light micrograph; 500X

b,c) Precrack zone; 800X, 4000X

d,e,f) Fatigue to fast fracture transition; 400X, 2000X, 800X

g,h,i,j) Fast fracture zone; 160X, 800X, 800X, 2000X

YS = 136 KSI

UTS = 153 KSI

K_{Ic} = 73.6 KSI$\sqrt{in}$

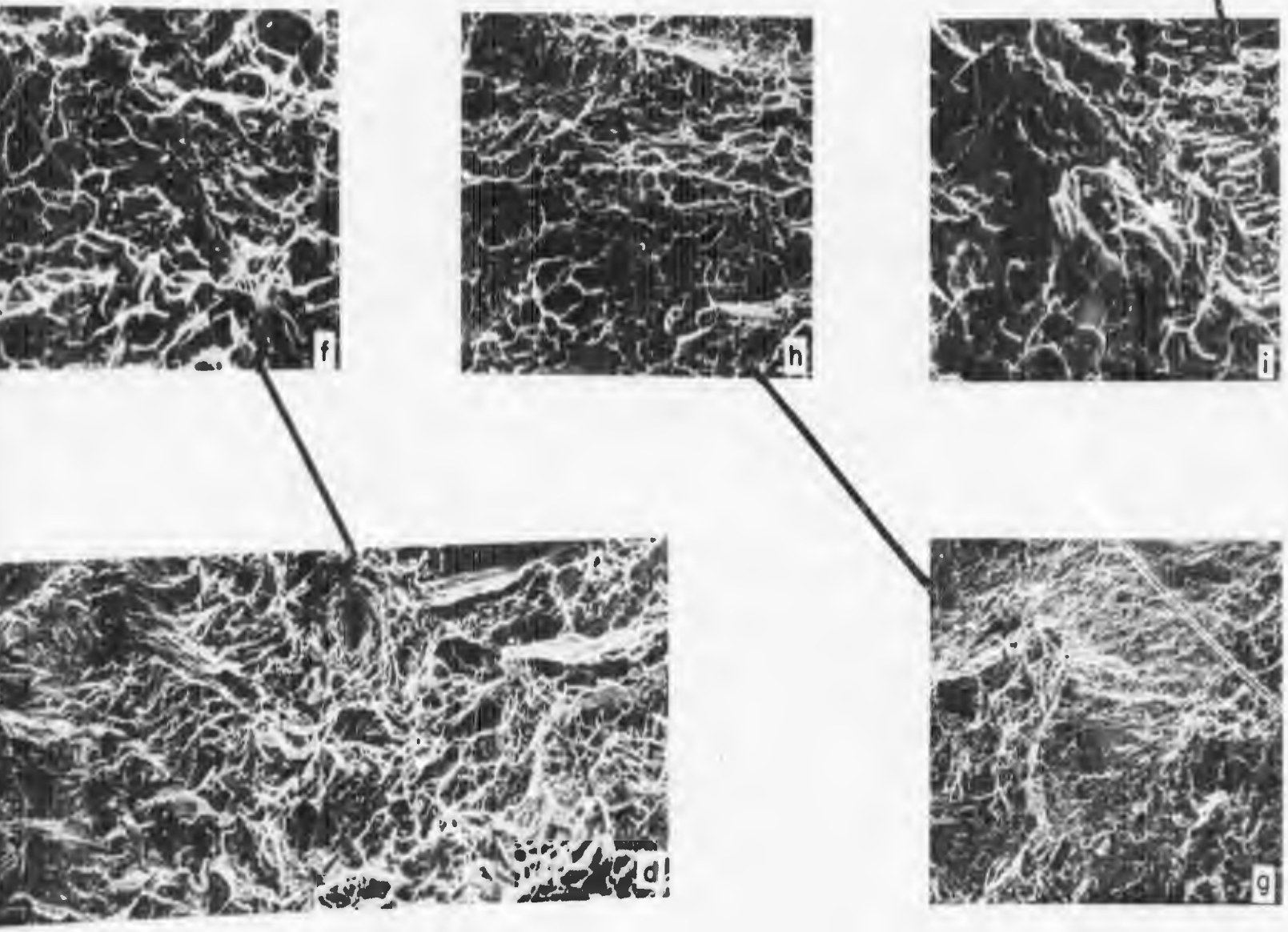

Figure 19

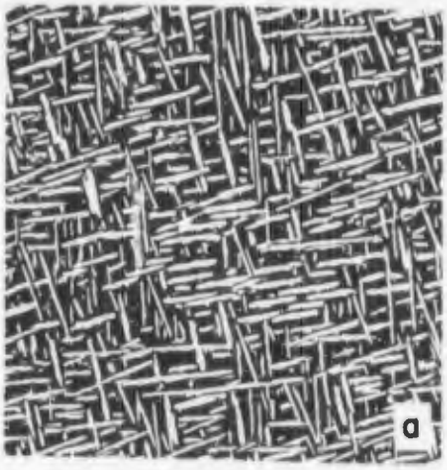

Ti-6Al-6V-2Sn Condition R, AC, STOA

a) Light micrograph; 500X

b) Precrack zone; 4000X

c,d,e) Fatigue to fast fracture transiti
200X, 400X, 1600X

f,g,h) Fast fracture zone; 800X, 400X,

YS = 140 KSI

UTS = 156 KSI

K_{Ic} = 73.6 KSI$\sqrt{in}$

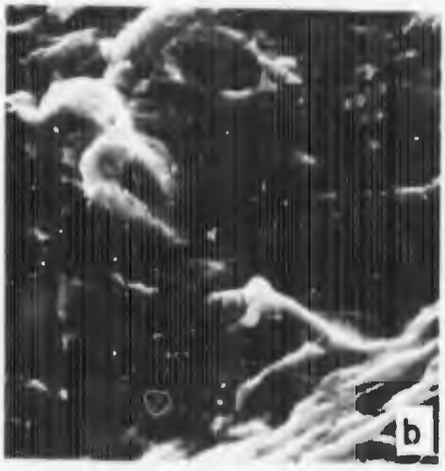

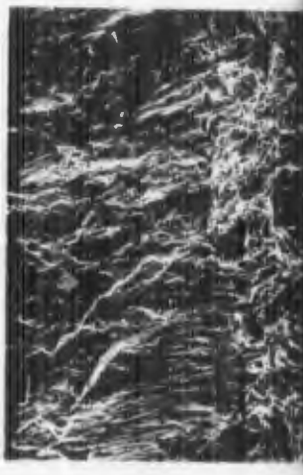

-6V-2Sn Condition R, AC, STOA

ght micrograph; 500X

crack zone; 4000X

) Fatigue to fast fracture transition;
200X, 400X, 1600X

) Fast fracture zone; 800X, 400X, 4000X

140 KSI

156 KSI

73.6 KSI$\sqrt{\text{in}}$

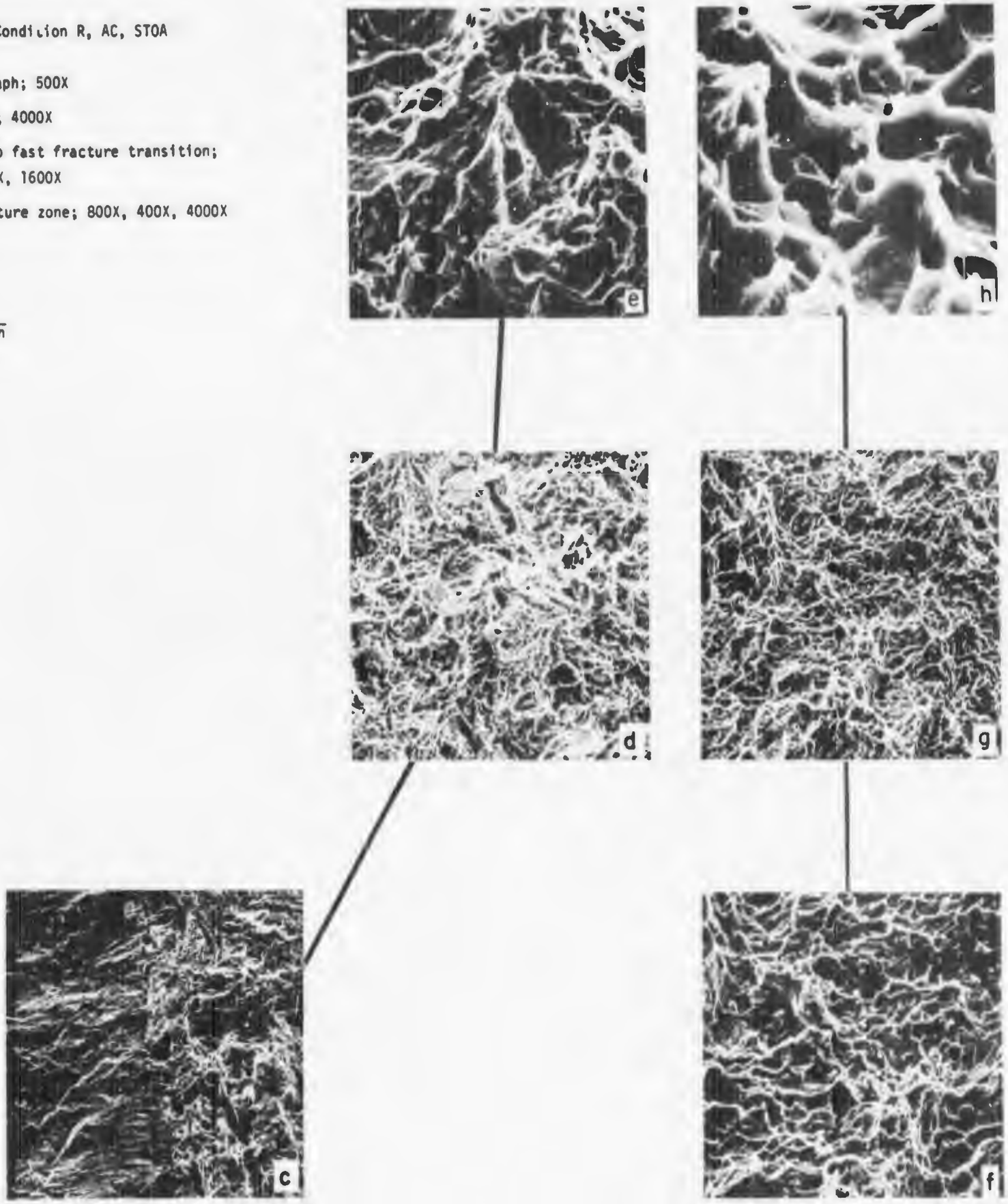

Figure 20

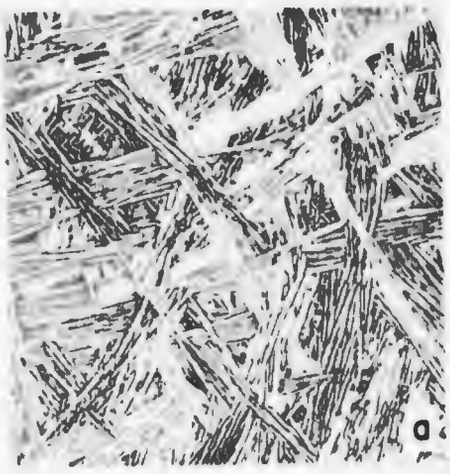
a

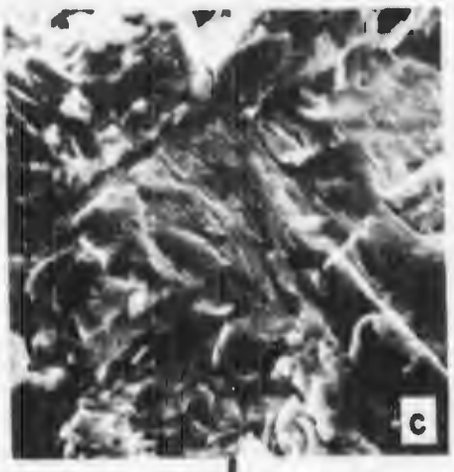
c

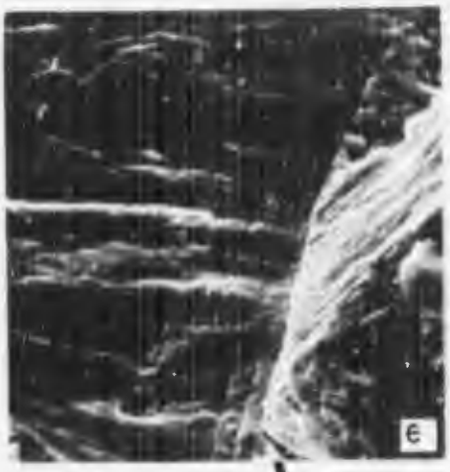
e

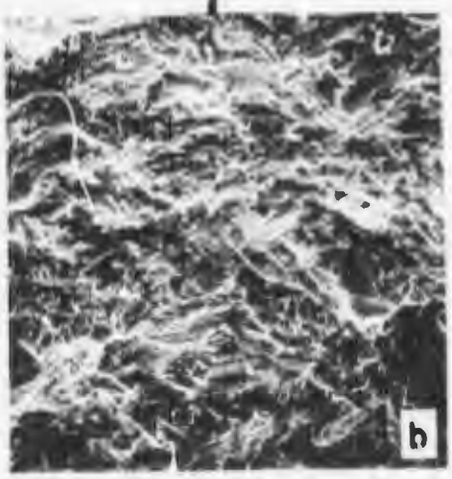
b

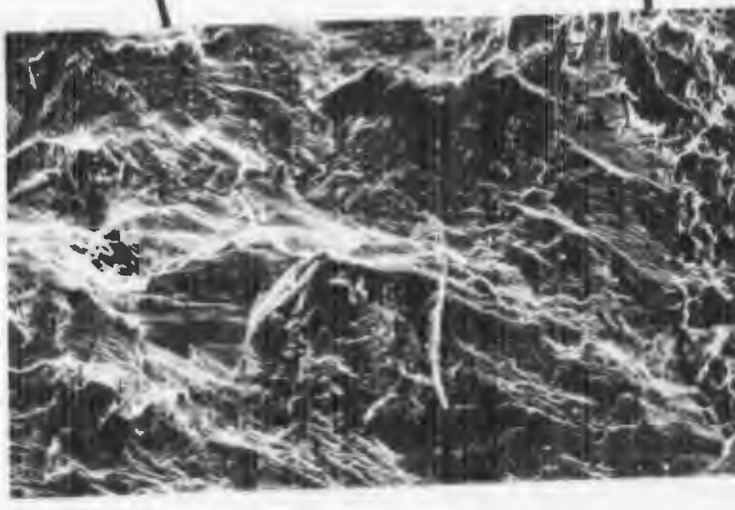

Ti-6Al-6V-2Sn Condition O, AC, ANN

a) Light micrograph; 500X

b,c) Precrack zone; 400X, 2000X

d,e,f,g) Fatigue to fast fracture transition;
400X, 2000X, 2000X, 2000X

h,i,j) Fast fracture zone; 80X, 400X, 2000X

YS = 136 KSI

UTS = 155 KSI

K_{Ic} = 71.7 KSI$\sqrt{in}$

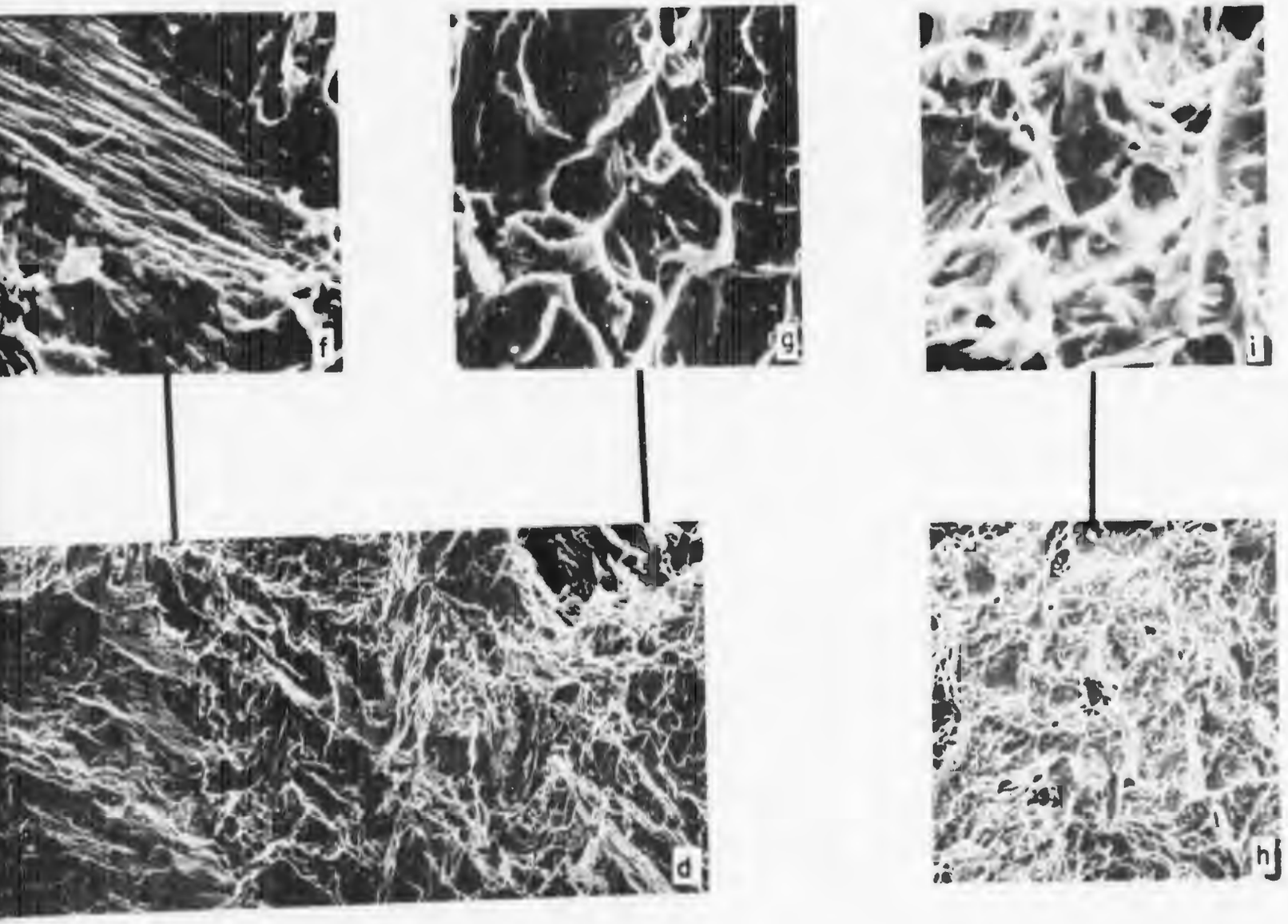

Figure 21

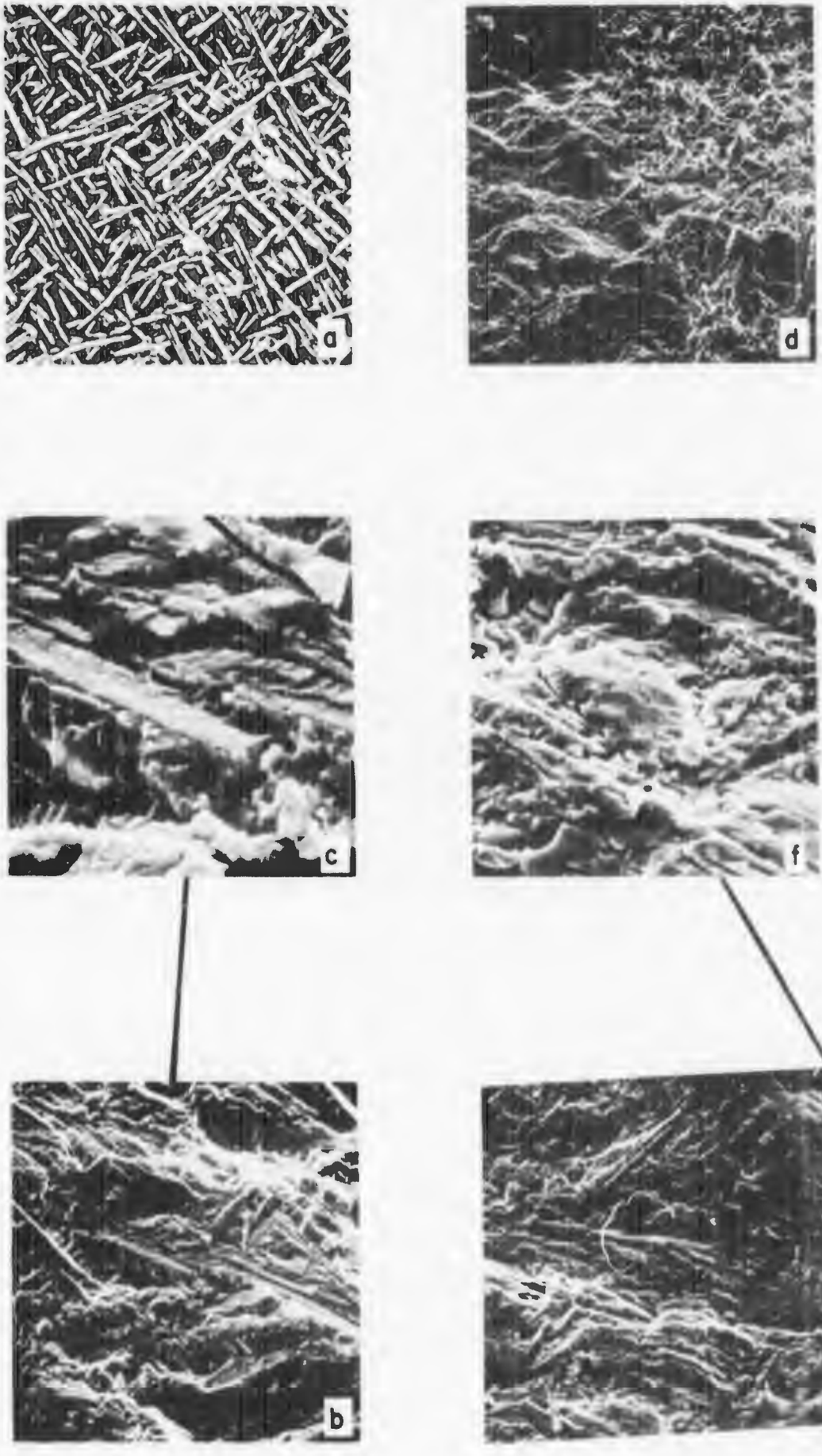
a
d
c
f
b

Ti-6Al-6V-2Sn Condition U, STOA

a) Light micrograph; 500X

b,c) Precrack zone; 800X, 4000X

d,e,f,g) Fatigue to fast fracture transition;
160X, 800X, 2000X, 2000X

h,i,j) Fast fracture zone; 2000X, 800X, 2000X

YS = 143 KSI

UTS = 159 KSI

K_{Ic} = 71.3 KSI$\sqrt{in}$

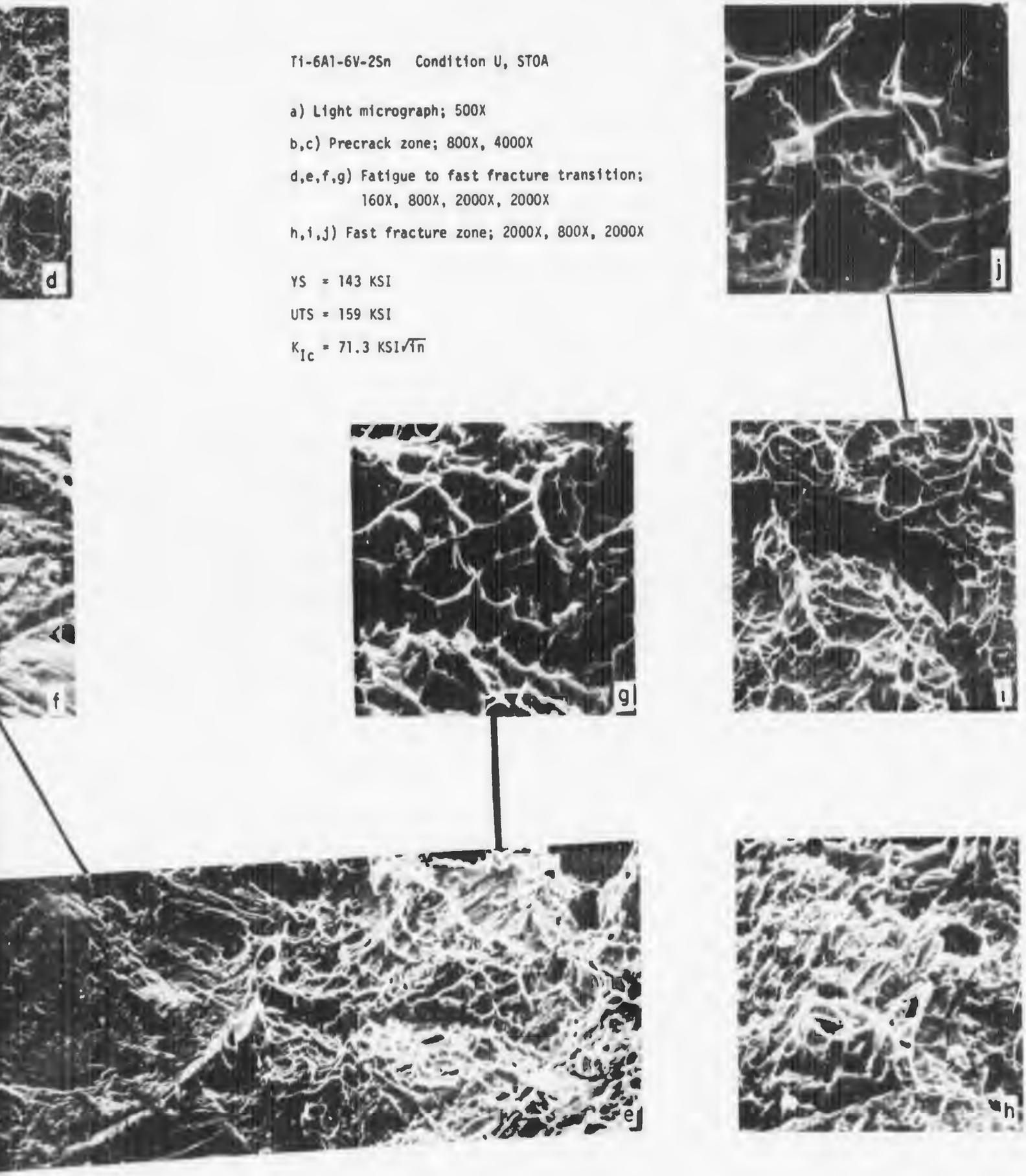

Figure 22

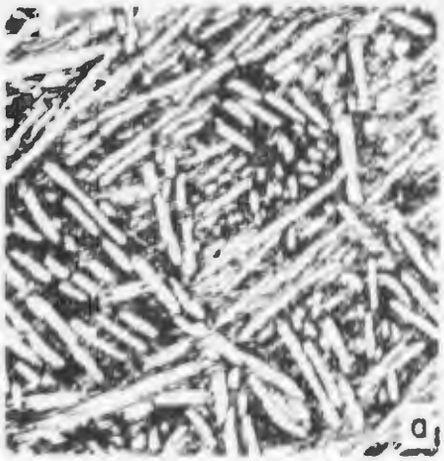

Ti-6Al-6V-2Sn Condition [illegible] STOA

a) Light micrograph; 500X

b,c,d) Fatigue to fast frac[illegible] transition
400X, 1600X, 1600X

e,f,g,h,i) Fast fracture zo[illegible] 400X,
1600X, 400X, 400

YS = 144 KSI

UTS = 160 KSI

K_{Ic} = 67.9 KSI$\sqrt{in}$

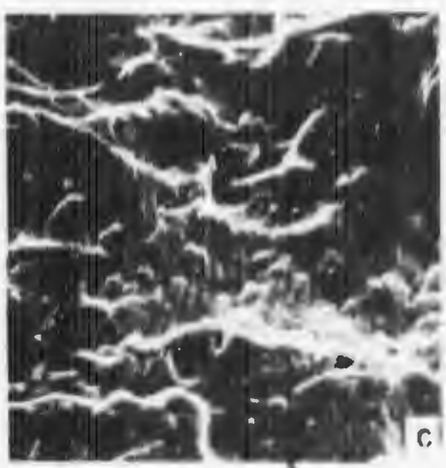

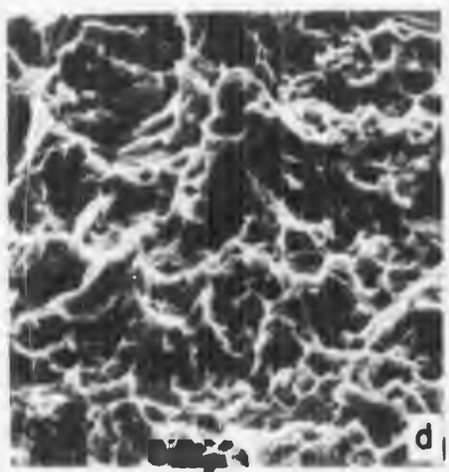

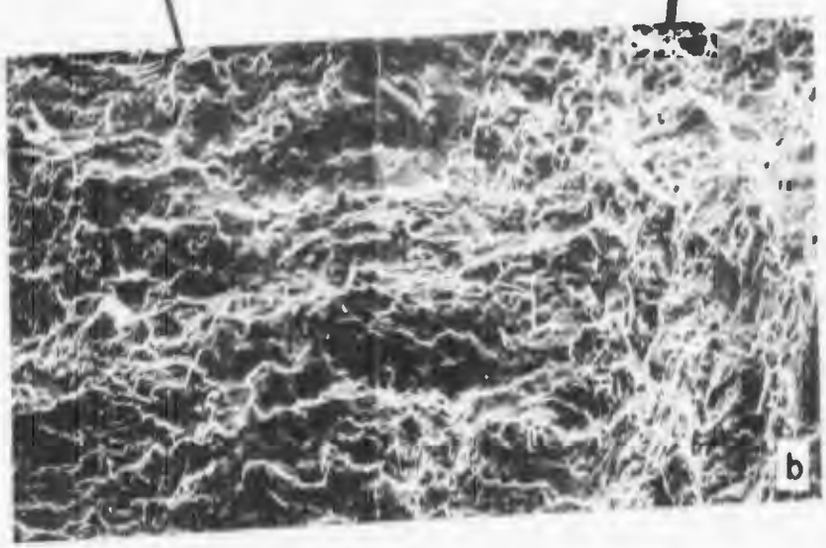

Preceding page blank

...tion M, WQ, STOA

...; 500X

...fast fracture transition;
...X, 1000X

...fracture zone; 80X, 400X,
...400X, 4000X

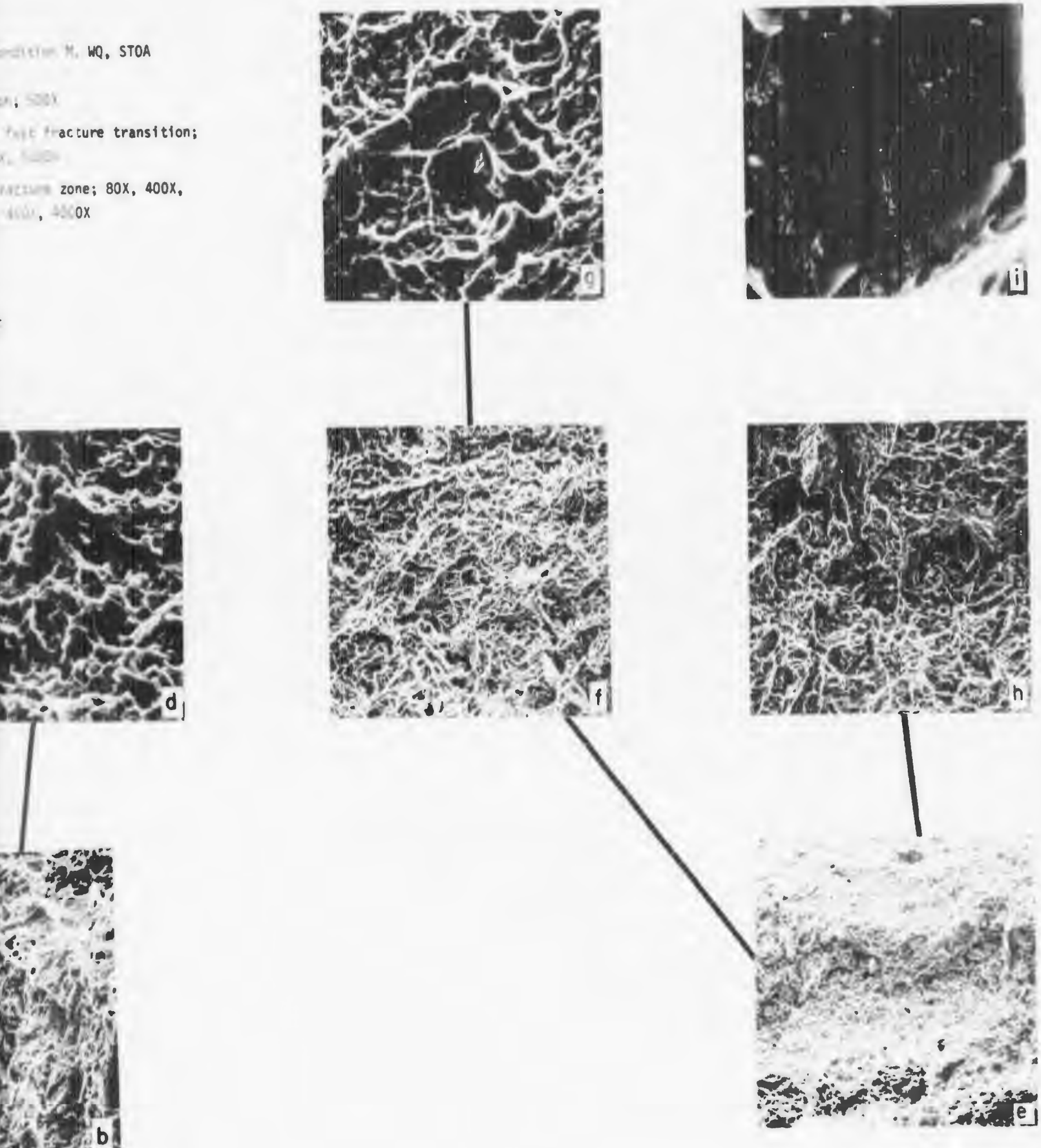

Figure 23

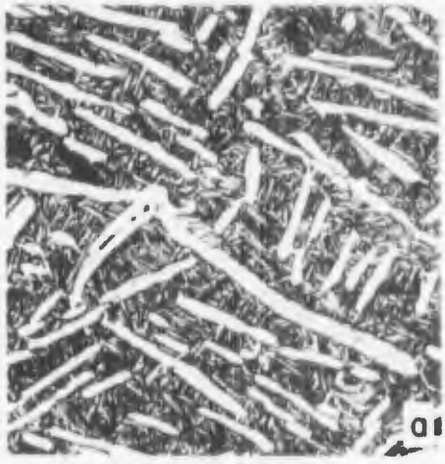

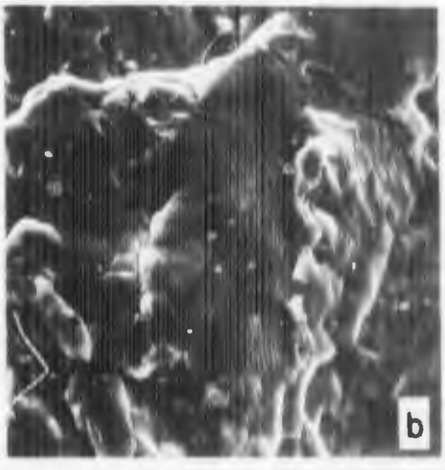

Ti-6Al-6V-2Sn Condition 5, AC, ANN

a) Light micrograph, 500X

b) Precrack zone, 2000X

c,d,e,f,g) Fatigue to fast fracture transition;
80X, 400X, 1600X, 400X, 1600X

h,i) Fast fracture zone, 400X, 1600X

YS = 142 KSI

UTS = 155 KSI

K_{Ic} = 65.4 KSI$\sqrt{In.}$

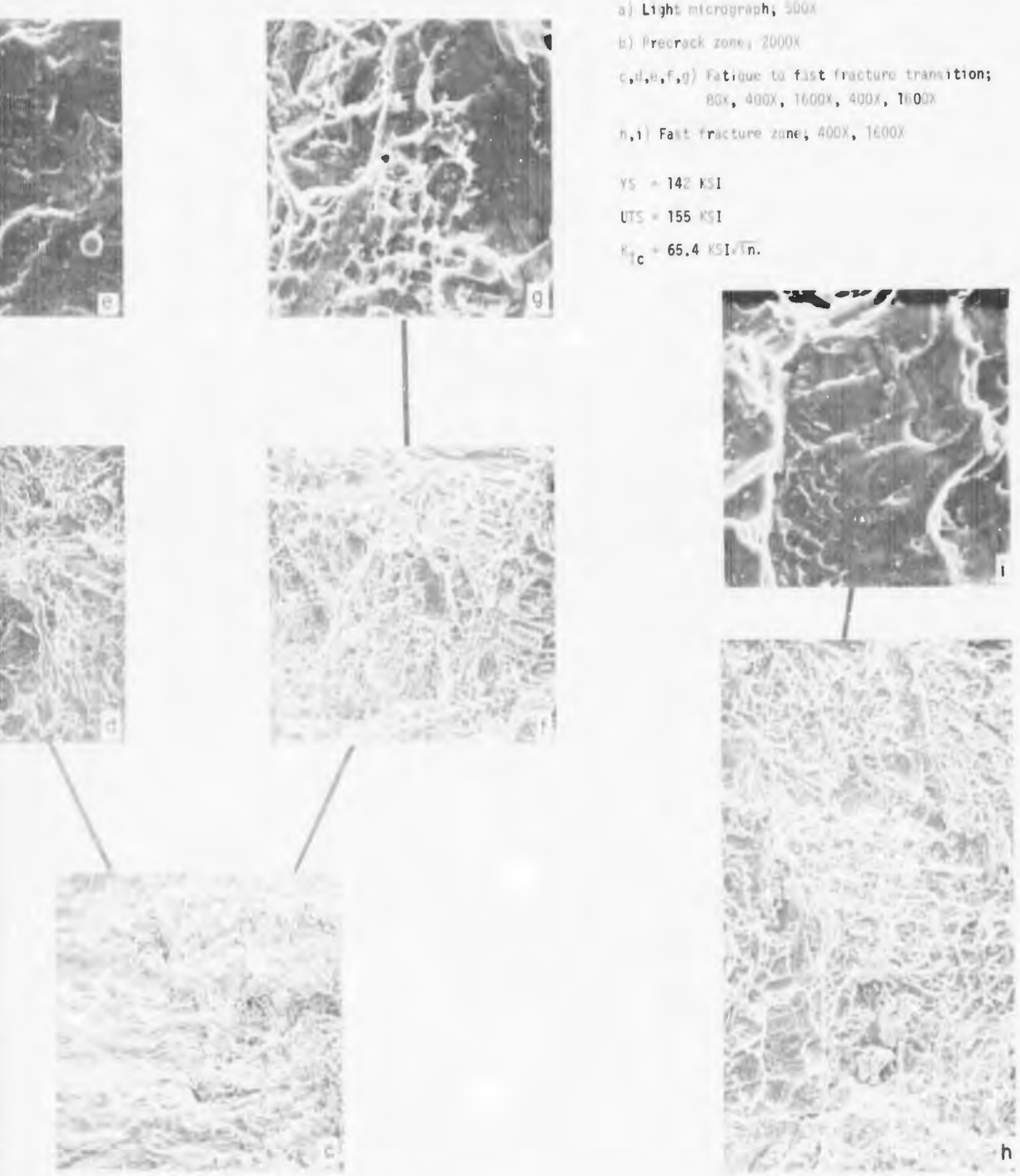

Figure 24

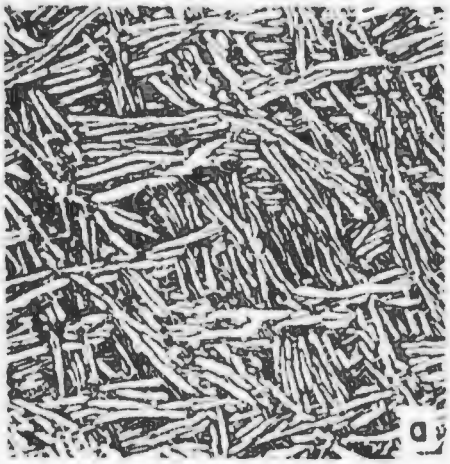

Ti-6Al-6V-2S Conditio

a) Light micrograph; 500

b,c) Precrack zone; 400X

d,e,f,g) Fatigue to fast
400X, 2000X, 80

h,i,j) Fast fracture zon

YS = 145 KSI

UTS = 158 KSI

K_{1c} = 64.4 KSI$\sqrt{in}$

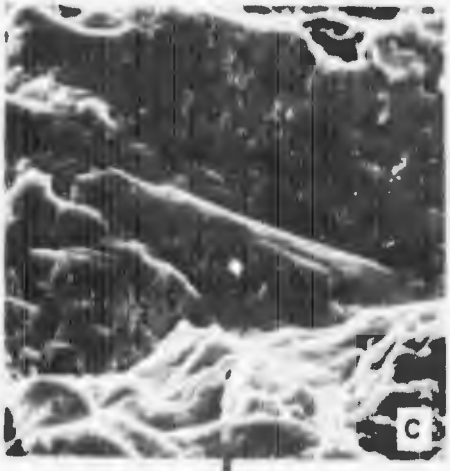

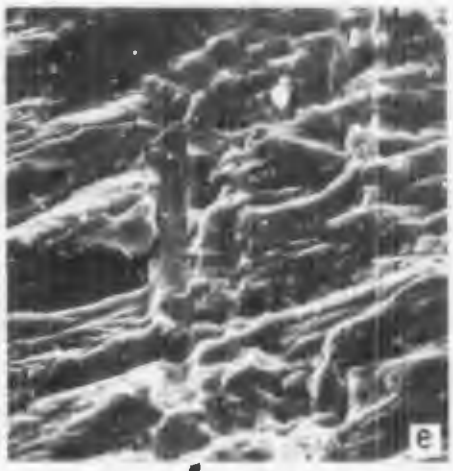

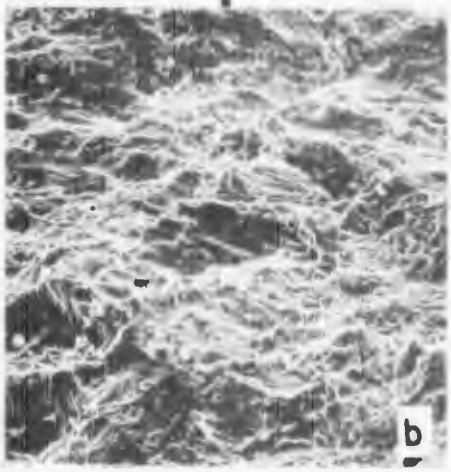

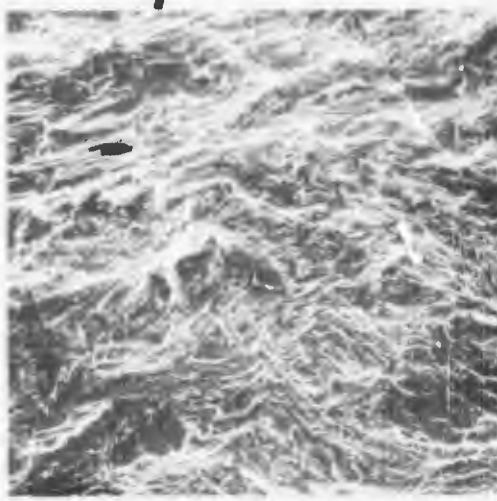

V-[illegible] Condition [illegible], AC, ANN

[illegible]icrograph; 500[illegible]

crack zone; 400[illegible], 2000X

Fa[illegible]igue t[illegible] fas[illegible] fracture transition;
400X, 2 00[illegible], 800[illegible], 2000X

ast fracture zone; 160X, 800X, 2000X

5 KSI

8 KSI

.4 KSI√[illegible]

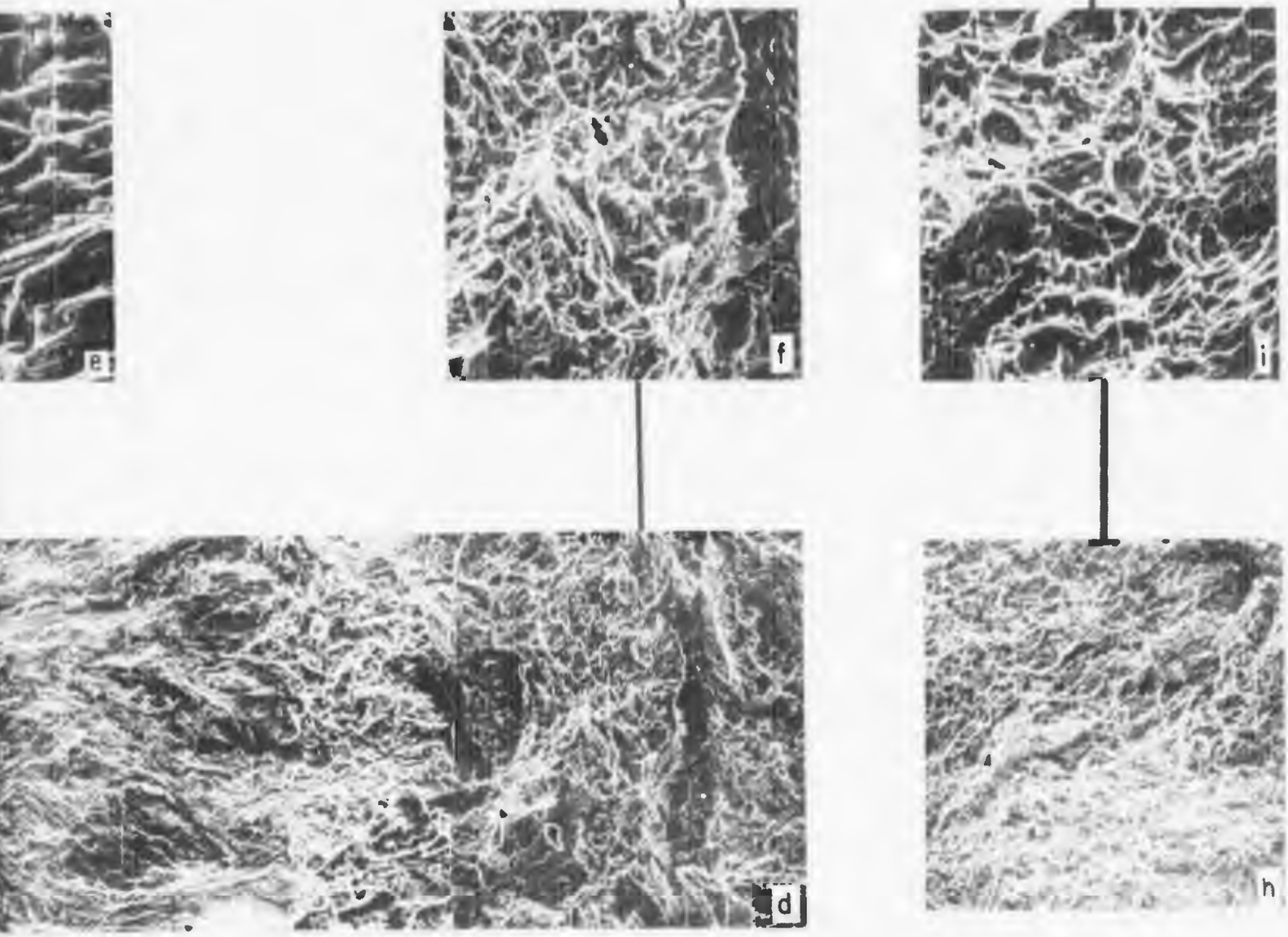

Figure 25

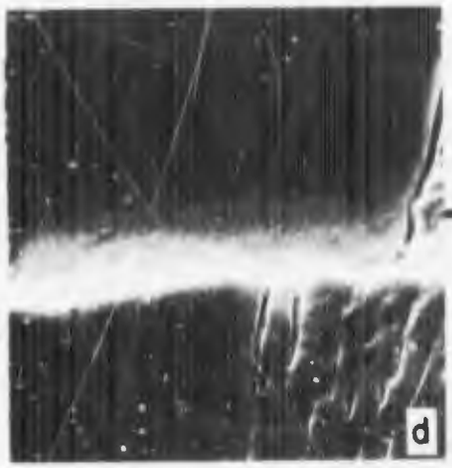

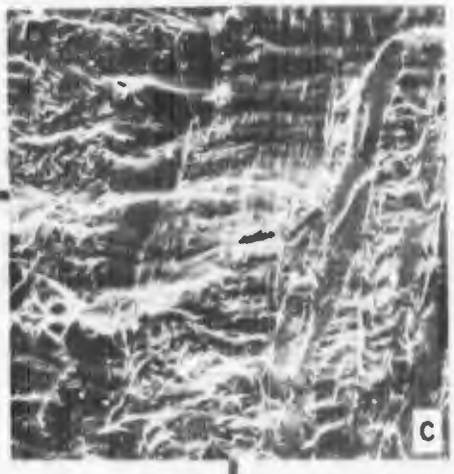

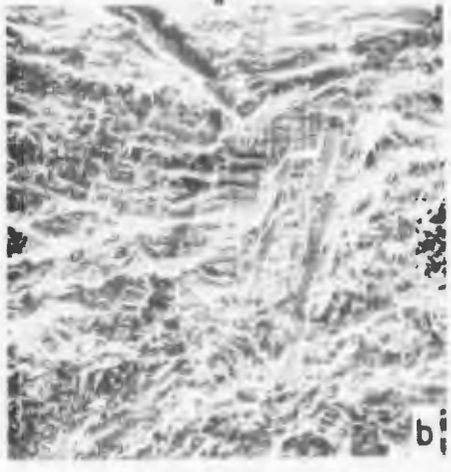

Ti-6Al-6V-2Sn Condition D, AC, ANN

a) Light micrograph; 500X

b,c,d,e,f) Fatigue to fast fracture transition;
160X, 400X, 2000X, 160X, 400X

g) Fast fracture zone; 400X

YS = 143 KSI

UTS = 155 KSI

K_{Ic} = 63.6 KSI$\sqrt{in}$

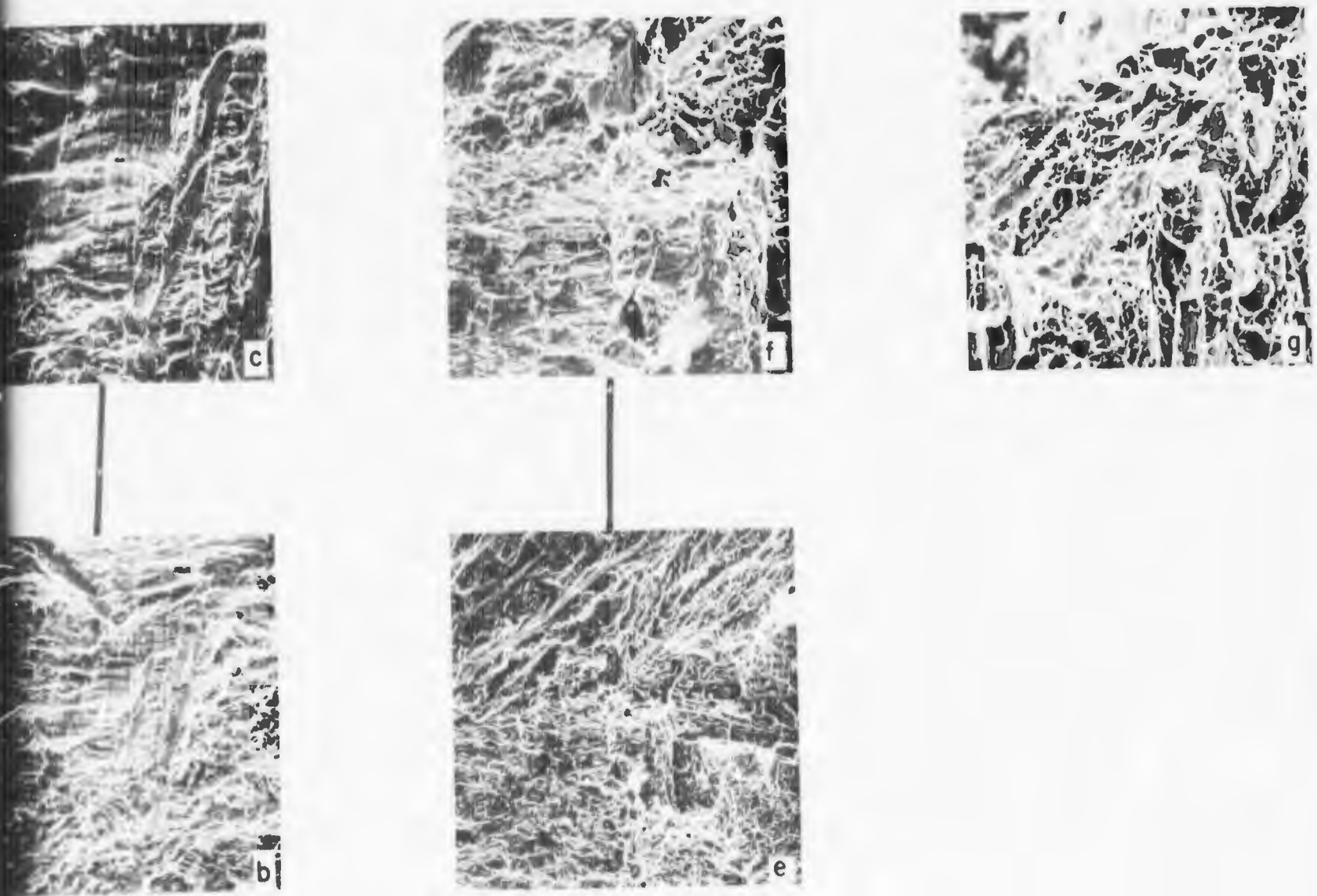

Figure 26

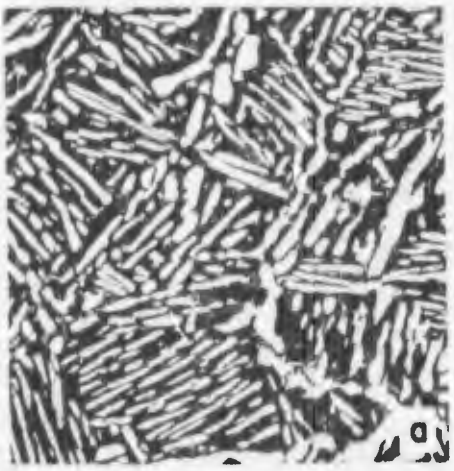
a


d

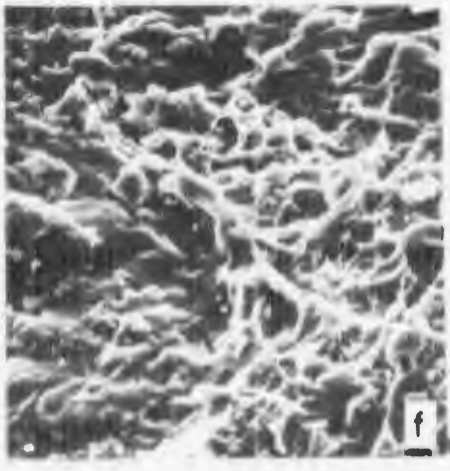
f

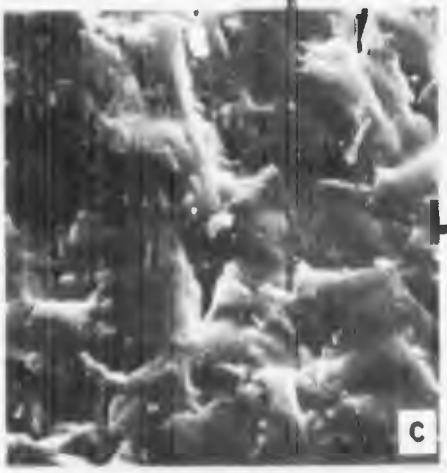
c

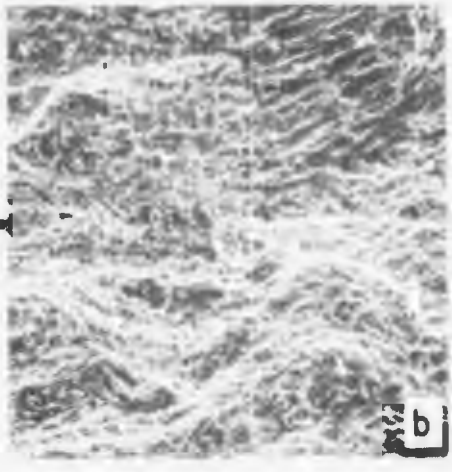
b

Ti-6Al-6V-2Sn Condition O, AC, STOA

a) Light micrograph; 500X

b,c,d) Precrack zone; 340X, 3600X, 14000X

e,f,g) Fatigue to fast fracture transition; 360X, 1450X, 1450X

n) Fast fracture zone; 1450X

YS = 148 KSI

UTS = 162 KSI

K_{Ic} = 60.8 KSI$\sqrt{in}$

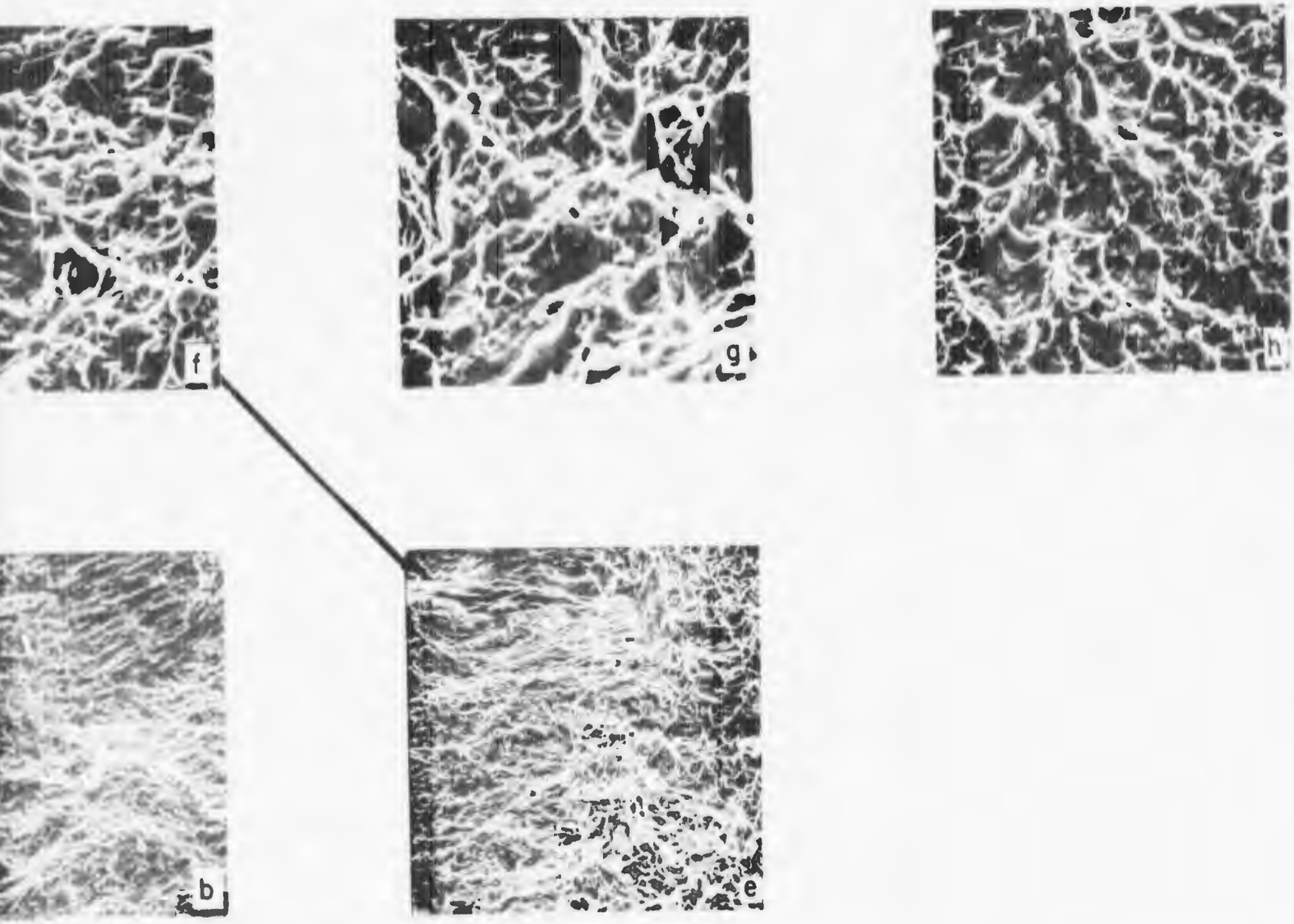

Figure 27

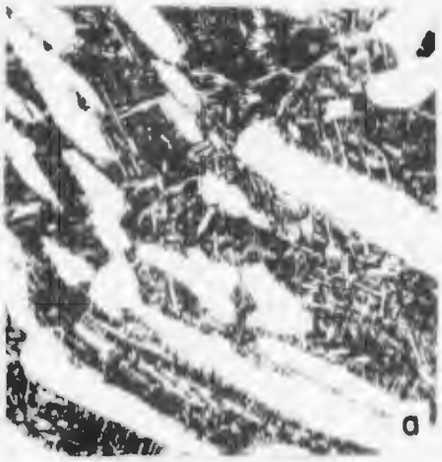
a


c

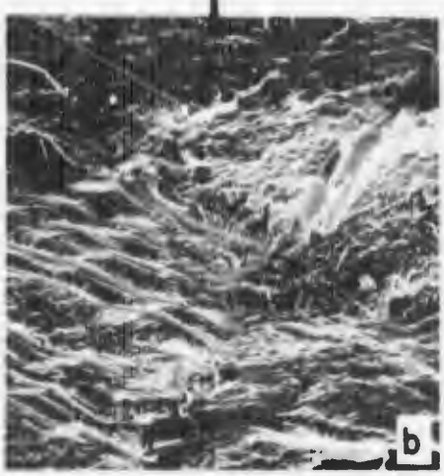
b

Ti-6Al-6V-2Sn Condition E, AC, STOA

a) Light micrograph; 500X

b,c) Precrack zone; 200X, 2000X

d,e) Fatigue to fast fracture transition;
800X, 4000X

f,g) Fast fracture zone; 200X, 800X

YS = 148 KSI

TS = 161 KSI

K_{Ic} = 56.5 KSI$\sqrt{in}$

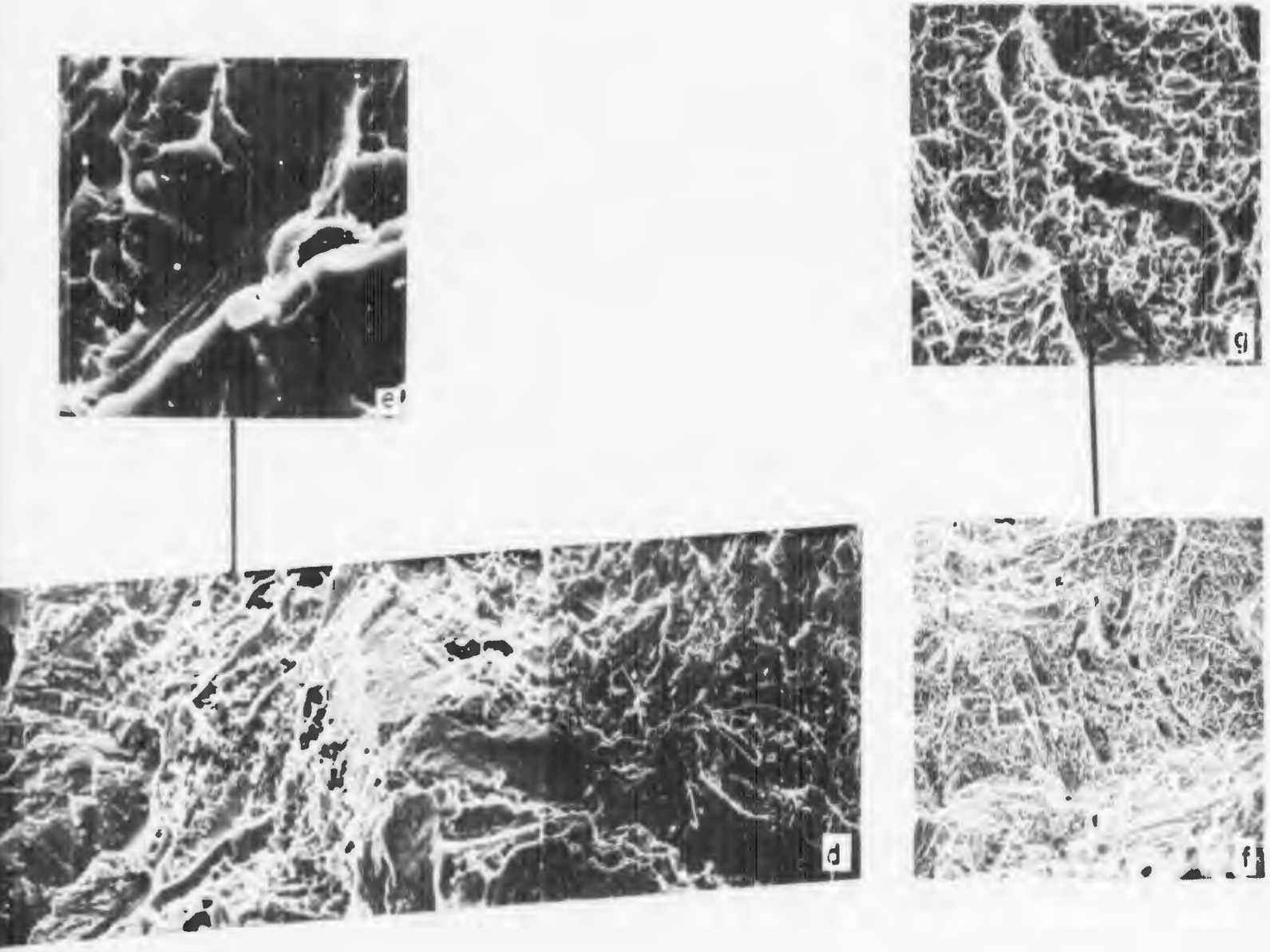

Figure 28

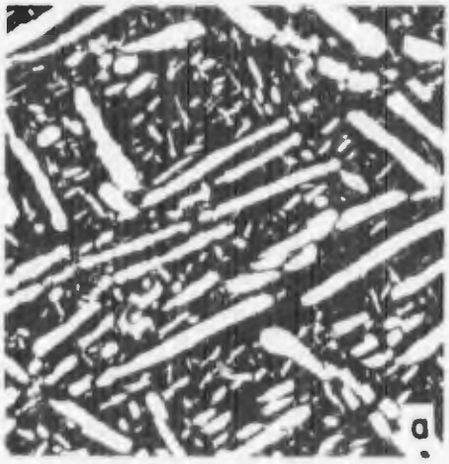
a

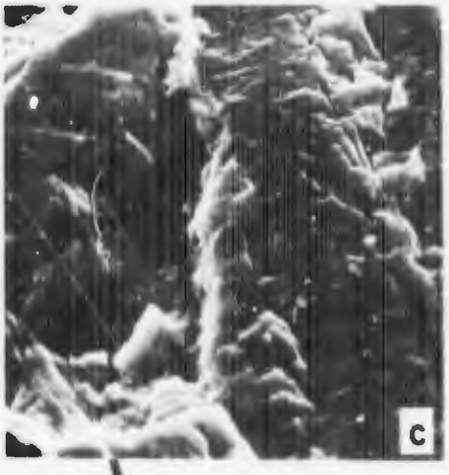
c

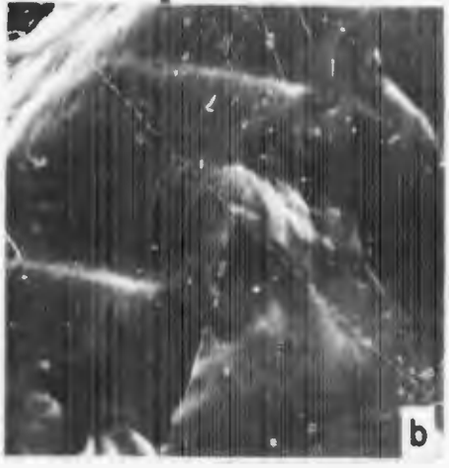
b

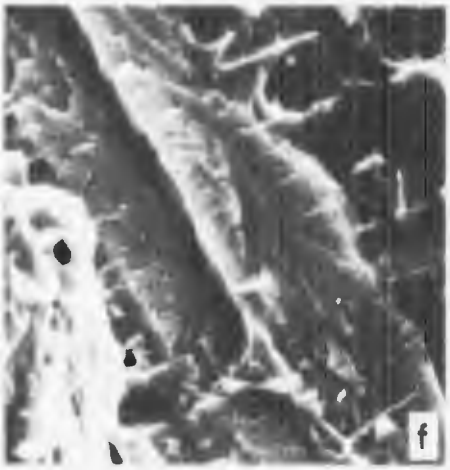

Ti-6Al-6V-2Sn Condition H, AC, STOA

a) Light micrograph; 500X

b,c) Precrack zone; 3400X, 6800X

d,e,f) Fatigue to fast fracture transition;
340X, 1400X, 3400X

g,h) Fast fracture zone; 340X, 1400X

YS = 150 KSI

UTS = 164 KSI

K_{Ic} = 55.2 KSI$\sqrt{in}$

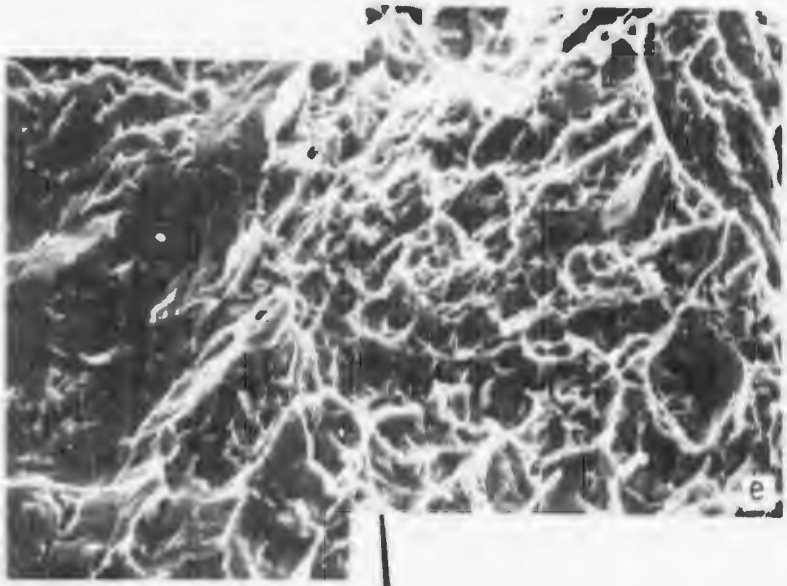

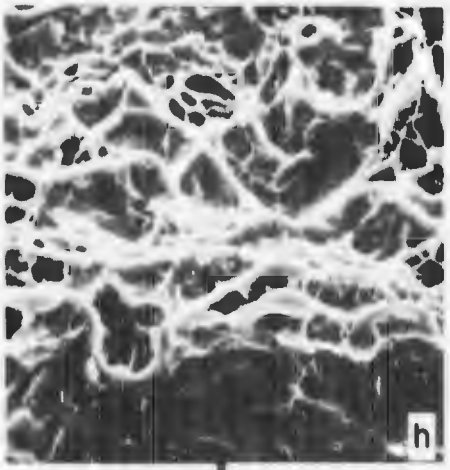

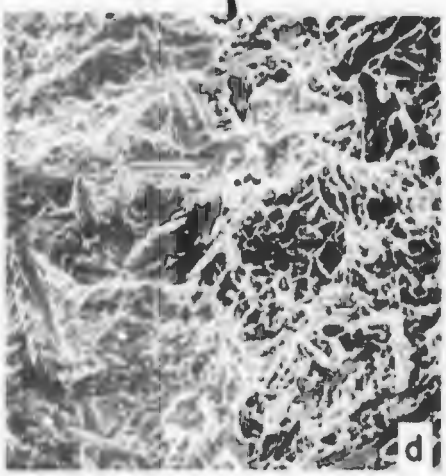

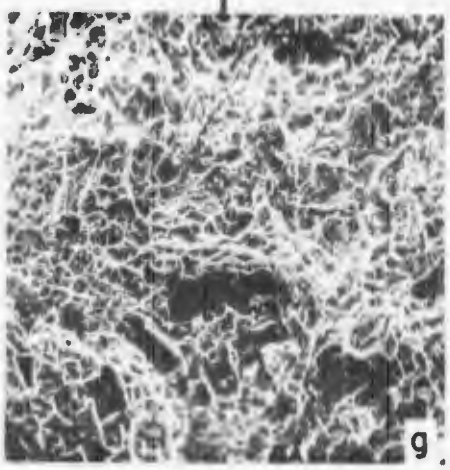

Figure 29

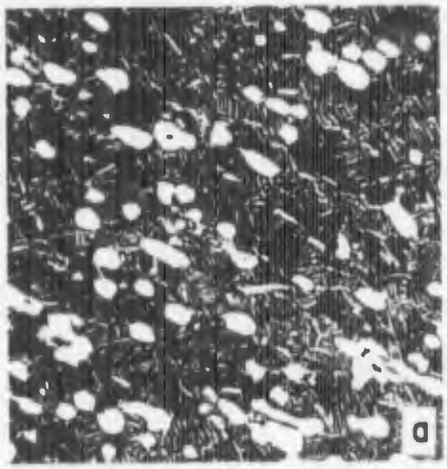

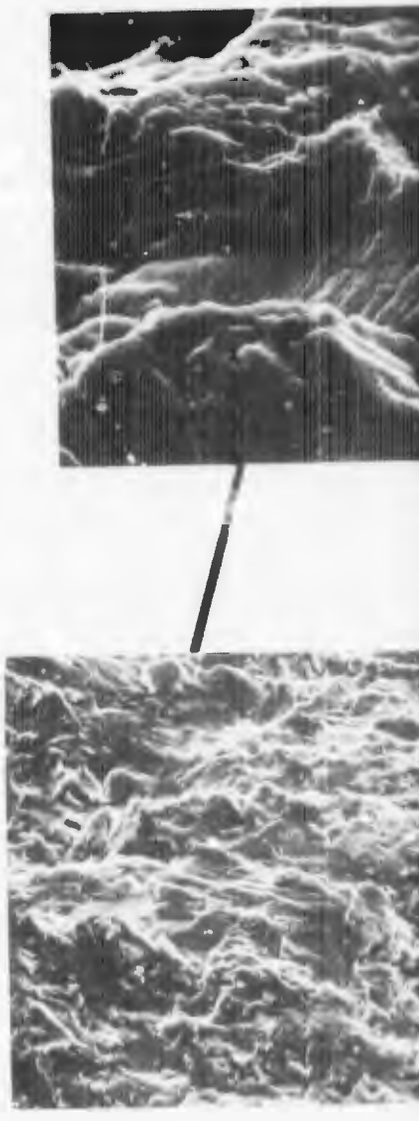

Preceding page blank

Ti-6Al-6V-2Sn Condition A, AC, ANN

a) Light micrograph; 500X

b,c,d) Fatigue to fast fracture transition;
800X, 4000X, 2000X

e,f) Fast fracture zone; 800X, 2000X

YS = 145 KSI

UTS = 158 KSI

K_{Ic} = 50.4 KSI$\sqrt{in}$

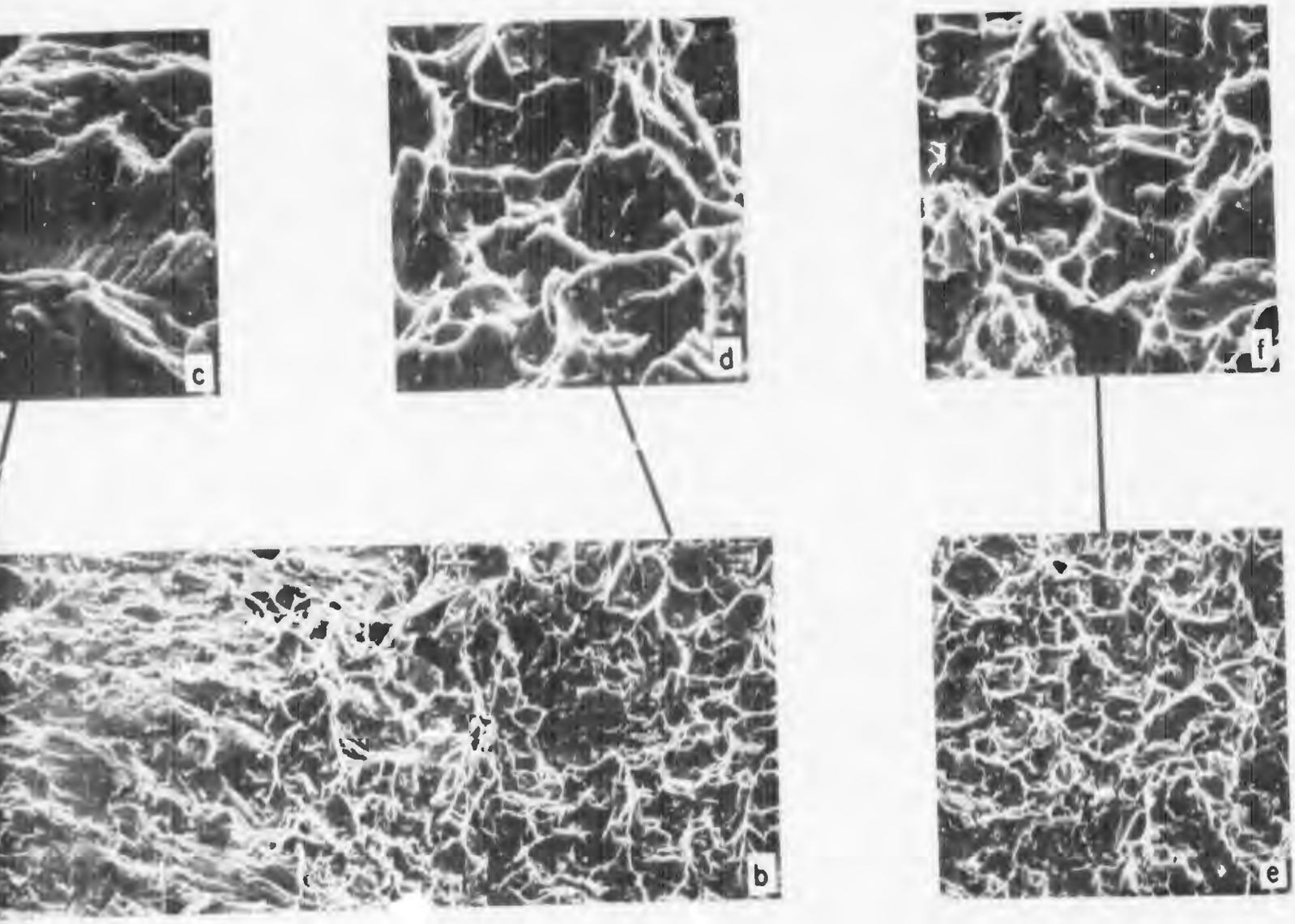

Figure 30

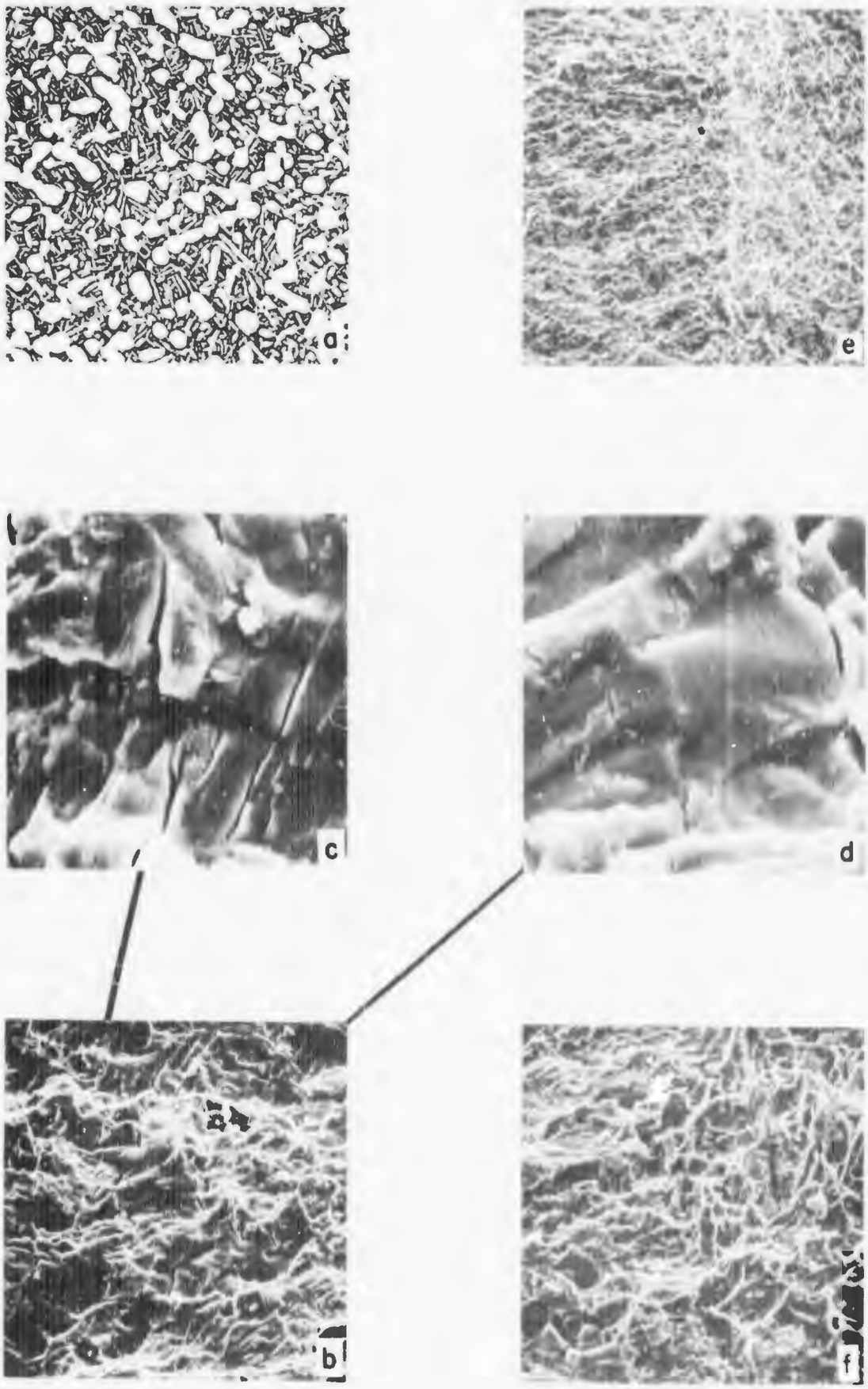

Preceding page blank

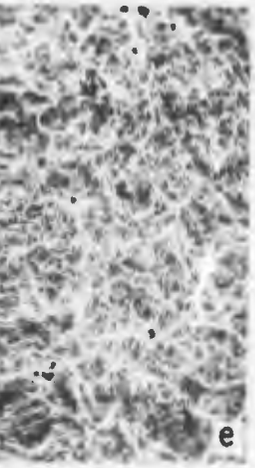

Ti-6Al-6V-2Sn Condition A-1, AC, ANN

a) Light micrograph; 500X

b,c,d) Precrack zone; 800X, 4000X, 4000X

e,f,g,h) Fatigue to fast fracture transition;
160X, 800X, 800X, 2000X

i,j) Fast fracture zone; 800X, 2000X

YS = 149 KSI

UTS = 159 KSI

K_{Ic} = 49.4 KSI$\sqrt{in}$

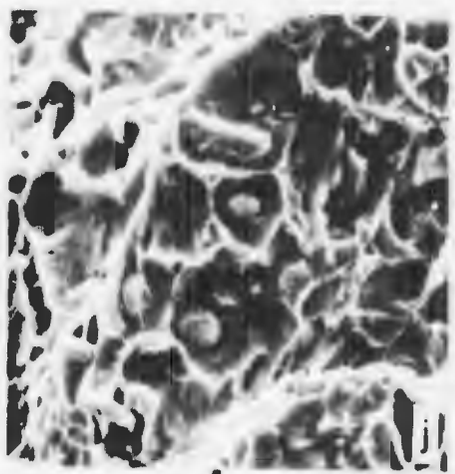

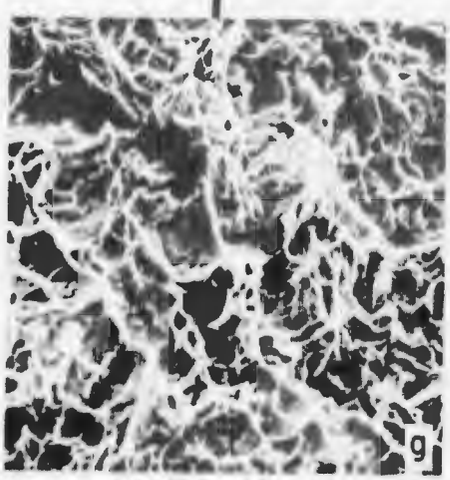

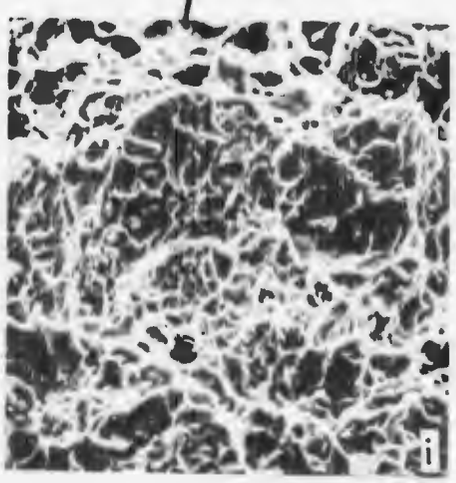

Figure 31

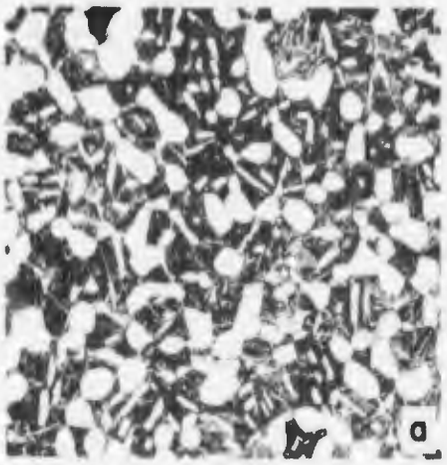

Ti-6Al-6V-2Sn Condit , AC, ST

a) Light micrograph; 50

b,c) Precrack zone; 800 4000X

d,e,f) Fatigue to fast ture tra
400X, 800X, 2000

g,h,i,j) Fast fracture zone; 400X,
400X, 800X

YS = 154 KSI

UTS = 165 KSI

K_{Ic} = 40.4 KSI$\sqrt{In}$

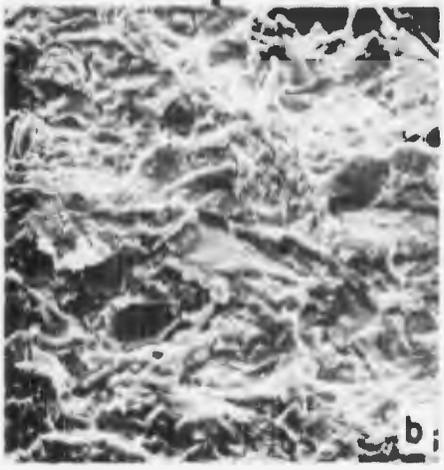

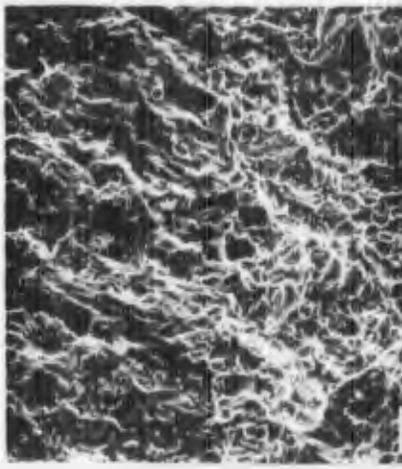

ndition B, AC, STOA

; 500X

ne; 800X, 4000X

o fast fracture transition;
2000X

acture zone; 400X, 1600X,
00

n

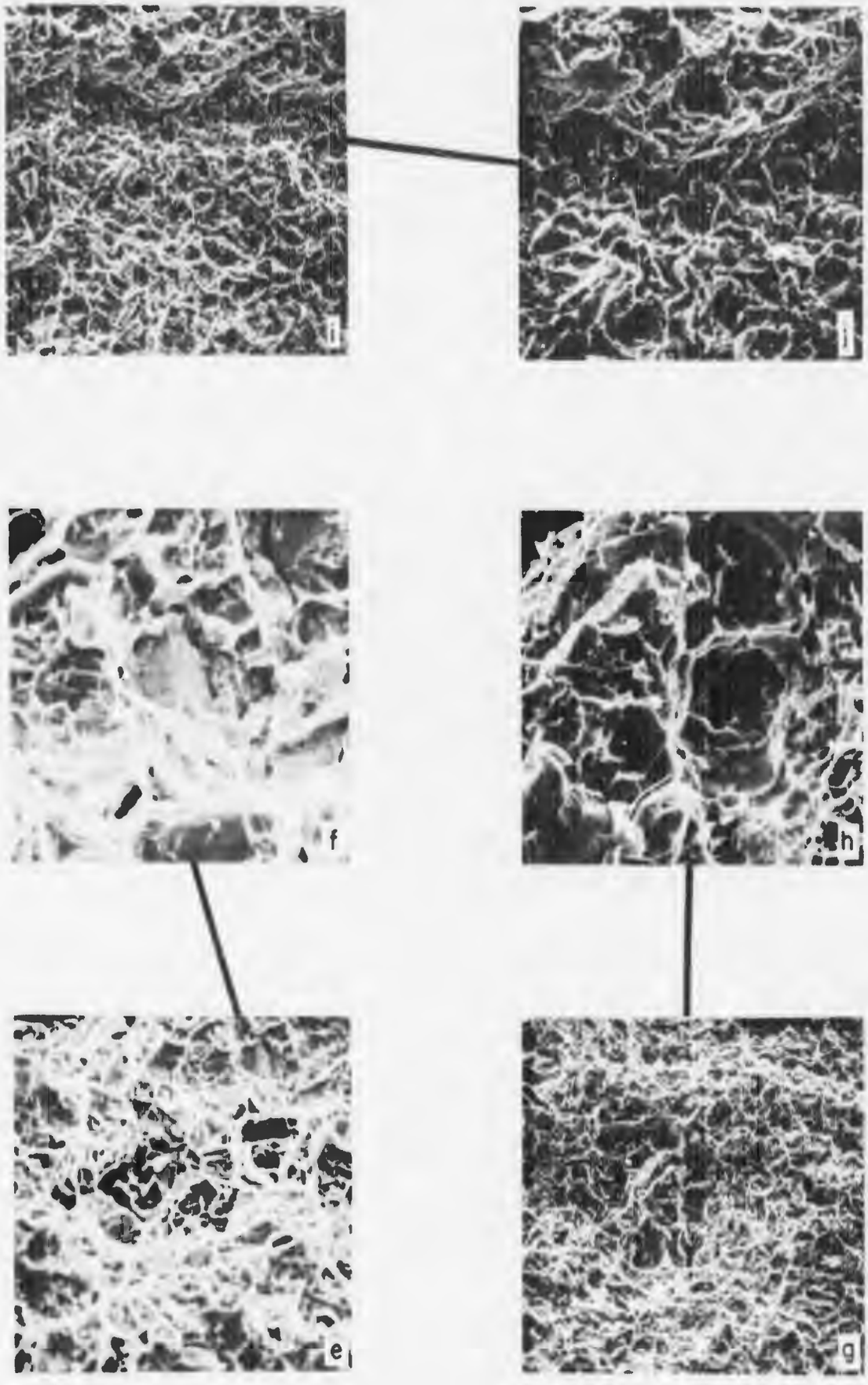

Figure 32

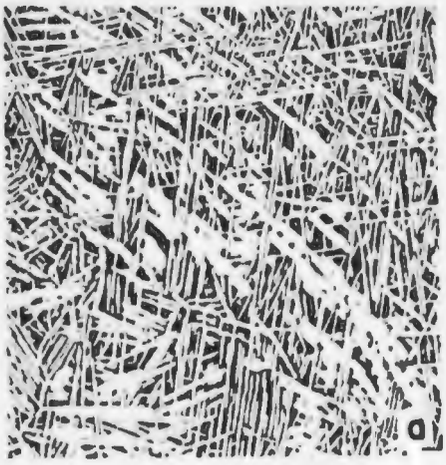
a

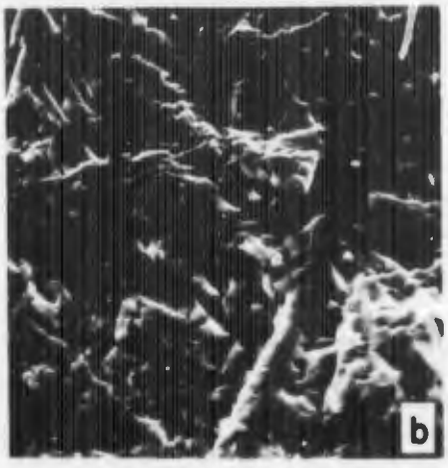
b

Ti-6Al-2Sn-4Zr-6Mo Condition G, STA

a) Light micrograph; 500X

b) Precrack zone; 2000X

c,d,e) Fatigue to fast fracture transition;
40X, 800X, 2000X

f) Fast fracture; 80X

YS = 152 KSI

UTS = 174 KSI

K_{Ic} = 51.4 KSI$\sqrt{in}$

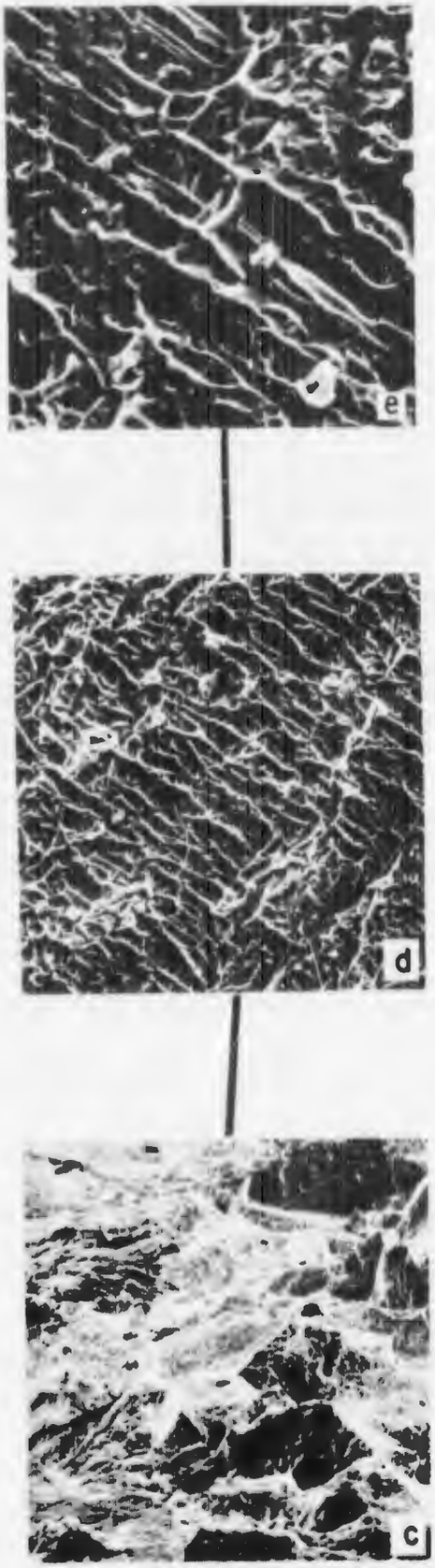

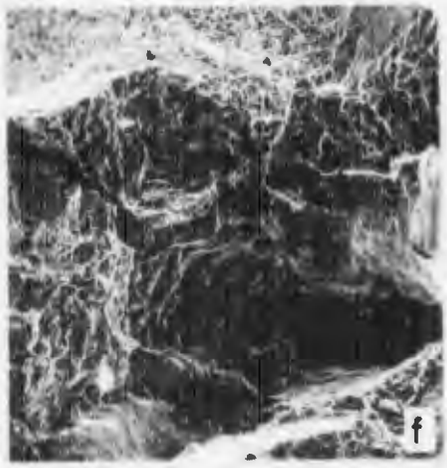

Figure 33

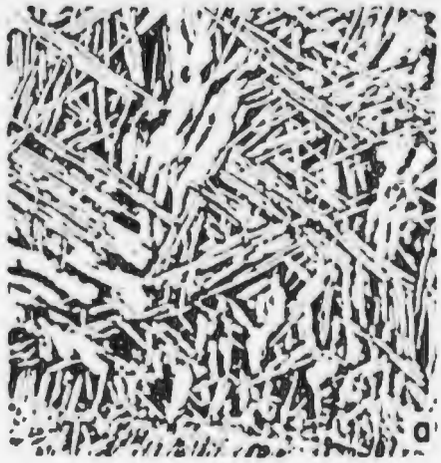

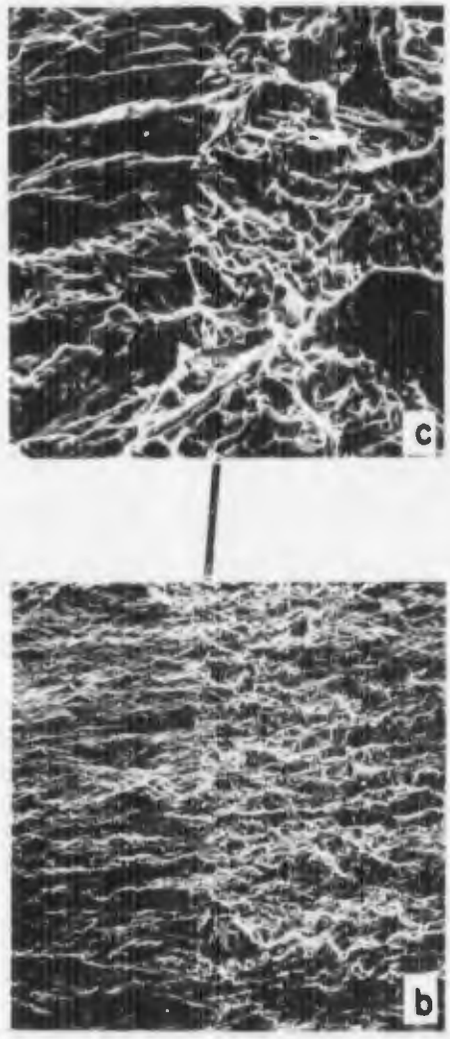

Ti-6Al-2Sn-4Zr-6Mo Condition E, STA

a) Light micrograph; 500X

b,c) Fatigue to fast fracture transition; 80X, 800X

d,e,f) Fast fracture zone near the transition; 200X, 800X, 2000X

g,h) Fast fracture zone; 80X, 80X

YS = 155 KSI

UTS = 171 KSI

K_{Ic} = 43.6 KSI$\sqrt{in}$

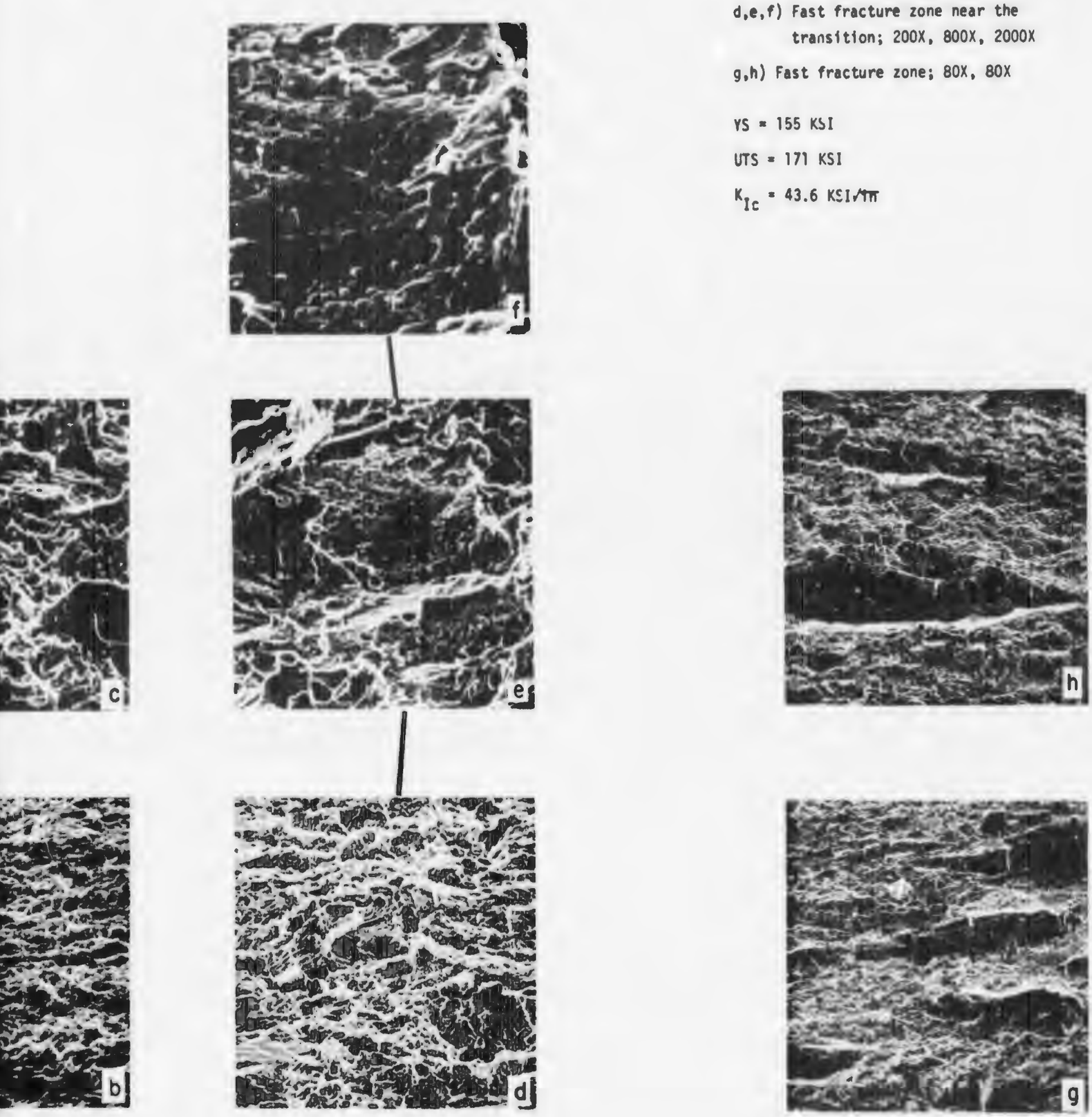

Figure 34

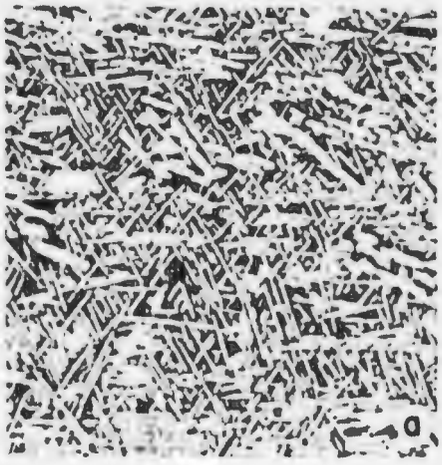

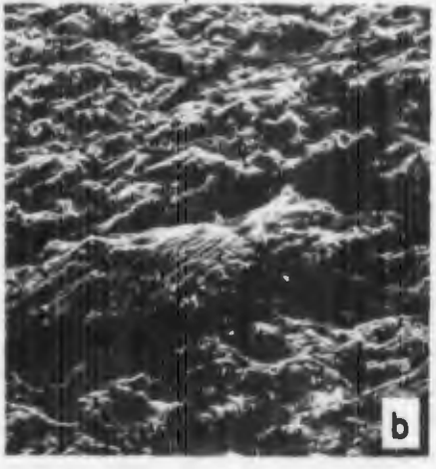

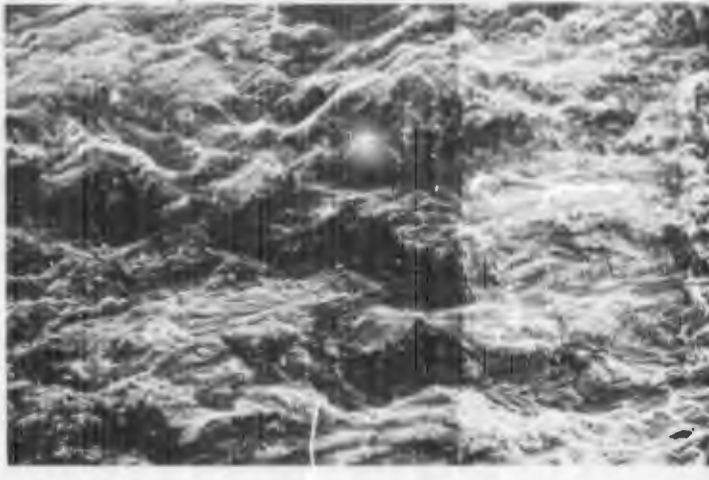

Preceding page blank

Ti-6Al-2Sn-4Zr-6Mo Condition C, STA

a) Light micrograph; 500X

b,c) Precrack zone; 400X, 2000X

d,e,f) Fatigue to fast fracture transition; 400X, 2000X, 2000X

g,h) Fast fracture; 400X, 2000X

YS = 159 KSI

UTS = 175 KSI

K_{Ic} = 40.5 KSI$\sqrt{in}$

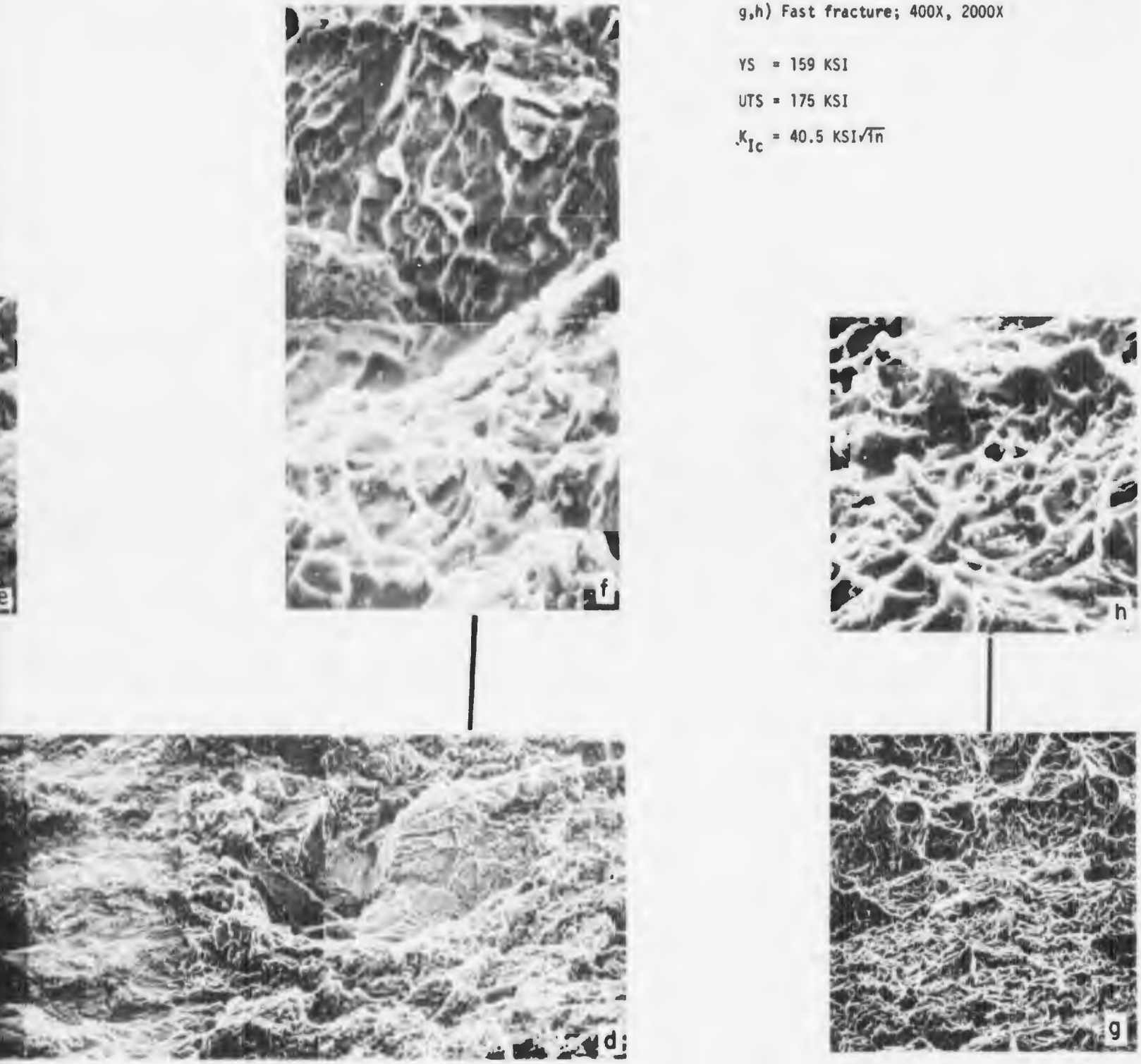

Figure 35

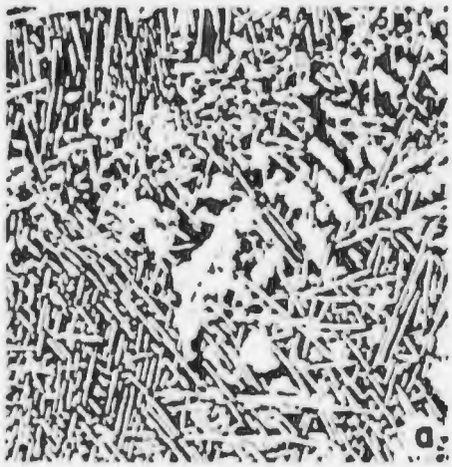
a


b

Ti-6Al-2Sn-4Zr-6Mo Condition D, STA

a) Light micrograph; 500X

b,c,d) Fatigue to fast fracture transition; 160X, 400X, 1600X

e) Fast fracture zone; 1600X

YS = 161 KSI

UTS = 175 KSI

K_{Ic} = 36.4 KSI$\sqrt{in}$

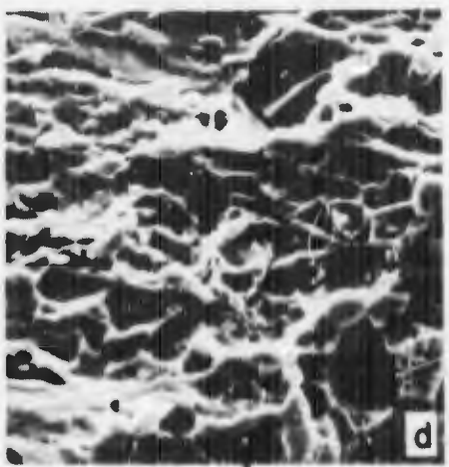

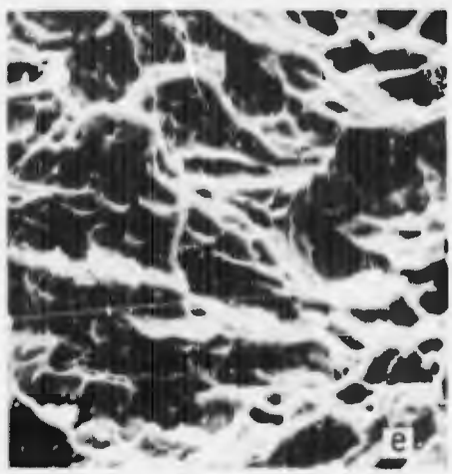

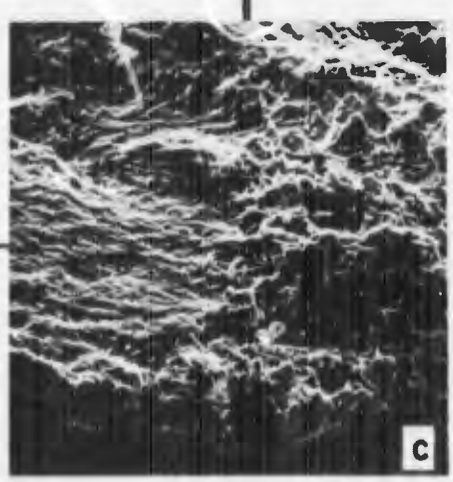

Figure 36

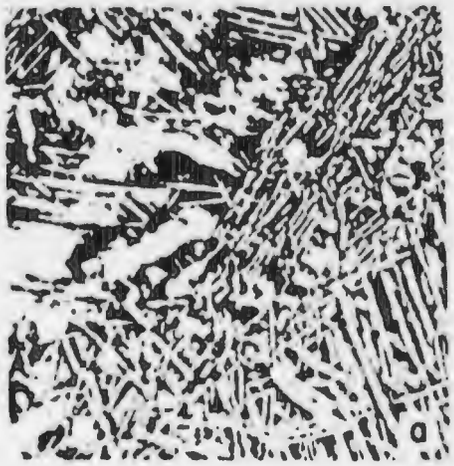
a


d

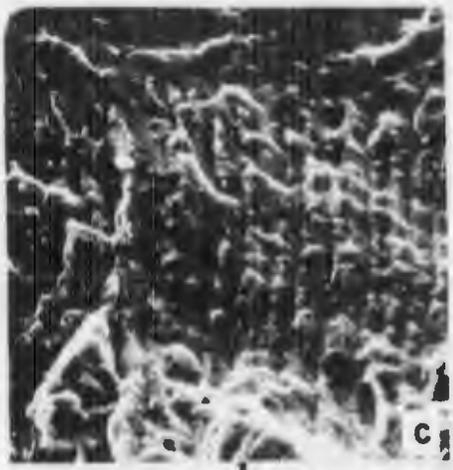
c


g

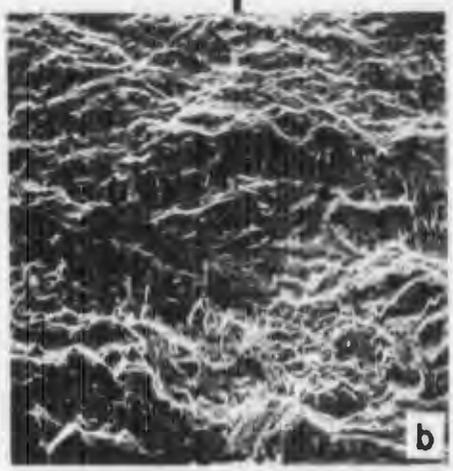
b

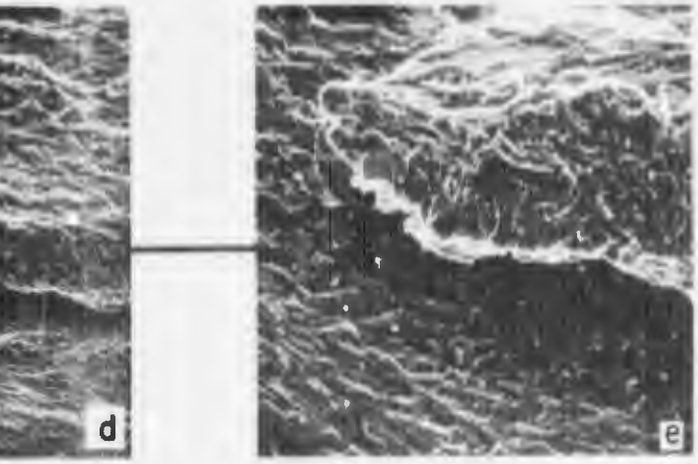

Ti-6Al-2Sn-4Zr-6Mo Condition F, STA

a) Light micrograph; 500X

b,c,d,e) Precrack zone; 400X, 2000X, 150X, 600X

f,g,h) Fatigue to fast fracture transition; 400X, 2000X, 2000X

i,j) Fast fracture zone; 400X, 4000X

YS = 161 KSI

UTS = 177 KSI

K_{Ic} = 31.6 KSI$\sqrt{in}$

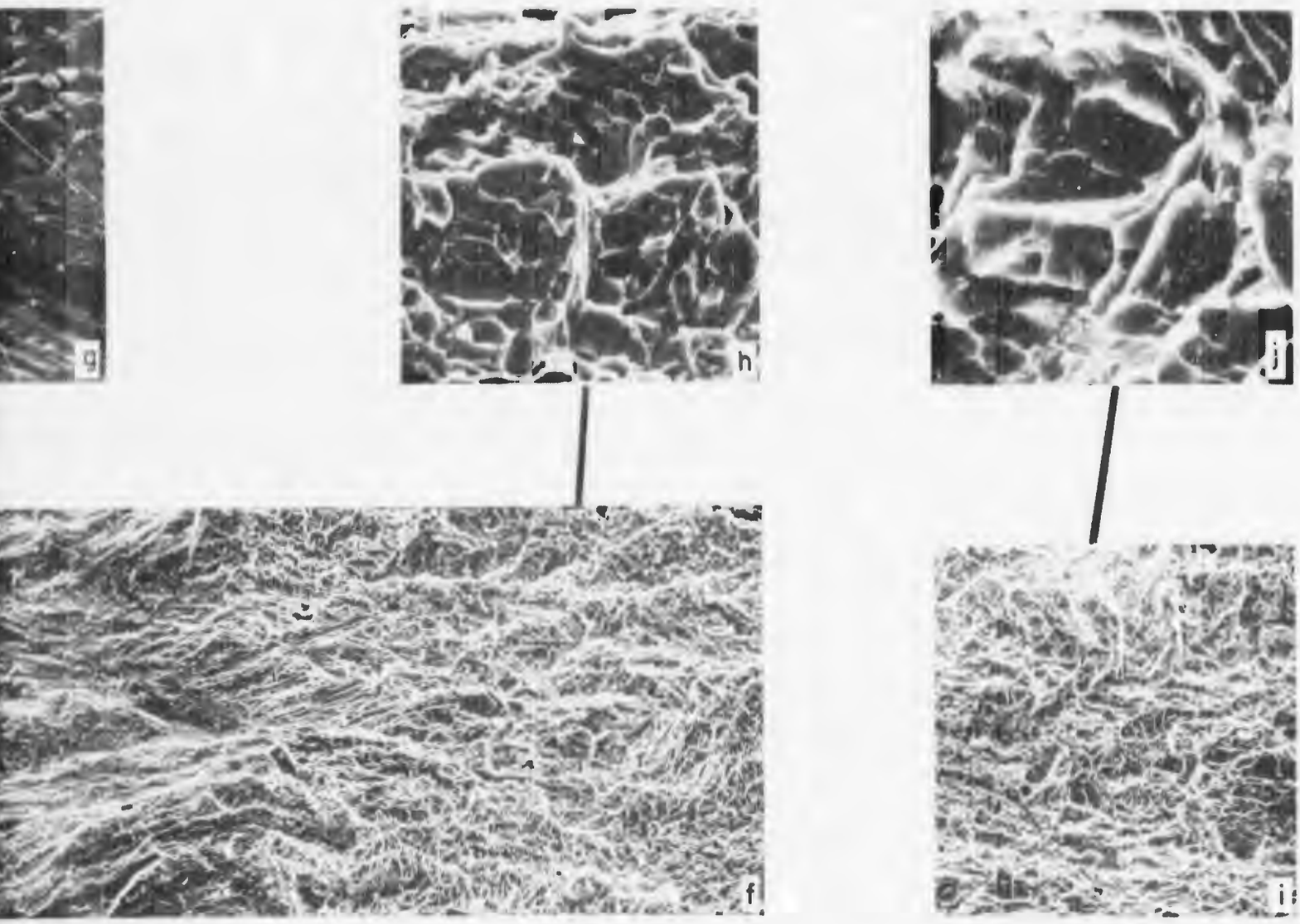

Figure 37

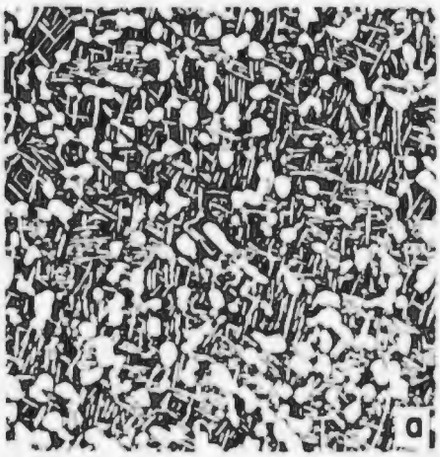

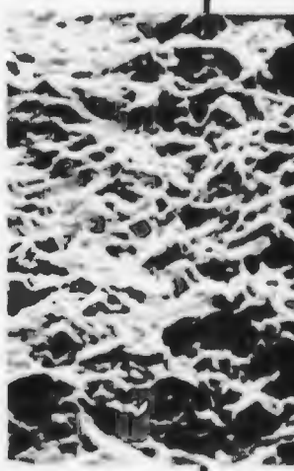

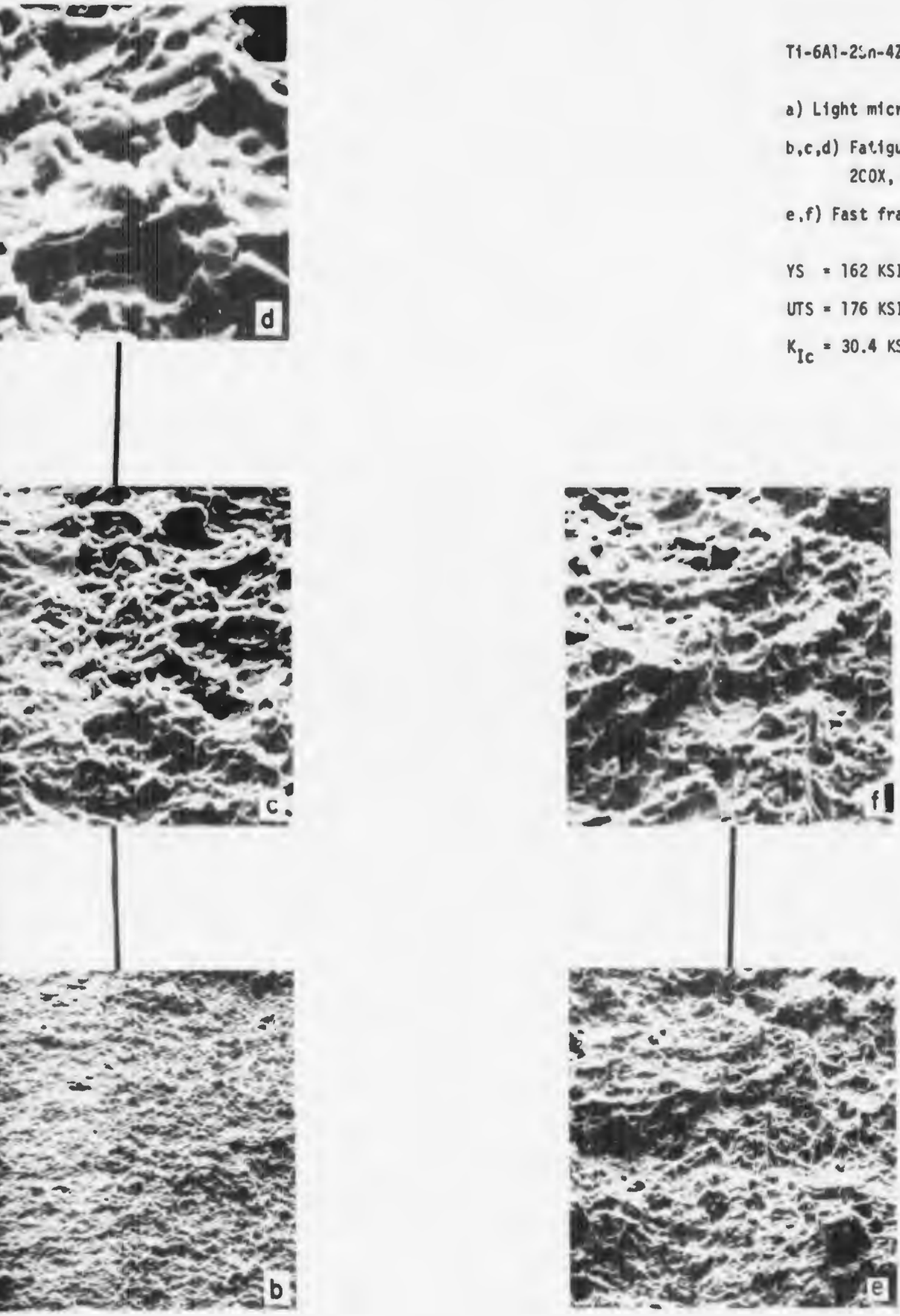

Ti-6Al-2Sn-4Zr-6Mo Condition A, STA

a) Light micrograph; 500X

b,c,d) Fatigue to fast fracture transition; 200X, 800X, 2000X

e,f) Fast fracture zone; 400X, 800X

YS = 162 KSI

UTS = 176 KSI

K_{Ic} = 30.4 KSI$\sqrt{in}$

Figure 38

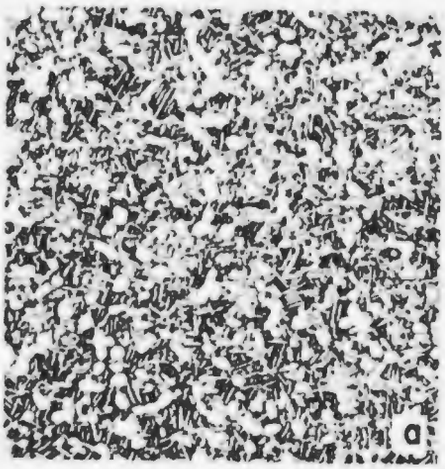
a

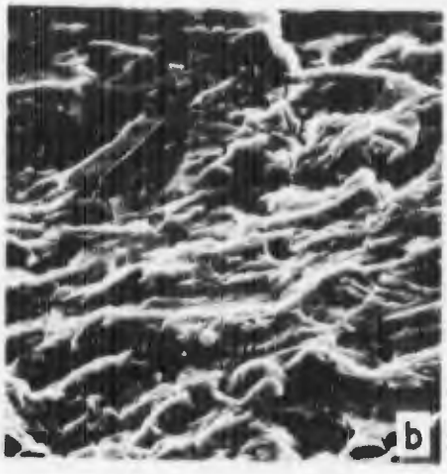
b

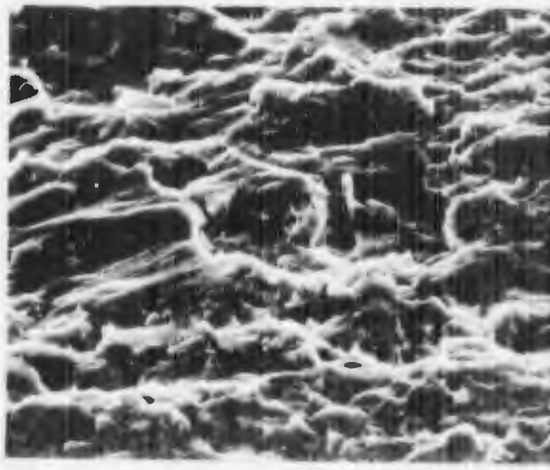

Ti-6Al-2Sn-4Zr-6Mo Condition A-2, STOA

a) Light micrograph; 500X

b) Precrack zone; 2000X

c,d) Fatigue to fast fracture transition; 400X, 2000X

e,f,g) Fast fracture zone; 200X, 800X, 2000X

YS = 148 KSI

UTS = 158 KSI

K_{Ic} = 27.1 KSI$\sqrt{in}$

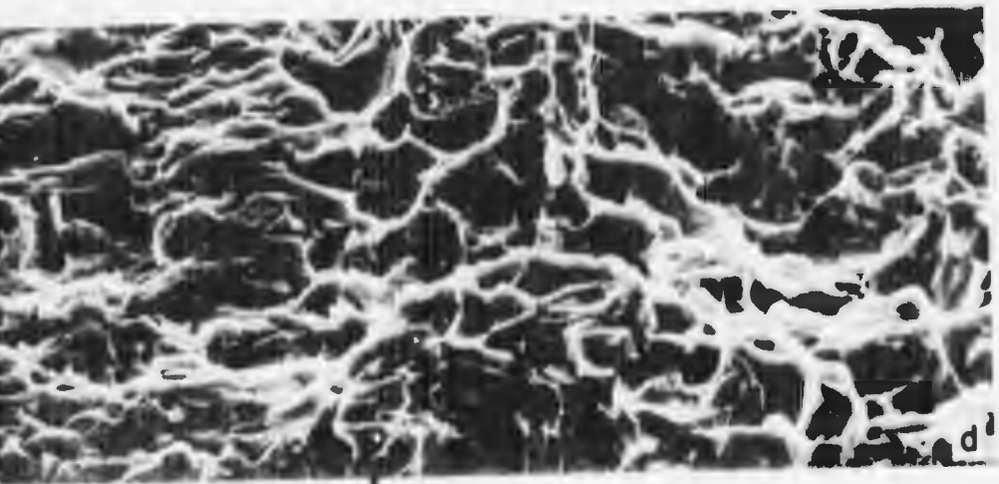

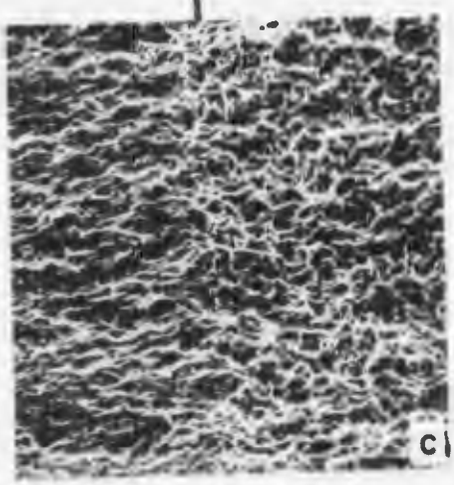

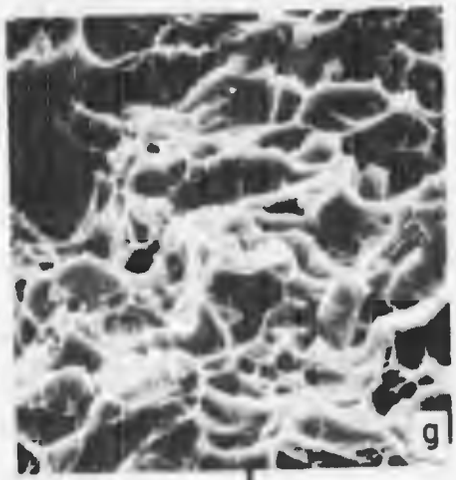

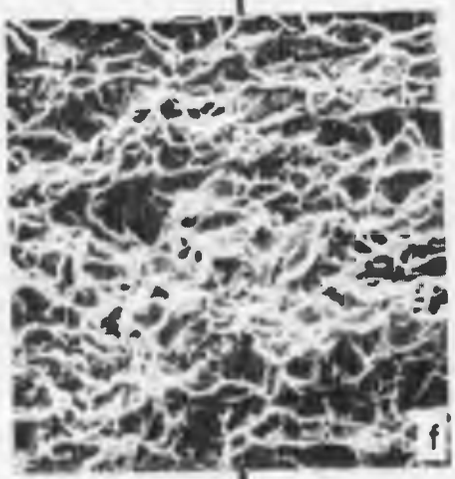

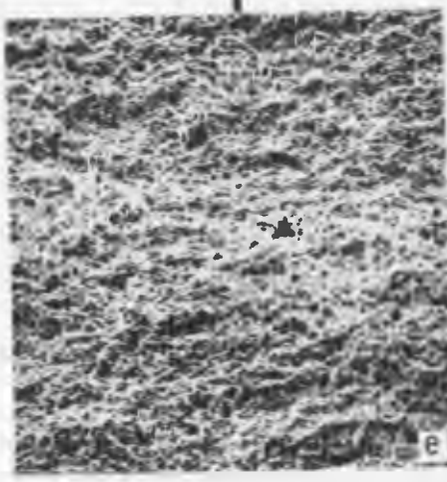

Figure 39

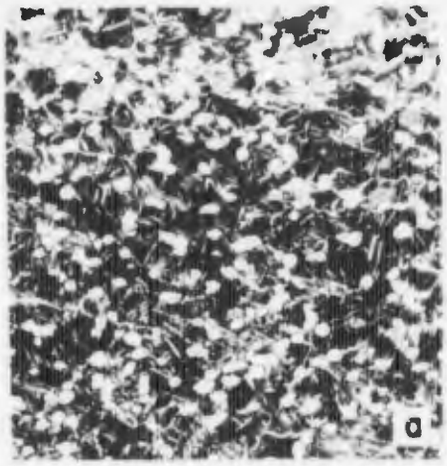
a

Ti-6Al-2Sn-4Zr-6Mo Condition A-1, ANN

a) Light micrograph; 500X

b,c) Precrack zone; 2000X, 4000X

d,e) Fatigue to fast fracture transition; 400X, 1600X

f,g) Fast fracture zone; 800X, 2000X

YS = 148 KSI

UTS = 161 KSI

K_{Ic} = 26.7 KSI$\sqrt{in}$

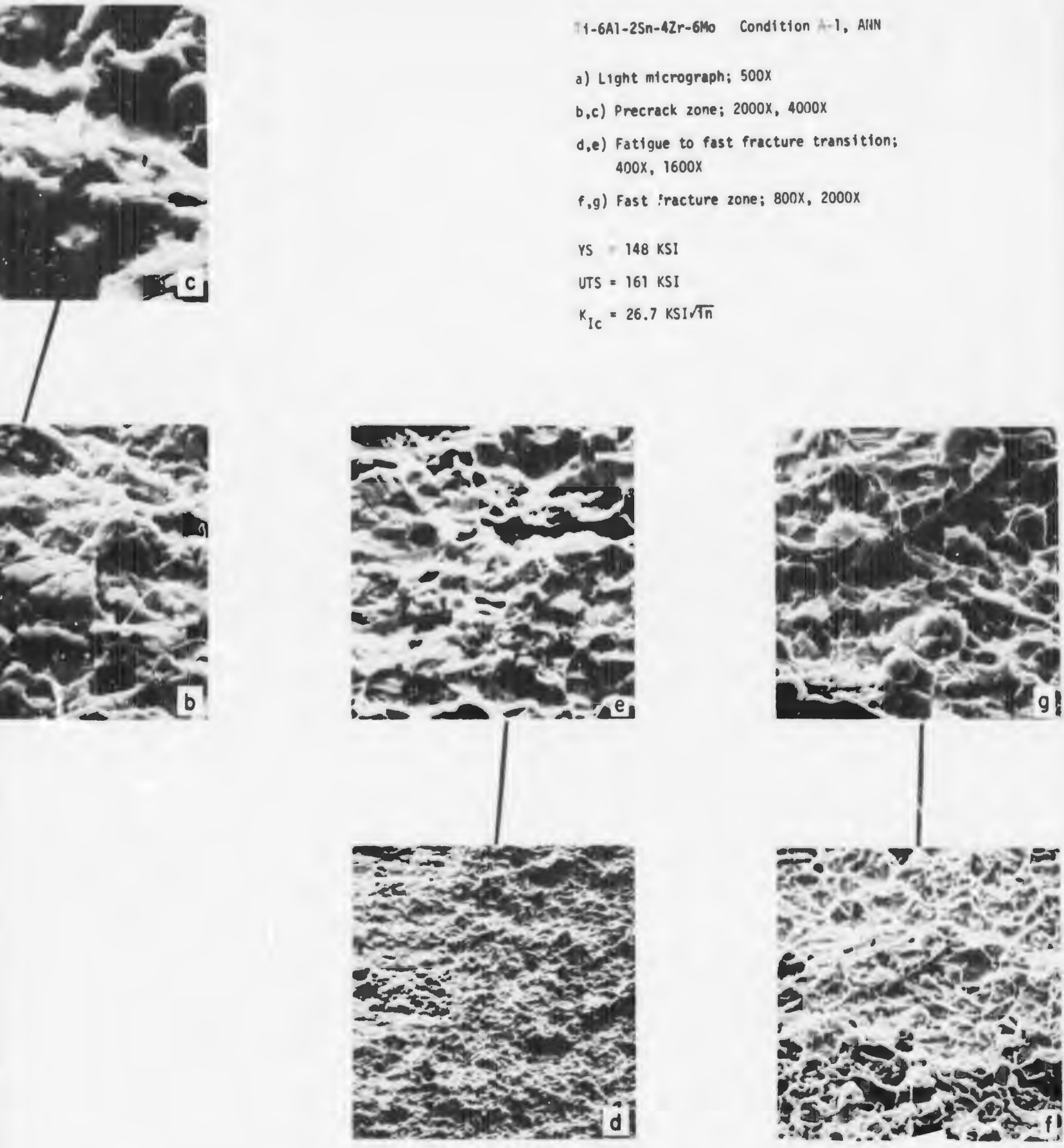

Figure 40

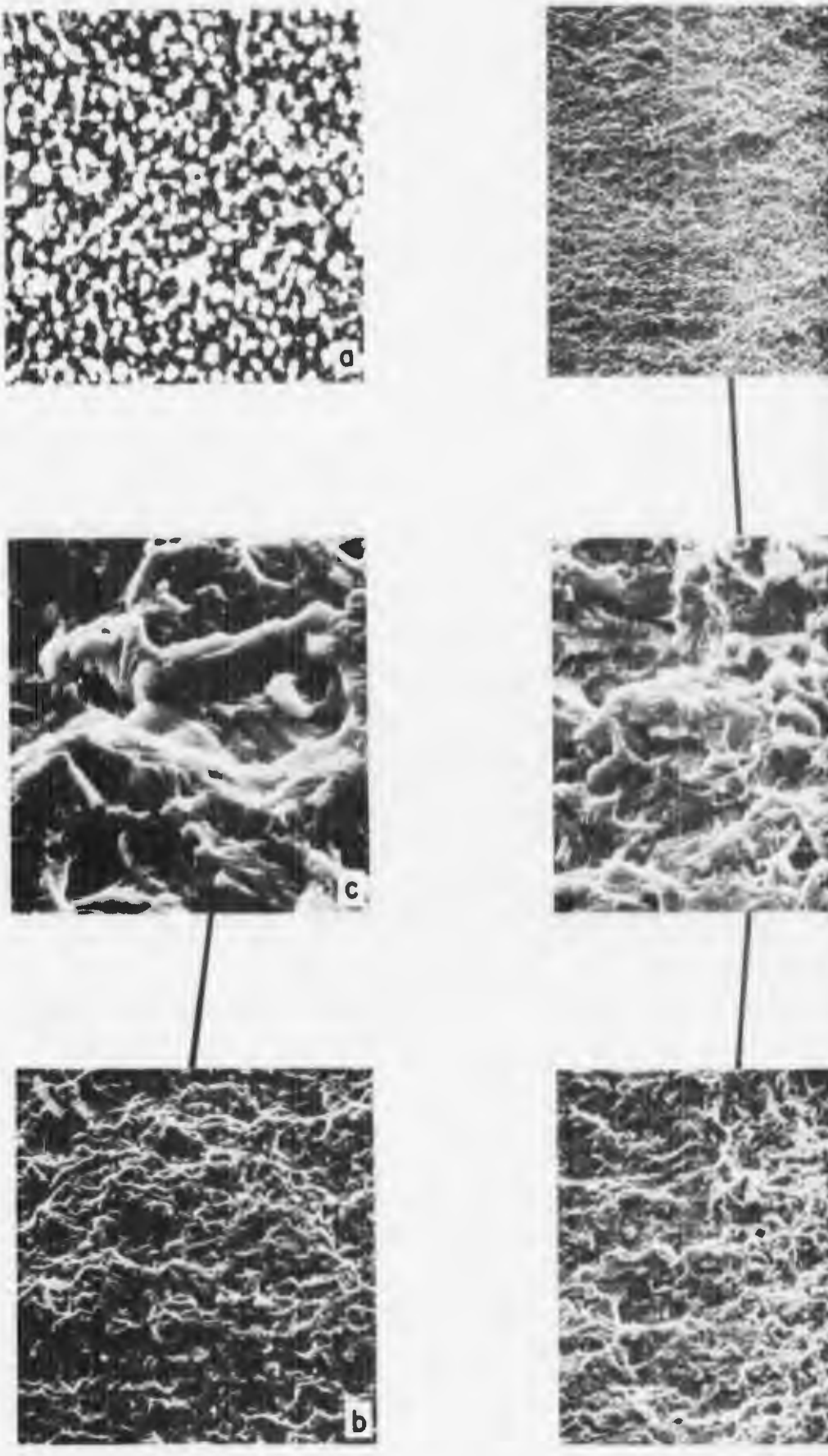
a
c
b

Ti-6A -2Sn-4Zr-6Mo Condition [illegible] TA

a) Light micrograph; 500X

b,c) Precrack zone; 800X, 4000X

d,e,f Fatigue to fast fracture transition; 200X, 800X, 2000X

g,h) [illegible]ast fracture zone near the transition; 800X, 4000X

i,j) Fast fracture zone; 800X, 4000X

YS = 167 KSI

UTS = 180 KSI

K_{Ic} = 24.8 KSI$\sqrt{in}$

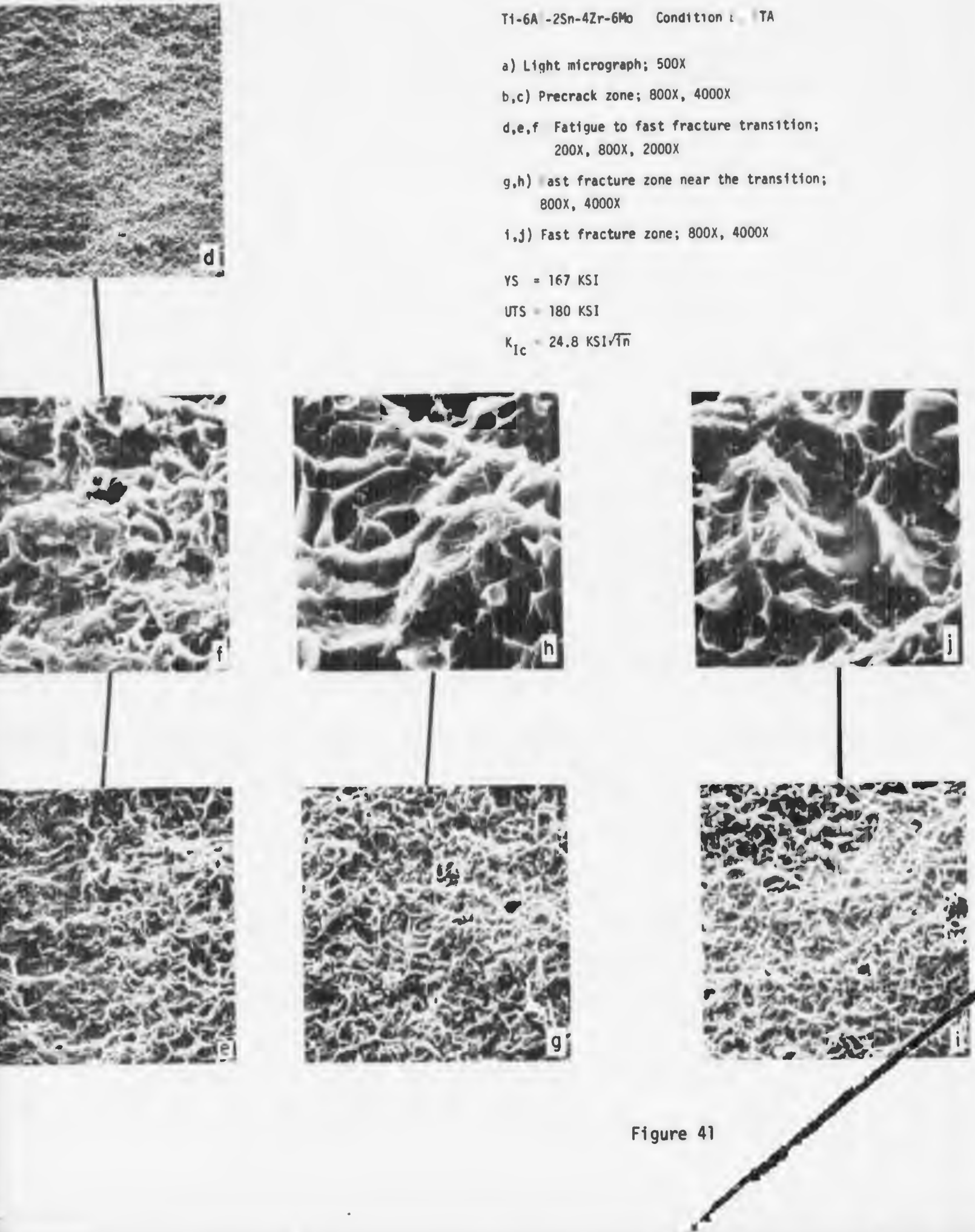

Figure 41

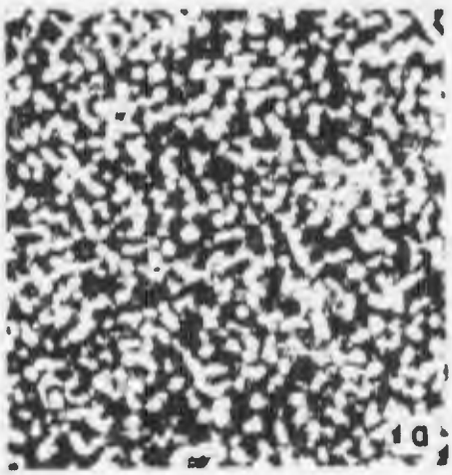

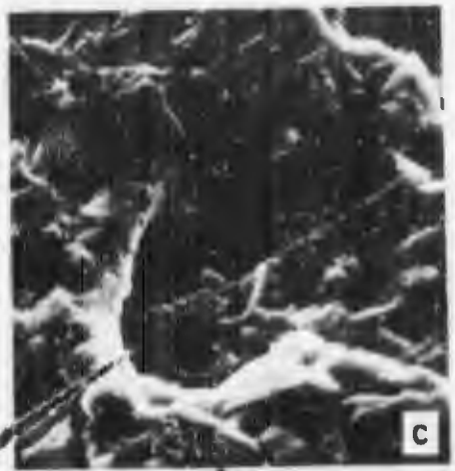

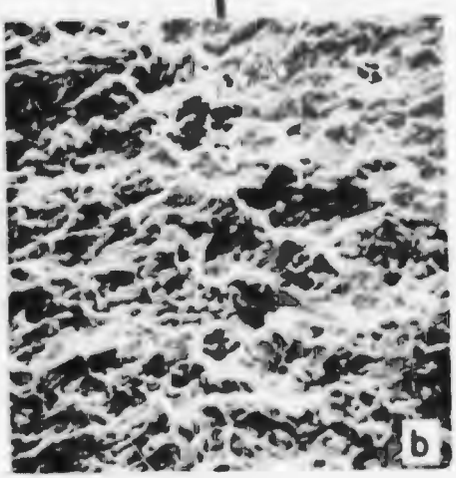

Preceding page blank

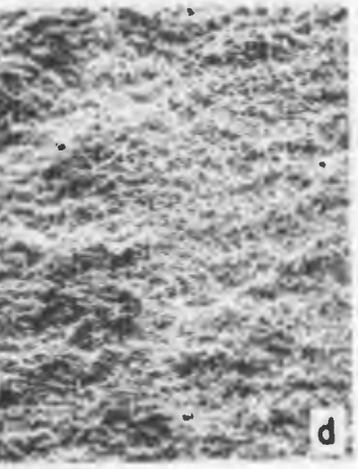

Ti-6Al-2Sn-4Zr-6Mo Condition B-2, STOA

a) Light micrograph; 500X

b,c) Precrack zone; 800X, 4000X

d,e) Fatigue to fast fracture transition; 160X, 800X

f,g) Fast fracture zone near the transition; 800X, 2000X

h,i) Fast fracture zone; 400X, 2000X

YS = 155 KSI

UTS = 166 KSI

K_{Ic} = 23.3 KSI$\sqrt{in}$

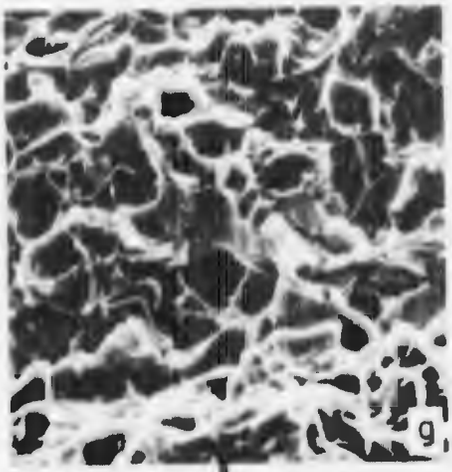

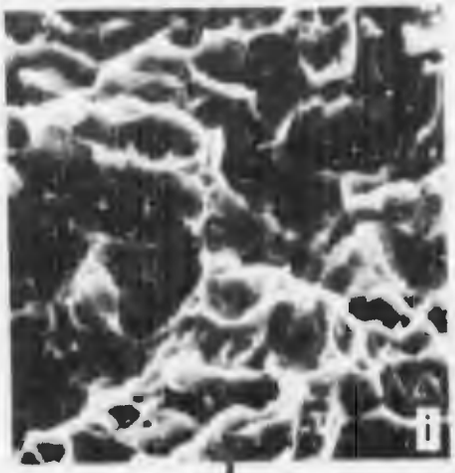

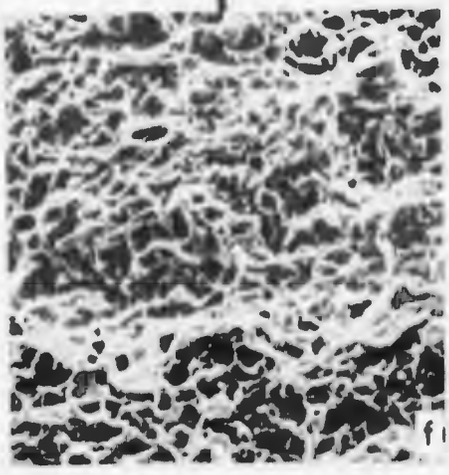

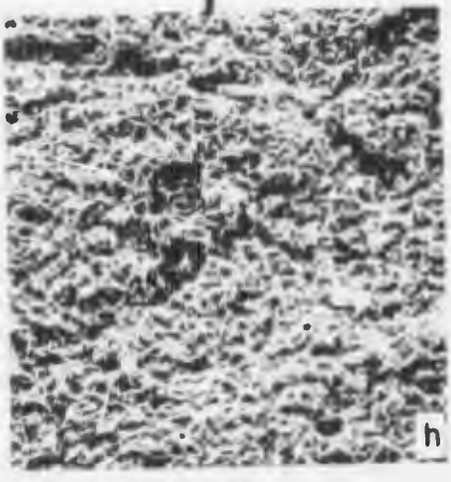

Figure 42

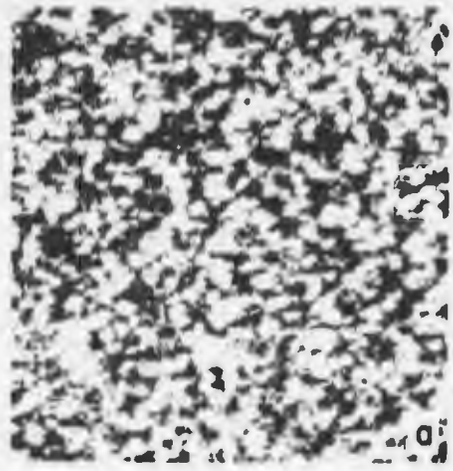

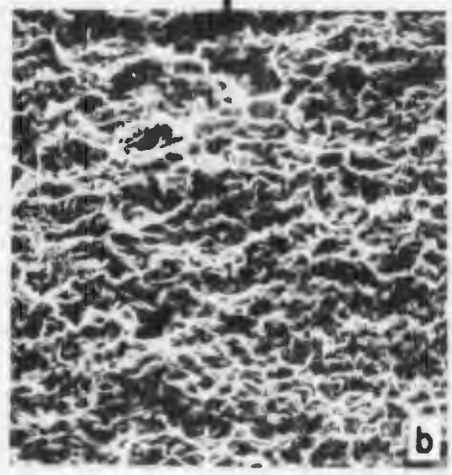

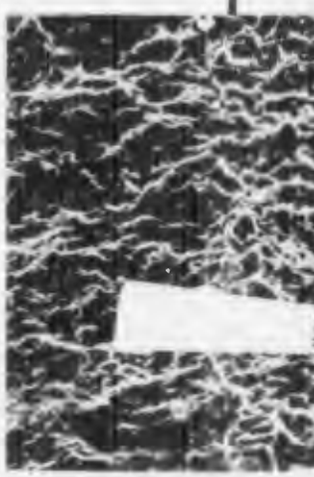

Preceding page blank

Ti-6Al-2Sn-4Zr-6Mo Condition B-1, ANN

a) Light micrograph; 500X

b,c) Precrack zone; 800X, 2000X

d,e) Fatigue to fast fracture transition; 800X, 1600X

f,g) Fast fracture near the transition;
800X, 4000X

h,i) Fast fracture zone; 800X, 4000X

YS = 154 KSI

UTS = 164 KSI

K_{Ic} = 22.7 KSI$\sqrt{in}$

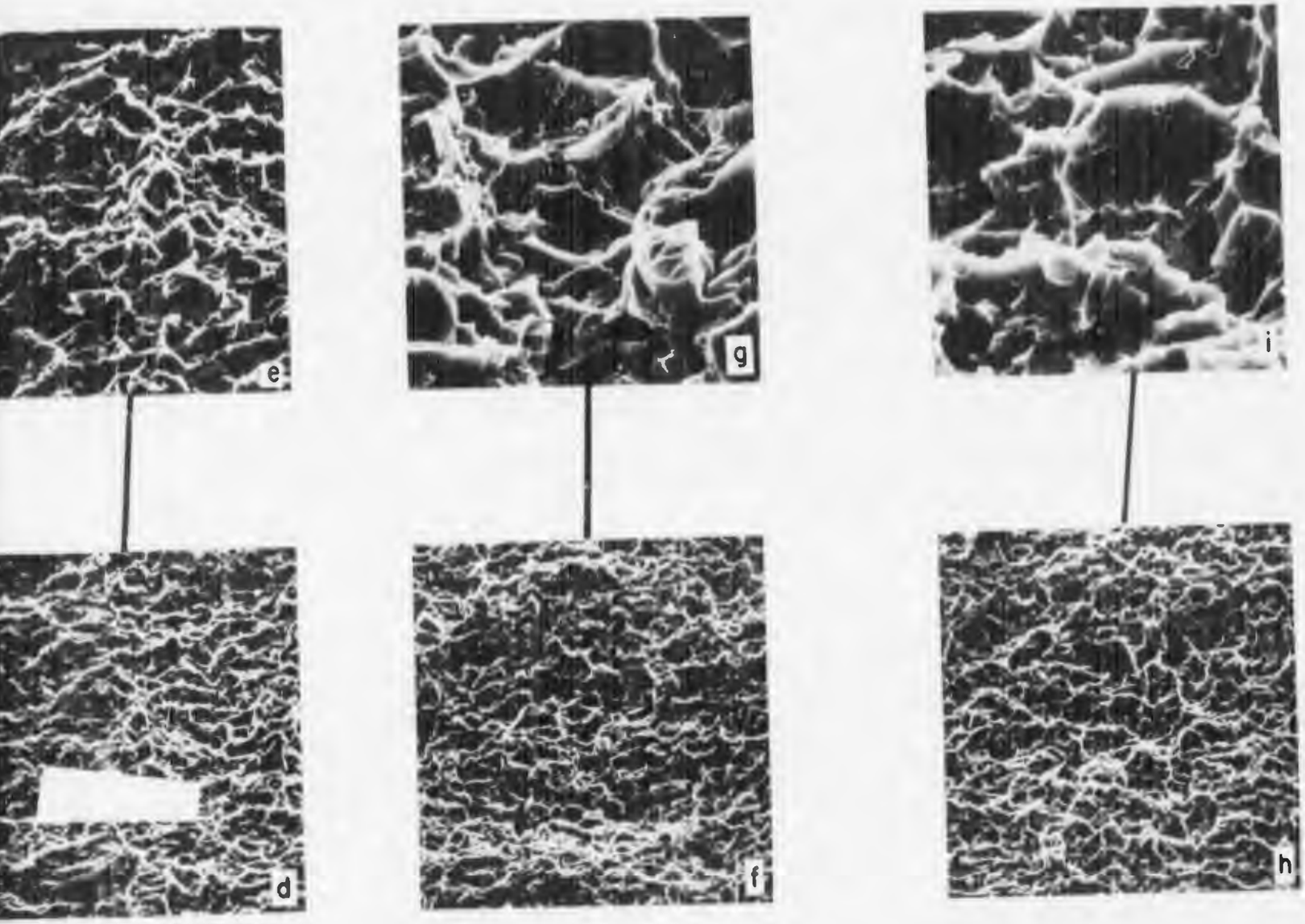

Figure 43